



**VNiVERSiDAD  
D SALAMANCA**

CAMPUS DE EXCELENCIA INTERNACIONAL

Facultad de Ciencias  
Departamento de Geología – Área de Paleontología

# **Estudio de un episodio de alta calcificación del nanoplancton calcáreo durante el Mid- Brunhes (Pleistoceno)**

**Alba González Lanchas**

TESIS DOCTORAL

Salamanca, 2021





**VNiVERSiDAD  
D SALAMANCA**

CAMPUS DE EXCELENCIA INTERNACIONAL

Facultad de Ciencias  
Departamento de Geología – Área de Paleontología

# **Estudio de un episodio de alta calcificación del nanoplancton calcáreo durante el Mid- Brunhes (Pleistoceno)**

Memoria de tesis en el formato de compendio de artículos presentada por  
**Alba González Lanchas** para optar al grado de **Doctor en Geología** por la  
Universidad de Salamanca con Mención Internacional

Directores de la Tesis:

**Dr. José-Abel Flores Villarejo**

Catedrático del Departamento de Geología (Área de Paleontología)  
Universidad de Salamanca

**Dr. Francisco Javier Sierro Sánchez**

Catedrático del Departamento de Geología (Área de Paleontología)  
Universidad de Salamanca

Salamanca, 2021



Los Doctores D. José-Abel Flores Villarejo y D. Francisco Javier Sierra Sánchez, catedráticos del Área de Paleontología en el Departamento de Geología de la Facultad de Ciencias de la Universidad de Salamanca

CERTIFICAN:

Que Dña. Alba González Lanchas ha realizado en el Área de Paleontología del Departamento de Geología de la Universidad de Salamanca y bajo nuestra supervisión el trabajo: **“Estudio de un episodio de alta calcificación del nanoplancton calcáreo durante el Mid-Brunhes (Pleistoceno)”**

y AUTORIZAN:

Su presentación mediante el formato de compendio de artículos/publicaciones según la normativa aprobada por la comisión de Doctorado y Posgrado de la Universidad de Salamanca el 25 de febrero de 2013, al considerar que se han alcanzado los objetivos inicialmente previstos.

Y para que así conste, firmamos el presente certificado en Salamanca, en noviembre de 2021

Los directores:

Fdo.: José-Abel Flores Villarejo

Fdo.: Francisco J. Sierra Sánchez

El doctorando:

Fdo.: Alba González Lanchas



Esta tesis doctoral se presenta como un compendio de **tres artículos publicados**:

**1. “A new perspective of the *Alboran Upwelling System* reconstruction during the Marine Isotope Stage 11: a high-resolution coccolithophore record”**

**Alba González-Lanchas**<sup>a</sup>, José-Abel Flores<sup>a</sup>, Francisco J. Sierro<sup>a</sup>, María Ángeles Bárcena<sup>a</sup>, Andrés S. Rigual-Hernández<sup>a</sup>, Dulce Oliveira<sup>b,c</sup>, Lucía A. Azibeiro<sup>a</sup>, Maria Marino<sup>d</sup>, Patrizia Maiorano<sup>d</sup>, Aleix Cortina<sup>e</sup>, Isabel Cacho<sup>f</sup> y Joan O. Grimalt<sup>e</sup>.

<sup>a</sup> Departamento de Geología, Universidad de Salamanca, 37008 Salamanca, España.

<sup>b</sup> Centro de Ciências do Mar (CCMAR), Universidade do Algarve, Campus de Gambelas, 8005-139 Faro, Portugal.

<sup>c</sup> Divisão de Geologia e Georecursos Marinhos, Instituto Português do Mar e da Atmosfera (IPMA), Av. Doutor Alfredo Magalhães Ramalho 6, 1495-165 Algés, Portugal.

<sup>d</sup> Dipartimento di Scienze della Terra e Geoambientali, Università degli Studi di Bari Aldo Moro, Bari, Italia.

<sup>e</sup> Department of Environmental Chemistry, IDAEA-CSIC, Barcelona, 08034, España.

<sup>f</sup> GRC Geociències Marines, Departament de Dinàmica de la Terra i de l'Oceà, Facultat de Ciències de la Terra, Universitat de Barcelona, Barcelona, 08028, España.

*Quaternary Science Reviews* 245, 106520.

DOI: [10.1016/j.quascirev.2020.106520](https://doi.org/10.1016/j.quascirev.2020.106520)

**2. “Control mechanisms of Primary Productivity revealed by calcareous nanoplankton from Marine Isotope Stages 12 to 9 at the Shackleton Site (IODP Site U1385)”**

**Alba González-Lanchas**<sup>a</sup>, José-Abel Flores<sup>a</sup>, Francisco J. Sierro<sup>a</sup>, María Fernanda Sánchez Goñi<sup>b,c</sup>, Teresa Rodrigues<sup>d,e</sup>, Blanca Ausin<sup>a</sup>, Dulce Oliveira<sup>d,e</sup>, Filipa Naughton<sup>e,f</sup>, Maria Marino<sup>f</sup>, Patrizia Maiorano<sup>f</sup> y Barbara Balestra<sup>g,h,i</sup>.

<sup>a</sup> Departamento de Geología, Universidad de Salamanca, 37008 Salamanca, España.

<sup>b</sup> École Pratique des Hautes Études (EPHE, PSL University), F-33615, Pessac, Francia.

<sup>c</sup> Université Bordeaux, EPOC, UMR 5805, F-33615, Pessac, Francia.

<sup>d</sup> CCMAR, Centro de Ciências do Mar, Universidade do Algarve, Campus de Gambelas, 8005-139, Faro, Portugal.

<sup>e</sup> Divisão de Geologia e Georecursos Marinhos, Instituto Português do Mar e da Atmosfera, Av. Doutor Alfredo Magalhães Ramalho 6, 1495-165, Algés, Portugal.

<sup>f</sup> Dipartimento di Scienze della Terra e Geoambientali, Università degli Studi di Bari Aldo Moro, Bari, Italia.

<sup>g</sup> American University, Department of Environmental Science, Washington, DC 20016, United States.

<sup>h</sup> National Museum of Natural History, (NMNH) Smithsonian, Paleobiology Department, Washington, DC 20560, United States.

<sup>i</sup> University of California Santa Cruz, Institute of Marine Sciences Department, Santa Cruz, CA 95064, United States.

*Paleoceanography and Paleoclimatology* 36(6), e2021PA004246.

DOI: [10.1029/2021PA004246](https://doi.org/10.1029/2021PA004246)

### 3. “Carbon Isotopic Fractionation of Alkenones and *Gephyrocapsa* Coccoliths Over the Late Quaternary (Marine Isotope Stages 12–9) Glacial-Interglacial Cycles at the Western Tropical Atlantic”

Alba González-Lanchas <sup>a</sup>, Iván Hernández-Alméida <sup>b</sup>, José-Abel Flores <sup>a</sup>, Francisco J. Sierra <sup>a</sup>, José Guitián <sup>b</sup> y Heather M. Stoll <sup>b</sup>

<sup>a</sup> Departamento de Geología, Universidad de Salamanca, 37008 Salamanca, España.

<sup>b</sup> Geological Institute, ETH Zürich, Zürich, Switzerland.

*Paleoceanography and Paleoclimatology* 36(8), e2020PA004175.

DOI: [10.1029/2020PA004175](https://doi.org/10.1029/2020PA004175)



Además, se presentan **dos artículos** en proceso de revisión y de preparación para envío:

**4. “Western Mediterranean deep paleoenvironmental conditions in response to surface organic productivity and regional deep dynamics during MIS 11”**

**Alba González-Lanchas**<sup>a</sup>, Javier Dorador<sup>b</sup>, Francisco J. Rodríguez-Tovar<sup>b</sup>, Francisco J. Sierro<sup>a</sup> y José-Abel Flores<sup>a</sup>

<sup>a</sup> Departamento de Geología, Universidad de Salamanca, 37008 Salamanca, España.

<sup>b</sup> Departamento de Estratigrafía y Paleontología, Universidad de Granada, 18002 Granada, España.

Artículo **en revisión** en *Marine Geology*

**5. “About the Mid-Brunhes interval and the role of the stumper coccolithophore *Gephyrocapsa* complex”**

**Alba González-Lanchas**<sup>a</sup>, Andrés S. Rigual-Hernández<sup>a</sup>, Francisco J. Sierro<sup>a</sup>, Montserrat Alonso-García<sup>a</sup> y José-Abel Flores<sup>a</sup>

<sup>a</sup> Departamento de Geología, Universidad de Salamanca, 37008 Salamanca, España

Artículo **en preparación** para ser enviado a *Nature Communications*

La realización del presente trabajo ha sido posible gracias a la concesión de un contrato predoctoral de Formación de profesorado Universitario (FPU17/03349) y la obtención de financiación para estancias breves (EST18/00842) por parte del Ministerio de Ciencia, Innovación y Universidades a la autora, Alba González Lanchas. La obtención de la Ayuda Predoctoral de la Junta de Castilla y León (Q3718001E) contribuyó, también al desarrollo inicial de este proyecto.

La investigación desarrollada ha estado asociada a los proyectos *Impacto de la inestabilidad climática milenaria en el intercambio de agua entre el Atlántico y el Mediterráneo* (CGL2015-68459-P) y *Circulation Termohalina del Mediterráneo durante los últimos 500 Ka: Implicaciones para el sistema del carbonato* (RTI2018-099489-B-100) financiados, respectivamente, por el Ministerio de Economía y Competitividad y el Ministerio de Ciencia, Innovación y Universidades del gobierno de España concedidos al grupo de Geociencias Oceánicas (GGO) de la Universidad de Salamanca. El desarrollo de la parte de este estudio correspondiente al análisis geoquímico isotópico de compuestos orgánicos e inorgánicos en el Atlántico tropical ha contado con la colaboración y supervisión de la Dr. Heather M. Stoll, a quien, además, se le agradece la oportunidad de integración en su grupo de investigación, *Climate Geology*, durante la estancia de investigación realizada en ETH – Zürich (Suiza), para la aplicación de dicha línea de investigación en esta tesis doctoral.

Agradecemos a *Integrated Ocean Drilling Program* (IODP) por facilitar las muestras analizadas en los diferentes trabajos. También agradecemos a María Ángeles Bárcena, Montserrat Alonso-García, Joan O. Grimalt, Aleix Cortina, Isabel Cacho, Dulce Oliveira, Filipa Naughton, Teresa Rodrigues, María Fernanda Sánchez-Goñi, Francisco J. Rodríguez-Tovar y Javier Dorador por la disponibilidad de sus datos, que han sido empleados como complemento en los artículos presentados en esta tesis doctoral.



# ÍNDICE

<b>Resumen</b>	<b>4</b>
<b>Abstract</b>	<b>8</b>
<b>Justificación e hipótesis</b>	<b>12</b>
<b>Objetivos</b>	<b>15</b>
<b>Estructura de la tesis doctoral</b>	<b>18</b>
<b>CAPÍTULO 1. INTRODUCCIÓN</b>	<b>23</b>
<b>1.1. El episodio del Mid-Brunhes</b>	<b>23</b>
<b>1.2. Cocolitóforos, definición general y funciones vitales</b>	<b>27</b>
<b>1.3. El complejo <i>Gephyrocapsa</i> y “<i>Gephyrocapsa caribbeanica</i>”</b>	<b>30</b>
1.3.1. Morfología y criterios para su clasificación	34
1.3.2. Producción de alquenonas	39
<b>1.4. Cocolitóforos en la reconstrucción paleoceanográfica y paleoclimática</b>	<b>40</b>
1.4.1. Reconstrucción de la productividad primaria con <i>Gephyrocapsa</i>	43
1.4.2. <i>Florisphaera profunda</i> vs. <i>Gephyrocapsa</i>	44
1.4.3. Grupos sensibles a la temperatura de las masas de agua superficiales	46
<b>1.5. Fraccionamiento isotópico del carbono durante la fotosíntesis</b>	<b>48</b>
1.5.1. Conceptos teóricos y aplicación para la reconstrucción de CO <sub>2</sub>	48
1.5.2. Análisis de la sensibilidad de $\epsilon_p$ a CO <sub>2</sub> y otros factores	49
<b>1.6. Variaciones en la calcificación de cocolitóforos</b>	<b>51</b>
1.6.1. Reconstrucción de la calcificación en cocolitos fósiles	53
<b>1.7. Efectos vitales de oxígeno y carbono en cocolitos</b>	<b>55</b>
<b>1.8. Materiales para el análisis</b>	<b>58</b>
1.8.1. Paleoceanografía de alta resolución en el Márgen Ibérico	59
1.8.2. Geoquímica orgánica y en cocolitos en el Atlántico tropical	60
1.8.3. Morfometría y calcificación en el Atlántico Norte y Mediterráneo	61
<b>Referencias</b>	<b>62</b>
<b>CAPÍTULO 2</b>	<b>77</b>
<b>"A new perspective of the <i>Alboran Upwelling System</i> reconstruction during the Marine Isotope Stage 11: a high-resolution coccolithophore record"</b>	
(González-Lanchas et al., 2020; <i>Quaternary Science Reviews</i> )	
<b>Resumen</b>	<b>78</b>
<b>Artículo</b>	<b>95</b>

<b>CAPÍTULO 3</b>	<b>84</b>
<b>"Control mechanisms of primary productivity revealed by calcareous nannoplankton from Marine Isotope Stages 12 to 9 at the Shackleton Site (IODP Site U1385)"</b>	
(González-Lanchas et al., 2021a; <i>Paleoceanography and Paleoclimatology</i> )	
<b>Resumen</b>	<b>102</b>
<b>Artículo</b>	<b>121</b>
<b>CAPÍTULO 4</b>	<b>130</b>
<b>"Carbon isotopic fractionation of alkenones and <i>Gephyrocapsa</i> coccoliths over the late Quaternary (Marine Isotope Stages 12 to 9) glacial-interglacial cycles at the Western Tropical Atlantic"</b>	
(González-Lanchas et al., 2021b; <i>Paleoceanography and Paleoclimatology</i> )	
<b>Resumen</b>	<b>131</b>
<b>Artículo</b>	<b>150</b>
<b>Información suplementaria</b>	
<b>CAPÍTULO 5</b>	<b>184</b>
<b>"Western Mediterranean deep-sea environmental conditions in response to surface organic productivity and regional circulation dynamics during the MIS 11"</b>	
(González-Lanchas et al., en revisión en <i>Marine Geology</i> )	
<b>Resumen</b>	<b>185</b>
<b>Artículo</b>	<b>201</b>
<b>CAPÍTULO 6</b>	<b>218</b>
<b>"About the Mid-Brunhes interval and the role of the stumper coccolithophore <i>Gephyrocapsa</i> complex"</b>	
(González-Lanchas et al., en preparación para envío a <i>Nature Communications</i> )	
<b>Resumen</b>	<b>219</b>
<b>Artículo</b>	<b>235</b>
<b>CAPÍTULO 7. CONCLUSIONES</b>	<b>262</b>
<b>CONCLUSIONS</b>	<b>266</b>
<b>ANEXOS</b>	<b>272</b>
<b>Anexo I. Sistemática de los taxones estudiados</b>	<b>272</b>
<b>Anexo II. Lámina fotográfica</b>	<b>274</b>

<b>Anexo III. Publicación adicional</b>	<b>276</b>
"Middle Eocene calcareous nannofossils in the Jaca transect (South-Central Pyrenees Eocene basin, Aragón River valley, Huesca)" (González-Lanchas et al., 2019; <i>Spanish Journal of Palaeontology</i> )	
<b>Anexo IV. Publicación adicional</b>	<b>293</b>
"Limited variability in the phytoplankton <i>Emiliana huxleyi</i> since the pre-industrial era in the subantarctic Southern Ocean" (Rigual-Hernández et al., 2020; <i>Anthropocene</i> )	
<b>Anexo V. Publicación adicional</b>	<b>310</b>
Preliminary results of Research Vessel (R/V) Meteor Cruise M149: Biostratigraphy	

## Resumen

El evento del Mid-Brunhes (MBE-*Mid Brunhes Event*), centrado en la edad de ~ 430 mil años (ka), es un proceso de cambio climático de entidad global en el que la ciclicidad glacial/interglacial (G/I) experimenta un significativo incremento en su amplitud. El intervalo que contiene este evento ilustra escenarios climáticos glaciales e interglaciales altamente contrastados dentro de la historia del Pleistoceno reciente, donde destacan las condiciones interglaciales altamente cálidas y duraderas del estadio isotópico marino (MIS-*Marine Isotope Stage*) 11. Dentro de los límites de este intervalo, tiene lugar la eclosión del complejo *Gephyrocapsa*, un grupo de especies de cocolitóforos (algas fitoplanctónicas calcificadoras) que domina los ambientes fitoplanctónicos globales y, en particular, la proliferación de la especie y/o morfotipo “*Gephyrocapsa caribbeanica*”. Esta tesis doctoral pretende contribuir a la discusión de cuestiones de alto grado de interés concernientes a este episodio, como la evolución climática del Atlántico Norte durante determinados estadios críticos, como en ya referido MIS 11 y los mecanismos de transferencia de la señal climática hacia las latitudes medias de la península ibérica, así como el papel jugado por las especies o morfotipos del complejo *Gephyrocapsa* durante este intervalo del Mid-Brunhes.

Para la realización de este trabajo, se han abordado diferentes casos de estudio específicos, mediante la aplicación de técnicas de análisis de diferente naturaleza, concretados en artículos científicos. Estos artículos pueden agruparse e identificarse con tres bloques generales de i) reconstrucción paleoceanográfica de alta resolución en el margen Ibérico a partir de la señal del complejo *Gephyrocapsa*, ii) evaluación de la sensibilidad fotosintética de *Gephyrocapsa* al CO<sub>2</sub>, a partir de la sensibilidad del fraccionamiento isotópico del carbono orgánico durante la fotosíntesis ( $\epsilon_p$ ) y de sus efectos vitales en los isótopos de oxígeno y carbono en el sector Oeste del Atlántico tropical y iii) caracterización morfométrica y de los cambios en la calcificación del complejo *Gephyrocapsa* en el Atlántico Norte y el sector occidental del mar Mediterráneo.

El primero de los bloques se desarrolla con la aplicación de un enfoque de análisis micropaleontológico de las asociaciones de cocolitóforos en los márgenes Mediterráneo

(testigo ODP *Site* 977, ubicado en el mar de Alborán) y Atlántico (testigo IODP *Site* U1385, ubicado en el sector sur de la costa portuguesa) de la península Ibérica. Los artículos científicos recogidos en los Capítulos 2, 3 y 5 se adscriben a este bloque. En ellos se emplea la señal de productividad del complejo *Gephyrocapsa* para la reconstrucción de la intensidad de los sistemas de surgencia o *upwelling* en ambas regiones. La integración de estos datos con indicadores geoquímicos isotópicos ( $\delta^{18}\text{O}$  y  $\delta^{13}\text{C}$ ), marcadores orgánicos para la reconstrucción del índice  $U^k_{37}$  y calibración de las temperaturas superficiales (SST-*Sea Surface Temperatures*), así como marcadores de origen terrestre (marcadores polínico y fitolitos silíceos), permite reconstruir las condiciones paleoceanográficas y atmosféricas regionales asociadas a los escenarios de producción e intensidad del *upwelling* durante el MIS 11 (430-376 ka), en el caso del margen ibérico Mediterráneo y del MIS 12 a 9 (420-397 ka) en el margen ibérico Atlántico. El mecanismo de transferencia de la señal climática hacia las latitudes ibéricas a escala G/I, es la intensificación de la célula atmosférica de altas presiones de Azores y su control sobre la circulación regional y los sistemas de *upwelling* en ambas regiones. Esta operación estaría potencialmente controlada por los cambios en los gradientes de presiones en el Atlántico Norte, que determinarían una variabilidad comparable a la Oscilación del Atlántico Norte (NAO-*North Atlantic Oscillation*) moderna, principalmente representada por la evolución hacia valores positivos durante el interglacial MIS 11. La prevalencia de este modelo de control atmosférico sobre la productividad en ambas regiones cesa durante los episodios de enfriamiento extremo y abrupto de tipo *Heinrich* (Ht-*Heinrich type*), a causa de diferentes impactos de tipo hidrológico y/o de los cambios en las temperaturas sobre los sistemas de *upwelling* y la producción nanoplanctónica en ambas regiones.

Para el segundo bloque, se lleva a cabo un enfoque de integración de técnicas de diferente naturaleza, con una especial relevancia de los análisis geoquímicos isotópicos sobre, las alquenonas ( $\delta^{13}\text{C}_{37:2}$ ), y los cocolitos producidos por el complejo *Gephyrocapsa* ( $\delta^{18}\text{O}$  y  $\delta^{13}\text{C}$ ), respectivamente. El artículo científico y material suplementario contenidos en el Capítulo 4 constituye íntegramente este bloque. El tratamiento, análisis y cálculos, a partir de estos datos medidos con un patrón de baja resolución en la región tropical del Atlántico Norte (testigo ODP *Site* 925) durante el intervalo comprendido entre el MIS 12 y 9 (454-334 ka) permite la obtención de medidas de la variabilidad de valor de



fraccionamiento isotópico del carbono orgánico durante la fotosíntesis ( $\epsilon_p$ ) y de los efectos vitales de los isótopos de oxígeno y carbono registrados en los cocolitos de *Gephyrocapsa*. Para llevar a cabo un ejercicio de análisis de la sensibilidad de estos valores a los cambios ambientales durante el intervalo y fisiológicos, por parte de este grupo, se llevó a cabo la medida directa o estimación de los principales parámetros influyentes, como los cambios en las tallas celulares de *Gephyrocapsa*, cambios en las condiciones de productividad, disponibilidad de luz y tasas de crecimiento celular. Los datos empleados para ello son de tipo micropaleontológico, como el análisis de la asociación de cocolitóforos, de tipo geoquímicos, como la medida de  $\delta^{18}\text{O}$  y  $\delta^{13}\text{C}$  en varias especies de foraminíferos planctónicos y cálculo de gradientes isotópicos, o el cálculo y calibración de  $U^{k'}_{37}$ -SST, así como de análisis de imagen, para la obtención de medidas morfométricas de talla, masa y espesor en los cocolitos de *Gephyrocapsa*. La disponibilidad de estos datos junto con la estimación directa de los cambios en la concentración de  $\text{CO}_2$  en el medio acuoso,  $\text{CO}_2$  [aq], durante el MIS 12 a 9 a partir de testigos de hielo, permite llevar a cabo la evaluación, mediante diferentes procedimientos de análisis, de la capacidad de los modelos disponibles para explicar las relaciones en este estudio. El modelo clásico de fraccionamiento de carbono orgánico durante la fotosíntesis, que conceptualiza la adquisición celular pasiva de  $\text{CO}_2$ , es incapaz de explicar las relaciones entre los parámetros, frente a un alto grado de semejanza con las relaciones recientemente observadas en cultivos. Este es un punto determinante que implica el cuestionamiento de los modelos clásicos para producir reconstrucciones de  $p\text{CO}_2$  plenamente aceptables, y que sustenta la aplicabilidad de nuevos modelos, donde las relaciones obtenidas para *Gephyrocapsa*, en este estudio, podrían incluirse. Por otro lado, los modelos de fraccionamiento isotópico inorgánico del oxígeno y carbono de la calcita de los cocolitos no explican la variación en los efectos vitales de *Gephyrocapsa* en este estudio. Sin embargo, la correlación entre ambos valores en la serie de tiempo analizada indica que las futuras propuestas deben entrañar, necesariamente, el acoplamiento entre ambos sistemas para oxígeno y carbono.

Para la caracterización morfométrica y de los cambios en la calcificación de las diferentes especies y/o morfotipos que constituyen el complejo *Gephyrocapsa* en el tercer bloque, se aplican técnicas de análisis de imagen. Los parámetros morfométricos medidos en los cocolitos analizados son: talla, masa, volumen y valor del ángulo de inclinación

del puente central que caracteriza a este grupo. Este análisis se lleva a cabo en regiones a diferente latitud y características ambientales, repartidas a lo largo del Atlántico Norte (IODP Sites U1314, U1385 y ODP Site 925) y el sector occidental del Mar Mediterráneo (ODP Site 977) para el intervalo de dominio del complejo *Gephyrocapsa* y de eclosión de “*G. caribbeanica*”, comprendido entre el MIS 14 y 7. Todo ello se integra en el artículo científico en preparación y material suplementario que constituye el Capítulo 6. Los datos morfométricos se combinan con el análisis micropaleontológico de la asociación de *Gephyrocapsa*, que posibilita la identificación de un patrón morfométrico de dominio de los especímenes de talla media común y con evolución comparable en todos los testigos estudiados. Los datos morfométricos permiten llevar a cabo el cálculo y discusión de los potenciales índices de calcificación: espesor normalizado a la talla (SN Thickness-Size Normalized Thickness), valor  $k$  y la estimación del ratio de carbono inorgánico/orgánico, “PIC/POC”. Se identifica un incremento en la calcificación del complejo *Gephyrocapsa* de carácter global o cuasi global, común a las diferentes regiones, que en este trabajo se discute como posiblemente resultante de un incremento en la alcalinidad del océano. Un potencial incremento en la entrada del compuesto ion bicarbonato ( $\text{HCO}_3^-$ ) responsable de este cambio estaría explicado por la intensificación en los procesos de meteorización terrestre y descarga fluvial de dicho compuesto, asociados a los mecanismos de regulación del ciclo del carbono a la escala de recurrencia de 400 kyr en la que este episodio del Mid-Brunhes tiene lugar. Este trabajo constituye una propuesta que evidencia la utilidad de los cambios en la calcificación de cocolitóforos para la inferencia de cambios en la química del océano asociados a la variabilidad climática y los procesos a escala orbital.

## Abstract

The Mid-Brunhes event (MBE), centered at ~ 430 thousand years (ka), is a global process of climate change, when glacial/interglacial (G/I) cyclicity recorded a distinct increase in amplitude. The interval containing this event is a key period of contrasted interglacial (warm) and glacial (cold) stages within the history of the late Pleistocene. The interglacial marine isotope stage (MIS) 11, right after the MBE, outstands among them by the long-lasting character of its extremely warm “full interglacial” conditions. The term “*Gephyrocapsa* complex” refers to a group of coccolithophores species (i.e., calcifying phytoplankton algae) that dominated the global phytoplanktonic environments during the interval neighboring the MBE. Conspicuous within this complex, is the proliferation (*bloom*) of species or morphotype “*Gephyrocapsa caribbeanica*”. This study aims to contribute to different key intervals, mainly focusing on the study of the climatic evolution in the North Atlantic during certain stages of interest, as the MIS 11, and the critical connection of this signal with the mid-latitude regions at the Iberian Margin. Also, the approach of the role and/or response of the *Gephyrocapsa* complex during the Mid-Brunhes interval.

Here we present different specific studies through the application of a suite of analytical techniques, which are specified and detailed in three already published scientific articles, one in a state of under review, and one in preparation to be submitted. These studies can be grouped and identified in three general blocks: i) high-resolution paleoceanographic reconstruction in the Iberian margin using the signal of *Gephyrocapsa* complex, ii) evaluation of the photosynthetic sensitivity of *Gephyrocapsa* to CO<sub>2</sub>, from the values of carbon isotopic fractionation during photosynthesis ( $\epsilon_p$ ), and the *Gephyrocapsa* coccolith vital effects at the western tropical Atlantic, and iii) characterization of the changes in morphometry and calcification of the *Gephyrocapsa* complex along the North to South transect through different regions in the North Atlantic and the western Mediterranean sea.

The first block was developed with the perspective of micropaleontological analysis of the coccolithophore assemblages in upwelling regions located in the Mediterranean and Atlantic Iberian margins, respectively: ODP Site 977, in the Alboran

sea and IODP Site U1385, in the southern Portuguese coast. This approach constitutes two published and one under review scientific articles, presented in Chapters 2, 3 and 5. As a common feature in these studies, the *Gephyrocapsa* complex is used to produce a proxy of primary productivity and reconstruct the degree of development and intensity of the upwelling systems in both regions. These data are integrated with geochemical isotope data ( $\delta^{18}\text{O}$  and  $\delta^{13}\text{C}$  in planktic foraminifers), organic compounds for the reconstruction of sea surface temperatures ( $U^{k'}_{37}$  - SST), and markers of terrestrial origin (pollen content and opal phytoliths). Such a multiproxy procedure allowed the reconstruction of regional palaeoceanographic, and atmospheric conditions associated with the upwelling development and productivity dynamics during Termination V (glacial to interglacial MIS 11/12 transition) and the MIS 11 (430-376 ka), in the case of the Mediterranean margin, and between MIS 12 and 9 (420-397 ka) in the Atlantic region. The intensification of the atmospheric Azores high-pressure (AH) cell is the main mechanism transferring the North Atlantic climatic signal towards the Iberian margin, on a G/I scale and controlling the regional circulation and upwelling systems in both regions. Such an operation would be potentially triggered by changes in the North-South atmospheric pressure gradients in the North Atlantic, in a manner comparable to the modern modes of the North Atlantic Oscillation (NAO), during MIS 11. The prevalence of this atmospheric pattern controlling the primary productivity in both regions, ceases through hydrological and/or temperature impacts during the occurrence of episodes of cooling and meltwater arrival through the Iberian latitudes, such as during the Heinrich *type* events (Ht).

For the second block, a multiproxy approach was conducted with relevance of organic and inorganic geochemical isotopical analysis over *Gephyrocapsa*-produced alkenones ( $\delta^{13}\text{C}_{37:2}$ ) and *Gephyrocapsa* coccoliths ( $\delta^{18}\text{O}$  and  $\delta^{13}\text{C}$ ). The scientific article and Supplementary material in Chapter 4 entirely constitutes this block. Data treatment and calculation from these values measured over a low-resolution pattern in the western tropical region of the North Atlantic region (ODP Site 925) during the interval between MIS 12 and 9 (454-334 ka), allowed the estimation of the variability in the value of carbon isotopic fractionation during photosynthesis ( $\epsilon_p$ ) and oxygen and carbon inorganic vital effects in *Gephyrocapsa*. We analyzed the sensitivity of these values to environmental changes and/or coccolithophore physiological control by direct comparison and evaluation of potential influencers, as the changes in *Gephyrocapsa* cell sizes, growth

rates and light availability during the interval, parameters that were directly measured in samples or estimated. Measurements for this purpose were obtained through micropaleontological analysis of the coccolithophore assemblages, isotopic measurement ( $\delta^{18}\text{O}$  and  $\delta^{13}\text{C}$ ) in planktonic foraminifera species of different depth habitat, organic geochemistry for  $U^{k'}_{37}$ -SST reconstruction, and image-analysis morphometrical measurements of size, mass, and thickness in *Gephyrocapsa* coccoliths. The estimation of  $\text{CO}_2$  [aq] through MIS 12 to 9 was produced from the ice-core  $p\text{CO}_2$  reference. These complete datasets enabled the evaluation of the available models to explain the relationships in this study. It follows that the classically accepted models for carbon isotopic fractionation during photosynthesis, which conceptualizes a purely passive cellular acquisition of  $\text{CO}_2$ , is unable to explain the relationships in this study. This critically suggests that the established models fail to produce fully acceptable  $p\text{CO}_2$  reconstructions in the past. The high degree of coherence in the relationships of this study with observations from culture, including the operation of mechanisms enhancing cellular carbon uptake, supports the suitability of new recently proposed models, where the relationships for *Gephyrocapsa* in this study are included. The available models do not explain, as well, the oxygen and carbon vital effects in *Gephyrocapsa* coccoliths in this study. However, the correlation between both carbon and oxygen values during MIS 12 to 9 indicates that future proposals should necessarily entail a coupled control for both systems.

To attempt the third block, about characterization of changes in morphometry and calcification in *Gephyrocapsa*, image analysis techniques were applied. The morphometric parameters measured were size, mass, volume, and the value of the angle between the central bridge (bar) in the coccoliths of this group and the major axis. This analysis was carried out in latitudinally and environmentally contrasted regions through the North Atlantic (IODP Sites U1314, U1385 and ODP Site 925) and the western Mediterranean Sea (ODP Site 977), during the complete interval of domain of the *Gephyrocapsa* complex, between MIS 14 and 7. This perspective integrates the article in preparation and supplementary material contained in Chapter 6. The obtained morphometric data is integrated with micropaleontological analysis of the *Gephyrocapsa* assemblages at the studied sites and dissolution approach, from foraminiferal fragmentation counts at IODP U1314, enabling the identification of a common

morphometrical pattern of domain of mid-sized *Gephyrocapsa* during the interval in all the studied locations. This morphometric data allowed the calculation of potential calcification proxies: Size Normalized (SN) Thickness,  $k$  value, and PIC/POC ratio. A global or quasi-global increase in the calcification of *Gephyrocapsa* complex is identified. In this study, a possible link of this feature with increase seawater alkalinity during the interval is discussed. We suggest this process to be the result of weathering strengthening and related processes at the 400 kyr low-eccentricity cycle of the Mid-Brunhes, triggering the addition of carbonate ion compound ( $\text{HCO}_3^-$ ) to the ocean. This study constitutes a proposal that evidences the potential usefulness of the changes in the coccolithophore calcification to infer changes in ocean chemistry during the past, associated with climate variability at orbital scale.

## Justificación e hipótesis

El intervalo del Pleistoceno que contiene el evento del Mid-Brunhes (MBE-*Mid Brunhes Event*) incluye extremos climáticos únicos y altamente contrastados en la historia climática del Pleistoceno reciente, que permite su consideración como un laboratorio natural para el análisis de la variabilidad climática desde múltiples perspectivas de análisis. La alta duración de las condiciones cálidas en el océano superficial y su inusual altas latitudes durante las fases interglaciales posteriores al MBE, es uno de los aspectos más significativos, donde el estadio isotópico marino (MIS-*Marine Isotope Stage*) 11 destaca como principal ejemplo. No obstante, existen ideas al respecto de una inicialmente insospechada complejidad para la evolución climática durante este estadio interglacial, siendo la duración y globalidad de sus condiciones cálidas y el tipo de procesos para la transmisión o refuerzo de esta señal climática en determinadas regiones, alguno de los elementos en actual discusión.

El episodio de diversificación y dominio de los ambientes fitoplanctónicos globales por parte del complejo *Gephyrocapsa* y la eclosión global de “*Gephyrocapsa caribbeanica*” añade al estudio de este intervalo la perspectiva adicional de la posible interconexión entre los cambios ambientales y los patrones evolutivos o de proliferación de este grupo, otorgando a este intervalo un interés añadido. La existencia de unas condiciones ambientales globales favorables para el desarrollo y la producción de determinadas especies y/o morfotipos de *Gephyrocapsa* es una idea ampliamente aceptada. A pesar de ello, el mecanismo o mecanismos por los cuales la proliferación de este grupo responde a cambios en las condiciones ambientales y químicas del océano, su globalidad y el posible papel dual, de amortiguación de estos cambios durante el Mid-Brunhes que este grupo pudo tener, no es una cuestión plenamente clarificada.

Por la particularidad de las condiciones registradas, el interés por el conocimiento y comprensión de este intervalo es un aspecto hoy en día en boga para la comunidad científica, como lo es, dentro de una perspectiva más general, el avance en el conocimiento de la respuesta y posible papel de los organismos fitoplanctónicos a los cambios climáticos futuros y, particularmente, al incremento antrópico en los niveles de CO<sub>2</sub> y la acidificación de los medios oceánicos. Así, este trabajo plantea el escenario

climático y ambiental del intervalo del Mid-Brunhes y las condiciones de dominio del complejo *Gephyrocapsa* como elemento troncal presente en los diferentes artículos científicos que, mediante compendio, constituyen esta tesis doctoral. Dada la variedad de los elementos de interés que engloba, son diferentes las cuestiones específicas, objetivos y desarrollo metodológico que se abordan, tratan y discuten en los diferentes artículos. En este apartado se presentan las tres principales hipótesis generales que subyacen al planteamiento de estos trabajos y que evidencian, de partida, la diversidad de la propuesta:

- i) Por la estrecha interconexión entre sus patrones de proliferación con el forzamiento climático durante el intervalo del Mid-Brunhes, el análisis de la representación de las diferentes especies y/o morfotipos pertenecientes al complejo *Gephyrocapsa* permite la inferencia de información paleoceanográfica fidedigna en regiones clave para el análisis de la variabilidad climática orbital (G/I) y suborbital (escala de milenios) durante el Cuaternario. Más específicamente, la señal de productividad a partir del análisis de *Gephyrocapsa*, es un índice aplicable para las reconstrucciones paleoceanográficas.
- ii) La abundancia y la casi monoespecificidad de los vestigios fósiles (i.e., cocolitos, nanofósiles) y compuestos orgánicos producidos por este grupo preservados en los sedimentos, ofrecen una base óptima para la evaluación de la respuesta de sensibilidad fotosintética, de calcificación y los efectos vitales de *Gephyrocapsa* en respuesta a los cambios en CO<sub>2</sub> y otros parámetros ambientales. Las relaciones obtenidas pueden servir como referencia para testar algunos modelos teóricos hoy en día en discusión, así como contribuir a la generación de nuevos.
- iii) Asumiendo la existencia de un control ambiental sobre la evolución morfométrica de los cocolitos producidos por los grupos de cocolitóforos pertenecientes a la familia Noëlaerhabdaceae, a la que *Gephyrocapsa* pertenece, el análisis del grado de homogeneidad o heterogeneidad en la evolución morfométrica de sus cocolitos preservados en sedimentos seleccionados en diferentes latitudes y ambientes se constituye como una herramienta para entender la escala y alcance de los procesos implicados en la variabilidad ambiental oceánica durante el Mid-Brunhes.



Además, el análisis morfométrico permite llevar a cabo una estimación cualitativa de los cambios en la calcificación, a partir del cálculo de índices numéricos que integran las relaciones dimensionales y volumétricas básicas para las formas de los cocolitos de *Gephyrocapsa*.

## Objetivos

El objetivo principal de esta tesis es la evaluación, desde diferentes perspectivas de análisis, de la capacidad de los nanofósiles calcáreos y compuestos orgánicos producidos por los organismos fitoplanctónicos pertenecientes al complejo *Gephyrocapsa* para proporcionar información i) paleoceanográfica de determinadas regiones de interés, ii) fisiológica, acerca de su sensibilidad ante parámetros ambientales cambiantes y iii) de evolución morfométrica de estos nanofósiles, todo ello (i – ii) durante diferentes intervalos próximos al MBE y en relación a las condiciones ambientales generales del intervalo. Estos ejercicios han sido llevados a cabo en los diferentes artículos científicos que componen esta tesis doctoral, en cada uno de los cuales subyace alguno de los tres grandes objetivos generales y objetivos específicos que se enumeran a continuación:

### **1. Reconstruir la evolución paleoceanográfica del margen ibérico a alta resolución a partir de la señal del complejo *Gephyrocapsa***

- Caracterizar las asociaciones de coccolitóforos a alta resolución en dos testigos sedimentarios de los márgenes ibéricos Mediterráneo (mar de Alborán, ODP Site 977) y Atlántico (sector sur de la costa portuguesa, IODP U1385) durante el MIS 11 y el intervalo entre MIS 12 y 9, respectivamente.
- Diferenciar exhaustivamente las especies y/o morfotipos contenidos en el complejo *Gephyrocapsa* y precisar el significado de su señal ambiental en cada una de las regiones de estudio.
- Elaborar un índice de productividad primaria a partir de la señal del complejo *Gephyrocapsa*.
- Integrar la señal de productividad con indicadores de naturaleza marina, como isotópicos de oxígeno y carbono y de temperaturas superficiales.
- Integrar la señal de productividad con indicadores de naturaleza terrestre, como marcadores de configuración atmosférica a partir del contenido de marcadores polínicos y/o de fitolitos silíceos.

- Identificar la variabilidad, escala e interconexión entre los indicadores de diferente naturaleza para ambos testigos.
- Reconstruir escenarios paleoceanográficos que expliquen la variabilidad en ambas regiones e identificar posibles patrones de teleconexión climática entre las latitudes estudiadas y el Atlántico Norte.

**2. Evaluar la sensibilidad del fraccionamiento isotópico del carbono orgánico ( $\epsilon_p$ ) al CO<sub>2</sub> y los efectos vitales de *Gephyrocapsa* en el sector Oeste del Atlántico tropical**

- Obtener una medida del fraccionamiento isotópico del carbono orgánico durante la fotosíntesis ( $\epsilon_p$ ) durante el intervalo comprendido entre MIS 12 y 9.
- Obtener una medida directa y/o diferentes estimaciones a partir de datos micropaleontológicos y geoquímicos de los diferentes parámetros principales involucrados en la modulación del valor de  $\epsilon_p$ : CO<sub>2</sub>, variación en las tallas celulares, variación de la talla de crecimiento celular y disponibilidad de luz.
- Reconstruir las condiciones de estratificación y disponibilidad de nutrientes a lo largo del intervalo a partir de la caracterización de la asociación de cocolitóforos y la evaluación de los gradientes obtenidos del análisis isotópico de diferentes especies de foraminíferos planctónicos.
- Desarrollar diferentes ejercicios y procedimientos analíticos para evaluar la capacidad de los modelos clásicos, de adquisición pasiva de CO<sub>2</sub> y los modelos recientes, basados en observaciones en cultivos, para explicar la sensibilidad a los cambios en CO<sub>2</sub> y el resto de los parámetros medidos o estimados.
- Obtener una medida de los efectos vitales de oxígeno y carbono en *Gephyrocapsa* con el empleo de valores isotópicos medidos en foraminíferos planctónicos como referencia isotópica durante la calcificación.
- Evaluar la capacidad de los modelos disponibles para explicar las relaciones entre ambos sistemas de fraccionamiento isotópico (oxígeno y carbono) y, por lo tanto, de los efectos vitales entre sí y con los parámetros ambientales medidos o estimados con anterioridad.

**3. Caracterizar la evolución de la morfométrica de los cocolitos que constituyen el complejo *Gephyrocapsa* y evaluar la capacidad de estos datos para proporcionar estimaciones de los cambios en la calcificación durante el Mid Brunhes**

- Caracterizar las asociaciones de cocolitóforos a baja resolución en los testigos en diferentes latitudes del Atlántico Norte y el sector occidental del Mediterráneo, IODP U1314, U1385, ODP 925 y 977, durante el intervalo contenido entre MIS 14 y 7.
- Documentar con el empleo de técnicas de polarización circular un alto número de campos visuales representativos de las asociaciones de cocolitos pertenecientes al complejo *Gephyrocapsa* en cada una de las muestras y para cada uno de los testigos.
- Obtener una medida directa de los parámetros morfométricos de talla, masa y volumen de un número representativo de cocolitos individuales pertenecientes al complejo *Gephyrocapsa* en cada una de las muestras.
- Analizar los datos para la extracción de las tendencias morfométricas generales y/o sus divergencias entre testigos.
- Explorar el potencial de los índices numéricos basados en las relaciones dimensionales y volumétricas de cocolitos para estimar los cambios en la calcificación: *Size Normalized (SN) Thickness*, valor  $k$  y PIC/POC.
- Identificar las posibles relaciones existentes entre los parámetros morfométricos y de cambios en la calcificación con las condiciones climáticas y ambientales durante el intervalo.

## Estructura de la tesis doctoral

Esta tesis doctoral se compone de siete capítulos y cinco anexos, cuyo contenido se presenta y resume a continuación:

En el **Capítulo 1** se introduce el periodo de tiempo estudiado y el problema de partida. Se presentan los organismos fitoplanctónicos estudiados, el complejo *Gephyrocapsa*, los principales conceptos taxonómicos y ecológicos acerca de las especies que lo componen y sobre otros taxones complementarios. A continuación, se presentan los testigos sedimentarios estudiados, emplazados en diferentes latitudes del Atlántico Norte y la región occidental del Mar Mediterráneo. Tras una presentación inicial, los testigos aparecen agrupados en los tres diferentes bloques generales de estudio, para cada uno de los cuales se determina la resolución en el muestro y se justifica los principales motivos para su selección e integración en los estudios. Más adelante, se presentan los conceptos teóricos y antecedentes principales previos al desarrollo completo e individual de los trabajos de investigación recogidos en los artículos que constituyen los capítulos siguientes, la aplicación de las asociaciones de cocolitóforos para la reconstrucción paleoceanográfica y paleoclimática, el fraccionamiento isotópico del carbono durante la fotosíntesis ( $\epsilon_p$ ), el análisis de los cambios en la calcificación de cocolitóforos y de sus efectos vitales.

El **Capítulo 2** lo compone el primer artículo científico publicado, que constituye una parte del primer bloque de estudio que aborda la reconstrucción paleoceanográfica de alta resolución en el margen ibérico, a partir de la señal de productividad primaria del complejo *Gephyrocapsa*. En él y, bajo esta perspectiva, se estudia el intervalo de tiempo contenido desde la Terminación V hasta la transición interglacial/glacial MIS 11/10 (430 – 376 ka) en el testigo ODP 977, ubicado en el mar de Alborán. En esta investigación se reconstruye la señal de productividad primaria y condiciones ambientales en la región y, a partir de su combinación con marcadores climáticos marinos y terrestres, se discuten las condiciones paleoceanográficas, a escala orbital y suborbital, en conexión con la evolución paleoclimática del intervalo a escala general del Atlántico Norte.

**González-Lanchas, A.**, Flores, J.-A., Sierro, F.J., Bárcena, M.A., Rigual-Hernández, A.S., Oliveira, D., Azibeiro, L.A., Marino, M., Maiorano, P., Cortina, A., Cacho, I. y Grimalt, J.O 2020. A new perspective of the *Alboran Upwelling System* reconstruction during the Marine Isotope Stage 11: A high-resolution coccolithophore record. *Quaternary Science Reviews*, 245, 106520.  
DOI: 10.1016/j.quascirev.2020.106520

El **Capítulo 3** queda integrado por el segundo artículo científico publicado, que constituye una parte del primer bloque de estudio que aborda la reconstrucción paleoceanográfica de alta resolución en el margen Ibérico, a partir de la señal de productividad primaria del complejo *Gephyrocapsa*. En él se lleva a cabo el estudio de alta resolución de las asociaciones de cocolitóforos, particularmente, del complejo de *Gephyrocapsa*, durante el intervalo de tiempo contenido desde la parte final del glacial MIS 12 hasta el comienzo del interglacial MIS 9 (420 – 397 ka), en el testigo IODP U1385, ubicado en el sector sur de la costa portuguesa. En esta investigación se reconstruye la señal de productividad primaria y condiciones ambientales en la región. La combinación de esta señal con marcadores climáticos de origen marinos y terrestres permite la discusión de los principales controles atmosféricos e hidrológicos en esta región, a escala orbital y suborbital y con relación a la evolución paleoclimática Atlántico Norte durante este intervalo.

**González-Lanchas, A.**, Flores, J.A., Sierro, F., Sánchez Goñi, M., Rodrigues, T., Ausin, B., Oliveira, D., Naughton, F., Marino, M., Maiorano, P. y Balestra, B., 2021a. Control mechanisms of Primary Productivity revealed by calcareous nannoplankton from Marine Isotope Stages 12 to 9 at the Shackleton Site (IODP Site U1385). *Paleoceanography and Paleoclimatology*, e2021PA004246.  
DOI: 10.1029/2021PA004246.

El **Capítulo 4** lo constituye el tercer artículo científico publicado que materializa íntegramente el segundo bloque de estudio orientado a la evaluación de la sensibilidad fotosintética al CO<sub>2</sub> de los cocolitóforos que componen el complejo *Gephyrocapsa*, a partir del valor de fraccionamiento isotópico del carbono orgánico durante la fotosíntesis ( $\epsilon_p$ ) medido en alquenonas y de sus efectos vitales de *Gephyrocapsa* durante el intervalo de tiempo desde el glacial MIS 12 hasta el interglacial MIS 9 (460 – 330 ka) en el testigo ODP 925, localizado en *Ceara Rise*, el sector Oeste del Atlántico Norte tropical. En este

estudio, se lleva a cabo el cálculo del valor de fraccionamiento isotópico del carbono durante la fotosíntesis ( $\epsilon_p$ ) y de los efectos vitales en *Gephyrocapsa* mediante análisis geoquímicos (inorgánicos y orgánicos) y la medida directa o estimación de los parámetros involucrados en su modulación, mediante la aplicación de técnicas micropaleontológicas, geoquímicas y de análisis de imagen. La aplicación de técnicas analíticas y diferentes ejercicios permiten evaluar la capacidad de los diferentes modelos teóricos existentes para explicar las relaciones obtenidas y se discute la validez de algunos indicadores para futuros trabajos. El desarrollo metodológico llevado a cabo en este estudio es extenso e innovador, motivo por el cual en este capítulo se incluye un apartado suplementario, también incluido en la versión publicada, donde se recoge una amplia variedad de información y discusión adicional acerca del trabajo presentado.

**González-Lanchas, A.**, Hernández-Alméida, I., Flores, J. A., Sierro, F. J., Guitián, J., y Stoll, H. M. 2021b. Carbon Isotopic Fractionation of Alkenones and *Gephyrocapsa* Coccoliths Over the Late Quaternary (Marine Isotope Stages 12–9) Glacial-Interglacial Cycles at the Western Tropical Atlantic. *Paleoceanography and Paleoclimatology*, 36(8), e2020PA004175. DOI:10.1029/2020PA004175.

En el **Capítulo 5** se encuentra el cuarto artículo científico. Este trabajo se encuentra en proceso de revisión y, en él, se materializa una parte del primer bloque de estudio, que aborda la reconstrucción paleoceanográfica de alta resolución en el margen Ibérico. En él se presenta un registro de alta resolución del contenido y preservación de la materia orgánica en el sedimento, a partir del análisis de trazas fósiles producidas por organismos macrobentónicos y de los cambios de color a partir de la aplicación de técnicas de análisis sobre las fotografías del sedimento procedente del testigo ODP 977 a alta resolución durante el mismo intervalo de tiempo abordado en el Capítulo 2. De este modo, y a partir de la integración con los datos publicados del capítulo anteriormente referido, se evalúa la transferencia de la señal de productividad primaria del complejo *Gephyrocapsa* y el efecto de la influencia de los procesos de oxigenación asociados a la circulación y procesos de renovación de las aguas profundas en el mar de Alborán.

**González-Lanchas, A.**, Dorador, J., Rodríguez-Tovar, F.J., Sierro, F.J. y Flores, J.A. Western Mediterranean deep-sea environmental conditions in response to surface organic productivity and regional circulation dynamics during the MIS 11. Artículo en revisión en *Marine Geology*.

El **Capítulo 6** lo compone la presentación del quinto artículo científico producido en esta tesis doctoral. Este trabajo se encuentra en proceso de preparación para ser enviado y sustenta el enfoque que se plantea en el tercer bloque de estudio. En él se exponen y discuten los principales resultados obtenidos acerca de la caracterización morfométrica del complejo *Gephyrocapsa* en los diferentes testigos previamente presentados y analizados en los trabajos anteriores además del testigo IODP *Site* U1314, localizado en altas latitudes del Atlántico Norte. Se obtienen datos de la evolución morfométrica de los cocolitos de *Gephyrocapsa* en las diferentes regiones y a partir de los mismos se calculan y evalúan diferentes índices para la reconstrucción de los cambios en la calcificación durante el intervalo comprendido entre MIS 14 y 7. El desarrollo metodológico llevado a cabo en este estudio es extenso e innovador, motivo por el cual en el capítulo se incluyen un apartado suplementario, donde se recogen métodos e información adicional acerca del trabajo presentado y de sus resultados.

**González-Lanchas, A.**, Rigual-Hernández, A.S., Sierro, F.J. Alonso-García y Flores, J.A. About the Mid-Brunhes interval and the role of the stumper coccolithophore *Gephyrocapsa* complex. Artículo en preparación para ser enviado a *Nature Communications*.

En el **Capítulo 7** se resumen las principales conclusiones derivadas de esta tesis doctoral, agrupadas para los diferentes bloques de estudio presentados.

Finalmente, se incluyen una serie de Anexos en los cuales se presenta información adicional que clarifica y/o complementa alguna de las partes de los capítulos precedentes. En el Anexo **I** se presenta la sistemática general de los grupos incluidos en esta tesis y en el Anexo **II** las imágenes de los cocolitos pertenecientes a algunos de los los taxones más representativos en las muestras estudiadas. Los Anexos **III** a **V** contienen dos artículos científicos publicados, de los que el doctorando es autor principal (**III**) y colaborador (**IV**), así como la memoria científica de una expedición oceanográfica en la que el doctorando participó y en la cual realizó las labores de bioestratigrafía (**V**), la parte de la



memoria que se incluye en este trabajo. Todos ellos están centrados en el análisis de coccolitóforos, como herramienta principal y se encuentran redactados en inglés, motivo por el cual se incluye, adicionalmente, un resumen en castellano en su presentación. Su cita completa se incluye, por orden de aparición en los anexos, a continuación:

**González-Lanchas, A.**, Remacha, E., Oms, O., Sierro, F. J., y Flores, J. A. 2019. Middle Eocene calcareous nannofossils in the Jaca transect (South-central Pyrenees Eocene Basin, Aragón River valley, Huesca). *Spanish Journal of Palaeontology*, 34(2), 229-240. DOI:10.7203/sjp.34.2.16096.

Rigual-Hernández, A.S., Sánchez-Santos, J.M., Eriksen, R., Moy, A.D., Sierro, F.J., Flores, J.-A., Abrantes, F., Bostook, H., Nodder, S.D., **González-Lanchas, A.** y Trull, T.W. 2020. Limited variability in the phytoplankton *Emiliana huxleyi* since the pre-industrial era in the Subantarctic Southern Ocean. *Anthropocene*, 31, 100254. DOI: 10.1016/j.ancene.2020.100254.

Hüpers, A., Brune, R., Magalhaes, V., Freitas, M., Fleischmann, T., Freudenthal, T., **González-Lanchas, A.**, Haberkorn, P., Heine, L., Klaembt, C., Mazerath, P., Menapace, W., Meservy, W., Moreno, K., Pereira, S., Schmidt, J. N., Stanislawski, K., Stelzner, M. 2020: Preliminary results of R/V METEOR cruise M149: Shipboard and Post-Cruise Analysis, Recurrence of tsunamigenic hazards from MeBo drilling records and hazard mitigation using MeBo observatories, Las Palmas (Canary Islands) – Cadiz (Spain), 24.07.2018 – 24.08.2018. *Berichte, MARUM-Zentrum für Marine Umweltwissenschaften, Fachbereich Geowissenschaften, Universität Bremen*, No. 324, 200 pages. Bremen, 2020. ISSN 2195-9633. DOI: 10.26092/elib/100.

# CAPÍTULO 1. Introducción

## 1.1. El episodio del Mid-Brunhes

Durante el Cuaternario, el periodo más reciente de la historia de la Tierra, que comienza hace 2.59 millones de años (Myr), el clima terrestre viene determinado por la instauración de la ciclicidad glacial/interglacial (G/I) en el hemisferio norte. Esta ciclicidad climática está principalmente materializada en el avance y retracción de las grandes masas de hielo, un proceso del cual tenemos evidencia, principalmente, a partir de los cambios en la signatura isotópica del oxígeno en el océano (relación  $^{18}\text{O}/^{16}\text{O}$ ), que queda registrada en el carbonato cálcico ( $\text{CaCO}_3$ ) (Lisiecki y Raymo, 2005). Estos patrones tienen su origen en los cambios latitudinales y estacionales de la distribución de la energía solar sobre la superficie terrestre, que están modulados, esencialmente, por las variaciones cíclicas en los parámetros orbitales de precesión, oblicuidad del eje de rotación y excentricidad de la órbita terrestre, con periodos de recurrencia de 19-23, 41 y 100-400 mil años (kyr), respectivamente. Específicamente, los cambios en la duración e intensidad de la tasa energética solar recibida durante la estación de verano en el hemisferio norte, representa el elemento crítico condicionante de esta variabilidad para la configuración continental existente durante el periodo Cuaternario (Milankovitch, 1930).

Lejos de tratarse de una pauta homogénea, la ciclicidad G/I durante el Cuaternario ha experimentado cambios en la simetría, cuyo origen se atribuye a las variaciones originales de los tres parámetros orbitales, pero también al efecto de otros componentes del sistema climático, que son capaces de ejercer una función de retroalimentación a partir del estímulo forzador externo como, por ejemplo, la insolación (Imbrie et al., 1993). El acceso a medidas directas de los cambios en la presión parcial de  $\text{CO}_2$  atmosférico ( $p\text{CO}_2$ ) durante el Cuaternario, a partir de testigos de hielo (Bereiter et al., 2015; Köhler et al., 2017), muestran la existencia de una pauta de ciclicidad G/I muy marcada, donde determinados cambios en  $p\text{CO}_2$  llegan, incluso, a anticiparse a la pauta isotópica G/I, lo que ha llevado a considerar los cambios en la concentración de  $\text{CO}_2$  como uno de los posibles elementos críticos en el forzamiento climático (Petit et al., 1999; Webb et al., 1997) e, incluso, en el origen de la ciclicidad durante el Cuaternario (Broecker y Henderson, 1998). Las causas específicas de los cambios G/I en  $p\text{CO}_2$  no han sido, sin embargo, aún identificadas (Sigman y Boyle, 2000), pero las hipótesis más viables al

respecto involucran, inequívocamente, a los cambios fisicoquímicos en el océano (Broecker, 1982), un proceso en el cual la retirada de carbono de la superficie oceánica mediante la producción biológica, se plantea como una de las posibles piezas de mayor influencia (Archer y Maier-Reimer, 1994; Broecker y Peng, 1987; Sigman y Boyle, 2000).

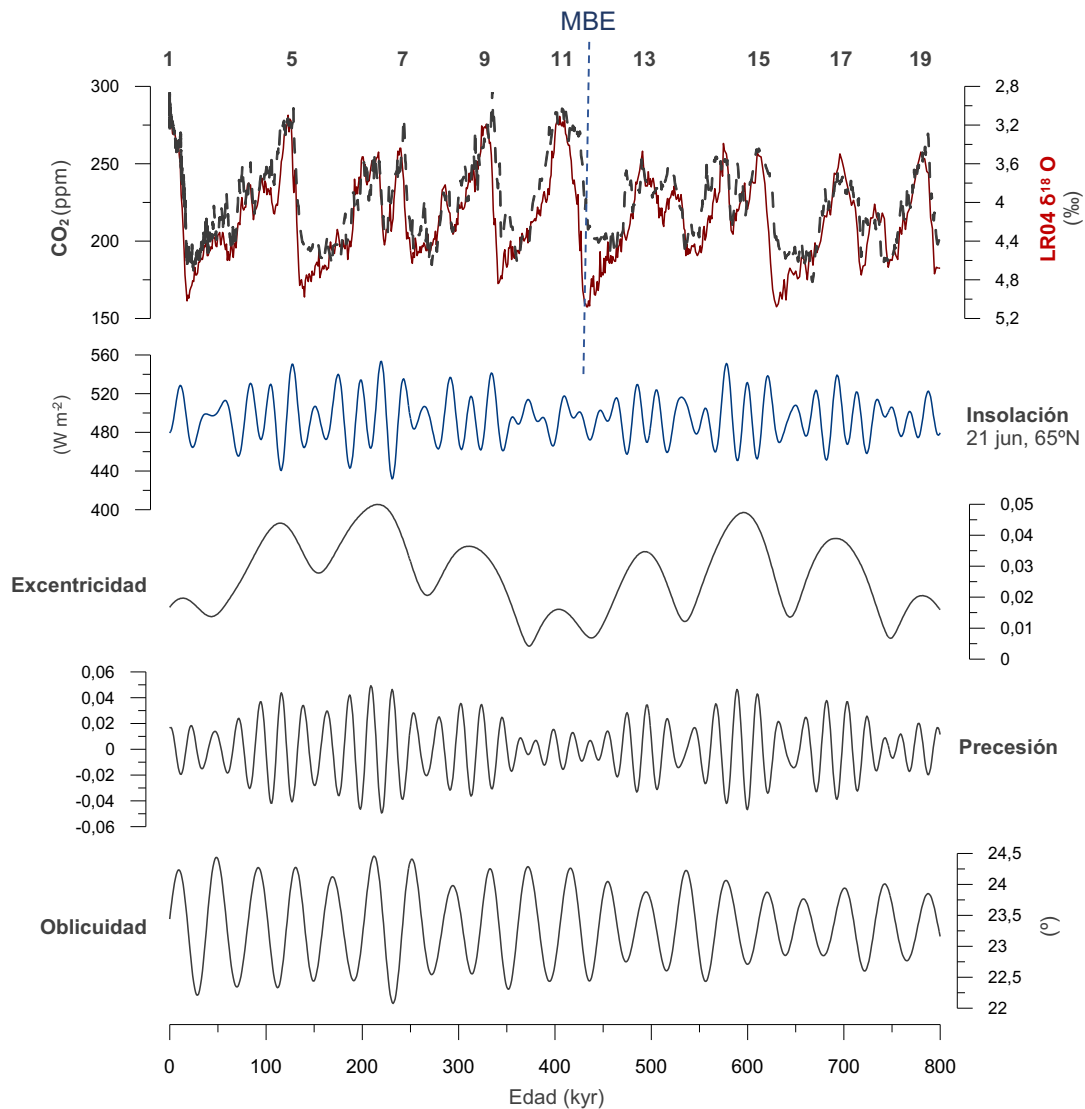


**Figura 1.** Comparación entre los ciclos de oblicuidad, precesión y excentricidad (parámetros astronómicos) tomados de Laskar et al. (2004), la variabilidad en la tasa de insolación que producen y la expresión de esa variabilidad en el registro global de isótopos de oxígeno marinos “LR04” de Lisiecki y Raymo, (2005) y la concentración de CO<sub>2</sub> atmosférica para los últimos 800 kyr (Bereiter et al., 2015). En la figura se representa la ubicación del evento del Mid-Brunhes (MBE), en ~ 430 ka, de acuerdo con Jansen et al. (1986)

Hacia la mitad del Pleistoceno, tiene lugar uno de los principales cambios en la simetría de la variabilidad G/I, que pasa de estar dominada por la ciclicidad de baja amplitud y alta frecuencia de 41 kyr, a la ciclicidad de alta amplitud y baja frecuencia de 100 kyr, un episodio correspondiente a la transición climática o revolución del Pleistoceno medio (Berger et al., 1993). Una vez la ciclicidad de 100 kyr se estabiliza por completo, a lo largo del Pleistoceno medio/superior, alrededor de ~ 430 kyr atrás, en la parte media del *cron* geomagnético “Brunhes”, tiene lugar un evento de amplificación en la ciclicidad G/I. Este es el denominado evento del Mid-Brunhes (Fig. 1) (*MBE-Mid-Brunhes Event* - MBE, Fig. 1; Jansen et al., 1986), a partir del cual tiene lugar la instauración de periodos interglaciales más cálidos que los registrados en fases anteriores al MBE, así como transiciones G/I (Terminaciones) de mayor amplitud (Lang y Wolff, 2011; Lisiecki y Raymo, 2005).

En términos isotópicos, el intervalo del Mid-Brunhes incluye, estrictamente, la franja temporal desde la transición G/I entre los estadios isotópicos marinos (*MIS-Marine Isotope Stage*) 12/11 o, también denominada Terminación V, hasta el estadio interglacial MIS 9 (Fig. 1). La Terminación V caracteriza plenamente este evento (MBE) de incremento en la amplitud G/I (Fig. 1) y se trata, por ello, de la deglaciación de mayor amplitud de los últimos 800 kyr (Droxler et al., 2003a; Droxler y Farrell, 2000). El fuerte calentamiento durante este episodio consumó un intenso transporte de aguas cálidas hacia altas latitudes, que conllevaría la fusión de Groenlandia y el sector occidental de la Antártida, con la consecuente subida del nivel del mar de entre 13 y 20 metros respecto al nivel eustático actual (Rohling et al., 1998). La respuesta a estos cambios, se expresa plenamente durante el subsecuente estadio interglacial MIS 11, en el que las condiciones de elevado calentamiento se mantienen de forma estable y prolongada durante, al menos, 30 kyr desde su comienzo, localizado, aproximadamente en la edad de ~ 424 ka, según el patrón isotópico de Lisiecki y Raymo (2005), una duración de estas condiciones que casi duplica la de otras fases interglaciales (Loutre y Berger, 2003; Mcmanus et al., 2003).

Durante el MIS 11 se identifican, además, otras particularidades de crítica importancia, como prominentes depósitos de carbonato en zonas de plataforma marina (Droxler et al., 2003a) coetáneos con condiciones de intensa disolución profunda en algunos puntos de diferentes latitudes (Crowley, 1985; Hodell et al., 2000) y de elevados niveles generales de productividad primaria y de exportación de carbonato pelágico en

los ambientes marinos (Wang et al., 2003). Todos estos elementos definen un escenario de alta complejidad, con cambios importantes afectando al océano superficial y profundo, difíciles de explicar atendiendo simplemente a la premisa que plantea la teoría climática orbital (Imbrie et al., 1993), por lo que el origen del evento del Mid-Brunhes continúa siendo una cuestión enigmática y en discusión, a día de hoy.

Las condiciones orbitales durante el MIS 11 son de excentricidad mínima (Fig. 1) y, por lo tanto, de modulación reducida del parámetro de precesión sobre la estacionalidad de la insolación (extremos de estacionalidad mínimos). De este modo, la insolación teórica estimada, siguiendo la teoría climática orbital, resulta insuficiente para ejercer como único elemento estimulante del elevado y prolongado calentamiento durante el intervalo. Esto ha llevado a diferentes autores a sugerir la necesidad de apelar a mecanismos adicionales como responsables de la amplificación del efecto de las condiciones orbitales (Imbrie et al., 1993). Significativamente, los niveles de CO<sub>2</sub> durante el MIS 11 parecen no alcanzar los niveles del Holoceno pre-industrial (Raynaud et al., 2005), lo cual eliminaría, aparentemente, la posibilidad de considerar éste como uno de los mecanismos de retroalimentación para el calentamiento. Entre las ideas al respecto, destacan las que apuntan a posibles perturbaciones en el reservorio de carbono oceánico y, por lo tanto, en sus condiciones químicas precediendo al MBE y, de este modo, condicionando este evento durante fases previas (Droxler et al., 2003b; Wang et al., 2003).

Por otro lado, la semejanza de las condiciones orbitales del MIS 11 con las del Holoceno preindustrial, ha llevado a muchos autores a considerar éste como un potencial análogo climático del presente y de su evolución futura (Candy et al., 2014; Loutre y Berger, 2003), motivo por el cual los estudios de alta resolución acerca de la evolución climática del MIS 11, en diferentes latitudes, han proliferado en los últimos años (Helmke et al., 2008; Kandiano et al., 2012; Oliveira et al., 2016; Saavedra-Pellitero et al., 2017). No obstante, y lejos de alcanzar un concilio, existen visiones contrapuestas, principalmente acerca de la duración de las condiciones cálidas y del comienzo de la inestabilidad climática operando a escala milenaria durante las fases tardías de este interglacial, así como la correspondencia de los patrones reconstruidos entre las diferentes latitudes o la entidad global de los procesos identificados (Helmke et al., 2008; Kandiano et al., 2012; Oliveira et al., 2016).

## 1.2. Cocolitóforos, definición general y funciones vitales

Los cocolitóforos, son organismos fitoplanctónicos algares calcificadores, de carácter unicelular, pertenecientes al filo Haptophyta y a la clase Prymnesiophyceae (Hibberd, 1976). El ciclo de vida de estos organismos, en términos generales, es heteromórfico, es decir, en él se alternan una fase diploide y una fase haploide (Green y Leadbeater, 1994). Su zona de hábitat se restringe a la parte superior de la columna de agua, donde este grupo encuentra una disponibilidad suficiente de luz y nutrientes, elementos básicos para el desarrollo de su actividad vital (Poulton et al., 2007; Winter y Siesser, 2006).

Morfológicamente, este grupo se caracteriza por la producción de escamas o placas de  $\text{CaCO}_3$ . Estas placas se denominan “cocolitos” y, aunque su producción tiene lugar por precipitación biomineral intracelular, estas estructuras son extruidas hacia fuera de la célula para formar una cubierta externa, o exosqueleto, denominado “cocosfera” (Fig. 2) (Brownlee and Taylor, 2004; Young y Henriksen, 2003) .

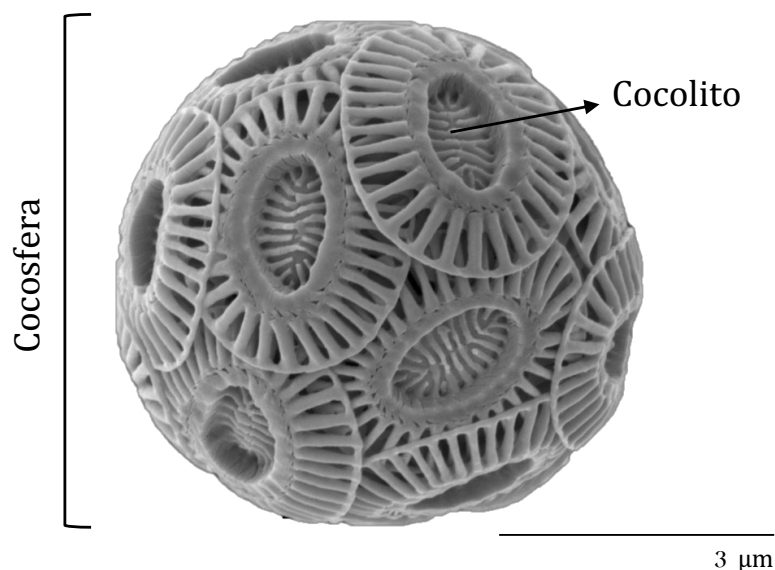


**Figura 2.** Imagen del aspecto de una cocosfera actual perteneciente a la especie de cocolitóforo *Emiliana huxleyi*. Fotografía de microscopio electrónico de transmisión (SEM-*Scanning Electron Microscope*) tomada de la guía online de biodiversidad y taxonomía de cocolitóforos, “Nannotax”.

Durante su ciclo de vida, estos organismos llevan a cabo dos funciones principales: fotosíntesis y calcificación. La función de fotosíntesis tiene lugar en los

cloroplastos y, mediante ella, los cocolitóforos toman el CO<sub>2</sub> disuelto en el medio acuoso superficial (CO<sub>2</sub> [aq]), para llevar a cabo la fijación y producción de carbono orgánico (POC-*Particulate Organic Carbon*). Este mecanismo, se denominado “bomba del carbono orgánico” (*organic carbon pump*) o “bomba biológica” (*biological pump*) (Rost y Riebesell, 2004), conlleva la retirada de una tasa de CO<sub>2</sub> de la superficie del océano (Fig. 3 y 4). La siguiente ecuación (1) sintetiza los procesos químicos que determina esta función:

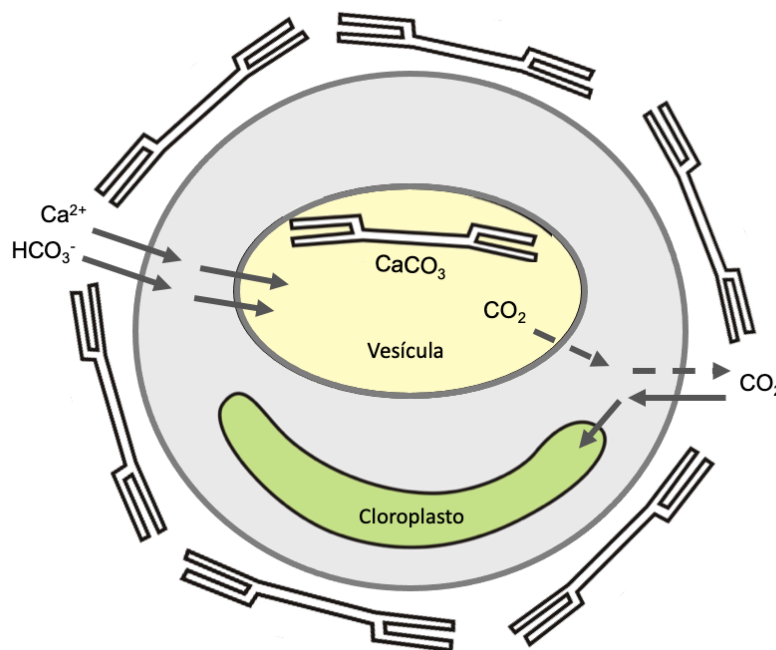


**Figura 3.** Esquema simple de los componentes de la célula de un cocolitóforo y de los flujos bioquímicos básicos y su dirección, relacionados con las funciones vitales de fotosíntesis y calcificación. Las ecuaciones (1) y (2) en el texto, estarían respectivamente ubicadas en el cloroplasto y en la vesícula de calcificación; se han omitido en la representación para mayor claridad. Figura modificada y simplificada a partir del esquema de Taylor et al. (2011).

Mediante la función de calcificación, conocida como “bomba del carbonato” o “bomba del carbono inorgánico” (*inorganic carbon pump*), los cocolitóforos biomineralizan intracelularmente carbono inorgánico particulado (PIC-*Particulate Inorganic Carbon*) a partir de la toma del carbono inorgánico disuelto en el medio acuoso (DIC-*Dissolved Inorganic Carbon*) (Volk y Hoffert, 1985). La toma de carbono inorgánico, en la forma de la especie del ion bicarbonato (HCO<sub>3</sub><sup>-</sup>), una de las especies

carbonatadas que constituye el DIC, se considera como base principal para la calcificación, aunque los procesos que rigen adquisición y distribución intracelular de este recurso puede variar en función de las condiciones geoquímicas y ambientales externas (ver Subepígrafe 1.6.). Esta función tiene lugar en la vesícula de calcificación (Fig. 3). El proceso de calcificación y biomineralización de cocolitos conlleva la generación de una porción variable de CO<sub>2</sub> como parte del proceso (Marsh, 2003). Por este motivo, la función de calcificación y producción de PIC es, también, denominada, “contra bomba del carbono” (*carbonate counter pump*). A continuación, se presenta la ecuación general (2) que define la función de calcificación:

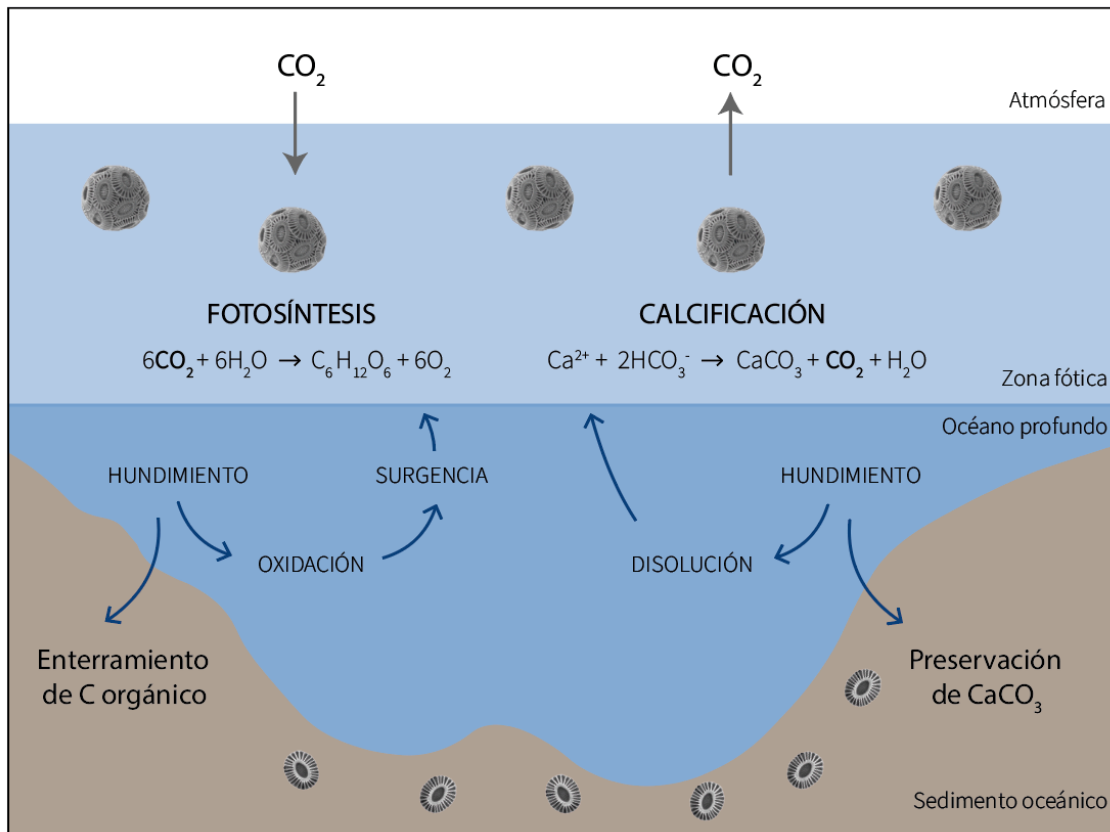
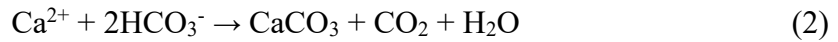


**Figura 4.** Esquema representativo del papel de los cocolitóforos en el ciclo del carbono, a partir de sus funciones vitales de fotosíntesis y calcificación. Para la elaboración de esta figura se siguió el esquema original de Baumann et al. (2004).

Los cocolitos son transportados hacia el fondo del océano, formando parte de agregados como “nieve marina” o agregados fecales que facilita su circulación y



transporte vertical (Broecker y Clark, 2009). Este proceso resulta en la acumulación y preservación de  $\text{CaCO}_3$  y en el enterramiento del carbono orgánico en el sedimento oceánico, culminando, con ello el proceso de retirada y disminución de  $\text{CO}_2$  que comienza en la superficie del océano (Fig. 4). El papel de este grupo supone una herramienta amortiguadora de la química oceánica, un elemento intermediario en la operación de los procesos que sustentan el ciclo del carbono y un sumidero de carbono, incluido en el reservorio oceánico (Fig. 4). De este modo, a la escala de tiempos geológica, los cambios en la intensidad relativa de las funciones vitales de producción de carbono orgánico (fotosíntesis) e inorgánico (calcificación) por parte de este grupo pudieron alterar profundamente el ciclo del carbono y las respuestas climáticas resultantes, como algunos autores sugieren (Archer y Maier-Reimer, 1994; Erba, 2006; Westbroek et al., 1993).

### **1.3. El complejo *Gephyrocapsa* y “*Gephyrocapsa caribbeanica*”**

Durante el intervalo del Mid Brunhes, las asociaciones de cocolitos fósiles se encuentran ampliamente dominadas por especímenes pertenecientes al género *Gephyrocapsa* (Kamptner, 1943). En términos sistemáticos, este género queda comprendido dentro de la familia de Noëlaerhabdaceae, también denominada Gephyrocapsaceae (Black, 1971). La primera aparición de esta familia tiene lugar hace 57.2 Myr, en el piso Thanetiense de la época Paleoceno, con especímenes pertenecientes al género *Reticulofenestra* (Hay et al., 1966). El género *Gephyrocapsa* aparece, por su parte, hace 7.3 Myr, en el piso Tortoniense de la época Mioceno (Rio, 1982) y su representación en las asociaciones de cocolitos fósiles y de cocolitóforos en los medios oceánicos se prolonga hasta día de hoy (Paasche, 2001).

Los nanofósiles pertenecientes al género *Gephyrocapsa* (Fig. 5) son especialmente abundantes en el sedimento durante el Cuaternario, donde evidencian patrones globales sincrónicos de rápidas reducciones e incrementos en sus rangos de tallas entre especies altamente emparentadas, potencialmente sustentado por procesos de radiación evolutiva, como el que comenzó hace 600 kyr e incluye el intervalo del Mid-Brunhes (Bendif et al., 2019), el cual resultaría correspondiente a los también observados para el género *Reticulofenestra* durante estadios anteriores del Cenozoico (Bendif et al., 2016). El término “complejo” *Gephyrocapsa* (*Gephyrocapsa* complex) aplicado en esta tesis doctoral, es frecuentemente empleado para referirse a la situación de dominio de este

grupo de especies variadas y semejantes, evidente en las asociaciones fósiles que incluyen este intervalo de estudio (Bollmann, 1997).

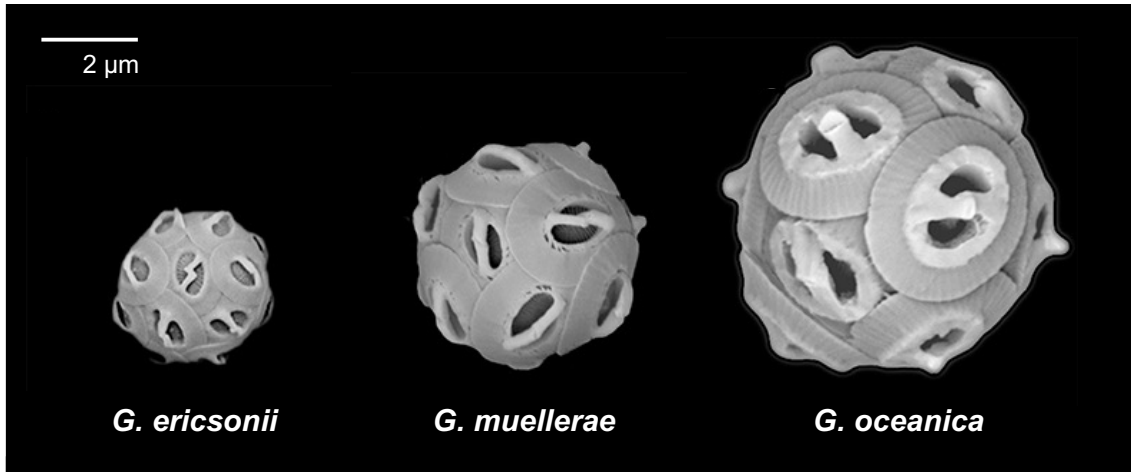


**Figura 5.** Cocosferas representativas de las especies modernas pertenecientes al género *Gephyrocapsa*: *G. ericsonii*, *G. muelleriae* y *G. oceanica*. Fotografía de SE; tomadas de Bendif et al. (2016).

Los organismos pertenecientes a la familia Noëlaerhabdaceae poseen, de forma general, una afinidad ecológica fuerte por los medios enriquecidos en nutrientes y una buena capacidad para el aprovechamiento rápido de estos recursos, características ecológicas propias de los organismos “estrategas de la r”, en el que las especies de esta familia quedan englobadas (Barber y Hiscock, 2006). Así, se han reconocido diferentes episodios de eclosión o alta proliferación (*bloom*) de determinadas especies o grupos de esta familia durante diferentes escenarios temporales, a lo largo del Cenozoico. El dominio de *Gephyrocapsa* durante el Mid-Brunhes se identifica con estos episodios de alta proliferación de Noëlaerhabdaceae, durante el cual la producción de los especímenes de *Gephyrocapsa* fue dominante en la producción de carbonato pelágico global, llegando a suponer, frecuentemente, una porción superior al 80 % de las asociaciones de cocolitóforos (Fig. 6) (Barker et al., 2006; Baumann y Freitag, 2004; Flores et al., 2012).

Dentro de este episodio, destaca, particularmente, la eclosión de “*Gephyrocapsa caribbeanica*”, un taxón o morfotipo de *Gephyrocapsa* que, a diferencia del resto, registra su primera y última aparición dentro de los límites del Mid-Brunhes, aproximadamente dentro de los estadios MIS 14 y 7 (rango de tiempo entre hace ~ 600 y 250 ka) (Fig. 6). De este modo, es frecuente encontrar referencias explícitas al episodio de alta

proliferación de *Gephyrocapsa* durante el Mid-Brunhes como de “*G. caribbeana*” (Flores et al., 2012).

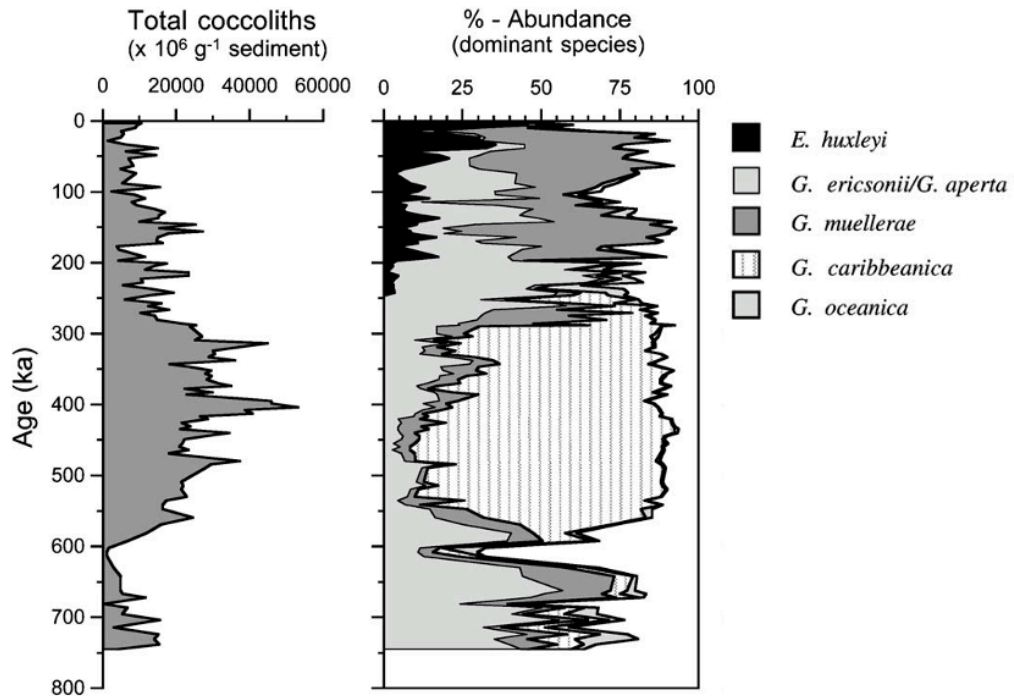


**Figura 6.** Concentración absoluta de cocolitos del conjunto total y porcentaje de abundancia (%) de las especies dominantes en las asociaciones de cocolitóforos estudiadas en el testigo ODP Site 1082, ubicado en el sistema de la corriente de Benguela (costa de Namibia, Atlántico Sur) en el intervalo comprendido desde el MIS 20 hasta la actualidad (para los últimos 750 kyr). La figura y los resultados descritos son autoría de Baumann y Freitag (2004).

Las principales hipótesis, hasta la fecha, acerca de los elementos que condicionaron la eclosión de *Gephyrocapsa* durante el Mid-Brunhes apuntan al control de la pauta orbital de la recurrencia cíclica en los valores de excentricidad mínima cada  $\sim 400$  kyr, condiciones orbitales que durante el Mid-Brunhes suceden, centradas alrededor de la edad de 400 ka (Fig. 1) y afectarían a determinados mecanismos que modificaron las condiciones de hábitat para esta especie como i) un incremento en la fuga de sílice en altas latitudes, que benefició la proliferación del fitoplancton silíceo en regiones polares y subpolares y la de fitoplancton calcáreo (cocolitóforos, *Gephyrocapsa*) en latitudes medias y bajas, ii) la mayor duración de la estación de crecimiento de estas especies, por la reducción de la estacionalidad durante el mínimo de excentricidad, iii) cambios en el tipo o cantidad de descarga de nutrientes por modificaciones en los

procesos de meteorización en bajas latitudes, y todos ellos (i-iii) resultantes en una substancial mejora de las condiciones que favorecieron el hábitat y la tasa de crecimiento de estas especies (Rickaby et al., 2007). Al respecto de esta cuestión, Flores et al. (2012) hipotetiza acerca de un incremento generalizado en el contenido de fosforo en las aguas superficiales, beneficiando la proliferación de determinados morfotipos de *Gephyrocapsa* capaces de maximizar su tasa de crecimiento ante estas condiciones.

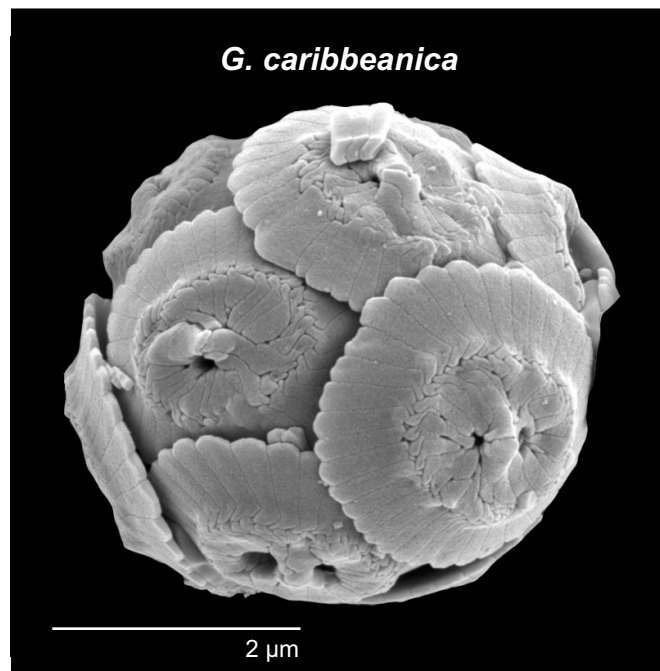


**Figura 6.** Imagen de una cocosfera de “*G. caribbeanica*”, ausente en las asociaciones modernas, pero dominante durante el intervalo de tiempo estudiado en este trabajo. Fotografía de SEM tomada de la guía online de biodiversidad y taxonomía de cocolitóforos, “*Nannotax*”.

Un elemento significativo durante el episodio del Mid-Brunhes, es el reconocimiento de condiciones de intensa disolución profunda en diferentes puntos del globo (Crowley, 1985; Hodell et al., 2000). Esta observación, junto con los valores de alta producción pelágica de *Gephyrocapsa* durante este intervalo, ha sido interpretada por algunos autores como indicativa de la interconexión existente entre su producción y la disolución de carbonato en los medios oceánicos, que podría desvelar la existencia de un papel clave de las eclosiones de Noëlaerhabdaceae en la regulación de la química del carbonato en el océano (Barker et al., 2006; Rickaby et al., 2007).

Los cocolitos producidos por “*G. caribbeanica*” se caracterizan, principalmente, por un alto grado de robustez (Fig. 6), debido al cierre total o parcial de su área central

(Subepígrafe 1.3.1.), lo que ha llevado a diferentes autores a definir “*G. caribbeanica*” como una especie o morfotipo de alta calcificación (Jin et al., 2018), para la cual también existen observaciones cualitativas acerca de una talla reducida de sus cocolitos (Bollmann, 1997; Flores et al., 2012). Aparte de las determinaciones anteriores, no existen referencias sólidas hasta la fecha acerca de precisiones morfométricas cuantitativas, más allá de valoraciones visuales (Saavedra-Pellitero et al., 2017), ni consenso claro acerca de su definición como especie independiente o como un morfotipo de respuesta ante un cambio ambiental acontecido durante el episodio del Mid-Brunhes.

### 1.3.1. Morfología y criterios para su clasificación

Al igual que los otros géneros pertenecientes a la familia Noëlaerhabdaceae, los cocolitos producidos por *Gephyrocapsa* pertenecen a la variedad genética de los “heterococolitos”, aquellos producidos durante la fase diploide de su ciclo de vida y característicamente compuestos de elementos, o unidades básicas de cristalización, que se disponen de forma radial (Young et al., 1999; Young y Henriksen, 2003) (Fig. 7). Morfológicamente, los cocolitos producidos por la familia de Noëlaerhabdaceae son de tipo “placolito”, aquellos compuestos por un escudo proximal y otro distal, dispuestos de perfil de forma paralela y perpendicular a una estructura en forma de tubo que define una abertura central (Young y Henriksen, 2003) (Fig. 7).

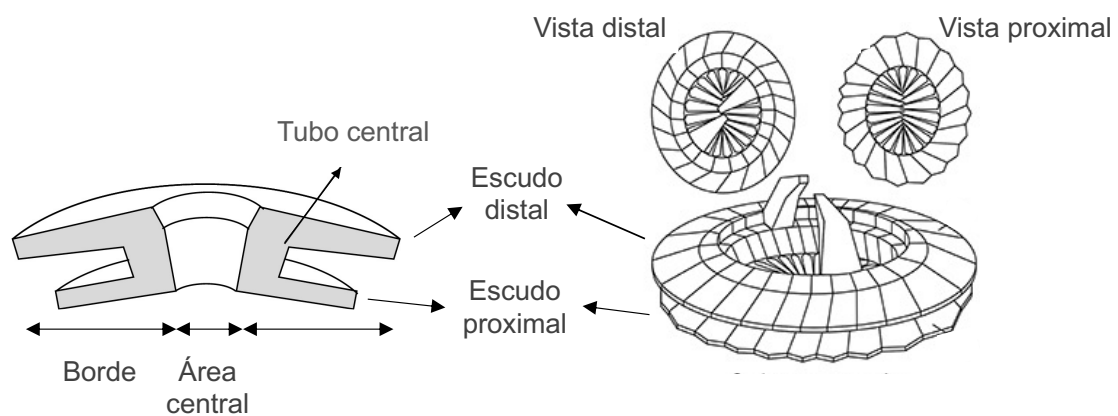


**Figura 7.** Estructura básica de un placolito producido por una especie perteneciente al género *Gephyrocapsa*. Figura compuesta a partir de esquemas originales tomadas de Young et al. (2003) y de Bendif et al. (2016).

En vista superior, el tubo central puede sobresalir, en mayor o menor medida, sobre el escudo distal, a modo de collar que bordea el área central. Los placolitos de este

tipo, producidos por *Gephyrocapsa*, se caracterizan, particularmente, por definir una forma elíptica o sub circular, así como por la presencia de una estructura en forma de barra central o puente, con una robustez variable, que cruza diagonalmente la abertura central. (Fig. 7).

Los criterios empleados para el reconocimiento de los placolitos pertenecientes a las diferentes especies o morfotipos que componen el género *Gephyrocapsa* son de tipo morfométrico y proceden de estudios biométricos convencionales (Bréhéret, 1978; Rio, 1982; Samtleben, 1980). Estos criterios son, principalmente y de forma cuantitativa, el tamaño del placolito, talla o medida del eje mayor de la elipse que conforma el escudo distal y el ángulo formado por el puente diagonal con respecto al eje mayor de la elipse que conforma el escudo distal del placolito (Fig. 8). El rango de tallas de estos placolitos, está comprendido entre las  $\sim 1.5$  y  $5.5 \mu\text{m}$  (Young et al., 2003). El grado de redondez del placolito y la abertura de su área central son criterios complementarios, aplicados de forma cualitativa. En este trabajo se ha adoptado, principalmente, la nomenclatura propuesta en los trabajos de Raffi et al. (1993) y de Flores et al. (2000a) para la clasificación de las diferentes especies, morfotipos o grupos, como se detalla a continuación.

El primer criterio morfométrico es la medida del eje mayor de la elipse que forma el placolito o talla (Fig. 8). Siguiendo los trabajos anteriormente referidos, el umbral de la medida de  $3 \mu\text{m}$  permite establecer la diferenciación general entre los placolitos de pequeño tamaño, de talla inferior a  $3 \mu\text{m}$ , incluidos en el grupo de *Gephyrocapsa* de tamaño pequeño o “small” *Gephyrocapsa* y los placolitos con una talla superior a  $3 \mu\text{m}$ , incluidos en el grupo de *Gephyrocapsa* de tamaño medio o “medium” *Gephyrocapsa*. Durante el episodio del Mid-Brunhes, el grupo de small *Gephyrocapsa* queda compuesto, de forma mayoritaria, por las especies *Gephyrocapsa aperta* y *Gephyrocapsa ericsonii* y, ocasionalmente, por morfotipos de talla pequeña, entre  $\sim 2.5$  y  $3 \mu\text{m}$ , pertenecientes a *Gephyrocapsa muelleriae*, una especie de talla regularmente medium. Las diferentes especies y morfotipos referidos dentro del grupo de small *Gephyrocapsa* se caracterizan por una afinidad ecológica semejante, por lo que, para fines de aplicación en estudios paleoecológicos y paleoceanográficos, los placolitos de *Gephyrocapsa* de este rango de

tamaños se agrupan tradicionalmente de forma conjunta para la generación de datos micropaleontológicos (Flores et al., 1999; Flores et al., 2000a,b).

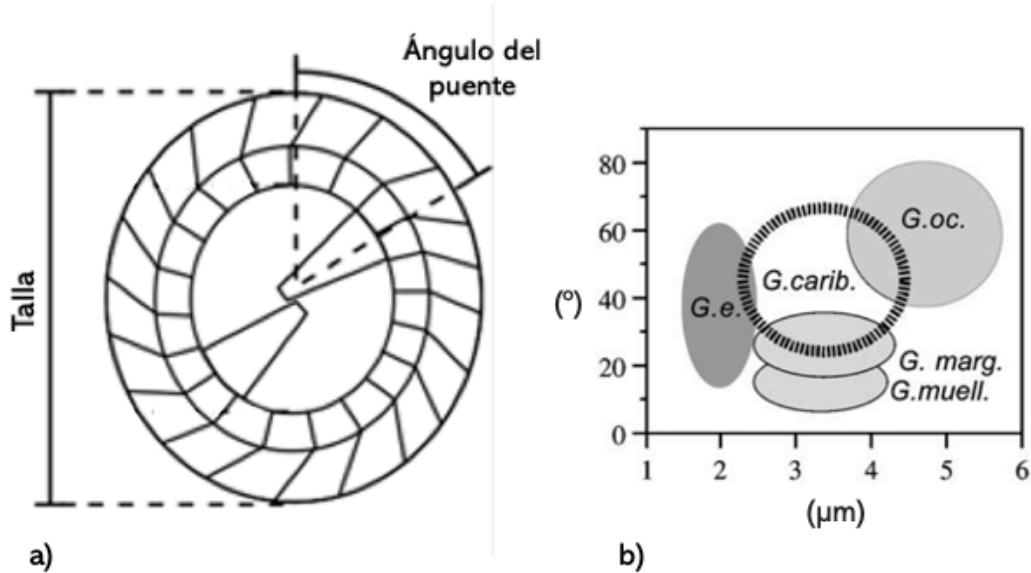


**Figura 8.** Figura compuesta a partir de esquemas originales tomados de (a) Bendif et al. (2019), para la representación esquemática de un cocolito perteneciente al género *Gephyrocapsa*, en el que los principales parámetros morfométricos empleados para la diferenciación de especies, morfotipos o grupos aparecen representados e indicados; y (b) Baumann y Freitag (2004), sobre la clasificación gráfica básica de las especies que constituyen el complejo *Gephyrocapsa* a partir de la aplicación de los criterios morfométricos.

Las especies y/o morfotipos de *Gephyrocapsa* que producen de placolitos de talla dentro del rango superior a 3  $\mu\text{m}$ , el grupo medium *Gephyrocapsa*, se caracterizan, sin embargo, por poseer afinidades ecológicas contrastadas. De este modo para la obtención de información completa acerca de este grupo en trabajos de índole micropaleontológica, es necesaria la diferenciación completa de taxones. El principal criterio morfométrico empleado para ello es la medida del ángulo del puente diagonal (Fig. 8). Así, dependiendo del valor de ángulo del puente podemos diferenciar entre las tres principales especies o morfotipos descritos a continuación, para los cuales se aporta una descripción morfométrica completa del resto de los elementos diagnósticos identificables con el empleo de técnicas de microscopía óptica:

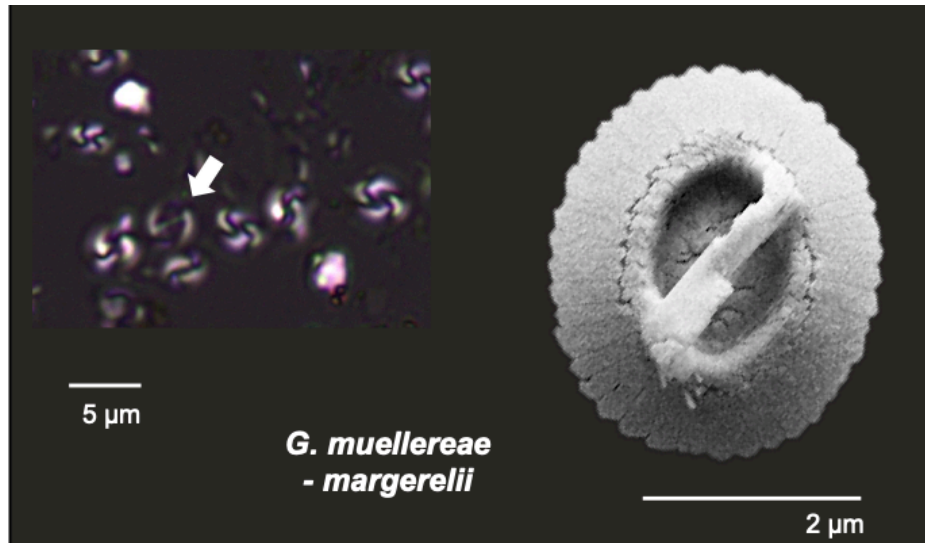


**Figura 9.** Aspecto de un cocolito perteneciente a la especie *G. muellerae-margerellii* observado mediante el empleo de técnicas de microscopía óptica (izquierda) y de SEM (derecha).

*Gephyrocapsa muellerae-margerellii*: El ángulo del puente es igual o inferior a 45°, regularmente comprendido entre los valores de 25 y 40° y con ocasionales especímenes con inclinación de bajo ángulo, inferior a 25°. El rango de tamaños de sus placolitos, que presentan un grado de elipticidad relativamente alta, queda comprendido entre 3 y 4 µm. Su área central es de pequeño tamaño (Fig. 9) (Bréhéret, 1978).

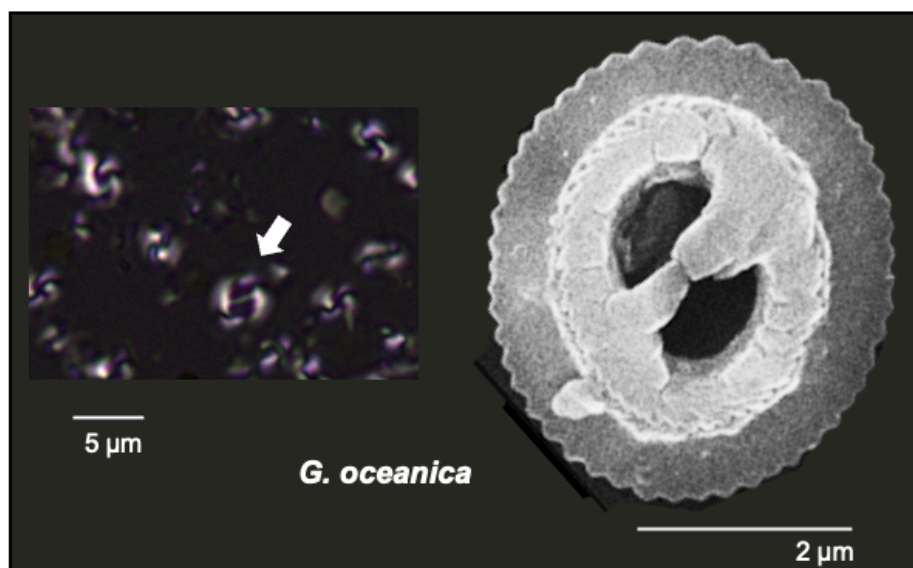


**Figura 10.** Aspecto de un cocolito perteneciente a la especie *G. oceanica* observado mediante el empleo de técnicas de microscopía óptica (izquierda) y de SEM (derecha).



*Gephyrocapsa oceánica*: El ángulo del puente es superior a 40 °. El rango de tamaños de sus placolitos queda comprendido entre 3.5 y 5.5  $\mu\text{m}$ , los cuales presentan un alto grado de circularidad (menos elípticos que la especie anterior), con un área central de grandes dimensiones (Kamptner, 1943). Cuando se observan con el empleo de técnicas de SEM, los placolitos de *G. oceánica* presentan, de forma característica, un collar central muy bien marcado (Fig. 10).

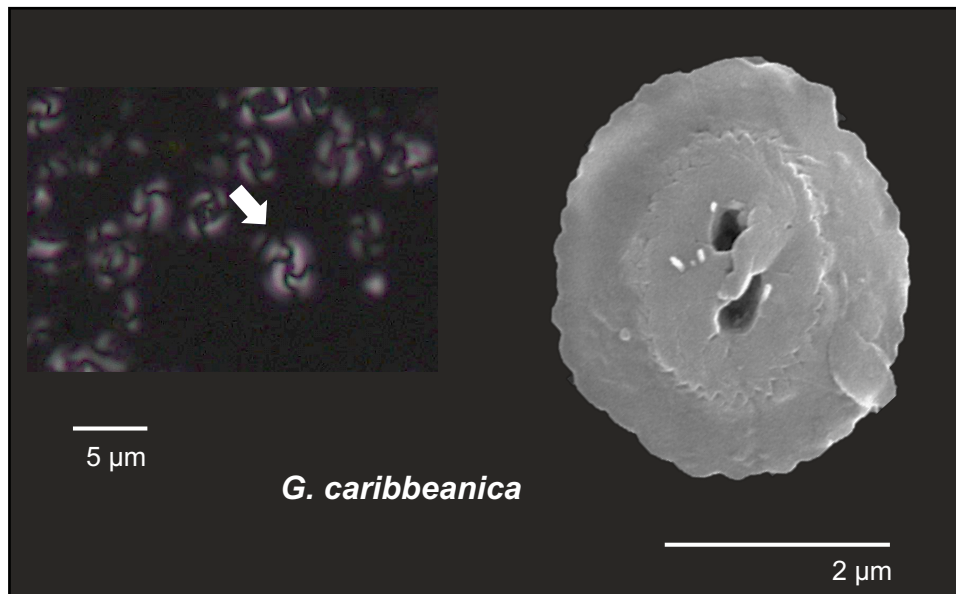


**Figura 11.** Aspecto de un coccolito perteneciente a la especie o morfotipo “*G. caribbeana*” observado mediante el empleo de técnicas de microscopía óptica (izquierda) y de electrónica de SEM (derecha).

“*Gephyrocapsa caribbeana*”: Los placolitos pertenecientes a esta especie o morfotipo presentan un valor de ángulo del puente que varía entre los valores de 30 y 65°, normalmente alrededor de 45°. El rango de tamaño de sus placolitos queda comprendido entre 3 y 5  $\mu\text{m}$  y su grado de elipticidad es bajo, semejante al de *G. oceánica*. El principal elemento diferenciador de los placolitos pertenecientes a “*G. caribbeana*” es su área central total o parcialmente ocluida (Fig. 10) (Hay et al., 1967).

A pesar de la preponderancia de los coccolitos procedentes de especies pertenecientes al género *Gephyrocapsa* durante el episodio e intervalo del Mid-Brunhes, otros taxones aparecen durante el análisis de asociaciones fósiles de este intervalo y han sido empleados como instrumentos complementarios para la reconstrucción paleoecológica y paleoceanográfica en esta tesis doctoral. El listado de estos aparece

recogido en el Anexo I, sobre la sistemática de los géneros y especies tratados en este estudio. Algunas precisiones relevantes al respecto de las particularidades ecológica de estas especies y/o grupos aparecen en el Epígrafe 1.4. y más ampliamente vinculadas a las particularidades ecológicas de los sectores estudiados en este trabajo, en los diferentes artículos que constituyen este compendio, localizados en los Capítulos 2 a 6.

### 1.3.2. Producción de alquenonas

Un aspecto característico del género *Gephyrocapsa* es su producción de alquenonas, compuestos orgánicos de tipo lipídico que quedan preservados en el sedimento (Volkman et al., 1995). La producción de estos compuestos se atribuye, generalmente, a diversos géneros y organismos de algas fitoplanctónicas procedentes de la clase Prymnesiophyceae y, dentro del grupo de los cocolitóforos, a algunas de las especies que constituyen la familia de Noëlaerhabdaceae, como *Emiliania huxleyi* y *G. oceanica* en la actualidad (Conte et al., 1998) y durante el pasado geológico, potencialmente, a otros organismos de esta familia pertenecientes a los géneros *Crenalithus*, *Dictyococcites*, *Reticulofenestra*, *Pseudoemiliania* y *Gephyrocapsa* (Brassell, 2014; Marlowe et al., 1990).

Las alquenonas, son moléculas de carbono de cadena larga: cetonas lineales con 37 átomos de carbono ( $C_{37}$ ) (Fig. 12), que pueden ser di, tri o tetra insaturadas ( $C_{37:2}$ ,  $C_{37:3}$  o  $C_{37:4}$ , respectivamente) es decir, pueden presentar dos, tres o cuatro enlaces dobles en la cadena (Fig. 12) (Volkman et al., 1980). Su función específica no ha sido aclarada por completo, aunque se encuentra hipotéticamente relacionada con el almacenamiento de material graso de reserva (Volkman, 2020).

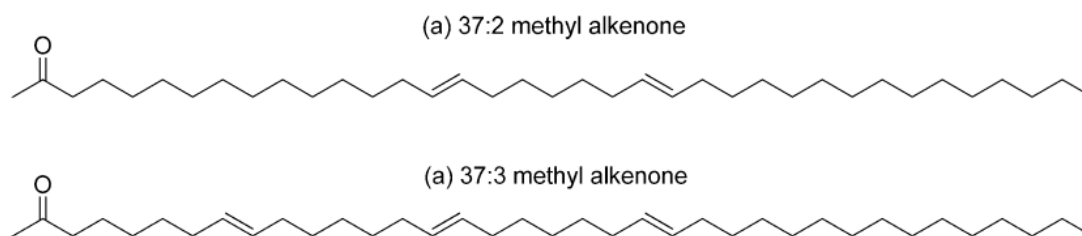


**Figure 12.** Estructura de los dos tipos de alquenonas más comunes: di insaturadas  $C_{37:2}$  (a) y tri insaturadas  $C_{37:3}$  (b). En la representación puede observarse la cadena de carbono larga y la posición de los dobles enlaces. Figura tomada de O’Neil et al. (2012).

El análisis geoquímico de estos biomarcadores ofrece herramientas ampliamente utilizada en estudios paleoceanográficos, como, por ejemplo, para la reconstrucción de los valores de temperatura superficial (SST-*Sea Surface Temperatures*), a partir de las relaciones de abundancias relativas entre las alquenonas C<sub>37:2</sub> y C<sub>37:3</sub> (Müller et al., 1998; Tierney y Tingley, 2018), o para llevar a cabo la estimación de los cambios en *p*CO<sub>2</sub> en el pasado, a partir de la medida de la composición isotópica del carbono en las alquenonas di insaturadas (<sup>13</sup>δ C<sub>37:2</sub>) (Pagani, 2014). Ambos procedimientos han sido aplicados en esta tesis doctoral, y la descripción completa de su desarrollo metodológico e integración en los estudios correspondientes aparece recogida en los Capítulos 2, 3 y 4.

#### **1.4. Cocolitóforos en la reconstrucción paleoceanográfica y paleoclimática**

Durante su vida, los cocolitóforos habitan en la zona fótica, una porción de la columna de agua en la que disponen de las condiciones suficientes de luz y cantidad de nutrientes, para llevar a cabo sus funciones vitales (McIntyre y Bé, 1967; Okada y McIntyre, 1977). De este modo, los cambios ambientales, incluyendo modificaciones en los parámetro anteriormente detallados, junto con cambios en la temperatura, salinidad y grado de turbiedad en las masas de agua superficiales, pueden repercutir en las asociaciones de cocolitóforos. Esto produce, principalmente, modificaciones en su proliferación y/o en el desarrollo preferente de una especie o grupo con capacidad para el desarrollo en una región o un sistema con determinadas condiciones concretas (Andruleit et al., 2003; Hagino et al., 2005; Takahashi y Okada, 2000).

En el océano moderno, existen especies de cocolitóforos con capacidad de adaptación, o sensibilidad, a condiciones diferentes, lo cual resulta en una distribución vertical (profundidad de hábitat) y horizontal (distribución biogeográfica) característica y ampliamente conocida (Young et al., 2003). En la Figura 13, puede observarse la distribución biogeográfica actual de algunas de ellas. Asumiendo una distribución ecológica de especies de cocolitóforos en el pasado comparable a la distribución y relaciones ecológicas de las asociaciones modernas, la distribución de los cocolitos fósiles preservados en el sedimento permite llevar a cabo la inferencia de cambios ambientales en los parámetros que controlaron su adaptación y hábitat durante el pasado, en el momento de su proliferación y desarrollo (Baumann y Freitag, 2004; Flores et al.,

2003; Kinkel et al., 2000). A escala de tiempo geológico, los cambios en la disponibilidad de nutrientes, luz, turbiedad, temperatura y salinidad vienen determinados, en gran medida, por modificaciones de índole oceanográfica y/o por cambios climáticos a escala regional, oceánica (p. ej., escala del océano Atlántico), o incluso a escala global. De este modo, el estudio de las asociaciones de cocolitos en el sedimento permite llevar a cabo inferencias acerca de cambios en las condiciones de carácter paleoceanográfico y/o paleoclimático durante el pasado, una perspectiva que se ha aplicado en este trabajo durante ciertos estadios de interés durante el intervalo del Mid-Brunhes.

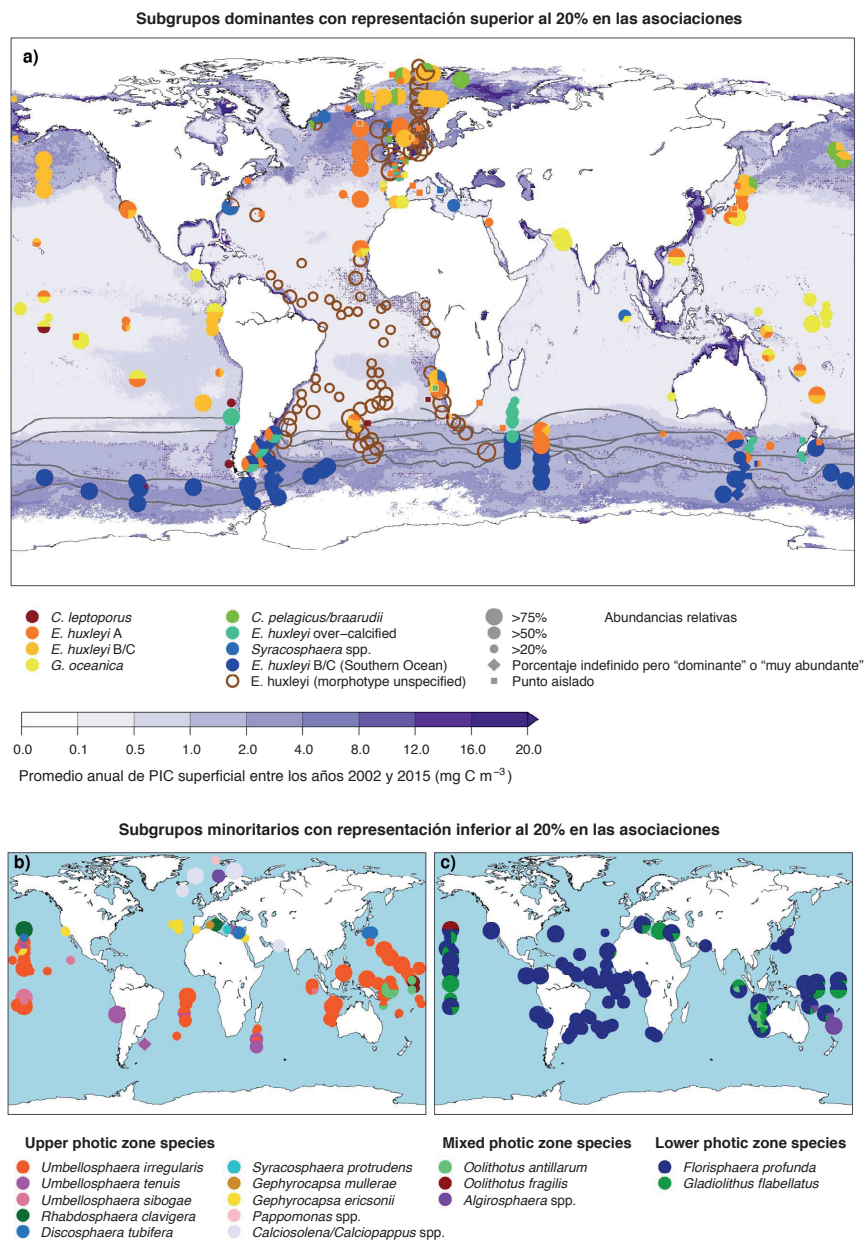


**Figura 13.** Distribución geográfica de los subgrupos de nanoplancton calcáreo dominantes (a) y minoritarios (b) en las asociaciones modernas. El tamaño de los puntos es proporcional a la abundancia relativa en la zona representada. La estimación de la concentración de carbono inorgánico (PIC) representada, puede considerarse una estimación cualitativa de la abundancia de nanoplancton calcáreo. Figura tomada de Krumhardt et al. (2017), donde pueden encontrarse las referencias específicas acerca de los datos representados.

Para llevar a cabo el análisis micropaleontológico de las asociaciones de cocolitos fósiles en el sedimento, se siguió el protocolo de preparación de muestras por decantación del material sedimentario estandarizado en la publicación de Flores y Sierro (1997) y el posterior recuento de la cantidad estadísticamente representativa de un mínimo de 400 cocolitos en cada muestra, con la aplicación de técnicas de microscopía óptica y polarización cruzada. Ya que esta técnica de preparación ofrece como resultado un distribución homogénea de los cocolitos en la muestra, los recuentos obtenidos son transferibles a medidas de la abundancia absoluta, o concentración de cocolitos por gramo de sedimento, siguiendo la formula en Flores y Sierro (1997) a continuación:

$$N = \frac{n * R^2 * V}{r^2 * g * v}$$

donde N es el valor de abundancia absoluta por gramo (cocolitos\*g<sup>-1</sup>), n es el número de cocolitos contados por campo visual, R es el radio de la placa de Petri utilizada (mm), V es el volumen de agua de la disolución inicial (μL), r es el radio del campo visual del microscopio (mm), g es el peso seco del sedimento de la disolución (g) y v es el volumen de muestra extraído con la micropipeta (μL).

A partir de este valor, la disponibilidad de un modelo de edad preciso que permita estimada la tasa de sedimentación para un intervalo estudiado y datos de densidad del sedimento, es posible llevar a cabo el cálculo de la tasa de acumulación de cocolitos o flujos (NAR-*Nannofossil Accumulation Rates*) durante el intervalo estudiado, por unidad de área (cm<sup>2</sup>) y tiempo (kyr) (Flores and Sierro, 1997):

$$NAR = N * d * s$$

donde NAR es el flujo o ratio de acumulación de cocolitos (cocolitos\*cm<sup>-2</sup>\*kyr<sup>-1</sup>), N la abundancia absoluta (cocolitos\*g<sup>-1</sup>), d la densidad de sedimento seco (g\*cm<sup>-3</sup>) y s la tasa de sedimentación lineal (cm\*kyr<sup>-1</sup>).

La aplicación metodológica de esta técnica de preparación y el análisis micropaleontológicos detallado asociado a este procedimiento se recoge en los Capítulos 2 a 6, junto con adaptaciones y precisiones específicas del método para cada uno de los estudios. Los detalles acerca de la resolución del muestro previa a la preparación de las muestras llevada a cabo para cada uno de los testigos sedimentarios estudiados en esta tesis doctoral se encuentran especificado en el Epígrafe 1.4. sobre materiales para el análisis.

#### 1.4.1. Reconstrucción de la productividad primaria con *Gephyrocapsa*

Los valores de N y NAR del total de cocolitos de una asociación fósil son, respectivamente, una medida de la concentración total de cocolitos en el sedimento y de la tasa total de acumulación de cocolitos en el tiempo. En ausencia de evidencias de procesos de disolución que conlleve la pérdida total de especímenes y/o de dilución, por aportes sedimentarios de diferente naturaleza, los valores de N y NAR total se considera como una buena estimación cualitativa de la productividad primaria acontecida en la zona fótica (Baumann et al., 2005; Saavedra-Pellitero et al., 2011). Así, cuando el proceso o procesos que ejercen el estímulo de fertilización sobre una asociación de cocolitóforos, en un lugar de estudio, es conocido o de posible precisión con el empleo de trazadores independientes, la variación en N y/o NAR durante un intervalo de tiempo estudiado permite llevar a cabo la reconstrucción cualitativa de la influencia del mecanismo sobre la productividad primaria de este grupo.

Las especies que componen el complejo *Gephyrocapsa* son de carácter cosmopolita, capaces de adaptarse a ambientes diversos, con una marcada afinidad por las condiciones de fertilización en la zona fótica superior y de rápido aprovechamiento de la disponibilidad de nutrientes (UPZ-Upper Photic Zone), de lo cual se benefician para la rápida proliferación, siguiendo la estrategia ecológica de la r (Barber y Hiscock, 2006). No obstante, existen ciertos parámetros ecológicos, como la temperatura, que controlan, en cierta medida, la proliferación de algunos de los taxones que integran el complejo *Gephyrocapsa* (Bollmann, 1995). En este trabajo, partiendo de la diferenciación exhaustiva de especies y/o morfotipos que componen el complejo *Gephyrocapsa*, previamente detallada en Subepígrafe 1.3.1., se precisa la información que los diferentes

taxones pueden aportar, y se aplica para la reconstrucción paleoceanográfica y paleoclimática durante el intervalo del Mid-Brunhes:

Las especies que componen el grupo de small *Gephyrocapsa* muestran una respuesta rápida ante los procesos de fertilización que ocurren en la UPZ, dónde este grupo habita (Okada y Honjo, 1973; Okada y Wells, 1997). La naturaleza y significado ecológico de “*G. caribbeanica*” es una cuestión altamente debatida. No obstante, el carácter cosmopolita de este taxón, comparable al de *E. huxleyi* en los nichos oceánicos actuales, es una noción ampliamente aceptada, llegándose a considerar a “*G. caribbeanica*” como análogo, en términos ecológicos, de dicha especie moderna (Saavedra-Pellitero et al., 2017). En este trabajo se ha considerado la suma de los valores absolutos conjuntos (N o NAR) de ambos grupos de small *Gephyrocapsa* y “*G. caribbeanica*” para la construcción de un índice de productividad (PPP-*Primary Productivity Proxy*), el cual se ha empleado como herramienta central en los trabajos orientados a la reconstrucción paleoceanográfica regional, a alta resolución, en los márgenes Mediterráneo y Atlántico de la península Ibérica, en los Capítulos 2 y 3. La capacidad de este indicador para delinear las condiciones de producción orgánica en el mar de Alborán ha sido, además, evaluada a partir del estudio de su relación de correspondencia con las condiciones de acumulación y preservación de materia orgánica en el sedimento, obtenidas a partir de datos de trazas fósiles y cambios de color en los sedimentos, un análisis cuyo desarrollo constituye el artículo científico que aparece en el Capítulo 5.

#### 1.4.2. *Florisphaera profunda* vs. *Gephyrocapsa*

*Florisphaera profunda* es una especie aún presente en las asociaciones de nannoplancton modernas, que habita la zona fótica inferior (LPZ-*Lower Photic Zone*), en profundidades regularmente inferiores a los 100 metros (Okada y Honjo, 1973; Okada and McIntyre, 1977; Venrick, 1982). Esta restricción de su hábitat se debe, principalmente, a su capacidad de supervivencia en condiciones de menor disponibilidad de luz, utilizando esencialmente las longitudes de onda del verde y del azul, en comparación con los taxones propios de la UPF, como las especies incluidas en el complejo *Gephyrocapsa* (Molfino y McIntyre, 1990). La proliferación de esta especie es superior cuando el nivel de máxima concentración de clorofila, localizado normalmente en la base de la capa de mezcla, se

profundiza y alcanza la zona de hábitat de *F. profunda* (Molfino y McIntyre, 1990). Esta configuración vertical de la columna de agua es propia de las regiones tropicales y/o subtropicales de baja latitud, donde predominan las condiciones de estratificación o ausencia de mezcla vertical (Fig. 14).

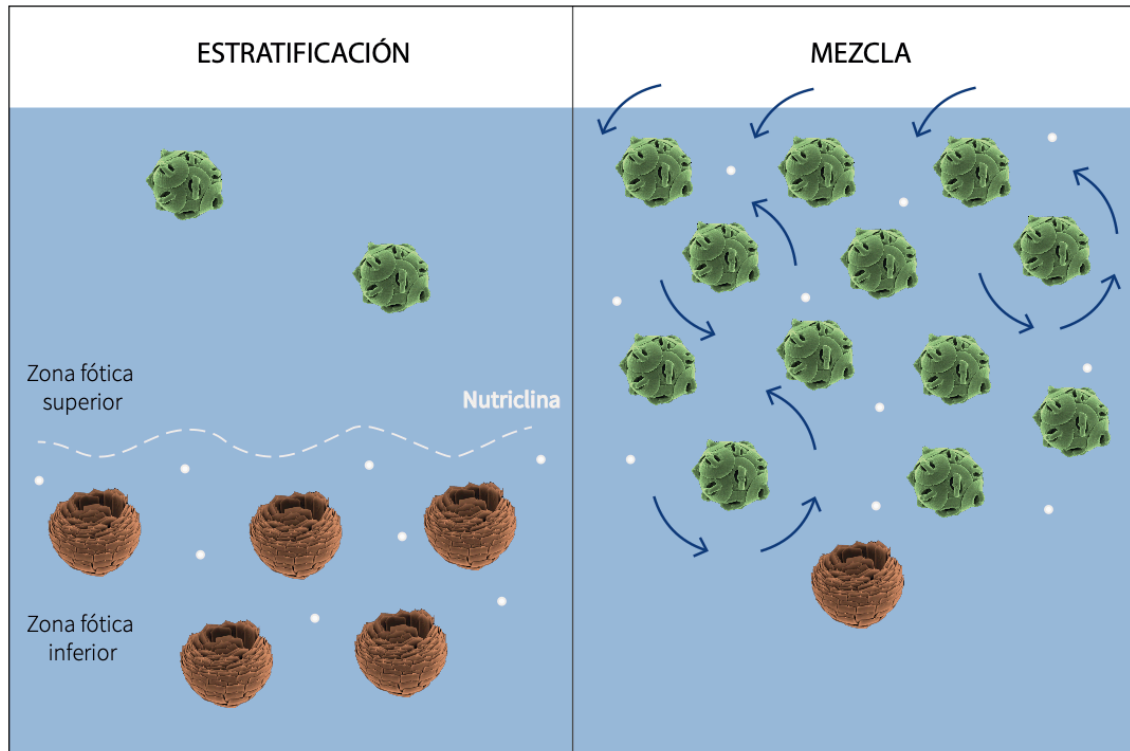


**Figura 14.** Representación esquemática de la relación de abundancia entre *Florisphaera profunda* (representada con color naranja) y *Gephyrocapsa* (representada con color verde) en respuesta a dos escenarios extremos: A la izquierda, estratificación de la columna de agua y restricción de nutrientes bajo la nutriclina profunda; a la derecha, ruptura de la nutriclina por fuerte mezcla vertical y distribución de nutrientes hacia la superficie.

El dominio o incremento de la representación de este taxón en las asociaciones de nanoplancton en el sedimento ha sido, por lo tanto, considerado indicativo de escenarios de incremento de la estratificación vertical (Fig. 14) con profundización de la nutriclina y consecuente reducción de la productividad primaria en la UPF e incremento en la LFZ (Molfino y McIntyre, 1990). Esta relación entre taxones cuantificados en el sedimento ha sido empleada para la estimación relativa de la profundidad de la nutriclina, mediante el cálculo del ratio N (N ratio), una medida relativa entre los valores de abundancia de ambos grupos de la UPZ, generalmente placolitos de pequeño tamaño y los de la LPF, constituido por *F. profunda*, propuesto por Flores et al. (2000b). Por su parte, la relación



entre los porcentaje de *F. profunda* y medidas de productividad y temperatura, a partir de indicadores independientes en sedimentos superficiales y asociaciones modernas, ha sido aplicado para la obtención de una transferencia hacia valores cuantitativos de productividad neta (Beaufort et al., 1997; Hernández-Almeida et al., 2019). En este trabajo se emplea el N ratio en el Capítulo 3, acerca de la reconstrucción de los mecanismos de control sobre la productividad primaria en el margen ibérico portugués (Site IODP U1385).

Entre los diferentes testigos sedimentarios estudiados en esta tesis doctoral (Epígrafe 1.8.), la representación de *F. profunda* es significativamente superior el ODP Site 925, localizado en la región tropical del Atlántico, en bajas latitudes (Epígrafe 1.8.2.). Así, los porcentajes de esta especie son empleados en el Capítulo 4, donde se analiza su potencialidad como indicador de los cambios en la tasa de crecimiento celular de los cocolitóforos (*growth rate*).

#### 1.4.3. Grupos sensibles a la temperatura de las masas de agua superficiales

Uno de los principales factores ambientales que ejerce control sobre la distribución vertical y horizontal de los géneros y especies de cocolitóforos, es la temperatura (Winter, 1994). Así, los cambios en la composición de una asociación actual, a lo largo del tiempo, o la observada en una asociación de cocolitos fósil durante un intervalo, puede entrañar una modificación de temperatura beneficiando y/o limitando el desarrollo de determinados taxones. Por otro lado, la temperatura es, junto con la salinidad, uno de los principales parámetros físicos para la caracterización de una masa de agua (Emery, 2001), motivo por el cual la reconstrucción de los cambios en la temperatura superficial durante el pasado es una herramienta relevante para la inferencia de los cambios en la influencia de las masas de agua superficiales en una región. De este modo, el análisis de la representación y cambios en el contenido de determinadas especies y/o grupos de cocolitóforos sensibles a los cambios de temperatura permite llevar a cabo la reconstrucción de la influencia de diferentes tipos de aguas superficiales, con posibles implicaciones paleoceanográficas, de mayor entidad, suprayacentes. Este enfoque se aplica en las reconstrucciones paleoceanográficas en los márgenes ibéricos mediterráneo (ODP 977) y portugués (IODP U1385), en los Capítulos 2 y 3. Ambos enclaves se ven influenciados por corrientes oceánicas superficiales semejantes y enmarcadas dentro del

sistema general del Atlántico Norte; por lo tanto, la explicación acerca de las relaciones y procedencia específica de las asociaciones indicadoras de temperatura, presentadas a continuación y desarrollada en los Capítulos 2 y 3, se lleva a cabo en relación con dichos sistemas.

Dentro del complejo *Gephyrocapsa*, el taxón *G. muelleriae-margerelli* es considerado un taxón propio de condiciones superficiales frías o transicionales, según el análisis y clasificación en el trabajo de Bollmann (1997). Por su parte, la subespecie *Coccolithus pelagicus pelagicus* habita en la región de límite del sector biogeográfica subártico (McIntyre and Bé, 1967; Winter, 1994). En latitudes ibéricas, ambas especies se consideran, conjuntamente, indicadoras de la presencia de masas de agua fría superficiales, de procedencia polar o subpolar. Esta discusión y referencias al respecto se encuentra incluida en los Capítulos 2 y 3.

Por su parte, los especímenes pertenecientes a los géneros y/o especies *Oolithotus* spp., *Umbilicosphaera* spp., *Umbilicosphaera sibogae*, *Umbilicosphaera foliosa*, *Rhabdosphaera clavigera*, *Umbellosphaera* spp. y *Calciosolenia* spp., poseen una afinidad común por las condiciones cálidas superficiales, propias de las regiones tropicales y subtropicales (Boeckel y Baumann, 2004; Winter, 1994). Tradicionalmente, estos taxones se agrupan conjuntamente como taxones de aguas cálidas (WWT-*Warm Water Taxa*) (Cachão et al., 2000; Winter, 1994) y, en los trabajos incluidos en los Capítulos 2 y 3, sus valores se emplean como indicadores del efecto de las masa de agua de procedencia subtropical afectando a los márgenes ibéricos.

En este estudio, los taxones o grupos previamente indicados como potenciales indicadores de temperaturas superficiales y de influencia de determinadas masas de agua se aplican, junto con los valores de reconstrucción de SST, obtenidos a partir del índice  $U^k_{37}$  procedente del análisis de alquenonas. Los métodos para su cálculo y diferentes procedimientos para su calibración aparecen incluidos en los Capítulos 2 a 4. La disponibilidad y aplicación conjunta de estos datos, ha permitido llevar a cabo la validación directa de la señal de sensibilidad a la temperatura de los grupos o especies de cocolitóforos, así como la extracción de información adicional y la discusión de nuevas relaciones ecológicas con la temperatura superficial.

## 1.5. Fraccionamiento isotópico del carbono durante la fotosíntesis

### 1.5.1. Conceptos teóricos y aplicación para la reconstrucción de CO<sub>2</sub>

El fraccionamiento isotópico del carbono durante la fotosíntesis, referido como  $\epsilon_p$ , es una aproximación del fraccionamiento isotópico entre el sustrato de carbono inorgánico empleado para la fotosíntesis – el carbono inorgánico disuelto, DIC, en el medio acuoso – y el carbono orgánico resultante de la fijación fotosintética llevada a cabo por el fitoplancton (Popp et al., 1998). La fórmula que sintetiza el proceso es:

$$\Delta_{\text{DIC} - \text{org}} = \delta^{13}\text{C}_{\text{DIC}} - \delta^{13}\text{C}_{\text{org}} \quad (3)$$

Particularmente,  $\epsilon_p$  está referido al valor de fraccionamiento obtenido a partir del CO<sub>2</sub> [aq], la fuente de carbono inorgánico básica para función de fotosíntesis (Freeman y Hayes, 1992):

$$\epsilon_p = [(\delta^{13}\text{C}_{\text{CO}_2[\text{aq}]} + 1000) / (\delta^{13}\text{C}_{\text{org}} + 1000)] * 1000 \quad (4)$$

De este modo, el valor de  $\epsilon_p$  viene determinado por la concentración ambiental de CO<sub>2</sub> [aq] y representa una medida del aporte de CO<sub>2</sub> a la célula relativa a la demanda de carbono celular. El mecanismo de adquisición de CO<sub>2</sub> por parte de la célula ha sido tradicionalmente considerado como pasivo, siguiendo los principios básicos del transporte por difusión (Rau et al., 1996), según lo cual se espera un aumento en los valores de  $\epsilon_p$  cuando la disponibilidad de CO<sub>2</sub> es superior en relación a la demanda celular. Por lo tanto, esta relación puede verse, además, influida por otros factores independientes al CO<sub>2</sub> que, en mayor o menor medida, afecten a los requerimientos de carbono celulares y a la dinámica de difusión. Entre ellos se incluye la permeabilidad de la membrana celular, la demanda celular de carbono o tasa de crecimiento celular (*growth rate*), así como la talla de la célula y su potencial capacidad para asimilar carbono de forma activa e independiente a la dinámica pasiva (Rau et al., 1996; Raven y Johnson, 1991).

El modelo de fraccionamiento clásico, de adquisición celular pasiva de CO<sub>2</sub> por difusión, ha sido ampliamente explotado como herramienta para la reconstrucción de niveles de  $p\text{CO}_2$  durante el pasado, a partir de la estimación de  $\epsilon_p$  (Pagani, 2014). Esta línea de estudio, denominada “paleobarometría” ha dado lugar a múltiples e importantes reconstrucciones de  $p\text{CO}_2$  desde el Eoceno (Pagani et al., 2005; Zhang et al., 2013). Bajo la pauta del modelo clásico por difusión, la influencia del resto de parámetros (diferentes a CO<sub>2</sub> [aq]) se considera mayoritariamente dependiente de las tasas de crecimiento celular

(Fig. 14). La “carga” impuesta por los posibles cambios en este parámetro, requerida para el cálculo de  $p\text{CO}_2$  con la aplicación del modelo, ha sido tradicionalmente considerada como un valor estable, englobado por un término denominado “ $b$ ” parametrizado, regularmente, a partir del valor de la concentración moderna de fosfato ( $[\text{PO}_4]$ ) en la zona de estudio (Bidigare et al., 1997; Rau et al., 1996),

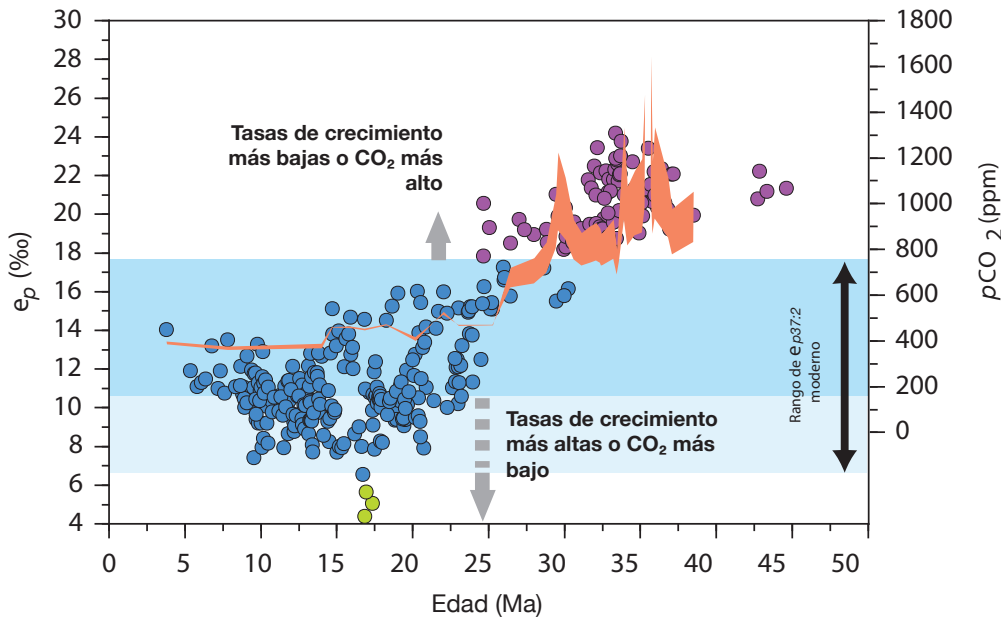


**Figura 15.** Ejemplo que ilustra la interpretación de un registro de fraccionamiento isotópico del carbono durante la fotosíntesis ( $\epsilon_p$ ) exclusivamente en términos de variación de las concentraciones de  $\text{CO}_2$  (y, por tanto, de  $\text{CO}_2$  [aq]) y de las tasas de crecimiento celular (*growth rate*). Figura modificada de Pagani (2014).

### 1.5.2. Análisis de la sensibilidad de $\epsilon_p$ a $\text{CO}_2$ y otros factores

Cuando el enfoque anterior se aplica durante el Pleistoceno y el Holoceno, la disponibilidad de medidas independientes de  $p\text{CO}_2$ , a partir de testigos de hielo (Köhler et al., 2017) permite realizar una comparación directa de los mismos con los valores  $\epsilon_p$  para analizar su relación de sensibilidad (la correspondencia existente entre ambas) e, incluso, llevar a cabo una comprobación directa de la validez de las reconstrucciones de  $p\text{CO}_2$ . De este modo, la obtención de una escasa variabilidad de los valores de  $\epsilon_p$  para los extremos de  $p\text{CO}_2$  mínimo durante los estadios glaciales, comenzó a suscitar dudas al respecto de la sensibilidad real de  $\epsilon_p$  a  $\text{CO}_2$ . Entre las principales líneas argumentales en el debate para explicar la aparente inconsistencia, se apela a la activación de los

mecanismos de concentración activa de carbono (CCM-*Carbon Concentration Mechanisms*) cuando los niveles de  $p\text{CO}_2$  son bajos, como sucede durante los estadios glaciales, lo cual representa la ruptura de las relaciones de adquisición pasiva de  $\text{CO}_2$  por parte de la célula y, por lo tanto, la incapacidad del modelo clásicos para englobar las relaciones y producir reconstrucciones sólidas de  $p\text{CO}_2$  (Badger et al., 2019; 2021). Otros autores han concentrado sus esfuerzos en el perfeccionamiento de la estimación de la carga fisiológica de cocolitóforos sobre el valor de  $\epsilon_p$ , donde destacan los recientes ejercicios para la obtención y calibración de valores de tasas de crecimiento celular, a partir de las medidas directas de la variación en los valores de talla celulares (Zhang et al., 2020) y a partir de datos micropaleontológicos, indicadores de la disponibilidad de nutrientes en el ambiente de hábitat del organismo fotosintético (Hernández-Almeida et al., 2020).

Un estudio basado en la observación de las relaciones empíricas de sensibilidad de los factores implicados en la modulación de  $\epsilon_p$  en cultivos, llevado a cabo en el grupo de investigación Climate Geology de ETH-Zürich, confirmó la importancia de la adquisición activa de  $\text{CO}_2$  [aq] cuando los niveles de  $p\text{CO}_2$  generales disminuyen (Stoll et al., 2019). La elaboración de un modelo estadístico de variable múltiple, a partir de estas observaciones permitió la integración de las relaciones empíricas implicadas en la modulación de  $\epsilon_p$ , generando un nuevo modelo de fraccionamiento potencialmente aplicable para la reconstrucción de  $p\text{CO}_2$  (Stoll et al., 2019).

Existen aún muchas preguntas abiertas acerca de la aplicabilidad de un modelo teórico fundamentalmente diferente al tradicionalmente aceptado, que requeriría de la evaluación de dichas relaciones de sensibilidad durante ciclos G/I con  $\text{CO}_2$  [aq] variable y conocido, junto a la incorporación de estimaciones fidedignas del resto de parámetros fisiológicos y ambientales implicados, principalmente: los cambios en las tasas de crecimiento celular, la disponibilidad de luz y la talla de las células de los organismos fotosintéticos. El intervalo del Mid-Brunhes ofrece importantes ventajas para este propósito, al incluir extremos contrastados de concentración de  $p\text{CO}_2$  atmosférico en el periodo Cuaternario, que podrían polarizar la carga fisiológica que se desea analizar, condiciones de excentricidad mínima que limitan la carga de la estacionalidad sobre los cambios en las condiciones de productividad y su efecto modificando las tasas de crecimiento celular y, de forma importante, el dominio del complejo *Gephyrocapsa* como

único grupo productor de alquenonas en este intervalo (Volkman et al., 1980), el elemento a partir del que se obtiene la medida isotópica inicial de  $\delta^{13}\text{C}$ , sobre la variedad de alquenonas di insaturadas,  $\delta^{13}\text{C}_{37:2}$ , a partir de la que se lleva a cabo la estimación del valor de  $\delta^{13}\text{C}_{\text{org}}$  necesario para llevar el cálculo de  $\epsilon_p$ . Este planteamiento y análisis se lleva a cabo en esta tesis doctoral y la descripción completa de su metodología, desarrollo, resultados y conclusiones se encuentra en el Capítulo 4.

## 1.6. Variaciones en la calcificación de cocolitóforos

En términos funcionales, la calcificación en cocolitóforos confiere, principalmente, un estatus de protección contra la depredación, los virus y bacterias y contra el exceso de radiación existente en la superficie de la zona fótica. Además, supone una herramienta de regulación de las condiciones de flotabilidad y hundimiento. Ya que la materialización de esta función conlleva un consumo energético determinado, un cambio en la intensidad de calcificación, podría conllevar la búsqueda de una ventaja o superación de unas condiciones ambientales, a priori, perjudiciales en términos de los parámetros anteriormente expuestos, o en respuesta a otros procesos aún desconocidos hasta la fecha (Monteiro et al., 2016).

El análisis de la variación en la calcificación de cocolitóforos se ha llevado a cabo, principalmente, a partir de estudios en cultivos (Bach et al., 2012; Bach et al., 2013). Estos análisis han demostrado un importante control en la calcificación por las condiciones de la química del carbono en el medio acuoso, particularmente referido a la concentración de  $\text{CO}_2$  [aq],  $\text{HCO}_3^-$  y  $\text{CO}_3^{2-}$ , las especies carbonatadas que constituyen el volumen total de carbono inorgánico disuelto en el medio acuoso, DIC, y las condiciones de pH y de alcalinidad, vinculadas al balance entre especies químicas carbonatadas (Bach et al., 2015) (Fig. 16).

En cuanto a la relación de los cambios en calcificación con el  $\text{CO}_2$ , los estudios han dado como resultado interpretaciones contrapuestas (Beaufort et al., 2011; Bolton et al., 2016; Iglesias-Rodríguez et al., 2008; Meier et al., 2014). En gran medida, esta controversia tiene que ver con las diferentes escalas de tiempo abordadas, las diferentes especies estudiadas e, incluso, en el caso de trabajos en cultivos, con las diferentes cepas empleadas para los análisis (Langer et al., 2009). Sin embargo, tanto los estudios en cultivos como en material fósil han concluido unánimemente acerca de la preponderancia

del control de la disponibilidad de  $\text{HCO}_3^-$  en el medio acuoso sobre los niveles de calcificación, con los que la tasas de calcificación intracelular mantienen una relación directa (Bach et al., 2015). Por su parte, la cantidad de iones  $\text{H}^+$  en las aguas, controla los niveles de pH, un parámetro que ejerce un efecto negativo o inhibitorio sobre la tasa de calcificación celular, a medida que la cantidad de  $\text{H}^+$  no neutralizados aumenta o, lo que es lo mismo, el pH disminuye (Bach et al., 2015). En segundo orden, dentro de los factores de naturaleza abiótica, los cambios en la temperatura pueden ejercer aceleración sobre los procesos metabólicos, afectando al grado de calcificación (Sett et al., 2014). Los cambios en las condiciones de estratificación y/u otros procesos limitando la disponibilidad de nutrientes pueden ejercer un control al afectar a las tasas de crecimiento y, por tanto, la fuente energética necesaria para sustentar las funciones intracelulares (Bach et al., 2015).

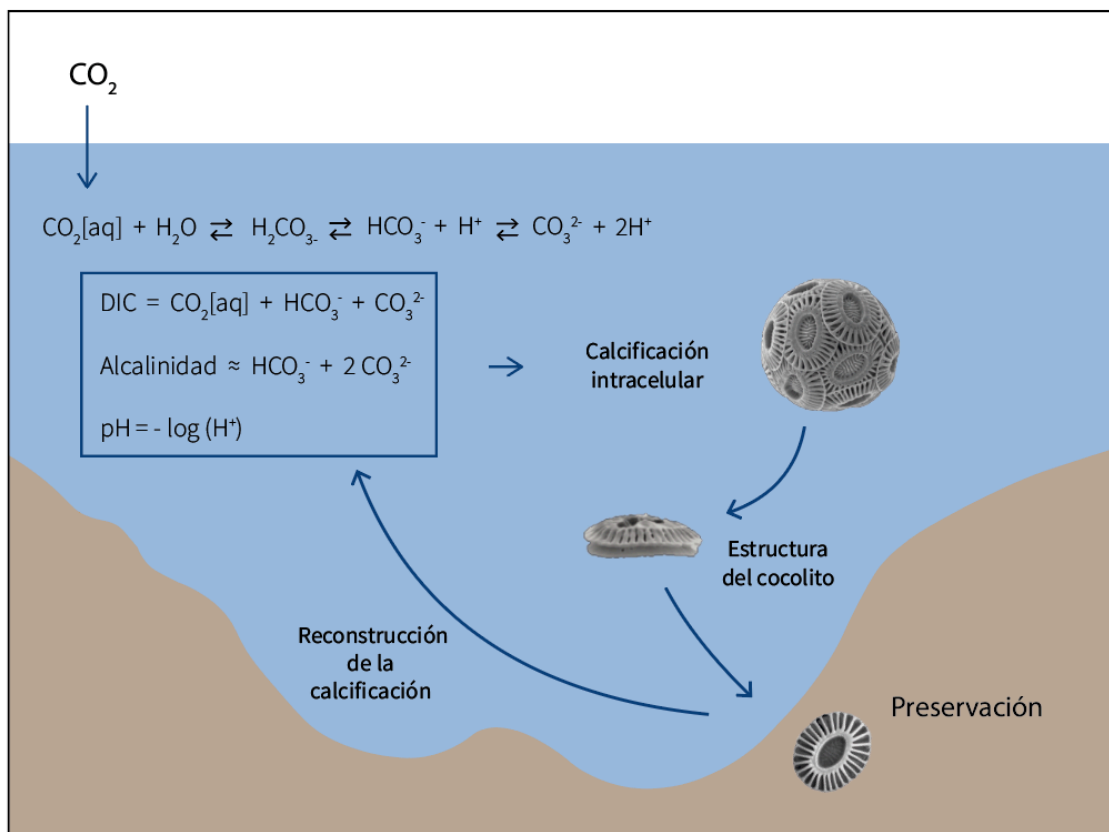


**Figura 16.** Representación simplificada de las reacciones básicas que rigen el sistema del carbonato oceánico y de cómo el enfoque de reconstrucción de la calcificación en cocolitóforos, a partir de cocolitos fósiles, puede contribuir a la inferencia de las condiciones geoquímicas del océano superficial.

No obstante, es importante tener en cuenta la existencia de un control añadido sobre la función de calcificación intracelular, por parte de factores de naturaleza biótica o fisiológica (McClelland et al., 2016). Estos factores pueden modular la relación directa con las condiciones químicas extracelulares. En este sentido, es conocida la existencia de mecanismos que aumentan la toma de carbono hacia la célula o que estimulan su transporte y distribución intracelular entre las funciones de calcificación y fotosíntesis, ante condiciones de limitación en la disponibilidad externa: este es el caso, por ejemplo, de la intensificación en la transferencia de  $\text{HCO}_3^-$  hacia la función de fotosíntesis, en detrimento de calcificación, ante condiciones de escasez en la disponibilidad de carbono extracelular por la reducción general de  $\text{CO}_2$  [aq] (Bolton and Stoll, 2013). Existen aún muchas cuestiones abiertas e incertidumbre al respecto del control fisiológico sobre la función de calcificación, los factores que lo estimulan y su cuantificación y la operación de este tipo de mecanismos debe tenerse en cuenta.

#### 1.6.1. Reconstrucción de la calcificación en cocolitos fósiles

Como se presenta en el apartado anterior, la reconstrucción de los cambios en la calcificación en cocolitóforos es una herramienta que puede ser de gran utilidad a la hora de inferir los cambios ambientales durante el pasado (Fig. 16). Además, este campo de estudio contribuye substancialmente al conocimiento de las posibles respuestas futuras de este grupo de fitoplancton ante el impacto antrópico, como el aumento en los niveles de  $\text{CO}_2$  atmosférico y la acidificación oceánica asociada, que realza su importancia.

Una de las técnicas empleadas para llevar a cabo la reconstrucción del grado de calcificación individual en cocolitóforos durante el pasado es el cálculo de índices de calcificación a partir de la caracterización morfométrica de los cocolitos fósiles preservados en el sedimento. Los parámetros morfométricos medidos para ello son, esencialmente, talla, volumen y masa del cocolito (Fig. 17).

En este trabajo, la obtención de los parámetros morfométricos procede de la aplicación de técnicas de análisis de imagen. Estas técnicas se basan en la aplicación, a las fotografías de cocolitos fósiles, tomadas al microscopio con el empleo de técnicas de polarización circular, de una relación de conversión del nivel de grises obtenido en dicha fotografía hacia un valor de espesor (Fuertes et al., 2014) (Fig. 17). Para la obtención de



dicha relación, o “calibración” del espesor de la calcita, en este estudio se ha aplicado i) la correlación de los valores directamente medidos sobre un nanolito perteneciente al género *Rhabdosphaera*, que presenta una estructura en forma cilíndrica óptima para la inferencia de la equivalencia entre la sección longitudinal medida en la superficie de la fotografía y el valor de espesor en profundidad (Fuertes et al., 2014), que aparece en el Capítulo 6 y a partir de ii) la medida del espesor conocido en un cuña de calcita inorgánica fotografiada (González-Lemos et al., 2018), en el Capítulo 4. Los dos trabajos referidos con anterioridad contienen la información completa y desarrollada sobre los procedimientos para la calibración del espesor. Para la automatización de la obtención de los valores morfométricos tras la obtención del valor de calibración, se empleó el software C-calcita (Fuertes et al., 2014)(Fig. 17).

A partir de los valores morfométricos de talla, masa y volumen, es posible llevar a cabo el cálculo de potenciales índices de calcificación, como la medida de espesor normalizado (SN Thickness-Size Normalized Thickness), el valor  $k$  y la estimación del ratio de carbono inorgánico/orgánico, “PIC/POC”. Los cálculos de estos parámetros provienen de la integración de las relaciones geométricas y volumétricas en cocolitos, propuestas en los trabajos originales de Young y Ziveri (2000), O’Dea et al. (2014), Aloisi (2015), y McClelland et al. (2016), revisadas por Bolton et al. (2016) y Jin et al. (2018), quienes definen y plantean la aplicabilidad de estos índices como estimaciones de la calcificación en cocolitóforos.

La aplicación y desarrollo de estas técnicas y procedimientos se llevan a cabo en los estudios orientados al análisis de la influencia de CO<sub>2</sub> y otros factores en el fraccionamiento isotópico durante la fotosíntesis y el análisis de efectos vitales en *Gephyrocapsa*, en el Capítulo 4, y en la reconstrucción de la evolución morfométrica y de la calcificación de las especies y/o morfotipos que constituyen el complejo *Gephyrocapsa* durante el intervalo del Mid-Brunhes, en el Capítulo 6. En estos capítulos señalados con anterioridad se encuentra la descripción metodológica completa del procedimiento para llevar a cabo estos cálculos, así como la discusión de su significado y validez para las diferentes zonas de estudio. Resulta importante destacar la escasez de múltiples referencias previas sobre el empleo de estas técnicas en material fósil, más allá de los trabajos de Bolton et al. (2016) y Jin et al. (2018), por lo que la contribución de los resultados y conclusiones en los artículos científicos incluidos en estas tesis doctoral

suponen un grado de innovación metodológica y de análisis para posteriores trabajos en este campo.

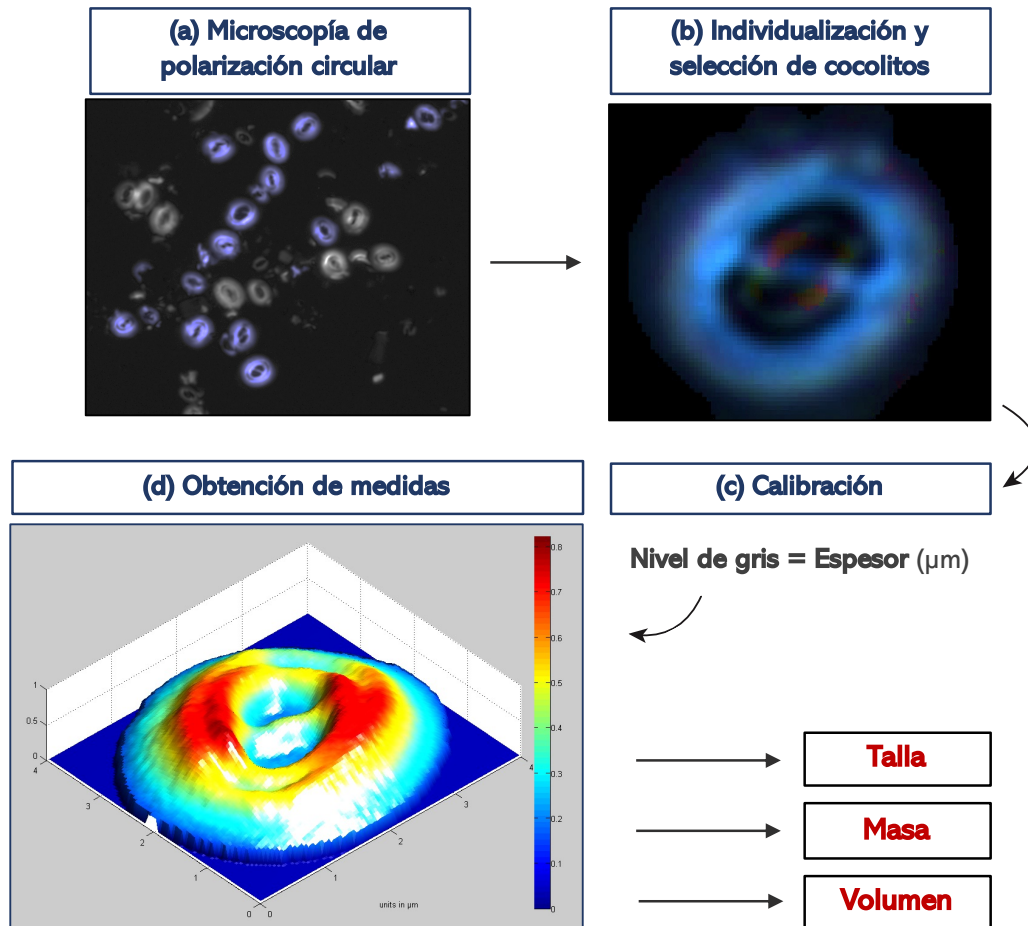


**Figura 17.** Esquema del procedimiento metodológico aplicado para la análisis de imagen de cocolitos pertenecientes al complejo *Gephyrocapsa* y obtención de medidas morfométricas (talla, masa y volumen), a partir del empleo del programa C-calcita (Fuertes et al., 2014) y los procedimientos para la calibración detallados en los trabajos de Fuertes et al. (2014) y González-Lemos et al. (2018), ambos aplicados en esta tesis doctoral y presentados en el texto.

### 1.7. Efectos vitales de oxígeno y carbono en cocolitos

Las estructuras biominerales producidas por los organismos calcificadores primarios se encuentran normalmente en condiciones de desequilibrio isotópico con el ambiente geoquímico marino durante su precipitación (Duplessy et al., 1970; Spero, 1998; Zeebe et al., 2008). Este desequilibrio se materializa como una diferencia entre las medidas isotópicas de  $\delta^{13}\text{C}$  y  $\delta^{18}\text{O}$ , obtenidas del carbonato y, respectivamente, el  $\delta^{13}\text{C}$  del DIC

( $\delta^{13}\text{C}_{\text{DIC}}$ ) y el  $\delta^{18}\text{O}$  del medio acuoso a la profundidad de hábitat y calcificación del organismo calcificador. A esta diferencia isotópica natural, que puede entrañar el control, tanto de parámetros ambientales, como fisiológicos propios del organismo, se hace referencia como “efectos vitales” (Dudley et al., 1986; Erez, 1978).

En el caso de los cocolitos, los efectos vitales detectados en la calcita son de una particular alta magnitud, que resulta incluso superior para grupos de especies que producen cocolitos de pequeñas dimensiones (valores de hasta  $\sim 5\%$  en cocolitos con tallas inferiores a  $3\ \mu\text{m}$ ; Bolton et al., 2012; Ziveri et al., 2003). Aparte del umbral impuesto por los diferentes tamaños, los diferentes géneros presentan un rango de fraccionamiento isotópico característicamente diferente (Rickaby et al., 2010).

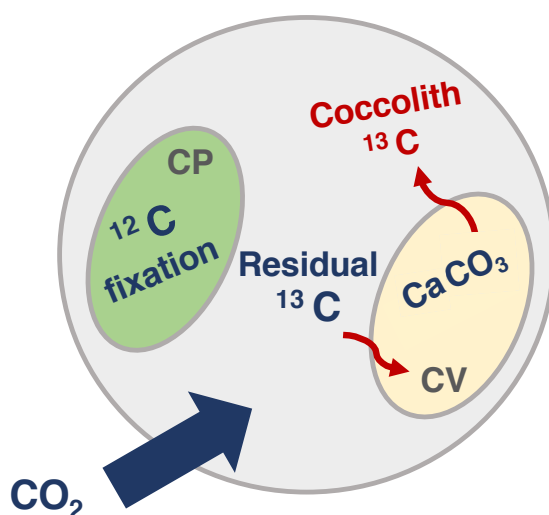


**Figura 18.** Esquema del mecanismo de fraccionamiento isotópico intracelular del carbono a partir de adquisición de  $\text{CO}_2$  pasiva. El reservorio de carbono intracelular queda, regularmente, enriquecido en  $^{13}\text{C}$  a medida que el proceso natural de producción de carbono orgánico, mediante fotosíntesis en el cloroplasto (CP-*Chloroplast*), fija el  $^{12}\text{C}$ . El carbono inorgánico intracelular, desde este reservorio, alimenta a la vesícula de calcificación (CV-*Coccolith Vesicle*) para la formación de cocolitos, cuyo  $\text{CaCO}_3$  registran la signatura isotópica,  $\delta^{13}\text{C}$ , intracelular.

La determinación del origen y control de estos factores es una cuestión altamente discutida, ante la cual no existe aún una idea plenamente concluyente acerca del significado de los efectos vitales ni diferenciación clara entre los controles variables, de tipología ambiental y/o fisiológica, de los puramente biológicos y propios de cada género y/o especie. Esto se debe, en parte, a la dificultad metodológica para la obtención de un

grado aceptable de aislamiento y extracción del sedimento y separación para el análisis a partir de material sedimentario fósil.

Los dos principales modelos teóricos acerca de efectos vitales en el fraccionamiento del oxígeno, predicen estos valores como indicativos de las condiciones de pH del DIC intracelular disponible para la calcificación, al existir fraccionamiento isotópico diferencial entre el agua y las diferentes especies carbonatadas que constituirán el reservorio intracelular para la calcificación (Langer et al., 2006; Ziveri et al., 2012) y/o los cambios en el tiempo de residencia del DIC intracelular, principalmente controlado por las tasas de crecimiento celular (Hermoso et al., 2014). En el caso del fraccionamiento del Carbono, los modelos disponibles vinculan la carga isotópica, que reflejan los efectos vitales, a cambios en la tasa de crecimiento celular, cambios en el balance entre las funciones de calcificación y fotosíntesis, la activación de estrategias fisiológicas para el incremento en la tasa de adquisición celular de carbono, más allá de la simple adquisición pasiva, y/o los cambios en su administración intracelular entre las funciones de calcificación y fotosíntesis, o condiciones de tipo ambiental, como cambios en la disponibilidad de CO<sub>2</sub> [aq] en el medio (Bolton y Stoll, 2013; Holtz et al., 2017; McClelland et al., 2017). Algunos trabajos evidencian la existencia de una correlación positiva entre los efectos vitales de los isótopos de oxígeno y de carbono medido para las diferentes especies en sedimentos (Bolton y Stoll, 2013; Hermoso et al., 2015) o en cultivo (Ziveri et al., 2003), lo que parece señalar la necesidad de un modelo integrado para explicar la operación de fraccionamiento para ambos elementos. No obstante, las últimas contribuciones han sugerido controles diferentes sobre ambos sistemas de fraccionamiento (Hermoso et al., 2020; Stoll et al., 2019; Tremblin et al., 2016).

El análisis de la composición geoquímica de estos nanofósiles ofrece una herramienta muy adecuada para la exploración y reconstrucción de los cambios ambientales acontecidos en el pasado (Hermoso, 2014;2020). No obstante, la clarificación de las cuestiones previamente planteadas es un paso previo de crítica importancia. Ante ello, la implementación de análisis isotópicos sobre concentraciones de cocolitos de carácter monoespecífico, restringida a un pequeño rango de tamaños y a lo largo de un intervalo de tiempo concreto es una de las vías de análisis más adecuadas, pero con escasas referencias hasta la fecha. El dominio casi monoespecífico de *Gephyrocapsa* en las asociaciones de cocolitos fósiles en el intervalo del Mid-Brunhes

ofrece una substancial ventaja, que, a priori resuelve algunas de las limitaciones metodológicas de base. Este enfoque se presenta en el Capítulo 4 de este trabajo, en el que los efectos vitales en *Gephyrocapsa*, calculados a partir de medidas isotópicas en la calcita, son comparados con los indicadores ambientales (temperatura y CO<sub>2</sub> [aq]) y fisiológicos (tasa de crecimiento celular, estimación de cambios en la calcificación, tamaño de la célula), directamente medidos o estimados, permitiendo la comprobación de los principales postulados a partir de los modelos de fraccionamiento.

### 1.8. Materiales para el análisis

En este trabajo, se ha estudiado el material procedente de un total de cuatro testigos sedimentarios marinos, tres de ellos localizados en diferentes latitudes del océano Atlántico Norte y uno en el sector oeste del Mar Mediterráneo (Fig. 19).

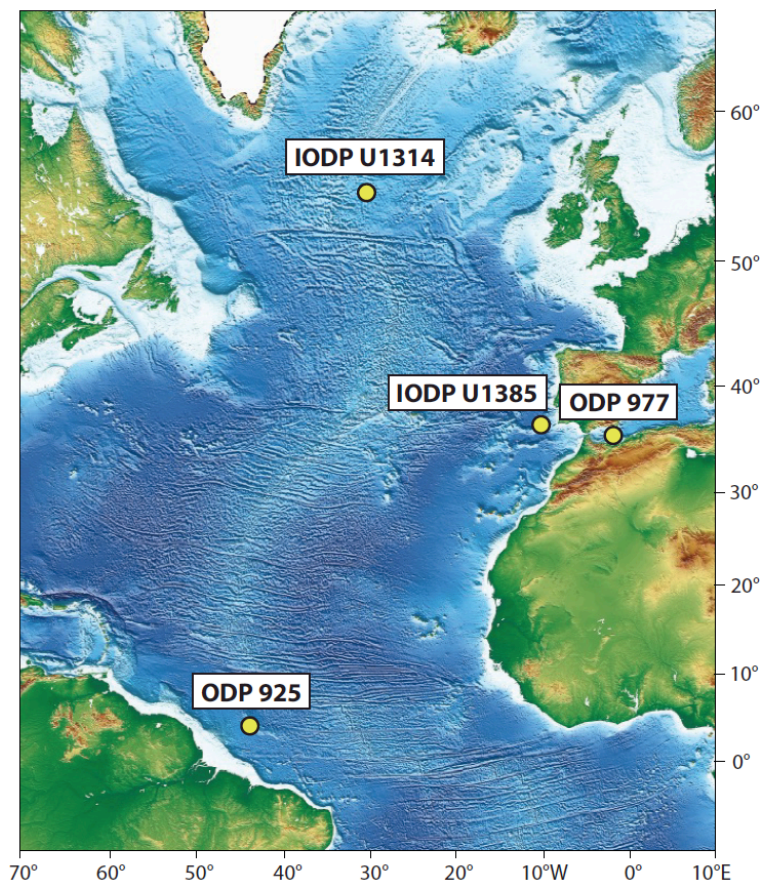


**Figura 19.** Mapa que muestra la ubicación de los diferentes testigos, ODP Site 977, 925, IODP Site U1385 y U1314, estudiados en esta tesis doctoral. Figura realizada a partir de un mapa original tomado de IODP ([www.iodp.org](http://www.iodp.org)).

En este apartado se presentan estos testigos agrupados en tres subsecciones correspondientes a cada uno de los tres bloques abordados en este trabajo. En estas subsecciones se incluyen las características básicas de estos materiales y de las regiones de estudio, así como las principales ventajas que impulsaron su elección para el desarrollo de cada uno de los casos de estudio presentados en los artículos que componen esta tesis doctoral y que se encuentran en los Capítulos 2 a 6. Es importante señalar que los capítulos anteriormente mencionados contienen la información completa y la descripción acerca de la oceanografía de cada una de las regiones estudiadas, con el grado de detalle requerido para cada uno de los trabajos.

### 1.8.1. Paleoceanografía de alta resolución en el margen ibérico

Los testigos ODP *Site 977* e IODP *Site U1385* se encuentran ubicados, respectivamente, en los márgenes Mediterráneo y Atlántico de la península ibérica. El material procedente de ambos testigos fue seleccionado para la reconstrucción de la evolución paleoceanográfica de alta resolución en el margen ibérico durante en intervalo del Mid-Brunhes. En el ODP *Site 977*, se estudio la Terminación V y el interglacial MIS 11, con un total de 181 muestras, que permitió abordar una resolución de 0.02 a 0.3 kyr entre muestra para el estudio (Capítulos 2 y 5). En el IODP *Site U1385*, se estudiaron 115 muestras para el intervalo comprendido entre el glacial MIS 12 y el interglacial MIS 9, que posibilitó una resolución de 0.4 a 0.7 kyr entre muestras para los análisis (Capítulo 3).

El testigo ODP *Site 977* está localizado en el sector Este del mar de Alborán (36° 1.9'N, 1° 57.3'W), al sur de la costa de Cabo de Gata (Almería) y a una profundidad de 1.984 metros bajo el nivel del mar (Comas et al., 1996). Ésta es la región de la cuenca Mediterránea más próxima al estrecho de Gibraltar, la única zona de conexión con el océano Atlántico, que registra la primera impronta de las aguas superficiales de procedencia Atlántica y el último registro de las aguas Mediterráneas, antes de su salida de la cuenca, en profundidad hacia el Golfo de Cádiz. En el mar de Alborán, tiene lugar el desarrollo de diferentes células de surgencia o *upwelling* de nutrientes profundos, asociados a diferentes estructuras oceanográficas permanentes o semipermanentes, principalmente el flujo de entrada de agua Atlántica y los dos giros anticiclónicos del oeste y este de la cuenca (Garcia-Gorriz y Carr, 1999; Sarhan et al., 2000) y a la influencia

de los vientos procedentes del Oeste (*westerlies*) sobre la geometría de la costa del Sur de la península ibérica (Parrilla y Kinder, 1987). A causa de la marcada influencia Atlántica en sus aguas superficiales y del desarrollo de los sistemas de *upwelling*, las condiciones generales para la productividad en el mar de Alborán son significativamente más ricas que en el resto de la cuenca Mediterránea (Siokou-Frangou et al., 2009).

El testigo IODP U1385 se ubica en la mitad Sur de la costa ibérica portuguesa (37° 34.285' N, 10° 7.562' W), a una profundidad de 2.578 metros bajo el nivel del mar (Hernández-Molina et al., 2012). Esta región queda comprendida dentro del sistema de borde del Este del giro subtropical del Atlántico Norte, caracterizado por el desarrollo de un sistema de *upwelling* costero (Mason et al., 2005). Esta zona se ve afectada por las corrientes superficiales y subsuperficiales procedentes de la corriente de Azores, al Sur, y también de la corriente del Atlántico Norte, al Norte (Peliz et al., 2005), cuya prevalencia influye, no solo en la regulación de las condiciones fisicoquímicas regionales (temperatura y cantidad de nutrientes según el tipo de aguas), sino también en el reparto físico de nutrientes procedentes del *upwelling* costero hacia posiciones más o menos distales de la costa (Relvas et al., 2007).

La conexión con las señales atmosféricas que opera en la actualidad en ambas regiones ha sido constatada durante intervalos pasados del Holoceno, y el Pleistoceno reciente en ambas regiones de ODP Site 977 (Cacho et al., 2001) e IODP U1385 (Pailler y Bard, 2002), revelando, en ambos casos, una importante conexión con las señales climáticas originadas en altas latitudes de la región Atlántica, a escala G/I y suborbital (milenarios). Estas regiones del margen ibérico fueron seleccionadas, por este motivo, para los estudios de alta resolución recogidos en los Capítulos 2, 3 y 5, centrados, principalmente, en el análisis de la evolución del complejo *Gephyrocapsa* y sus condiciones de productividad primaria, además del resto de la asociación de cocolitóforos, como principal herramienta para la reconstrucción paleoceanográfica de los intervalos de estudio seleccionados, bajo la perspectiva de análisis detallada en el Epígrafe 1.2.

### 1.8.2. Geoquímica orgánica y en cocolitos en el Atlántico tropical

El testigo ODP Site 925 se encuentra ubicado en el sector Oeste de la región tropical del Atlántico (4° 12.2' N/43° 29.3' W). Está localizado en la parte más somera del

promontorio oceánico de *Ceara Rise*, a una profundidad de 3.040 metros bajo el nivel del mar (Shackleton et al., 1998). El material procedente de este sondeo fue seleccionado para el análisis de la sensibilidad fotosintética de *Gephyrocapsa* al CO<sub>2</sub> y efectos vitales en sus cocolitos durante el intervalo del Mid-Brunhes, como parte de esta tesis doctoral, un estudio que se encuentra recogido y detallado en el Capítulo 4. Para este propósito, se diseñó un patrón de muestreo a baja resolución, consistente en doce muestras para el intervalo comprendido entre el glacial MIS 12 y el interglacial MIS 9, que posibilitó la captura de los cambios en los parámetros y relaciones medidas a escala G/I

El sector oeste del Atlántico Norte Tropical, donde este testigo se ubica, se caracteriza por el mantenimiento de unas condiciones de alta estabilidad y estratificación de la columna de agua, que limitan la transferencia de nutrientes hacia la superficie y, con ello, la productividad primaria en la zona fótica (Mann y Lazier, 2006; Philander y Pacanowski, 1986). La modesta variabilidad G/I en las temperaturas superficiales en estas latitudes (Rehfeld et al., 2018), la ausencia de actividad de *upwelling* y las condiciones de intercambio de CO<sub>2</sub> entre la atmósfera y la superficie oceánica próximas al equilibrio, o con una muy pequeña variabilidad (Takahashi et al., 2009) favorecen que el principal elemento estimulante de los cambios en el CO<sub>2</sub> [aq] en la superficie oceánica sea, directamente, el pCO<sub>2</sub> atmosférico. Estas condiciones de estabilidad ofrecen ventajas críticas a la hora de estudiar el efecto del cambio en CO<sub>2</sub> [aq] sobre la fisiología de cocolitóforos, lo cual justifica la selección de este testigo para la aplicación de la perspectiva de análisis que fueron presentados en los Epígrafes 1.6. y 1.7.,

### 1.8.3. Morfometría y calcificación en el Atlántico Norte y Mediterráneo

El testigo IODP *Site* U1314 se ubica en la región Norte del océano Atlántico, en la zona sur de *Gardar Drift*, al sur de Islandia, (56° 21.8' N, 27° 53.3' W), a una profundidad de 2.820 metros bajo el nivel del mar (Channell et al., 2006). Este testigo representa el extremo de alta latitud que completa el transecto de diferentes latitudes, a lo largo del Atlántico Norte y el Oeste Mediterráneo, que constituyen todos los *Sites* analizados en esta tesis doctoral y que, de forma conjunta, han sido empleados para la caracterización morfométrica del complejo *Gephyrocapsa* y la reconstrucción de sus cambios en calcificación durante el intervalo del Mid-Brunhes. Este aspecto aparece recogido en el Capítulo 6. Para cada uno de los cuatro testigos incluidos en este análisis – IODP *Sites*



U1314 y U1385, y ODP Sites 977 y 925 – se seleccionaron un total de dieciséis muestras con edades correspondientes, para el intervalo comprendido entre los subestadios glaciales MIS 14 y MIS 7, que posibilitó la captura de los cambios morfométricos y de la contribución de especies y/o morfotipos al complejo *Gephyrocapsa*, a escala G/I orbital, en las diferentes regiones de estudio.

La profundidad de estos testigos es, en todos los casos, más somera que la profundidad de la lisoclina actual en cada una de las regiones de estudio, una característica que, minimiza, en parte, el posible efecto la disolución en profundidad sobre el material fósil analizado. El planteamiento teórico y el enfoque correspondiente a este estudio se presentó en el Epígrafe 1.6.

## Referencias

- Aloisi, G., 2015. Covariation of metabolic rates and cell size in coccolithophores. *Biogeosciences* 12, 4665-4692.
- Andrulleit, H., Stäger, S., Rogalla, U., Čepek, P., 2003. Living coccolithophores in the northern Arabian Sea: ecological tolerances and environmental control. *Marine Micropaleontology* 49, 157-181.
- Archer, D., Maier-Reimer, E., 1994. Effect of deep-sea sedimentary calcite preservation on atmospheric CO<sub>2</sub> concentration. *Nature* 367, 260-263.
- Bach, L.T., Bauke, C., Meier, K., Riebesell, U., Schulz, K.G., 2012. Influence of changing carbonate chemistry on morphology and weight of coccoliths formed by *Emiliana huxleyi*. *Biogeosciences* (BG) 9, 3449-3463.
- Bach, L.T., Mackinder, L.C., Schulz, K.G., Wheeler, G., Schroeder, D.C., Brownlee, C., Riebesell, U., 2013. Dissecting the impact of CO<sub>2</sub> and pH on the mechanisms of photosynthesis and calcification in the coccolithophore *Emiliana huxleyi*. *New Phytologist* 199, 121-134.
- Bach, L.T., Riebesell, U., Gutowska, M.A., Federwisch, L., Schulz, K.G., 2015. A unifying concept of coccolithophore sensitivity to changing carbonate chemistry embedded in an ecological framework. *Progress in Oceanography* 135, 125-138.
- Badger, M.P., 2021. Alkenone isotopes show evidence of active carbon concentrating mechanisms in coccolithophores as aqueous carbon dioxide concentrations fall below 7 μmol L<sup>-1</sup>. *Biogeosciences* 18, 1149-1160.
- Badger, M.P., Chalk, T.B., Foster, G.L., Bown, P.R., Gibbs, S.J., Sexton, P.F., Schmidt, D.N., Pälike, H., Mackensen, A., Pancost, R.D., 2019. Insensitivity of alkenone carbon isotopes to atmospheric CO<sub>2</sub> at low to moderate CO<sub>2</sub> levels. *Climate of the Past* 15, 539-554.

- Barber, R., Hiscock, M., 2006. A rising tide lifts all phytoplankton: Growth response of other phytoplankton taxa in diatom-dominated blooms. *Global Biogeochemical Cycles* 20 (4).
- Barker, S., Archer, D., Booth, L., Elderfield, H., Henderiks, J., Rickaby, R.E., 2006. Globally increased pelagic carbonate production during the Mid-Brunhes dissolution interval and the CO<sub>2</sub> paradox of MIS 11. *Quaternary Science Reviews* 25, 3278-3293.
- Baumann, K.-H., Andruleit, H., Böckel, B., Geisen, M., Kinkel, H., 2005. The significance of extant coccolithophores as indicators of ocean water masses, surface water temperature, and palaeoproductivity: a review. *Paläontologische Zeitschrift* 79, 93-112.
- Baumann, K.-H., Böckel, B., Frenz, M., 2004. Coccolith contribution to South Atlantic carbonate sedimentation, *Coccolithophores*. Springer, pp. 367-402.
- Baumann, K.-H., Freitag, T., 2004. Pleistocene fluctuations in the northern Benguela Current system as revealed by coccolith assemblages. *Marine Micropaleontology* 52, 195-215.
- Beaufort, L., 2005. Weight estimates of coccoliths using the optical properties (birefringence) of calcite. *Micropaleontology* 51, 289-297.
- Beaufort, L., Barbarin, N., Gally, Y., 2014. Optical measurements to determine the thickness of calcite crystals and the mass of thin carbonate particles such as coccoliths. *Nature protocols* 9, 633-642.
- Beaufort, L., Lancelot, Y., Camberlin, P., Cayre, O., Vincent, E., Bassinot, F., Labeyrie, L., 1997. Insolation cycles as a major control of equatorial Indian Ocean primary production. *Science* 278, 1451-1454.
- Beaufort, L., Probert, I., de Garidel-Thoron, T., Bendif, E.M., Ruiz-Pino, D., Metzl, N., Goyet, C., Buchet, N., Coupel, P., Grelaud, M., 2011. Sensitivity of coccolithophores to carbonate chemistry and ocean acidification. *Nature* 476, 80-83.
- Bendif, E.M., Nevado, B., Wong, E.L., Hagino, K., Probert, I., Young, J.R., Rickaby, R.E., Filatov, D.A., 2019. Repeated species radiations in the recent evolution of the key marine phytoplankton lineage *Gephyrocapsa*. *Nature communications* 10, 1-9.
- Bendif, E.M., Probert, I., Díaz-Rosas, F., Thomas, D., Van Den Engh, G., Young, J.R., Von Dassow, P., 2016. Recent reticulate evolution in the ecologically dominant lineage of Coccolithophores. *Frontiers in microbiology* 7, 784.
- Bereiter, B., Eggleston, S., Schmitt, J., Nehrbass-Ahles, C., Stocker, T.F., Fischer, H., Kipfstuhl, S., Chappellaz, J., 2015. Revision of the EPICA Dome C CO<sub>2</sub> record from 800 to 600 kyr before present. *Geophysical Research Letters* 42, 542-549.
- Berger, W., Bickert, T., Jansen, E., Wefer, G., Yasuda, M., 1993. The central mystery of the Quaternary ice age: a view from the South Pacific. *Oceanus* 36, 53-57.
- Bidigare, R.R., Fluegge, A., Freeman, K.H., Hanson, K.L., Hayes, J.M., Hollander, D., Jasper, J.P., King, L.L., Laws, E.A., Milder, J., 1997. Consistent fractionation of

- <sup>13</sup>C in nature and in the laboratory: Growth-rate effects in some haptophyte algae. *Global Biogeochemical Cycles* 11, 279-292.
- Black, M., 1971. The systematics of coccoliths in relation to the paleontological record. *The Micropaleontology of the Oceans*, 611-624.
- Boeckel, B., Baumann, K.-H., 2004. Distribution of coccoliths in surface sediments of the south-eastern South Atlantic Ocean: ecology, preservation and carbonate contribution. *Marine Micropaleontology* 51, 301-320.
- Bollmann, J., 1995. *Biogeography and morphological variation of the genus Gephyrocapsa (Prymnesiophyceae) today and during its late Pleistocene dominance interval* (Doctoral dissertation, ETH Zurich).
- Bollmann, J., 1997. Morphology and biogeography of *Gephyrocapsa* coccoliths in Holocene sediments. *Marine Micropaleontology* 29, 319-350.
- Bolton, C.T., Hernández-Sánchez, M.T., Fuertes, M.-A., González-Lemos, S., Abrevaya, L., Mendez-Vicente, A., Flores, J.-A., Probert, I., Giosan, L., Johnson, J., 2016. Decrease in coccolithophore calcification and CO<sub>2</sub> since the middle Miocene. *Nature communications* 7, 1-13.
- Bolton, C.T., Stoll, H.M., 2013. Late Miocene threshold response of marine algae to carbon dioxide limitation. *Nature* 500, 558-562.
- Bolton, C.T., Stoll, H.M., Mendez-Vicente, A., 2012. Vital effects in coccolith calcite: Cenozoic climate-*p*CO<sub>2</sub> drove the diversity of carbon acquisition strategies in coccolithophores? *Paleoceanography* 27.
- Brassell, S.C., 2014. Climatic influences on the Paleogene evolution of alkenones. *Paleoceanography* 29, 255-272.
- Bréhéret, J.G., 1978. Formes nouvelles quaternaires et actuelles de la famille des *Gephyrocapsaceae* (Coccolithophorides).
- Broecker, W., Clark, E., 2009. Ratio of coccolith CaCO<sub>3</sub> to foraminifera CaCO<sub>3</sub> in late Holocene deep sea sediments. *Paleoceanography* 24.
- Broecker, W.S., 1982. Glacial to interglacial changes in ocean chemistry. *Progress in Oceanography* 11, 151-197.
- Broecker, W.S., Henderson, G.M., 1998. The sequence of events surrounding Termination II and their implications for the cause of glacial-interglacial CO<sub>2</sub> changes. *Paleoceanography* 13, 352-364.
- Broecker, W.S., Peng, T.H., 1987. The role of CaCO<sub>3</sub> compensation in the glacial to interglacial atmospheric CO<sub>2</sub> change. *Global Biogeochemical Cycles* 1, 15-29.
- Brownlee, C., Taylor, A., 2004. Calcification in coccolithophores: a cellular perspective, *Coccolithophores*. Springer, pp. 31-49.
- Cachão, M., Oliveira, A., Vitorino, J., 2000. Subtropical winter guests, offshore Portugal. *Journal of Nannoplankton Research* 22, 19-26.
- Cacho, I., Grimalt, J.O., Canals, M., Saffi, L., Shackleton, N.J., Schönfeld, J., Zahn, R., 2001. Variability of the Western Mediterranean sea surface temperature during the last 25,000 years and its connection with the Northern Hemisphere climatic changes. *Paleoceanography* 16, 40-52.

- Candy, I., Schreve, D.C., Sherriff, J., Tye, G.J., 2014. Marine Isotope Stage 11: Palaeoclimates, palaeoenvironments and its role as an analogue for the current interglacial. *Earth-Science Reviews* 128, 18-51.
- Channell, J., Kanamatsu, T., Sato, T., Stein, R., Zarikian, C.A., Malone, M., Scientists, T., 2006. 303/306 Expedition Reports, North Atlantic Climate, *Proceedings of the Integrated Ocean Drilling Program*.
- Comas, M., Zahn, R., Klaus, A., 1996. Preliminary results of ODP Leg 161. *Proceeding Ocean Drilling Program*, Preliminary Results 161, 1-1679.
- Conte, M.H., Thompson, A., Lesley, D., Harris, R.P., 1998. Genetic and physiological influences on the alkenone/alkenoate versus growth temperature relationship in *Emiliana huxleyi* and *Gephyrocapsa oceanica*. *Geochimica et Cosmochimica Acta* 62, 51-68.
- Crowley, T.J., 1985. Late Quaternary Carbonate Changes in the North Atlantic and Atlantic/Pacific Comparisons, *The Carbon Cycle and Atmospheric CO<sub>2</sub>: Natural Variations Archean to Present*, pp. 271-284.
- Droxler, A.W., Alley, R.B., Howard, W.R., Poore, R.Z., Burckle, L.H., 2003a. Unique and exceptionally long interglacial marine isotope stage 11: Window into earth warm future climate, *Geophysical Monograph Series*, pp. 1-14.
- Droxler, A.W., Farrell, J.W., 2000. Marine Isotope Stage 11 (MIS 11): new insights for a warm future. *Global and Planetary Change* 24, 1-5.
- Droxler, A.W., Poore, R.Z., Burckle, L.H., 2003b. Earth's climate and orbital eccentricity: The marine isotope stage 11 question. *Washington DC American Geophysical Union Geophysical Monograph Series* 137.
- Dudley, W.C., Blackwelder, P., Brand, L., Duplessy, J.-C., 1986. Stable isotopic composition of coccoliths. *Marine micropaleontology* 10, 1-8.
- Duplessy, J.C., Lalou, C., Vinot, A.C., 1970. Differential isotopic fractionation in benthic foraminifera and paleotemperatures reassessed. *Science* 168, 250-251.
- Emery, W.J., 2001. Water types and water masses. *Encyclopedia of ocean sciences* 6, 3179-3187.
- Erba, E., 2006. The first 150 million years history of calcareous nannoplankton: biosphere–geosphere interactions. *Palaeogeography, Palaeoclimatology, Palaeoecology* 232, 237-250.
- Erez, J., 1978. Vital effect on stable-isotope composition seen in foraminifera and coral skeletons. *Nature* 273, 199-202.
- Fairbanks, R.G., Sverdrlove, M., Free, R., Wiebe, P.H., Bé, A.W., 1982. Vertical distribution and isotopic fractionation of living planktonic foraminifera from the Panama Basin. *Nature* 298, 841-844.
- Flores, J., Sierro, F., 1997. Revised technique for calculation of calcareous nannofossil accumulation rates. *Micropaleontology*, 321-324.
- Flores, J.-A., Gersonde, R., Sierro, F., Niebler, H.-S., 2000a. Southern Ocean Pleistocene calcareous nannofossil events: calibration with isotope and geomagnetic stratigraphies. *Marine Micropaleontology* 40, 377-402.

- Flores, J.-A., Gersonde, R., Sierro, F.J., 1999. Pleistocene fluctuations in the Agulhas Current Retroflexion based on the calcareous plankton record. *Marine Micropaleontology* 37, 1-22.
- Flores, J.-A., Marino, M., Sierro, F.J., Hodell, D.A., Charles, C.D., 2003. Calcareous plankton dissolution pattern and coccolithophore assemblages during the last 600 kyr at ODP Site 1089 (Cape Basin, South Atlantic): paleoceanographic implications. *Palaeogeography, Palaeoclimatology, Palaeoecology* 196, 409-426.
- Flores, J.A., Bárcena, M.A., Sierro, F.J., 2000b. Ocean-surface and wind dynamics in the Atlantic Ocean off Northwest Africa during the last 140 000 years. *Palaeogeography, Palaeoclimatology, Palaeoecology* 161, 459-478.
- Flores, J.A., Filippelli, G.M., Sierro, F.J., Latimer, J.C., 2012. The “White Ocean” hypothesis: a late Pleistocene Southern Ocean governed by coccolithophores and driven by phosphorus. *Frontiers in microbiology* 3, 233.
- Freeman, K.H., Hayes, J., 1992. Fractionation of carbon isotopes by phytoplankton and estimates of ancient CO<sub>2</sub> levels. *Global biogeochemical cycles* 6, 185-198.
- Fuertes, M.-Á., Flores, J.-A., Sierro, F.J., 2014. The use of circularly polarized light for biometry, identification and estimation of mass of coccoliths. *Marine Micropaleontology* 113, 44-55.
- García-Gorrioz, E., Carr, M.E., 1999. The climatological annual cycle of satellite-derived phytoplankton pigments in the Alboran Sea. *Geophysical Research Letters* 26, 2985-2988.
- González-Lemos, S., Guitián, J., Fuertes, M.-Á., Flores, J.-A., Stoll, H.M., 2018. An empirical method for absolute calibration of coccolith thickness. *Biogeosciences*, 15.
- Green, J.C., Leadbeater, B.S., 1994. *The haptophyte algae*. Systematics Association.
- Hagino, K., Okada, H., Matsuoka, H., 2005. Coccolithophore assemblages and morphotypes of *Emiliania huxleyi* in the boundary zone between the cold Oyashio and warm Kuroshio currents off the coast of Japan. *Marine Micropaleontology* 55, 19-47.
- Hay, W.W., Mohler, H., Wade, M.E., 1966. Calcareous nannofossils from Nal'chik (northwest Caucasus). *Eclogae Geologicae Helvetiae* 59, 379-399.
- Hay, W.W., Mohler, H.P., Roth, P.H., Schmidt, R.R., Boudreaux, J.E., 1967. Calcareous Nannoplankton Zonation of the Cenozoic of the Gulf Coast and Caribbean-Antillean Area, and Transoceanic Correlation (1).
- Helmke, J.P., Bauch, H.A., Röhl, U., Kandiano, E.S., 2008. Uniform climate development between the subtropical and subpolar Northeast Atlantic across marine isotope stage 11. *Climate of the Past Discussions* 4, 433-457.
- Hermoso, M., 2014. Coccolith-derived isotopic proxies in palaeoceanography: where geologists need biologists. *Cryptogamie, Algologie* 35, 323-351.

- Hermoso, M., Horner, T.J., Minoletti, F., Rickaby, R.E.M., 2014. Constraints on the vital effect in coccolithophore and dinoflagellate calcite by oxygen isotopic modification of seawater. *Geochimica et Cosmochimica Acta* 141, 612-627.
- Hermoso, M., 2015. Control of ambient pH on growth and stable isotopes in phytoplanktonic calcifying algae. *Paleoceanography*, 30(8), 1100–1112.
- Hermoso, M., McClelland, H.-L.O., Hirst, J.S., Minoletti, F., Bonifacie, M., Rickaby, R.E.M., 2020. Towards the use of the coccolith vital effects in palaeoceanography: A field investigation during the middle Miocene in the SW Pacific Ocean. Deep Sea Research Part I: *Oceanographic Research Papers* 160, 103262.
- Hernández-Almeida, I., Ausín, B., Saavedra-Pellitero, M., Baumann, K.-H., Stoll, H.M., 2019. Quantitative reconstruction of primary productivity in low latitudes during the last glacial maximum and the mid-to-late Holocene from a global *Florisphaera profunda* calibration dataset. *Quaternary Science Reviews* 205, 166-181.
- Hernández-Molina, F.J., Stow, D.A., Zarikian, C.A., Williams, T., Lofi, J., Acton, G.D., Bahr, A., Balestra, B., Ducassou, E., Flood, R.D., 2012. Mediterranean outflow: Environmental significance of the Mediterranean Outflow Water and its global implications (Integrated Ocean Drilling Program Expedition 339 Preliminary Report).
- Hernández-Almeida, I., Krumhardt, K., Zhang, H., Stoll, H., 2020. Estimation of physiological factors controlling carbon isotope fractionation in coccolithophores in photic zone and core-top samples. *Geochemistry, Geophysics, Geosystems*, e2020GC009272.
- Hibberd, D., 1976. The ultrastructure and taxonomy of the Chrysophyceae and Prymnesiophyceae (Haptophyceae): a survey with some new observations on the ultrastructure of the Chrysophyceae. *Botanical Journal of the Linnean Society* 72, 55-80.
- Hodell, D.A., Charles, C.D., Ninnemann, U.S., 2000. Comparison of interglacial stages in the South Atlantic sector of the southern ocean for the past 450 kyr: implications for Marine Isotope Stage (MIS) 11. *Global and Planetary Change* 24, 7-26.
- Holtz, L.-M., Wolf-Gladrow, D., Thoms, S., 2017. Stable carbon isotope signals in particulate organic and inorganic carbon of coccolithophores – A numerical model study for *Emiliana huxleyi*. *Journal of Theoretical Biology* 420, 117-127.
- Iglesias-Rodriguez, M.D., Halloran, P.R., Rickaby, R.E., Hall, I.R., Colmenero-Hidalgo, E., Gittins, J.R., Green, D.R., Tyrrell, T., Gibbs, S.J., von Dassow, P., 2008. Phytoplankton calcification in a high-CO<sub>2</sub> world. *Science* 320, 336-340.
- Imbrie, J., Berger, A., Boyle, E.A., Clemens, S., Duffy, A., Howard, W., Kukla, G., Kutzbach, J., Martinson, D., McIntyre, A., 1993. On the structure and origin of major glaciation cycles 2. The 100,000-year cycle. *Paleoceanography* 8, 699-735.
- Jansen, J., Kuijpers, A., Troelstra, S., 1986. A mid-Brunhes climatic event: Long-term changes in global atmosphere and ocean circulation. *Science* 232, 619-622.

- Jerkovic, L., 1970. Noelaerhabdus nov. gen. Type d'une nouvelle famille de coccolithophoridés fossiles: Noëlaerhabdaceae du Miocène supérieur de Yougoslavie. *CR Acad Sci Paris* 270, 468-470.
- Jin, X., Liu, C., Zhang, H., Zhou, C., Jiang, X., Wu, Z., Xu, J., 2018. Evolutionary driven of Gephyrocapsa coccolith isotopic vital effects over the past 400 ka. *Earth and Planetary Science Letters* 503, 236-247.
- Kamptner, E., 1943. Zur Revision der Coccolithineen-Spezies Pontosphaera huxleyi Lohm. *Anzeiger der Akademie der Wissenschaften, Wien* 80, 43-49.
- Kamptner, E., 1962. Coccolithineen-Skelettreste aus Tiefseeablagerungen des Pazifischen Ozeans Eine nannopaläontologische Untersuchung. *Annalen des Naturhistorischen Museums in Wien*, 139-206.
- Kandiano, E.S., Bauch, H.A., Fahl, K., Helmke, J.P., Röhl, U., Pérez-Folgado, M., Cacho, I., 2012. The meridional temperature gradient in the eastern North Atlantic during MIS 11 and its link to the ocean-atmosphere system. *Palaeogeography, Palaeoclimatology, Palaeoecology* 333, 24-39.
- Kinkel, H., Baumann, K.-H., Cepek, M., 2000. Coccolithophores in the equatorial Atlantic Ocean: response to seasonal and Late Quaternary surface water variability. *Marine Micropaleontology* 39, 87-112.
- Köhler, P., Nehrbass-Ahles, C., Schmitt, J., Stocker, T.F., Fischer, H., 2017. A 156 kyr smoothed history of the atmospheric greenhouse gases CO<sub>2</sub>, CH<sub>4</sub>, and N<sub>2</sub>O and their radiative forcing. *Earth System Science Data* 9, 363-387.
- Krumhardt, K.M., Lovenduski, N.S., Iglesias-Rodriguez, M.D., Kleypas, J.A., 2017. Coccolithophore growth and calcification in a changing ocean. *Progress in oceanography* 159, 276-295.
- Lang, N., Wolff, E.W., 2011. Interglacial and glacial variability from the last 800 ka in marine, ice and terrestrial archives. *Climate of the Past* 7, 361-380.
- Langer, G., Geisen, M., Baumann, K.H., Kläs, J., Riebesell, U., Thoms, S., Young, J.R., 2006. Species-specific responses of calcifying algae to changing seawater carbonate chemistry. *Geochemistry, geophysics, geosystems* 7.
- Langer, G., Nehrke, G., Probert, I., Ly, J., Ziveri, P., 2009. Strain-specific responses of *Emiliania huxleyi* to changing seawater carbonate chemistry. *Biogeosciences* 6, 2637-2646.
- Laskar, J., Robutel, P., Joutel, F., Gastineau, M., Correia, A., Levrard, B., 2004. A long-term numerical solution for the insolation quantities of the Earth. *Astronomy & Astrophysics* 428, 261-285.
- Lisiecki, L.E., Raymo, M.E., 2005. A Pliocene-Pleistocene stack of 57 globally distributed benthic  $\delta^{18}\text{O}$  records. *Paleoceanography* 20.
- Lohmann, H., 1902. Die Coccolithophoridae: eine Monographie der *Coccolithen bildenden Flagellaten, Zugleich ein Beitrag zur Kenntnis des Mittelmeerauftriebs*. Fischer.
- Loutre, M.-F., Berger, A., 2003. Marine Isotope Stage 11 as an analogue for the present interglacial. *Global and planetary change* 36, 209-217.

- Mann, K., Lazier, J., 2006. Vertical Structure of the Open Ocean: Biology of the Mixed Layer. *Dynamics of Marine Ecosystems*. Oxford: Blackwell Publishing.
- Marlowe, I., Brassell, S., Eglinton, G., Green, J., 1990. Long-chain alkenones and alkyl alkenoates and the fossil coccolith record of marine sediments. *Chemical Geology* 88, 349-375.
- Marsh, M., 2003. Regulation of CaCO<sub>3</sub> formation in coccolithophores. *Comparative Biochemistry and Physiology Part B: Biochemistry and Molecular Biology* 136, 743-754.
- Mason, E., Coombs, S., Oliveira, P., 2005. An overview of the literature concerning the oceanography of the eastern North Atlantic region. *Relatórios Científicos e Técnicos IPIMAR Serie Digital* 33, 59.
- McClelland, H., Barbarin, N., Beaufort, L., Hermoso, M., Ferretti, P., Greaves, M., Rickaby, R., 2016. Calcification response of a key phytoplankton family to millennial-scale environmental change. *Scientific reports* 6, 1-11.
- McClelland, H., Bruggeman, J., Hermoso, M., Rickaby, R., 2017. The origin of carbon isotope vital effects in coccolith calcite. *Nature communications* 8, 1-16.
- McIntyre, A., Bé, A.W., 1967. Modern coccolithophoridae of the Atlantic Ocean—I. Placoliths and cyrtoliths, *Deep Sea Research and Oceanographic Abstracts*. Elsevier, pp. 561-597.
- Mcmanus, J., Oppo, D., Cullen, J., Healey, S., 2003. Marine isotope stage 11 (MIS 11): analog for Holocene and future Climate? *Washington DC American Geophysical Union Geophysical Monograph Series* 137, 69-85.
- Meier, K., Berger, C., Kinkel, H., 2014. Increasing coccolith calcification during CO<sub>2</sub> rise of the penultimate deglaciation (Termination II). *Marine Micropaleontology* 112, 1-12.
- Milankovitch, M., 1930. Mathematische klimalehre und astronomische theorie der klimaschwankungen. *Handbuch der Klimatologie* 1.
- Molfino, B., McIntyre, A., 1990. Precessional forcing of nutricline dynamics in the equatorial Atlantic. *Science* 249, 766-769.
- Monteiro, F.M., Bach, L.T., Brownlee, C., Bown, P., Rickaby, R.E.M., Poulton, A.J., Tyrrell, T., Beaufort, L., Dutkiewicz, S., Gibbs, S., Gutowska, M.A., Lee, R., Riebesell, U., Young, J., Ridgwell, A., 2016. Why marine phytoplankton calcify. *Science Advances* 2, e1501822.
- Müller, P.J., Kirst, G., Ruhland, G., Von Storch, I., Rosell-Melé, A., 1998. Calibration of the alkenone paleotemperature index U<sub>37K'</sub> based on core-tops from the eastern South Atlantic and the global ocean (60° N-60° S). *Geochimica et Cosmochimica Acta* 62, 1757-1772.
- O'Dea, S.A., Gibbs, S.J., Bown, P.R., Young, J.R., Poulton, A.J., Newsam, C., Wilson, P.A., 2014. Coccolithophore calcification response to past ocean acidification and climate change. *Nature communications* 5, 1-7.
- O'Neil, G. W., Carmichael, C. A., Goepfert, T. J., Fulton, J. M., Knothe, G., Pui Ling Lau, C., ... & Reddy, C. M. (2012). Beyond fatty acid methyl esters: Expanding



- the renewable carbon profile with alkenones from *Isochrysis* sp. *Energy & fuels*, 26(4), 2434-2441
- Okada, H., Honjo, S., 1973. The distribution of oceanic coccolithophorids in the Pacific, *Deep Sea Research and Oceanographic Abstracts*. Elsevier, pp. 355-374.
- Okada, H., McIntyre, A., 1977. Modern coccolithophores of the Pacific and North Atlantic oceans. *Micropaleontology*, 1-55.
- Okada, H., Wells, P., 1997. Late Quaternary nannofossil indicators of climate change in two deep-sea cores associated with the Leeuwin Current off Western Australia. *Palaeogeography, Palaeoclimatology, Palaeoecology* 131, 413-432.
- Oliveira, D., Desprat, S., Rodrigues, T., Naughton, F., Hodell, D., Trigo, R., Rufino, M., Lopes, C., Abrantes, F., Goni, M.F.S., 2016. The complexity of millennial-scale variability in southwestern Europe during MIS 11. *Quaternary Research* 86, 373-387.
- Paasche, E., 2001. A review of the coccolithophorid *Emiliana huxleyi* (Prymnesiophyceae), with particular reference to growth, coccolith formation, and calcification-photosynthesis interactions. *Phycologia* 40, 503-529.
- Pagani, M., 2014. 12.13 Biomarker-based inferences of past climate: The alkenone  $p\text{CO}_2$  proxy. *Treatise on Geochemistry, edited by: Holland, HD and Turekian, KK, Elsevier, Oxford*, 361-378.
- Pagani, M., Zachos, J.C., Freeman, K.H., Tipler, B., Bohaty, S., 2005. Marked decline in atmospheric carbon dioxide concentrations during the Paleogene. *Science* 309, 600-603.
- Pailler, D., Bard, E., 2002. High frequency palaeoceanographic changes during the past 140 000 yr recorded by the organic matter in sediments of the Iberian Margin. *Palaeogeography, Palaeoclimatology, Palaeoecology* 181, 431-452.
- Parrilla, G., Kinder, T.H., 1987. Oceanografía física del mar de Alborán. *Boletín del Instituto Español de Oceanografía* 4, 133-165.
- Peliz, Á., Dubert, J., Santos, A.M.P., Oliveira, P.B., Le Cann, B., 2005. Winter upper ocean circulation in the Western Iberian Basin—Fronts, Eddies and Poleward Flows: an overview. *Deep sea research Part I: Oceanographic research papers* 52, 621-646.
- Petit, J.-R., Jouzel, J., Raynaud, D., Barkov, N.I., Barnola, J.-M., Basile, I., Bender, M., Chappellaz, J., Davis, M., Delaygue, G., 1999. Climate and atmospheric history of the past 420,000 years from the Vostok ice core, Antarctica. *Nature* 399, 429-436.
- Philander, S., Pacanowski, R., 1986. A model of the seasonal cycle in the tropical Atlantic Ocean. *Journal of Geophysical Research: Oceans* 91, 14192-14206.
- Popp, B.N., Laws, E.A., Bidigare, R.R., Dore, J.E., Hanson, K.L., Wakeham, S.G., 1998. Effect of phytoplankton cell geometry on carbon isotopic fractionation. *Geochimica et cosmochimica acta* 62, 69-77.
- Poulton, A.J., Adey, T.R., Balch, W.M., Holligan, P.M., 2007. Relating coccolithophore calcification rates to phytoplankton community dynamics: Regional differences

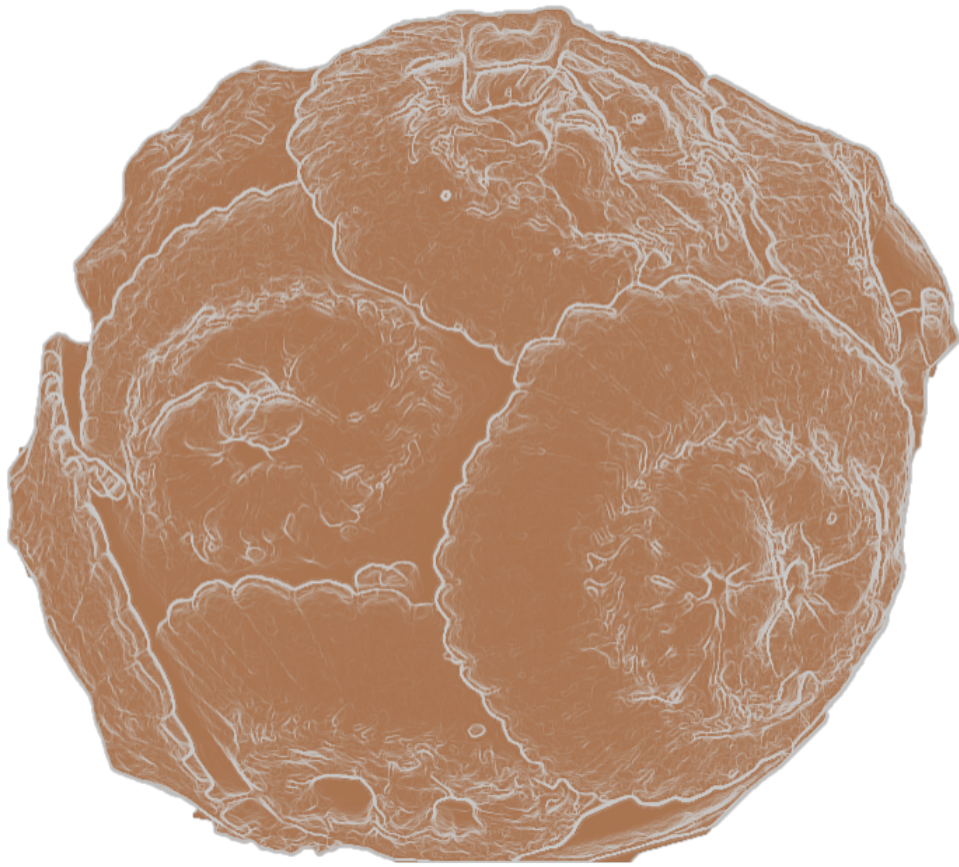
- and implications for carbon export. *Deep Sea Research Part II: Topical Studies in Oceanography* 54, 538-557.
- Raffi, I., Backman, J., Rio, D., Shackleton, N.J., 1993. Plio-Pleistocene Nannofossil Biostratigraphy and Calibration to Oxygen Isotope Stratigraphies from Deep Sea Drilling Project Site 607 and Ocean Drilling Program Site 677. *Paleoceanography* 8, 387-408.
- Rau, G.H., Riebesell, U., Wolf-Gladrow, D., 1996. A model of photosynthetic  $^{13}\text{C}$  fractionation by marine phytoplankton based on diffusive molecular  $\text{CO}_2$  uptake. *Marine Ecology Progress Series* 133, 275-285.
- Raven, P., Johnson, G.B., 1991. *Understanding biology*. (No. QH308. 2. R381 1991.).
- Raynaud, D., Barnola, J.-M., Souchez, R., Lorrain, R., Petit, J.-R., Duval, P., Lipenkov, V.Y., 2005. Palaeoclimatology: The record for marine isotopic stage 11. *Nature* 436, 39.
- Rehfeld, K., Münch, T., Ho, S.L., Laepple, T., 2018. Global patterns of declining temperature variability from the Last Glacial Maximum to the Holocene. *Nature* 554, 356-359.
- Relvas, P., Barton, E.D., Dubert, J., Oliveira, P.B., Peliz, A., Da Silva, J., Santos, A.M.P., 2007. Physical oceanography of the western Iberia ecosystem: latest views and challenges. *Progress in Oceanography* 74, 149-173.
- Rickaby, R., Bard, E., Sonzogni, C., Rostek, F., Beaufort, L., Barker, S., Rees, G., Schrag, D., 2007. Coccolith chemistry reveals secular variations in the global ocean carbon cycle? *Earth and Planetary Science Letters* 253, 83-95.
- Rickaby, R.E., Henderiks, J., Young, J.N., 2010. Perturbing phytoplankton: response and isotopic fractionation with changing carbonate chemistry in two coccolithophore species. *Climate of the Past* 6, 771-785.
- Rio, D., 1982. The fossil distribution of coccolithophore genus *Gephyrocapsa* Kamptner and related Plio-Pleistocene chronostratigraphic problems. *Init. Repts. DSDP* 68, 325-343.
- Rohling, E.J., Fenton, M., Jorissen, F.J., Bertrand, P., Ganssen, G., Caulet, J.P., 1998. Magnitudes of sea-level lowstands of the past 500,000 years. *Nature* 394, 162-165.
- Rost, B., Riebesell, U., 2004. Coccolithophores and the biological pump: responses to environmental changes, *Coccolithophores*. Springer, pp. 99-125.
- Saavedra-Pellitero, M., Baumann, K.-H., Ullermann, J., Lamy, F., 2017. Marine Isotope Stage 11 in the Pacific sector of the Southern Ocean; a coccolithophore perspective. *Quaternary Science Reviews* 158, 1-14.
- Saavedra-Pellitero, M., Baumann, K.H., Lamy, F., Köhler, P., 2017. Coccolithophore variability across Marine Isotope Stage 11 in the Pacific sector of the Southern Ocean and its potential impact on the carbon cycle. *Paleoceanography* 32, 864-880.

- Saavedra-Pellitero, M., Flores, J., Lamy, F., Sierro, F., Cortina, A., 2011. Coccolithophore estimates of paleotemperature and paleoproductivity changes in the southeast Pacific over the past~ 27 kyr. *Paleoceanography* 26.
- Samtleben, C., 1980. Die Evolution der Coccolithophoriden-Gattung *Gephyrocapsa* nach Befunden im Atlantik. *Paläontologische Zeitschrift* 54, 91-127.
- Sarhan, T., Lafuente, J.G., Vargas, M., Vargas, J.M., Plaza, F., 2000. Upwelling mechanisms in the northwestern Alboran Sea. *Journal of Marine Systems* 23, 317-331.
- Sett, S., Bach, L.T., Schulz, K.G., Koch-Klavsen, S., Lebrato, M., Riebesell, U., 2014. Temperature modulates coccolithophorid sensitivity of growth, photosynthesis and calcification to increasing seawater  $p\text{CO}_2$ . *PLoS one* 9, e88308.
- Shackleton, N., Curry, W., Richter, C., Bralower, T., 1998. Proceedings, scientific results, Ocean Drilling Program, Leg 154, Ceara Rise. *Oceanographic Literature Review* 4, 639.
- Sigman, D.M., Boyle, E.A., 2000. Glacial/interglacial variations in atmospheric carbon dioxide. *Nature* 407, 859-869.
- Siokou-Frangou, I., Christaki, U., Mazzocchi, M., Montresor, M., d'Alcalá, M.R., Vaqué, D., Zingone, A., 2009. Plankton in the open Mediterranean Sea: a review. *Biogeosciences Discussions* 6.
- Spero, H.J., 1998. Life history and stable isotope geochemistry of planktonic foraminifera. *The Paleontological Society Papers* 4, 7-36.
- Stoll, H.M., Guitian, J., Hernandez-Almeida, I., Mejia, L.M., Phelps, S., Polissar, P., Rosenthal, Y., Zhang, H., Ziveri, P., 2019. Upregulation of phytoplankton carbon concentrating mechanisms during low  $\text{CO}_2$  glacial periods and implications for the phytoplankton  $p\text{CO}_2$  proxy. *Quaternary Science Reviews* 208, 1-20.
- Takahashi, K., Okada, H., 2000. Environmental control on the biogeography of modern coccolithophores in the southeastern Indian Ocean offshore of Western Australia. *Marine Micropaleontology* 39, 73-86.
- Takahashi, T., Sutherland, S.C., Wanninkhof, R., Sweeney, C., Feely, R.A., Chipman, D.W., Hales, B., Friederich, G., Chavez, F., Sabine, C., 2009. Climatological mean and decadal change in surface ocean  $p\text{CO}_2$ , and net sea-air  $\text{CO}_2$  flux over the global oceans. *Deep Sea Research Part II: Topical Studies in Oceanography* 56, 554-577.
- Taylor, A.R., Chrachri, A., Wheeler, G., Goddard, H., Brownlee, C., 2011. A voltage-gated  $\text{H}^+$  channel underlying pH homeostasis in calcifying coccolithophores. *PLoS biology* 9, e1001085.
- Tierney, J.E., Tingley, M.P., 2018. BAYSPLINE: A new calibration for the alkenone paleothermometer. *Paleoceanography and Paleoclimatology* 33, 281-301.
- Tremblin, M., Hermoso, M., Minoletti, F., 2016. Equatorial heat accumulation as a long-term trigger of permanent Antarctic ice sheets during the Cenozoic. *Proceedings of the National Academy of Sciences of the United States of America* 113, 11782-11787.

- Venrick, E., 1982. Phytoplankton in an Oligotrophic Ocean: Observations and Questions: Ecological Archives M052-002. *Ecological Monographs* 52, 129-154.
- Volk, T., Hoffert, M.I., 1985. Ocean carbon pumps: Analysis of relative strengths and efficiencies in ocean-driven atmospheric CO<sub>2</sub> changes. *The carbon cycle and atmospheric CO<sub>2</sub>: natural variations Archean to present* 32, 99-110.
- Volkman, J.K., 2020. Lipids of geochemical interest in microalgae. *Hydrocarbons, Oils and Lipids: Diversity, Origin, Chemistry and Fate*, 159-191.
- Volkman, J.K., Barrerr, S.M., Blackburn, S.I., Sikes, E.L., 1995. Alkenones in *Gephyrocapsa oceanica*: Implications for studies of paleoclimate. *Geochimica et Cosmochimica Acta* 59, 513-520.
- Volkman, J.K., Eglinton, G., Corner, E.D., Forsberg, T., 1980. Long-chain alkenes and alkenones in the marine coccolithophorid *Emiliana huxleyi*. *Phytochemistry* 19, 2619-2622.
- Wang, P., Tian, J., Cheng, X., Liu, C., Xu, J., 2003. Carbon reservoir changes preceded major ice-sheet expansion at the mid-Brunhes event. *Geology* 31, 239-242.
- Webb, R.S., Rind, D.H., Lehman, S.J., Healy, R.J., Sigman, D., 1997. Influence of ocean heat transport on the climate of the Last Glacial Maximum. *Nature* 385, 695-699.
- Westbroek, P., Brown, C.W., van Bleijswijk, J., Brownlee, C., Brummer, G.J., Conte, M., Egge, J., Fernández, E., Jordan, R., Knappertsbusch, M., 1993. A model system approach to biological climate forcing. The example of *Emiliana huxleyi*. *Global and planetary change* 8, 27-46.
- Winter, A., 1994. Biogeography of living coccolithophores in ocean waters. *Coccolithophores*.
- Winter, A., Siesser, W.G., 2006. *Coccolithophores*. Cambridge University Press.
- Young, J., Bown, P., 1997. Cenozoic calcareous nannoplankton classification. *Journal of nannoplankton Research* 19, 36-47.
- Young, J., Geisen, M., Cros, L., Kleijne, A., Sprengel, C., Probert, I., Østergaard, J., 2003. A guide to extant coccolithophore taxonomy. *Journal of Nannoplankton Research*, Special Issue 1, 1-132.
- Young, J.R., Davis, S.A., Bown, P.R., Mann, S., 1999. Coccolith ultrastructure and biomineralisation. *Journal of structural biology* 126, 195-215.
- Young, J.R., Henriksen, K., 2003. Biomineralization within vesicles: the calcite of coccoliths. *Reviews in mineralogy and geochemistry* 54, 189-215.
- Young, J.R., Ziveri, P., 2000. Calculation of coccolith volume and its use in calibration of carbonate flux estimates. *Deep Sea Research Part II: Topical Studies in Oceanography* 47, 1679-1700.
- Young, J.R., Bown, P.R. & Lees, J.A. (eds.) 2021. Nannotax3 website. International Nannoplankton Association. 1 Sep.2021. URL: <http://ina.tmsoc.org/Nannotax3>.
- Zeebe, R.E., Bijma, J., Hönisch, B., Sanyal, A., Spero, H.J., Wolf-Gladrow, D.A., 2008. Vital effects and beyond: a modelling perspective on developing palaeoceanographical proxy relationships in foraminifera. *Geological Society, London, Special Publications* 303, 45-58.

- Zhang, Y.G., Henderiks, J., Liu, X., 2020. Refining the alkenone- $p\text{CO}_2$  method II: Towards resolving the physiological parameter 'b'. *Geochimica et Cosmochimica Acta* 281, 118-134.
- Zhang, Y.G., Pagani, M., Liu, Z., Bohaty, S.M., DeConto, R., 2013. A 40-million-year history of atmospheric  $\text{CO}_2$ . *Philosophical Transactions of the Royal Society A: Mathematical, Physical and Engineering Sciences* 371, 20130096.
- Ziveri, P., Stoll, H., Probert, I., Klaas, C., Geisen, M., Ganssen, G., Young, J., 2003. Stable isotope 'vital effects' in coccolith calcite. *Earth and planetary science letters* 210, 137-149.
- Ziveri, P., Thoms, S., Probert, I., Geisen, M., Langer, G., 2012. A universal carbonate ion effect on stable oxygen isotope ratios in unicellular planktonic calcifying organisms. *Biogeosciences* 9, 1025-1032.





**A new perspective of the *Alboran Upwelling System*  
reconstruction during the Marine Isotope Stage 11: a  
high-resolution coccolithophore record**

(González-Lanchas et al., 2020)

*Quaternary Science Reviews*

## CAPÍTULO 2. Artículo científico

### **“A new perspective of the *Alboran Upwelling System* reconstruction during the marine isotope stage 11: a high resolution coccolithophore record”**

**Alba González-Lanchas**<sup>a</sup>, José-Abel Flores<sup>a</sup>, Francisco J. Sierro<sup>a</sup>, María Ángeles Bárcena<sup>a</sup>, Andrés S. Rigual-Hernández<sup>a</sup>, Dulce Oliveira<sup>b,c</sup>, Lucía A. Azibeiro<sup>a</sup>, Maria Marino<sup>d</sup>, Patrizia Maiorano<sup>d</sup>, Aleix Cortina<sup>e</sup>, Isabel Cacho<sup>f</sup>, Joan O. Grimalt<sup>e</sup>.

<sup>a</sup> Departamento de Geología, Universidad de Salamanca, 37008 Salamanca, España.

<sup>b</sup> Centro de Ciências do Mar (CCMAR), Universidade do Algarve, Campus de Gambelas, 8005-139 Faro, Portugal.

<sup>c</sup> Divisão de Geologia e Georecursos Marinhos, Instituto Português do Mar e da Atmosfera (IPMA), Av. Doutor Alfredo Magalhães Ramalho 6, 1495-165 Algés, Portugal.

<sup>d</sup> Dipartimento di Scienze della Terra e Geoambientali, Università degli Studi di Bari Aldo Moro, Bari, Italia.

<sup>e</sup> Department of Environmental Chemistry, IDAEA-CSIC, Barcelona, 08034, España.

<sup>f</sup> GRC Geociències Marines, Departament de Dinàmica de la Terra i de l'Oceà, Facultat de Ciències de la Terra, Universitat de Barcelona, Barcelona, 08028, España.

*Quaternary Science Reviews* 245, 106520.

DOI: [10.1016/j.quascirev.2020.106520](https://doi.org/10.1016/j.quascirev.2020.106520)



## Resumen

El Mar de Alborán es el sector más occidental de la cuenca Mediterránea. Esta región experimenta el efecto de la circulación estuarina que caracteriza a la cuenca Mediterránea, registrando en su estructura hidrológica vertical la impronta de la entrada en superficie de las aguas ligeras de procedencia Atlántica, y la salida en profundidad de las aguas más densas formadas en la cuenca Mediterránea. Las tasas de producción primaria en esta región son superiores a las del resto de zonas Mediterránea, por la operación de diferentes mecanismos que estimulan la mezcla vertical y la surgencia de nutrientes profundos (*upwelling*). Estos sistemas de *upwelling* son i) el asociado a la formación completa de dos giros geostróficos superficiales (*Western/Estern Alboran Gyre-WAG* y *EAG*), principalmente estimulado por la intensidad de la circulación superficial en la región y ii) el *upwelling* costero, estimulado por el efecto de los vientos procedentes del oeste (contraalísios, *westerlies*) sobre la costa (Heburn y La Violette, 1990; Sarhan et al., 2000; Siokou-Frangou et al., 2009). Las condiciones ambientales en la región, incluyendo la operación de los mecanismos anteriores, dependen ampliamente de las condiciones climáticas en el Atlántico Norte, con una importante influencia de la variabilidad en los modos positivo (+) y negativo (-) de oscilación del Atlántico Norte (*North Atlantic Oscillation* – *NAO*) durante los meses de invierno, que controlan el gradiente de presiones y, por lo tanto, la configuración atmosférica y disposición de los sistemas de vientos sobre la región (Lionello, 2012). Asumiendo el mantenimiento de esta interconexión en el tiempo, el Mar de Alborán representa un área estratégica y de interés para el estudio de la variabilidad paleoceanográfica y paleoclimática de alta frecuencia en intervalos de tiempo de interés durante el pasado (Cacho et al., 2001; Moreno et al., 2002).

El estadio isotópico marino (*Marine Isotope Stage* – *MIS*) 11 se localiza después del evento de incremento de la amplitud de la ciclicidad glacial/interglacial del Mid-Brunhes, y es uno de los estadios interglaciales de calentamiento más elevado y prolongado del Pleistoceno reciente (PAGES, 2016). No obstante, diversos trabajos han evidenciado discrepancias al respecto de la estabilidad de estas condiciones interglaciales y su duración, dejando abierta la discusión acerca de la homogeneidad global de estas condiciones (Desprat et al., 2007; Tzedakis et al., 2009). Por otro lado, la fase final del MIS 11 se caracteriza por la ocurrencia de eventos de deshielo en altas latitudes, cuyo

impacto en latitudes medias podría ser semejante al de los eventos de deshielo del último ciclo glacial (eventos *Heinrich*) (Rodrigues et al., 2011).

En este trabajo se realiza un estudio a alta resolución del intervalo comprendido entre la transición glacial/interglacial MIS 12/11, o Terminación V, y el interglacial MIS 11 completo hasta su transición al glacial MIS 10, entre las edades de 430 y 374 ka, con la reconstrucción de las condiciones de productividad primaria como principal herramienta para la inferencia de las condiciones paleoceanográficas en el Mar de Alborán en relación con la evolución climática del Atlántico Norte durante el intervalo. Para ello, se estudió la asociación de cocolitóforos, organismos fitoplanctónicos de alta sensibilidad a los cambios en las condiciones de temperatura, disponibilidad de nutrientes, salinidad y turbulencia, en muestras sedimentarias obtenidas del testigo ODP Site 977, ubicado en la subcuenca Este del Mar de Alborán.

En esta región la proliferación de cocolitóforos principalmente controlada por la intensidad de funcionamiento de los sistemas de upwelling, aquí referidos conjuntamente como *Alboran Upwelling System*. El estudio micropaleontológico se llevó a cabo mediante el recuento de individuos fósiles, cocolitos, en las muestras, con el empleo de técnicas de microscopía óptica. El intervalo de estudio se encuentra dominado por las especies pertenecientes al género *Gephyrocapsa*, comúnmente denominado complejo *Gephyrocapsa*. Las diferentes especies contenidas en el complejo presentan una afinidad ecológica diferente e interesante para la inferencia de las condiciones de disponibilidad de nutrientes en la zona de estudio, tipo y procedencia de aguas superficiales e intensidad de su influencia en la región. De este modo, se llevó a cabo una exhaustiva diferenciación de especímenes dentro del complejo con la aplicación de criterios taxonómicos clásicos. Los datos micropaleontológicos sustentaron el cálculo de las concentraciones de cocolitos fósiles por gramo, un dato considerado como representativo de las condiciones de productividad en la zona fótica. Para precisar la representatividad de esta señal como indicativa de la intensidad del *Alboran Upwelling System*, en este trabajo se emplearon los datos de las especies del grupo de small *Gephyrocapsa* y “*Gephyrocapsa caribbeanica*”, ecológicamente vinculadas a los estímulos procedentes del upwelling. A este índice se le denominó *Primary Productivity Proxy* (PPP).

La señal de productividad e intensidad del *Alboran Upwelling System* se combinó con i) análisis geoquímicos de isótopos estables de oxígeno y carbono, del  $\delta^{18}\text{O}$  y  $\delta^{13}\text{C}$ ,

en la especie de foraminífero planctónico *Globigerina bulloides* de alquenonas, compuestos orgánicos producidos por coccolitóforos. La cuantificación tras la extracción de alquenonas sustentó el cálculo del índice  $U^{k'}_{37}$  y su calibración hacia datos de evolución de las temperaturas superficiales, SST (Müller et al., 1998). El perfil de SST en el Site ODP 977 permitió la elaboración de un modelo de edad para los sedimentos, mediante su correlación con el perfil equivalente del intervalo en el testigo IODP Site U1313 (Stein et al., 2009), para el cual se dispone de un modelo de edad preciso (Voelker et al., 2010) vinculado a la curva isotópica global (Lisiecki y Raymo, 2005). Las medidas de  $\delta^{18}\text{O}$  *G. bulloides* sirvieron para la identificación de subestadios isotópicos en el intervalo y, todos estos datos –  $\delta^{18}\text{O}$ ,  $\delta^{13}\text{C}$  y SST – para sustentar la discusión acerca de la evolución de las condiciones oceánicas superficiales en este trabajo. La señal de productividad se combina, además, con ii) marcadores terrestres para precisar la configuración atmosférico en la latitud de estudio durante el intervalo, como las abundancias de marcadores polínicos procedentes de bosque Mediterráneo en el testigo U1385 (Oliveira et al., 2016), indicativo de la influencia de los *Westerlies* sobre Iberia y el contenido de fitolitos silíceos en las muestras de estudio, cuya abundancia es procedente del Norte de África y, por lo tanto, indicativa de la intensidad de las rutas de transporte aéreo hacia la región.

La actividad de mezcla vertical y transferencia de nutrientes profundos se incrementa durante las fases de intensificación de los gradientes meridionales, equiparable al modo + de la NAO moderna, que resulta en la estimulación de las condiciones de aridez de invierno: Estas condiciones generan aumento en la formación de aguas profundas del oeste Mediterráneo (*WMDW-Western Mediterranean Deep Waters*) y de circulación termohalina en el Mediterráneo, estimulando por completo el desarrollo y la alta intensidad del *Alboran Upwelling System*. Este escenario se identificó durante la transición entre MIS 12 / MIS 11 o Terminación V, en el subestadio final del intervalo de condiciones interglaciales plenas, MIS 11c, y en la parte final del interglacial, en las fases correspondientes a los subestadios MIS 11 b a MIS 11a hacia la transición con el MIS 10.

La actividad de mezcla vertical y transferencia de nutrientes profundos disminuye durante las fases de desintensificación de los gradientes meridionales, equiparable al modo - de la NAO moderna, que resulta en la estimulación de las condiciones de humedad

de invierno: Estas condiciones promueven la reducción en la formación de WMDW y circulación termohalina menos intensa en el sector occidental del Mediterráneo, que obstaculiza el desarrollo completo del *Alboran Upwelling System*. Este escenario se identifica durante la primera fase de periodo interglacial completo, MIS 11c.

Durante el subestadio MIS 11b se identifican dos mínimos de corta duración en la productividad primaria, centrados en 390 y 383 ka, coincidentes con sendos mínimos en SST, correspondientes a los eventos de tipo *Heinrich* Ht3 y Ht2. El aumento de la representación de especies propias de aguas superficiales frías de tipo subpolar, como *G. muelleriae* y la subespecie *C. pelagicus pelagicus* es consistente con la entrada de este tipo de aguas en el Mar Mediterráneo. Las condiciones de circulación y estimulación del sistema de upwelling se mantienen, no obstante, activas durante estos episodios y la reducción en la productividad es producida por la limitación térmica de las bajas temperaturas para el desarrollo de las asociaciones de coccolitóforos.

## Referencias

- Cacho, I., Grimalt, J.O., Canals, M., Sbaiffi, L., Shackleton, N.J., Schönfeld, J., Zahn, R., 2001. Variability of the Western Mediterranean sea surface temperature during the last 25,000 years and its connection with the Northern Hemisphere climatic changes. *Paleoceanography* 16, 40-52.
- Desprat, S., Goñi, M.S., Naughton, F., Turon, J.-L., Duprat, J., Malaizé, B., Cortijo, E., Peypouquet, J.-P., 2007. 25. Climate variability of the last five isotopic interglacials: Direct land-sea-ice correlation from the multiproxy analysis of North-Western Iberian margin deep-sea cores, *Developments in Quaternary Sciences*. Elsevier, pp. 375-386.
- Heburn, G.W., La Violette, P.E., 1990. Variations in the structure of the anticyclonic gyres found in the Alboran Sea. *Journal of Geophysical Research: Oceans* 95, 1599-1613.
- Lionello, P., 2012. *The climate of the Mediterranean region: From the past to the future*. Elsevier.
- Lisiecki, L.E., Raymo, M.E., 2005. A Pliocene-Pleistocene stack of 57 globally distributed benthic  $\delta^{18}O$  records. *Paleoceanography* 20.
- Moreno, A., Cacho, I., Canals, M., Prins, M.A., Sánchez-Goñi, M.-F., Grimalt, J.O., Weltje, G.J., 2002. Saharan dust transport and high-latitude glacial climatic variability: the Alboran Sea record. *Quaternary Research* 58, 318-328.
- Müller, P.J., Kirst, G., Ruhland, G., Von Storch, I., Rosell-Melé, A., 1998. Calibration of the alkenone paleotemperature index U37K' based on core-tops from the eastern

- South Atlantic and the global ocean (60° N-60° S). *Geochimica et Cosmochimica Acta* 62, 1757-1772.
- Oliveira, D., Desprat, S., Rodrigues, T., Naughton, F., Hodell, D., Trigo, R., Rufino, M., Lopes, C., Abrantes, F., Goni, M.F.S., 2016. The complexity of millennial-scale variability in southwestern Europe during MIS 11. *Quaternary Research* 86, 373-387.
- Past International Working Group of PAGES, 2016. Interglacials of the last 800,000 years. *Reviews of Geophysics* 54, 162-219.
- Rodrigues, T., Voelker, A., Grimalt, J., Abrantes, F., Naughton, F., 2011. Iberian Margin sea surface temperature during MIS 15 to 9 (580–300 ka): Glacial suborbital variability versus interglacial stability. *Paleoceanography* 26.
- Sarhan, T., Lafuente, J.G., Vargas, M., Vargas, J.M., Plaza, F., 2000. Upwelling mechanisms in the northwestern Alboran Sea. *Journal of Marine Systems* 23, 317-331.
- Siokou-Frangou, I., Christaki, U., Mazzocchi, M., Montresor, M., d'Alcalá, M.R., Vaqué, D., Zingone, A., 2009. Plankton in the open Mediterranean Sea: a review. *Biogeosciences Discussions* 6.
- Stein, R., Hefter, J., Grützner, J., Voelker, A., Naafs, B.D.A., 2009. Variability of surface water characteristics and Heinrich-like events in the Pleistocene midlatitude North Atlantic Ocean: Biomarker and XRD records from IODP Site U1313 (MIS 16–9). *Paleoceanography* 24.
- Tzedakis, P., Pälike, H., Roucoux, K., De Abreu, L., 2009. Atmospheric methane, southern European vegetation and low-mid latitude links on orbital and millennial timescales. *Earth and Planetary Science Letters* 277, 307-317.
- Voelker, A.H.L., Rodrigues, T., Billups, K., Oppo, D., McManus, J., Stein, R., Hefter, J., Grimalt, J.O., 2010. Variations in mid-latitude North Atlantic surface water properties during the mid-Brunhes (MIS 9-14) and their implications for the thermohaline circulation. *Climate of the Past* 6, 531-552.





# A new perspective of the Alboran Upwelling System reconstruction during the Marine Isotope Stage 11: A high-resolution coccolithophore record

Alba González-Lanchas<sup>a,\*</sup>, José-Abel Flores<sup>a</sup>, Francisco J. Sierro<sup>a</sup>,  
 María Ángeles Bárcena<sup>a</sup>, Andrés S. Rigual-Hernández<sup>a</sup>, Dulce Oliveira<sup>b,c</sup>,  
 Lucía A. Azibeiro<sup>a</sup>, Maria Marino<sup>d</sup>, Patrizia Maiorano<sup>d</sup>, Aleix Cortina<sup>e</sup>, Isabel Cacho<sup>f</sup>,  
 Joan O. Grimalt<sup>e</sup>

<sup>a</sup> Departamento de Geología, Universidad de Salamanca, 37008, Salamanca, Spain

<sup>b</sup> Centro de Ciências do Mar (CCMAR), Universidade do Algarve, Campus de Gambelas, 8005-139, Faro, Portugal

<sup>c</sup> Divisão de Geologia e Georecursos Marinhos, Instituto Português do Mar e da Atmosfera (IPMA), Av. Doutor Alfredo Magalhães Ramalho 6, 1495-165, Algés, Portugal

<sup>d</sup> Dipartimento di Scienze della Terra e Geoambientali, Università degli Studi di Bari Aldo Moro, Bari, Italy

<sup>e</sup> Department of Environmental Chemistry, IDAEA-CSIC, Barcelona, 08034, Spain

<sup>f</sup> GRC Geociències Marines, Departament de Dinàmica de la Terra i de l'Oceà, Facultat de Ciències de la Terra, Universitat de Barcelona, Barcelona, 08028, Spain

## ARTICLE INFO

### Article history:

Received 5 March 2020

Received in revised form

23 July 2020

Accepted 23 July 2020

Available online 3 September 2020

### Keywords:

Palaeoceanography

Interglacial

Marine isotope stage 11

Alboran sea

Western europe

Micropaleontology

Coccolithophore primary productivity

North atlantic oscillation

## ABSTRACT

A high-resolution study of the MIS 12/MIS 11 transition and the MIS 11 (430–376 kyr) coccolithophore assemblages at Ocean Drilling Program Site 977 was conducted to reconstruct the palaeoceanographic and climatic changes in the Alboran Sea from the variability in surface water conditions. The nannofossil record was integrated with the planktonic oxygen and carbon stable isotopes, as well as the  $U^{K-37}$  Sea Surface Temperature (SST) at the studied site during the investigated interval. The coccolithophore primary productivity, reconstructed from the PPP (primary productivity proxy = absolute values of *Gephyrocapsa caribbeanica* + small *Gephyrocapsa* group) revealed pronounced fluctuations, that were strongly associated with variations in the intensity of the regional *Alboran Upwelling System*. The comparison of the nanoplankton record with opal phytolith content for the studied site and the already available pollen record at the nearby Integrated Ocean Drilling Program Site U1385, suggests an association of the upwelling dynamics with the variability of the North Atlantic Oscillation-like (NAO-like) phase. High PPP during positive (+) NAO-like phases is the result of intensified upwelling, owing to the complete development of the surface hydrological structures at the Alboran Sea. This scenario was identified during the MIS 12/MIS 11 transition (428–422 kyr), the late MIS 11c (405–397 kyr), and MIS 11b to MIS 11a (397–376 kyr). Two short-term minima in the PPP and SST were observed during MIS 11b and were coeval with the North Atlantic Heinrich-type (Ht) events Ht3 (~390 kyr) and Ht2 (~384 kyr). Increased abundance of the subpolar *Coccolithus pelagicus* subsp. *pelagicus* and *Gephyrocapsa muelleriae* was consistent with the inflow of cold surface waters into the Mediterranean Sea during the Ht events. Lowered PPP during negative (–) NAO-like phases is the result of moderate upwelling by the incomplete development of surface hydrological structures at the Alboran Sea. This scenario is expressed during the early MIS 11c (422–405 kyr). Overall, the results of our study provide evidence of the important role of atmospheric circulation patterns in the North Atlantic region for controlling phytoplankton primary production and oceanographic circulation dynamics in the Western Mediterranean during MIS 11.

© 2020 Elsevier Ltd. All rights reserved.

## 1. Introduction

The Mid-Brunhes interval, spanning from Pleistocene Marine

\* Corresponding author.

E-mail address: [lanchas@usal.es](mailto:lanchas@usal.es) (A. González-Lanchas).

Isotope Stages (MIS) 14 to 9 (Barker et al., 2006; Jansen et al., 1986), is a critical period for global climate change. Following the Mid-Pleistocene transition, this interval contains the shift in ice age cycles, that lengthened from ~ 40 to ~100 kyr, leading to warmer interglacial phases (Berger and Wefer, 2003; Jansen et al., 1986; Lisiecki and Raymo, 2005) and glacial terminations of greater amplitude (Terminations I–V; Past Interglacials Working Group of PAGES, 2016) than before. Among the other interglacial periods of the Mid-Brunhes, MIS 11 (424–374 kyr; Lisiecki and Raymo, 2005) has been proposed as a model to analyse the natural climate variability for several reasons: (i) the intensity and duration of the warming (Bauch et al., 2012; Hodell et al., 2000; PAGES, 2016); (ii) the enhanced penetration of the warm waters poleward (Berger and Wefer, 2003); and (iii) the increase in atmospheric greenhouse gas concentrations (Raynaud et al., 2005; Yin and Berger, 2012). All these processes are considered as main drivers of the collapse of the Greenland and west Antarctica ice sheets, and resulted in the eustatic sea-level rising about 20 m higher than it currently is (Olson and Hearty, 2009; Raymo and Mitrovica, 2012; Reyes et al., 2014; Roberts et al., 2012). Termination V, at the MIS 12/MIS 11 transition (424 kyr; Lisiecki and Raymo, 2005), is furthermore regarded as the largest amplitude glacial/interglacial transition of the last 800 kyr (PAGES, 2016).

MIS 11 is often considered a potential analogue for the Holocene as there are multiple similarities between both intervals, including: (i) the similar orbital forcing parameters of low eccentricity, high obliquity, low precessional amplitude, and insolation geometry (Berger and Loutre, 1991; Loutre and Berger, 2003); (ii) the elevated atmospheric CO<sub>2</sub> levels (Droxler and Farrell, 2000); and (iii) a small amount of continental ice (Loutre and Berger, 2003) similar to present conditions (Candy et al., 2014; Rohling et al., 2010; Yin and Berger, 2012).

Several paleoclimate records evidence the prevalence of long-lasting (~30 kyr) warm and stable conditions during the early substage of the full interglacial, MIS 11c period (Desprat et al., 2007; Martrat et al., 2007; McManus et al., 2003; Oppo et al., 1998; Stein et al., 2009; Voelker et al., 2010). Nevertheless, mid-latitude terrestrial climate-records indicate contrasting early climate instabilities during MIS 11c on centennial (Koutsodendris et al., 2010; Prokopenko et al., 2010; Tye et al., 2016) to millennial time-scales (Oliveira et al., 2016; Tzedakis et al., 2009), keeping the discussion open regarding the homogeneity of the latitudinal extent of the full interglacial conditions. Suborbital-scale climate instabilities are comparatively well recorded during MIS 11 b and MIS 11a (~395–374 kyr), in the North Atlantic to the Iberian latitudes (de Abreu et al., 2005; Hodell et al., 2013; Martrat et al., 2007; Palumbo et al., 2013; Rodrigues et al., 2011; Stein et al., 2009; Voelker et al., 2010) and the western Mediterranean (Marino et al., 2018). The origin of these instabilities has been associated with the southward incursion of waters with an Arctic origin (e.g. Oppo et al., 1998), and their effect on weakening the North Atlantic Meridional Overturning Circulation and coupled atmospheric interactions (Barker et al., 2015; McManus et al., 2003).

The Alboran Sea is the westernmost basin of the Mediterranean Sea, and hence, it has a crucial role in forming climate connections with the North Atlantic (Cacho et al., 1999, 2000; Martrat et al., 2004; Sierro et al., 2005). The Alboran Sea thus represents a strategic location for the reconstruction of palaeoceanographic and paleoclimatic variability for the whole Mediterranean Basin (e.g., Ausín et al., 2015a,b; Bazzicalupo et al., 2018; Colmenero-Hidalgo et al., 2004). Currently, the variability in sea-level, temperature, and precipitation in the region is partially controlled by fluctuations in the atmospheric gradient between the Azores High-pressure (AH) and the Icelandic Low-pressure (IL) cells, which constitutes the North Atlantic Oscillation mode (NAO) of winter

climate variability in the North Atlantic region (Hurrell, 1995; Lionello, 2012). The changing NAO-like phase has been identified as a triggering mechanism for paleoenvironmental oscillations in the western Mediterranean during the Holocene (Fletcher et al., 2013; Frigola et al., 2007), with effects on primary productivity in the Alboran Sea (e.g., Ausín et al., 2015b; Bazzicalupo et al., 2020).

The sensitivity of coccolithophores to the changing surface ocean physicochemical conditions (temperature, salinity, nutrient-concentrations, and turbulence) makes them a valuable tool for the reconstruction of rapid palaeoceanographic fluctuations (Baumann et al., 2005). The high accumulation rate and adequate preservations of nannofossil (calcite plates termed coccoliths) in sediments throughout the Atlantic and Mediterranean Iberian margins have allowed for a number of studies, revealing the strong dependence of the coccolithophore primary productivity and assemblage-structure on the global climate at orbital and suborbital/millennial-scale (Amore et al., 2012; Ausín et al., 2015a,b; Bazzicalupo et al., 2018; Colmenero-Hidalgo et al., 2004; Marino et al., 2018; Palumbo et al., 2013).

The main objective of the present study was the high-resolution reconstruction of environmental and climatic changes in the Alboran Sea during the MIS 12/MIS 11 transition and MIS 11. Considering the coccolithophore primary productivity patterns as a proxy to monitor the changes in the surface and subsurface water column conditions, we attempted to unravel the past variations in the oceanographic circulation and its atmospheric configuration forcing at the western Mediterranean region. We integrated the high-resolution coccolithophore primary productivity record –inferred from the nannofossil characterization and quantification–, with the high-resolution records of the stable  $\delta^{18}\text{O}$  and  $\delta^{13}\text{C}$  isotopes from the planktonic foraminifera *Globigerina bulloides* and the alkenone  $U^k_{37}$  Sea Surface Temperatures (SST) at Ocean Drilling Program (ODP) Site 977. Additionally, the record of the opal phytolith content at ODP Site 977 together with the Mediterranean forest pollen taxa at the Portuguese Iberian margin Integrated Ocean Drilling Program (IODP) Site U1385 from Oliveira et al. (2016), were used to reconstruct the response of the Alboran Sea to atmospheric precipitation and wind track configuration during the MIS 12/MIS 11 transition and MIS 11 and their connections with the paleoclimate and palaeoceanographic processes of the North Atlantic.

## 2. The Alboran Sea

### 2.1. Oceanographic and atmospheric setting

ODP Site 977 is located in the Alboran Sea, a transitional area between the semi-enclosed Mediterranean Sea and the adjacent Atlantic Ocean. As such, the circulation in this region is intense and characterized by an anti-estuarine model, with surface inflow of relatively low saline waters from the Atlantic (Atlantic Water, AW), and the outflow in depth of highly saline Mediterranean waters (Mediterranean Outflow Water, MOW) through the narrow and shallow Strait of Gibraltar (Pistek et al., 1985). The eastern branch of the Azores Current (AzC; Johnson and Stevens, 2000) is the main source of the AW that flow into the Alboran Sea as a strong Atlantic Jet (AJ) though the upper ~200 m of the water column (Lafuente et al., 2000). The confluence of the Atlantic and Mediterranean waters results in the formation of two quasi-permanent anti-cyclonic gyres: the Western and Eastern anti-cyclonic Alboran Gyres (WAG and EAG, respectively; Heburn and La Violette, 1990; Fig. 1a). These gyres mix in the upper 300 m of the water column, resulting in pronounced variations in temperature, salinity, and nutrient distributions (Modified Atlantic Water, MAW).

The development, extension, and position of these hydrological



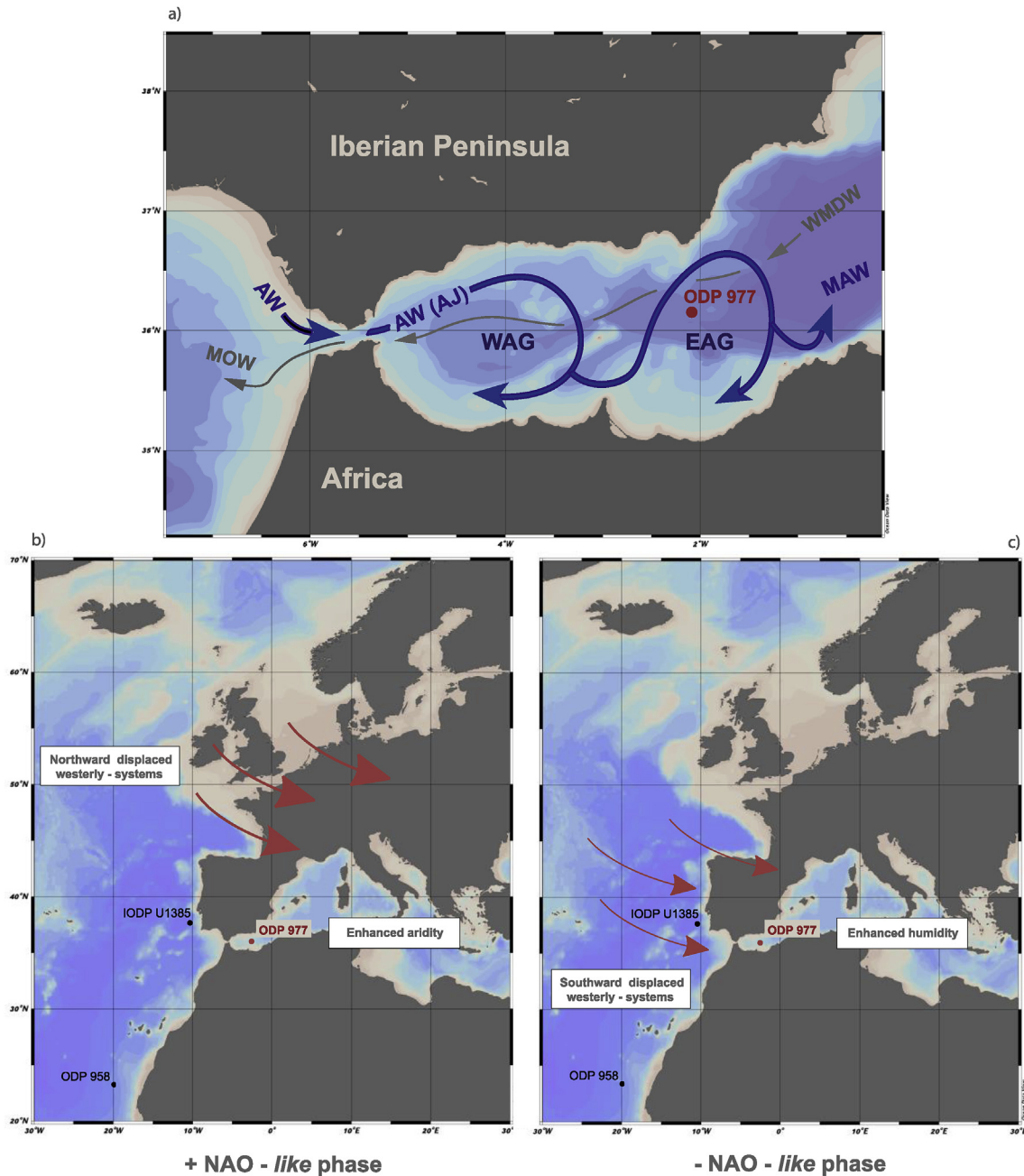


**Fig. 1.** (a) Geographic location and modern oceanographic circulation scheme of the study area. Arrows indicate the theoretical trajectories of water masses. Blue lines represent the surface circulation. Grey lines trace the circulation at depth. AW (Atlantic Water); MOW (Mediterranean Outflow Water); MAW (Modified Atlantic Water); WAG (Western Alboran Gyre); EAG (Eastern Alboran Gyre); WMDW (Western Mediterranean Deep Water). (b) and (c) Schematic NAO-like phase scenarios that synthesize the main processes controlling the activation of the *Alboran Upwelling System* during (b) +NAO-like phase and (c) -NAO-like phase. Location of ODP Site 977 (red dot, this study) and the IODP Site U1385 and ODP Site 958 (black dot) discussed in the text. (For interpretation of the references to colour in this figure legend, the reader is referred to the Web version of this article.)

structures is unstable and highly variable (Heburn and La Violette, 1990; Perkins et al., 1990). In the deeper layers of the water column (>300 m), the dense MOW, which is a mixture of Levantine Intermediate Water (LIW) and Western Mediterranean Deep Water (WMDW), exits the Strait of Gibraltar, flowing into the Atlantic and forming a distinct water mass whose imprint can be identified in much of the North Atlantic (Millot et al., 2008).

The climatic seasonality of the western Mediterranean is influenced by the Azores atmospheric high-pressure cell, resulting in warm-dry summers and mild-humid winters (Quézel and Médail, 2003; Sarnthein et al., 1982; Sumner et al., 2001), which control

the wind circulation/intensities and the moisture availability (Lionello, 2012). At decadal and longer timescales, the climate variability in the Mediterranean and the North Atlantic region is triggered by the winter atmospheric pressure gradient between the Azores High (AH) and the Iceland Low (IL) systems, which defines the North Atlantic Oscillation (NAO; Hurrell et al., 1995). Currently, the fluctuations in the NAO phase largely modulate the position and strength of the westerlies, the seasonal mean heat and moisture transport over the ocean and the path and frequency of storms. They can also be responsible for important changes in ocean temperature and sea-ice cover in the Arctic region (Hurrell, 1995; Trigo

et al., 2002). In the modern Mediterranean, a positive (+) phase of the NAO (Fig. 1b) leads to drier and cooler conditions during the winter, due to a northward positioning of the westerly and north-westerly winds and storm tracks over the northern European latitudes. In contrast, the negative (−) phase of the NAO (Fig. 1c) generates wetter and warmer winter conditions over the Mediterranean, caused by the weakening and southward positioning of the westerly and northwesterly systems and storm tracks across the North Atlantic (Dai et al., 1997; Hurrell, 1995; Rodó et al., 1997). These winter anomalies are involved in deep-water convection and WMDW formation in the Northwestern (NW) Mediterranean (Millot, 1999) and the net water influx across the Strait of Gibraltar (Fenoglio-Marc et al., 2013); mechanisms that ultimately control the intensity of the circulation in the Alboran Sea (Pistek et al., 1985).

## 2.2. The Alboran Upwelling System

The Mediterranean Sea is classified as an oligotrophic basin, owing to its extremely low nutrient concentrations that limit phytoplankton growth. There are, however, a few regions with high algal biomass accumulations, including the Alboran Sea (see Siokou-Frangou et al., 2009 for a review). In the Alboran Sea, vertical mixing is the main mechanism fuelling phytoplankton production (Packard et al., 1988). The two main upwelling mechanisms in operation are: (i) the offshore upwelling associated with the formation of the two Alboran gyres, which is mainly controlled by the intensity of the AJ (García-Gorriz and Carr, 1999; Sarhan et al., 2000); and (ii) the wind-induced coastal upwelling in the north western Alboran Sea, driven by the westerly winds blowing along the southern Iberian coast (Parrilla and Kinder, 1987). These mechanisms are referred to hereinafter as the *Alboran Upwelling System*. The intensity of this system and, consequently, the phytoplankton distributions in the Alboran Sea, are ultimately dependent on atmospheric circulation over the western Mediterranean (d'Ortenzio and Ribera d'Alcalà, 2009; García-Gorriz and Carr, 1999; Lafuente et al., 2000).

In the Alboran Sea, the strong wind force and decrease in solar irradiance during the winter results in a replenishment of nutrients in the surface layer, favouring a spring peak of primary productivity and coccolithophore export to deeper levels, as documented in other Mediterranean regions of high productivity such as the NW Mediterranean (d'Ortenzio and Ribera d'Alcalà, 2009; Rigual-Hernández et al., 2013). Nevertheless, exceptional production during anti-cyclonic conditions over the region suggests that the surface Atlantic flux plays a major role in the stimulation of phytoplankton blooms (d'Ortenzio and Ribera d'Alcalà, 2009). The incoming AW not only introduces high amounts of nutrients, but is also responsible for the eastward transport and distribution of biogenic materials produced in the westernmost sector of the basin (García-Gorriz and Carr, 1999; Salat and Cruzado, 1981).

## 3. Material and methods

### 3.1. Site location and core materials

ODP Site 977 is located in the eastern basin of the Alboran Sea (36° 1.9'N, 1° 57.3'W; Figs. 1), 1984 m below sea level. The sediment composition of the studied interval corresponds to 67.49–58.64 corrected meters below sea floor (cmbsf) from cores 8 and 7 of hole 977 A. The correction was made to adjust the 10.01 and 10.03 m of recovery, respectively in core 8 and 7, to the standard core length of 9.5 m.

The core materials are composed by an open marine-

hemipelagic facies of nannofossil-rich to calcareous silty clay, with CaCO<sub>3</sub> content varying between 43.2 and 57.7 wt % (Comas et al., 1996).

### 3.2. Coccolith sample preparation and analysis

A total of 181 samples for the coccolithophore analyses were selected, each at 4–6 cm spacings from the hole 977 A. Slides for nannoplankton analysis were prepared following the random settling technique outlined by Flores and Sierro (1997). Coccolith identification and counting were carried out using a cross polarized-light Nikon Eclipse 80i petrographic microscope at 1000× magnification. All slides were analysed by counting a minimum of 400 coccoliths in a variable number of fields of view. A second supplementary count of 10 fields of view was performed to accurately determine the abundance of the rarer taxa. Reworked nannofossils were counted separately and expressed as absolute concentrations, (N), and as a percentage of the total concentration. A semiquantitative estimation of the coccolith preservation was applied using the scanning electron microscope (SEM) visual observation and following the scale established by Flores and Marino (2002).

A total of 21 taxa were recognized. Identification of the coccolithophore species followed Young et al. (2003), and the guide to the biodiversity and taxonomy of coccolithophores Nannotax 3 (ina.tmsoc.org/Nannotax3/index.html). Further considerations were made for the *Gephyrocapsa* specimen classification, following Flores et al. (2000). Only mid-sized specimens (3–4.5 μm) with closed or very small central openings were considered as *Gephyrocapsa caribbeanica*; all the *Gephyrocapsa* individuals that were <3 μm, with both open and closed central openings, were grouped as 'small *Gephyrocapsa*'. *Oolithotus* spp., *Umbilicosphaera sibogae*, *Umbilicosphaera foliosa* (both as *Umbilicosphaera* spp.), *Rhabdosphaera clavigera*, *Umbellosphaera* spp., and *Calciosolenia* spp. were lumped together in the Warm Water Taxa (WWT) group. *Coccolithus pelagicus* was subdivided into the subspecies *C. pelagicus* subsp. *pelagicus* (5–10 μm), *C. pelagicus* subsp. *braarudii* (<13 μm), and *C. pelagicus* subsp. *azorinus* (15–16 μm) (Geisen et al., 2002; Parente et al., 2004).

### 3.3. Coccolithophore paleoenvironmental considerations

Variations in the coccolith abundances were estimated using percentages, coccolith absolute values (N) and nannofossil accumulation rates (NAR). N and NAR were calculated according to Flores and Sierro (1997) (Fig. 3c and d). For NAR calculations, the bulk density was obtained from the gamma-ray attenuation density (Comas et al., 1996), and the linear sedimentation rates were calculated from the age model (Fig. 3a). NAR is considered to be an estimate of paleoproductivity (Steinmetz, 1994; Baumann et al., 2004), as it depends on the surface water conditions controlling the proliferation of coccolithophores (Flores et al., 1997; Baumann et al., 2005; Stolz and Baumann, 2010). Following previous studies in the region (Colmenero-Hidalgo et al., 2004; Ausín et al., 2015a,b), these parameters were considered indicators of the coccolithophore primary productivity variability through time.

Eutrophic conditions in the upper photic zone are known to favour coccolithophore proliferation (Barber and Hiscock, 2006; Baumann et al., 2005), in particular the r-selected coccolithophore species, such as those belonging to the *Gephyrocapsa* genus (Young et al., 2000). The small *Gephyrocapsa* group refers to a cluster of opportunistic species dwelling in the uppermost photic zone (Gartner, 1988; Takahashi and Okada, 2000), with affinity for strong vertical mixing, and surface eutrophication in the Alboran Sea

(Hernández-Almeida et al., 2011; Knappertsbusch, 1993). *G. caribbeanica* dominates the coccolith fossil assemblages during the interglacial stages of the Mid-Brunhes interval, including the MIS 11 (e.g., Amore et al., 2012; Marino et al., 2014), although its nature and ecological roles are debated (Bollmann et al., 1998; Flores et al., 2012). Due to the cosmopolitan distribution of *G. caribbeanica*, the ecology of this species is considered analogous to the modern *Emiliania huxleyi* (e.g., Saavedra-Pellitero et al., 2017) and, therefore its N values are grouped together with those of the small *Gephyrocapsa* in the primary productivity proxy (PPP; Fig. 3f). The PPP is used to trace the activation of the Alboran Upwelling System, increasing the accuracy of the net coccolithophore primary productivity signal by removing the load of minor species not completely related to the autochthonous coccolith production at the Alboran Sea. Proportions of small *Gephyrocapsa* up to the threshold of 40% are interpreted as intensified activation of the Alboran Upwelling System, following the observations by Bárcena et al. (2004) during pronounced active upwelling periods in the region inferred from sediment trap records.

The coccolithophore temperature-sensitive assemblage refers to species with ecological requirements associated with a specific temperature range. For instance, the presence of the subpolar water taxon *C. pelagicus* subsp. *pelagicus* is interpreted as a tracer of pulses of polar/subpolar water inflow into the Iberian latitudes (e.g., Amore et al., 2012; Marino et al., 2018; Marino et al., 2014). The tropical/subtropical species composing the WWT group have a common ecological affinity for tropical-subtropical surface waters (Baumann et al., 2004; Boeckel and Baumann, 2004; Winter 1994). The presence of WWT in living and Holocene coccolith assemblages in the Mediterranean is scarce (Knappertsbusch, 1993). Therefore, an increased abundance of these species in our record is considered as a proxy of the enhanced influence of the warm AzC current across the Strait of Gibraltar.

#### 3.4. Opal phytolith analysis

Opal phytoliths are siliceous biogenic particles formed in the aerial tissues of plants, and are particularly abundant and characteristic of the Poaceae family (Carter and Lian, 2000; Twiss, 1992). Since there are no important river systems in the region, the phytolith content in the Alboran Sea is considered to be a wind-transported microfossils that are likely to be sourced from North Africa (Bárcena et al., 2001 and references therein). During periods of dry conditions and marked seasonality over the NW African region, large amounts of phytoliths from tall-grass savannah produced during the humid season are injected into the atmosphere (Flores et al., 2000). The phytolith profile in the Alboran Sea is thus considered to trace the more arid conditions and intensified winds from North Africa.

A set of 35 samples from the hole 977 A were analysed for the content of opal phytolith particles in the sediments. Samples were prepared according to the randomly distributed method outlined in Bárcena and Abrantes (1998). Several transects, accounting for a total surface of 8 mm<sup>2</sup> per slide, were studied. Quantitative analyses were performed at 1000 × , using a Leica DMLB with phase-contrast illumination. The absolute values are expressed as the number of phytoliths per gram (phytolith g<sup>-1</sup>; Fig. 6f).

#### 3.5. Stable isotopes

The Stable isotope analyses were carried out in 272 samples from 977 A at intervals of 2–5 cm. A number of 11 hand-picked specimens of *Globigerina bulloides* per sample were measured. The individuals were separated from the >300 μm size fraction and

crushed and cleaned with methanol and ultrasonicated for a few minutes. The δ<sup>18</sup>O and δ<sup>13</sup>C measurements were performed on an IRMS (isotope-ratio mass spectrometry). Finnigan-MAT 252 coupled to a single acid bath CarboKiel-III carbonate preparation device at the Scientific and Technological Centre of the University of Barcelona (CCiT-UB). Analytical uncertainties were obtained by means of an in-house carbonate standard that is calibrated to NBS-19 international standard (Coplen, 1996). The uncertainties were 0.04‰ VPDB for δ<sup>13</sup>C and 0.08‰ VPDB for δ<sup>18</sup>O.

#### 3.6. Alkenone U<sup>k</sup><sub>37</sub> for SST reconstruction

Biomarker extraction was carried out on the same samples selected for coccolithophore analysis following the protocol described by Villanueva et al. (1997). An internal standard (n-nonadecan-1-ol, n-hexatriacontane and n-dotetracontane) was added to about 2.5 g of sediment, which was extracted with dichloromethane in an ultrasonic bath. The extracts were saponified with 10% KOH in methanol. The extraction of the neutral lipid fraction was performed with the use of hexane and dried under a gentle flow of nitrogen. After that, toluene solvent was used to redissolve and the compounds were derivatized with bis(trimethylsilyl)trifluoroacetamide. The gas chromatography analysis was carried out on a Varian 3800 equipped with a CPSIL-5 CB column coated with 100% dimethylsiloxane (film thickness 0.12 mm) using hydrogen as carrier gas (50 cm/s). Analytical errors were <10% and the uncertainty in the U<sup>k</sup><sub>37</sub> determinations lower than 0.015 (ca. ± 0.5 °C). The complete procedure and analysis were performed at the department of environmental chemistry (IDAEA-CSIC) of Barcelona.

The U<sup>k</sup><sub>37</sub> index (Brassel et al., 1986; Prahl and Wakeham, 1987) was calculated after quantification of [C<sub>37:2</sub>], that indicates the concentration of (E,E)-15,22-heptatriacontadien-2-one and [C<sub>37:3</sub>], referred to the concentration of (E,E,E)-8,15,22-heptatriacontatrien-2-one. The values were converted into Sea Surface Temperatures (SST) using a calibration equation from sediment samples and annual average SST of overlying waters (Müller et al., 1998).

## 4. Results

### 4.1. Chronological framework

The chronology of the sediments was established by correlating the SSTs of both ODP Site 977 and the North Atlantic mid latitude IODP Site U1313 (Stein et al., 2009), for which the available age model is based on the correlation of the benthic δ<sup>18</sup>O with the global LR04 stack (Voelker et al., 2010). As the SST at Sites 977 and 1313 is controlled by the Azores Current, we assumed that there would be synchronous variations. The adjustments for the studied interval were made by including five primary control points (Fig. 2 Table 1), while the age of each sample was calculated using linear interpolations between the age control points.

The studied interval spans were from 429.7 kyr at the MIS 12/MIS 11 transition to 376.3 kyr, near the isotopically MIS 11/MIS 10 boundary (Lisiecki and Raymo, 2005). The nomenclature of Railsback et al. (2015) was used for the identification of substages MIS 11c, 11 b, and 11a over the δ<sup>18</sup>O *G. bulloides* of ODP Site 977 (Fig. 3h).

The high temporal resolution of the coccolithophore record, ranging between 0.02 and 0.3 kyr, provides an exceptional opportunity to reconstruct the environmental conditions in the Alboran Sea at a millennial to centennial scale.

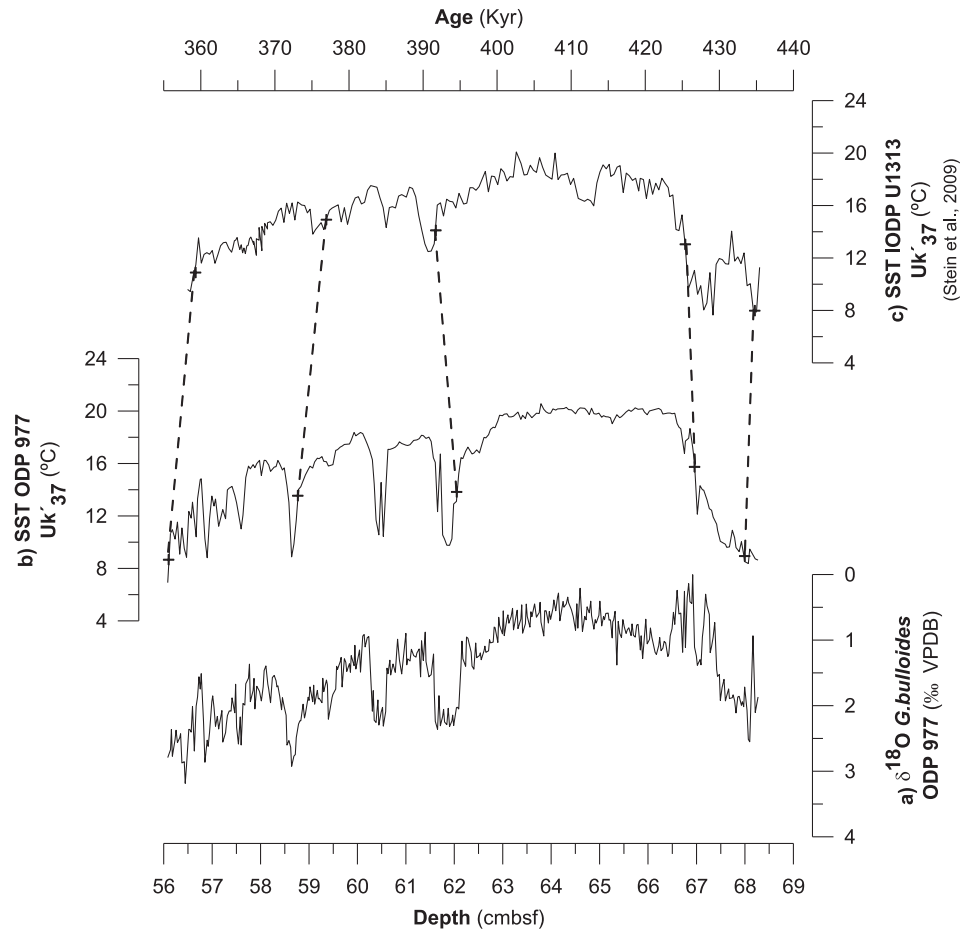


**Fig. 2.** Chronological framework of the studied materials. In depth scale (a) planktonic foraminifera  $\delta^{18}\text{O}$  (‰ VPDB) from *G. bulloides* at ODP Site 977 and (b)  $U^k_{37}$  Sea Surface Temperature (SST) at ODP Site 977. In age scale (c)  $U^k_{37}$  SST at Site U1313 by Stein et al. (2009). Age assignment from correlation of the changes in SST at Site 977 with SST at Site U1313 (Stein et al., 2009). Control points used for the correlation are identified with the dashed lines.

#### 4.2. Coccolithophore assemblages

Species of the genus *Gephyrocapsa* dominated the coccolithophore assemblages during the entire analysed interval (Fig. 4). The small *Gephyrocapsa* group and *G. caribbeanica* are the major contributors, accounting respectively for 46 and 20% of the average relative abundances (Fig. 4c and d). The proportion of the small *Gephyrocapsa* group was over the threshold of 40% at the MIS 12/MIS 11 transition (429.7–418 kyr), during the late MIS 11c (from 405 kyr), and between 396–388 kyr and 385–376 kyr during the MIS 11 b and MIS 11a (Fig. 4c). The proportion of *G. caribbeanica* was over 30% during the MIS 11c (420–400 kyr), and between 389–384 kyr and 383–380 kyr within MIS 11 b (Fig. 4d). The average contribution of *G. oceanica* was ~16%, displaying values over 20% from 405 kyr, during the late MIS 11c and MIS 11 b (Fig. 4e). *G. muelleriae* is the least abundant *Gephyrocapsa* species, averaging 3% (Fig. 4f). Increased percentages are recorded during the MIS12/MIS11 transition (430–422 kyr), briefly at 384 kyr within MIS 11 b, and from 378 kyr within MIS 11a (Fig. 4f).

The WWT % increases during the MIS12/MIS11 transition (426–423.5 kyr) and within the late MIS 11c (412–392.5 kyr; Fig. 5c). *C. pelagicus* subsp. *pelagicus* is scarcely recorded at MIS 11c (until 413.5 kyr) and around 391 and 385 kyr during MIS 11 b (Fig. 5d). The abundance of *Helicosphaera carteri* and *Syracosphaera* spp. increases at the end of the MIS 12/MIS 11 transition and from 405 kyr, during the late MIS 11c and MIS 11 b (Fig. 5e and f).

*C. pelagicus* subsp. *azorinus* increases its numbers during MIS 11 b (from 397 kyr; Fig. 5g). Reworked nanofossils are present in low proportions over the complete studied period (Fig. 3e). The highest percentages are registered at MIS 11c until 414 kyr, and secondary maxima are observed at 391 and 385 kyr within MIS 11 b (Fig. 3e).

#### 4.3. Coccolith absolute values and primary productivity proxy

The preservation of coccoliths in samples is good. The absence of dissolution affecting the nanofossil concentration in samples is further in favour of the usefulness of N as a reference of the coccolithophore primary productivity across the interval. The average of the total N ranged between  $10 \times 10^9$  and  $60 \times 10^9$  coccoliths  $\text{g}^{-1}$  (Fig. 3c). Enhanced PPP values above the threshold of  $20 \times 10^9$  coccoliths  $\text{g}^{-1}$  were observed between 428 and 422 kyr during the MIS 12/MIS 11 transition, between 405 and 397.5 kyr in the late MIS 11c, and during three short intervals at 397.5–392 and 388–386 kyr in MIS 11 b and at 382–376 kyr in MIS 11a (Fig. 3f and 6c). The lowest recorded PPP were during the early MIS 11c (422–405 kyr) and two abrupt drops centred at ~390 and 383 kyr (Fig. 3f). Maximum values for the N of *G. oceanica* were recorded up to the late MIS 11c, and then there were three pulses of enhanced abundance around 396, 388, and 380 kyr (Fig. 4e and 6h). The highest N of *G. muelleriae* occurs at the MIS 12/MIS 11 transition and MIS 11a (Fig. 4f).

The N values of the WWT increased during the final part of the

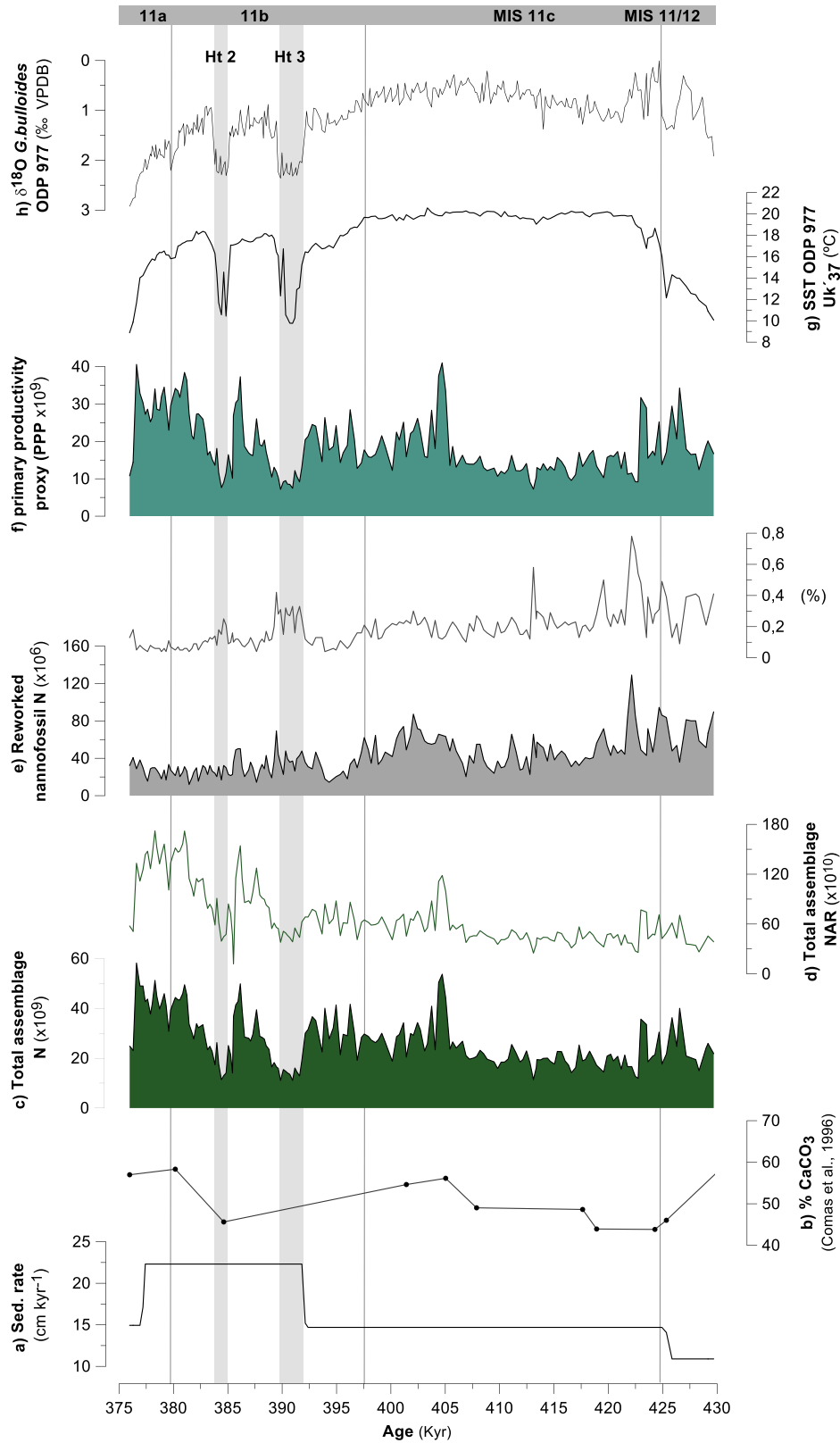


**Fig. 3.** Characterization of the calcareous nanofossil content in the sedimentary record: **a)** Sedimentation rate (cm kyr<sup>-1</sup>); **b)** carbonate content (% CaCO<sub>3</sub>) from Comas et al. (1996); **c)** number of coccoliths per gram of sediment (N; [coccolith g<sup>-1</sup>]) of the total assemblage; **d)** Nanofossil Accumulation Rates (NAR; [coccolith cm<sup>-2</sup> kyr<sup>-1</sup>]) of the total assemblage; **e)** Reworked nanofossils as absolute values (N; [coccolith g<sup>-1</sup>]) and relative abundance (%); **f)** primary productivity proxy (PPP = N small *Gephyrocapsa* + N *G. caribbeanica*; [coccolith g<sup>-1</sup>]); **g)** *U*<sup>k</sup><sub>37</sub> Sea Surface Temperature (°C) at ODP Site 977; **h)** planktonic foraminifera δ<sup>18</sup>O (‰ VPDB) from *G. bulloides* at ODP Site 977. Substages are indicated according to Railsback et al. (2015). Grey bands represent the Heinrich-type events 3 and 2.

**Table 1**  
Primary control points used to correlate the SST values at IODP Site U1313 (Stein et al., 2009) and ODP Site 977. Cmbfs: corrected meters below seafloor.

ODP Site 977 depth (cmbfs)	Age (kyr)	Sed. Rate (cm/kyr)
56.107	359.00	14.94
58.812	377.11	22.31
62.096	391.82	14.69
67.009	425.26	10.90
68.070	435	7.63

MIS 12/MIS 11 transition, and from 413 kyr during the late MIS 11c (Fig. 5c). *C. pelagicus* subsp. *pelagicus* exhibited a decrease in its N from the early MIS 12/MIS 11 transition, towards MIS 11c (Fig. 5d). The N of the *H. carteri* and *Syracosphaera* spp. exhibited high values at the MIS 12/MIS 11 transition and marked pulses of increased abundance during the late MIS 11c (Fig. 5e and f). *C. pelagicus* subsp. *azorinus* increased above the MIS 11 b/MIS 11c transition (Fig. 5g).

#### 4.4. Phytolith content

The highest phytolith content (over  $40 \times 10^4$  phytolith  $g^{-1}$ ) was recorded at the MIS 12/MIS 11 transition (429.7–422 kyr), from the late MIS 11c to MIS 11c/MIS 11 b transition (at 407, 404, and between 397–393 kyr), during the Ht2 (~383 kyr), and the MIS 11a (~376 kyr) (Fig. 6f). The phytolith record displays low values between 420 and 408 kyr in the early MIS 11c, between 389 and 384 in MIS 11 b, and 382–378 kyr towards MIS 11a (Fig. 6f).

## 5. Discussion

### 5.1. Atmospheric control mechanisms on the Alboran Upwelling System

The recorded PPP values, ranging from  $7 \times 10^9$  to  $41 \times 10^9$  coccolith  $g^{-1}$  (Fig. 3f and 6c), are of similar or higher magnitude than those documented in the Alboran Sea during periods of enhanced primary productivity, such as the Holocene (e.g. Colmenero-Hidalgo et al., 2004; Ausín et al., 2015a,b). Thus, it can be concluded that MIS 11 was a period of high coccolithophore primary productivity, most likely owing to the complete development of the Alboran Upwelling System (Fig. 6c). This observation is in agreement with earlier work in the western Mediterranean (e.g., Gironé et al., 2013; Marino et al., 2018), and in the Portuguese Iberian margin (e.g., Amore et al., 2012; Maiorano et al., 2015; Palumbo et al., 2013), that also described MIS 11 as an interglacial period of high primary productivity.

Notably, the high resolution of our analysis reveals substantial intra-interglacial fluctuations in coccolithophore productivity, within the overall highly productive conditions during the MIS 12/MIS 11 transition and MIS 11 (430–376 kyr). Our data suggest that these fluctuations are intimately related to changes in the regional atmospheric circulation. In the modern North Atlantic, the winter + NAO phase is associated with an intensification and northward positioning of the westerly and northwesterly systems, while the winter - NAO phase is related to the weakening of the northwesterly winds that are conveyed towards midlatitudes, leading to an increase in the precipitations in the Mediterranean region and North Africa (Hurrell et al., 1995).

Periods of increased PPP (Fig. 6c) and when the percentage of small *Gephyrocapsa* reached the 40% threshold (Fig. 6d), are associated with the intensification of the Alboran Upwelling System (Fig. 7a). These time intervals are coupled with the increased content of wind-transported phytoliths (Fig. 6f). We propose that + NAO-like conditions were dominant during these intervals of

increasing winter pressure gradients, and thereby favouring the transport of dry winds from the North African region (i.e. Saharan dust transport; Moulin et al., 1997, Fig. 7a). This concept is supported by pollen records at the nearby IODP Site U1385 (Oliveira et al., 2016, Fig. 6g), that suggests Mediterranean forest contractions are consistent with the northward displacement of westerly wind system during + NAO-like phases. In turn, the low PPP (Fig. 6c) and the decreased proportion of small *Gephyrocapsa* (Fig. 6d), were determined to be caused by the moderate activation of the Alboran Upwelling System (Fig. 7b). These intervals are coupled with low phytolith content, owing to a stronger influence of moist air masses over the western Mediterranean (Fig. 6f; Fig. 7b). This idea is consistent with the expansion of the Mediterranean forest during these intervals, strongly suggesting a southward positioning of the westerly winds (Oliveira et al., 2016, Fig. 6g).

The variability of westerly and northwesterly wind systems over the NW Mediterranean has an impact on the thermohaline overturning systems in the western Mediterranean (Cacho et al., 2000; Millot, 1999; Moreno et al., 2002). WMDW convection takes place during winter when the dry and cold northwesterly winds intensify, inducing cooling and evaporation of the surface waters in the NW Mediterranean (Cacho et al., 2000; Fenoglio-Marc et al., 2013; Rogerson et al., 2012; Rohling et al., 1998). Increased winter pressure gradients associated with + NAO-like conditions (Fig. 7a) intensify these mechanisms and surface circulation systems (Cacho et al., 2000), ultimately inducing a more vigorous AJ flux in the western Mediterranean. These conditions most likely result in the complete gyre development and associated upwelling systems, thereby favouring a more intense activation of the Alboran Upwelling System (Fig. 7a). As a feedback mechanism, the complete WAG activity may increase the admixture and acceleration in the WMDW (Lafuente et al., 2000). The N values and percentages of *Gephyrocapsa oceanica* can be used as a tracer of the surface Atlantic waters in the region (Alvarez et al., 2010; Knappertsbusch, 1993; Bazzicalupo et al., 2018, 2020) (Fig. 6h). The reduced winter pressure during the - NAO-like phases (Fig. 7b) results in mild winter conditions and a consequent reduction in WMDW formation, exerting a slowdown in the western Mediterranean circulation and regional AJ intensities (Cacho et al., 2000). The incomplete development of the Alboran gyres (and associated upwelling cells) and the sole coastal wind-induced upwelling development, is considered to weaken the activation of the Alboran System, limiting the overall regional coccolithophore primary productivity (Fig. 7b).

In the following sections we provide a chronological description for our high-resolution signal and a detailed discussion of its relationship with such fluctuations in the Mediterranean atmospheric and oceanographic circulation patterns.

### 5.2. MIS 12/MIS 11 transition (Termination V)

Between 428 and 422 kyr, the high PPP and percentages of small *Gephyrocapsa* (Fig. 6c and d), together with the increased phytolith concentrations (Fig. 6f) and a reduction in Mediterranean forest pollen records at Site U1385 (Fig. 6g), suggests an intensification of the Alboran Upwelling System triggered by more intense trade winds, as a result of + NAO-like conditions. A latitudinal aridification affecting the western Mediterranean across deglaciation is in agreement with the dry and cold midland conditions of SW Iberia (Oliveira et al., 2016) and the iron-enriched sediments affected by the enhanced Saharan dust fluxes at ODP Site 958 off NW Africa (Helmke et al., 2008).

A northward shift of the temperate westerlies is more likely to have resulted in an intensified AJ inflow into the Alboran Sea, stimulating the Alboran Upwelling System. The increased

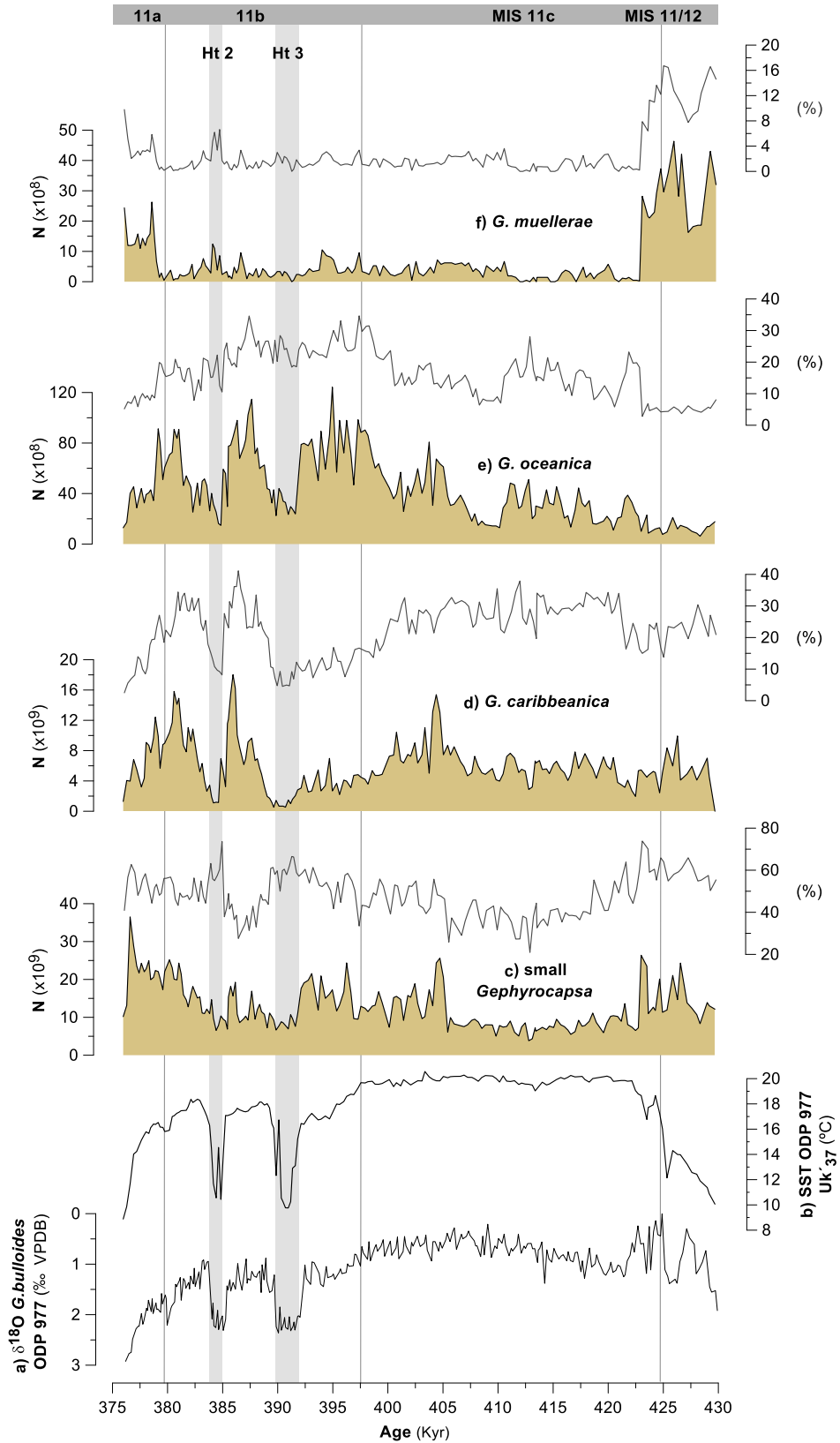


**Fig. 4.** Characterization of the major coccolithophore species of the assemblages during MIS 12/MIS11 and MIS 11 at ODP Site 977. (a) planktonic foraminifera  $\delta^{18}\text{O}$  (‰ VPDB) from *G. bulloides* at ODP Site 977; (b)  $U^{K_{37}}$  Sea Surface Temperature ( $^{\circ}\text{C}$ ) at ODP Site 977. Absolute values (N [coccolith  $g^{-1}$ ]; filled areas) and relative abundances ([%]; grey lines) of (c) small *Gephyrocapsa* group; (d) *Gephyrocapsa caribbeana*; (e) *Gephyrocapsa oceanica*; (f) *Gephyrocapsa muelleriae*.

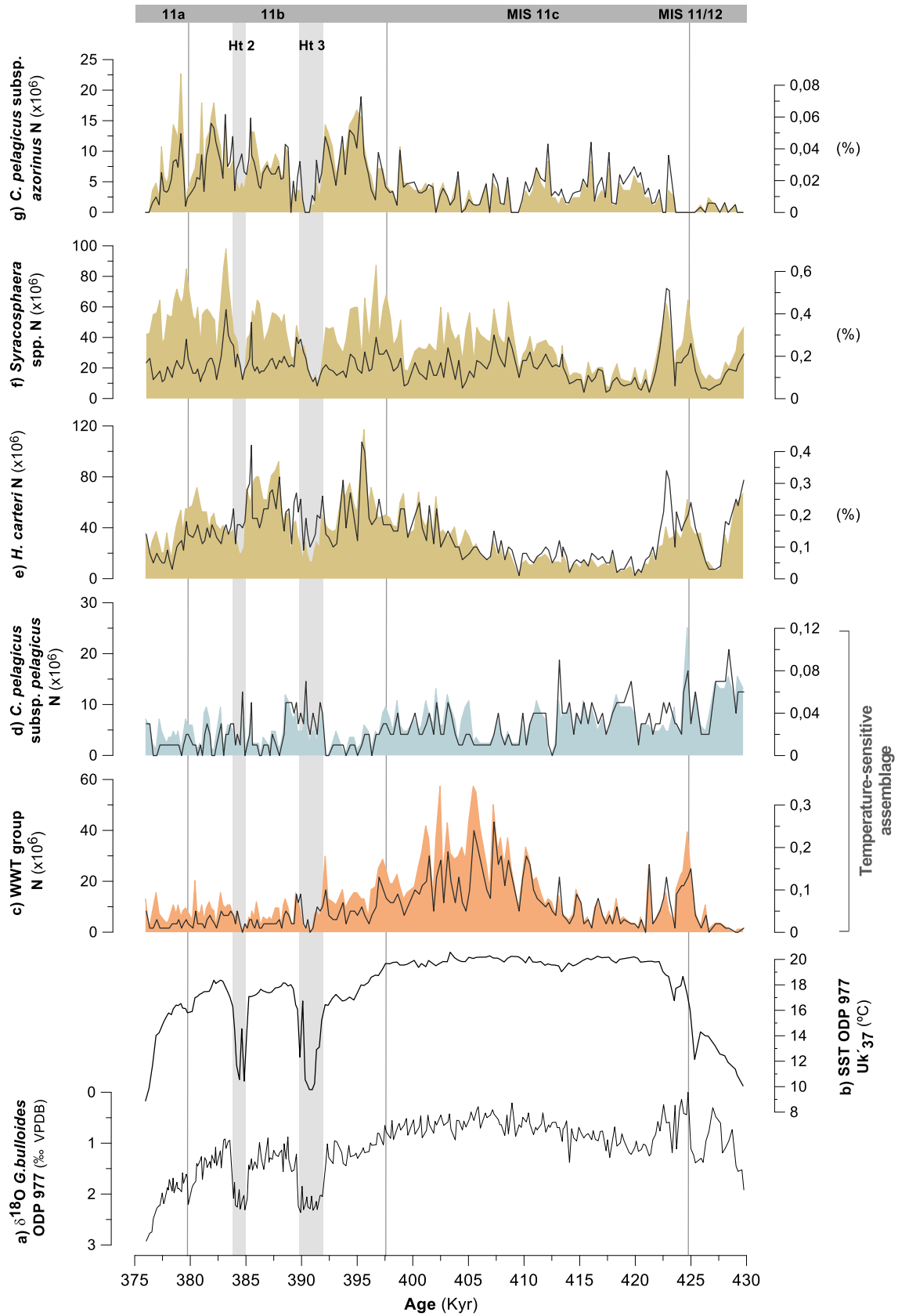


**Fig. 5.** Variations in the absolute abundance of minor coccolithophore species of the assemblages during MIS 12/MIS11 and MIS 11 at ODP Site 977. Absolute values (N [coccolith  $g^{-1}$ ]; filled areas) and relative abundance ([%]; grey lines). **(a)** planktonic foraminifera  $\delta^{18}O$  (‰ VPDB) from *G. bulloides* at ODP Site 977; **(b)**  $U^k_{37}$  Sea Surface Temperature ( $^{\circ}C$ ) at ODP Site 977; **(c)** Warm Water Taxa (WWT) group; **(d)** *Coccolithus pelagicus* subspecies *pelagicus* **(e)** *Helicosphaera carteri*; **(f)** *Syracosphaera* spp.; **(g)** *Coccolithus pelagicus* subspecies *azorinus*.



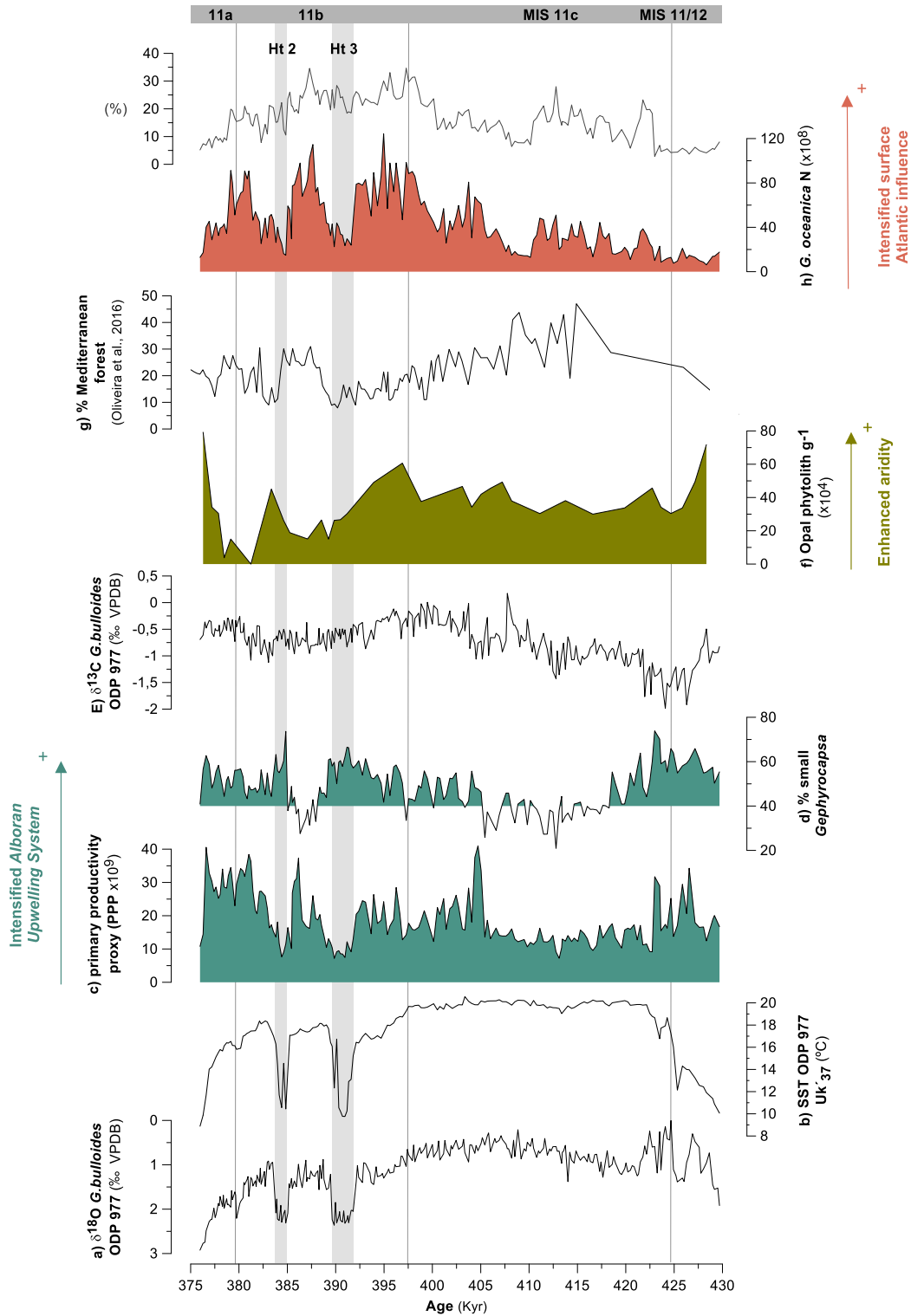


**Fig. 6.** Atmospheric and oceanographic proxies and their relationships with the Alboran Upwelling System. (a)  $U^k_{37}$  Sea Surface Temperature ( $^{\circ}\text{C}$ ) at ODP Site 977; (b) planktonic foraminifera  $\delta^{18}\text{O}$  ( $\text{‰ VPDB}$ ) from *G. bulloides* at ODP Site; (c) primary productivity proxy ( $\text{N small Gephyrocapsa} + \text{N Gephyrocapsa caribbeanica}$ ; [coccolith  $\text{g}^{-1}$ ]); (d) relative abundances (%) of small *Gephyrocapsa*; (e) planktonic foraminifera  $\delta^{13}\text{C}$  ( $\text{‰ VPDB}$ ) from *G. bulloides* at ODP Site 977; (f) Opal phytolith content at ODP Site 977 (phytolith  $\text{g}^{-1}$ ); (g) relative abundances (%) of Mediterranean forest taxa at IODP Site U1385 (Oliveira et al., 2016); (h) absolute values ( $\text{N [coccolith } \text{g}^{-1}]$ ) and relative abundances (%) of *Gephyrocapsa oceanica*.

concentration of reworked nanofossil during the MIS 12/MIS 11 transition (Fig. 3e) is tentatively suggested to be conditioned by depositional processes related to intensified deep circulation in the

Alboran Sea. This idea agrees with a conspicuous MOW intensification during Termination V reported by Sánchez-Goñi et al. (2016). Timing of the restoration of the water exchange across the Strait of

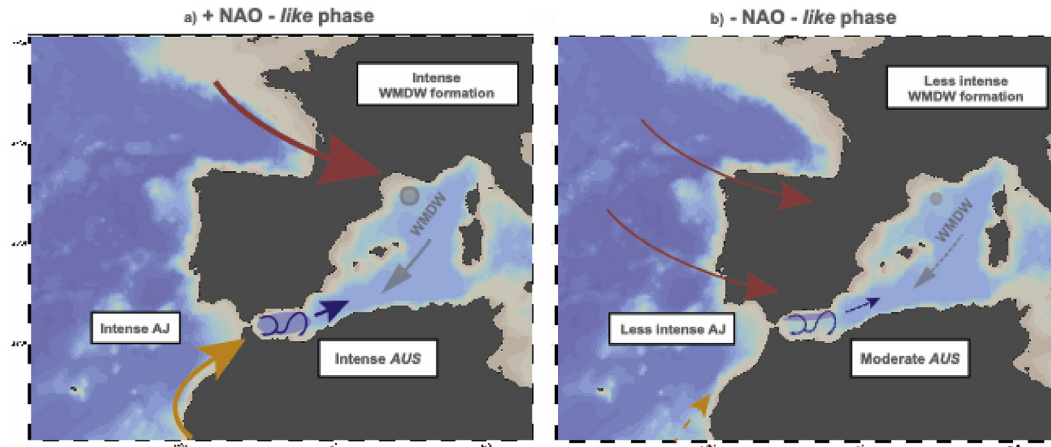


**Fig. 7.** NAO-like scenarios that summarize the main processes controlling the intensity of the Alboran Upwelling System and the coccolithophore primary productivity record during the MIS 12/MIS 11 and the MIS 11. AUS (Alboran Upwelling System); AJ (Atlantic Jet); WMDW (Western Mediterranean Deep Water).

Gibraltar during Termination V (Rohling et al., 1998, 2010) could contribute to the intensified AJ. In this sense, the intense surface influence of the AzC across the deglaciation promoting higher SST (Fig. 5b) is well identified by the increased percentages and N of the WWT group between 426 and 422 kyr (Fig. 5c). The coeval decrease in percentages and N of *G. muelleriae*, associated with colder surface conditions in the region (Weaver and Pujol, 1988), evidences a reversal in the temperature-sensitive species comparable to that observed during the last glacial/interglacial transition of the Mediterranean (Incarbona et al., 2009).

Surface water nutrient-enrichment by the river discharges is not considered to be a regular factor controlling the regional primary productivity in the Alboran Sea (Sanchez-Vidal et al., 2005). Nonetheless, the higher abundances of *H. carteri* and *Syracosphaera* spp. (Fig. 5e and f), species which benefit from turbid, fresher, and productive surface conditions (Colmenero-Hidalgo et al., 2004; Giraudeau, 1992; Hernández-Almeida et al., 2011), suggest an exceptional continental discharge throughout the deglaciation. Nevertheless, the enhanced regional freshwater input due to the intensification of the surface Atlantic influence is regarded as the main driver of these processes.

### 5.3. MIS 11c

A moderate Alboran Upwelling System between 422 and 405 kyr of the early MIS 11c is recognized because of the lowered PPP and percentages of small *Gephyrocapsa* (Fig. 6c and d). Its control by -NAO-like configuration is suggested from the less intense wind supply from N Africa into the Alboran Sea and the consequent decrease in phytolith content (Fig. 6f) and the increased Mediterranean forest pollen record at Site U1385 (Fig. 6g). In line with this interpretation is the timing of changes leading to a more intense rainfall seasonality at the Iberian Peninsula, as suggested by pollen records (Oliveira et al., 2016; Desprat et al., 2004; Tzedakis et al., 2009) and the description of early MIS 11c as a humid period affecting the Mediterranean and the North Atlantic region (Helmke et al., 2008; Kandiano et al., 2012).

The prolonged mild conditions during winter and reduced wind field over the NW Mediterranean most likely resulted in a decreased WMDW formation. A low AJ influx has clearly been traced by the low N and percentages of *G. oceanica* (Fig. 6h). The decrease in abundance of *H. carteri* and *Syracosphaera* spp. (Fig. 5e and f) suggests less turbid and fresher surface layer conditions than during the MIS 12/MIS 11 transition. An extended surface warm

water scenario, as indicated by the high SST (Fig. 6b), is somewhat at odds with the decrease in percentages and N of the WWT until 413 kyr in our coccolithophore record (Fig. 5c) and the parallel rise in  $\delta^{18}\text{O}$  from TV (Fig. 6a). Reconciliations of these results may lie in the reduction inflow of surface AW into the Alboran Sea. Indeed, the decrease in  $\delta^{13}\text{C}$  from *G. bulloides* at 413.5 kyr (Fig. 6e) could be interpreted as the expression of the transference of reduced intermediate water ventilation to surface. Sediment trap studies in the region reported a high affinity of this foraminifera species for upwelling conditions (Bárcena et al., 2004; Hernández-Almeida et al., 2011); thus, an imprint of the subsurface geochemical conditions in its isotopic profile is considered. This pattern was furthermore coeval with the deposition of sapropel S11 and the weak ventilation of intermediate and bottom waters in the eastern Mediterranean (Konijnendijk et al., 2014). A similar  $\delta^{13}\text{C}$  response in the western Mediterranean was described at nearby Site 975 during the humid period of the early Holocene and the deposition of ORL 1 (Jimenez-Espejo et al., 2008). Furthermore, the coccolithophore primary productivity reconstruction by Colmenero-Hidalgo et al. (2004) during this early Holocene period also agrees with the lower PPP observed here during the early MIS 11c (Fig. 5c). The suggested limitation in the western Mediterranean circulation ultimately agrees with the weakening in the intensity of the MOW after Termination V, as reported by Sánchez-Goñi et al. (2016).

A shift to a more intense Alboran Upwelling System from 405 kyr across the late MIS 11c is suggested from an increase in the PPP and the percentages of small *Gephyrocapsa* (Fig. 6c and d). A relationship with an intra-interglacial northward shift of the temperate westerlies through a + NAO-like phase is evidenced by the increased phytolith content (Fig. 6f) and the long-term forest decline at Site U1385 (Fig. 6g). These results point to a latitudinal aridification and are in agreement with the terrestrial moisture decrease and cooling of SW Iberia (Oliveira et al., 2016) and the enhanced Saharan dust flux towards Site 958 from ~405 kyr (Helmke et al., 2008). More constant peaks of heavy planktonic  $\delta^{13}\text{C}$  values (Fig. 6e) indicate intense surface nutrient supply coupled with high nutrient consumption rates, that further support the occurrence of an additional nutrient fertilization by the Saharan dust supply into the Alboran Sea. The high N and percentages of *G. oceanica* (Fig. 6h), together with the high abundances of *H. carteri* and *Syracosphaera* spp. (Fig. 4e and f), shows an intensified AJ and surface circulation. The moderate increase in the N of the reworked nannofossils is tentatively proposed to be linked to the depositional

processes related to intensified deep circulation in the Alboran Sea.

The increased percentages and N maxima of the WWT, from 410 kyr onwards (Fig. 5c), are interpreted to reflect an intensification of the AzC over the study region and are in agreement with previous studies (Marino et al., 2018). From a coccolithophore perspective, the intra-interglacial intensification of the *Alboran Upwelling System* shares many similarities with the timing of the development of the Alboran Gyres during the Holocene (Rohling et al., 1995; Pérez-Folgado et al., 2003), which were described by marked increases in coccolithophore productivity between 8.2 kyr (Colmenero-Hidalgo et al., 2004) and 7.7 kyr (Ausín et al., 2015b). This Holocene hydrological shift has been suggested to be related to cold and arid continental conditions (cold and arid Holocene 8.2 kyr event; Alley et al., 1997). The terrestrial climate during MIS 11c is characterized in several records by a vegetation setback during the “Older Holsteinian Oscillation” event (Koutsodendris et al., 2012). The comparable response of the *Alboran Upwelling System* supports the previously proposed relationship of the “Older Holsteinian Oscillation” event of the late MIS 11 (Koutsodendris et al., 2012) and the middle (8.2 kyr; Koutsodendris et al., 2012) to the late (Combourieu-Nebout et al., 2009; Desprat et al., 2013) Holocene arid event (see Oliveira et al., 2016 and references therein).

#### 5.4. MIS 11 b and MIS 11a

During MIS 11 b and MIS 11a, an intense *Alboran Upwelling System* is identified from the high PPP and percentages of small *Gephyrocapsa* (Fig. 6c and d). There are two important exceptions that are coeval with the Heinrich-type events 3 and 2, that are discussed in section 5.5. A maintained + NAO-like atmospheric configuration phase after 397 kyr at the MIS 11c/MIS 11 b transition is suggested by the high phytolith content (Fig. 6f) and the long-term decline in Mediterranean forest pollen at Site U1385 (Fig. 6g). A shift towards year-round sustained humidity in SW Iberia (Oliveira et al., 2016) may have affected the phytolith transport activity and explain the decrease in records for 389–384 kyr and 382–376 kyr (Fig. 6f). The increased coccolith N and NAR (Fig. 3c and d), together with the lowered magnetic susceptibilities of the core sediments between 61.504–61.104 and 60.405–59.544 mbsf (Comas et al., 1996), reflect an enhancement in the biogenic carbonate sedimentation. This may explain a dilution of the phytolith concentrations in the sediments. The recovered increase in phytolith concentrations during MIS 11a (Fig. 6f) was consistent with the timing of increased aridification in N Africa, as described by Helmke et al. (2008) at ODP Site 958 towards the end of MIS 11.

While we lack direct evidences of MOW intensities during MIS 11 b and MIS 11a, the increased N and percentages of *G. oceanica* (Fig. 6h) are in agreement with the strengthening of the Mediterranean circulation and intensification of the AJ inflow, ultimately resulting in an intensification of the *Alboran Upwelling System*. We propose that cooler and more intense and prolonged evaporative conditions in the NW Mediterranean would have intensified the outflow of Mediterranean waters through the Strait of Gibraltar. Further evidence for the increased influence of the surface AW over the Alboran Sea is provided by the notable increase in the N values and percentages of *C. pelagicus* subsp. *azorinus* (Fig. 5g). This idea is supported by the findings of Parente et al. (2004), who proposed the use of this taxon as a proxy for the intensification of AH cells and the more vigorous influence of the Atlantic Azores Front over the Iberian margin.

#### 5.5. Heinrich – type 3 and 2

Two pronounced drops in PPP centred at 390 and 383 kyr

suggest an abrupt reduction in the activity of the *Alboran Upwelling System* (Fig. 6c and d). This shift was coeval with two rapid SST cooling events (Fig. 6b) and is accompanied by slight increases in the temperature-sensitive cold species *C. pelagicus* subsp. *pelagicus* (Fig. 5d) and *G. muelleriae* (Fig. 4f), suggesting an influence of sub-polar meltwaters in the western Mediterranean. The timing of these episodes is related to Heinrich-type (Ht) events 3 and 2 (Ht3 and Ht2), identified at the Portuguese Iberian margin Site MD03-2699, based on Rodrigues et al. (2011). These events have been linked to disruptions in the Atlantic Meridional Overturning Circulation, from iceberg discharge that originates from the British ice sheet (Rodrigues et al., 2011 and references therein).

The phytolith content was particularly increased during the Ht2 event (Fig. 6f), suggesting an enhancement in wind-driven transport from North Africa. Interestingly, the Ht3 and Ht2 events corresponded to the most severe and longest forest setbacks in SW Iberia (U1385-11-fe5 and fe6; Oliveira et al., 2016). The influences on both the terrestrial and marine ecosystems had significant similarities with the last glacial Heinrich stadial (HS; Cacho et al., 2000), suggesting a comparable atmospheric scenario of intensification and northward displacement of westerlies (Margari et al., 2010; Sánchez-Goñi et al., 2002; Oliveira et al., 2016). The moderate phytolith content of our record during this interval was thought to be due to the moderate degree of semi-desertic conditions in Iberia during the Ht3 and Ht2 events of MIS 11 in comparison with the HS of the last glacial period (Combourieu-Nebout et al., 2002; Sánchez Goñi et al., 2002).

According to our model, a persistent + NAO-like phase during these short stages is proposed. Analogous with that described during the HS events in the Mediterranean (Cacho et al., 2000), a consequent enhancement in the WMDW formation should occur. This hypothetical intensification in the western Mediterranean circulation during the Ht3 and Ht2 events is not clearly evidenced by a more intense *Alboran Upwelling System*, since our data suggests low PPP (Fig. 6c). However, high proportions of small *Gephyrocapsa*, reaching ~70% (Fig. 6d) provide evidence for an intense *Alboran Upwelling System*. We cannot discard the effects of temperature reductions on the production of *G. caribbeanica*, resulting in an overall decrease in PPP (Fig. 4d), as the species composing the small *Gephyrocapsa* group are better adapted to such abrupt temperature drops (Fig. 4c). The moderate increase in N and percentages of reworked nannofossils may indicate an intensification of deep circulations in the Alboran Sea during the Ht3 and Ht2 events (Fig. e).

## 6. Conclusions

Variations in the primary productivity proxy (PPP) and percentages of small *Gephyrocapsa* trace the changes in the coccolithophore paleoproductivity, triggered by the variations in the state of activation of the *Alboran Upwelling System* during the MIS 12/MIS 11 transition and MIS 11. A two-phase atmospheric scenario linked with the intensity of meridional atmospheric pressure gradients, NAO-like, is proposed to explain the changes in the state of activation of the *Alboran Upwelling System*:

- 1) Intensification in the activation of the *Alboran Upwelling System* corresponds with + NAO-like phase conditions, as evidenced by the enhanced phytolith content together with a decrease in the Mediterranean forest pollen records at IODP Site U1385. The more vigorous western Mediterranean circulation, induced by the enhanced WMDW formation in the NW Mediterranean during arid periods, is proposed to be a mechanism stimulating the complete gyre and offshore upwelling development from the intensified AJ influx. This scenario was identified during the

MIS 12/MIS 11 transition (428–422 kyr), the late MIS 11c (405–397 kyr), and MIS 11 b to MIS 11a (397–376).

- 2) Moderate activation of the *Alboran Upwelling System* corresponds with a -NAO-like phase, as suggested by a decrease in the phytolith content and maxima in the Mediterranean forest pollen record, at IODP Site U1385. The attenuated western Mediterranean circulation, due to a reduction of the WMDW formation during humid periods, is thought to hamper the complete upwelling development because there is a less intense AJ influx. This scenario is identified during the early MIS 11c (422–405 kyr).

During MIS 11 b, two short-term minima in PPP and SSTs, whose occurrences are centred 390 and 383 kyr, appear to be comparable with the Heinrich-type events Ht3 and Ht2 (Rodrigues et al., 2011 and references therein). Increased abundances of *C. pelagicus* subsp. *pelagicus* and *G. muelleriae* is consistent with the inflow of cold surface waters into the Mediterranean Sea. A prolonged +NAO-like phase affecting the *Alboran Upwelling System* during these events is discussed.

### Author statement

Coccolithophore sample analysis was made by AGL. Phytolith sample analysis was made by MAB. IC performed the isotopic analyses. JOG and AC processed and analysed the biomarkers for SST reconstruction. AGL integrated the data and conducted the research with the supervision of JAF. DO, ARH, MM, PM and LAA provided resources. AGL visualized and wrote the paper with the supervision of JAF and FJS and the input of coauthors. Founding acquisition leading to this publication was achieved by FJS and JAF.

### Data statement

All data used in this study are available in the public repository PANGAEA® as: González-Lanchas, Alba; Flores, José-Abel; Sierro, Francisco J.; Bárcena, María Ángeles; Cortina, Aleix; Cacho, Isabel; Grimalt, Joan O (2020): Nannofossil, opal phytolith, stable isotopes and  $U^{K}_{37}$  Sea Surface Temperature record from ODP Site 977 during the MIS 11 <https://doi.org/10.1594/PANGAEA.921235>.

### Declaration of competing interest

The authors declare that they have no known competing financial interests or personal relationships that could have appeared to influence the work reported in this paper.

### Acknowledgments

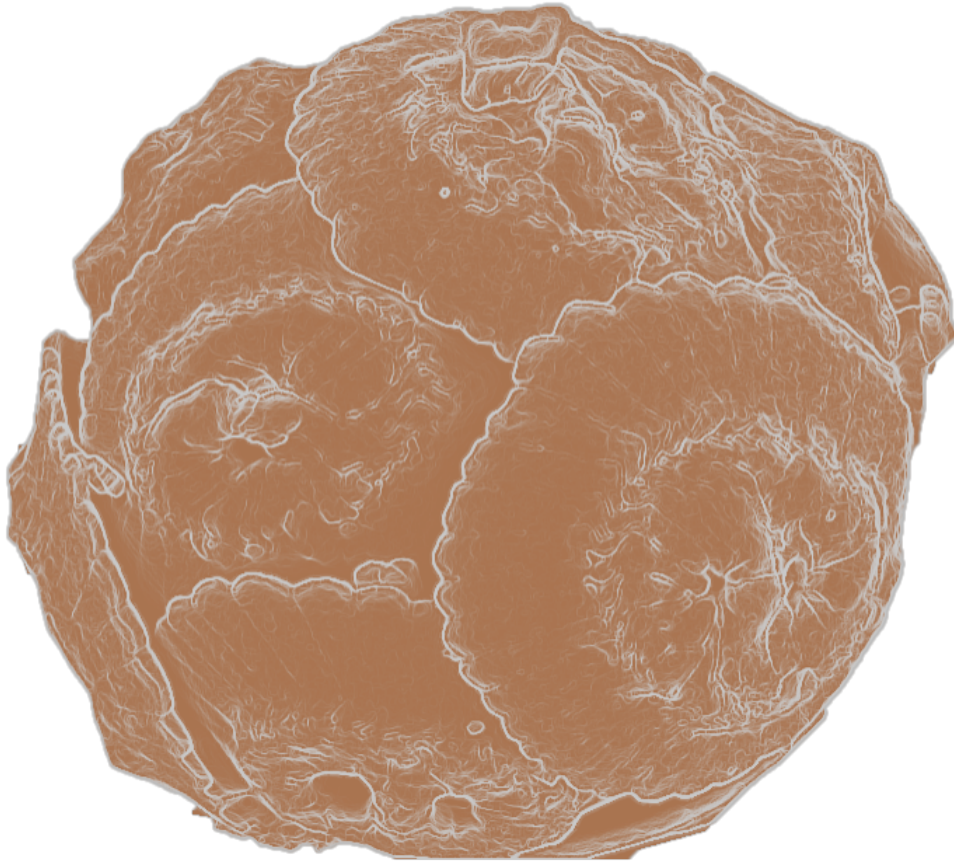
This work was supported by the FPU contract of the Ministry of Education and Professional Formation of the Spanish government [FPU17/03349] awarded to A. González-Lanchas and by the financing infrastructure provided by the programs of the Ministry of Economy and Competitiveness [CGL 2015-68459-P] and the Ministry of Science, Innovation and Universities [RTI 2018-099489-B-100] granted to the GGO (Grupo de Geociencias Oceánicas) of the University of Salamanca. DO acknowledges funding from Portuguese Foundation for Science and Technology (FCT) through the CCMAR Research Unit - project UIDB/04326/2020 and contract (CEECIND/02208/2017). The authors thank Editor Antje Voelker and the two anonymous reviewers for their valuable comments and suggestions.

### References

- Alley, R.B., Mayewski, P.A., Sowers, T., Stuiver, M., Taylor, K.C., Clark, P.U., 1997. Holocene climatic instability: A prominent, widespread event 8200 yr ago. *Geology* 25 (6), 483–486.
- Álvarez, M.C., Amore, F.O., Cros, L., Alonso, B., Alcántara-Carrió, J., 2010. Coccolithophore biogeography in the Mediterranean Iberian margin. *Revista Española de Micropaleontología* 42 (3), 359–371.
- Amore, F.O., Flores, J.A., Voelker, A.H.L., Lebreiro, S.M., Palumbo, E., Sierro, F.J., 2012. A middle Pleistocene northeast Atlantic coccolithophore record: paleoclimatology and paleoproductivity aspects. *Mar. Micropaleontol.* 90–91, 44–59.
- Ausín, B., Flores, J.-A., Sierro, F.-J., Bárcena, M.-A., Hernández-Almeida, I., Francés, G., Gutiérrez-Arnillas, E., Martrat, B., Grimalt, J.O., Cacho, I., 2015a. Coccolithophore productivity and surface water dynamics in the Alboran Sea during the last 25 kyr. *Palaeogeogr. Palaeoclimatol. Palaeoecol.* 418, 126–140.
- Ausín, B., Flores, J.A., Sierro, F.J., Cacho, I., Hernández-Almeida, I., Martrat, B., Grimalt, J.O., 2015b. Atmospheric patterns driving holocene productivity in the Alboran Sea (western mediterranean): a multiproxy approach. *Holocene* 25, 583–595.
- Barber, R., Hiscock, M., 2006. A rising tide lifts all phytoplankton: growth response of other phytoplankton taxa in diatom-dominated blooms. *Global Biogeochem. Cycles* 20.
- Bárcena, M.A., Abrantes, F., 1998. Evidence of a high-productivity area off the coast of Málaga from studies of diatoms in surface sediments. *Mar. Micropaleontol.* 35 (1–2), 91–103.
- Bárcena, M., Cacho, I., Abrantes, F., Sierro, F., Grimalt, J., Flores, J., 2001. Paleoproductivity variations related to climatic conditions in the Alboran Sea (western Mediterranean) during the last glacial–interglacial transition: the diatom record. *Palaeogeogr. Palaeoclimatol. Palaeoecol.* 167, 337–357.
- Bárcena, M., Flores, J., Sierro, F., Pérez-Folgado, M., Fabres, J., Calafat, A., Canals, M., 2004. Planktonic response to main oceanographic changes in the Alboran Sea (Western Mediterranean) as documented in sediment traps and surface sediments. *Mar. Micropaleontol.* 53, 423–445.
- Barker, S., Archer, D., Booth, L., Elderfield, H., Henderiks, J., Rickaby, R.E., 2006. Globally increased pelagic carbonate production during the Mid-Brunhes dissolution interval and the CO<sub>2</sub> paradox of MIS 11. *Quat. Sci. Rev.* 25, 3278–3293.
- Barker, S., Chen, J., Gong, X., Jonkers, L., Knorr, G., Thornalley, D., 2015. Icebergs not the trigger for North Atlantic cold events. *Nature* 520, 333.
- Bauch, H.A., Kandiano, E.S., Helmke, J.P., 2012. Contrasting ocean changes between the subpolar and polar North Atlantic during the past 135 ka. *Geophys. Res. Lett.* 39.
- Baumann, K.-H., Andruleit, H., Böckel, B., Geisen, M., Kinkel, H., 2005. The significance of extant coccolithophores as indicators of ocean water masses, surface water temperature, and paleoproductivity: a review. *Palaeontol. Z.* 79, 93–112.
- Baumann, K.-H., Böckel, B., Frenz, M., 2004. Coccolith Contribution to South Atlantic Carbonate Sedimentation, Coccolithophores. Springer, pp. 367–402.
- Bazzicalupo, P., Maiorano, P., Girona, A., Marino, M., Combouirieu-Nebout, N., Incarbona, A., 2018. High-frequency climate fluctuations over the last deglaciation in the Alboran Sea, Western Mediterranean: evidence from calcareous plankton assemblages. *Palaeogeogr. Palaeoclimatol. Palaeoecol.* 506, 226–241.
- Bazzicalupo, P., Maiorano, P., Girona, A., Marino, M., Combouirieu-Nebout, N., Pelosi, N., Salgueiro, E., Incarbona, A., 2020. Holocene climate variability of the Western Mediterranean: surface water dynamics inferred from calcareous plankton assemblages. *Holocene*, 0959683619895580.
- Berger, A., Loutre, M.F., 1991. Insolation values for the climate of the last 10 million years. *Quat. Sci. Rev.* 10 (4), 297–317.
- Berger, W., Wefer, G., 2003. On the dynamics of the ice ages: stage-11 paradox, mid-Brunhes climate shift, and 100-ky cycle. *GEOPHYSICAL MONOGRAPH-AMERICAN GEOPHYSICAL UNION* 137, 41–60.
- Boeckel, B., Baumann, K.-H., 2004. Distribution of coccoliths in surface sediments of the south-eastern South Atlantic Ocean: ecology, preservation and carbonate contribution. *Mar. Micropaleontol.* 51, 301–320.
- Bollmann, J., Baumann, K.H., Thierstein, H.R., 1998. Global dominance of Gephyrocapsa coccoliths in the late Pleistocene: selective dissolution, evolution, or global environmental change? *Paleoceanography* 13, 517–529.
- Brassell, S.C., Eglinton, G., Marlowe, I.T., Pflaumann, U., Sarnthein, M., 1986. Molecular stratigraphy: a new tool for climatic assessment. *Nature* 320 (6058), 129–133.
- Cacho, I., Grimalt, J.O., Pelejero, C., Canals, M., Sierro, F.J., Flores, J.A., Shackleton, N., 1999. Dansgaard-oeschger and Heinrich event imprints in Alboran Sea paleotemperatures. *Paleoceanography* 14, 698–705.
- Cacho, I., Grimalt, J.O., Sierro, F.J., Shackleton, N., Canals, M., 2000. Evidence for enhanced Mediterranean thermohaline circulation during rapid climatic coolings. *Earth Planet Sci. Lett.* 183, 417–429.
- Candy, I., Schreve, D.C., Sherriff, J., Tye, G.J., 2014. Marine Isotope Stage 11: palaeoclimates, palaeoenvironments and its role as an analogue for the current interglacial. *Earth Sci. Rev.* 128, 18–51.
- Carter, J.A., Lian, O.B., 2000. Palaeoenvironmental reconstruction from the last interglacial using phytolith analysis, southeastern North Island, New Zealand. *J. Quat. Sci.: Published for the Quaternary Research Association* 15, 733–743.
- Combouirieu-Nebout, N., Turon, J.-L., Zahn, R., Capotondi, L., Londeix, L., Pahnke, K., 2002. Enhanced aridity and atmospheric high-pressure stability over the western Mediterranean during the North Atlantic cold events of the past 50 ky.

- Geology 30, 863–866.
- Combourieu-Nebout, N., Peyron, O., Dormoy, I., Desprat, S., Beaudouin, C., Kotthoff, U., Marret, F., 2009. Rapid climatic variability in the west Mediterranean during the last 25 000 years from high resolution pollen data. *Climate Past* 5, 503–521.
- Colmenero-Hidalgo, E., Flores, J.-A., Sierro, F.J., Bárcena, M.A., Löwemark, L., Schönfeld, J., Grimalt, J.O., 2004. Ocean surface water response to short-term climate changes revealed by coccolithophores from the Gulf of Cadiz (NE Atlantic) and Alboran Sea (W Mediterranean). *Palaeogeogr. Palaeoclimatol. Palaeoecol.* 205, 317–336.
- Comas, M., Zahn, R., Klaus, A., 1996. Preliminary results of ODP leg 161. *Proceeding Ocean Drilling Program, Preliminary Results* 161, 1–1679.
- Coplen, T.B., 1996. New guidelines for reporting stable hydrogen, carbon, and oxygen isotope-ratio data. *Geochem. Cosmochim. Acta* 60 (17), 3359–3360.
- d'Ortenzio, F., Ribera d'Alcalá, M., 2009. On the trophic regimes of the Mediterranean Sea: a satellite analysis. *Biogeosciences* 6, 139–148.
- Dai, A., Funk, I.Y., Del Genio, A.D., 1997. Surface observed global land precipitation variations during 1900–88. *J. Clim.* 10, 2943–2962.
- de Abreu, L., Abrantes, F.F., Shackleton, N.J., Tzedakis, P.C., McManus, J.F., Oppo, D.W., Hall, M.A., 2005. Ocean climate variability in the eastern North Atlantic during interglacial marine isotope stage 11: a partial analogue to the Holocene? *Palaeoceanography* 20, 1–15.
- Desprat, S., Goñi, M.S., Naughton, F., Turon, J.-L., Duprat, J., Malaizé, B., Cortijo, E., Peypouquet, J.-P., 2007. Climate variability of the last five isotopic interglacials: direct land-sea-ice correlation from the multiproxy analysis of North-Western Iberian margin deep-sea cores. In: *Developments in Quaternary Sciences*. Elsevier, pp. 375–386.
- Desprat, S., Sánchez Goñi, M.F., Naughton, F., Turon, J.-L., Duprat, J., Malaizé, B., Peypouquet, J.-P., Pujol, C., 2004. Climatic variability of the last five isotopic interglacials: direct land-sea-ice correlation from multiproxy analyses of north-western Iberian margin deep-sea cores. In: *8th International Conference on Paleocceanography: ICP-8*.
- Desprat, S., Combourieu-Nebout, N., Essallami, L., Sicre, M.A., Dormoy, I., Peyron, O., Siani, G., Bout Roumazielles, V., Turon, J.L., 2013. Deglacial and Holocene vegetation and climatic changes in the southern central Mediterranean from a direct land-sea correlation. *Climate Past* 9, 767–787.
- Droxler, A.W., Farrell, J.W., 2000. Marine Isotope Stage 11 (MIS 11): new insights for a warm future. *Global Planet. Change* 24, 1–5.
- Fenoglio-Marc, L., Mariotti, A., Sannino, G., Meyssignac, B., Carillo, A., Struglia, M.V., Rixen, M., 2013. Decadal variability of net water flux at the Mediterranean Sea Gibraltar Strait. *Global Planet. Change* 100, 1–10.
- Fletcher, W.J., Debret, M., Sánchez-Goñi, M.F., 2013. Mid-Holocene emergence of a low-frequency millennial oscillation in western Mediterranean climate: implications for past dynamics of the North Atlantic atmospheric westerlies. *Holocene* 23, 153–166.
- Flores, J., Sierro, F., 1997. Revised technique for calculation of calcareous nannofossil accumulation rates. *Micropaleontology* 321–324.
- Flores, J.A., Bárcena, M.A., Sierro, F.J., 2000. Ocean-surface and wind dynamics in the atlantic ocean off northwest Africa during the last 140 000 years. *Palaeogeogr. Palaeoclimatol. Palaeoecol.* 161 (3–4), 459–478.
- Flores, J.A., Filippelli, G.M., Sierro, F.J., Latimer, J.C., 2012. The “White Ocean” hypothesis: a late Pleistocene Southern Ocean governed by coccolithophores and driven by phosphorus. *Front. Microbiol.* 3, 233.
- Flores, J.A., Marino, M., 2002. Pleistocene calcareous nannofossil stratigraphy for ODP leg 177 (atlantic sector of the southern ocean). *Mar. Micropaleontol.* 45, 191–224.
- Frigola, J., Moreno, A., Cacho, I., Canals, M., Sierro, F.J., Flores, J.A., Grimalt, J.O., Hodell, D.A., Curtis, J.H., 2007. Holocene climate variability in the western Mediterranean region from a deepwater sediment record. *Paleoceanography* 22.
- García-Gorri, E., Carr, M.E., 1999. The climatological annual cycle of satellite-derived phytoplankton pigments in the Alboran Sea. *Geophys. Res. Lett.* 26, 2985–2988.
- Gartner, S., 1988. Paleocceanography of the mid-Pleistocene. *Mar. Micropaleontol.* 13, 23–46.
- Geisen, M., Billard, C., Broerse, A.T., Cros, L., Probert, I., Young, J.R., 2002. Life-cycle associations involving pairs of holococcolithophorid species: intraspecific variation or cryptic speciation? *Eur. J. Phycol.* 37, 531–550.
- Giraudeau, J., 1992. Distribution of recent nannofossils beneath the Benguela system: southwest African continental margin. *Mar. Geol.* 108, 219–237.
- Girone, A., Maiorano, P., Marino, M., Kucera, M., 2013. Calcareous plankton response to orbital and millennial-scale climate changes across the Middle Pleistocene in the western Mediterranean. *Palaeogeogr. Palaeoclimatol. Palaeoecol.* 392, 105–116.
- Heburn, G.W., La Violette, P.E., 1990. Variations in the structure of the anticyclonic gyres found in the Alboran Sea. *J. Geophys. Res.: Oceans* 95, 1599–1613.
- Helmke, J.P., Bauch, H.A., Röhl, U., Kandiano, E.S., 2008. Uniform climate development between the subtropical and subpolar Northeast Atlantic across marine isotope stage 11. *Clim. Past Discuss* 4, 433–457.
- Hernández-Almeida, I., Bárcena, M., Flores, J., Sierro, F., Sanchez-Vidal, A., Calafat, A., 2011. Microplankton response to environmental conditions in the Alboran Sea (Western Mediterranean): one year sediment trap record. *Mar. Micropaleontol.* 78, 14–24.
- Hodell, D.A., Charles, C.D., Ninnemann, U.S., 2000. Comparison of interglacial stages in the South Atlantic sector of the southern ocean for the past 450 kyr: implications for Marine Isotope Stage (MIS) 11. *Global Planet. Change* 24, 7–26.
- Hodell, D., Crowhurst, S., Skinner, L., Tzedakis, P.C., Margari, V., Channell, J.E., Kamenov, G., Maclachlan, S., Rothwell, G., 2013. Response of Iberian Margin sediments to orbital and suborbital forcing over the past 420 ka. *Paleoceanography* 28, 185–199.
- Hurrell, J.W., 1995. Decadal trends in the North Atlantic Oscillation: regional temperatures and precipitation. *Science* 269, 676–679.
- Incarbona, A., Di Stefano, E., Bonomo, S., 2009. Calcareous nannofossil biostratigraphy of the central Mediterranean Basin during the last 430 000 years. *Stratigraphy* 6 (1), 33–34.
- Jansen, J., Kuijpers, A., Troelstra, S., 1986. A mid-Brunhes climatic event: long-term changes in global atmosphere and ocean circulation. *Science* 232, 619–622.
- Jimenez-Espejo, F., Martinez-Ruiz, F., Rogerson, M., González-Donoso, J., Romero, O., Linares, D., Sakamoto, T., Gallego-Torres, D., Rueda Ruiz, J., Ortega-Huertas, M., 2008. Detrital input, productivity fluctuations, and water mass circulation in the westernmost Mediterranean Sea since the Last Glacial Maximum. *G-cubed* 9.
- Johnson, J., Stevens, I., 2000. A fine resolution model of the eastern North Atlantic between the Azores, the canary islands and the Gibraltar strait. *Deep Sea Res. Oceanogr. Res. Pap.* 47 (5), 875–899.
- Kandiano, E.S., Bauch, H.A., Fahl, K., Helmke, J.P., Röhl, U., Pérez-Folgado, M., Cacho, I., 2012. The meridional temperature gradient in the eastern North Atlantic during MIS 11 and its link to the ocean–atmosphere system. *Palaeogeogr. Palaeoclimatol. Palaeoecol.* 333, 24–39.
- Knappertsbusch, M., 1993. Geographic distribution of living and holocene coccolithophores in the Mediterranean Sea. *Mar. Micropaleontol.* 21, 219–247.
- Konijnendijk, T.Y.M., Ziegler, M., Lourens, L.J., 2014. Chronological constraints on Pleistocene sapropel depositions from high-resolution geochemical records of ODP sites 967 and 968. *Newsl. Stratigr.* 47, 263–282.
- Koutsodendris, A., Müller, U.C., Pross, J., Brauer, A., Kotthoff, U., Lotter, A.F., 2010. Vegetation dynamics and climate variability during the Holsteinian interglacial based on a pollen record from Dethlingen (northern Germany). *Quat. Sci. Rev.* 29, 3298–3307.
- Koutsodendris, A., Pross, J., Müller, U.C., Brauer, A., Fletcher, W.J., Köhl, N., Kirilova, E., Verhagen, F.T.M., Lücke, A., Lotter, A.F., 2012. A short-term climate oscillation during the Holsteinian interglacial (MIS 11c): an analogy to the 8.2ka climatic event? *Glob. Planet. Change* 92–93, 224–235.
- Lafuente, J.G., Vargas, J.M., Plaza, F., Sarhan, T., Candela, J., Bascheck, B., 2000. Tide at the eastern section of the Strait of Gibraltar. *J. Geophys. Res.: Oceans* 105, 14197–14213.
- Lionello, P., 2012. The Climate of the Mediterranean Region: from the Past to the Future. Elsevier.
- Lisiecki, L.E., Raymo, M.E., 2005. A Pliocene-Pleistocene stack of 57 globally distributed benthic  $\delta^{18}O$  records. *Paleoceanography* 20.
- Loutre, M.-F., Berger, A., 2003. Marine Isotope Stage 11 as an analogue for the present interglacial. *Global Planet. Change* 36, 209–217.
- Maiorano, P., Marino, M., Balestra, B., Flores, J.A., Hodell, D.A., Rodrigues, T., 2015. Coccolithophore variability from the shackleton site (IODP site U1385) through MIS 16–10. *Global Planet. Change* 133, 35–48.
- Margari, V., Skinner, L., Tzedakis, P., Ganopolski, A., Vautravers, M., Shackleton, N., 2010. The nature of millennial-scale climate variability during the past two glacial periods. *Nat. Geosci.* 3, 127.
- Marino, M., Girone, A., Maiorano, P., Di Renzo, R., Piscitelli, A., Flores, J.A., 2018. Calcareous plankton and the mid-Brunhes climate variability in the Alboran Sea (ODP Site 977). *Palaeogeogr. Palaeoclimatol. Palaeoecol.* 508, 91–106.
- Marino, M., Maiorano, P., Tarantino, F., Voelker, A., Capotondi, L., Girone, A., Lirer, F., Flores, J.A., Naafs, B.D.A., 2014. Coccolithophores as proxy of seawater changes at orbital-to-millennial scale during middle Pleistocene Marine Isotope Stages 14–9 in North Atlantic core MD01-2446. *Paleoceanography* 29, 518–532.
- Martrat, B., Grimalt, J.O., Lopez-Martinez, C., Cacho, I., Sierro, F.J., Flores, J.A., Zahn, R., Canals, M., Curtis, J.H., Hodell, D.A., 2004. Abrupt temperature changes in the Western Mediterranean over the past 250,000 years. *Science* 306, 1762–1765.
- Martrat, B., Grimalt, J.O., Shackleton, N.J., de Abreu, L., Hutterli, M.A., Stocker, T.F., 2007. Four climate cycles of recurring deep and surface water destabilizations on the Iberian margin. *Science* 317, 502–507.
- McManus, J., Oppo, D., Cullen, J., Healey, S., 2003. Marine isotope stage 11 (MIS 11): analog for holocene and future climate? *Geophys. Monogr.* 69–85.
- Millot, C., 1999. Circulation in the western Mediterranean Sea. *J. Mar. Syst.* 20, 423–442.
- Millot, C., 2008. Short-term variability of the Mediterranean in-and out-flows. *Geophys. Res. Lett.* 35 (15).
- Moreno, A., Cacho, I., Canals, M., Prins, M.A., Sánchez-Goñi, M.-F., Grimalt, J.O., Weltje, G.J., 2002. Saharan dust transport and high-latitude glacial climatic variability: the Alboran Sea record. *Quat. Res.* 58, 318–328.
- Moulin, C., Lambert, C.E., Dulac, F., Dayan, U., 1997. Control of atmospheric export of dust from North Africa by the north atlantic oscillation. *Nature* 387, 691.
- Müller, P.J., Kirst, G., Ruhland, G., Von Storch, I., Rosell-Melé, A., 1998. Calibration of the alkenone paleotemperature index U37K' based on core-tops from the eastern South Atlantic and the global ocean (60° N–60° S). *Geochimica et Cosmochimica Acta* 62 (10), 1757–1772.
- Oliveira, D., Desprat, S., Rodrigues, T., Naughton, F., Hodell, D., Trigo, R., Rufino, M., Lopes, C., Abrantes, F., Sánchez-Goñi, M.F., 2016. The complexity of millennial-scale variability in southwestern Europe during MIS 11. *Quat. Res.* 86, 373–387.

- Olson, S.L., Hearty, P.J., 2009. A sustained +21m sea-level highstand during MIS 11 (400ka): direct fossil and sedimentary evidence from Bermuda. *Quat. Sci. Rev.* 28, 271–285.
- Oppo, D., McManus, J., Cullen, J., 1998. Abrupt climate events 500,000 to 340,000 years ago: evidence from subpolar North Atlantic sediments. *Science* 279, 1335–1338.
- Packard, T.T., Minas, H., Coste, B., Martinez, R., Bonin, M., Gostan, J., Garfield, P., Christensen, J., Dortch, Q., Minas, M., 1988. formation of the alboran oxygen minimum zone. Deep sea research Part A. *Oceanographic Research Papers* 35, 1111–1118.
- Past Interglacials Working Group of PAGES, 2016. Interglacials of the last 800,000 years. *Rev. Geophys.* 54 (1), 162–219.
- Palumbo, E., Flores, J.A., Perugia, C., Emanuele, D., Petrillo, Z., Rodrigues, T., Voelker, A.H., Amore, F.O., 2013. Abrupt variability of the last 24 ka BP recorded by coccolithophore assemblages off the Iberian Margin (core MD03-2699). *J. Quat. Sci.* 28, 320–328.
- Parente, A., Cachão, M., Baumann, K.-H., de Abreu, L., Ferreira, J., 2004. Morphometry of *Coccolithus pelagicus* sl (Coccolithophore, Haptophyta) from offshore Portugal, during the last 200 kyr. *Micropaleontology* 50, 107–120.
- Parrilla, G., Kinder, T.H., 1987. Oceanografía física del mar de Alborán, vol. 4. Boletín del Instituto Español de Oceanografía, pp. 133–165.
- Perkins, H., Kinder, T., Violette, P.L., 1990. The atlantic inflow in the western Alboran Sea. *J. Phys. Oceanogr.* 20, 242–263.
- Pérez-Folgado, M., Sierro, F.J., Flores, J.A., Cacho, I., Grimalt, J.O., Zahn, R., Shackleton, N., 2003. WesternMediterranean planktonic foraminifera events and millennial climatic variability during the last 70 kyr. *Mar. Micropaleontol.* 48, 49–70.
- Pistek, P., De Strobel, F., Montanari, C., 1985. Deep-sea circulation in the Alboran Sea. *J. Geophys. Res.: Oceans* 90, 4969–4976.
- Prahl, F.G., Wakeham, S.G., 1987. Calibration of unsaturation patterns in long-chain ketone compositions for palaeotemperature assessment. *Nature* 330 (6146), 367–369.
- Prokopenko, A., Bezrukova, E., Khursevich, G., Solotchina, E., Kuzmin, M., Tarasov, P., 2010. Climate in continental interior Asia during the longest interglacial of the past 500 000 years: the new MIS 11 records from Lake Baikal, SE Siberia. *Clim. Past* 6, 31–48.
- Quézel, P., Médail, F., 2003. Que faut-il entendre par "forêts méditerranéennes. Forêt méditerranéenne 24, 11–31.
- Railsback, L.B., Gibbard, P.L., Head, M.J., Voarintsoa, N.R.G., Toucanne, S., 2015. An optimized scheme of lettered marine isotope substages for the last 1.0 million years, and the climatostatigraphic nature of isotope stages and substages. *Quat. Sci. Rev.* 111, 94–106.
- Raymo, M.E., Mitrovica, J.X., 2012. Collapse of polar ice sheets during the stage 11 interglacial. *Nature* 483, 453.
- Raynaud, D., Barnola, J.-M., Souchez, R., Lorrain, R., Petit, J.-R., Duval, P., Lipenkov, V.Y., 2005. Palaeoclimatology: the record for marine isotopic stage 11. *Nature* 436, 39.
- Reyes, A.V., Carlson, A.E., Beard, B.L., Hatfield, R.G., Stoner, J.S., Winsor, K., Welke, B., Ullman, D.J., 2014. South Greenland ice-sheet collapse during marine isotope stage 11. *Nature* 510, 525.
- Rigual-Hernández, A.S., Bárcena, M.A., Jordan, R.W., Sierro, F.J., Flores, J.A., Meier, K.S., Heussner, S., 2013. Diatom fluxes in the NW Mediterranean: evidence from a 12-year sediment trap record and surficial sediments. *J. Plankton Res.* 35 (5), 1109–1125.
- Roberts, D.L., Karkanis, P., Jacobs, Z., Mearns, C.W., Roberts, R.G., 2012. Melting ice sheets 400,000 yr ago raised sea level by 13 m: Past analogue for future trends. *Earth Planet Sci. Lett.* 357, 226–237.
- Rodó, X., Baert, E., Comin, F., 1997. Variations in seasonal rainfall in southern Europe during the present century: relationships with the north atlantic oscillation and the el niño-southern oscillation. *Clim. Dynam.* 13, 275–284.
- Rodrigues, T., Voelker, A., Grimalt, J., Abrantes, F., Naughton, F., 2011. Iberian Margin sea surface temperature during MIS 15 to 9 (580–300 ka): glacial suborbital variability versus interglacial stability. *Paleoceanography* 26.
- Rogerson, M., Rohling, E., Bigg, G.R., Ramirez, J., 2012. Paleoceanography of the Atlantic-Mediterranean exchange: overview and first quantitative assessment of climatic forcing. *Rev. Geophys.* 50.
- Rohling, E.J., Den Dulk, M., Pujol, C., Vergnaud-Grazzini, C., 1995. Abrupt hydrographic change in the Alboran Sea (western Mediterranean) around 8000 yrs BP. *Deep-Sea Res. I Oceanogr. Res. Pap.* 42, 1609–1619.
- Rohling, E.J., Fenton, M., Jorissen, F.J., Bertrand, P., Ganssen, G., Caulet, J.P., 1998. Magnitudes of sea-level lowstands of the past 500,000 years. *Nature* 394, 162–165.
- Rohling, E.J., Braun, K., Grant, K., Kucera, M., Roberts, A.P., Siddall, M., Trommer, G., 2010. Comparison between holocene and marine isotope stage-11 sea-level histories. *Earth Planet Sci. Lett.* 291, 97–105.
- Saavedra-Pellitero, M., Baumann, K.H., Lamy, F., Köhler, P., 2017. Coccolithophore variability across marine isotope stage 11 in the Pacific sector of the southern ocean and its potential impact on the carbon cycle. *Paleoceanography* 32, 864–880.
- Salat, J., Cruzado, A., 1981. Masses d'eau dans la Méditerranée Occidentale: mer Catalane et eaux adjacentes. *Rapp. Comm. Int. Exploit. Sci. Mer Méditerranée* 27, 201–209.
- Sánchez-Goni, M.F., Cacho, I., Turon, J.-L., Guiot, J., Sierro, F., Peyrouquet, J., Grimalt, J., Shackleton, N., 2002. Synchronicity between marine and terrestrial responses to millennial scale climatic variability during the last glacial period in the Mediterranean region. *Clim. Dynam.* 19, 95–105.
- Sánchez-Goni, M.F., Llave, E., Oliveira, D., Naughton, F., Desprat, S., Ducassou, E., et al., 2016. Climate changes in south western Iberia and Mediterranean Outflow variations during two contrasting cycles of the last 1 Myrs: MIS 31–MIS 30 and MIS 12–MIS 11. *Global Planet. Change* 136, 18–29.
- Sanchez-Vidal, A., Calafat, A., Canals, M., Frigola, J., Fabres, J., 2005. Particle fluxes and organic carbon balance across the eastern Alboran Sea (SW Mediterranean Sea). *Continental Shelf Res.* 25, 609–628.
- Sarhan, T., Lafuente, J.G., Vargas, M., Vargas, J.M., Plaza, F., 2000. Upwelling mechanisms in the northwestern Alboran Sea. *J. Mar. Syst.* 23, 317–331.
- Sarnthein, M., Thiede, J., Pflaumann, U., Erlenkeuser, H., Fütterer, D., Koopmann, B., Lange, H., Seibold, E., 1982. Atmospheric and Oceanic Circulation Patterns off Northwest Africa during the Past 25 Million Years, Geology of the Northwest African Continental Margin. Springer, pp. 545–604.
- Sierro, F.J., Hodell, D.A., Curtis, J.H., Flores, J.A., Reguera, I., Colmenero-Hidalgo, E., Bárcena, M.A., Grimalt, J.O., Cacho, I., Frigola, J., Canals, M., 2005. Impact of iceberg melting on Mediterranean thermohaline circulation during Heinrich events. *Paleoceanography* 20, 1–13.
- Siokou-Frangou, I., Christaki, U., Mazzocchi, M., Montresor, M., d'Alcalá, M.R., Vaqué, D., Zingone, A., 2009. Plankton in the open Mediterranean Sea: a review. *Biogeosci. Discuss.* 6.
- Stein, R., Hefter, J., Grützner, J., Voelker, A., Naafs, B.D.A., 2009. Variability of surface water characteristics and heinrich-like events in the Pleistocene midlatitude North Atlantic ocean: biomarker and XRD records from IODP site U1313 (MIS 16–9). *Paleoceanography* 24.
- Steinmetz, J.C., 1994. Sedimentation of coccolithophores. In: *Coccolithophores*. Cambridge University Press, Cambridge, pp. 179–197.
- Stolz, K., Baumann, K.H., 2010. Changes in palaeoceanography and palaeoecology during Marine Isotope Stage (MIS) 5 in the eastern North Atlantic (ODP Site 980) deduced from calcareous nannoplankton observations. *Paleoogeogr. Palaeoclimatol. Palaeoecol.* 292 (1–2), 295–305.
- Sumner, G., Homar, V., Ramis, C., 2001. Precipitation seasonality in eastern and southern coastal Spain. *Int. J. Climatol.* 21, 219–247.
- Takahashi, K., Okada, H., 2000. Environmental control on the biogeography of modern coccolithophores in the southeastern Indian Ocean offshore of Western Australia. *Mar. Micropaleontol.* 39, 73–86.
- Trigo, R.M., Osborn, T.J., Corte-Real, J.M., 2002. The North Atlantic Oscillation influence on Europe: climate impacts and associated physical mechanisms. *Clim. Res.* 20, 9–17.
- Twiss, P.C., 1992. Predicted World Distribution of C 3 and C 4 Grass Phytoliths, *Phytolith Systematics*. Springer, pp. 113–128.
- Tye, G., Sherriff, J., Candy, I., Coxon, P., Palmer, A., McClymont, E., Schreve, D., 2016. The  $\delta^{18}O$  stratigraphy of the Hoxnian lacustrine sequence at Marks Tey, Essex, UK: implications for the climatic structure of MIS 11 in Britain. *J. Quat. Sci.* 31, 75–92.
- Tzedakis, P.C., Pälike, H., Roucoux, K.H., de Abreu, L., 2009. Atmospheric methane, southern European vegetation and low-mid latitude links on orbital and millennial timescales. *Earth Planet Sci. Lett.* 277, 307–317.
- Villanueva, J., Pelejero, C., Grimalt, J.O., 1997. Clean-up procedures for the unbiased estimation of C37 alkenone sea surface temperatures and terrigenous n-alkane inputs in paleoceanography. *J. Chromatogr. A* 757 (1–2), 145–151.
- Voelker, A.H., Rodrigues, T., Billups, K., Oppo, D.W., McManus, J.F., Stein, R., Hefter, J., Grimalt, J.O., 2010. Variations in mid-latitude North Atlantic surface water properties during the mid-Brunhes (MIS 9–14) and their implications for the thermohaline circulation. *Clim. Past* 6, 531–552.
- Weaver, P., Pujol, C., 1988. History of the last deglaciation in the Alboran Sea (western Mediterranean) and adjacent North Atlantic as revealed by coccolith floras. *Paleoogeogr. Palaeoclimatol. Palaeoecol.* 64, 35–42.
- Winter, A., 1994. Biogeography of Living Coccolithophores in Ocean Waters. *Coccolithophores*.
- Yin, Q.Z., Berger, A., 2012. Individual contribution of insolation and CO2 to the interglacial climates of the past 800,000 years. *Clim. Dynam.* 38, 709–724.
- Young, J., Geisen, M., Cros, L., Kleijne, A., Sprengel, C., Probert, I., Østergaard, J., 2003. A guide to extant coccolithophore taxonomy. *Journal of Nannoplankton Research*, Special Issue 1, 1–132.
- Young, J.R., Thierstein, H.R., Winter, A., 2000. Nannoplankton ecology and palaeoecology. *Mar. Micropaleontol.* 39, vii–ix.



**Control mechanisms of primary productivity revealed  
by calcareous nannoplankton from Marine Isotope  
Stages 12 to 9 at the Shackleton site (IODP Site U1385)**

(González-Lanchas et al., 2021a)

*Paleoceanography and Paleoclimatology*





## CAPÍTULO 3. Artículo científico

### “Control mechanisms of primary productivity revealed by calcareous nanoplankton from Marine Isotope Stages 12 to 9 at the Shackleton Site (IODP Site U1385)”

Alba González-Lanchas <sup>a</sup>, José-Abel Flores <sup>a</sup>, Francisco J. Sierro <sup>a</sup>, María Fernanda Sánchez Goñi <sup>b, c</sup>, Teresa Rodrigues <sup>d, e</sup>, Blanca Ausin <sup>a</sup>, Dulce Oliveira <sup>d, e</sup>, Filipa Naughton <sup>e, f</sup>, Maria Marino <sup>f</sup>, Patrizia Maiorano <sup>f</sup> y Barbara Balestra <sup>g, h, i</sup>.

<sup>a</sup> Departamento de Geología, Universidad de Salamanca, 37008 Salamanca, España.

<sup>b</sup> École Pratique des Hautes Études (EPHE, PSL University), F-33615, Pessac, Francia.

<sup>c</sup> Université Bordeaux, EPOC, UMR 5805, F-33615, Pessac, Francia.

<sup>d</sup> CCMAR, Centro de Ciências do Mar, Universidade do Algarve, Campus de Gambelas, 8005-139, Faro, Portugal.

<sup>e</sup> Divisão de Geologia e Georecursos Marinhos, Instituto Português do Mar e da Atmosfera, Av. Doutor Alfredo Magalhães Ramalho 6, 1495-165, Algés, Portugal.

<sup>f</sup> Dipartimento di Scienze della Terra e Geoambientali, Università degli Studi di Bari Aldo Moro, Bari, Italia.

<sup>g</sup> American University, Department of Environmental Science, Washington, DC 20016, United States.

<sup>h</sup> National Museum of Natural History, (NMNH) Smithsonian, Paleobiology Department, Washington, DC 20560, United States.

<sup>i</sup> University of California Santa Cruz, Institute of Marine Sciences Department, Santa Cruz, CA 95064, United States.

*Paleoceanography and Paleoclimatology* 36(6), e2021PA004246.

DOI: [10.1029/2021PA004246](https://doi.org/10.1029/2021PA004246)

## Resumen

El sector sur de margen Ibérico portugués forma parte de importantes sistemas atmosféricos e hidrológicos cruciales en la dinámica oceanográfica y de circulación del Atlántico norte, que hacen de éste un enclave de alto interés para el estudio de las señales climáticas de interconexión entre altas latitudes y latitudes medias. Entre ellos, destaca la pertenencia de esta región al sistema de surgencia (*upwelling*) del límite Atlántico oriental, que da lugar a la convección de aguas profundas enriquecidas en nutrientes hacia

la superficie durante los meses de primavera/verano, con el consecuente incremento de la tasa de producción en los sectores de proximidad costera del margen ibérico portugués (Mason et al., 2005; Relvas et al., 2007). Este enclave se ve, además, afectado, con variabilidad estacional, por las masas de agua superficiales y subsuperficiales de procedencia subtropical y subártico (Peliz et al., 2005), llegando a representar durante el Cuaternario el límite septentrional de alcance y fusión de los icebergs tras eventos de desprendimiento de los casquetes de regiones árticas, como evidencian los depósitos de materiales líticos (*IRD-ice-rafted detritus*) identificados en los sedimentos oceánicos profundos en estas latitudes (Lebreiro et al., 1996; Vautravers y Shackleton, 2006).

El intervalo comprendido entre los estadios isotópicos marinos (*MIS-Marine Isotope Stage*) 12 a 9, entre las edades de 445 y 320 kyr contiene el denominado evento del Mid-Brunhes, de incremento en la amplitud de la ciclicidad G/I, centrado en la Terminación V (~ 430 ka), que da lugar a los estadios interglaciales MIS 11 y 9 de más alto calentamiento y niveles de CO<sub>2</sub> atmosférico (*pCO<sub>2</sub>*) durante el Pleistoceno reciente, que contrasta con las condiciones glaciales extremas durante el MIS 12 (PAGES, 2016). En contraste con el MIS 12, el glacial MIS 10, también contenido en el intervalo, se caracteriza por unas condiciones glaciales más suaves, donde destaca la recurrencia de eventos de variabilidad climática de alta frecuencia desde la inceptión en la fase final del MIS 11 (Voelker et al., 2010). Así, este intervalo puede considerarse un laboratorio natural para el análisis de escenarios con condiciones de base altamente contrastadas durante el Pleistoceno final. Para intervalos más recientes, algunos estudios previos evidenciaron la existencia de un impacto de la variabilidad en la configuración atmosférica en el Atlántico Norte a escala G/I sobre la productividad primaria regional, por su control sobre el sistema de *upwelling* costero (Pailler y Bard, 2002) y de un impacto de naturaleza hidrológica, a escala milenaria suborbital, sobre el *upwelling*, cuya activación quedaría paralizada, o incluso suprimida, ante la llegada de aguas de fusión de icebergs hacia la región (Ausín et al., 2020; Voelker et al., 2009). De este modo, ambos controles atmosféricos e hidrológicos debieron tener un papel clave sobre la productividad primaria regional durante el Pleistoceno. Hasta la fecha, existen referencias acerca del efecto de la evolución climática en el Atlántico Norte, entre el MIS 12 y 9, sobre los sistemas de circulación superficial en la región y su efecto sobre las asociaciones de cocolitóforos (Amore et al., 2012; Maiorano et al., 2015; Palumbo et al., 2013), pero

ninguna al respecto del análisis de su influencia sobre las condiciones de productividad en la región y los mecanismos de transferencia intermediarios.

En este trabajo se analiza, principalmente, los cambios en las condiciones de productividad primaria en el sector sur de margen Ibérico Portugués durante este intervalo. Para ello, se estudió la asociación de nannoplancton calcáreo, organismos fitoplanctónicos calcificadores, en materiales sedimentarios procedentes del testigo IODP Site U1385. En esta región, la proliferación de estos organismos está principalmente controlada por la actividad del *upwelling* costero y, los mecanismos de transporte superficial de los nutrientes hacia la zona de estudio. El intervalo de estudio se encuentra dominado por las especies pertenecientes al género *Gephyrocapsa*, comúnmente denominado complejo *Gephyrocapsa*. Con el fin de obtener información pormenorizada a partir de las diferentes afinidades ecológicas de las especies que constituyen este complejo, se llevó a cabo una diferenciación completa de especímenes con la aplicación de criterios taxonómicos clásicos. Además, se caracterizó el contenido de otras especies de nanoplancton calcáreo representadas en las muestras, principalmente *Florisphaera profunda* y grupos asociados a condiciones de temperatura variable, vinculados, en esta región, a la influencia de las diferentes masas de aguas superficiales y subsuperficiales (de procedencia subtropical o subpolar). Los datos micropaleontológicos sustentaron el cálculo de las concentraciones de cocolitos fósiles por gramo y esto, junto con el empleo del modelo de edad previamente disponible para las muestras (Hodell et al., 2015) y los valores de densidad del sedimento (<http://www-odp.tamu.edu>), el cálculo de las tasas de acumulación de nanofósiles en el tiempo (por cada mil años, kyr), un valor considerado una buena estimación de las condiciones de productividad en la zona fótica (Baumann et al., 2004). De forma semejante al procedimiento seguido en González-Lanchas et al. (2020), las especies del grupo de small *Gephyrocapsa* y “*Gephyrocapsa caribbeanica*” se emplearon para el cálculo del *Primary Productivity Proxy* (PPP), a fin de precisar la señal de la intensidad del *upwelling* costero. El valor de esta señal de productividad obtenida mediante análisis micropaleontológico se contrasta con la señal de productividad obtenida a partir del análisis del contenido de compuestos orgánicos en el sedimento, analizadas en este estudio tras el procedimiento de extracción del contenido lipídico y la cuantificación de alquenonas. Además, se calculó el índice N de Flores et al. (2000), un valor relativo entre la representación de *F. profunda* y las especies que

constituyen el grupo small *Gephyrocapsa*, ambos respectivamente indicativos de las condiciones de productividad en la zona fótica inferior y superior, empleado como indicador cualitativo del grado de estabilidad de la columna de agua (grado de estratificación o mezcla, como términos extremos). También se consideraron las abundancias relativas de aquellas especies sensibles a los cambios de temperaturas superficiales y subsuperficiales.

La señal de productividad primaria y los datos micropaleontológicos adicionales procedentes del estudio de la asociación, se combinaron con i) datos geoquímicos, como los valores de isótopos estables de oxígeno,  $\delta^{18}\text{O}$ , en foraminíferos planctónicos y bentónicos (Hodell et al., 2013), la relación entre el contenido de calcio y titanio en el sedimento,  $\text{Log Ca/Ti}$  (Hodell et al., 2015), la reconstrucción de temperaturas superficiales, SST, a partir del índice  $U^{k'}_{37}$  y de la representación de la variedad tetra insaturada,  $\%C_{37:4}$  (Rodrigues et al., 2017) y ii) marcadores de origen terrestres, como las abundancias polínicas procedentes del bosque mediterráneo, indicativas de los cambios en la vegetación ibérica y, por lo tanto, aplicables para la precisión de la configuración atmosférica durante el intervalo (Desprat et al., 2017; Oliveira et al., 2016; Sánchez Goñi, 2020; Sánchez Goñi et al., 2016). Todos los datos anteriores, previamente disponibles o generados para este estudio, son procedentes del mismo testigo IODP *Site* U1385.

La integración de los datos evidencia la fuerte influenciada de la configuración atmosférica, particularmente, del desplazamiento e intensidad de la célula de altas presiones de Azores (AH- *Azores High*) sobre las condiciones ambientales, siendo este el principal control sobre la productividad primaria a escala G/I. Durante las etapas tempranas de los periodos de condiciones interglaciales plenas MIS 11c (~ 420-405 ka) y MIS 9e (~ 337-320 ka), la productividad primaria es moderada, producto de la disminución en la disponibilidad de nutrientes a causa de la reducción en la intensidad de la mezcla vertical y el transporte en superficie desde la costa hacia la zona de estudio. Estas condiciones son atribuidas a la limitación de la estimulación del *upwelling* costero a los meses de verano, a causa de la exclusiva intensificación y desplazamiento hacia el norte de la AH durante ese periodo del año, una configuración comparable a las condiciones identificadas durante el Holoceno y en la actualidad en la región, y posiblemente atribuible a una disminución del gradiente de presiones con altas latitudes,

comparable al establecido durante el modo negativo (-) de la Oscilación del Atlántico Norte (NAO-*North Atlantic Oscillation*) moderna.

La etapa tardía del periodo interglacial pleno del MIS 11c (~ 405-392 ka), registra un incremento en la productividad primaria y una mayor disponibilidad de nutrientes en superficie. Estas condiciones se atribuyen a la posible intensificación intra-interglacial de la AH, que condicionaría la prolongación en la estimulación del *upwelling* estacional más allá de los meses de verano. Esta configuración promovería una intensificación del gradiente de presiones, en relación con las células de altas latitudes, comparable a la prolongación del modo positivo (+) de la NAO moderna identificado, en este estudio, hacia la fase final de periodo de condiciones interglaciales plenas del MIS 11.

El significativo aumento de la productividad primaria y la disponibilidad de nutrientes durante el periodo de establecimiento de las condiciones glaciales, desde el final del MIS 11 y durante el comienzo del MIS 10 (~ 392-356 ka), es indicativa de una significativa intensificación de la actividad del *upwelling* costero. Esta intensificación se vincula a la posible ampliación de las dimensiones de las células de surgencia, su desplazamiento mar adentro hacia la zona de estudio en respuesta al fortalecimiento general de la circulación atmosférica e intensificación generalizada de los gradientes de presiones en el Atlántico norte durante esta fase de transición hacia condiciones glaciales.

Las reducciones bruscas, a escala suborbital milenaria, de la productividad primaria y disponibilidad de nutrientes superficiales, junto con la estabilización de las condiciones de mezcla, se identifican durante el establecimiento de condiciones subpolares en las latitudes estudiadas, durante la sucesión de los eventos de tipo *Heinrich* (Ht) 4 a 1 (~ 436, 392, 384 y 339 ka), durante otros episodios de enfriamiento a corto plazo (~ 378, 372, 364, 350 y 355 ka) y, de forma más prolongada, durante las Terminaciones glacial/interglacial V y IV. Estas condiciones pueden ser indicativas de la formación de una haloclina regional, comparable a la descrita durante episodios semejantes del último ciclo glacial (s. str. eventos *Heinrich*), restringiendo el transporte vertical de nutrientes hacia la superficie, a pesar de contar con unas condiciones atmosféricas potencialmente favorables para la estimulación del *upwelling* costero.

## Referencias

- Amore, F.O., Flores, J.A., Voelker, A.H.L., Lebreiro, S.M., Palumbo, E., Sierro, F.J., 2012. A Middle Pleistocene Northeast Atlantic coccolithophore record: Paleoclimatology and paleoproductivity aspects. *Marine Micropaleontology* 90-91, 44-59.
- Ausín, B., Hodell, D.A., Cutmore, A., Eglinton, T.I., 2020. The impact of abrupt deglacial climate variability on productivity and upwelling on the southwestern Iberian margin. *Quaternary Science Reviews* 230, 106139.
- Baumann, K.-H., Böckel, B., Frenz, M., 2004. Coccolith contribution to South Atlantic carbonate sedimentation, *Coccolithophores*. Springer, pp. 367-402.
- Desprat, S., Oliveira, D., Naughton, F., Sánchez Goñi, M.F., 2017. L'étude du pollen des séquences sédimentaires marines pour la compréhension du climat: l'exemple des périodes chaudes passées. *Quaternaire. Revue de l'Association française pour l'étude du Quaternaire* 28, 259-269.
- Flores, J.A., Bárcena, M.A., Sierro, F.J., 2000. Ocean-surface and wind dynamics in the Atlantic Ocean off Northwest Africa during the last 140 000 years. *Palaeogeography, Palaeoclimatology, Palaeoecology* 161, 459-478.
- González-Lanchas, A., Flores, J.-A., Sierro, F.J., Bárcena, M.Á., Rigual-Hernández, A.S., Oliveira, D., Azibeiro, L.A., Marino, M., Maiorano, P., Cortina, A., Cacho, I., Grimalt, J.O., 2020. A new perspective of the Alboran Upwelling System reconstruction during the Marine Isotope Stage 11: A high-resolution coccolithophore record. *Quaternary Science Reviews* 245, 106520.
- Hodell, D., Lourens, L., Crowhurst, S., Konijnendijk, T., Tjallingii, R., Jiménez-Espejo, F., Skinner, L., Tzedakis, P., Members, T.S.S.P., Abrantes, F., 2015. A reference time scale for Site U1385 (Shackleton Site) on the SW Iberian Margin. *Global and Planetary Change* 133, 49-64.
- Hodell, D., Lourens, L., Stow, D., Hernández-Molina, F.J., Alvarez-Zarikian, C., Abrantes, F., Acton, G., Bahr, A., Balestra, B., Llave Barranco, E., 2013. The "Shackleton Site"(IODP Site U1385) on the Iberian Margin. *Scientific Drilling* 16, 13-19.
- Lebreiro, S., Moreno, J., McCave, I., Weaver, P., 1996. Evidence for Heinrich layers off Portugal (Tore Seamount: 39 N, 12 W). *Marine Geology* 131, 47-56.
- Maiorano, P., Marino, M., Balestra, B., Flores, J.-A., Hodell, D., Rodrigues, T., 2015. Coccolithophore variability from the Shackleton Site (IODP Site U1385) through MIS 16-10. *Global and Planetary Change* 133, 35-48.
- Mason, E., Coombs, S., Oliveira, P., 2005. An overview of the literature concerning the oceanography of the eastern North Atlantic region. *Relatórios Científicos e Técnicos IPIMAR Serie Digital* 33, 59.
- Oliveira, D., Desprat, S., Rodrigues, T., Naughton, F., Hodell, D., Trigo, R., Rufino, M., Lopes, C., Abrantes, F., Goni, M.F.S., 2016. The complexity of millennial-scale

- variability in southwestern Europe during MIS 11. *Quaternary Research* 86, 373-387.
- Past International Working Group of PAGES, 2016. Interglacials of the last 800,000 years. *Reviews of Geophysics* 54, 162-219.
- Pailler, D., Bard, E., 2002. High frequency palaeoceanographic changes during the past 140 000 yr recorded by the organic matter in sediments of the Iberian Margin. *Palaeogeography, Palaeoclimatology, Palaeoecology* 181, 431-452.
- Palumbo, E., Flores, J., Perugia, C., Petrillo, Z., Voelker, A., Amore, F., 2013. Millennial scale coccolithophore paleoproductivity and surface water changes between 445 and 360 ka (Marine Isotope Stages 12/11) in the Northeast Atlantic. *Palaeogeography, Palaeoclimatology, Palaeoecology* 383, 27-41.
- Peliz, Á., Dubert, J., Santos, A.M.P., Oliveira, P.B., Le Cann, B., 2005. Winter upper ocean circulation in the Western Iberian Basin—Fronts, Eddies and Poleward Flows: an overview. *Deep sea research Part I: Oceanographic research papers* 52, 621-646.
- Relvas, P., Barton, E.D., Dubert, J., Oliveira, P.B., Peliz, A., Da Silva, J., Santos, A.M.P., 2007. Physical oceanography of the western Iberia ecosystem: latest views and challenges. *Progress in Oceanography* 74, 149-173.
- Rodrigues, T., Alonso-García, M., Hodell, D.A., Rufino, M., Naughton, F., Grimalt, J.O., Voelker, A.H.L., Abrantes, F., 2017. A 1-Ma record of sea surface temperature and extreme cooling events in the North Atlantic: A perspective from the Iberian Margin. *Quaternary Science Reviews* 172, 118-130.
- Sánchez Goñi, M.F., 2020. Regional impacts of climate change and its relevance to human evolution. *Evolutionary Human Sciences* 2, e55.
- Sánchez Goñi, M.F., Llave, E., Oliveira, D., Naughton, F., Desprat, S., Ducassou, E., Hodell, D.A., Hernández-Molina, F.J., 2016. Climate changes in south western Iberia and Mediterranean Outflow variations during two contrasting cycles of the last 1 Myrs: MIS 31-MIS 30 and MIS 12-MIS 11. *Global and Planetary Change* 136, 18-29.
- Vautravers, M.J., Shackleton, N.J., 2006. Centennial-scale surface hydrology off Portugal during marine isotope stage 3: Insights from planktonic foraminiferal fauna variability. *Paleoceanography* 21.
- Voelker, A., De Abreu, L., Schönfeld, J., Erlenkeuser, H., Abrantes, F., 2009. Hydrographic conditions along the western Iberian margin during marine isotope stage 2. *Geochemistry, Geophysics, Geosystems* 10.
- Voelker, A.H., Rodrigues, T., Billups, K., Oppo, D.W., McManus, J.F., Stein, R., Hefter, J., Grimalt, J.O., 2010. Variations in mid-latitude North Atlantic surface water properties during the mid-Brunhes (MIS 9–14) and their implications for the thermohaline circulation. *Climate of the Past*, 6, 531–552.





# Paleoceanography and Paleoclimatology

## RESEARCH ARTICLE

10.1029/2021PA004246

### Key Points:

- High-resolution calcareous nannoplankton record reveal upwelling-related primary productivity variations not previously described
- Multiproxy integration allows the assessment of the control by major atmospheric circulation changes at orbital and suborbital timescales
- Reductions in surface productivity during abrupt cold episodes is the result of upwelling limitation by hydrological changes

### Correspondence to:

A. González-Lanchas,  
[lanchas@usal.es](mailto:lanchas@usal.es)

### Citation:







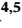


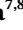

González-Lanchas, A., Flores, J.-A., Sierro, F. J., Sánchez Goñi, M. F., Rodrigues, T., Ausín, B., et al. (2021). Control mechanisms of primary productivity revealed by calcareous nannoplankton from marine isotope stages 12 to 9 at the Shackleton Site (IODP Site U1385). *Paleoceanography and Paleoclimatology*, 36, e2021PA004246. <https://doi.org/10.1029/2021PA004246>

Received 20 FEB 2021  
 Accepted 23 MAY 2021

© 2021. The Authors.

This is an open access article under the terms of the [Creative Commons Attribution License](#), which permits use, distribution and reproduction in any medium, provided the original work is properly cited.

## Control Mechanisms of Primary Productivity Revealed by Calcareous Nannoplankton From Marine Isotope Stages 12 to 9 at the Shackleton Site (IODP Site U1385)

A. González-Lanchas<sup>1</sup> , J.-A. Flores<sup>1</sup> , F. J. Sierro<sup>1</sup> , M. F. Sánchez Goñi<sup>2,3</sup> , T. Rodrigues<sup>4,5</sup> , B. Ausín<sup>1</sup> , D. Oliveira<sup>4,5</sup> , F. Naughton<sup>4,5</sup> , M. Marino<sup>6</sup> , P. Maiorano<sup>6</sup> , and B. Balestra<sup>7,8,9</sup> 

<sup>1</sup>Departamento de Geología, Universidad de Salamanca, Salamanca, Spain, <sup>2</sup>École Pratique des Hautes Études (EPHE, PSL University), Pessac, France, <sup>3</sup>Université Bordeaux, Environnements et Paléoenvironnements Océaniques et Continentaux (EPOC), UMR 5805, Pessac, France, <sup>4</sup>Centro de Ciências do Mar (CCMAR), Universidade do Algarve, Faro, Portugal, <sup>5</sup>Divisão de Geologia e Georecursos Marinhos, Instituto Português do Mar e da Atmosfera (IPMA), Algés, Portugal, <sup>6</sup>Dipartimento di Scienze della Terra e Geoambientali, Università degli Studi di Bari Aldo Moro, Bari, Italy, <sup>7</sup>Department of Environmental Science, American University, Washington, DC, USA, <sup>8</sup>Paleobiology Department, National Museum of Natural History (NMNH) Smithsonian, Washington, DC, USA, <sup>9</sup>Institute of Marine Sciences Department, University of California Santa Cruz, Santa Cruz, CA, USA

**Abstract** Nowadays, primary productivity variations at the SW Iberian Margin (IbM) are primarily controlled by wind-driven upwelling. Thus, major changes in atmospheric circulation and wind regimes between the Marine Isotope Stages (MIS) 12 and 9 could have driven substantial changes in phytoplankton productivity which remains poorly understood. We present a high-resolution calcareous nannofossil record from the Shackleton Site Integrated Ocean Discovery Program Site U1385 that allow the assessment of primary productivity and changing surface conditions on orbital and suborbital timescales over the SW IbM. These records are directly compared and integrated with terrestrial – Mediterranean forest pollen – and marine – benthic and planktic oxygen stable isotopes ( $\delta^{18}\text{O}$ ), alkenone concentration [ $\text{C}_{37}$ ],  $U^{k}_{37}$ –Sea Surface Temperature and %  $\text{C}_{37:4}$  – proxy records from Site U1385. Our results indicate intra-interglacial increase in primary productivity together with intensification of the Azores anticyclonic high-pressure cell beyond the summer that suggests a two-phase upwelling behavior during the full interglacial MIS 11c (~420–397 ka), potentially driven by atmospheric NAO-like variability. Primary productivity is largely enhanced during the inception of glacial MIS 10 and the early MIS 10 (~392–356 ka), linked to intensified upwelling and associated processes during a period of strengthened atmospheric circulation. In agreement with the conditions observed during Heinrich events of the last glacial cycle, primary productivity reductions during abrupt cold episodes, including the Heinrich-type (Ht) events 4 to 1 (~436, 392, 384 and 339 ka) and the Terminations V and IV, seems to be the result of halocline formation induced by meltwater arrival, reducing the regional upward nutrient transference.

## 1. Introduction

Reconstruction of changes in marine primary productivity during the Pleistocene is crucial for understanding the climate dynamics on glacial/interglacial (G/I) and suborbital timescales (e.g., Beaufort et al., 1997; Kinkel et al., 2000; Molino & McIntyre, 1990) and the effect of the ocean biological pump on the evolution of atmospheric  $\text{CO}_2$  (e.g., Mix, 1989). Given proliferation of coccolithophores, a major group of calcifying phytoplankton, is tightly related to changing surface physicochemical conditions (i.e., light, nutrient concentration, salinity, temperature and turbulence), high resolution records of coccolithophore calcite plates (coccoliths) provide a valuable tool for paleoclimate and paleoceanographic reconstructions (e.g., Baumann & Freitag, 2004; Flores et al., 1997).

The Iberian Margin (IbM) is a benchmark region for the assessment of possible links between Northern Hemisphere and mid-latitude climatic signals (e.g., Martrat et al., 2007; Rodrigues et al., 2011). Crucial atmospheric and hydrological systems in the North Atlantic affect the IbM, as (i) the Iberian Canary Current eastern boundary upwelling (see Relvas et al., 2007) triggering the upwelling of cold and nutrient-rich subsurface waters during spring/summer at the IbM (May to September; Abrantes & Moita, 1999; Moita

et al., 2010; Silva et al., 2009); (ii) the surface ocean boundary between the subpolar and subtropical gyres (Ruddiman & McIntyre, 1981) and (iii) the proximity to the southernmost limit where northern hemisphere icebergs have reached and melted, favoring the accumulation of high quantities of ice-rafted detritus (IRD) and the surface influence of meltwaters in this region (e.g., Lebreiro et al., 1996; Martrat et al., 2007; Shackleton et al., 2000; Vautravers & Shackleton, 2006). Thus, primary productivity variations at the IbM during extended intervals of the Pleistocene could be the result of substantial atmospheric and hydrological changes in the North Atlantic region.

Previous studies for the last glacial cycle and former periods of the Pleistocene at the IbM (e.g., Incarbona et al., 2010; Pailler & Bard, 2002) observed contrasted scenarios of reduced/increased primary productivity during respectively interglacials/transitional stages and glacials. Pailler and Bard (2002) linked this to the enhanced wind-driven upwelling controlled by shifts in the atmospheric circulation patterns over the North Atlantic, that were favored by substantial changes in northern hemisphere ice volume. Further work of Cavaleiro et al. (2020) observed similar patterns of coccolithophore productivity in response to G/I and millennial-scale variability, primarily attributed to variations in the dominant surface water masses and their influence (i.e., changes in nutrient content) on the state of competition between phytoplankton groups, but suggested to be connected to wind-driven upwelling. However, in these studies a clear determination of the mechanisms controlling vertical mixing dynamics and fertilization was severely hampered by the absence of direct information about prevailing wind regimes and atmospheric configuration. Addressing this question requires direct comparison of primary productivity records with those of continental and oceanic conditions derived from the same marine sequence, allowing a better evaluation of the interactions between the atmosphere, ocean and land systems, and modeling validation (e.g., Hernandez et al., 2021). Furthermore, extreme episodes of iceberg calving, such as the Heinrich events of the last glacial cycle or the Heinrich stadial-type events up to the middle Pleistocene, when subpolar fronts experimented marked southward displacements down to 40°N (e.g., Eynaud et al., 2009; Naughton et al., 2009; Rodrigues et al., 2011), are known to lead coastal upwelling weakening or cessation by the southward incursion of iceberg-melting waters (e.g., Ausín et al., 2020; Voelker et al., 2010).

The interval between the Marine Isotope Stages (MIS) 12 to 9 (from 450 to 320 ka) is a key period of contrasted warm and cold stages associated with different baseline conditions (i.e., orbital, ice volume, CO<sub>2</sub>). It encompasses the Mid-Brunhes event during the glacial/interglacial Termination V (MBE, MIS 12/11, ~430 ka), one of the most puzzling transition of the last 1 million years leading to interglacials marked by warmer climates and higher atmospheric concentrations of pCO<sub>2</sub> than previous interglacials (Barker et al., 2006; Jansen et al., 1986; Jouzel et al., 2007). As such, the full interglacials MIS 11c and MIS 9e were characterized by extreme warming and early temperature maxima, long-lasting stable climate conditions, greenhouse gas concentrations over the pre-industrial Holocene levels, and higher-than-present sea level (McManus et al., 1999; Petit et al., 1999). Indeed, these interglacials have been frequently considered as potential analogs of the Holocene (e.g., Candy et al., 2014; Loutre & Berger, 2003). The later phases of MIS 11 and the inception of glacial MIS 10 is marked by abrupt millennial-scale variability contemporaneous to the ice-sheet build-up (e.g., McManus et al., 1999; Oppo et al., 1998). In contrast with MIS 10, MIS 12 is the most extreme glacial of the Pleistocene, as many marine, ice and terrestrial proxy records evidence (e.g., Lang & Wolff, 2011). A wide array of high-resolution proxy records from marine sedimentary sequences at the IbM has provided extensive knowledge on the impact of these scenarios in the North Atlantic (e.g., de Abreu et al., 2005; Martrat et al., 2007; Rodrigues et al., 2011, 2017). Among them, those from the Shackleton Site Integrated Ocean Discovery Program (IODP) U1385, located at the SW IbM, outstands by the record of millennial-scale climate variability as a prominent feature (e.g., Hodell et al., 2015; Maiorano et al., 2015; Martin-Garcia et al., 2015; Oliveira et al., 2016; Rodrigues et al., 2017). Interestingly, the hydrological fluctuations conditioned by these shifts (e.g., Rodrigues et al., 2011; Voelker et al., 2010) has been recognized to produce major changes in the phytoplankton communities in the region (e.g., Amore et al., 2012; Maiorano et al., 2015; Marino et al., 2014; Palumbo, Flores, Perugia, Petrillo, et al., 2013b). However, little is known about the impacts of such differentiated climate conditions between MIS 12 and 9 on primary productivity through atmospheric and/or hydrologically forced changes on vertical mixing and nutrient fueling.

Here, we present high-resolution calcareous nannofossil records to reconstruct variations in primary productivity and corresponding changes in surface-water dynamics between MIS 12 and MIS 9 (450–320 ka).

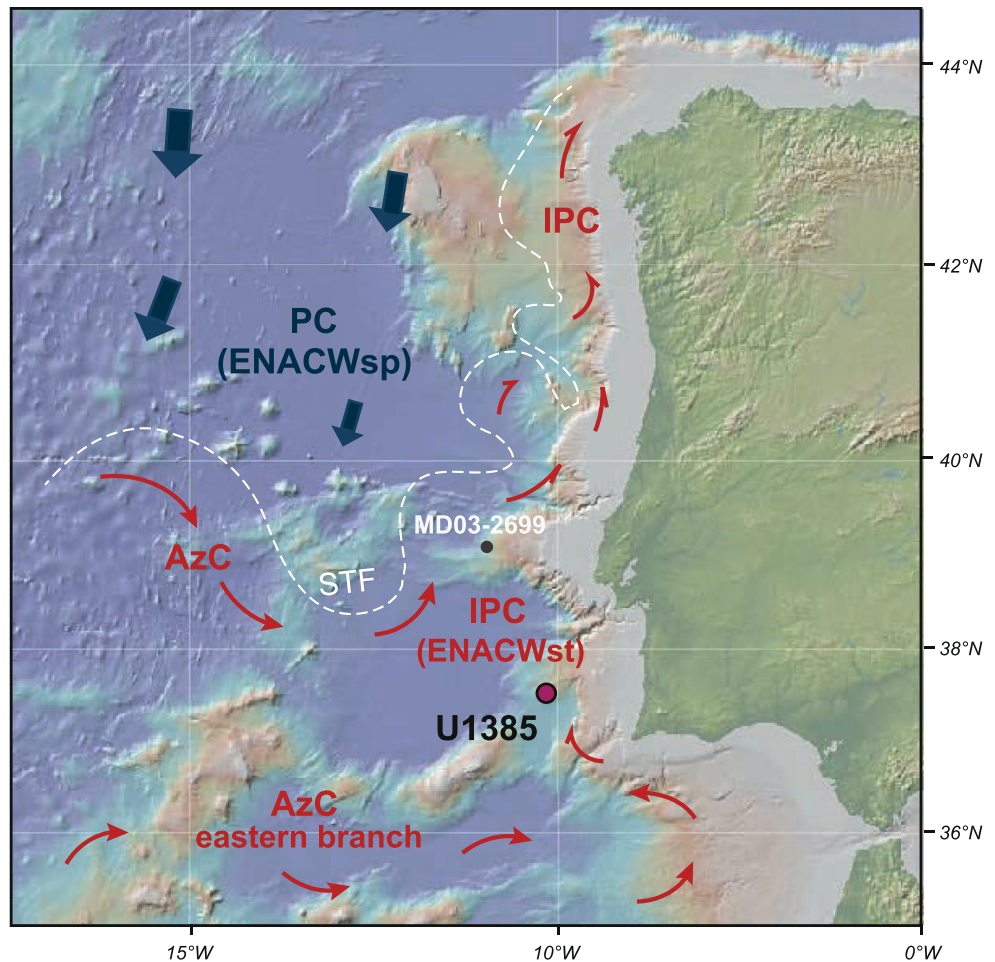


**Figure 1.** Location of IODP Site U1385 (red dot) and regional winter surface and subsurface circulation scheme off Portugal after Peliz et al. (2005). Modified from Voelker et al. (2010). AzC: Azores Current; ENACW: Eastern North Atlantic Central Water of subtropical (st) or subpolar (sp) component; PC: Portugal Current; IPC: Iberian Poleward Current and STF: Subtropical Front. Site MD03-2699 mentioned in the text is marked with a gray dot. Map source <http://www.geomapapp.org/>.

These data are compared with marine proxies such as alkenone concentration and  $U^{k_{37}}$  - Sea Surface Temperature (SST) (Rodrigues et al., 2017) and benthic and planktonic stable oxygen isotope records (Hodell et al., 2015) and terrestrial atmospherically driven vegetation changes from Site U1385 (Desprat et al., 2017; Oliveira et al., 2016; Sánchez-Goñi et al., 2016, 2020). This multi-proxy approach provides an excellent opportunity to evaluate the influence of both atmospheric and hydrological forcing in response to climate oscillations on marine primary productivity in the context of G-I to suborbital/millennial-scale variability.

## 2. The SW Iberian Margin

The SW IbM is part of the North Atlantic eastern boundary system (Figure 1). The upper 500 m of the water column, including the surface mixed layer and the upper thermocline, is constituted by the Eastern North Atlantic Central Water (ENACW; Fiúza et al., 1998; van Aken, 2001).

Surface to subsurface circulation is modulated by the atmospheric pressure gradients controlled by the relative position and intensity between the Azores High- (AH) and the Iceland Low- (IL) atmospheric pressure cells and the dominant wind patterns (Barton et al., 2001; Fiúza et al., 1998; Relvas et al., 2007). During the winter months, the AH moves southward while IL intensifies, promoting a dominant southerly wind regime over the region (Mason et al., 2005). This configuration results in coastal downwelling conditions

and enhanced northward flux of the Iberian Poleward Current (IPC; Figure 1; Fiúza, 1983). The latter is a recirculating branch of the eastern Azores Current (AzC; Figure 1) that flows northward from September/October to April/March (AzC; Figure 1; Peliz et al., 2005) and includes a subsurface subtropical component of the ENACW (ENACWst) formed by winter cooling at the Azores front (Ríos et al., 1992). As a result, relatively warmer, saltier and oligotrophic surface to subsurface waters bath the region (e.g., van Aken, 2001). During the late spring and summer months (May to September), the northward migration and strengthening of the AH toward the central Atlantic results in prevailing northerly winds. This provokes the intensification of the Portuguese Current (PC; Figure 1), a year-long southward flowing branch of the North Atlantic Current, as well as upwelling of colder and nutrient-rich subsurface waters occurs along the coast (Haynes & Barton, 1990; Peliz et al., 2005; Pérez et al., 2001). The PC involves a subsurface subpolar component of ENACW (ENACWsp) formed by winter cooling in the eastern North Atlantic (McCartney & Talley, 1982). This situation is characterized by the advection of relatively colder, fresher and nutrient-rich waters leading to high primary production (Alvarez et al., 2011; Figueiras et al., 2002; McCartney & Talley, 1982). The resulting upwelling filaments reach up to 200 km offshore (Coste et al., 1986; Fiúza, 1983), a surface distribution covering the location of the Site U1385.

### 3. Materials and Methods

#### 3.1. Core Material and Chronology

We analyzed sediment samples from Site U1385 (37°34.285' N, 10°7.562'W; 2.578 m below sea level; Figure 1) recovered by the advanced piston corer system of the RV Joides Resolution during IODP Expedition 339 in the SW IbM (Expedition 339 Scientists, 2013). Our study interval corresponds to the depth between 56.34 and 45.9 corrected revised meters composite depth (crmcD).

The lithology of the studied sediments is composed of nannofossil clays and muds, with a variable proportion of biogenic carbonates and terrigenous material (Expedition 339 Scientists, 2013).

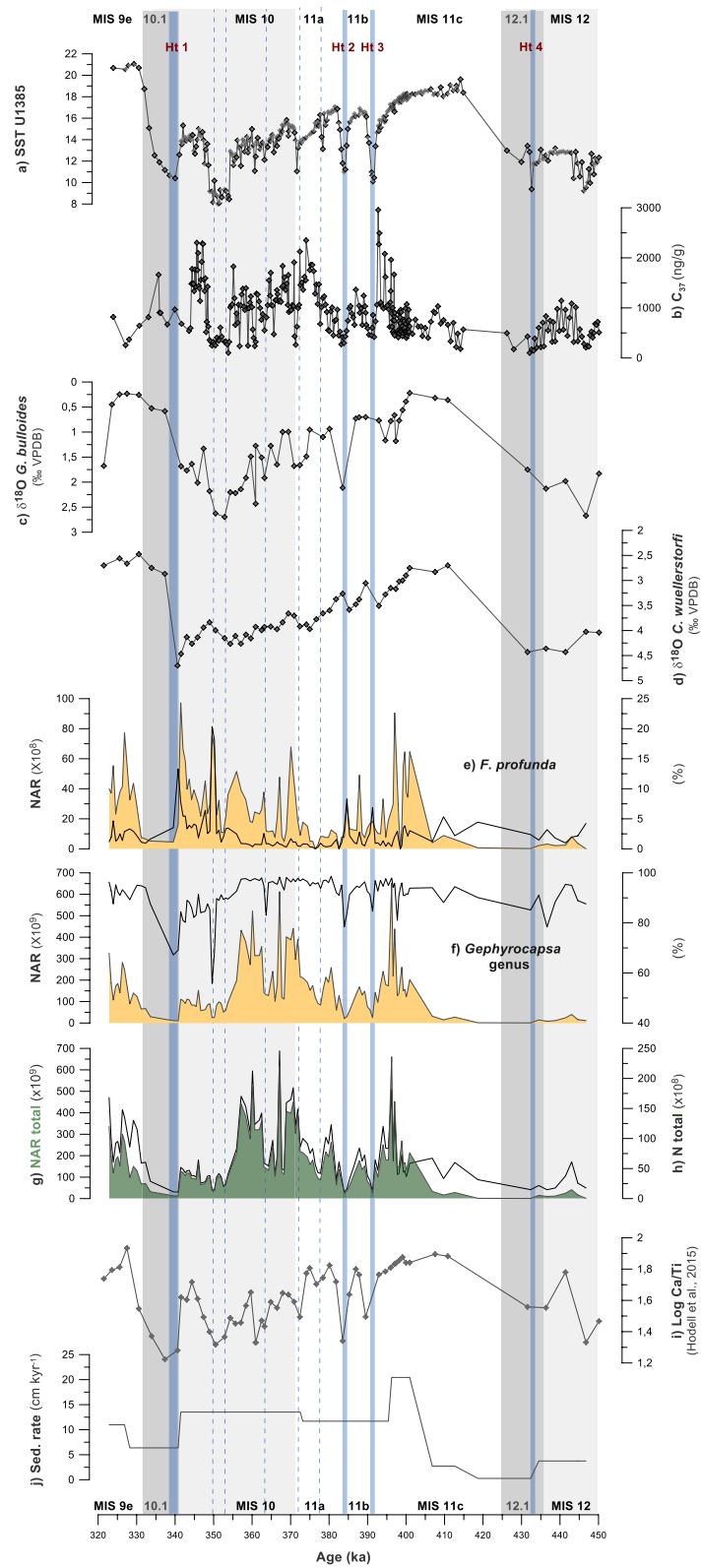
The chronostratigraphic framework followed the age model produced by Hodell et al. (2015), based on the correlation of the benthic oxygen isotope record of Site U1385 with the reference LR04 stack (Lisiecki & Raymo, 2005). The investigated interval spans from 447 ka (late MIS 12) to 323 ka (MIS 9; Lisiecki & Raymo, 2005). G/I stage identification and determination of terminal stadial events 12.1 and 10.1 (corresponding to Terminations V and IV, respectively) in the benthic  $\delta^{18}\text{O}$  followed Hodell et al. (2015). The MIS substages corresponds to the nomenclature of Railsback et al. (2015).

Extremely low sedimentation rates are recorded during Termination V and the early MIS 11c (~434–406 ka; Figure 2j), described by Hodell et al. (2015) as a condensed section or hiatus. Thus, interpretations regarding this part of the record – particularly the absolute values of proxies – must be taken with caution.

#### 3.2. Calcareous Nannofossil Analysis

For calcareous nannofossil analyses, a set of 115 samples were subsampled from Holes U1385 A and B evenly spaced every 8 cm. The corresponding temporal resolution of 0.4–0.7 ka (excluding the condensed section) provided the required high-resolution to explore in detail both orbital and millennial-scale climatic variability.

Samples were prepared following the random settling technique outlined by Flores and Sierro (1997). Coccolith identification and quantitative analysis were carried out by using a double polarized-light Nikon Eclipse 80i petrographic microscope at 1000x magnification at the University of Salamanca. A minimum of 400 coccoliths per sample were identified in a variable number of fields of view. A supplementary census count of 10 fields of view was performed to accurately determine the abundance of minor taxa accounting less than 1% of the assemblage. The abundance of specimens from older stratigraphic levels prior to the studied interval, termed reworked nannofossils, were estimated separately. A semiquantitative estimation of coccolith preservation was applied using Scanning Electron Microscope visual observation, following the criteria by Flores and Marino (2002).



Identification of coccolithophore species followed Young et al. (2003) and the guide of coccolithophore biodiversity and taxonomy Nannotax 3 ([ina.tmsoc.org/Nannotax3/index.html](http://ina.tmsoc.org/Nannotax3/index.html); Young et al., 2020). Placoliths <3  $\mu\text{m}$  of *Gephyrocapsa* genus were grouped as small *Gephyrocapsa* group following Flores, Bárcena, and Sierro (2000). This cluster mainly contains specimens of *G. aperta* and *G. ericsonii*, and those specimens with a closed central area widely considered as small *G. caribbeanica* (e.g., Saavedra-Pellitero et al., 2017). Occasional small-sized (<3  $\mu\text{m}$ ) *G. muelleriae*/*G. margereli* are, as well, included in this cluster; the specimens  $\geq 3 \mu\text{m}$  of *G. muelleriae*/*G. margereli* are considered themselves in their own group. *Coccolithus pelagicus* subspecies (subsp.) *pelagicus* corresponds to the variety of sizes <10  $\mu\text{m}$  (Geisen et al., 2002; Parente et al., 2004)

Coccolith abundances are presented as percentages (%), coccolith concentration (N; coccolith  $\text{g}^{-1}$ ) and Nannofossil Accumulation Rates (NAR; coccolith  $\text{cm}^{-2} \text{kyr}^{-1}$ ; Figures 2g and 2h). N and NAR were calculated according to Flores and Sierro (1997). In the absence of dry bulk density, NAR was calculated considering wet bulk density from the shipboard Gamma Ray Attenuation and the sedimentation rate derived from the age model (Figure 2g). Wet bulk density is regularly used to estimate coccolithophore production (see Grelaud et al., 2009; Maiorano et al., 2015; Marino et al., 2014; Stolz & Baumann, 2010).

### 3.3. Nannoplankton-Based Proxies and Primary Productivity

Total NAR is a proxy for paleoproductivity reconstruction (e.g., Baumann & Freitag, 2004), whose suitability at the IBM relies on several previous studies (e.g., Amore et al., 2012; Ausín et al., 2020; Marino et al., 2014; Palumbo, Flores, Perugia, Emanuele, et al., 2013a). Higher concentration of coccoliths in surface sediments off Portugal is associated to enhanced nannoplankton production in the overlying water column during upwelling events (e.g., Abrantes & Moita, 1999; Moita, 1993).

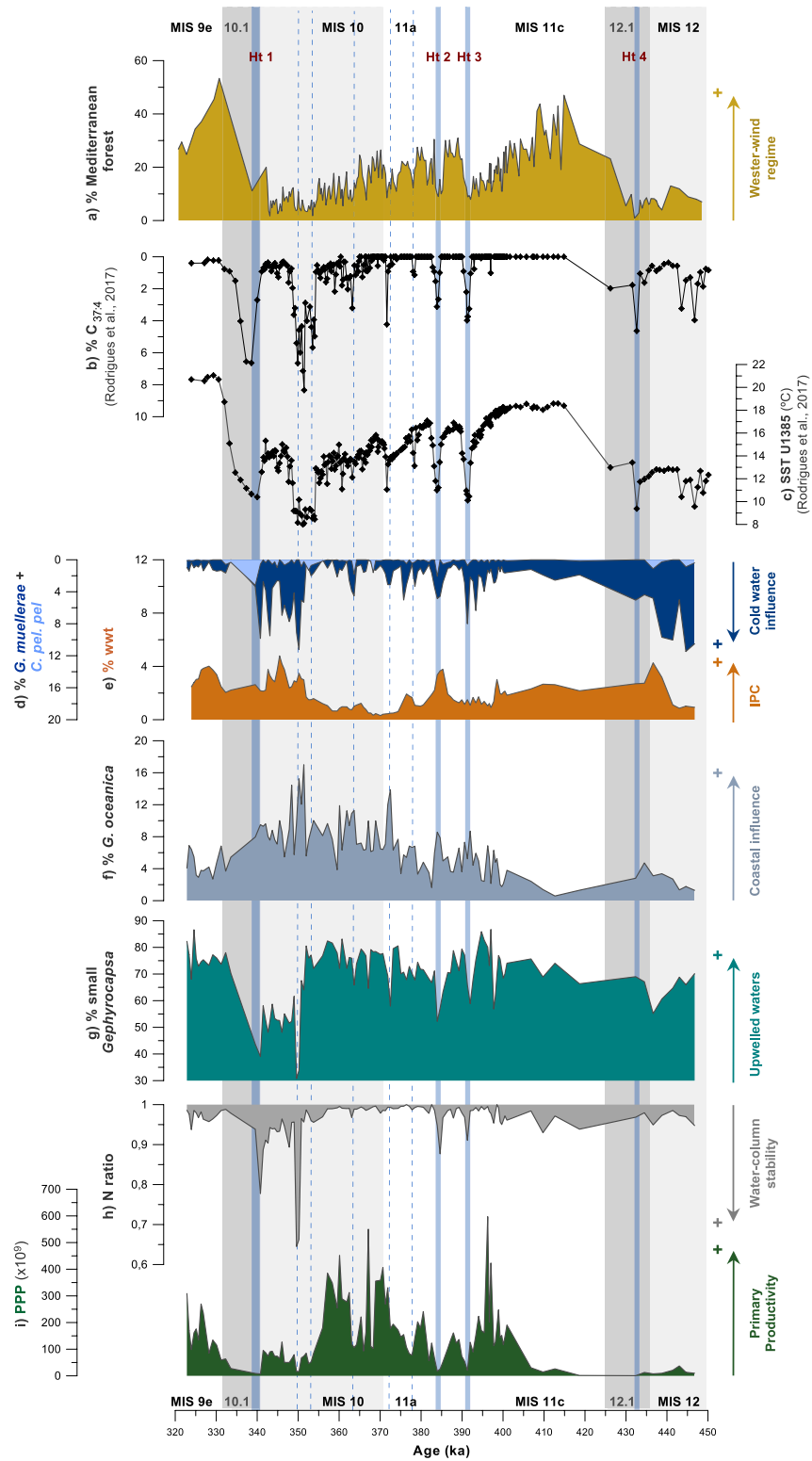
The dominant small *Gephyrocapsa* group (Section 4) is a cluster of r-strategist species with a high affinity for enhanced vertical mixing and/or the availability of highly fertilized upwelled waters in the upper water column (Gartner, 1988; Okada & Wells, 1997). The proportions of this group are here considered an indicator of the availability of highly fertilized surface waters of upwelling origin over the Site U1385. The extant *G. caribbeanica* is believed to have an affinity for ecological conditions comparable to those of the blooming *Emiliana huxleyi* (e.g., Saavedra-Pellitero et al., 2017). In the modern IBM, maximum cell densities of *E. huxleyi* are closely associated with the highest Chl-*a* concentrations (e.g., Guerreiro et al., 2014). Based on these observations, the NAR of small *Gephyrocapsa* and *G. caribbeanica* are grouped together in the primary productivity proxy (PPP; Figure 3i) to increase the accuracy of the upwelling-stimulated coccolithophore primary productivity signal. The species *Gephyrocapsa oceanica* are known to benefit from highly fertilized mature coastal upwelled waters in the modern IBM (Silva et al., 2008).

The species *Florisphaera profunda* is a common inhabitant of the lower photic zone (Kinkel et al., 2000; Okada & Honjo, 1973) widely considered as a tracer of the nutricline depth (e.g., Beaufort et al., 1997; Molino & McIntyre, 1990). We calculated the N ratio, a proxy for nutricline depth fluctuations, following Flores, Bárcena, and Sierro (2000):

$$\text{N ratio} = \text{small placoliths} / \text{small placoliths} + F. \textit{profunda}$$

Small placoliths correspond to specimens of small *Gephyrocapsa*. Higher values of N ratio (Figure 3h) are indicative of a shallower nutricline (Flores, Gersonde, et al., 2000), implying increased availability of nutrients in surface waters.

**Figure 2.** Calcareous nannoplankton content in the sedimentary record in comparison with sedimentological and geochemical data at Site U1385. (a) Alkenone-based Sea Surface Temperature (SST; Rodrigues et al., 2017). (b) Total alkenone [ $\text{C}_{37}$ ] concentration [ng/g]. (c) Planktic oxygen isotopes ( $\text{‰ VPDB}$ ) from *G. bulloides* (Hodell et al., 2015). (d) Benthic oxygen isotopes ( $\text{‰ VPDB}$ ) from *Cibicoides wuellerstorfi* (Hodell et al., 2015). Nannofossil Accumulation Rates (NAR; [coccolith  $\text{g}^{-1} \text{kyr}^{-1}$ ]) and relative abundances (%) of (e) *Florisphaera profunda* and (f) *Gephyrocapsa* genus. (g) Nannofossil Accumulation Rates (NAR; [coccolith  $\text{g}^{-1} \text{kyr}^{-1}$ ]) of the total assemblage. (h) Number of coccoliths per gram of sediment (N; [coccolith  $\text{g}^{-1}$ ]) of the total assemblage. (i) Log Ca/Ti (Hodell et al., 2015) and (j) Sedimentation rate ( $\text{cm kyr}^{-1}$ ). Blue bands represent the Heinrich-type (Ht) events 1 to 4 and dashed lines represent other major drops in temperature mentioned in the text.



The species *Oolithotus* spp., *Umbilicosphaera sibogae*, *Umbilicosphaera foliosa* (both grouped here as *Umbilicosphaera* spp.), *Syracosphaera* spp., *Rhabdosphaera clavigera*, *Umbellosphaera* spp. and *Calciosolenia* spp. were lumped together as the warm water taxa (wwt) group (e.g., Amore et al., 2012). This group has a common ecological affinity for tropical to subtropical surface waters (e.g., Baumann et al., 2004; Boeckel & Baumann, 2004; Cachão et al., 2000; Winter, 1994). At the SW IbM, these species are typical in late summer/autumn assemblages (Cachão et al., 2000; Moita et al., 2010; Silva et al., 2008, 2009), tracing the subsurface influence of ENACWst (Fiúza, 1983). Following previous studies (e.g., Amore et al., 2012; Maiorano et al., 2015; Marino et al., 2014; Palumbo, Flores, Perugia, Petrillo, et al., 2013b), the relative abundance of this group in sediments has been already proposed to estimate the influence of the northward flowing IPC and the associated surface to subsurface conditions of lowered nutrient concentration at the studied latitudes. Both, *Gephyrocapsa muelleriae* and *C. pelagicus* subsp. *pelagicus*, are typical markers of cold and less saline surface waters of polar to subpolar origin reaching the IbM latitudes (e.g., Amore et al., 2012; Balestra et al., 2017; Maiorano et al., 2015; Marino et al., 2014; Rodrigues et al., 2010). We consider the relative abundance of these cold temperature-sensitive coccolithophore species to trace the southward displacements of the polar front (PF) and cold-water influence over the studied latitudes.

### 3.4. Organic Biomarker Analysis

Alkenones are organic biomass compounds synthesized by certain coccolithophore species from the coccolithophore Noëlaerhabdaceae family that remain preserved in sediments (Volkman et al., 1980). The species composing the *Gephyrocapsa* genus are considered to be the main alkenone producers during the studied interval (see Marlowe et al., 1990).

The analytical procedure used for determining alkenone content in sediments is described in detail elsewhere (see Rodrigues et al., 2009; Villanueva et al., 1997). Biomarker analyses were performed in the laboratory of Biogeochemistry at Div.GM-IPMA in 307 sediment levels sampled from Holes U1385 D and E, every 3–4 cm between 56.54 to 46.02 crmd. The total organic compounds were extracted and separated using organic solvents, then identified using Bruker Mass spectrometer detector and quantified with Varian Gas chromatograph Model 3800 equipped with a septum programmable injector and a flame ionization detector with a CPSIL-5 CB column. The concentration of alkenones were determined using *n*-hexatriacontane as an internal standard.

Following different authors (Schubert et al., 1998; Schulte et al., 1999; Villanueva et al., 1998, 2001), the total alkenone concentration [ $C_{37}$ ] could be representative of the phytoplankton paleoproductivity in open ocean areas.

## 4. Results

### 4.1. Nannofossil Assemblages and Proxies

Coccolithophore assemblages at Site U1385 are dominated by *Gephyrocapsa* genus (91.3% on average; Figure 2f). The PPP records  $155 \times 10^9$  coccoliths  $\text{cm}^{-2} \text{kyr}^{-1}$  on average, in the range of previous studies in the region that include this interval of high clacareous nannoplankton production (e.g., Marino et al., 2014). Maxima values are recorded during the late MIS 11, centered at 397 ka, and MIS 10, between 374 and 355 ka, whereas low-to-intermediate values are registered (i) until 400 ka during the early MIS 11c and (ii) MIS 9e, from 332 ka toward the end of the studied interval. Lowest PPP are recorded: (i) throughout the late MIS 12 and TV, between 445 and 425 ka, (ii) in two short episodes centered at 391 and 384 ka during the late MIS 11, and (iii) late MIS 10 and TIV, between 355 and 332 ka (Figure 3i).

**Figure 3.** Atmospheric and oceanographic proxies at the Site U1385. (a) Relative abundances (%) of mediterranean forest pollen (Desprat et al., 2017; Oliveira et al., 2016; Sánchez Goñi, 2016, 2020). (b) Relative abundances (%) of tetra-unsaturated alkenone ( $C_{37:4}$ ; Rodrigues et al., 2017). (c) Alkenone-based Sea Surface Temperature (SST; Rodrigues et al., 2017). Relative abundance (%) of (d) *G. muelleriae* + *C. pelagicus* subsp. *pelagicus*; (e) warm water taxa (wwt; smoothed curve); (f) *G. oceanica* and (g) small *Gephyrocapsa*. (h) N ratio. (i) Primary productivity proxy (PPP;  $\text{NAR small } Gephyrocapsa \times 10^9 + \text{NAR } Gephyrocapsa \text{ caribbeanica} \times 10^9$  [coccolith  $\text{cm}^2 \text{kyr}^{-1}$ ]). Substages are indicated according to Railsback et al. (2015). Blue bands represent the Heinrich-type (Ht) events 1 to 4 and dashed lines represent other major drops in temperature mentioned in the text.



The contribution of *F. profunda* accounts for 2.3% of the total assemblage on average, reaching values over 5% at 409, 391 and 384 ka during MIS 11, and at 350 and 341 ka during MIS 10 and MIS 10/MIS 9 transition (Figure 2e). The N ratio oscillates slightly around 0.9 throughout most of the record (Figure 3h). In general, the highest N ratio  $\sim 0.95$  accompanies periods of PPP maxima, while lowered values under 0.9 are identified as short-term episodes together with PPP reductions (Figures 3h and 3i). The lowest N ratio  $\sim 0.6$ , which correspond to the highest percentages of *F. profunda*, are recorded during the MIS 10/MIS 9 transition (TIV) and are accompanied by increases in the NAR of *F. profunda* (Figures 2e and 3h).

Relative abundance of small *Gephyrocapsa* averages 69.2% (with maxima and minima of 86.62% and 30.73%, respectively) through the studied interval, with substantial reductions only recorded during short episodes around 425 ka of the late MIS 12; 397, 391 and 384 ka at MIS 11; 371 ka at MIS 11/MIS 10 and within a more continuous and much lower reduction toward values below 50% between 350 to 338 ka, across MIS 10 (Figure 3g). The percentages of *G. oceanica* averages 6.2% and evidence a strong control for G/I variability (Figure 3f). There is a marked progressive increasing trend from minima values below 5% at the full interglacial MIS 11c to maxima values  $\sim 18\%$  at 350 ka during MIS 10 (Figure 3f). Short-term increases are in phase with rapid reductions in % of small *Gephyrocapsa* (Figures 3f and 3g).

The wwt is recorded in low proportion (0.86% on average). The profile is characterized by higher abundances during the late glacial to interglacial periods MIS 12 to MIS 11 ( $\sim 443$ – $400$  ka) and MIS 10 to MIS 9 ( $\sim 352$ – $320$  ka). Lowest values are observed between  $\sim 375$  and  $352$  ka during the MIS 11/10 transition (Figure 3e). Percentages of *G. muelleriae* + *C. pelagicus* subsp. *pelagicus*, with contribution to assemblages of, respectively 2.9% and 0.3%, evidence a pattern of short-term moderate increases, with summed values slightly over 10% between  $\sim 446$  and  $431$  ka during MIS 12, from  $\sim 391$  to  $384$  ka during late MIS 11,  $\sim 364$  ka during MIS 10 and a more continuous increase between  $\sim 352$  and  $339$  ka over late MIS 10 and TIV (Figure 3d).

#### 4.2. Alkenone-Based Paleoproductivity

Total alkenone concentration [ $C_{37}$ ] changes between 101.95 and 2955.57 ng/g through the record, evidencing a pattern of high frequency variability (Figure 2b). The maximum values are detected at the intervals between 396 and 393 ka during the late MIS 11c, 374–355 ka during the MIS 11/10 transition and 347–345 ka at MIS 10. The lowest alkenone concentrations are recorded between 432 and 427 ka during the terminal stadial 12.1, at 414 ka at MIS 11c, at 391, 384 ka during late MIS 11 and between 371 and 353 ka during MIS 10 (Figure 2b).

### 5. Discussion

The overall G-I variability observed in the PPP record is superimposed by millennial-scale changes (Figure 3i), concomitant to oscillations in other nannoplankton-based proxy records, SST (Rodrigues et al., 2017) and Mediterranean forest percentage profiles from Site U1385 (Desprat et al., 2017; Oliveira et al., 2016; Sánchez Goñi et al., 2016, 2020; Figures 3a and 3c). In general, high PPP values coincide with reduced Mediterranean forest development, (i.e., cold and weak winter precipitation, and low SST during glacials) whereas interglacials are marked by lower PPP values and significant expansion of the Mediterranean forest (i.e., warm and wet winters, and warm SST; Rodrigues et al., 2017; Figures 3a, 3c and 3i).

A prominent feature in our record is the occurrence of abrupt cold events, primarily recognized as abrupt drops in SST (Rodrigues et al., 2017) having a large impact on PPP, which shows substantial reductions (Figures 3c and 3i). The occurrence of Heinrich-type (Ht) events 1 to 4 ( $\sim 436$ , 392, 384 and 339 ka) is recognized by the record of abrupt drops in SST together with increased %  $C_{37:4}$  (Rodrigues et al., 2017) in comparison with the reference record by Rodrigues et al. (2011) at MD03-2699 (blue bands in Figures 2 and 3). Other short-term SST drops previously described by (Rodrigues et al., 2011;  $\sim 372$ , 350 and 355 ka), or observed in the temperature record for this interval (Rodrigues et al., 2017;  $\sim 378$  and 364 ka) are here identified to have a similar correspondence with lowered PPP (dashed lines in Figures 2 and 3). All these short-term episodes are also detected in the terrestrial realm by strong contraction of the Mediterranean forest, (i.e., winter precipitation decrease, colder atmospheric temperatures; Figure 3a).

The detailed assessment of the control mechanisms on primary productivity in the area of study requires multiple non-excluding influencing factors to be considered: (i) changes in the dominant wind systems and wind-stress stimulating vertical mixing (e.g., Incarbona et al., 2010; Pailler & Bard, 2002); (ii) the nutrient content of the subsurface waters fueling the upwelling (e.g., Palumbo, Flores, Perugia, Petrillo, et al., 2013b); (iii) shifts in the regional hydrological configuration and associated surface-nutrient transport (e.g., Amore et al., 2012; Maiorano et al., 2015; Palumbo, Flores, Perugia, Emanuele, et al., 2013a); (iv) changes in the extension and/or offshore displacement of the coastal upwelling influence area (e.g., Salgueiro et al., 2014); (v) arrival of iceberg-melting waters leading to vertical mixing weakening or even cessation, as observed during extreme deglacial episodes (e.g., Voelker et al., 2009).

In the following sections we provide a detailed discussion about these records and the main processes at hand during G/I cycles, and millennial-scale timescales.

### 5.1. Atmospheric Patterns Driving Primary Productivity During Interglacials

The parallelism observed between primary productivity, hydrological and atmospheric records (Figure 3) suggests that, as demonstrated for the modern setting (e.g., Guerreiro et al., 2014; Lopes et al., 2009; Oliveira et al., 2009), the intensity and position of the Azores High (AH) pressure cell played a significant role on the vertical mixing and surface nutrient availability at the IbM over different timescales.

Present-day and past changes in the Mediterranean forest composition and development are mainly controlled by winter precipitation and seasonal climate contrast, reflecting changes in the position of the west-erlies led by the AH during the winter (Gouveia et al., 2008; Naughton et al., 2009; Oliveira et al., 2018). According to Oliveira et al. (2016), the expansion of the Mediterranean forest, as observed during the early full interglacials MIS 11c and 9e (values over 20%; Figure 3a), is indicative of higher winter precipitation, which, in turn, indicates increased influence of the westerly wind systems and related southward winter position of the AH (Figure 4a). Conversely, forest reductions without a counterpart cooling in the SST, as recorded during the late phase of MIS 11c (Rodrigues et al., 2017; Figures 3a and 3c), are associated with an intensified and northward positioned AH during the winter, with consequent reduction of large-scale winter precipitation in SW Iberia (Oliveira et al., 2016; Figure 4b).

Today, the North Atlantic and Iberian climate are closely coupled through the North Atlantic Oscillation (NAO), the variable pressure gradient between the AH and Icelandic Low (IL) centers during the winter season (Hurrell, 1995; Hurrell et al., 2003). A negative (−) NAO mode implies a weakened North Atlantic atmospheric circulation and the southward displacement of the westerly wind systems down to southern Europe and North Africa during winter (Figure 4a). During a positive (+) NAO mode, the North Atlantic atmospheric circulation is strengthened during the winter and the westerly wind systems are displaced further north (Figure 4b; Hurrell, 1995; Trigo et al., 2002). Consequently, the regional seasonal atmospheric circulation is modulated at decadal to centennial timescales and causes a regional hydrological impact, implying an intensified winter northward IPC, as the result of the southward position and weakening of AH (Barton et al., 2001; Haynes & Barton, 1990; Figure 4a). The prevalence of northerly trade wind regime aside the summer season during + NAO (Figure 4b) has been shown to increase the frequency of the upwelling events in the region (e.g., Alvarez et al., 2009; Barton, 2001; Silva et al., 2008; Vitorino et al., 2002).

#### 5.1.1. Early Interglacials

The early interglacial substages at MIS 11c (~420–400 ka) and MIS 9e (~337–320 ka) are characterized by low to intermediate PPP and a relatively deep nutricline with moderate surface nutrient availability (Figures 3g–3i), also supported by a reduction in the  $C_{37}$  alkenone concentration (Figure 2b). These conditions suggest a substantial weakening in the upwelling regime by a weaker northerly trade influence over SW Iberia due to the winter southern position of AH and enhanced westerly influence (Figures 3a and 4a). Such conditions probably led to moderate surface-water stratification, resulting in a prolonged warming of surface waters (Figure 3c). Surface to subsurface oligotrophy and decline in regional vertical mixing were also promoted by the long-term intensified influence of the winter IPC and ENACWst (Figure 3e) and, potentially, by a shallower position of this subsurface water mass system in absence of a strong northerly trade influence during winter (Barton, 2001; Figure 4a). The hampering effect of this hydrological configuration seems to reduce, as well, the arrival of nutrient-rich waters from the PC and/or surface offshore transport

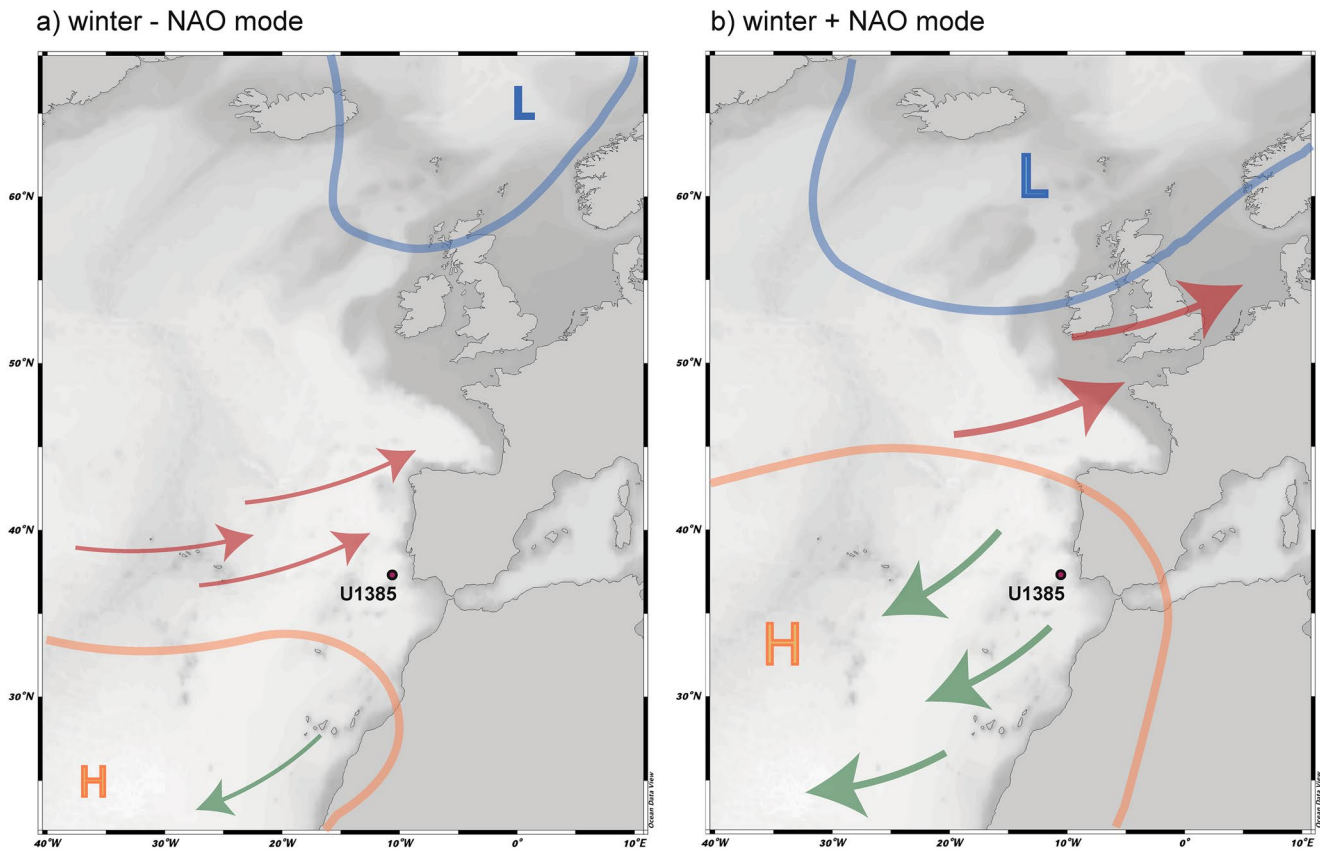


**Figure 4.** Simplified scheme of the modern patterns of the intensity and position of the Azores anticyclone high-pressure cell (AH) and associated wind regimes at the Iberian Margin (IbM) during the winter entailed by the modern North Atlantic Oscillation (NAO) variability, as in Wanner et al. (2001). Arrow thickness indicates intensity of wind systems. Red: westerly wind system; green: northerly trades. (a) Winter weakening and southward movement of the AH during a negative (–) NAO mode. (b) Winter intensification and northward movement of the AH during a positive (+) NAO mode.

from the neighbor coastal upwelling, a fact that is also sustained by the reduced % *G. oceanica* together with the increased % wwt (Figures 3f and 3e); this later group has been considered to trace intensified ENACWst water mass transport towards Iberia during the winter (e.g., Cachão et al., 2000). Ultimately, both interglacial sea-level high stands during the early MIS 11c and MIS 9e (Rohling et al., 2009) exclude any offshore displacement of the coastal upwelling cells through the position of the Site U1385. A recently suggested increased influence of nutrient-poorer subtropical waters during the full interglacial MIS 11 and 9 to the north of our Site (Cavaleiro et al., 2020) is consistent with our observations. As well, similar primary productivity scenario and associated upwelling conditions was described at the IbM during other more recent interglacial periods (i.e., MIS 5; Pailler & Bard, 2002) and the Holocene (Incarbona et al., 2010).

By analogy with the present-day conditions, the enhanced winter westerlies influence over the IbM, reconstructed during the early stages of interglacials MIS 11c and 9e (Figures 3a and 4a), suggest a control of a prevalent winter – NAO-like (Figure 4a), reducing primary productivity at Site U1385 by the balanced restriction of the upwelling season and associated fertilization processes to the summer months, when the AH intensification occurred.

### 5.1.2. Intra-Interglacial Shift to the Late MIS 11c

The late phase of the full interglacial MIS 11c (~405–392 ka) is characterized by a shift to high PPP corresponding to a shallow nutricline and consequent increased surface nutrient availability in comparison to the early phase of this substage (Figures 3g–3i). This is also supported by progressively increased  $C_{37}$  alkenone concentration (Figure 2b). Increased percentages of cold temperature-sensitive coccolithophore taxa (Figure 3d) are consistent with slightly cooler surface waters. By contrast, the SST record shows a moderate ocean cooling toward the end of the full interglacial (Rodrigues et al., 2017; Figures 3c and 3d).

A reduced influence of the oligotrophic IPC during the winter (Figure 3e) might have provoked a regional eutrophication. The high % of small *Gephyrocapsa* (Figure 3g) characterizes, beyond the general availability of upwelled surface waters, a link for these conditions with an enhanced influence of the nutrient-richer PC (e.g., Amore et al., 2012; Palumbo, Flores, Perugia, Petrillo, et al., 2013b).

A more intense and northernmost positioned AH during winter reduced the westerly influence (Figure 3a) and enhanced the winter northerly trades, that may progressively extend its effect over SW Iberia (Figure 4b). As proposed by Oliveira et al. (2016), this intra-interglacial shift (Figure 3a) without a counterpart cooling in the SST (Rodrigues et al., 2017; Figure 3c) could be explained by a progression toward the prevalence of a + NAO mode (Figure 4b). In agreement with present day observations in the region (e.g., Alvarez et al., 2009; Barton, 2001; Silva et al., 2008; Vitorino et al., 2002), an increased frequency of the upwelling events beyond the summer season is observed coupled to the positive modes of the modern NAO. The increased effect of northerly trades by maintained AH northward position is here interpreted with the prevalence of a + NAO-like mode (Figures 3a and 4b), considered responsible of the enhanced upwelling and increased PPP in a comparable way to the modern conditions. Additionally, widening of the coastal upwelling zones could have occurred as a result of strengthened atmospheric circulation (e.g., Pailler & Bard, 2002), complementary favoring the conditions for primary productivity at Site U1385.

The effect of this intra-interglacial atmospherically shift at the full interglacial MIS 11c over primary productivity records has been similarly identified in the Alboran Sea (González-Lanchas et al., 2020) at around 406 ka via enhanced western Mediterranean circulation and complete upwelling development controlled by this atmospheric shift towards a prevalent + NAO-like configuration.

## 5.2. Enhanced Primary Productivity at the Onset of Glacial MIS 10

The interval spanning from ~392 to 356 ka from the late MIS 11 to early full glacial MIS 10 (inception to glacial MIS 10) is characterized by a long-term increase in PPP and a shallow nutricline with enhanced surface nutrient availability (Figures 3g–3i), also supported by relatively high values in C<sub>37</sub> alkenone concentration (Figure 2b). A progressively reduced influence of the AzC waters through the IbM by reduced IPC effect over the studied area during the beginning of MIS 10 is observed from the lowered % wwt (Figure 3e) along with a gradual SST cooling (Rodrigues et al., 2017; Figure 3c).

Growing of ice sheets toward the glacial period, as recorded by the long-term trend toward heavier values of benthic  $\delta^{18}\text{O}$  (Figure 2d) in agreement with other isotopic records (e.g., Elderfield, et al., 2012; Lisiecki & Raymo, 2005) and the sea-level stack of Spratt and Lisiecki (2016), probably led to an increased meridional air pressure gradient between the high and low latitudes in the North Atlantic (Keffer et al., 1988; Ruddiman, 1977). This atmospheric trend and the climate shift toward cooler and drier conditions in SW Iberia affected the regional vegetation, as evidenced by the reduction of the Mediterranean forest (Figure 3a). Nonetheless, this vegetation pattern toward the glacial (Figure 3a) cannot be solely interpreted as the result of a reduction in the winter humidity (Figure 4), as evidenced by the parallel reduction in SST throughout the glacial onset (Rodrigues et al., 2017; Figure 3c). However, the higher wind stress during transitional and glacial phases is considered a crucial factor determining intensified wind-driven upwelling at the North Atlantic eastern boundary system (e.g., Abrantes, 2000; Bradtmiller et al., 2016; Pailler & Bard, 2002; Romero et al., 2008; Sarnthein et al., 1988). This process could explain the increased PPP and high nutrient content in surface waters through this interval (Figures 3g–3i). Models for the LGM suggest intensification in the AH and the IL (e.g., Hewitt et al., 2001); in this sense, strengthening of the northerly trades over the IbM could explain the enhanced upwelling in a comparable way that the record by Pailler and Bard (2002) at the onset of glacials MIS 4 and 2 at MD9-2042.

Strengthened wind-stress together with reduced winter IPC (Figure 3e), promoting the maintained influence of the surface PC, is considered, as well, to result in the prevalent upward advection of deeper and nutrient-richer subsurface ENACWsp fueling the regional upwelling. This observation is in agreement with nutrient-richer surface waters favoring coccolithophore proliferation against diatoms discussed by Cavaleiro et al. (2020) at the nearby site MD03-2699. Additionally, the strengthened atmospheric circulation could have resulted in substantial widening of the coastal upwelling (e.g., Pailler & Bard, 2002), benefiting eutrophication at Site U1385 due to greater proximity of the upwelled filaments (or area of influence of the upwelling). Ultimately, we cannot discard the possible impact of an offshore displacement of the coastal upwelling cells

during the long-term sea-level drop through glacial MIS 10 (Rohling et al., 2009). The increased percentages of *G. oceanica* toward MIS 10 from the MIS 11 transition (Figure 3f) could be a potential indicator of an increase in the coastal influence, entailing coastal upwelling processes, over the studied location. A similar process was already proposed by Salgueiro et al. (2014) for the LGM. The considerable increase in coccolith accumulation and primary productivity through this interval in comparison with more inshore locations at the early MIS 10 (e.g., Amore et al., 2012; Palumbo, Flores, Perugia, Petrillo, et al., 2013b) supports this process.

Summarizing, a scenario comparable to that observed during the LGM (Ausín et al., 2020; Incarbona et al., 2010; Salgueiro et al., 2014) is proposed for the inception of glacial MIS 10 and the early full glacial MIS 10, in which the enhanced PPP is considered to be the result of several potentially active mechanisms intensifying fertilization due to either increased wind-induced upwelling, increased nutrient content in the source of upwelling and/or enhanced surface nutrient arrival to the Site U1385.

### 5.3. Impact of Surface Water Conditions on Primary Productivity During Abrupt Cold Events

The availability of upwelled waters reaching Site U1385 is constant through almost the entire interval (Figure 3g), driving eutrophication of the uppermost water column where the dominant *Gephyrocapsa* species inhabits. However, significant reductions in surface water fertilization occurred during the Ht events 4 to 1 (~436, 392, 384 and 339 ka) and other short-term cold episodes, reflected as abrupt decreases in PPP, also supported by reduced  $C_{37}$  alkenone concentration, and limited nutrient availability, as recorded by the lowered values in the N ratio and decrease in % *small Gephyrocapsa* (Figures 2d and Figures 3a–3i). The higher percentages of cold-water coccolithophore species (Figure 3d) together with severe SST coolings and increased % of  $C_{37:4}$  (Rodrigues et al., 2017; Figures 3c and 3b) suggest pronounced southward shifts of the PF. The influence of ice rafting and the presence of meltwaters at the studied latitudes during extreme cooling events at the studied interval has been already detailed and discussed (de Abreu et al., 2005; Rodrigues et al., 2011, 2017; Voelker et al., 2010). The observed decrease in Ca/Ti (Figure 2h) is indicative of the reduction in carbonate burial, as a result of the reduced surface production (Figures 2b and 3i), but also of the enhancement in detrital input (Hodell et al., 2013, 2015).

Extreme continental aridity and cold atmospheric conditions on land during Ht 4, 3 and 2 (Oliveira et al., 2016; Sánchez Goñi et al., 2016) are here similarly recognized by the abrupt reduction of the Mediterranean forest (Figure 3a) together with low SST (Rodrigues et al., 2017; Figure 3c) during Ht 1, and probably during the other short-term abrupt coolings during the glacial inception of MIS 10 (Figures 2 and 3; dashed lines). The prevailing northerly trade regime over SW Iberia from the extended aridity indicated by the pollen record (Figure 3a) is expected to intensify the coastal upwelling, however, this notion contrast with the lowest PPP and the reduced surface nutrient availability recorded during these episodes (Figures 3f–3i).

The rapid evolution toward surface subpolar cold-water conditions is known to result in unfavorable conditions for calcareous nanoplankton growth in the region (i.e., cold, turbid, and low salinity; see Maiorano et al., 2015; Marino et al., 2014 and references therein). In particular, the higher abundances of *F. profunda* (Figure 2e) in the North Atlantic during the occurrence of Heinrich events are consistent with enhanced upper water-column stability (e.g., Colmenero-Hidalgo et al., 2004; Marino et al., 2014). Synchronous short-term increases in the relative abundances of *G. oceanica* (Figure 3f) could be tentatively interpreted as the effect of a reduction in surface-water salinity (Ausín et al., 2015; Jordan & Winter, 2000) in response to the freshwater advection. However, as suggested by previous authors, a better adaptation of this *Gephyrocapsa* species by means of vertical migration and affinity of this species to deeper water layers in the proximity of the thermocline (e.g., Girardeau et al., 1993), or the variable tolerance of hypothetical sub-species included in this group (e.g., Andrulleit et al., 2003) could not be discarded. The formation of a halocline led by surface freshening, as occurred during the Heinrich events of the last glacial cycle (see Voelker et al., 2009), could explain the recorded conditions where, despite a plausible favorable wind stimulation (Figure 3a), the water column vertical structure with a shallower mixed layer separated from deep nutrient-rich levels would reduce the upward nutrient transference. As in Voelker et al., (2009), the presence of higher-temperature ENACWst underneath the halocline could particularly explain the favorable thermal conditions for the proliferation of *F. profunda* (Figure 2d) and the eventual increases in % wwt observed during the occurrence of these episodes (Figure 3e).

The most extreme and long-lasting of these conditions occurred between 350 ka, at the end of MIS 10, and TIV at the onset of MIS 9 (Figure 3). As previously pointed out (Maiorano et al., 2015), there is a good correspondence of these conditions at ~ 349 ka with IRD deposition at MD01-2446 (Voelker et al., 2010) and Site U1313 (Naafs et al., 2011, 2013; Stein et al., 2009), suggesting analogous conditions with a Heinrich stadial. During the late glacial MIS 12 and TV, despite important SST cooling is solely recorded at ~445 and Ht4 (Rodrigues et al., 2017; Figures 3b and 3c), the PPP, N ratio and cold-water coccolithophore species (Figures 3d and 3h) evidence an important reduction in surface production and implementation of surface subpolar conditions between 445 and 425 ka (Figure 3). Among both Terminations, conditions of primary productivity after cold deglacial episodes seems to be more rapidly increased after TIV toward MIS 9 (Figure 3), while TV show a more persistent limited surface-nutrient fertilization into the MIS 11 (Figure 3).

Overall, productivity reduction and associated hydrological and paleoceanographic conditions observed during these abrupt cold events of different duration for the studied interval impacted nanoplankton assemblages on a regional level, as proven by the consistency of our record with that from core MD03-2699 (Cavaleiro et al., 2020). The mechanism that reduces primary productivity is probably comparable to that proposed during the Heinrich episodes of the last glacial (e.g., Ausin et al., 2020; Incarbona et al., 2010).

## 6. Conclusions

Changes in primary productivity related to variation in wind-induced upwelling at the Site U1385 at the SW IbM during the MIS 12 to 9 interval are reconstructed from the study of calcareous nanoplankton assemblages. The integration with previously published SST and pollen-based vegetation and climate records at the same site evidence that the environmental conditions controlling phytoplankton production were largely influenced by the prevailing atmospheric configuration. During the early stages of the full interglacial MIS 11c (~420–405 ka) and MIS 9e (~337–320 ka), moderate primary productivity and surface nutrient availability is the result of reduced vertical mixing and offshore nutrient transport by a restriction of the upwelling stimulation to the summer months own by an atmospheric configuration comparable to a prevailing – NAO-like mode. The full interglacial MIS 11c registers a shift to increased primary productivity and surface nutrient availability (~405–392 ka), which is attributed to an intra-interglacial AH intensification beyond the summer comparable to a progression to prevailing + NAO modetowards the end of MIS 11. Enhanced primary productivity and surface nutrient availability through the inception and early MIS 10 (~392–356 ka) indicate upwelling offshore displacement and intensification in the context of strengthened atmospheric circulation during the glacial transition. Significant abrupt reductions in primary productivity and enhanced surface stability are identified during the occurrence of Heinrich-type (Ht) events 4 to 1 (~436, 392, 384 and 339 ka), other short-term cold episodes (~378, 372, 364, 350 and 355 ka) and more prolonged during the Terminations V and IV. The establishment of cold surface subpolar conditions and increased %  $C_{37:4}$  indicates that, as during the Heinrich stadials of the last glacial cycle, the regional halocline formation induced by meltwater arrival restricted the nutrient upward advection.

## Data Availability Statement

All original data produced for this work is available at <https://data.mendeley.com/datasets/kv85rjj4y7/3> archived at the public repository Mendeley as: González-Lanchas, Alba; Flores, José-Abel; Sierro, Francisco J. (2021), “High-resolution calcareous nannofossil record between the Marine Isotope Stage (MIS) 12 to 9 from the IODP Site U1385”, Mendeley Data, V3, doi: [10.17632/kv85rjj4y7.3](https://doi.org/10.17632/kv85rjj4y7.3)”.

## References

- Abrantes, F. (2000). 200 000 yr diatom records from Atlantic upwelling sites reveal maximum productivity during LGM and a shift in phytoplankton community structure at 185 000 yr. *Earth and Planetary Science Letters*, 176, 7–16. [https://doi.org/10.1016/S0012-821X\(99\)00312-X](https://doi.org/10.1016/S0012-821X(99)00312-X)
- Abrantes, F., & Moita, M. T. (1999). Water column and recent sediment data on diatoms and coccolithophorids, off Portugal, confirm sediment record of upwelling events. *Oceanologica Acta*, 22, 319–336. [https://doi.org/10.1016/S0399-1784\(99\)80055-3](https://doi.org/10.1016/S0399-1784(99)80055-3)
- Alvarez, I., Gomez-Gesteira, M., DeCastro, M., Lorenzo, M., Crespo, A., & Dias, J. (2011). Comparative analysis of upwelling influence between the western and northern coast of the Iberian Peninsula. *Continental Shelf Research*, 31, 388–399. <https://doi.org/10.1016/j.csr.2010.07.009>

## Acknowledgments

This study was supported by the predoctoral FPU contract FPU17/03349 awarded to A. González-Lanchas by the Spanish Ministry of Science, Innovation and Universities. Essential financial infrastructure was provided by the programs RTI2018-099489-B-100 of the Spanish Ministry of Science, Innovation and Universities granted to GGO (Grupo de Geociencias Oceánicas de la Universidad de Salamanca). T. Rodrigues received funds from Portuguese National Foundation for Science and Technology FCT - through projects: Warm World (PTDC/CTA-GEO/29897/2017) and CCMAR UIDB/04326/2020. D. Oliveira acknowledges funding from Portuguese Foundation for Science and Technology (FCT) through the CCMAR Research Unit - project UIDB/04326/2020 and contract (CEECIND/02208/2017). The authors are grateful to IODP for inviting some of the coauthors to participate in Expedition 339 and providing the samples used in this study. The authors also thank two anonymous reviewers and Carlos Jaramillo, whose constructive comments and suggestions improved the quality of this study.

- Alvarez, I., Ospina-Alvarez, N., Pazos, Y., deCastro, M., Bernardez, P., Campos, M. J., et al. (2009). A winter upwelling event in the Northern Galician Rias: Frequency and oceanographic implications. *Estuarine, Coastal and Shelf Science*, 82, 573–582. <https://doi.org/10.1016/j.eess.2009.02.023>
- Amore, F. O., Flores, J. A., Voelker, A. H. L., Lebreiro, S. M., Palumbo, E., & Sierro, F. J. (2012). A Middle Pleistocene Northeast Atlantic coccolithophore record: Paleoclimatology and paleoproductivity aspects. *Marine Micropaleontology*, 90–91, 44–59. <https://doi.org/10.1016/j.marmicro.2012.03.006>
- Andruleit, H., Stäger, S., Rogalla, U., & Čepek, P. (2003). Living coccolithophores in the northern Arabian Sea: Ecological tolerances and environmental control. *Marine Micropaleontology*, 49(1–2), 157–181. [https://doi.org/10.1016/s0377-8398\(03\)00049-5](https://doi.org/10.1016/s0377-8398(03)00049-5)
- Ausin, B., Hernández-Almeida, I., Flores, J.-A., Sierro, F.-J., Grosjean, M., Francés, G., & Alonso, B. (2015). Development of coccolithophore-based transfer functions in the western Mediterranean sea: A sea surface salinity reconstruction for the last 15.5 kyr. *Climate of the Past*, 11, 1635–1651. <https://doi.org/10.5194/cp-11-1635-2015>
- Ausin, B., Hodell, D. A., Cutmore, A., & Eglinton, T. I. (2020). The impact of abrupt deglacial climate variability on productivity and upwelling on the southwestern Iberian margin. *Quaternary Science Reviews*, 230, 106139. <https://doi.org/10.1016/j.quascirev.2019.106139>
- Balestra, B., Grunert, P., Ausin, B., Hodell, D., Flores, J. A., Alvarez-Zarikian, C. A., et al. (2017). Coccolithophore and benthic foraminifera distribution patterns in the Gulf of Cadiz and western Iberian margin during Integrated Ocean Drilling Program (IODP) expedition 339. *Journal of Marine Systems*, 170, 50–67. <https://doi.org/10.1016/j.jmarsys.2017.01.005>
- Barker, S., Archer, D., Booth, L., Elderfield, H., Henderiks, J., & Rickaby, R. E. M. (2006). Globally increased pelagic carbonate production during the Mid-Brunhes dissolution interval and the CO<sub>2</sub> paradox of MIS 11. *Quaternary Science Reviews*, 25, 3278–3293. <https://doi.org/10.1016/j.quascirev.2006.07.018>
- Barton, E. D. (2001). Canary and Portugal Currents. In J. H. Steele (Ed.) *Encyclopedia of Ocean Sciences*, (pp. 380–389). Oxford: Academic Press. <https://doi.org/10.1006/rwos.2001.0360>
- Barton, E., Inall, M., Sherwin, T., & Torres, R. (2001). Vertical structure, turbulent mixing and fluxes during Lagrangian observations of an upwelling filament system off Northwest Iberia. *Progress in Oceanography*, 51, 249–267. [https://doi.org/10.1016/s0079-6611\(01\)00069-6](https://doi.org/10.1016/s0079-6611(01)00069-6)
- Baumann, K.-H., Böckel, B., Frenz, M. (2004). *Coccolith contribution to South Atlantic carbonate sedimentation, Coccolithophores*, pp. 367–402. Springer. [https://doi.org/10.1007/978-3-662-06278-4\\_14](https://doi.org/10.1007/978-3-662-06278-4_14)
- Baumann, K.-H., & Freitag, T. (2004). Pleistocene fluctuations in the northern Benguela Current system as revealed by coccolith assemblages. *Marine Micropaleontology*, 52, 195–215. <https://doi.org/10.1016/j.marmicro.2004.04.011>
- Beaufort, L., Lancelot, Y., Camberlin, P., Cayre, O., Vincent, E., Bassinot, F., & Labeyrie, L. (1997). Insolation cycles as a major control of equatorial Indian Ocean primary production. *Science*, 278, 1451–1454. <https://doi.org/10.1126/science.278.5342.1451>
- Boeckel, B., & Baumann, K.-H. (2004). Distribution of coccoliths in surface sediments of the south-eastern South Atlantic Ocean: Ecology, preservation and carbonate contribution. *Marine Micropaleontology*, 51, 301–320. <https://doi.org/10.1016/j.marmicro.2004.01.001>
- Bradt Miller, L. I., McGee, D., Awalt, M., Evers, J., Yerxa, H., Kinsley, C. W., & deMenocal, P. B. (2016). Changes in biological productivity along the northwest African margin over the past 20,000 years. *Paleoceanography*, 31, 185–202. <https://doi.org/10.1002/2015pa002862>
- Cachão, M., Oliveira, A., & Vitorino, J. (2000). Subtropical winter guests, offshore Portugal. *Journal of Nanoplankton Research*, 22, 19–26.
- Candy, I., Schreve, D. C., Sherriff, J., & Tye, G. J. (2014). Marine Isotope Stage 11: Palaeoclimates, palaeoenvironments and its role as an analogue for the current interglacial. *Earth-Science Reviews*, 128, 18–51. <https://doi.org/10.1016/j.earscirev.2013.09.006>
- Cavaleiro, C., Voelker, A. H., Stoll, H., Baumann, K.-H., & Kucera, M. (2020). Coccolithophore productivity at the western Iberian Margin during the Middle Pleistocene (310–455 ka)–evidence from coccolith Sr/Ca data. *Climate of the Past*, 16, 2017–2037. <https://doi.org/10.5194/cp-16-2017-2020>
- Colmenero-Hidalgo, E., Flores, J.-A., Sierro, F. J., Bárcena, M. A., Löwemark, L., Schönfeld, J., & Grimalt, J. O. (2004). Ocean surface water response to short-term climate changes revealed by coccolithophores from the Gulf of Cadiz (NE Atlantic) and Alboran Sea (W Mediterranean). *Palaeogeography, Palaeoclimatology, Palaeoecology*, 205, 317–336. <https://doi.org/10.1016/j.palaeo.2003.12.014>
- Coste, B., Fiuza, A., & Minas, H. (1986). Conditions hydrologiques et chimiques associées à l’upwelling côtier du Portugal en fin d’été. *Oceanologica Acta*, 9, 149–158.
- de Abreu, L., Abrantes, F. F., Shackleton, N. J., Tzedakis, P. C., McManus, J. F., Oppo, D. W., & Hall, M. A. (2005). Ocean climate variability in the eastern North Atlantic during interglacial marine isotope stage 11: A partial analogue to the Holocene? *Paleoceanography*, 20(3). <https://doi.org/10.1029/2004pa001091>
- Desprat, S., Oliveira, D., Naughton, F., & Sánchez Goñi, M. F. (2017). L’étude du pollen des séquences sédimentaires marines pour la compréhension du climat: L’exemple des périodes chaudes passées. *Quaternaire. Revue de l’Association française pour l’étude du Quaternaire*, 28, 259–269. <https://doi.org/10.4000/quaternaire.8102>
- Elderfield, H., Ferretti, P., Greaves, M., Crowhurst, S., McCave, I. N., Hodell, D., & Piotrowski, A. M. (2012). Evolution of ocean temperature and ice volume through the mid-Pleistocene climate transition. *Science*, 337(6095), 704–709. <https://doi.org/10.1126/science.1221294>
- Expedition 339 Scientists. (2013). Site U1385. In D. A. V. Stow, F. J. Hernández-Molina, C. A. Alvarez Zarikian, & Expedition 339 Scientists (Eds.). *Proceedings of the integrated ocean drilling program*. 339. Tokyo: Integrated Ocean Drilling Program Management International, Inc. <https://doi.org/10.2204/iodp.proc.339.103.2013>
- Eynaud, F., De Abreu, L., Voelker, A., Schönfeld, J., Salgueiro, E., Turon, J. L., et al. (2009). Position of the Polar Front along the western Iberian margin during key cold episodes of the last 45 ka. *Geochemistry, Geophysics, Geosystems*, 10, Q07U05. <https://doi.org/10.1029/2009gc002398>
- Figueiras, F., Labarta, U., & Reiriz, M. F. (2002). Coastal upwelling, primary production and mussel growth in the Rias Baixas of Galicia. In *Sustainable increase of marine harvesting: fundamental mechanisms and new concepts*, pp. 121–131. Springer. [https://doi.org/10.1007/978-94-017-3190-4\\_11](https://doi.org/10.1007/978-94-017-3190-4_11)
- Fiúza, A. F. (1983). *Upwelling patterns off Portugal, Coastal Upwelling its sediment record*. Springer, pp. 85–98. [https://doi.org/10.1007/978-1-4615-6651-9\\_5](https://doi.org/10.1007/978-1-4615-6651-9_5)
- Fiúza, A. F. G., Hamann, M., Ambar, I., Díaz del Río, G., González, N., & Cabanas, J. M. (1998). Water masses and their circulation off western Iberia during May 1993. *Deep Sea Research Part I: Oceanographic Research Papers*, 45, 1127–1160. [https://doi.org/10.1016/s0967-0637\(98\)00008-9](https://doi.org/10.1016/s0967-0637(98)00008-9)
- Flores, J. A., Bárcena, M. A., & Sierro, F. J. (2000). Ocean-surface and wind dynamics in the Atlantic Ocean off Northwest Africa during the last 140 000 years. *Palaeogeography, Palaeoclimatology, Palaeoecology*, 161, 459–478. [https://doi.org/10.1016/s0031-0182\(00\)00099-7](https://doi.org/10.1016/s0031-0182(00)00099-7)
- Flores, J. A., Gersonde, R., Sierro, F., & Niebler, H.-S. (2000). Southern Ocean Pleistocene calcareous nannofossil events: Calibration with isotope and geomagnetic stratigraphies. *Marine Micropaleontology*, 40, 377–402. [https://doi.org/10.1016/s0377-8398\(00\)00047-5](https://doi.org/10.1016/s0377-8398(00)00047-5)
- Flores, J. A., & Marino, M. (2002). Pleistocene calcareous nannofossil stratigraphy for ODP Leg 177 (Atlantic sector of the Southern Ocean). *Marine Micropaleontology*, 45, 191–224. [https://doi.org/10.1016/s0377-8398\(02\)00030-0](https://doi.org/10.1016/s0377-8398(02)00030-0)

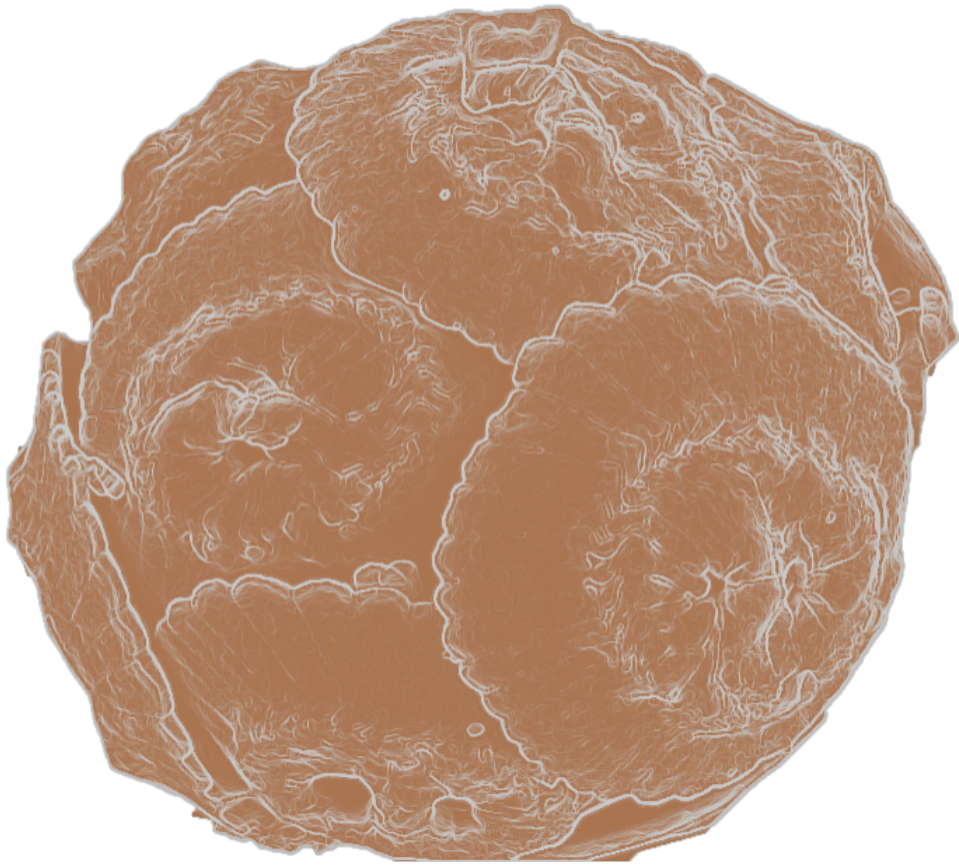
- Flores, J. A., & Sierro, F. J. (1997). Revised technique for calculation of calcareous nannofossil accumulation rates. *Micropaleontology*, *43*, 321–324. <https://doi.org/10.2307/1485832>
- Flores, J. A., Sierro, F. J., Francés, G., Vázquez, A., & Zamarreno, I. (1997). The last 100,000 years in the western Mediterranean: Sea surface water and frontal dynamics as revealed by coccolithophores. *Marine Micropaleontology*, *29*, 351–366. [https://doi.org/10.1016/s0377-8398\(96\)00029-1](https://doi.org/10.1016/s0377-8398(96)00029-1)
- Gartner, S. (1988). Paleoceanography of the mid-Pleistocene. *Marine Micropaleontology*, *13*, 23–46. [https://doi.org/10.1016/0377-8398\(88\)90011-4](https://doi.org/10.1016/0377-8398(88)90011-4)
- Geisen, M., Billard, C., Broerse, A. T., Cros, L., Probert, I., & Young, J. R. (2002). Life-cycle associations involving pairs of holococcolithophorid species: Intraspecific variation or cryptic speciation?. *European Journal of Phycology*, *37*, 531–550. <https://doi.org/10.1017/s0967026202003852>
- Girardeau, J., Monteiro, P. M., & Nikodemus, K. (1993). Distribution and malformation of living coccolithophores in the northern Benguela upwelling system off Namibia. *Marine Micropaleontology*, *22*(1–2), 93–110.
- González-Lanchas, A., Flores, J.-A., Sierro, F. J., Bárcena, M. Á., Rigual-Hernández, A. S., Oliveira, D., et al. (2020). A new perspective of the Alboran Upwelling System reconstruction during the Marine Isotope Stage 11: A high-resolution coccolithophore record. *Quaternary Science Reviews*, *245*. art. no. 106520. <https://doi.org/10.1016/j.quascirev.2020.106520>
- Gouveia, C., Trigo, R. M., DaCamara, C. C., Libonati, R., & Pereira, J. M. (2008). The North Atlantic oscillation and European vegetation dynamics. *International Journal of Climatology: A Journal of the Royal Meteorological Society*, *28*, 1835–1847. <https://doi.org/10.1002/joc.1682>
- Grelaud, M., Schimmelmann, A., & Beaufort, L. (2009). Coccolithophore response to climate and surface hydrography in Santa Barbara Basin, California, AD 1917–2004. *Biogeosciences*, *6*(10), 2025–2039. <https://doi.org/10.5194/bg-6-2025-2009>
- Guerreiro, C., Sá, C., de Stigter, H., Oliveira, A., Cachão, M., Cros, L., et al. (2014). Influence of the Nazaré Canyon, central Portuguese margin, on late winter coccolithophore assemblages. *Deep Sea Research Part II: Topical Studies in Oceanography*, *104*, 335–358. <https://doi.org/10.1016/j.dsr2.2013.09.011>
- Haynes, R., & Barton, E. D. (1990). A poleward flow along the Atlantic coast of the Iberian Peninsula. *Journal of Geophysical Research*, *95*, 11425–11441. <https://doi.org/10.1029/jc095ic07p11425>
- Hernández, A., Cachão, M., Sousa, P., Trigo, R. M., Luterbacher, J., Vaquero, J. M., & Freitas, M. C. (2021). External forcing mechanisms controlling the North Atlantic coastal upwelling regime during the mid-Holocene. *Geology*, *49*(4), 433–437. <https://doi.org/10.1130/g48112.1>
- Hewitt, C. D., Broccoli, A. J., Mitchell, J. F., & Stouffer, R. J. (2001). A coupled model study of the last glacial maximum: Was part of the North Atlantic relatively warm? *Geophysical Research Letters*, *28*, 1571–1574. <https://doi.org/10.1029/2000gl012575>
- Hodell, D., Crowhurst, S., Skinner, L., Tzedakis, P. C., Margari, V., Channell, J. E., et al. (2013). Response of Iberian Margin sediments to orbital and suborbital forcing over the past 420 ka. *Paleoceanography*, *28*, 185–199. <https://doi.org/10.1002/palo.20017>
- Hodell, D., Lourens, L., Crowhurst, S., Konijnendijk, T., Tjallingii, R., Jiménez-Espejo, F., et al. (2015). A reference time scale for Site U1385 (Shackleton Site) on the SW Iberian Margin. *Global and Planetary Change*, *133*, 49–64. <https://doi.org/10.1016/j.gloplacha.2015.07.002>
- Hurrell, J. W. (1995). Decadal trends in the North Atlantic Oscillation: Regional temperatures and precipitation. *Science*, *269*, 676–679. <https://doi.org/10.1126/science.269.5224.676>
- Hurrell, J. W., Kushnir, Y., Ottersen, G., & Visbeck, M. (2003). An overview of the North Atlantic oscillation. *Geophysical Monograph-American Geophysical Union*, *134*, 1–35. <https://doi.org/10.1029/134gm01>
- Incarbona, A., Martrat, B., Di Stefano, E., Grimalt, J. O., Pelosi, N., Patti, B., & Tranchida, G. (2010). Primary productivity variability on the Atlantic Iberian Margin over the last 70,000 years: Evidence from coccolithophores and fossil organic compounds. *Paleoceanography*, *25*(2). <https://doi.org/10.1029/2008pa001709>
- Jansen, J. H. F., Kuijpers, A., & Troelstra, S. R. (1986). A Mid-Brunhes Climatic Event: Long-Term Changes in Global Atmosphere and Ocean Circulation. *Science*, *232*, 619–622. <https://doi.org/10.1126/science.232.4750.619>
- Jordan, R., & Winter, A. (2000). Assemblages of coccolithophorids and other living microplankton off the coast of Puerto Rico during January–May 1995. *Marine Micropaleontology*, *39*, 113–130. [https://doi.org/10.1016/s0377-8398\(00\)00017-7](https://doi.org/10.1016/s0377-8398(00)00017-7)
- Jouzel, J., Masson-Delmotte, V., Cattani, O., Dreyfus, G., Falourd, S., Hoffmann, G., et al. (2007). Orbital and millennial Antarctic climate variability over the past 800,000 years. *Science*, *317*, 793–796. <https://doi.org/10.1126/science.1141038>
- Keffer, T., Martinson, D., & Corliss, B. (1988). The position of the Gulf Stream during Quaternary glaciations. *Science*, *241*, 440–442. <https://doi.org/10.1126/science.241.4864.440>
- Kinkel, H., Baumann, K.-H., & Cepek, M. (2000). Coccolithophores in the equatorial Atlantic Ocean: Response to seasonal and Late Quaternary surface water variability. *Marine Micropaleontology*, *39*, 87–112. [https://doi.org/10.1016/s0377-8398\(00\)00016-5](https://doi.org/10.1016/s0377-8398(00)00016-5)
- Lang, N., & Wolff, E. W. (2011). Interglacial and glacial variability from the last 800 ka in marine, ice and terrestrial archives. *Climate of the Past*, *7*, 361–380. <https://doi.org/10.5194/cp-7-361-2011>
- Lebreiro, S., Moreno, J., McCave, I., & Weaver, P. (1996). Evidence for Heinrich layers off Portugal (Tore Seamount: 39 N, 12 W). *Marine Geology*, *131*, 47–56. [https://doi.org/10.1016/0025-3227\(95\)00142-5](https://doi.org/10.1016/0025-3227(95)00142-5)
- Lisiecki, L. E., & Raymo, M. E. (2005). A Pliocene-Pleistocene stack of 57 globally distributed benthic  $\delta^{18}O$  records. *Paleoceanography*, *20*(1). <https://doi.org/10.1029/2004pa001071>
- Lopes, J. F., Cardoso, A. C., Moita, M. T., Rocha, A. C., & Ferreira, J. A. (2009). Modelling the temperature and the phytoplankton distributions at the Aveiro near coastal zone, Portugal. *Ecological Modelling*, *220*, 940–961. <https://doi.org/10.1016/j.ecolmodel.2008.11.024>
- Loutre, M.-F., & Berger, A. (2003). Marine Isotope Stage 11 as an analogue for the present interglacial. *Global and Planetary Change*, *36*, 209–217. [https://doi.org/10.1016/s0921-8181\(02\)00186-8](https://doi.org/10.1016/s0921-8181(02)00186-8)
- Maiorano, P., Marino, M., Balestra, B., Flores, J.-A., Hodell, D., & Rodrigues, T. (2015). Coccolithophore variability from the Shackleton Site (IODP Site U1385) through MIS 16–10. *Global and Planetary Change*, *133*, 35–48. <https://doi.org/10.1016/j.gloplacha.2015.07.009>
- Marino, M., Maiorano, P., Tarantino, F., Voelker, A., Capotondi, L., Giron, A., et al. (2014). Coccolithophores as proxy of seawater changes at orbital-to-millennial scale during middle Pleistocene Marine Isotope Stages 14–9 in North Atlantic core MD01-2446. *Paleoceanography*, *29*, 518–532. <https://doi.org/10.1002/2013pa002574>
- Marlowe, I. T., Brassell, S. C., Eglinton, G., & Green, J. C. (1990). Long-chain alkenones and alkyl alkenoates and the fossil coccolith record of marine sediments. *Chemical Geology*, *88*(3–4), 349–375. [https://doi.org/10.1016/0009-2541\(90\)90098-r](https://doi.org/10.1016/0009-2541(90)90098-r)
- Martin-Garcia, G. M., Alonso-Garcia, M., Sierro, F. J., Hodell, D. A., & Flores, J. A. (2015). Severe cooling episodes at the onset of deglaciations on the Southwestern Iberian margin from MIS 21 to 13 (IODP site U1385). *Global and Planetary Change*, *135*, 159–169. <https://doi.org/10.1016/j.gloplacha.2015.11.001>



- Martrat, B., Grimalt, J. O., Shackleton, N. J., de Abreu, L., Hutterli, M. A., & Stocker, T. F. (2007). Four climate cycles of recurring deep and surface water destabilizations on the Iberian margin. *Science*, *317*, 502–507. <https://doi.org/10.1126/science.1139994>
- Mason, E., Coombs, S., & Oliveira, P. (2005). An overview of the literature concerning the oceanography of the eastern North Atlantic region. *Relatórios Científicos e Técnicos IPIMAR Serie Digital*, *33*, 59.
- McCartney, M. S., & Talley, L. D. (1982). The subpolar mode water of the North Atlantic Ocean. *Journal of Physical Oceanography*, *12*, 1169–1188. [https://doi.org/10.1175/1520-0485\(1982\)012<1169:tsmwot>2.0.co;2](https://doi.org/10.1175/1520-0485(1982)012<1169:tsmwot>2.0.co;2)
- McManus, J. F., Oppo, D. W., & Cullen, J. L. (1999). A 0.5-million-year record of millennial-scale climate variability in the North Atlantic. *Science*, *283*, 971–975. <https://doi.org/10.1126/science.283.5404.971>
- Mix, A. C. (1989). Influence of productivity variations on long-term atmospheric CO<sub>2</sub>. *Nature*, *337*, 541–544. <https://doi.org/10.1038/337541a0>
- Moita, M., Silva, A., Palma, S., & Vilarinho, M. (2010). The coccolithophore summer–autumn assemblage in the upwelling waters of Portugal: Patterns of mesoscale distribution (1985–2005). *Estuarine, Coastal and Shelf Science*, *87*, 411–419. <https://doi.org/10.1016/j.ecss.2010.01.025>
- Moita, T. (1993). Spatial variability of phytoplankton communities in the upwelling region off Portugal. *Proceeding of the International Council for the Exploration of the Sea L*, *64*, 1–20.
- Molfino, B., & McIntyre, A. (1990). Precessional forcing of nutricline dynamics in the equatorial Atlantic. *Science*, *249*, 766–769. <https://doi.org/10.1126/science.249.4970.766>
- Naafs, B. D. A., Hefter, J., Ferretti, P., Stein, R., & Haug, G. H. (2011). Sea surface temperatures did not control the first occurrence of Hudson Strait Heinrich Events during MIS 16. *Paleoceanography*, *26*(4). <https://doi.org/10.1029/2011pa002135>
- Naafs, B. D. A., Hefter, J., Grützner, J., & Stein, R. (2013). Warming of surface waters in the mid-latitude North Atlantic during Heinrich events. *Paleoceanography*, *28*, 153–163. <https://doi.org/10.1029/2012pa002354>
- Naughton, F., Goñi, M. S., Kageyama, M., Bard, E., Duprat, J., Cortijo, E., et al. (2009). Wet to dry climatic trend in north-western Iberia within Heinrich events. *Earth and Planetary Science Letters*, *284*, 329–342. <https://doi.org/10.1016/j.epsl.2009.05.001>
- Okada, H., & Honjo, S. (1973). The distribution of oceanic coccolithophorids in the Pacific. *Deep Sea Research and Oceanographic Abstracts*, *20*, 355–374. [https://doi.org/10.1016/0011-7471\(73\)90059-4](https://doi.org/10.1016/0011-7471(73)90059-4)
- Okada, H., & Wells, P. (1997). Late Quaternary nannofossil indicators of climate change in two deep-sea cores associated with the Leeuwin Current off Western Australia. *Palaeogeography, Palaeoclimatology, Palaeoecology*, *131*, 413–432. [https://doi.org/10.1016/s0031-0182\(97\)00014-x](https://doi.org/10.1016/s0031-0182(97)00014-x)
- Oliveira, D., Desprat, S., Rodrigues, T., Naughton, F., Hodell, D., Trigo, R., et al. (2016). The complexity of millennial-scale variability in southwestern Europe during MIS 11. *Quaternary Research*, *86*, 373–387. <https://doi.org/10.1016/j.yqres.2016.09.002>
- Oliveira, D., Desprat, S., Yin, Q., Naughton, F., Trigo, R., Rodrigues, T., et al. (2018). Unraveling the forcings controlling the vegetation and climate of the best orbital analogues for the present interglacial in SW Europe. *Climate Dynamics*, *51*, 667–686. <https://doi.org/10.1007/s00382-017-3948-7>
- Oliveira, P. B., Nolasco, R., Dubert, J., Moita, T., & Peliz, A. (2009). Surface temperature, chlorophyll and advection patterns during a summer upwelling event off central Portugal. *Continental Shelf Research*, *29*, 759–774. <https://doi.org/10.1016/j.csr.2008.08.004>
- Oppo, D., McManus, J., & Cullen, J. (1998). Abrupt climate events 500,000 to 340,000 years ago: Evidence from subpolar North Atlantic sediments. *Science*, *279*, 1335–1338. <https://doi.org/10.1126/science.279.5355.1335>
- Pailler, D., & Bard, E. (2002). High frequency palaeoceanographic changes during the past 140 000 yr recorded by the organic matter in sediments of the Iberian Margin. *Palaeogeography, Palaeoclimatology, Palaeoecology*, *181*, 431–452. [https://doi.org/10.1016/s0031-0182\(01\)00444-8](https://doi.org/10.1016/s0031-0182(01)00444-8)
- Palumbo, E., Flores, J. A., Perugia, C., Emanuele, D., Petrillo, Z., Rodrigues, T., et al. (2013a). Abrupt variability of the last 24 ka BP recorded by coccolithophore assemblages off the Iberian Margin (core MD03-2699). *Journal of Quaternary Science*, *28*, 320–328. <https://doi.org/10.1002/jqs.2623>
- Palumbo, E., Flores, J. A., Perugia, C., Petrillo, Z., Voelker, A., & Amore, F. (2013b). Millennial scale coccolithophore paleoproductivity and surface water changes between 445 and 360 ka (Marine Isotope Stages 12/11) in the Northeast Atlantic. *Palaeogeography, Palaeoclimatology, Palaeoecology*, *383*, 27–41. <https://doi.org/10.1016/j.palaeo.2013.04.024>
- Parente, A., Cachão, M., Baumann, K.-H., de Abreu, L., & Ferreira, J. (2004). Morphometry of *Coccolithus pelagicus* sl (Coccolithophore, Haptophyta) from offshore Portugal, during the last 200 kyr. *Micropaleontology*, *50*, 107–120. [https://doi.org/10.2113/50.suppl\\_1.107](https://doi.org/10.2113/50.suppl_1.107)
- Peliz, Á., Dubert, J., Santos, A. M. P., Oliveira, P. B., & Le Cann, B. (2005). Winter upper ocean circulation in the Western Iberian Basin—Fronts, Eddies and Poleward Flows: An overview. *Deep Sea Research Part I: Oceanographic Research Papers*, *52*, 621–646. <https://doi.org/10.1016/j.dsr.2004.11.005>
- Pérez, F. F., Castro, C. G., Álvarez-Salgado, X. A., & Ríos, A. F. (2001). Coupling between the Iberian basin — scale circulation and the Portugal boundary current system: A chemical study. *Deep Sea Research Part I: Oceanographic Research Papers*, *48*, 1519–1533. [https://doi.org/10.1016/s0967-0637\(00\)00101-1](https://doi.org/10.1016/s0967-0637(00)00101-1)
- Petit, J.-R., Jouzel, J., Raynaud, D., Barkov, N. I., Barnola, J.-M., Basile, I., et al. (1999). Climate and atmospheric history of the past 420,000 years from the Vostok ice core, Antarctica. *Nature*, *399*, 429–436. <https://doi.org/10.1038/20859>
- Railsback, L. B., Gibbard, P. L., Head, M. J., Voarintsoa, N. R. G., & Toucanne, S. (2015). An optimized scheme of lettered marine isotope substages for the last 1.0 million years, and the climatostratigraphic nature of isotope stages and substages. *Quaternary Science Reviews*, *111*, 94–106. <https://doi.org/10.1016/j.quascirev.2015.01.012>
- Relvas, P., Barton, E. D., Dubert, J., Oliveira, P. B., Peliz, A., Da Silva, J., & Santos, A. M. P. (2007). Physical oceanography of the western Iberia ecosystem: Latest views and challenges. *Progress in Oceanography*, *74*, 149–173. <https://doi.org/10.1016/j.pocean.2007.04.021>
- Ríos, A. F., Pérez, F. F., & Fraga, F. (1992). Water masses in the upper and middle North Atlantic Ocean east of the Azores. *Deep Sea Research Part A: Oceanographic Research Papers*, *39*(3–4), 645–658. [https://doi.org/10.1016/0198-0149\(92\)90093-9](https://doi.org/10.1016/0198-0149(92)90093-9)
- Rodrigues, T., Alonso-García, M., Hodell, D. A., Rufino, M., Naughton, F., Grimalt, J. O., et al. (2017). A 1-Ma record of sea surface temperature and extreme cooling events in the North Atlantic: A perspective from the Iberian Margin. *Quaternary Science Reviews*, *172*, 118–130. <https://doi.org/10.1016/j.quascirev.2017.07.004>
- Rodrigues, T., Grimalt, J. O., Abrantes, F. G., Flores, J. A., & Lebreiro, S. M. (2009). Holocene interdependences of changes in sea surface temperature, productivity, and fluvial inputs in the Iberian continental shelf (Tagus mud patch). *Geochemistry, Geophysics, Geosystems*, *10*, Q07U06. <https://doi.org/10.1029/2008gc002367>
- Rodrigues, T., Grimalt, J. O., Abrantes, F., Naughton, F., & Flores, J.-A. (2010). The last glacial–interglacial transition (LGIT) in the western mid-latitudes of the North Atlantic: Abrupt sea surface temperature change and sea level implications. *Quaternary Science Reviews*, *29*, 1853–1862. <https://doi.org/10.1016/j.quascirev.2010.04.004>

- Rodrigues, T., Voelker, A., Grimalt, J., Abrantes, F., & Naughton, F. (2011). Iberian Margin sea surface temperature during MIS 15 to 9 (580–300 ka): Glacial suborbital variability versus interglacial stability. *Paleoceanography*, 26(1). <https://doi.org/10.1029/2010pa001927>
- Rohling, E. J., Grant, K., Bolshaw, M., Roberts, A., Siddall, M., Hemleben, C., & Kucera, M. (2009). Antarctic temperature and global sea level closely coupled over the past five glacial cycles. *Nature Geoscience*, 2, 500–504. <https://doi.org/10.1038/ngeo557>
- Romero, O. E., Kim, J. H., & Donner, B. (2008). Submillennial-to-millennial variability of diatom production off Mauritania, NW Africa, during the last glacial cycle. *Paleoceanography*, 23(3). <https://doi.org/10.1029/2008pa001601>
- Ruddiman, W. F. (1977). Late Quaternary deposition of ice-rafted sand in the subpolar North Atlantic (lat 40 to 65 N). *Geological Society of America Bulletin*, 88, 1813–1827. [https://doi.org/10.1130/0016-7606\(1977\)88<1813:lqdois>2.0.co;2](https://doi.org/10.1130/0016-7606(1977)88<1813:lqdois>2.0.co;2)
- Ruddiman, W. F., & McIntyre, A. (1981). The mode and mechanism of the last deglaciation: Oceanic evidence. *Quaternary Research*, 16, 125–134. [https://doi.org/10.1016/0033-5894\(81\)90040-5](https://doi.org/10.1016/0033-5894(81)90040-5)
- Saavedra-Pellitero, M., Baumann, K. H., Lamy, F., & Köhler, P. (2017). Coccolithophore variability across Marine Isotope Stage 11 in the Pacific sector of the Southern Ocean and its potential impact on the carbon cycle. *Paleoceanography*, 32, 864–880. <https://doi.org/10.1002/2017pa003156>
- Salgueiro, E., Naughton, F., Voelker, A. H. L., de Abreu, L., Alberto, A., Rossignol, L., et al. (2014). Past circulation along the western Iberian margin: A time slice vision from the Last Glacial to the Holocene. *Quaternary Science Reviews*, 106, 316–329. <https://doi.org/10.1016/j.quascirev.2014.09.001>
- Sánchez Goñi, M. F. (2020). Regional impacts of climate change and its relevance to human evolution. *Evolutionary Human Sciences*, 2, e55. <https://doi.org/10.1017/ehs.2020.56>
- Sánchez Goñi, M. F., Llave, E., Oliveira, D., Naughton, F., Desprat, S., Ducassou, E., et al. (2016). Climate changes in south western Iberia and Mediterranean Outflow variations during two contrasting cycles of the last 1 Myrs: MIS 31-MIS 30 and MIS 12-MIS 11. *Global and Planetary Change*, 136, 18–29. <https://doi.org/10.1016/j.gloplacha.2015.11.006>
- Sarnthein, M., Winn, K., Duplessy, J.-C., & Fontugne, M. R. (1988). Global variations of surface ocean productivity in low and mid latitudes: Influence on CO<sub>2</sub>. *Paleoceanography*, 3, 361–399. <https://doi.org/10.1029/pa003i003p00361>
- Schubert, C., Villanueva, J., Calvert, S., Cowie, G., Von Rad, U., Schulz, H., et al. (1998). Stable phytoplankton community structure in the Arabian Sea over the past 200,000 years. *Nature*, 394, 563–566. <https://doi.org/10.1038/29047>
- Schulte, S., Rostek, F., Bard, E., Rullkötter, J., & Marchal, O. (1999). Variations of oxygen-minimum and primary productivity recorded in sediments of the Arabian Sea. *Earth and Planetary Science Letters*, 173, 205–221. [https://doi.org/10.1016/s0012-821x\(99\)00232-0](https://doi.org/10.1016/s0012-821x(99)00232-0)
- Shackleton, N. J., Hall, M. A., & Vincent, E. (2000). Phase relationships between millennial-scale events 64,000–24,000 years ago. *Paleoceanography*, 15, 565–569. <https://doi.org/10.1029/2000pa000513>
- Silva, A., Palma, S., & Moita, M. (2008). Coccolithophores in the upwelling waters of Portugal: Four years of weekly distribution in Lisbon bay. *Continental Shelf Research*, 28, 2601–2613. <https://doi.org/10.1016/j.csr.2008.07.009>
- Silva, A., Palma, S., Oliveira, P., & Moita, M. (2009). Composition and interannual variability of phytoplankton in a coastal upwelling region (Lisbon Bay, Portugal). *Journal of Sea Research*, 62, 238–249. <https://doi.org/10.1016/j.seares.2009.05.001>
- Spratt, R. M., & Lisiecki, L. E. (2016). A Late Pleistocene sea level stack. *Climate of the Past*, 12(4), 1079–1092. <https://doi.org/10.5194/cp-12-1079-2016>
- Stein, R., Heftner, J., Grütznert, J., Voelker, A., & Naafs, B. D. A. (2009). Variability of surface water characteristics and Heinrich-like events in the Pleistocene midlatitude North Atlantic Ocean: Biomarker and XRD records from IODP Site U1313 (MIS 16–9). *Paleoceanography*, 24(2). <https://doi.org/10.1029/2008pa001639>
- Stolz, K., & Baumann, K. H. (2010). Changes in palaeoceanography and palaeoecology during Marine Isotope Stage (MIS) 5 in the eastern North Atlantic (ODP Site 980) deduced from calcareous nannoplankton observations. *Palaeogeography, Palaeoclimatology, Palaeoecology*, 292(1–2), 295–305. <https://doi.org/10.1016/j.palaeo.2010.04.002>
- Trigo, R. M., Osborn, T. J., & Corte-Real, J. M. (2002). The North Atlantic Oscillation influence on Europe: Climate impacts and associated physical mechanisms. *Climate Research*, 20, 9–17. <https://doi.org/10.3354/cr020009>
- van Aken, H. M. (2001). The hydrography of the mid-latitude northeast Atlantic Ocean—Part III: The subducted thermocline water mass. *Deep Sea Research Part I: Oceanographic Research Papers*, 48, 237–267. [https://doi.org/10.1016/s0967-0637\(00\)00059-5](https://doi.org/10.1016/s0967-0637(00)00059-5)
- Vautravers, M. J., & Shackleton, N. J. (2006). Centennial-scale surface hydrology off Portugal during marine isotope stage 3: Insights from planktonic foraminiferal fauna variability. *Paleoceanography*, 21(3). <https://doi.org/10.1029/2005pa001144>
- Villanueva, J., Calvo, E., Pelejero, C., Grimalt, J., Boelaert, A., & Labeyrie, L. (2001). A latitudinal productivity band in the central North Atlantic over the last 270 kyr: An alkenone perspective. *Paleoceanography*, 16, 617–626. <https://doi.org/10.1029/2000pa000543>
- Villanueva, J., Grimalt, J. O., Labeyrie, L. D., Cortijo, E., Vidal, L., & Louis-Turon, J. (1998). Precessional forcing of productivity in the North Atlantic Ocean. *Paleoceanography*, 13, 561–571. <https://doi.org/10.1029/98pa02318>
- Villanueva, J., Pelejero, C., & Grimalt, J. O. (1997). Clean-up procedures for the unbiased estimation of C37 alkenone sea surface temperatures and terrigenous n-alkane inputs in paleoceanography. *Journal of Chromatography*, 757, 145–151. [https://doi.org/10.1016/s0021-9673\(96\)00669-3](https://doi.org/10.1016/s0021-9673(96)00669-3)
- Vitorino, J., Oliveira, A., Jouanneau, J. M., & Drago, T. (2002). Winter dynamics on the northern Portuguese shelf. Part 1: Physical processes. *Progress in Oceanography*, 52, 129–153. [https://doi.org/10.1016/s0079-6611\(02\)00003-4](https://doi.org/10.1016/s0079-6611(02)00003-4)
- Voelker, A. H. L., De Abreu, L., Schönfeld, J., Erlenkeuser, H., & Abrantes, F. (2009). Hydrographic conditions along the western Iberian margin during marine isotope stage 2. *Geochemistry, Geophysics, Geosystems*, 10, Q12U08. <https://doi.org/10.1029/2009gc002605>
- Voelker, A. H. L., Rodrigues, T., Billups, K., Oppo, D. W., McManus, J. F., Stein, R., et al., 2010. Variations in mid-latitude North Atlantic surface water properties during the mid-Brunhes (MIS 9–14) and their implications for the thermohaline circulation. *Climate of the Past*, 6, 531–552.
- Volkman, J. K., Eglinton, G., Corner, E. D., & Forsberg, T. (1980). Long-chain alkenes and alkenones in the marine coccolithophorid *Emiliania huxleyi*. *Phytochemistry*, 19, 2619–2622. [https://doi.org/10.1016/s0031-9422\(00\)83930-8](https://doi.org/10.1016/s0031-9422(00)83930-8)
- Wanner, H., Brönnimann, S., Casty, C., Gyalistras, D., Luterbacher, J., Schmutz, C., et al. (2001). North Atlantic Oscillation—concepts and studies. *Surveys in Geophysics*, 22, 321–381. <https://doi.org/10.1023/a:1014217317898>
- Winter, A. (1994). Biogeography of living coccolithophores in ocean waters. *Coccolithophores*.
- Young, J. R., Bown, P. R., & Lees, J. A. (2020). *Nannotax3 website*. International Nannoplankton Association. Retrieved from <http://www.mikrotax.org/Nannotax3>. Accessed 10 Feb. 2021. URL.
- Young, J. R., Geisen, M., Cros, L., Kleijne, A., Sprengel, C., Probert, I., & Østergaard, J. (2003). A guide to extant coccolithophore taxonomy. *Journal of Nannoplankton Research, Special Issue, 1*, 1–132.





**Carbon isotopic fractionation of alkenones and  
*Gephyrocapsa* coccoliths over the late Quaternary  
(Marine Isotope Stages 12 to 9) glacial-interglacial  
cycles at the Western Tropical Atlantic**

(González-Lanchas et al., 2021b)

*Paleoceanography and Paleoclimatology*

## **CAPÍTULO 4. Artículo científico**

### **“Carbon isotopic fractionation of alkenones and *Gephyrocapsa* coccoliths over the Late Quaternary glacial-interglacial cycles at the Western Tropical Atlantic”**

**Alba González-Lanchas**<sup>a</sup>, Iván Hernández-Alméida<sup>b</sup>, José-Abel Flores<sup>a</sup>, Francisco J. Sierra<sup>a</sup>, José Guitián<sup>b</sup> y Heather M. Stoll<sup>b</sup>

<sup>a</sup> Departamento de Geología, Universidad de Salamanca, 37008 Salamanca, España.

<sup>b</sup> Geological Institute, ETH Zürich, Zürich, Switzerland.

*Paleoceanography and Paleoclimatology* 36(8), e2020PA004175.

DOI: [10.1029/2020PA004175](https://doi.org/10.1029/2020PA004175)

## Resumen

El fraccionamiento isotópico del carbono durante la fotosíntesis en haptofitas,  $\epsilon_p$ , queda registrado en las alquenonas, compuestos orgánicos de tipo lipídico producidos por los organismos pertenecientes a este grupo que aparecen preservadas en los sedimento. El valor de  $\epsilon_p$  medido en archivos de este tipo se ha empleado como una herramienta importante para la reconstrucción de la presión parcial atmosférica,  $p\text{CO}_2$ , durante el pasado (Pagani, 2014). Sin embargo, la recientemente observada discrepancia entre las reconstrucciones de  $p\text{CO}_2$  atmosférico durante el Pleistoceno, obtenidas con este método, y los niveles de  $p\text{CO}_2$  medidos directamente en testigos de hielo, ha llevado a la comunidad científica a cuestionar la fiabilidad del indicador de  $\epsilon_p$  (Badger et al., 2019), y a tratar de refinar este método a partir de un mayor conocimiento de la sensibilidad de  $\epsilon_p$  a los cambios en  $\text{CO}_2$  y a la influencia de otros parámetros de naturaleza ecológica y/o fisiológica (Badger, 2021; Hernández-Almeida et al.; Stoll et al., 2019; Zhang et al., 2020). Este estudio trata de esclarecer estas cuestiones a partir de la medida directa de  $\epsilon_p$  y la reconstrucción del resto de parámetros implicados en su modulación durante el intervalo comprendido entre los estadios isotópicos marinos (MIS) 12 a 9, entre los 430 y 330 mil años (ka), en el que los niveles de  $p\text{CO}_2$  son conocidos y empleados como referencia. La zona de estudio seleccionada fue el sector Oeste de la región tropical del Atlántico, donde la relación de intercambio océano-atmósfera de  $\text{CO}_2$  se considera, al igual que sucede en la actualidad, próxima al equilibrio.

Los valores de  $\epsilon_p$  fueron calculados a partir de la medida de  $\delta^{13}\text{C}$  en las alquenonas di insaturadas,  $\text{C}_{37:2}$ , extraídas del sedimento, como estimación de  $\delta^{13}\text{C}$  en la materia orgánica producida durante la fotosíntesis. Para la obtención del  $\delta^{13}\text{C}$  en  $\text{C}_{37:2}$ , se llevó a cabo un proceso de extracción, aislamiento y separación del contenido lipídico total y de los diferentes compuestos orgánicos en la muestra, y su medida a partir de técnicas espectrometría de masas. El  $\delta^{13}\text{C}$  del  $\text{CO}_2$  disuelto en el medio acuoso,  $\text{CO}_2$  [aq], de hábitat del organismo fotosintético, se requiere como referencia para el cálculo de  $\epsilon_p$ . Para su estimación, se empleó el valor de  $\delta^{13}\text{C}$  en el carbono inorgánico disuelto,  $\delta^{13}\text{C}_{\text{DIC}}$ , a la profundidad de hábitat de organismo fotosintético, un valor obtenido mediante la corrección sobre los valores  $\delta^{13}\text{C}$  en la especie de foraminífero planctónico *Trilobatus sacculifer*. Un análisis de las diferencias relativas de temperatura de calcificación,

calculadas a partir del  $\delta^{18}\text{O}$  medido en varias especies de foraminíferos planctónicos, extraídos de las mismas muestras, y cocolitos aislados del sedimento, pertenecientes al género *Gephyrocapsa* (ver texto suplementario) permitió precisar la profundidad de hábitat de *Trilobatus sacculifer* en la región de estudio como la más próxima a *Gephyrocapsa*. Las especies de foraminíferos planctónicos extraídos, seleccionados y analizados fueron *G. ruber*, *T. sacculifer* y *N. dutertrei*. Para la extracción de cocolitos del género *Gephyrocapsa*, se aplicó la técnica de microfiltrado del sedimento y concentración de la fracción entre 3 y 5  $\mu\text{m}$ . Las medidas isotópicas en la calcita de foraminíferos y cocolitos se realizó mediante técnicas de GasBench.

La correlación existente entre  $\epsilon_p$  y los niveles de  $\text{CO}_2$  [aq], es del 48 %, lo cual indica un control cercano al 50 % por parte de  $p\text{CO}_2$  y del 50 % por parte de otros parámetros de diferente naturaleza. Los valores de  $\text{CO}_2$  [aq] durante el intervalo de estudio fueron calculados a partir de las concentraciones de  $p\text{CO}_2$  en testigos de hielo, específicamente, aplicando la ecuación de la regresión entre los valores de  $\delta^{18}\text{O}$  bentónico en el Atlántico (Lisiecki y Stern, 2016) y los valores de  $p\text{CO}_2$  para los últimos 40 kyr, cuya edad fue asignada mediante técnicas de datación por radiocarbono (Köhler et al., 2017), a los valores de  $\delta^{18}\text{O}$  bentónico disponibles para las muestras en el testigo estudiado (Wilkens et al., 2017; ver texto suplementario)

Aparte de los cambios en  $p\text{CO}_2$  las tasas de crecimiento celular (*growth rate*), la disponibilidad de luz en la zona de hábitat y los cambios en la talla de la célula del organismo son otros de los parámetros potencialmente influyentes en  $\epsilon_p$ . En este estudio se analiza la capacidad del modelo clásico, que asume una adquisición pasiva del  $\text{CO}_2$  hacia la célula por mecanismos de difusión (Rau et al., 1996; sección 6.2.1.) y el modelo basado en las relaciones empíricas observadas en cultivos (Stoll et al., 2019; secciones 6.2.2. y 6.2.3.) para integrar y explicar las relaciones entre los factores influyentes en  $\epsilon_p$  directamente medidas y modelizadas en nuestro análisis.

Para comprobar la capacidad del modelo de adquisición de  $\text{CO}_2$  por difusión para explicar las relaciones medidas en este estudio (sección 6.2.1.), se calcularon diferentes predicciones de  $\epsilon_p$  empleando el modelo de Rau et al., (1996). Para ello, se incorporaron los datos de talla celular en *Gephyrocapsa*, las variaciones en  $\text{CO}_2$  [aq] estimadas, los valores experimentales de permeabilidad celular de Blanco-Ameijeiras et al. (2020), junto con diferentes opciones para la modelización de la variación en las tasas de crecimiento

celular, el único parámetro del que no se dispone de una medida directa. Estas modelizaciones se realizaron sobre parámetros directamente medidos en este estudio, como las tallas de los cocolitos de *Gephyrocapsa* y las SST, a partir del índice  $U^{k'}_{37}$  calculado a partir de las medidas de la concentración de alquenonas, o empleando datos de condiciones actuales en la región, como las concentraciones superficiales de fosfato ( $[PO_4]$ ). La estimación de las tallas celulares en *Gephyrocapsa* se llevó a cabo aplicando la relación dimensional propuesta por Henderiks y Pagani (2007) sobre los valores de talla de los cocolitos directamente medidos, con el empleo de técnicas de análisis de imagen (C-calcita; Fuertes et al., 2014). El factor de fraccionamiento enzimático eficaz de Rubisco,  $\epsilon_f$ , fue modulado en los cálculos de las predicciones entre el valor máximo de 25 %, según trabajos clásicos, y otros valores inferiores, según estudios recientes (Boller et al., 2015). Los resultados y análisis de sensibilidad llevados a cabo sugieren i) la inconsistencia del modelo clásico para explicar las relaciones en el conjunto de datos en este estudio y ii) la incapacidad del método recientemente propuesto por Zhang et al. (2020) para la conversión de las tallas celulares en tasas de crecimiento celular.

El valor de la pendiente de la regresión entre  $\epsilon_p$  y  $CO_2$  [aq] es similar al observado en cultivos, y esto sustenta la capacidad de un nuevo modelo estadístico de variable múltiple, basado en la integración de dichas relaciones (Stoll et al., 2019) para “acomodar” el efecto de los parámetros que influyen a  $\epsilon_p$ . Esta semejanza sustenta su aplicación en este estudio para analizar el efecto de otros factores, diferentes a  $CO_2$ , sobre la variabilidad restante, del  $\sim 50$  %, en  $\epsilon_p$ . Incluyendo los valores disponibles de talla celular y  $CO_2$  [aq] en el modelo estadístico basado en cultivos, se obtuvo un valor de  $\epsilon_p$  “estadístico” correspondiente a la “carga” impuesta por estos parámetros que sí se controlan. La diferencia entre este valor y  $\epsilon_p$  directamente medido en nuestro estudio, denominado “ $\epsilon_p$  residual”, permite, así, aislar la parte de la variabilidad correspondiente a las tasas de crecimiento celular y a la disponibilidad de luz, parámetros altamente vinculados a la evolución de las condiciones ambientales y ecológicas del medio a lo largo del intervalo. En este estudio no se dispone de una medida directa de dichas variables, pero su variación durante el intervalo estudiado se discute a partir de potenciales indicadores de condiciones derivadas o relacionadas, como los cambios de estratificación y disponibilidad de nutrientes en la zona fótica superior, a partir del análisis micropaleontológico sobre la asociación de microfósiles de las especies que componen el



complejo *Gephyrocapsa* y análisis geoquímicos en las muestras. Así, los valores de variación SST, muestran escasa variabilidad, coherente con la también limitada variabilidad en las condiciones de estratificación, a partir de los gradientes isotópicos en foraminíferos planctónicos calculados a partir de las medidas isotópicas de  $\delta^{18}\text{O}$ ,  $\Delta\delta^{18}\text{O}_{N. dutertrei-G. ruber}$  y  $\Delta\delta^{18}\text{O}_{N. dutertrei-T. sacculifer}$ . Por su parte, la variabilidad observada en los indicadores micropaleontológicos de % *Florisphaera profunda* y N (concentración de cocolitos por gramo) de *Gephyrocapsa* parecen indicar una coherente relación con los aportes en superficie de nutrientes procedentes de las descargas de río Amazonas, que muestra una reducción de la fertilización a la zona eufótica de hábitat de *Gephyrocapsa* hacia el final del intervalo por una limitación en la influencia de este tipo de nutrientes o una ligera profundización de la nutriclina, ambos procesos coherentes con una limitación en la influencia de este tipo de aguas superficiales a lo largo del intervalo. La comparación de  $\epsilon_p$  residual, antes calculado y descrito, con estos datos, evidenció que las variaciones en % *F. profunda* y la ratio entre la concentración de alquenonas C37/38. et son capaces de explicar una parte de esta variabilidad en  $\epsilon_p$ .

Las relaciones de sensibilidad entre los parámetros medidos en este estudio son incorporadas en la ecuación de Stoll et al. (2019) para calcular el rango de  $\text{CO}_2$  [aq] y su transferencia hacia consistente con las medidas de  $\epsilon_p$  para el Neógeno, disponibles a partir del estudio previo en la región de Zhang et al. (2013). Para la incorporación del margen de incertidumbre correspondiente a la carga de los parámetros medidos en nuestro estudio, se emplea la técnica de propagación de error de Monte Carlo, que también incluye la incertidumbre asociada a la conversión final de valores de  $\text{CO}_2$  [aq] a  $p\text{CO}_2$  (a partir de la ley de Henry; ver texto suplementario). Estos valores evidencian una mayor amplitud en la de reducción de  $p\text{CO}_2$  durante los últimos 5 Myr, en comparación con los valores de  $p\text{CO}_2$  obtenidos mediante cálculos basados en modelo de  $\epsilon_p$  por Zhang et al., (2013) y en coherencia con otros métodos de reconstrucción de  $p\text{CO}_2$  para el intervalo (Mejía et al., 2017; Sosdian et al., 2018). Estas observaciones sugieren que, al menos en localidades oligotróficas tropicales, la aplicación de la sensibilidad impuesta por el modelo clásico puede subestimar significativamente la variabilidad y los valores de concentración absolutas de  $p\text{CO}_2$ .

Otro bloque de este trabajo se centra en el análisis de los efectos vitales de oxígeno y carbono en *Gephyrocapsa*: la diferencia entre los valores isotópicos,  $\delta^{18}\text{O}$  y  $\delta^{13}\text{C}$ ,

medidos en los cocolitos de *Gephyrocapsa* y el valor isotópico de las condiciones isotópicas de equilibrio. El valor de referencia isotópica para la estimación de los efectos vitales en *Gephyrocapsa* en este estudio se obtuvo a partir de la normalización de los valores de  $\delta^{18}\text{O}$  y  $\delta^{13}\text{C}$  medidos en *T. sacculifer*, la especie con el hábitat de profundidad más próximo a *Gephyrocapsa* en la zona de estudio y, por tanto, de valores isotópicos más semejantes a las condiciones químicas del medio acuoso a la profundidad de calcificación. Los efectos vitales en el oxígeno (referida como  $\Delta\delta^{18}\text{O}_{\text{Gephyrocapsa-T. sacculifer}}$ ) y en el carbono (referida como  $\epsilon_{\text{cocolith}}$ ) son representativos de las condiciones de fraccionamiento isotópico intracelular del  $\delta^{18}\text{O}$  y  $\delta^{13}\text{C}$  que se incorpora a la calcita en formación, cuya variación puede estar modulada por una conexión con parámetros de índole ambiental, como los niveles cambiantes de temperatura,  $\text{CO}_2$  [aq] y tasas de crecimiento celular y/o de índole fisiológica, como cambios en las tallas celulares, los niveles de pH intracelular, y los procesos de calcificación intracelular. En este trabajo, se realiza una comparación de los valores de efectos vitales en *Gephyrocapsa* con el conjunto de datos medidos en las muestras, representativos o indicativos de algunos de los parámetros anteriormente mencionados. El índice de calcificación empleado en este trabajo es el índice de espesor normalizado en cocolitos (*Size Normalized-SN-Thickness*) y se calculó a partir de las medidas morfométricas de talla y masa en cocolitos de *Gephyrocapsa* en las muestras, mediante el empleo de técnicas de análisis de imagen y el programa C-Calcita (Fuertes et al., 2014). El conjunto de datos en este trabajo supone una de las escasas referencias disponibles para la evaluación directa de estas relaciones en material fósil, a partir de una separación de cocolitos casi monoespecífica. Los resultados proporcionan una clara evidencia de la existencia de un modelo de fraccionamiento isotópico intracelular acoplado para oxígeno y carbono en *Gephyrocapsa* durante el intervalo de estudio, a la luz de la correlación existente entre ambos efectos vitales de oxígeno y carbono en el tiempo. No obstante, la ausencia de correlación clara con los parámetros ambientales y fisiológicos disponibles en este estudio sugiere que todavía se requieren evaluaciones adicionales sobre los procesos intracelulares de fraccionamiento para una comprensión completa y cuantitativa de los impulsores de estos efectos vitales.

## Referencias

- Badger, M.P., 2021. Alkenone isotopes show evidence of active carbon concentrating mechanisms in coccolithophores as aqueous carbon dioxide concentrations fall below 7  $\mu\text{mol L}^{-1}$ . *Biogeosciences* 18, 1149-1160.
- Badger, M.P., Chalk, T.B., Foster, G.L., Bown, P.R., Gibbs, S.J., Sexton, P.F., Schmidt, D.N., Pälike, H., Mackensen, A., Pancost, R.D., 2019. Insensitivity of alkenone carbon isotopes to atmospheric CO<sub>2</sub> at low to moderate CO<sub>2</sub> levels. *Climate of the Past* 15, 539-554.
- Blanco-Ameijeiras, S., Stoll, H.M., Zhang, H., Hopkinson, B.M., 2020. Influence of Temperature and CO<sub>2</sub> On Plasma-membrane Permeability to CO<sub>2</sub> and HCO<sub>3</sub><sup>-</sup> in the Marine Haptophytes *Emiliana huxleyi* and *Calcidiscus leptoporus* (Prymnesiophyceae). *Journal of Phycology*. 56(5), 1283-1294
- Boller, A., Thomas, P., Cavanaugh, C., Scott, K., 2015. Isotopic discrimination and kinetic parameters of R ubis CO from the marine bloom-forming diatom, *Skeletonema costatum*. *Geobiology* 13, 33-43.
- Fuertes, M.-Á., Flores, J.-A., Sierro, F.J., 2014. The use of circularly polarized light for biometry, identification and estimation of mass of coccoliths. *Marine Micropaleontology* 113, 44-55.
- Henderiks, J., Pagani, M., 2007. Refining ancient carbon dioxide estimates: Significance of coccolithophore cell size for alkenone-based pCO<sub>2</sub> records. *Paleoceanography* 22.
- Hernández-Almeida, I., Krumhardt, K., Zhang, H., Stoll, H., 2020. Estimation of physiological factors controlling carbon isotope fractionation in coccolithophores in photic zone and core-top samples. *Geochemistry, Geophysics, Geosystems*, e2020GC009272.
- Köhler, P., Nehrbass-Ahles, C., Schmitt, J., Stocker, T., Fischer, H., 2017. Continuous record of the atmospheric greenhouse gas carbon dioxide (CO<sub>2</sub>), raw data, In supplement to: Köhler, P et al.(2017): A 156 kyr smoothed history of the atmospheric greenhouse gases CO<sub>2</sub>, CH<sub>4</sub>, and N<sub>2</sub>O and their radiative forcing. *Earth Syst. Sci. Data* 9, 363-387.
- Lisiecki, L.E., Stern, J.V., 2016. Regional and global benthic  $\delta^{18}\text{O}$  stacks for the last glacial cycle. *Paleoceanography* 31, 1368-1394.
- Mejía, L.M., Méndez-Vicente, A., Abrevaya, L., Lawrence, K.T., Ladlow, C., Bolton, C., Cacho, I., Stoll, H., 2017. A diatom record of CO<sub>2</sub> decline since the late Miocene. *Earth and Planetary Science Letters* 479, 18-33.
- Pagani, M., 2014. 12.13 Biomarker-based inferences of past climate: The alkenone pCO<sub>2</sub> proxy. *Treatise on Geochemistry*, edited by: Holland, HD and Turekian, KK, Elsevier, Oxford, 361-378.
- Rau, G.H., Riebesell, U., Wolf-Gladrow, D., 1996. A model of photosynthetic <sup>13</sup>C fractionation by marine phytoplankton based on diffusive molecular CO<sub>2</sub> uptake. *Marine Ecology Progress Series* 133, 275-285.

- Sosdian, S.M., Greenop, R., Hain, M., Foster, G.L., Pearson, P.N., Lear, C.H., 2018. Constraining the evolution of Neogene ocean carbonate chemistry using the boron isotope  $\delta^{11}\text{B}$  proxy. *Earth and Planetary Science Letters* 498, 362-376.
- Stoll, H.M., Guitian, J., Hernandez-Almeida, I., Mejia, L.M., Phelps, S., Polissar, P., Rosenthal, Y., Zhang, H., Ziveri, P., 2019. Upregulation of phytoplankton carbon concentrating mechanisms during low  $\text{CO}_2$  glacial periods and implications for the phytoplankton  $p\text{CO}_2$  proxy. *Quaternary Science Reviews* 208, 1-20.
- Wilkens, R.H., Westerhold, T., Drury, A.J., Lyle, M., Gorgas, T., Tian, J., 2017. Revisiting the Ceara Rise, equatorial Atlantic Ocean: isotope stratigraphy of ODP Leg 154 from 0 to 5Ma. *Climate of the Past* 13, 779-793.
- Zhang, Y.G., Henderiks, J., Liu, X., 2020. Refining the alkenone- $p\text{CO}_2$  method II: Towards resolving the physiological parameter 'b'. *Geochimica et Cosmochimica Acta* 281, 118-134.
- Zhang, Y.G., Pagani, M., Liu, Z., Bohaty, S.M., DeConto, R., 2013. A 40-million-year history of atmospheric  $\text{CO}_2$ . *Philosophical Transactions of the Royal Society A: Mathematical, Physical and Engineering Sciences* 371, 20130096.



# Paleoceanography and Paleoclimatology



## RESEARCH ARTICLE

10.1029/2020PA004175

### Key Points:

- Coccolithophore  $\epsilon_p$  sensitivity to  $\text{CO}_2[\text{aq}]$  is consistent with that observed in cultures but contrasts with predictions of classical diffusive models of  $\text{CO}_2$  acquisition
- Geochemical, micropaleontological, and morphometrical proxies are assessed as indicators of the non- $\text{CO}_2$  effects on  $\epsilon_p$
- *Gephyrocapsa* coccoliths show coupled variations in oxygen and carbon isotope vital effects over the time series

### Supporting Information:

Supporting Information may be found in the online version of this article.

### Correspondence to:

A. González-Lanchas,  
[lanchas@usal.es](mailto:lanchas@usal.es)

### Citation:

González-Lanchas, A., Hernández-Almeida, I., Flores, J.-A., Sierro, F. J., Guitián, J., & Stoll, H. M. (2021). Carbon isotopic fractionation of alkenones and *Gephyrocapsa* coccoliths over the Late Quaternary (marine isotope stages 12–9) glacial-interglacial cycles at the western tropical Atlantic. *Paleoceanography and Paleoclimatology*, 36, e2020PA004175. <https://doi.org/10.1029/2020PA004175>

Received 9 DEC 2020

Accepted 5 JUL 2021

© 2021. The Authors.

This is an open access article under the terms of the [Creative Commons Attribution-NonCommercial License](#), which permits use, distribution and reproduction in any medium, provided the original work is properly cited and is not used for commercial purposes.

## Carbon Isotopic Fractionation of Alkenones and *Gephyrocapsa* Coccoliths Over the Late Quaternary (Marine Isotope Stages 12–9) Glacial-Interglacial Cycles at the Western Tropical Atlantic

A. González-Lanchas<sup>1</sup> , I. Hernández-Almeida<sup>2</sup> , J.-A. Flores<sup>1</sup> , F. J. Sierro<sup>1</sup> , J. Guitián<sup>2</sup> , and H. M. Stoll<sup>2</sup> 

<sup>1</sup>Departamento de Geología, Universidad de Salamanca, Salamanca, Spain, <sup>2</sup>Geological Institute, ETH Zürich, Zürich, Switzerland

**Abstract** The sensitivity of coccolithophores to changing  $\text{CO}_2$  and its role modulating cellular photosynthetic carbon isotopic fractionation ( $\epsilon_p$ ) is crucial to understand the future adaptation of these organisms to higher  $\text{CO}_2$  world and to assess the reliability of  $\epsilon_p$  for past  $\text{CO}_2$  estimation. Here, we present  $\epsilon_p$  measured on natural fossil samples across the glacial-interglacial (G-I)  $\text{CO}_2$  variations of marine isotope stages 12 to 9 interval (454–334 ka) at the western tropical Atlantic Ocean Drilling Program Site 925 together with a set of organic and inorganic geochemical, micropaleontological and morphometrical data from *Gephyrocapsa* coccoliths in the same samples. The  $\sim 2\text{‰}$  variation in  $\epsilon_p$  is significantly correlated with the  $\text{CO}_2[\text{aq}]$  concentrations calculated from assumption of air-sea equilibrium with measured ice core  $p\text{CO}_2$  concentrations. The sensitivity of  $\epsilon_p$  to  $\text{CO}_2[\text{aq}]$  is similar to that derived from a multiple regression model of culture observations and is not well simulated with the classical purely diffusive model of algal  $\text{CO}_2$  acquisition. The measured range of *Gephyrocapsa* cell sizes is insufficient to explain the non- $\text{CO}_2$  effects on  $\epsilon_p$  at this location, via either direct size effect or growth rate correlated to cell size. Primary productivity, potentially triggered by shifting growth rates and light levels, may also affect  $\epsilon_p$ . Proposed productivity proxies % *Florisphaera profunda* and the ratio between the  $\text{C}_{37}$  to  $\text{C}_{38,\text{et}}$  alkenone ( $\text{C}_{37}/\text{C}_{38,\text{et}}$  ratio) both correlates modestly with the non- $\text{CO}_2$  effects on  $\epsilon_p$ . When the observed G-I  $\epsilon_p$  to  $\text{CO}_2$  sensitivity at this site is used to estimate  $p\text{CO}_2$  from  $\epsilon_p$  since the Miocene, the inferred  $p\text{CO}_2$  declines are larger in amplitude compared to that calculated from a theoretical  $\epsilon_p$  diffusive model. We find that oxygen and carbon stable isotope vital effects in the near monogeneric-separated *Gephyrocapsa* coccoliths (respectively  $\Delta\delta^{18}\text{O}_{\text{Gephyrocapsa-Trilobatus sacculifer}}$  and  $\epsilon_{\text{coccolith}}$ ) are coupled through the time series, but the origins of these vital effects are not readily explained by existing models.

## 1. Introduction

Coccolithophores, single-celled marine phytoplankton, play a unique role in the marine carbon cycle because their primary production contributes to both the operation of the carbonate counter pump and the biological organic carbon pump during their lifecycle. There is considerable interest in understanding their past role in the carbon cycle and how their growth and calcification may have been affected by changing oceanographic conditions and changing  $\text{CO}_2$  availability (e.g., Bach et al., 2011, 2013; Rigual-Hernández et al., 2020).

At the same time, they produce alkenones, organic biomarkers preserved in sediments, which have been widely applied for two proxies: (a) using the unsaturation ratio of  $\text{C}_{37}$  ketones ( $U_{37}^k$ ), as a proxy for temperature (Müller et al., 1998; Prahl & Wakeham, 1987) and (b) using the photosynthetic carbon isotopic fractionation of alkenones ( $\epsilon_p$ ), to estimate past changes in carbon limitation of algae as an indicator of changing  $p\text{CO}_2$  (e.g., Pagani et al., 1999, 2011; Seki et al., 2010; Y. G. Zhang et al., 2013).

In addition, the carbon and oxygen isotopic composition of their intracellularly produced coccoliths (calcite platelets) are being explored to evaluate if they might provide additional paleoclimatic information. Early studies (e.g., Dudley et al., 1986; Ziveri et al., 2003) documented that the coccolith isotopic composition did not reflect equilibrium precipitation from seawater but was offset due to “vital effects.” Recent models

(Bolton & Stoll, 2013; Hermoso et al., 2014; Holtz et al., 2017; McClelland et al., 2017; Ziveri et al., 2012) have explored whether such vital effects might record different aspects of coccolithophore physiology during cellular growth, such as the ratio of calcification to photosynthesis, carbon uptake and allocation strategies or changes in the dissolved (aqueous) seawater concentration of  $\text{CO}_2$  (hereafter referred as  $\text{CO}_2[\text{aq}]$ ).

While the alkenone temperature proxy is widely applied as a standard temperature indicator, many open questions remain regarding the application of  $\epsilon_p$  for  $p\text{CO}_2$  estimation. The  $\epsilon_p$  is expected to increase with a higher  $\text{CO}_2$  supply to photosynthesis relative to the cellular carbon demand (see Pagani, 2014 for a review). Traditionally, this dependence has been modeled as a passive cellular  $\text{CO}_2$  acquisition by diffusive transport, in which  $\epsilon_p$  varies as a function of  $\text{CO}_2[\text{aq}]$  and the physiological parameter  $b$  (Bidigare et al., 1997; Rau et al., 1996). According to the physical diffusive model,  $b$  is most sensitive to cell size, algal growth rate and the cell permeability to  $\text{CO}_2[\text{aq}]$ ; whereas abiotic factors such as ocean temperature, pH and salinity only exert a minor influence on  $b$  (Bidigare et al., 1997). Under the perspective of this classical model, the limited variation in  $\epsilon_p$  over known quaternary glacial-interglacial (G-I) variations in  $p\text{CO}_2$  has led some to question the suitability of  $\epsilon_p$  as a  $p\text{CO}_2$  proxy (see Badger et al., 2019). Recent aggregate analysis of a large experimental culture data set suggest that the  $\epsilon_p$  dependence on  $\text{CO}_2$  does not follow a purely diffusive model, and that similarly,  $\epsilon_p$  is less sensitive to glacial  $\text{CO}_2$  variations in some sites than predicted by this classical approach (Stoll et al., 2019). One explanation is that intracellular active carbon transport systems sustain carbon concentrating mechanisms (CCM; Cassar et al., 2006; Laws et al., 2002), resulting in the observed lowered sensitivity of  $\epsilon_p$  to  $\text{CO}_2$  within the low  $\text{CO}_2$  range. Among recent contributions considering the role of CCM on  $\epsilon_p$  for  $p\text{CO}_2$  reconstruction, Badger (2021) suggested a  $7 \mu\text{mol L}^{-1}$  threshold for the operation of the CCM, proposing the breakdown of the diffusive alkenone  $p\text{CO}_2$  approach below this threshold concentration. The culture-based regression of the  $\epsilon_p$  dependence on  $\text{CO}_2[\text{aq}]$  by Stoll et al. (2019) incorporates the operation of these non-diffusive mechanisms, regardless of the existence of a threshold, and offers the opportunity to evaluate the implication of further reconstructed coccolithophore physiological (i.e., cell size and growth rate) and environmental (i.e., light) constraints affecting  $\epsilon_p$ .

The most important physiological and environmental processes contributing to carbon and oxygen isotope vital effects in coccoliths remain under investigation. Coccolith oxygen isotopic vital effects have been proposed to reflect the intracellular pH of the calcification space due to the pH effect on the relative contribution of the different carbonate species to calcification (e.g., Langer et al., 2006; Ziveri et al., 2012). This mechanism is analogous to that proposed in planktic foraminifera (e.g., Zeebe, 1999) and arises because of varying fractionation factors between water and the different dissolved carbon species. Alternatively, changes in the intracellular residence time of dissolved carbon species related to cellular growth rates was proposed to regulate oxygen isotope vital effects (e.g., Hermoso et al., 2014). Carbon isotopic fractionation of coccoliths is modeled to be controlled by several factors, such as intracellular  $\text{HCO}_3^-$  allocation between photosynthesis and calcification, the significance of  $\text{HCO}_3^-$  pumping into the cell,  $\text{CO}_2[\text{aq}]$ , organic carbon fixation rate, and the calcification/photosynthesis ratio (e.g., Bolton & Stoll, 2013; Holtz et al., 2017; McClelland et al., 2017), but experimental confirmation of these processes in culture studies remains sparse, and only few studies have explored the effects in coccoliths produced in the ocean under known  $\text{CO}_2$  conditions, as reviewed in Stoll et al. (2019).

In this contribution, we explore the processes influencing the variations in  $\epsilon_p$  and vital effects in *Gephyrocapsa* coccolith carbon and oxygen isotopes in natural samples recovered from sediments from the Western Tropical Atlantic (WTA) warm pool between the Marine Isotope Stage (MIS) 12 to MIS 9 (454–334 ka). The low amplitude of the eccentricity changes during this interval (e.g., Jansen et al., 1986) minimizes the effect of the variance in the magnitude of precessional forcing on productivity and potentially growth rate, increasing the signal/noise ratio for the main research question in this study: the relationship between  $\epsilon_p$  and  $\text{CO}_2$ . This period contains, furthermore, strong contrasts from the extreme glacial MIS 12 to the longest interglacial MIS 11 (e.g., Lang & Wolff, 2011; Yin & Berger, 2012), that provides a broad spectrum to test our results under high and low  $\text{CO}_2$  endmembers during the late Quaternary. A conspicuous feature of this interval is the dominance of the *Gephyrocapsa* genus in the global ocean (Baumann & Freitag, 2004; Bollmann et al., 1998), the main coccolithophore alkenone producer prior to the appearance and proliferation of *Emiliana huxleyi* at  $\sim 280$  ka (e.g., Volkman, 2000). As a result, coccolith assemblages in sediment records are nearly monogeneric, facilitating the generation of coccolith geochemical records derived from

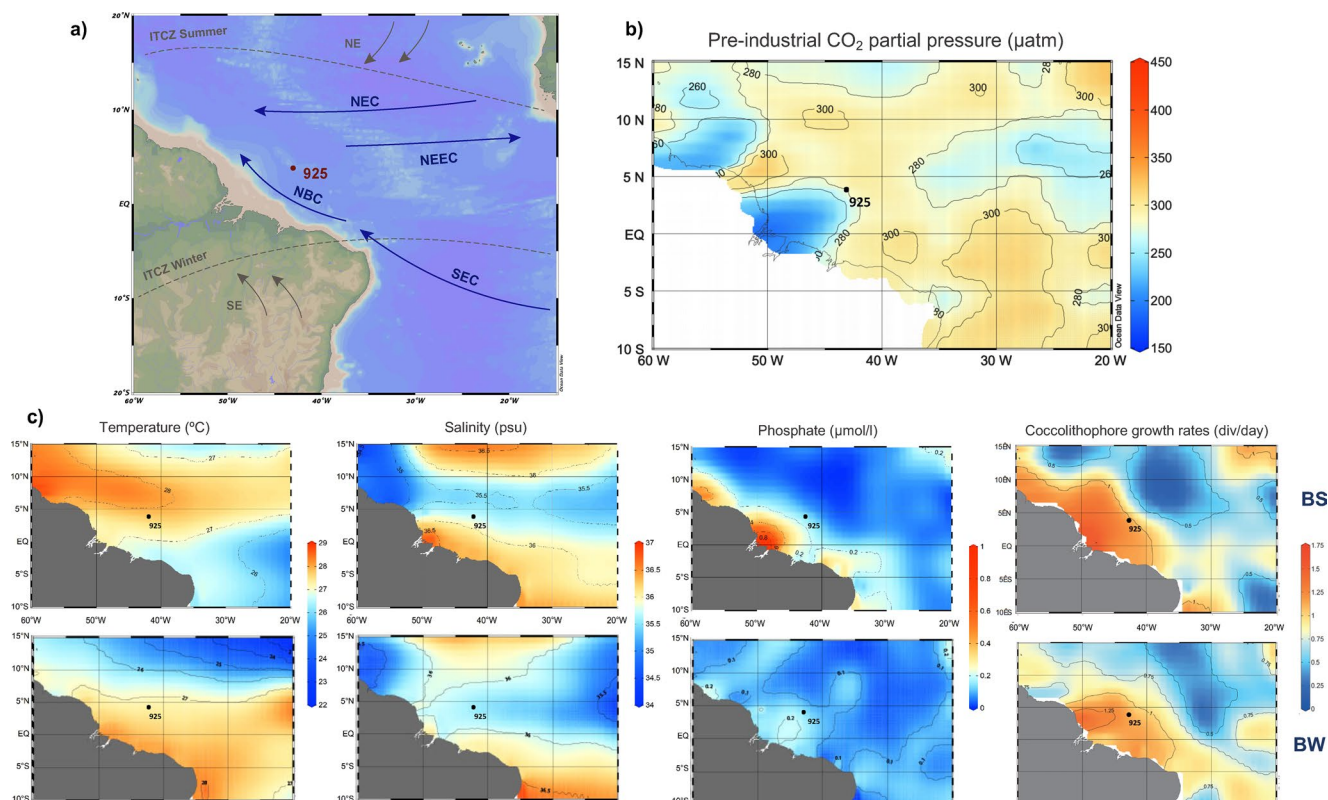


**Figure 1.** (a) Geographic location of the ODP Site 925 and modern oceanographic and climatic scheme. Arrows indicates the trajectories of water masses (in blue) and wind systems (in gray). North Equatorial Current; North Equatorial Counter Current; North Brazilian Current; South Equatorial Current; and Intertropical Convergence Zone. (b) Pre-industrial  $\text{CO}_2$  partial pressure ( $\mu\text{atm}$ ) in the regional ocean surface calculated with MOCSY 2.0 (Orr & Epitalon, 2015) using SST and salinity from GLODAP (Olsen et al., 2016; Key et al., 2015). (c) Seasonal variability at 10 m depth of temperature ( $^{\circ}\text{C}$ ), salinity (psu), phosphate concentration ( $\mu\text{mol l}^{-1}$ ), and coccolithophore growth rate (divisions  $\text{day}^{-1}$ ; Krumhardt et al., 2017). Temperatures, salinities, and  $[\text{PO}_4^{3-}]$  were extracted from the Locarnini et al. (2013) and were plotted using Ocean Data View (Schlitzer, 2008). BS, Boreal summer; BW, Boreal winter.

few closely related *Gephyrocapsa* species (e.g., Bendif et al., 2019), and assessing a unique haptophyte group as alkenone source.

The ODP Site 925 has been previously selected for the reconstruction of  $\text{CO}_2$ , using both boron isotope (Foster et al., 2012; Sosdian et al., 2018) and the alkenone  $p\text{CO}_2$  proxy, including the longest single site  $p\text{CO}_2$  record from present to 40 my (Y. G. Zhang et al., 2013). This site has been chosen for these studies because it is not affected by upwelling and sufficiently distant from coastal influences, so that it is interpreted to have remained close to equilibrium with atmospheric  $\text{CO}_2$ . It maintains very low ( $<18 \mu\text{atm}$ ) post-industrial air-sea  $p\text{CO}_2$  difference (Takahashi et al., 2009) and a low air-sea disequilibrium in the pre-industrial (Figure 1b). It has been, as well, considered for the study of long term evolution of coccolithophore stable isotope vital effects and cellular calcification (e.g., Bolton et al., 2016). In general, tropical sites offer some advantages for the study of the effect of varying  $\text{CO}_2[\text{aq}]$  on coccolithophore proxies: temperature changes are lower than high latitude locations because they are much less affected by the G-I movements of the polar fronts (e.g., Rehfeld et al., 2018), so  $p\text{CO}_2$  is the main driver of  $\text{CO}_2[\text{aq}]$  variations. However, at the location of Site 925, there is only limited published data of  $\epsilon_p$  and coccolith stable isotope fractionation during a quaternary G-I (e.g., Stoll et al., 2019; Y. G. Zhang et al., 2013) to evaluate these proxies against independently constrained variations in  $p\text{CO}_2$  from available ice core records.

We therefore provide new determinations of  $\epsilon_p$  from biomarker analyses and new determinations of carbon and oxygen vital effects from separated coccoliths of the genus *Gephyrocapsa*; hence, we provide matched records of the organic and inorganic carbon isotopic fractionation in coccoliths. The sea surface temperature (SST) and productivity conditions are well reconstructed from  $U_{37}^{k'}$  index, the  $\delta^{18}\text{O}$  gradients between surface and intermediate dwelling planktic foraminifera species, coccolith counts, % *Florisphaera profunda*



and the ratio between the  $C_{37}$  to  $C_{38.et}$  alkenone ( $C_{37}/C_{38.et}$  ratio). *Gephyrocapsa* coccolith morphometry (coccolith length, mass, and thickness) and coccolith assemblage characterization provide additional information on the production environment and surface ocean conditions. The integration of all of these proxies gives us a unique opportunity to parse out the effect of the changing environmental conditions at the WTA and the physiological modulation from *Gephyrocapsa* on  $\epsilon_p$  across the investigated period. Specifically, we are able to compare the new  $\epsilon_p$  observations with the predictions of the diffusive and culture-derived models of the relationship between  $\epsilon_p$  and  $CO_2[aq]$ . In addition, we evaluate whether other independent proxies have power to predict the non- $CO_2$  influences on  $\epsilon_p$ .

## 2. Modern Oceanographic Setting of the Western Tropical Atlantic

The studied ODP Site 925 (4°12.249'N; 43°29.334'W) is located in Ceara Rise, the western sector of the tropical Atlantic Ocean (WTA; Figure 1a). Surface circulation in the region is characterized by the preferential westward flow of the North Equatorial Current (NEC; Figure 1a). South of the NEC, the North Equatorial Counter Current (NECC; Figure 1a), flows in a counter direction (Stramma & Schott, 1999). The North Brazilian Current (NBC; Figure 1a) is the northward bifurcation of the South Equatorial Current (SEC; Peterson & Stramma, 1991).

The seasonal variability in surface ocean conditions is driven by the seasonal shifts in the intensities of SE and NE trade winds and the coupled migration of the Intertropical Convergence Zone (ITCZ; Figure 1a). During boreal summer and fall, the strengthening of SE trade wind system promotes the northernmost movement of the ITCZ and intensification of the westward circulation. In turn, this is the time of NECC development (Hastenrath & Merle, 1987). The NBC experiences a detachment from its Brazilian-coast pathway and retroflects eastward into the NECC (Richardson & Reverdin, 1987). Most of the Amazon discharges concentrate in the shelf, but 7%–17% of terrigenous particles are transported northwest through NBC as dispersion plumes. During boreal winter and spring, when the NE trade winds intensify, the ITCZ reach its southwardmost position (Figure 1a). This causes the disappearance of the NECC. At this time, the NBC continues to flow north-westward off the South American coasts (Philander, 2001; Richardson & Reverdin, 1987).

In the modern WTA, the depth of the mixed layer is stable, with near-permanent highly stratified surface conditions through the entire year (Philander & Pacanowski, 1986). A strong thermocline and nutricline below the photic zone (>100 m) limits the nutrient renewal and the primary productivity in the upper photic zone (see Mann & Lazier, 2006). Surface temperatures and salinities are high and stable throughout the year, with a small temperature increase during the summer (Figure 1c; Locarnini et al., 2013) most likely related to the slight thermocline deepening by pileup of SEC waters (Hastenrath & Merle, 1987). As light and temperature are not limiting factors in the region, changes in coccolithophore growth and production rates are controlled by the changes in nutrient distribution through the euphotic zone (Kinkel et al., 2000). Surface phosphate concentrations and coccolithophore growth rates seasonally range around 0.1–0.2  $\mu\text{mol l}^{-1}$  (Locarnini et al., 2013) and 1–1.25  $\text{day}^{-1}$  (Krumhardt et al., 2017), respectively, with slight increases during the summer (Figure 1c). Despite modest changes, coccolithophore fluxes are highest during the summer and fall, when the water column is stabilized by the northward positioning of ITCZ and weaker influence of NE trades (Guerreiro et al., 2017). Minima in coccolithophore fluxes were found during winter and spring, associated with water column instabilities due to the southward displacement of ITCZ and intensified influence of NE trade winds (Guerreiro et al., 2017).

As important feature in the modern setting, significant stimulation of coccolithophore primary productivity is driven by the eventual nutrient input of Amazon origin (Korte et al., 2020). Higher fluxes of opportunistic species like *Emiliania huxleyi* and those belonging to the *Gephyrocapsa* genus were consistently described as fast productivity response to the increased input of low-salinity and nutrient-enriched waters within the upper ~50 m (e.g., Demaster & Pope, 1996; Guerreiro et al., 2017).

### 3. Sediments and Inference of $p\text{CO}_2$ for Sampled Intervals

The studied materials were retrieved during the expedition ODP 154. The ODP Site 925 is located at 3.040 m water depth, in the shallowest part of Ceara Rise, well above the modern carbonate lysocline (at 4.500 m; Bickert et al., 1997). The studied interval, from 12.96 to 18.80 mcd (meters composite depth) of the splice, corresponds to holes B and C. Sediments are characterized by a continuous alternation of nannofossil clay and nannofossil ooze (Curry et al., 1995).

Twelve samples were selected following the available age model by Wilkens et al. (2017), covering the interval between MIS 12 to MIS 10/MIS 9 (454.24–334.69 ka).

A critical step is the proper assignment of a reference ice core  $p\text{CO}_2$  value for each of the samples considered in this study. To minimize uncertainty due to absolute chronology in both the marine record and Antarctic ice cores, the  $p\text{CO}_2$  corresponding to each sample age was derived from the regression between the deep North Atlantic  $\delta^{18}\text{O}$  benthic stack LS16 (Lisiecki & Stern, 2016) and the  $p\text{CO}_2$  ice core compilation by Köhler et al. (2017) for the last 40 kyr, which is constrained by  $^{14}\text{C}$  dates in the marine archive and layer counted Antarctic ice core chronology back to 30 ka. Results and calibration are shown in Text S1 and Figures S1 and S2. The corresponding  $\text{CO}_2[\text{aq}]$  values for our samples are calculated using Henry's law. We use the alkenone-derived SST at Site 925 for the calculation of  $\text{CO}_2$  solubility. Detailed information and the conversion of values from  $p\text{CO}_2$  to  $\text{CO}_2[\text{aq}]$  for each sample is included in Text S1 and Table S1.

## 4. Analytical Methods and Calculations

### 4.1. Alkenone Analysis and Proxies

Lipids were extracted from 20 g freeze-dried sediment at ETH Zürich with the use of an *Accelerated Solvent Extraction 350*. The lipids were saponified using  $\sim 2$  ml of a 0.5 M solution of potassium hydroxide (KOH) in 95:5 methanol (MeOH)/ $\text{H}_2\text{O}$  and the neutral fraction extracted with hexane ( $\text{C}_6\text{H}_4$ ). The hydrocarbon, ketone and polar organic fractions were separated through silica gel columns, respectively eluted with 4 ml of  $\text{C}_6\text{H}_4$ , dichloromethane ( $\text{CH}_2\text{Cl}_2$ ), and MeOH. The ketone quantification was carried out on a *Thermo Scientific Trace 1310 Gas Chromatograph* (GC) coupled to a Flame Ionization Detector (FID). GC-FID was equipped with an Agilent capillary column (60 m  $\times$  0.25 mm  $\times$  0.25  $\mu\text{m}$ ) *VF-200 ms* and a 5-m guard column. Helium (He) at 2 ml  $\text{min}^{-1}$  was used as carrier gas flow. GC oven was set at 60°C for a minute after injection and then ramped at 20°C  $\text{min}^{-1}$  to 255°C, 3°C  $\text{min}^{-1}$  to 300°C, and finally 10°C  $\text{min}^{-1}$  to 320°C to be held 5 min.

The  $U_{37}^{k'}$  index (Brassell et al., 1986) was calculated after the abundance of the  $\text{C}_{37}$  di- and triunsaturated ketones.  $\text{C}_{39}$   $n$ -alkane was added to every sample as internal standard, and replicates and an in-house alkenone standard was injected at every sequence to determine the analytical accuracy of 0.025  $U_{37}^{k'}$  units. The  $U_{37}^{k'}$  index was converted into SST values with the BAYSPLINE calibration (Tierney & Tingley, 2018), which re-examined available core top data and improves the attenuation observed at high  $U_{37}^{k'}$  with classical linear calibrations, producing a better fit for the SST changes in tropical regions.

Following the connection between the ratio of production of  $\text{C}_{37}$  to  $\text{C}_{38}$  organic compounds with haptophyte growth rates proposed by Herbert et al. (2018), the proportion of  $\text{C}_{37}$  to  $\text{C}_{38,\text{et}}$  ( $\text{C}_{37}/\text{C}_{38,\text{et}}$ ) was calculated; it was proposed that the increase in the value of this ratio implies an increase in the growth rate of the producers that, in this case, corresponds to *Gephyrocapsa*.

The carbon isotopic composition of the diunsaturated alkenone  $\text{C}_{37:2}$  ( $\delta^{13}\text{C}_{37:2}$ ) was analyzed on a Delta V isotope-ratio mass spectrometer coupled to a *Trace 1310 GC* (GC-IRMS) from *Thermo Scientific* at ETH Zürich. Combustion reactor was oxidized for one hour and seed oxidized during one minute before each sequence and injection respectively with equivalent purge of He backflush time. GC was equipped as the GC-FID previously described. Oven temperature was set at 90°C for injection to be ramped after 1 min to 250°C at 25°C  $\text{min}^{-1}$ , 1°C  $\text{min}^{-1}$  to 305°C, and finally to 320°C at 10°C  $\text{min}^{-1}$ . The temperature was kept isothermal for 10 min. To determine analytical precision of the measurements, molecular standards A6 and B4, containing  $n$ -alkanes of known isotopic mixtures (supplied by Arndt Schimmelmann, University of Indiana) replicates and an in-house standard were injected in every sequence to determine the analytical

accuracy. Values are reported relative to the Vienna Pee Dee Belemnite (VPDB) standard. Measurement replicates yielded a mean difference of 0.5‰.

#### 4.2. Planktic Foraminifers

Bulk samples were sieved through 425, 350, 250 and 150  $\mu\text{m}$  with DI water and oven dried overnight at 50°C. Foraminifers were picked from narrow size ranges to minimize large changes in the isotope signal due to size variations (Ezard et al., 2015). Approximately, 15 specimens of *Neogloboquadrina dutertrei* were extracted from the 425–350  $\mu\text{m}$  fraction and the same number of specimens of *Trilobatus sacculifer* (without sac, var. *Trilobatus inmaturus*; Leroy, 1939) and *Globigerinoides ruber* (“white” sensu stricto; Aurahs et al., 2011) from the 350–250  $\mu\text{m}$  fraction. The foraminifer specimens were crushed with two clean moistened glass-slides and rinsed two times in ultrapure MilliQ water. After adding 500  $\mu\text{l}$  of methanol, samples were ultrasonicated for 1 min. Clays were removed with a pipet as an overlying residue. The remaining carbonate content was oven dried overnight at 50°C. Stable isotope analyses were carried out at ETH Zurich (see Section 4.4. for further instrumental details).

The selected species *G. ruber* and *T. sacculifer* dwell near the surface, from 0 to 50 m (Ravelo & Fairbanks, 1992), while *N. dutertrei* is a common thermocline dweller, between 60 and 150 m (Steph et al., 2009). A foraminifer multispecies isotopic approach allows to trace the physical and chemical structure of the mixed layer and thermocline across during the interval. To correct for the influence of species-specific fractionation factors on oxygen isotopes, we applied the species-specific normalization values at 25°C summarized by Spero et al. (2003) to the measured isotope values (Figure 2c). For  $\delta^{18}\text{O}$ , these normalization factors are derived from empirical culture or plankton tow regressions of temperature and foraminiferal  $\delta^{18}\text{O}$  and normalize the other species to the *G. ruber* calibration; that is, we apply the correction factors of  $-0.11\text{‰}$  and  $+0.05\text{‰}$ , respectively to *T. sacculifer* and *N. dutertrei* (see Spero et al., 2003 and references therein).

#### 4.3. *Gephyrocapsa* Coccolith Microfiltration

The coccolith assemblages were extracted and size-separated to isolate the fraction containing the species belonging to the *Gephyrocapsa* genus (see Text S3). An amount of 0.5 g of bulk sample was disaggregated by suspension in 2% ammonia solution and ultrasonication. Larger-sized particles were removed by filtering through a 20  $\mu\text{m}$  nylon mesh. The  $<2\ \mu\text{m}$  fraction, which includes *Florisphaera profunda*, was removed on the basis of its slow settling velocity (H. Zhang et al., 2018). Subsequently, we used 5 and 3  $\mu\text{m}$  polycarbonate membranes to filter a 2 L suspension of the sediment in 2% ammonia to produce a 3–5  $\mu\text{m}$  coccolith fraction. Size fractions were collected by high-speed (4000 RPM) centrifugation, and pellets were rinsed with ultrapure water (Milli-Q). After removing the liquid with a pipette, the coccolith fractions were oven-dried overnight at 50°.

The separation efficiency was checked in smear slides and confirmed that the 3–5  $\mu\text{m}$  fraction is dominated by the *Gephyrocapsa* genus with an average proportion of 86.6%. The  $<3\ \mu\text{m}$  fraction, which also contains *Gephyrocapsa* individuals of 2–3  $\mu\text{m}$ , was not further analyzed as it contained a proportion of undetermined small carbonate fragments.

#### 4.4. Stable Isotope Analysis on Planktic Foraminifers and *Gephyrocapsa* Coccoliths

Carbonate samples from *Gephyrocapsa* coccolith and planktic foraminifers were analyzed at ETH Zürich on a GasBench II coupled to a Delta V isotope-ratio mass spectrometer, as described by Breitenbach and Bernasconi (2011) for small carbonate samples. The instrument was calibrated with the internal standards MS2 ( $\delta^{18}\text{O} = -1.81\text{‰}$ ) and ETH-4 ( $\delta^{18}\text{O} = -18.71\text{‰}$ ) to the international reference materials NBS 19 ( $\delta^{18}\text{O} = -2.2\text{‰}$ ) and NBS 18 ( $\delta^{18}\text{O} = -23.00\text{‰}$ ), yielding a precision of 0.07‰ for both isotopes. Values are reported in relative to the VPDB standard. Measurement replicates yielded a mean difference for oxygen and carbon isotopes of 0.04‰.

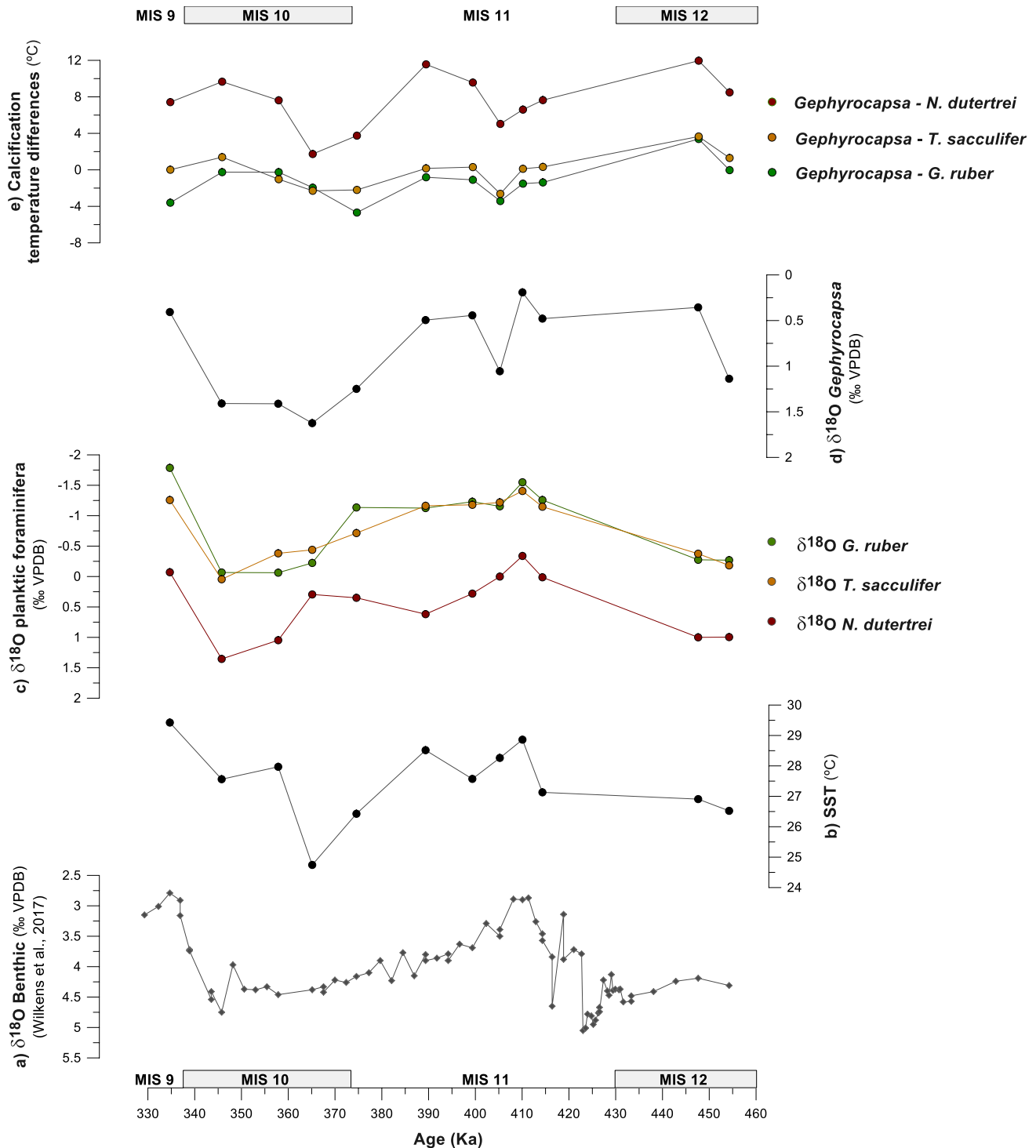


**Figure 2.** Changes in surface water properties across the MIS 12 to MIS 9. (a) spliced  $\delta^{18}\text{O}$  benthic profile at Site 925 (‰ VPDB) by Wilkins et al. (2017); (b)  $U_{37}^k$  alkenone-derived SST (°C); (c) species-specific corrected  $\delta^{18}\text{O}$  values of planktic foraminifera species (‰ VPDB); (d)  $\delta^{18}\text{O}$  *Gephyrocapsa* (‰ VPDB); and (e) paired equilibrium calcification temperature relationships between *Gephyrocapsa* and the planktic foraminifera species (°C). Error bars of inorganic isotopic measurements are omitted for clarity and the values can be found in methods.

#### 4.5. Calculation of $\epsilon_p$ and Vital Effects in Coccolith Carbon and Oxygen Isotopes

The carbon isotopic fractionation during photosynthesis ( $\epsilon_p$ ) is calculated from the carbon isotopic composition of  $\text{CO}_2[\text{aq}]$ ,  $\delta^{13}\text{C}_{\text{CO}_2}$  and the carbon isotopic composition of the haptophyte biomass,  $\delta^{13}\text{C}_{\text{org}}$ , using the following equation by Jasper et al. (1994):

$$\epsilon_p = \left[ \left( \delta^{13}\text{C}_{\text{CO}_2}[\text{aq}] + 1000 \right) / \left( \delta^{13}\text{C}_{\text{org}} + 1000 \right) - 1 \right] \times 1000 \quad (1)$$

For the estimation of  $\delta^{13}\text{C}_{\text{DIC}}$ , the  $\delta^{13}\text{C}$  values of the planktic foraminifer *T. sacculifer* species were used. Given uncertainty about the offset between  $\delta^{13}\text{C}$  *T. sacculifer* and  $\delta^{13}\text{C}_{\text{DIC}}$  (e.g., Birch et al., 2013; Spero et al., 2003), we follow the practice of previous studies (Badger et al., 2019; Y. G. Zhang et al., 2020) and apply the 1‰ calcite- $\text{HCO}_3^-$  fractionation factor, following Romanek et al. (1992), on  $\delta^{13}\text{C}$  *T. sacculifer* for  $\delta^{13}\text{C}_{\text{DIC}}$  estimation. Applying a different fractionation factor between foraminiferal calcite  $\delta^{13}\text{C}$  and  $\delta^{13}\text{C}_{\text{DIC}}$  could lead to slightly different absolute  $\epsilon_p$  values, but would not affect the trends, neither their correlation with any variables which are discussed below. The  $\delta^{13}\text{C}_{\text{CO}_2}[\text{aq}]$  is calculated from  $\delta^{13}\text{C}_{\text{DIC}}$ , as in Benthien et al. (2002). The required temperature values are derived from the  $U_{37}^k$  SST at Site 925.

The  $\delta^{13}\text{C}_{\text{org}}$  is obtained from the  $\delta^{13}\text{C}$  of the alkenone,  $\delta^{13}\text{C}_{37:2}$ , following the equation that integrates the 4.2‰ fractionation factor between alkenones and cellular particulate organic carbon (Jasper et al., 1994; Popp et al., 1998):

$$\delta^{13}\text{C}_{\text{org}} = \left[ \left( \delta^{13}\text{C}_{37:2} + 1000 \right) \times \left( \left( 4.2/1000 \right) + 1 \right) \right] - 1000 \quad (2)$$

The carbon isotope vital effects in *Gephyrocapsa* are calculated as the isotopic offset between the  $\delta^{13}\text{C}$  *Gephyrocapsa* and  $\delta^{13}\text{C}_{\text{DIC}}$  ( $\Delta\delta^{13}\text{C}_{\text{Gephyrocapsa-DIC}}$ ), which approximates  $\epsilon_{\text{coccolith}}$ . The oxygen isotope vital effect in *Gephyrocapsa* is here reported as  $\Delta\delta^{18}\text{O}_{\text{Gephyrocapsa-T. sacculifer}}$ , the isotopical offset in values between  $\delta^{18}\text{O}$  *Gephyrocapsa* and the normalized to equilibrium  $\delta^{18}\text{O}$  of the planktic foraminifer species *T. sacculifer*.

#### 4.6. Coccolith Micropaleontological Analysis and Proxies

Slides for microscopic nanoplankton analysis were prepared following the random settling technique outlined by Flores & Sierro (1997). The abundance of the assemblages was estimated by counting a minimum of 400 coccoliths in a variable number of fields of view with the use of a double polarized-light *Nikon Eclipse 80i* microscope at 1000X magnification at the University of Salamanca. For coccolithophore species identification, we followed Young et al. (2003) and the guide of biodiversity the guide of biodiversity and taxonomy of coccolithophores Nannotax 3 (ina.tmsoc.org/Nannotax3). Further considerations for the recognition and classification of the species belonging to the *Gephyrocapsa* genus and grouping are found in Text S3.

The absolute coccolith abundances (coccolith  $\text{g}^{-1}$  sediment), referred as N, are calculated following Flores and Sierro (1997). N values of the total assemblage could be considered as an estimate of paleoproductivity (e.g., Baumann et al., 2005; Kinkel et al., 2000; Stolz & Baumann, 2010). From the general dependence of the r-strategists *Gephyrocapsa* species on eutrophic conditions in the upper photic zone (e.g., Barber & Hiscock, 2006; Baumann et al., 2005; Young et al., 2000), we use the N *Gephyrocapsa* spp. as a proxy to estimate the degree of nutrient-enriched surface condition in the region.

The species *F. profunda* is a common inhabitant of the deep photic zone (Kinkel et al., 2000; Okada & Honjo, 1973). Following previous authors (Beaufort et al., 1997; Molino & McIntyre, 1990), the relationship between the percentages of *F. profunda* is used to monitor the changes in depth of the nutricline due to water column stratification.

#### 4.7. *Gephyrocapsa* Coccolith Size, Mass, and Thickness

Slides were imaged using a *Zeiss Axiocam 506 color* camera coupled to a *Zeiss Axio Scope HAL100 POL* microscope configured with circular polarization and *Zeiss Plan-APOCHROMAT 100x/1.4 Oil* objective at ETH Zürich. Coccolith length, volume and mass were obtained by processing images with the C-Calcita

software (Fuertes et al., 2014). For thickness calibration, a calcite wedge manufactured at ETH Zürich was used as independent reference, giving its robust relationship between gray level and thickness (González Lemos et al., 2018). A minimum of 100 *Gephyrocapsa* coccoliths between 3 and 5  $\mu\text{m}$  was analyzed. Coccolith lengths serve to derive the *Gephyrocapsa* coccolithophore cellular sizes (radius), following the dimensional relation in Noëlaerhabdaceae by Henderiks and Pagani (2007).

Following Bolton et al. (2016) and references therein, the coccolith thickness is considered as representative of the degree of calcification of coccolithophore cell. Size normalized thickness (SN thickness) was calculated to accurate the size relation of calcification for every measured coccolith by following the equation by O'Dea et al. (2014):

$$\text{SN thickness} = \left[ (\text{ML} - \text{CL}) \times S \right] + \text{CT} \quad (3)$$

where ML = mean coccolith length; CL = length of each individual coccolith in sample;  $S$  = slope of the regression between length and thickness for all coccoliths in sample; and CT = original thickness of each individual coccolith in sample.

#### 4.8. Statistical Analyses

The Pearson correlation coefficient ( $R$ ) and its level of significance ( $p$ -values) are shown to assess the relationship between the proxy data produced and discussed in this study (e.g., Table 2; Figures 5, 6, 9, S7, and S8). This analysis was performed using the package GGally (<https://cran.r-project.org/web/packages/GGally/index.html>) in R software (R core Team, 2021). Correlations with  $p$ -values lower than or equal to the threshold of 0.05 ( $p \leq 0.05$ ) are considered as statistically representative in this study.

Coefficients of determination ( $R^2$ ) were calculated to determine how much of the variation of the predicted variable is explained by the response variable or variables (e.g., Figure 7; Tables S3–S6).

Monte Carlo error propagation was employed to constrain the uncertainty associated with the calculation of  $\epsilon_p$  when we apply the relationships identified during the Late Quaternary (this study) on  $p\text{CO}_2$  estimation back to the Neogene (see Section 6.4).

## 5. Results

### 5.1. Planktic $\delta^{18}\text{O}$ and Surface Ocean Temperature

Planktic foraminifer  $\delta^{18}\text{O}$  and  $U_{37}^{k'}$  alkenone-derived SST temperature record G-I oscillations (Figures 2b and 2c) and show significant correlations with the benthic  $\delta^{18}\text{O}$  ( $R = 0.92/p \leq 0.05$  and  $R = -0.66/p \leq 0.05$ , respectively; Figure 6). The SST records oscillate between 24 and 27°C in glacials MIS 10 and 12 and 27 and 29°C in interglacials MIS 9 and 11, with the coldest temperatures recorded at the early MIS 10 and sustained warmth during the MIS 11 interglacial (Figure 2b). The  $\delta^{18}\text{O}$  trends in the three studied planktic foraminifer species closely parallel the G-I cycles observed in the benthic  $\delta^{18}\text{O}$  record at Site 925 (Figures 2a and 2c). Following correction for species-specific vital effects, trends and values of *G. ruber* and *T. sacculifer* are similar, whereas *N. dutertrei* has  $\delta^{18}\text{O}$  more positive than both *G. ruber* and *T. sacculifer* (by +1.3‰ and +1.24‰, respectively; Figure 2c).

The  $\delta^{18}\text{O}$  *Gephyrocapsa* records a comparable G-I trend to the planktic foraminifer *G. ruber* and *T. sacculifer*, but offset to higher absolute values (Figure 2d). When specific  $\delta^{18}\text{O}$  temperature calibration equations for each taxa are used to estimate calcification temperature relationships (see protocol of calculation in Text S2), assuming similar  $\delta^{18}\text{O}_{\text{sw}}$  in foraminiferal and coccolithophore habitats across the photic zone, as suggested by modern monitoring (Waelbroeck et al., 2014), the calcification temperature of *Gephyrocapsa* is most similar to that of *G. ruber* and *T. sacculifer* and significantly warmer than that of *N. dutertrei* (Figure 2e).

## 5.2. Stratification and Export Production and *Gephyrocapsa* Morphometries

Temporal variations in the indicators of water column stratification and export production exhibit some similarities but also significant divergences. There is a large range (from 0.6‰ to 1.8‰) in the  $\delta^{18}\text{O}$  gradient between *N. dutertrei* and *G. ruber* or *T. sacculifer* (Figure 3b). The lowest gradients coincide with the coldest  $U_{37}^k$  SST, early in MIS 10 (Figures 2b and 3b). In contrast to this large variability in the isotopic indicators of stratification, the coccolith-derived proxy of stratification, *F. profunda*, is more stable (Figure 3c). The coccolith assemblage is dominated by the *Gephyrocapsa* genus (average 70%; Figure 3d and Text S3) and the relative abundance of *F. profunda* varies only slightly between 20% and 32% (Figure 3c). These modest variations in the percentages of *F. profunda* show no consistent relationship with G-I cycles (Figure 3c), nor with the higher amplitude variations in  $\Delta^{18}\text{O}_{N. dutertrei-G. ruber}$  (Figures 2b and 6).

The N of the total assemblage and *Gephyrocapsa* species is high during MIS 12 and progressively decreases by 40% within MIS 11 and MIS 10 (Figure 3f). A moderate final increase is observed at MIS 10/MIS 9 (334 ka; Figure 3f). The maintenance of high values around 1 in the CEX dissolution index (Text S4 and Figure S5) indicates a negligible dissolution effect. The alkenone C37/C38. et ratio exhibits high values from 1.75‰ to 1.95‰ at MIS 12 and generally decreases through MIS 11 and MIS 10, from 1.95‰ to 1.6‰, but exhibits more structure than the N coccolith, with local maxima at 447, 399, 374, and 357 ka (Figure 3g).

Maximum length and mass of *Gephyrocapsa* coccoliths are attained during the glacial periods (Figures 3i and 3j). A maximum mass of 8 pg characterizes the coldest part of MIS 10 glacial at 365 ka, whereas minimum mass of 6.5 pg occurs during the earlier MIS 11, at 414 ka (Figure 3j); length is significantly correlated with the benthic  $\delta^{18}\text{O}$  as an indicator of G-I stages ( $R = 0.56/p \leq 0.05$ ; Figure 6). In comparison with the measured range in modern Noëlaerhabdaceae (González Lemos et al., 2018), the SN thickness in *Gephyrocapsa* coccoliths does not vary significantly at Site 925 (Figure 3h). There is no overall correspondence between the changes in the *Gephyrocapsa* morphometrical parameters and the changes in the species composition of the *Gephyrocapsa* assemblage, because the assemblage variations are minor and not dominated by G-I cyclicity (Text S3 and Figure S5).

## 5.3. $\epsilon_p$ and Vital Effects in *Gephyrocapsa* Coccolith Carbon and Oxygen Isotopes

$\epsilon_p$  and  $\epsilon_{\text{coccolith}}$  are calculated using the  $\delta^{13}\text{C}$  of *T. sacculifer* (Figure 4b) as an indicator of the  $\delta^{13}\text{C}_{\text{DIC}}$ . As this planktic foraminifer species shows a similar calcification temperature as *Gephyrocapsa* through the interval (Figure 2e), it is considered to share the most similar production depth and season as the alkenone producers.  $\epsilon_p$  ranges from 12.1‰ to 14.3‰, and is dominantly driven by the 3‰ variation in  $\delta^{13}\text{C}_{37:2}$  (Figures 4c and 4d).  $\epsilon_p$  is higher during interglacials and lower during glacials (Figure 4d) and is significantly correlated with the benthic  $\delta^{18}\text{O}$  ( $R = -0.7/p \leq 0.05$ ; Figures 5a and 6) and the  $\delta^{18}\text{O}$  of *G. ruber* ( $R = -0.61/p \leq 0.05$ ; Figures 5b and 6).

The *Gephyrocapsa* carbon vital effects from  $\epsilon_{\text{coccolith}}$  ranges from 0.47‰, recorded at MIS 12, to 2.32‰ at MIS 10 (Figure 4f). The *Gephyrocapsa* oxygen vital effects, from  $\Delta\delta^{18}\text{O}_{\text{Gephyrocapsa-T. sacculifer}}$  range from +0.7 to +2.2 (Figure 4g). Both the carbon and oxygen vital effect profiles increase from the lowest values at MIS 12 (447 ka) to the highest at MIS 10 (365 ka; Figures 4f and 4g).

## 6. Discussion

### 6.1. Evolution of Surface Production Environment From MIS 12 to MIS 9

Both the relative abundance of deep photic zone coccolithophore species *F. profunda* and the isotopic  $\Delta\delta^{18}\text{O}$  gradient between the shallow living species *G. ruber* and *T. sacculifer* and the thermocline-dwelling *N. dutertrei* (Figures 3b and 3c) are proposed as indicators of upper water column stratification. Higher values of  $\Delta\delta^{18}\text{O}_{N. dutertrei-G. ruber}$  and  $\Delta\delta^{18}\text{O}_{N. dutertrei-T. sacculifer}$  are indicative of large temperature gradients that imply increased stratification (Vink et al., 2002). In oligotrophic water masses, higher percentages of *F. profunda* are linked to a deep nutricline, while low percentages characterize a shallow nutricline (e.g., Ahagon et al., 1993; Beaufort et al., 1997; Molino & McIntyre, 1990). Compared with other oceanographic regions, the maxima  $\Delta\delta^{18}\text{O}_{N. dutertrei-G. ruber}$  (1.7‰) and  $\Delta\delta^{18}\text{O}_{N. dutertrei-T. sacculifer}$  (1.78‰) in this study (Figure 3b)

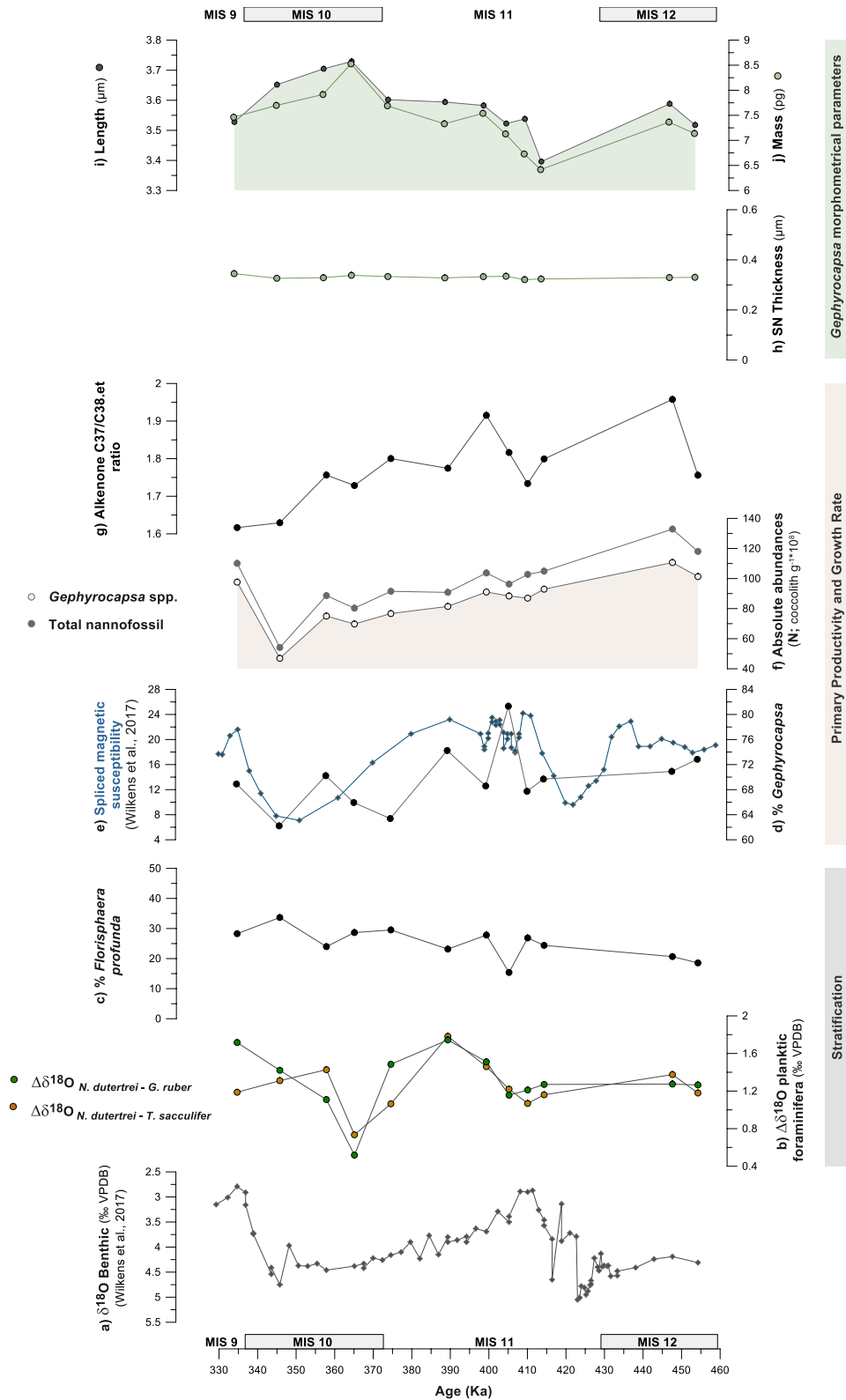


Figure 3



are intermediate between those of intensely upwelled waters of the Arabian sea (1‰; Prell & Curry, 1981) and the highly stratified surface waters of the northern Panama basin (2‰; Curry et al., 1983). However, our G-I  $\Delta\delta^{18}\text{O}$  estimates for the MIS 12–9 at Site 925 are similar to those observed in core tops in the region (Dekens et al., 2002) and during the last glacial cycle, from comparable  $\Delta\delta^{18}\text{O}_{T. \text{sacculifer-G. truncatulinoides}}$  (Wilson et al., 2011).

The relative abundance of *F. profunda* at Site 925 is also intermediate between the low values of upwelling regions and the very high values of strongly stratified regions. Application of the global calibration of % *F. profunda* by Hernández-Almeida et al. (2019) suggests an average primary productivity of  $760 \text{ mgC m}^{-2} \text{ day}^{-1}$ , also corresponding to a moderate supply of deep nutrients into the upper photic zone. These estimates are consistent with the modest growth rates modeled for Site 925 today, which are also in the intermediate range compared to other tropical settings (Krumhardt et al., 2017, Figure 1c). Although these proxies agree on the intermediate average rate of nutrient supply to the surface photic zone,  $\Delta\delta^{18}\text{O}_{N. dutertrei-G. ruber}$  and  $\Delta\delta^{18}\text{O}_{N. dutertrei-T. sacculifer}$  are much more variable than percentages of *F. profunda* (Figures 3b and 3c). We suggest that the minimum in  $\Delta\delta^{18}\text{O}_{N. dutertrei-G. ruber}$  and  $\Delta\delta^{18}\text{O}_{N. dutertrei-T. sacculifer}$  at 365 ka, coincident with the lowest SST of the record (Figures 2b and 3b) may reflect a shallowing of the depth habitat of *N. dutertrei* in response to the intense cooling, rather than a true reduction in stratification. We, therefore, more confidently interpret the *F. profunda* record and infer that the stratification and rate of mixing of the upper water column has not varied significantly at this site through MIS 12–9.

While stratification was invariant over time, the abundance of coccoliths in sediments decreases progressively from MIS 12 through MIS 9, a trend also observed as a decrease in the alkenone C37/C38.et ratio (Figures 3f and 3g). This suggests potential variation in algal growth rates and export production unrelated to changes in stratification. At the Site 925 setting, the Amazon River plume represents another source of nutrients to the upper photic zone, which are distributed in the upper 50 m of water column (e.g., Boyle et al., 1977; DeMaster et al., 1986). The magnetic susceptibility at Site 925, inferred as an indicator of Amazon-derived detrital magnetic minerals (Francois & Bacon, 1991), is significantly correlated to N *Gephyrocapsa* ( $R = 0.68/p \leq 0.05$ ; Figure 6) and has a correspondence with the percentages of *Gephyrocapsa* (Figures 3e and 3d). This positive correlation trend is opposite to that expected if coccoliths were diluted by terrigenous input or carbonate dissolution were controlling the concentration of magnetic minerals.

The multiple linear regression of magnetic susceptibility and percentages of *F. profunda* explains 62% of the variability of N *Gephyrocapsa* (Table S3). We suggest that the decrease in *Gephyrocapsa* production was mainly triggered by a decline in delivery of nutrients from Amazon plume waters to the surface above the Site 925. The increase in percentages of *F. profunda* and decrease of N *Gephyrocapsa* from MIS 12 to MIS 9 (Figures 3c and 3f) is coherent with reduced euphotic zone fertilization, either from a decline in the surface delivery of nutrients by a limitation in the influence of Amazon plume waters above the Site 925 (Figure 3e) or a slight general deepening of the nutricline.

## 6.2. CO<sub>2</sub> and Other Environmental Influences on $\epsilon_p$ at Site 925

At Site 925, 48% of the variability of the measured  $\epsilon_p$  record is explained by  $\ln(\text{CO}_2[\text{aq}])$ ,  $R^2 = 0.48$  (Figure 7), confirming a significant influence of the changes in  $\text{CO}_2[\text{aq}]$  on  $\epsilon_p$  across the MIS 12 to MIS 9.

The mechanistic interpretation of the relationship between  $\epsilon_p$  and  $\text{CO}_2[\text{aq}]$  is still under debate (e.g., Badger, 2021; Stoll et al., 2019). Traditionally, the relationship has been interpreted to arise from a purely diffusive  $\text{CO}_2$  supply across a cell into a single intracellular space in which carbon was fixed (e.g., Rau et al., 1996). Subsequently, multiple-compartment cellular models revealed that, in addition to diffusion into the cell, enhancement of the concentration of dissolved inorganic carbon in intracellular compartments, including the site of carbon fixation, could regulate the relationship between  $\epsilon_p$  and  $\text{CO}_2[\text{aq}]$  (e.g., Cassar et al., 2006;

**Figure 3.** Surface production proxies: (a) spliced  $\delta^{18}\text{O}$  benthic profile at Site 925 (‰ VPDB) by Wilkens et al. (2017); (b)  $\Delta\delta^{18}\text{O}_{N. dutertrei-G. ruber}$  (green dots) and  $\Delta\delta^{18}\text{O}_{N. dutertrei-T. sacculifer}$  (yellow dots) (‰ VPDB); (c) % *Florisphaera profunda*; (d) % *Gephyrocapsa*; (e) spliced magnetic susceptibilities at Site 925 by Wilkens et al. (2017); (f) absolute abundances, N (coccolith  $\text{g}^{-1}$  sediment), of *Gephyrocapsa* (colored section) and the total assemblage (black dots); and (g) alkenone C37/38.et ratio. *Gephyrocapsa* coccolith morphometries in samples (h) average size normalized (SN) thickness ( $\mu\text{m}$ ). The scale is adjusted to the range of variability of modern Noëlaerhabdaceae by González Lemos et al. (2018); (i) average coccolith length ( $\mu\text{m}$ ); and (j) average coccolith mass (pg).

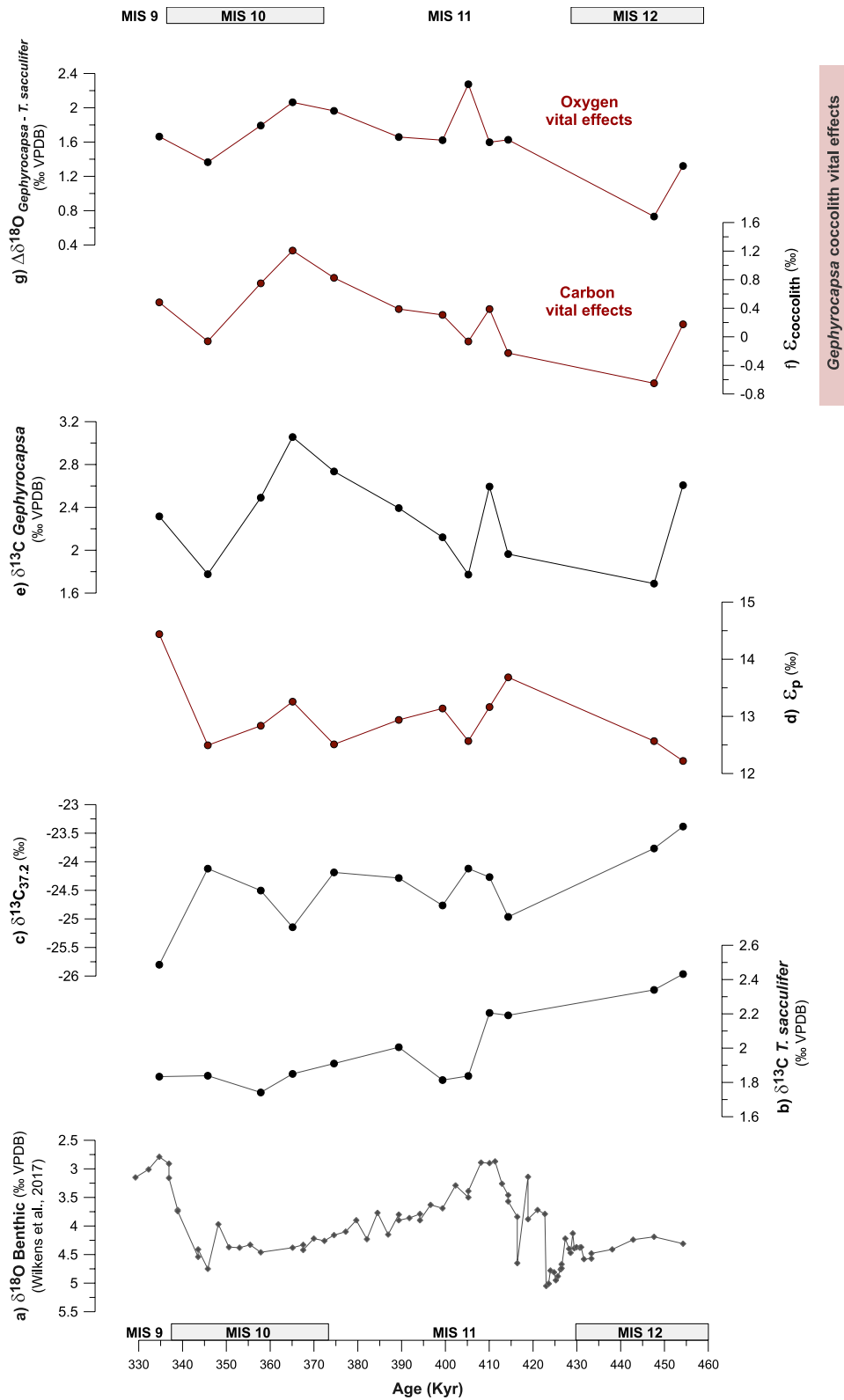
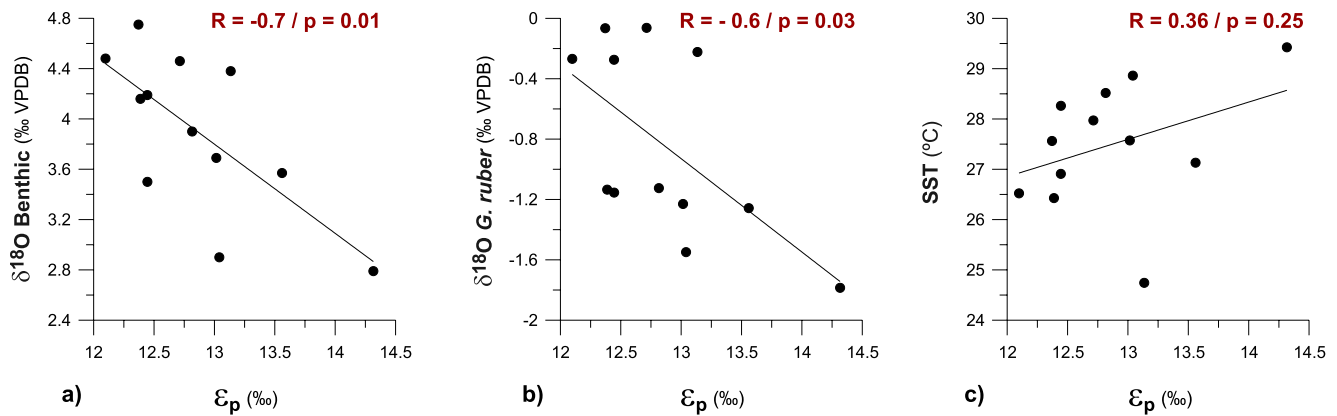


Figure 4



**Figure 5.** Relationship of  $\epsilon_p$  with regional proxies at Site 925: (a)  $\delta^{18}\text{O}$  benthic at Site 925 (Wilkins et al., 2017); (b)  $\delta^{18}\text{O}$  *G. ruber*; and (c)  $U_{37}^k$  alkenone-derived SST ( $^{\circ}\text{C}$ ).

Hopkinson et al., 2011). The relationship between  $\epsilon_p$  and  $\text{CO}_2[\text{aq}]$  found in cultured phytoplankton appears inconsistent with a purely diffusive acquisition (Stoll et al., 2019).

In this section, we review the degree to which the new data of  $\epsilon_p$  from fossil record at Site 925 could be consistent with (a) the diffusive model (Rau et al., 1996) with varying assumptions of growth rate and the Rubisco fractionation factor (Section 6.2.1) and (b) the empirical dependence observed in laboratory cultures (Stoll et al., 2019), which is known to respond to the operation of carbon concentrating mechanisms (Section 6.2.2).

### 6.2.1. $\epsilon_p$ Compared to Predictions From Diffusive Model

According to the diffusive model of phytoplankton carbon acquisition, the increasing  $\text{CO}_2[\text{aq}]$  promotes a higher relative carbon supply to cellular demand, resulting in higher  $\epsilon_p$  (Rau et al., 1996). Beyond this control, other environmental and physiological parameters can modify this relationship if cellular carbon requirements change: smaller cell sizes, entailing a higher surface area/volume (SA/V) ratio, or lower growth rates, would both be expected to maintain a high ratio of diffusive  $\text{CO}_2$  supply relative to cellular carbon demand, leading as well to higher  $\epsilon_p$ .

Using the model of Rau et al. (1996), we incorporate the measured *Gephyrocapsa* cell radius and  $\epsilon_p$  at Site 925 together with the estimated  $\text{CO}_2[\text{aq}]$ , and the recent experimental determinations of cell permeability to  $\text{CO}_2$  by Blanco-Ameijeiras et al. (2020) to evaluate if the response of  $\epsilon_p$  is consistent with the physical diffusive model. There are no independent determinations of absolute growth rates across the MIS 12–9 at the studied location, so we explore possible values, including (a) the application of a recently suggested regression to infer growth rates from coccolithophore cell size by Y. G. Zhang et al. (2020) (simulations A and F in Table 1 and Figure 8), (b) growth rates estimated using the  $\text{PO}_4$  and temperature formulation by Krumhardt et al. (2017) with constant modern  $\text{PO}_4$  (Figure 1c) and either average constant temperature (simulation E in Table 1; Figure 8b) or the  $U_{37}^k$  SST temperature variation at Site 925 (simulations B and G in Table 1; Figure 8), and (c) absolute growth rates used as a tuning parameter to improve agreement between the modeled and observed  $\epsilon_p$  (simulations C and D in Table 1; Figure 8a).

When the diffusive model is applied assuming a maximum effective enzymatic Rubisco fractionation factor ( $\epsilon_r$ ) of 25‰, as traditionally simulated (Figure 8a) the modeled  $\epsilon_p$  is significantly higher than the

**Figure 4.**  $\epsilon_p$  and vital effects in *Gephyrocapsa* coccolith carbon and oxygen stable isotopes: (a) spliced  $\delta^{18}\text{O}$  benthic profile at Site 925 (‰ VPDB) by Wilkins et al. (2017); (b)  $\delta^{13}\text{C}_{\text{DIC}}$  calculated from  $\delta^{13}\text{C}$  *T. sacculifer* (‰ VPDB); (c)  $\delta^{13}\text{C}_{37:2}$  (‰ VPDB); (d)  $\epsilon_p$  measured at Site 925 (‰ VPDB); (e)  $\delta^{13}\text{C}$  *Gephyrocapsa* (‰ VPDB); (f) *Gephyrocapsa* carbon vital effects, as  $\epsilon_{\text{coccolith}}$  (‰ VPDB); and (g) *Gephyrocapsa* oxygen vital effects as  $\Delta\delta^{18}\text{O}_{\text{Gephyrocapsa-T. sacculifer}}$  (‰ VPDB). Error bars of organic isotopic measurements are omitted for clarity and the values can be found in methods; error on  $\epsilon_p$  is typically  $<0.5\%$ , smaller than the size of the symbol.

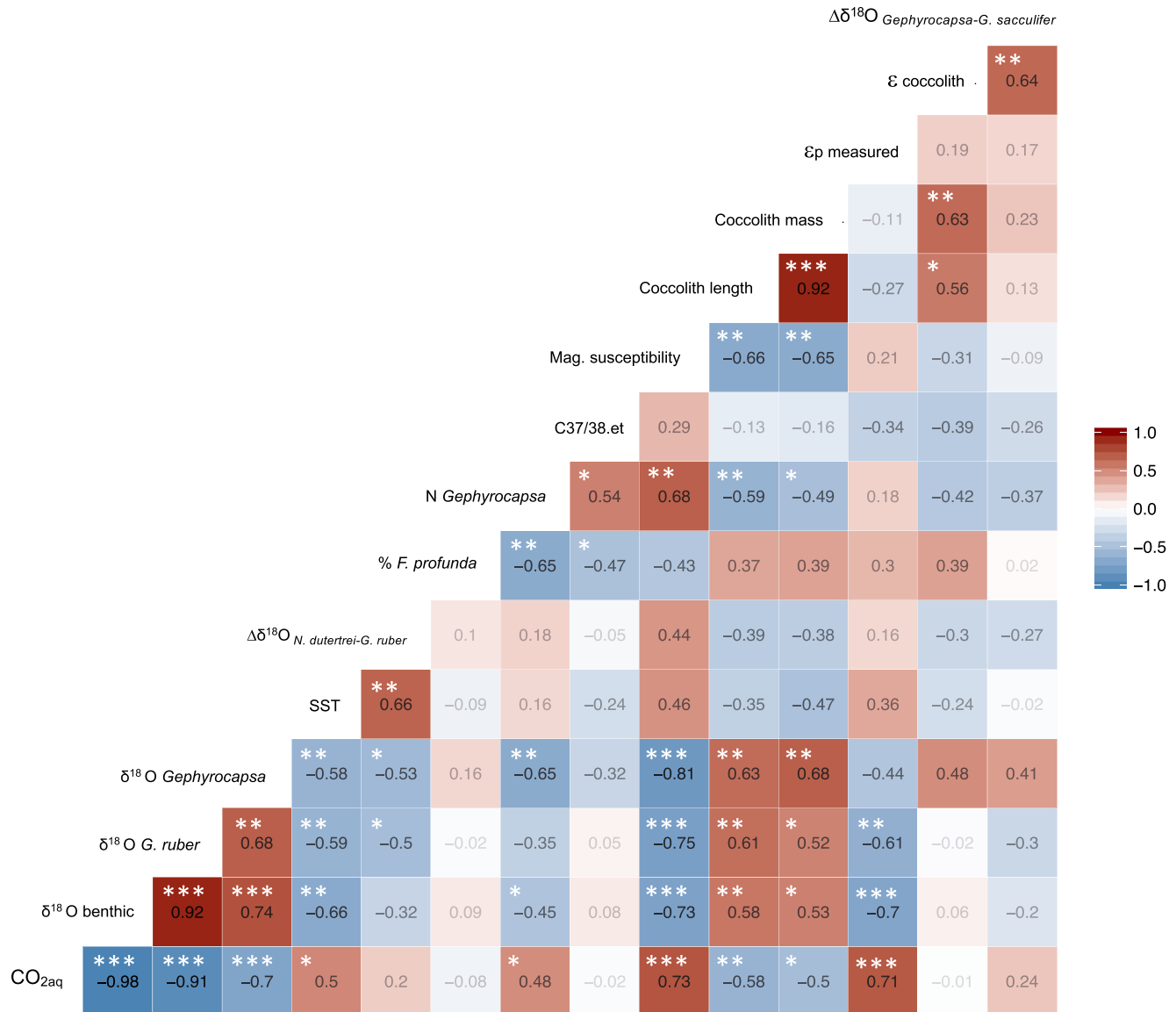


**Figure 6.** Pearson correlation matrix of the proxies and data in this study: CO<sub>2</sub>[aq], δ<sup>18</sup>O *G. ruber*, δ<sup>18</sup>O *Gephyrocapsa*, U<sub>37</sub><sup>k'</sup> alkenone-derived SST, Δδ<sup>18</sup>O<sub>N. dutertrei-G. ruber</sub>, % *F. profunda*, absolute values (N; coccolith g<sup>-1</sup> sediment) of *Gephyrocapsa*, alkenone C37/38.et ratio, average *Gephyrocapsa* coccolith length and mass, ε<sub>p</sub>, ε<sub>coccolith</sub>, and Δδ<sup>18</sup>O<sub>*Gephyrocapsa-G. sacculifer*</sub>. The spliced δ<sup>18</sup>O benthic and magnetic susceptibilities at Site 925 by Wilkens et al. (2017) are also included. Symbols represent the statistical significance: \*\*\*p ≤ 0.01; \*\*p ≤ 0.05 and \*p ≤ 0.1.

observations at Site 925 when growth rates are estimated (a) using the cell size regression by Y. G. Zhang et al. (2020) from the *Gephyrocapsa* cell radius at Site 925 (simulation A; Figure 8a) or (b) following Krumhardt et al. (2017) with constant modern PO<sub>4</sub> (Figure 1c) and variable temperature from SST at Site 925 (simulation B; Figure 8a). With ε<sub>f</sub> of 25‰, only significantly higher growth rates lead to ε<sub>p</sub> close to the measured values at Site 925: a constant high growth rate of 2.2 days<sup>-1</sup> matches the average measured ε<sub>p</sub>, but features a much higher than observed slope of ε<sub>p</sub> versus CO<sub>2</sub>[aq] (simulation C; Figure 8a). However, while this growth rate matches ε<sub>p</sub>, it is not consistent with independent estimates of the growth rate in this setting (e.g., Krumhardt et al., 2017). Only a model in which the growth rate is high but decreases significantly (26%) as CO<sub>2</sub>[aq] decreases to glacial values, is able to reproduce the slope and absolute values of the measured ε<sub>p</sub> at Site 925 (simulation D; Figure 8a), that is, the low sensitivity of ε<sub>p</sub> to CO<sub>2</sub> would need to be caused by a compensating depression of growth rate during the low CO<sub>2</sub> periods. However, laboratory experiments based on half-saturation constant (K<sub>M</sub>) for CO<sub>2</sub> from observations by Sett et al. (2014) suggest that growth rate is much less sensitive to CO<sub>2</sub> (around 6% reduction in growth rates over this range of CO<sub>2</sub>[aq]).

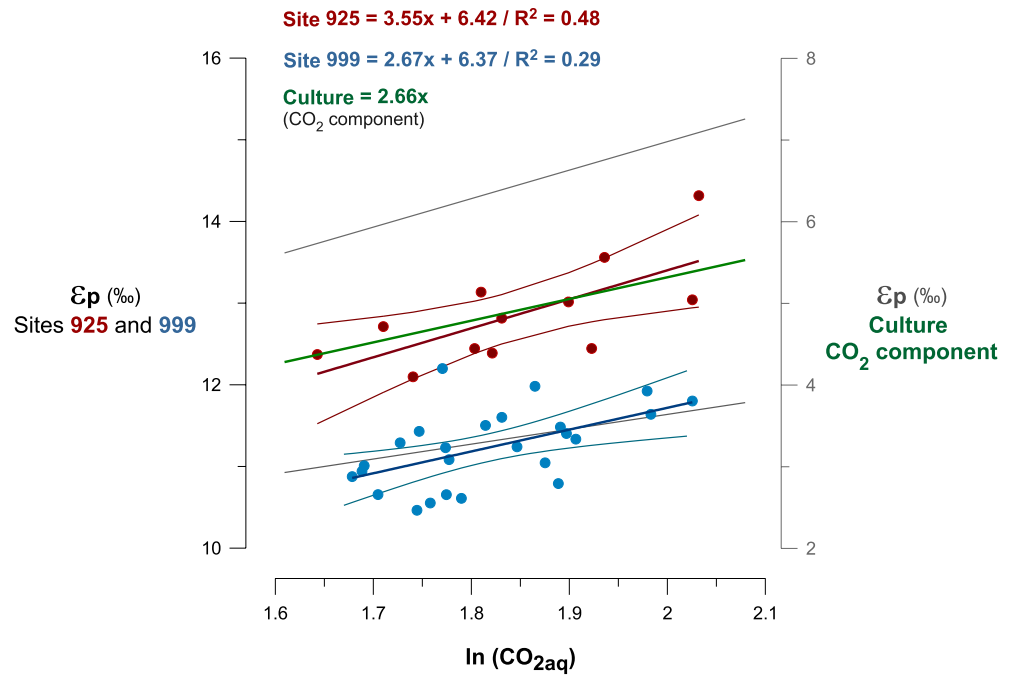


**Figure 7.** On the left y-axis: Regression of  $\epsilon_p$  measured at Site 925 and  $\ln(CO_{2aq})$  during the MIS 12–9, in red; regression of  $\epsilon_p$  at the nearby Site 999 and  $\ln(CO_{2aq})$  during the G-I period between MIS 8–5 (Badger et al., 2019), in blue. The best fit (lineal equation) and 95% confidence intervals are represented for both data sets. On the right y-axis: slope of the culture regression between the  $CO_2$  component on  $\epsilon_p$  and  $\ln(CO_{2aq})$  (Stoll et al., 2019), in green; the black lines represent the range of culture  $\epsilon_p$  obtained from the upper and lower confidence interval (95% CI: 3.5 and 1.83, respectively) of the slope of the culture dependence of  $\epsilon_p$  on  $CO_2$  ( $\epsilon_p$  vs.  $\ln(CO_{2aq})$ )).

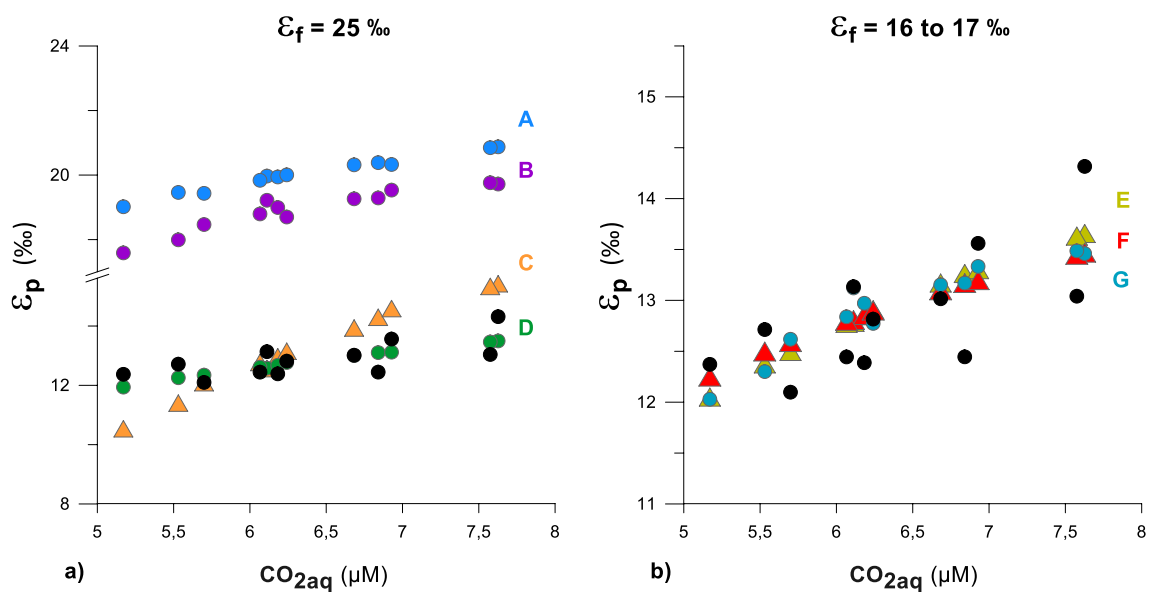


**Figure 8.** Regression of  $\epsilon_p$  measured at Site 925 and  $CO_{2aq}$ , in black dots, in comparison with the  $\epsilon_p$  predicted from the diffusive model given different assumptions of (a) large Rubisco fractionation ( $\epsilon_f = 25\%$ ) or (b) lower fractionation ( $\epsilon_f = 16\text{--}17\%$ ). The different assumptions and estimations for growth rate carried out for each  $\epsilon_p$  simulation (a) to (g) are indicated with colored symbols in the figure detailed in Table 1.

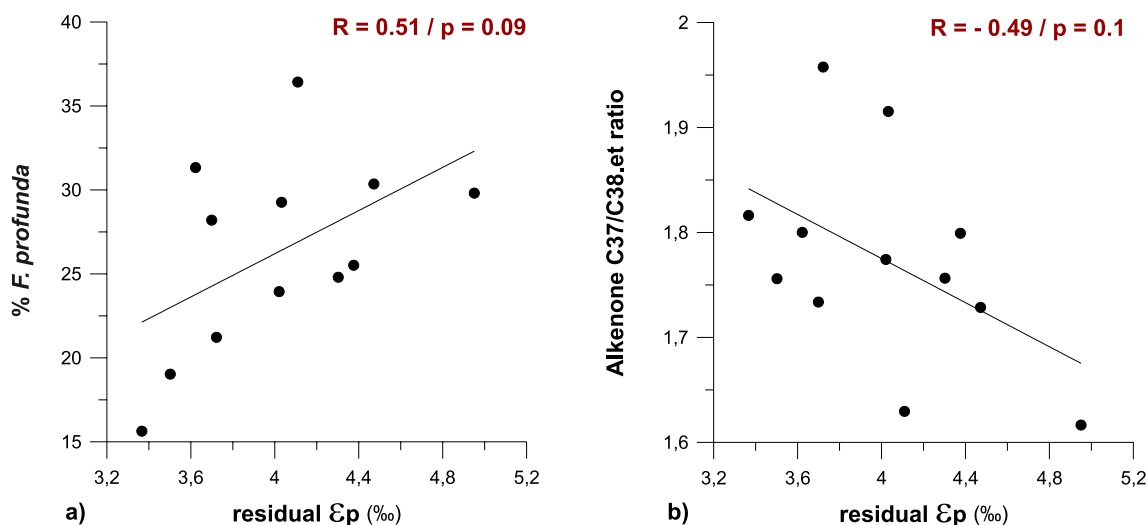


**Figure 9.** Correlation  $R$  of the non- $\text{CO}_2$  variation in  $\epsilon_p$  (residual  $\epsilon_p$  variation) with the surface production and growth rate proxies (a) % *Florispheera profunda* and (b) alkenone C37/38.etc ratio.

Alternatively, the low observed  $\text{CO}_2$  sensitivity of  $\epsilon_p$  could arise in a diffusive model due not to the influence of compensating effects of growth rate, but rather to a lower slope of the  $\epsilon_p$  to  $\text{CO}_2$  relationship, as would occur if  $\epsilon_f$  were lower than 25‰ (Figure 8b). There are no  $\epsilon_f$  data for *Gephyrocapsa* species to date, but some recent studies of Rubisco fractionation in marine eukaryotes suggest values lower than 25‰, which yield a range of 11‰–18‰ from the study of the coccolithophore species *E. huxleyi* and the diatom species *Skellonema costatum* (Boller et al., 2011, 2015). With growth rates in the range of 0.9–1.14  $\text{day}^{-1}$ , as obtained when estimating growth rates following both Y. G. Zhang et al. (2020) and Krumhardt et al. (2017 Table S2), the  $\epsilon_p$  measured at Site 925 and the observed slope of  $\epsilon_p$  versus  $\text{CO}_2[\text{aq}]$  are well matched by the  $\epsilon_p$  diffusive simulations when  $\epsilon_f$  values are in the range of 16‰–17‰ (simulations E–G; Figure 8b), an intermediate value between 11‰ and 18‰, which we incorporate as a sensitivity analysis. This suggests that, if the observations are to be described by diffusive model, much lower  $\epsilon_f$  than 25‰ (Figure 8b), or a much stronger growth rate dependence on  $\text{CO}_2$ , must be used (simulations C and D; Figure 8a). However, in the Oligocene at Site 925, the measured  $\epsilon_p$  values of 18‰–25‰ (Y. G. Zhang et al., 2013) are not compatible with an  $\epsilon_f$  of

**Table 1**

Compilation of Detailed Information of  $\epsilon_p$  Simulations From the Different Assumptions of Rubisco Fractionation ( $\epsilon_f$ ) and Growth Rate ( $\mu$ ) Applied to Evaluate the Adequacy of the Physical Diffusive Model (Rau et al., 1996) to Explain the Variability in  $\epsilon_p$  Measured in Site 925.

Simulations	RMSE	$\epsilon_f$ (‰)	Estimation or assumption for $\mu$ ( $\text{day}^{-1}$ )	$\mu$ variation (%)	$\mu$ average ( $\text{day}^{-1}$ )
A	7.51	25	Cell size regression by Y. G. Zhang et al. (2020) from <i>Gephyrocapsa</i> cell radius at Site 925	10	0.92
B	6.38	25	Estimation by Krumhardt et al. (2017) with constant modern $\text{PO}_4$ and temperature variation from SST at Site 925	14	1.14
C	1.24	25	Constant high $\mu$ to minimize RMSE	0	2.2
D	0.46	25	High $\mu$ that decreases during low $\text{CO}_2$ (compensating depression of $\mu$ )	26	2.32
E	0.46	17	Estimation by Krumhardt et al. (2017) with constant modern $\text{PO}_4$ and constant temperature from average SST at Site 925	0	1.14
F	0.46	16	Average $\mu$ from cell size regression by Y. G. Zhang et al. (2020) from <i>Gephyrocapsa</i> cell radius at Site 925	0	0.92
G	0.48	17	Estimation by Krumhardt et al. (2017) with constant modern $\text{PO}_4$ and temperature variation from SST at Site 925	14	1.14

Note. A constant value of cell permeability ( $P$ ) of  $1 \times 10^{-4} \text{ cm s}^{-1}$  is taken from experimental determinations by Blanco-Ameijeiras et al (2020). The  $\epsilon_p$  simulations A to G are plotted in Figure 8.

Abbreviation: RMSE, root mean square error.

**Table 2**  
Pearson Correlation  $R$  Between the Residual  $\epsilon_p$  and the Set of Proxies for Surface Production and Growth Rate

	$\Delta\delta^{18}\text{O}_{\text{N. duertrei-G. ruber}} (\text{‰ VPDB})$	% <i>F. profunda</i>	C37/38.et	N <i>Gephyrocapsa</i>	<i>Gephyrocapsa</i> cell radius ( $\mu\text{m}$ )
Residual $\epsilon_p$	0.0013	<b>0.51</b>	<b>-0.49</b>	-0.17	0.15

Note. The level of significance ( $p$ -values) is over the threshold of 0.05 in all cases, whereas bold values correspond to  $p$  values at least  $\leq 0.1$ .

16‰, suggesting either that this is not the mechanistically correct explanation for the low G-I  $\epsilon_p$  sensitivity or that long-term evolution of enzymes involved in carbon isotopic fractionation of alkenone producers has occurred.

In summary, the observed  $\epsilon_p$  variations at Site 925 are not consistent with the application of the classical diffusive model, nor growth rate as a function of coccolith size, as recently proposed for other locations (Y. G. Zhang et al., 2020).

### 6.2.2. Comparison With Culture Observations of $\epsilon_p$ Dependence on $\text{CO}_2$

While agreeing on the influence of these same factors on  $\epsilon_p$ , a recent culture reanalysis suggests a non-diffusive logarithmic dependence of  $\epsilon_p$  on  $\text{CO}_2$  (see Stoll et al., 2019).

In the regression between the  $\epsilon_p$  record at Site 925 and  $\ln(\text{CO}_2[\text{aq}])$  across the MIS 12 to MIS 9, we obtained a slope value of 3.55 (Figure 7). Our estimated slope is on the upper end of that inferred from laboratory cultures (95% confidence interval; 1.83 to 3.5) by Stoll et al. (2019), suggesting (a) a similar sensitivity of  $\epsilon_p$  to  $\text{CO}_2[\text{aq}]$  on  $\epsilon_p$  at Site 925 as observed in cultures and (b) supporting the further application of the  $\epsilon_p$  multiple regression statistical model by Stoll et al. (2019) to provide a suitable quantification of the effect of other non- $\text{CO}_2$  parameters on  $\epsilon_p$  at Site 925.

The slope between  $\epsilon_p$  and  $\ln(\text{CO}_2[\text{aq}])$  of 2.67 at the Site 999 through the MIS 8 to MIS 5 G-I cycles studied by Badger et al. (2019, Figure 7), is within the 95% confidence interval by Stoll et al. (2019). This record comes from the western Caribbean Sea, so both locations of Sites 925 and 999 are assumed to share comparable air-sea equilibrium conditions and absence of remarkable upwelling activity across the Pleistocene (see Badger et al., 2019 and references therein). The comparison suggests a similar phytoplankton sensitivity to changing G-I  $p\text{CO}_2$  across the Pleistocene, from the MIS 12 to MIS 9 in our record and through the MIS 8–5.  $\epsilon_p$  over the interval between 20 and 430 ka (from MIS 12 to the last glacial maximum) at ODP 925 was reported by Y. G. Zhang et al. (2013), and although the absence of reported benthic  $\delta^{18}\text{O}$  for the sampled intervals leads to greater uncertainty in the estimation of the  $\text{CO}_2[\text{aq}]$ , these data also show a similar sensitivity of  $\epsilon_p$  to  $\text{CO}_2[\text{aq}]$  (see Text S1 and Figure S3).

### 6.2.3. Evaluating the Non- $\text{CO}_2$ Influences on $\epsilon_p$ and Potential Proxies for Them

Because the slope of  $\epsilon_p$  relative to  $\text{CO}_2[\text{aq}]$  at 925 is similar to that of cultures by Stoll et al. (2019), but the cultures are defined by a larger data set and, therefore, a narrower confidence interval, we employ the slope from cultures to evaluate the non- $\text{CO}_2$  influences on  $\epsilon_p$  in our record at Site 925. Unlike the diffusive model, the regression model is empirical and not dependent on quantifying the  $\epsilon_p$ , nor *a priori* assumptions about the significance of diffusive versus active carbon supply (CCMs) to photosynthesis. We have chosen the culture regression with a limited range of  $\delta^{13}\text{C}_{\text{DIC}}$ , consistent with expectations for the Late Quaternary, and the model which provided the highest experimental  $R^2$  value (see Stoll et al., 2019). In this model,  $\epsilon_p$  is a combination of the influence of  $\text{CO}_2[\text{aq}]$ , growth rate ( $\mu$ ), cell radius and light as:

$$\epsilon_p \sim a \times \ln\text{CO}_2 + b \times \ln \text{light} + c \times \mu + d \times \text{radius} \quad (4)$$

As approximately 50% of variance on  $\epsilon_p$  at Site 925 is attributed to  $\text{CO}_2$  (Figure 7), the remaining 50% may arise due to temporal variation in cell radius, light, or growth rate. Of these parameters, we have direct estimates only for *Gephyrocapsa* cell radius from coccolith length (Figure 3i), in which increasing radius toward MIS 10, from minima values at MIS 11, is similar to that shown for the same time interval in the equatorial Pacific by Beaufort et al. (2020). The *Gephyrocapsa* cell radius values at Site 925 from coccolith length show, however, a non-significant correlation with  $\epsilon_p$  ( $R = -0.27/p \geq 0.05$ ; Figure 6). This fact suggests that such

changes across the MIS 12 to MIS 9 did not exert significant modulation on  $\epsilon_p$ . In effect, the calculation of the effect of *Gephyrocapsa* cell radius on  $\epsilon_p$  at 925 by applying the slope of size effect from the culture observations by Stoll et al. (2019) suggests that such a small size variation would affect  $\epsilon_p$  by less than 0.14‰, a difference that we consider negligible.

Using the estimated  $\text{CO}_2[\text{aq}]$  and the values of *Gephyrocapsa* cell radius for each sample, we predict the  $\text{CO}_2$  and cell size components of  $\epsilon_p$  at Site 925 by applying the  $\epsilon_p$  multiple regression model with the coefficient values and a fixed intercept from culture ( $a = 2.66$ ,  $d = -1.28$  and intercept = 6.30; see Stoll et al., 2019). The residual difference of the measured  $\epsilon_p$  at Site 925 minus this calculated variation in  $\epsilon_p$  (residual  $\epsilon_p$  variation) reflects the summed effects of light and growth rate contributing to  $\epsilon_p$  at Site 925.

Analysis of  $\epsilon_p$  in core tops suggests that some micropaleontological proxies have a strong correlation with spatial variations in the light or growth rate effects on  $\epsilon_p$  in the modern ocean (Hernández-Almeida et al., 2020). For our sample set, the residual  $\epsilon_p$  variation has not statistically significant correlation with some proxies for surface production and growth rate ( $p > 0.05$ ; Table 2). However, some relationships are observed. The comparison with percentages of *F. profunda* results in some correlation of  $R = 0.51$  ( $p > 0.05$ ; Table 2 and Figure 9a). In addition, the alkenone C37/C38.et ratio has an inverse relationship with the residual non- $\text{CO}_2$  variation in  $\epsilon_p$ ,  $R = -0.49$  ( $p > 0.05$ ; Table 2 and Figure 9b). On the other hand, the residual non- $\text{CO}_2$  variation in  $\epsilon_p$  is not significantly correlated with the  $\Delta\delta^{18}\text{O}_{\text{N. duterrei-G. ruber}}$ ,  $R = 0.001$  ( $p > 0.05$ ; Table 2), nor with N *Gephyrocapsa*,  $R = -0.17$  ( $p > 0.05$ ; Table 2). It is important to note that N *Gephyrocapsa* may not accurately reflect the production of *Gephyrocapsa* if the growth rate may be decoupled from the standing stock and total biogenic export.

The positive relationship between the percentages of *F. profunda* and the non- $\text{CO}_2$   $\epsilon_p$  is consistent with lower growth rates (or higher light) during periods of increased % *F. profunda*. The inverse relationship between the alkenone C37/C38.et ratio is consistent with higher growth rates (or lower light) during periods of higher C37/C38.et. This is in agreement with Herbert et al. (2018), who proposed a correlation of the C37 to C38 organic compounds with algal growth rates. The combination of percentages of *F. profunda* and the values of C37/C38.et does not explain additional variation nor increased significance, with  $R^2 = 0.34$  (Table S4), suggesting that both are indicating similar aspects of *Gephyrocapsa* growth and that other factors influencing  $\epsilon_p$  are not yet resolved by the existing proxy suite.

We next evaluate if we can establish a quantitative estimation of the growth rate  $\epsilon_p$  variation from the use of micropaleontological proxies in this study. On a regional scale, the percentages of *F. profunda* has been established as a proxy for surface ocean  $[\text{PO}_4^{3-}]$  from the study of surface sediment samples by Hernández-Almeida et al. (2020). When the  $[\text{PO}_4^{3-}]$  obtained applying that same regression (0.28–0.38  $\mu\text{M}$ ; Figure S6c) is incorporated into the growth rate parametrization by Krumhardt et al. (2017), we estimate growth rates ranging from 1.4 to 1.6  $\text{day}^{-1}$  (Figure S6d). According to the steep dependence of  $\epsilon_p$  on growth rate in cultures, this 0.2  $\text{day}^{-1}$  variation in growth rate would be expected to lead to 1.4‰ variations in  $\epsilon_p$ , similar to 1.5‰ found in this study. However, comparing the growth rates values estimated from this calculation with the measured  $\epsilon_p$  at Site 925 is more difficult because the light level during *Gephyrocapsa* growth is not independently constrained. If *Gephyrocapsa* was produced at 50 m depth under modern conditions, yearly average light would be 113  $\mu\text{E m}^{-2} \text{s}^{-1}$ , whereas if it was deeper between 60 and 70 m, the value would be lower, between 62 and 84  $\mu\text{E m}^{-2} \text{s}^{-1}$  (further details on this calculation and resulting values are included in Text S6 and Table S7). Nevertheless, we note that the parametrized growth rates using the estimation of  $[\text{PO}_4^{3-}]$  from percentages of *F. profunda* are higher than the modern modeled values (1–1.25  $\text{day}^{-1}$ ; Krumhardt et al., 2017, Figure 1c), suggesting that the approach using *F. profunda* may overestimate  $[\text{PO}_4^{3-}]$  at this location during MIS 12–9 compared to the more open ocean settings from which the calibration was developed.

We finally explore if there is a relationship between the variability in *Gephyrocapsa* cell radius and growth rate during the MIS 12 to MIS 9, since larger cell sizes have higher nutrient requirements to attain a given growth rate. For this, we used the culture regression from different studies of the  $K_M$  for growth limited by the concentration of  $\text{NO}_3$  as a function of the cell radius (Cermeño et al., 2011; Eppley et al., 1969; Perrin et al., 2016; Riegman et al., 2000). The difference between the derived  $K_M \text{NO}_3$  values from the smallest and largest size values at Site 925 is of about 0.075  $\mu\text{M}$ , a maximum variability of too small magnitude to



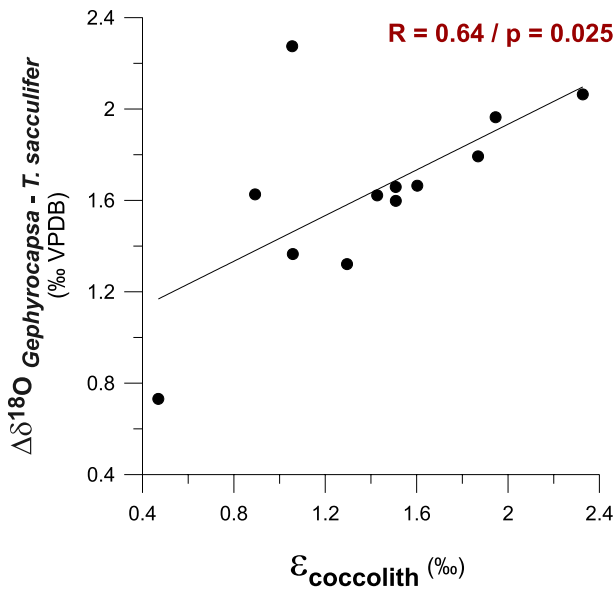


**Figure 10.** Correlation R between carbon and oxygen vital effects in *Gephyrocapsa* coccolith calcite at Site 925, respectively, represented from  $\epsilon_{\text{coccolith}}$  and  $\Delta\delta^{18}\text{O}_{\text{Gephyrocapsa-T. sacculifer}}$ .

exert a significant modulation on the *Gephyrocapsa* growth rates across the interval. We neither find a significant correlation between the *Gephyrocapsa* size trends and the residual  $\epsilon_p$  ( $R = 0.15/p > 0.05$ ; Table 2). This suggests that *Gephyrocapsa* cell sizes is a poor predictor of the growth rate or light variation effects on  $\epsilon_p$  through MIS 12 to MIS 9 at Site 925.

### 6.3. Carbon and Oxygen Vital Effects in *Gephyrocapsa* Coccolith Calcite

Until this study, well-separated near monogeneric coccolith records examined for *Gephyrocapsa* vital effects spanning G-I cycles had been only made by Jin et al. (2018). Some previous studies have used bulk carbonate samples from the Caribbean Sea without quantification of the relative abundance of different coccolith species (e.g., Hermoso, 2016) or, alternatively, fine fractions in which analyses of the species abundances revealed systematic variation in assemblage (i.e., *F. profunda*) over G-I cycles (e.g., Mejía et al., 2014; Stoll et al., 2019). Because different coccolith sizes and genera are known to have contrasting isotopic fractionation (e.g., Candelier et al., 2013; Dudley et al., 1986; Hermoso et al., 2014; Rickaby et al., 2010; Ziveri et al., 2003), in mixtures with varying contribution of different groups, it is not possible to distinguish the effect of species-specific offsets from changes in stable isotope vital effects due to environmental and biological factors. Here, the specimens of the genus *Gephyrocapsa* represent the 84%–91% of the 3–5- $\mu\text{m}$  microfiltered coccolith size fraction. We therefore examine to what extent the isotopic composition differs from that of coeval planktic foraminifera, to evaluate possible environmental influences on the vital effects in carbon and oxygen isotopes.

The carbon isotope vital effect from  $\epsilon_{\text{coccolith}}$  is significantly correlated with the vital effect in oxygen isotopes in coccoliths from  $\Delta\delta^{18}\text{O}_{\text{Gephyrocapsa-T. sacculifer}}$  ( $R = 0.64/p \leq 0.05$ ; Figures 6 and 10). There is no correlation between the vital effects in *Gephyrocapsa* and the changes in the assemblage structure in our record (Figures 4f, 4g, and S5), so we suggest that the vital effect is not controlled by the changes in the species composition of the *Gephyrocapsa* assemblage through time. In contrast we suggest a variable physiological effect in Noëlaerhabdaceae on the magnitude of stable isotope fractionation in coccolith calcite, in agreement with previous studies (e.g., Bolton & Stoll, 2013; Hermoso et al., 2015).

The carbon isotope vital effect from  $\epsilon_{\text{coccolith}}$  is significantly correlated with the vital effect in oxygen isotopes in coccoliths from  $\Delta\delta^{18}\text{O}_{\text{Gephyrocapsa-T. sacculifer}}$  ( $R = 0.64/p \leq 0.05$ ; Figures 6 and 10). There is no correlation between the vital effects in *Gephyrocapsa* and the changes in the assemblage structure in our record (Figures 4f, 4g, and S5), so we suggest that the vital effect is not controlled by the changes in the species composition of the *Gephyrocapsa* assemblage through time. In contrast we suggest a variable physiological effect in Noëlaerhabdaceae on the magnitude of stable isotope fractionation in coccolith calcite, in agreement with previous studies (e.g., Bolton & Stoll, 2013; Hermoso et al., 2015).

#### 6.3.1. Carbon Isotope Vital Effects

Cell modeling suggests that the  $\epsilon_{\text{coccolith}}$  may increase with higher photosynthetic rates and low  $\text{CO}_2[\text{aq}]$  (Bolton & Stoll, 2013; Holtz et al., 2017; McClelland et al., 2017). The reason is that photosynthesis fractionates against the heavy isotope, so the intracellular DIC pool is more positive when there is a higher photosynthetic rate, resulting in higher  $\delta^{13}\text{C}$  of the carbon available for calcification. In this sense, faster growth rates may result in a higher  $\epsilon_{\text{coccolith}}$  (Holtz et al., 2017). When the  $\text{CO}_2[\text{aq}]$  is low and the diffusive  $\text{CO}_2$  flux is low, this isotopically heavy carbon may remain a more significant fraction of the intracellular DIC pool; conversely, at high  $\text{CO}_2[\text{aq}]$ , a significant  $\text{CO}_2$  influx may dilute the intracellular carbon pool. These processes driving an internal isotopically heavy signature could be incorporated into coccolith vesicle and recorded by  $\epsilon_{\text{coccolith}}$ . In addition, the inorganic/organic carbon (PIC/POC) ratio in some circumstances is modeled to affect as well the  $\epsilon_{\text{coccolith}}$ : a higher  $\epsilon_{\text{coccolith}}$  is expected to result from low PIC/POC (McClelland et al., 2017).

However, the variations in  $\epsilon_{\text{coccolith}}$  in our new record are not readily explained by the processes simulated in models. For example, although  $\epsilon_{\text{coccolith}}$  varies by over 1‰ in our record (Figure 4f), we observe a non-significant correlation with  $\text{CO}_2[\text{aq}]$ ,  $R = -0.01$  ( $p > 0.05$ ; Figures 6 and S8a). This contrasts with the previous results on non-monogeneric coccolith fractions from the last 200 kyr at Site 925, which evidenced correlation of higher  $\epsilon_{\text{coccolith}}$  with lower  $\text{CO}_2[\text{aq}]$  (Stoll et al., 2019). We suggest that the resulting  $\epsilon_{\text{coccolith}}$  record for the samples younger than 200 ka not dominated by species of the genus *Gephyrocapsa* may reflect the impact of major changes in the coccolithophore assemblages rather than  $\text{CO}_2$  on isotopic fractionation in a given

species. Thus, our new results suggest that non-CO<sub>2</sub> aspects of the surface production conditions may exert dominant effect on the *Gephyrocapsa*  $\epsilon_{\text{coccolith}}$  across the MIS 12 to MIS 9. For example, while low CO<sub>2</sub>[aq] is expected to increase  $\epsilon_{\text{coccolith}}$ , such a signal could be obscured if there were a compensating process working to decrease  $\epsilon_{\text{coccolith}}$  at low CO<sub>2</sub> effect, such as (a) a reduced growth rate or (b) an increase in PIC/POC. Regarding the latter mechanism, since coccolith SN thickness has a negligible variation among our samples (Figure 3h), we have no evidence for significant changes in the degree of cellular calcification (PIC/cell surface area) or PIC/POC. There are positive correlations between  $\epsilon_{\text{coccolith}}$  and *Gephyrocapsa* coccolith length  $R = 0.56$  (Figure 6) and mass  $R = 0.63$  (Figure 6). If the ratio of cellular carbon supply to demand correlated with coccolith size and SA/V ratio, then larger sizes might be expected to increase the  $\epsilon_{\text{coccolith}}$  (McClelland et al., 2017), as we observe (Figures 3i and 4f). However, while this process is working in the expected direction, its magnitude may not be sufficient: in cellular process models, a 1‰ shift in  $\epsilon_{\text{coccolith}}$  would require a 60% increase in carbon utilization (McClelland et al., 2017). The maximum range in *Gephyrocapsa* coccolith length (size) is <10% (Figure 3i).

$\epsilon_{\text{coccolith}}$  shows a non-significant correlation with the surface production proxies of % *F. profunda* ( $R = 0.39/p > 0.05$ ; Figure 6) and *N Gephyrocapsa* ( $R = -0.42/p > 0.05$ ; Figure 6), and the growth rate proxy C37/C38.et ( $R = -0.39/p > 0.05$ ; Figure 6) and the sign of this relationship is opposite to that predicted by cellular process models. It is important to note that the percentages of *F. profunda* and C37/C38.et have the expected correlation for growth rate effect on  $\epsilon_p$  (Section 6.2.3). These results evidence that the variations in growth rate or production indicated by these proxies do not influence  $\epsilon_{\text{coccolith}}$  in the manner predicted by cellular process models, as neither have a significant influence individually on  $\epsilon_{\text{coccolith}}$ . However, it is possible that these growth rate and production proxies contain complementary information that helps to explain a higher proportion of the  $\epsilon_{\text{coccolith}}$  variance when they are combined. Thus, when we combine in a multiple linear regression model the *Gephyrocapsa* coccolith mass and the C37/C38.et to predict  $\epsilon_{\text{coccolith}}$ , the explained variance is higher,  $R^2 = 0.49$  (Table S5), and even higher with the addition of CO<sub>2</sub>[aq] to the previous variables, improving the performance of the multiple linear regression model ( $R^2 = 0.59$ ; Table S6).

### 6.3.2. Oxygen Isotope Vital Effects

The  $\Delta\delta^{18}\text{O}_{\text{Gephyrocapsa-T. sacculifer}}$  values (Figure 4g) are consistent with previous studies, showing *Gephyrocapsa* to have higher  $\delta^{18}\text{O}$  than equilibrium calcite (Dudley et al., 1986; Hermoso et al., 2015; Ziveri et al., 2003). The temporal variation in  $\Delta\delta^{18}\text{O}_{\text{Gephyrocapsa-T. sacculifer}}$  is >1‰, suggesting that recent assumptions of a constant  $\Delta\delta^{18}\text{O}_{\text{Gephyrocapsa-T. sacculifer}}$  for paleoceanographic studies (e.g., Hermoso et al., 2020; Tremblin et al., 2016 and references therein) may require reevaluation. More specifically, our results from time series are in agreement with core-top calibration by Hermoso et al. (2015), in which Noëlaerhabdaceae  $\delta^{18}\text{O}$  may be controlled by multiple factors in addition to temperature.

Positive correlation between oxygen and carbon isotope vital effects among coeval coccolith populations of different species from sediments (Bolton & Stoll, 2013), core top sediments (Hermoso et al., 2015), or among species in culture (Ziveri et al., 2003) has been widely described but seldom documented in time series (e.g., Hermoso et al., 2020; Jin et al., 2018; Liu et al., 2002). The main physiological mechanisms alluded as triggering Noëlaerhabdaceae  $\delta^{18}\text{O}$  enrichment from equilibrium has been (a) intracellular pH reduction in the coccolith vesicle (Hermoso et al., 2015; Ziveri et al., 2003, 2012) and (b) the effect of fast growth rates on the DIC pool signature (e.g., Hermoso et al., 2014). However, coupled models of carbon and oxygen isotope vital effects are not yet published. This data set could be an important model target.

As observed for  $\epsilon_{\text{coccolith}}$ , CO<sub>2</sub>[aq] is not a main control of the oxygen vital effects from a low and non-significant correlation  $R = 0.23$  ( $p > 0.05$ ; Figures 6 and S8b). As suggested by Jin et al. (2018) for the Western Equatorial Pacific, it is possible that the narrow range of CO<sub>2</sub>[aq] variability across the studied interval (~5–8  $\mu\text{M}$ ; Figure S2) was not significant enough to affect the  $\delta^{18}\text{O}$  *Gephyrocapsa*. Whereas some albeit limited correlations between productivity proxies and carbon isotope vital effects were found, there are no significant correlations between the oxygen isotope vital effects and the surface production and growth rate proxies in our study as % *F. profunda* ( $R = 0.02/p > 0.05$ ; Figure 6), *N Gephyrocapsa* ( $R = -0.37/p > 0.05$ ; Figure 6), and C37/C38.et ( $R = -0.28/p > 0.05$ ; Figure 6).

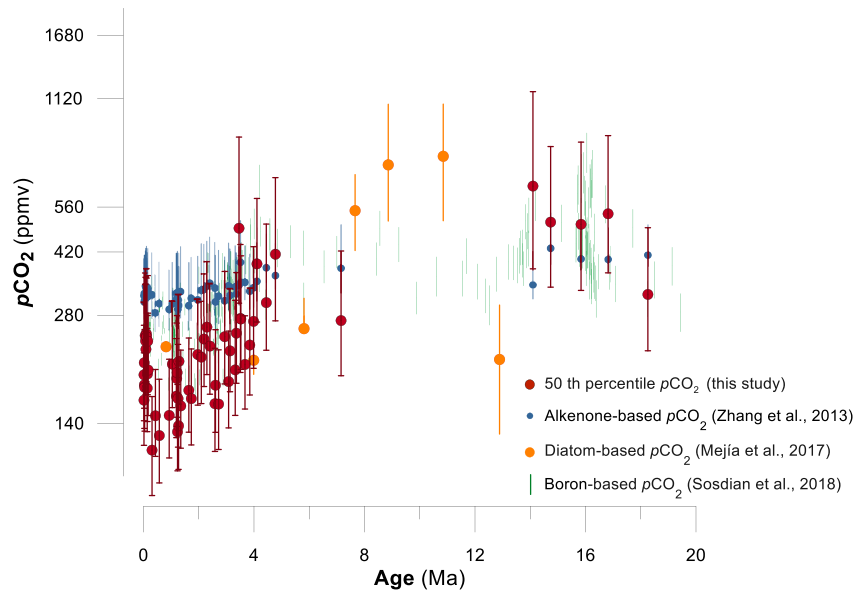


**Figure 11.**  $p\text{CO}_2$  estimated at Site 925 from the MIS 12 to MIS 9 (Late Quaternary) data set and Monte Carlo error propagation through the Neogene: red dots are the 50th percentile resulting from  $p\text{CO}_2$  estimates and the red bars represent the Monte Carlo error propagation between the 16th and 84th percentiles. Previously published  $p\text{CO}_2$  records are shown for comparison as colored symbols: blue = alkenone  $\epsilon_p$ -based  $p\text{CO}_2$  by Y. G. Zhang et al. (2013); yellow = diatom  $\epsilon_p$ -based  $p\text{CO}_2$  by Mejía et al. (2017); and green = boron-based  $p\text{CO}_2$  updated calculations reported in Sosdian et al. (2018).

#### 6.4. Implications for Neogene $p\text{CO}_2$ Estimation at Site 925

At Site 925, previous studies reported alkenone  $\epsilon_p$  through the Neogene (e.g., Pagani et al., 2011; Y. G. Zhang et al., 2013). Our results spanning MIS 12 to MIS 9 at Site 925 confirm that  $\epsilon_p$  at this location is significantly influenced by the changes in  $\text{CO}_2[\text{aq}]$ , with a sensitivity similar to that inferred through culture regressions (Stoll et al., 2019). So, we aim to evaluate the implications of the relationships identified in this fossil proxy data set during the Late Quaternary for longer term Neogene  $p\text{CO}_2$  reconstruction.

From this relationship, we calculate the range of  $\text{CO}_2[\text{aq}]$  consistent with Neogene  $\epsilon_p$  to compare it with previous calculations, which employed the classical diffusive model to derive the  $\text{CO}_2[\text{aq}]$ . The Neogene data set does not include potential proxies for growth rate, such as % *F. profunda* nor alkenone C37/38:et ratio, nor continuous data on the size of coccoliths in the time slices for which  $\epsilon_p$  was analyzed. Consequently, as in previous interpretations, this exercise assumes that the magnitude of growth rate and other non- $\text{CO}_2$  contributions to  $\epsilon_p$  has remained invariable through the Neogene. Regardless of whether this assumption is correct, we can evaluate the effect of applying an  $\epsilon_p$  to  $\text{CO}_2$  calibration similar to the sensitivity observed during the MIS 12 to MIS 9 glacial, versus applying a calibration based on using the classic diffusive model.

As there are no size, growth rate, or light data, we simplify the culture-based statistical calibration equation by Stoll et al. (2019) to:

$$\epsilon_p = m(\ln \text{CO}_2[\text{aq}]) + I \quad (5)$$

where  $m$  is the slope ( $2.66 \pm 0.42$  1 s.d.) derived from cultures (see Stoll et al., 2019) and  $I$  is the intercept which encompasses, in aggregate, all other controls on  $\epsilon_p$ . We estimate  $I$  from the Late Quaternary data set in this study ( $7.88 \pm 0.4$  1 s.d.). Given uncertainty about the offset between foraminiferal calcite  $\delta^{13}\text{C}$  and  $\delta^{13}\text{C}_{\text{DIC}}$ , a slightly different  $I$  value from the Late Quaternary anchoring would be obtained from an initial selection of a different fractionation factor; however, it is important to note that this it would not change the slope of the  $\epsilon_p$  versus  $\text{CO}_2[\text{aq}]$  relationship during the Late Quaternary, nor the  $p\text{CO}_2$  estimate from Neogene recalculated  $\epsilon_p$  data. We implement this equation in a Monte Carlo error propagation, which also incorporates the following normally distributed uncertainty in terms employed for  $\epsilon_p$  calculation and for

$p\text{CO}_2$  calculation using Henry's Law: salinity: (s.d. = 1 psu), temperature (s.d. = 2°),  $\delta^{13}\text{C}_{37.2}$  (as reported or s.d. = 0.2‰), and  $\delta^{13}\text{C}$  foraminifera (s.d. = 0.1‰).

When calculated with the sensitivity observed in cultures (Stoll et al., 2019) and over the MIS 12–9, Neogene  $p\text{CO}_2$  declined over the last 5 Myr at an average rate of 26 ppm per Myr (50th percentile values; Figure 11). The values for the four points in the mid-Miocene (~14–17 Ma) range from 500 to 640 ppmv, with one significantly higher  $p\text{CO}_2$  estimate of 836 ppm in the earliest Miocene (Figure 11). Further comparison to other  $p\text{CO}_2$  proxy records can be found in the recent review by Rae et al. (2021).

The temperature history at this site suggests minimal cooling over the Neogene (e.g., Y. G. Zhang et al., 2013), in contrast to mid and high latitude sites (e.g., Herbert et al., 2016). If the temperature change over the Neogene at Site 925 is underestimated and Miocene temperatures were significantly warmer than estimated (Y. G. Zhang et al., 2013), then the  $\text{CO}_2$  solubility would be underestimated and the absolute  $p\text{CO}_2$  likewise underestimated. Furthermore, if higher temperatures would suggest a higher growth rate, the use of constant growth rate over time might underestimate the amplitude of  $p\text{CO}_2$  change.

From the relationships observed in our fossil data set, we suggest that (a) the diffusive model and conventional parameters ( $\epsilon_f = 25\%$ ) provide a poor fit to the  $\epsilon_p$  during the Late Quaternary  $\text{CO}_2$  variations (Section 6.2.1) and consequently (b) the previously published Neogene  $p\text{CO}_2$  estimates calculated with these parameters reveal more stable  $p\text{CO}_2$  estimates, particularly over the last 5 Myr (e.g., Y. G. Zhang et al., 2013). Alternatively, if the diffusive model was configured to fit Late Quaternary observations, for example, with  $\epsilon_f = 16\%$ , it would imply mean  $b$  values of 19 ( $\pm 3.15$  s.d.) for the Late Quaternary. Application of this parameter set would yield an average decline of 37 ppm per Myr in the last 5 Myr, and mid-Miocene  $p\text{CO}_2$  estimates around 500 ppmv. Therefore, when the parameters for calculation of Neogene  $p\text{CO}_2$  are adjusted to fit the observed Late Quaternary G-I  $\epsilon_p$  sensitivity at Site 925 (Figure 11), similar  $p\text{CO}_2$  estimates are obtained regardless of whether a diffusive-based or empirical culture-based calibration approach is employed. However, because  $\epsilon_f = 16\%$  is not consistent with Paleogene  $\epsilon_p$ , we suggest that tuning  $\epsilon_f$  is not the optimal approach for past  $p\text{CO}_2$  reconstruction.

## 7. Conclusions

The integration of organic geochemical (SST from alkenone  $U_{37}^{k'}$  and the C37/C38.et ratio), micropaleontological (amount of *Gephyrocapsa* per gram and % *F. profunda*), geochemical (stable isotope  $\delta^{18}\text{O}$  and  $\delta^{13}\text{C}$  in planktic foraminifera species), and *Gephyrocapsa* coccolith morphometrical (average length, mass, and SN thickness) data analyzed on the same samples allowed us to explore different options to differentiate and evaluate the load of  $\text{CO}_2$  and non- $\text{CO}_2$  effects on  $\epsilon_p$ .

We found that phytoplankton  $\epsilon_p$  sensitivity on  $\text{CO}_2[\text{aq}]$  across the G-I cycles from MIS 12 to MIS 9 (454–334 ka) at the Western Tropical Atlantic is consistent with the observation in cultures (Stoll et al., 2019) and in the western Caribbean (Badger et al., 2019). This sensitivity is much lower than that predicted by the classically applied model of diffusive phytoplankton  $\text{CO}_2$  acquisition. The diffusive model, with or without the effect of cell size or growth rate variations estimated by size, provides a poor fit to our  $\epsilon_p$  data. This result suggests that if  $\epsilon_p$  is to be applied for  $\text{CO}_2$  estimation, at least in tropical oligotrophic settings, the classic diffusive model may significantly underestimate both the variability and absolute  $p\text{CO}_2$  concentrations. For such sites, either empirical relationships anchored to known Late Quaternary ice core  $p\text{CO}_2$  concentrations, or the empirical multiple regression model from cultures by Stoll et al. (2019), may provide more robust estimates, at least for the late Neogene. We provide an example of the recalculated  $p\text{CO}_2$  since the Miocene from published  $\epsilon_p$  at Site 925, illustrating solely the effect of the  $\epsilon_p$  sensitivity to  $\text{CO}_2$  on the calculation.

Our analysis suggests that, at least at some sites, further improvements to  $p\text{CO}_2$  estimation may be possible using additional indicators of non- $\text{CO}_2$  effects on  $\epsilon_p$ . We found that % *F. profunda* and the alkenone C37/38.et ratio were able to explain part of the non- $\text{CO}_2$  variability. At Site 925, this may reflect a marked fertilization response of the coccolithophore species of the *Gephyrocapsa* genus to the surface nutrient input triggered by Amazon-affected waters that may have an effect on the changes in growth rate and light levels through the interval.

This data set further provides clear evidence of coupled models of carbon and oxygen isotope vital effects in *Gephyrocapsa* coccolith calcite through the MIS 12 to MIS 9, but further evaluation with cellular process models for vital effects is needed for a quantitative understanding of the drivers of these effects.

## Data Availability Statement

All original data produced for this work is available at the public repository Mendeley as: González-Lanchas, Alba; Stoll, Heather; Hernández-Alméida, Iván; Flores, José-Abel; Sierro, Francisco J.; Guitián, José (2020), “Carbon isotopic fractionation of alkenones and *Gephyrocapsa* coccoliths over the Late Quaternary (Marine Isotope Stages 12 to 9) glacial-interglacial cycles at the western tropical Atlantic,” Mendeley Data (<https://data.mendeley.com/datasets/zhmwhjjs63>).

## Acknowledgments

This study was supported by the predoctoral FPU contract FPU17/03349 and the program EST18/00842 for a research stay at Climate Geology Group (ETH Zürich), both awarded to A. González-Lanchas by the Spanish Ministry of Science, Innovation and Universities. Financing infrastructure was provided by the programs RTI2018-099489-B-I00 of the Spanish Ministry of Science, Innovation and Universities granted to GGO (Grupo de Geociencias Oceánicas de la Universidad de Salamanca) and by the Swiss National Science Foundation award 200021\_182070 granted to H.M. Stoll. Authors appreciate the suggestions and comments of the four anonymous reviewers, which benefited the manuscript. The authors also thank Madalina Jaggi for her assistance in the laboratory and Thomas Tanner for the guidelines on the procedure for the extraction and treatment of organic compounds.

## References

- Ahagon, N., Tanaka, Y., & Ujiie, H. (1993). Florisphaera profunda, a possible nannoplankton indicator of late Quaternary changes in sea-water turbidity at the northwestern margin of the Pacific. *Marine Micropaleontology*, 22, 255–273. [https://doi.org/10.1016/0377-8398\(93\)90047-2](https://doi.org/10.1016/0377-8398(93)90047-2)
- Aurachs, R., Treis, Y., Darling, K., & Kucera, M. (2011). A revised taxonomic and phylogenetic concept for the planktonic foraminifer species Globigerinoides ruber based on molecular and morphometric evidence. *Marine Micropaleontology*, 79, 1–14. <https://doi.org/10.1016/j.marmicro.2010.12.001>
- Bach, L. T., Mackinder, L. C., Schulz, K. G., Wheeler, G., Schroeder, D. C., Brownlee, C., & Riebesell, U. (2013). Dissecting the impact of CO<sub>2</sub> and pH on the mechanisms of photosynthesis and calcification in the coccolithophore *Emiliana huxleyi*. *New Phytologist*, 199, 121–134. <https://doi.org/10.1111/nph.12225>
- Bach, L. T., Riebesell, U., & Schulz, K. G. (2011). Distinguishing between the effects of ocean acidification and ocean carbonation in the coccolithophore *Emiliana huxleyi*. *Limnology & Oceanography*, 56, 2040–2050. <https://doi.org/10.4319/lo.2011.56.6.2040>
- Badger, M. P. (2021). Alkenone isotopes show evidence of active carbon concentrating mechanisms in coccolithophores as aqueous carbon dioxide concentrations fall below 7 μmol L<sup>-1</sup>. *Biogeosciences*, 18(3), 1149–1160. <https://doi.org/10.5194/bg-18-1149-2021>
- Badger, M. P., Chalk, T. B., Foster, G. L., Bown, P. R., Gibbs, S. J., Sexton, P. F., et al. (2019). Insensitivity of alkenone carbon isotopes to atmospheric CO<sub>2</sub> at low to moderate CO<sub>2</sub> levels. *Climate of the Past*, 15, 539–554. <https://doi.org/10.5194/cp-15-539-2019>
- Barber, R. T., & Hiscock, M. R. (2006). A rising tide lifts all phytoplankton: Growth response of other phytoplankton taxa in diatom-dominated blooms. *Global Biogeochemical Cycles*, 20(4). <https://doi.org/10.1029/2006gb002726>
- Baumann, K.-H., Andruleit, H., Böckel, B., Geisen, M., & Kinkel, H. (2005). The significance of extant coccolithophores as indicators of ocean water masses, surface water temperature, and palaeoproductivity: A review. *Paläontologische Zeitschrift*, 79, 93–112. <https://doi.org/10.1007/bf03021756>
- Baumann, K.-H., & Freitag, T. (2004). Pleistocene fluctuations in the northern Benguela Current system as revealed by coccolith assemblages. *Marine Micropaleontology*, 52, 195–215. <https://doi.org/10.1016/j.marmicro.2004.04.011>
- Beaufort, L., Bolton, C., Sarr, A.-C., Souchères-Marx, B., Rosenthal, Y., Donnadieu, Y., et al. (2020). Cyclic evolution of phytoplankton forced by changes in tropical seasonality.
- Beaufort, L., Lancelot, Y., Camberlin, P., Cayre, O., Vincent, E., Bassinot, F., & Labeyrie, L. (1997). Insolation cycles as a major control of equatorial Indian Ocean primary production. *Science*, 278, 1451–1454. <https://doi.org/10.1126/science.278.5342.1451>
- Bendif, E. M., Nevado, B., Wong, E. L., Hagino, K., Probert, I., Young, J. R., et al. (2019). Repeated species radiations in the recent evolution of the key marine phytoplankton lineage *Gephyrocapsa*. *Nature Communications*, 10, 1–9. <https://doi.org/10.1038/s41467-019-12169-7>
- Benthien, A., Andersen, N., Schulte, S., Müller, P. J., Schneider, R. R., & Wefer, G. (2002). Carbon isotopic composition of the C<sub>37:2</sub> alkenone in core top sediments of the South Atlantic Ocean: Effects of CO<sub>2</sub> and nutrient concentrations. *Global Biogeochemical Cycles*, 16, 11–12. <https://doi.org/10.1029/2001gb001433>
- Bickert, T., Curry, W., & Wefer, G. (1997). Late Pliocene to Holocene (2.6–0 Ma) western equatorial Atlantic deep-water circulation: Inferences from benthic stable isotopes. In *Proceedings of the ocean drilling program. Scientific results* (pp. 239–253). <https://doi.org/10.2973/odp.proc.sr.154.110.1997>
- Bidigare, R. R., Fluegge, A., Freeman, K. H., Hanson, K. L., Hayes, J. M., Hollander, D., et al. (1997). Consistent fractionation of <sup>13</sup>C in nature and in the laboratory: Growth-rate effects in some haptophyte algae. *Global Biogeochemical Cycles*, 11, 279–292. <https://doi.org/10.1029/96gb03939>
- Birch, H., Coxall, H. K., Pearson, P. N., Kroon, D., & O'Regan, M. (2013). Planktonic foraminifera stable isotopes and water column structure: Disentangling ecological signals. *Marine Micropaleontology*, 101, 127–145. <https://doi.org/10.1016/j.marmicro.2013.02.002>
- Blanco-Ameijeiras, S., Stoll, H. M., Zhang, H., & Hopkinson, B. M. (2020). Influence of temperature and CO<sub>2</sub> on plasma-membrane permeability to CO<sub>2</sub> and HCO<sub>3</sub><sup>-</sup> in the marine haptophytes *Emiliana huxleyi* and *Calcidiscus leptoporus* (Prymnesiophyceae). *Journal of Phycology*, 56(5).
- Boller, A. J., Thomas, P. J., Cavanaugh, C. M., & Scott, K. M. (2011). Low stable carbon isotope fractionation by coccolithophore *RubisCO*. *Geochimica et Cosmochimica Acta*, 75, 7200–7207. <https://doi.org/10.1016/j.gca.2011.08.031>
- Boller, A. J., Thomas, P. J., Cavanaugh, C. M., & Scott, K. M. (2015). Isotopic discrimination and kinetic parameters of *RubisCO* from the marine bloom-forming diatom, *Skeletonema costatum*. *Geobiology*, 13, 33–43. <https://doi.org/10.1111/gbi.12112>
- Bollmann, J., Baumann, K. H., & Thierstein, H. R. (1998). Global dominance of *Gephyrocapsa* coccoliths in the Late Pleistocene: Selective dissolution, evolution, or global environmental change? *Paleoceanography*, 13, 517–529. <https://doi.org/10.1029/98pa00610>
- Bolton, C. T., Hernández-Sánchez, M. T., Fuertes, M.-A., González-Lemos, S., Abrevaya, L., Mendez-Vicente, A., et al. (2016). Decrease in coccolithophore calcification and CO<sub>2</sub> since the middle Miocene. *Nature Communications*, 7, 1–13. <https://doi.org/10.1038/ncomms10284>
- Bolton, C. T., & Stoll, H. M. (2013). Late Miocene threshold response of marine algae to carbon dioxide limitation. *Nature*, 500, 558–562. <https://doi.org/10.1038/nature12448>
- Boyle, E., Edmond, J., & Sholkovitz, E. (1977). The mechanism of iron removal in estuaries. *Geochimica et Cosmochimica Acta*, 41, 1313–1324. [https://doi.org/10.1016/0016-7037\(77\)90075-8](https://doi.org/10.1016/0016-7037(77)90075-8)
- Brassell, S., Brereton, R., Eglinton, G., Grimalt, J., Liebezeit, G., Marlowe, I., et al. (1986). Paleoclimatic signals recognized by chemometric treatment of molecular stratigraphic data. *Organic Geochemistry*, 10, 649–660. [https://doi.org/10.1016/s0146-6380\(86\)80001-8](https://doi.org/10.1016/s0146-6380(86)80001-8)
- Breitenbach, S. F., & Bernasconi, S. M. (2011). Carbon and oxygen isotope analysis of small carbonate samples (20 to 100 μg) with a Gas-Bench II preparation device. *Rapid Communications in Mass Spectrometry*, 25, 1910–1914. <https://doi.org/10.1002/rcm.5052>

- Candelier, Y., Minoletti, F., Probert, I., & Hermoso, M. (2013). Temperature dependence of oxygen isotope fractionation in coccolith calcite: A culture and core top calibration of the genus *Calcidiscus*. *Geochimica et Cosmochimica Acta*, *100*, 264–281. <https://doi.org/10.1016/j.gca.2012.09.040>
- Cassar, N., Laws, E. A., & Popp, B. N. (2006). Carbon isotopic fractionation by the marine diatom *Phaeodactylum tricornutum* under nutrient- and light-limited growth conditions. *Geochimica et Cosmochimica Acta*, *70*(21), 5323–5335. <https://doi.org/10.1016/j.gca.2006.08.024>
- Cermeño, P., Lee, J.-B., Wyman, K., Schofield, O., & Falkowski, P. G. (2011). Competitive dynamics in two species of marine phytoplankton under non-equilibrium conditions. *Marine Ecology Progress Series*, *429*, 19–28. <https://doi.org/10.3354/meps09088>
- Curry, W. B., Shackleton, N. J., Richter, C., & Party, S. S. (1995). Ocean drilling program. In *Proceedings of ODP, Initial Reports*. Citeseer.
- Curry, W. B., Thunell, R. C., & Honjo, S. (1983). Seasonal changes in the isotopic composition of planktonic foraminifera collected in Panama Basin sediment traps. *Earth and Planetary Science Letters*, *64*(1), 33–43. [https://doi.org/10.1016/0012-821x\(83\)90050-x](https://doi.org/10.1016/0012-821x(83)90050-x)
- Dekens, P. S., Lea, D. W., Pak, D. K., & Spero, H. J. (2002). Core top calibration of Mg/Ca in tropical foraminifera: Refining paleotemperature estimation. *Geochemistry, Geophysics, Geosystems*, *3*, 1–29. <https://doi.org/10.1029/2001gc000200>
- DeMaster, D. J., Kuehl, S. A., & Nittrouer, C. A. (1986). Effects of suspended sediments on geochemical processes near the mouth of the Amazon River: Examination of biological silica uptake and the fate of particle-reactive elements. *Continental Shelf Research*, *6*, 107–125. [https://doi.org/10.1016/0278-4343\(86\)90056-7](https://doi.org/10.1016/0278-4343(86)90056-7)
- Demaster, D. J., & Pope, R. H. (1996). Nutrient dynamics in Amazon shelf waters: Results from AMASSEDs. *Continental Shelf Research*, *16*, 263–289. [https://doi.org/10.1016/0278-4343\(95\)00008-0](https://doi.org/10.1016/0278-4343(95)00008-0)
- Dudley, W. C., Blackwelder, P., Brand, L., & Duplessy, J.-C. (1986). Stable isotopic composition of coccoliths. *Marine Micropaleontology*, *10*, 1–8. [https://doi.org/10.1016/0377-8398\(86\)90021-6](https://doi.org/10.1016/0377-8398(86)90021-6)
- Eppley, R. W., Rogers, J. N., & McCarthy, J. J. (1969). Half-saturation constants for uptake of nitrate and ammonium by marine phytoplankton. *Limnology & Oceanography*, *14*, 912–920. <https://doi.org/10.4319/lo.1969.14.6.0912>
- Ezard, T. H., Edgar, K. M., & Hull, P. M. (2015). Environmental and biological controls on size-specific  $\delta^{13}\text{C}$  and  $\delta^{18}\text{O}$  in recent planktonic foraminifera. *Paleoceanography*, *30*, 151–173. <https://doi.org/10.1002/2014pa002735>
- Flores, J., & Sierro, F. (1997). Revised technique for calculation of calcareous nannofossil accumulation rates. *Micropaleontology*, 321–324. <https://doi.org/10.2307/1485832>
- Foster, G. L., Lear, C. H., & Rae, J. W. (2012). The evolution of pCO<sub>2</sub>, ice volume and climate during the middle Miocene. *Earth and Planetary Science Letters*, *341*, 243–254. <https://doi.org/10.1016/j.epsl.2012.06.007>
- Francois, R., & Bacon, M. P. (1991). Variations in terrigenous input into the deep equatorial Atlantic during the past 24,000 years. *Science*, *251*, 1473–1476. <https://doi.org/10.1126/science.251.5000.1473>
- Fuertes, M.-Á., Flores, J.-A., & Sierro, F. J. (2014). The use of circularly polarized light for biometry, identification and estimation of mass of coccoliths. *Marine Micropaleontology*, *113*, 44–55. <https://doi.org/10.1016/j.marmicro.2014.08.007>
- González Lemos, S., Guitián, J., Fuertes, M.-Á., Flores, J.-A., & Stoll, H. M. (2018). An empirical method for absolute calibration of coccolith thickness. *Biogeosciences*, *15*. <https://doi.org/10.5194/bg-15-1079-2018>
- Guerreiro, C. V., Baumann, K.-H., Brummer, G.-J. A., Fischer, G., Korte, L. F., Merkel, U., et al. (2017). Coccolithophore fluxes in the open tropical North Atlantic: Influence of thermocline depth, Amazon water, and Saharan dust. *Biogeosciences*, *14*, 4577–4599. <https://doi.org/10.5194/bg-14-4577-2017>
- Hastenrath, S., & Merle, J. (1987). Annual cycle of subsurface thermal structure in the tropical Atlantic Ocean. *Journal of Physical Oceanography*, *17*, 1518–1538. [https://doi.org/10.1175/1520-0485\(1987\)017<1518:acosts>2.0.co;2](https://doi.org/10.1175/1520-0485(1987)017<1518:acosts>2.0.co;2)
- Henderiks, J., & Pagani, M. (2007). Refining ancient carbon dioxide estimates: Significance of coccolithophore cell size for alkenone-based pCO<sub>2</sub> records. *Paleoceanography*, *22*(3). PA3202. <https://doi.org/10.1029/2006pa001399>
- Herbert, T., George, S. E., Marino, M., Maiorano, P., & Thunell, R. (2018). Alkenone-based approaches to productivity and growth rate. In AGU Fall Meeting (Vol. 2018, p. PP24B-02).
- Herbert, T. D., Lawrence, K. T., Tzanova, A., Peterson, L. C., Caballero-Gill, R., & Kelly, C. S. (2016). Late Miocene global cooling and the rise of modern ecosystems. *Nature Geoscience*, *9*, 843–847. <https://doi.org/10.1038/ngeo2813>
- Hermoso, M. (2015). Control of ambient pH on growth and stable isotopes in phytoplanktonic calcifying algae. *Paleoceanography*, *30*(8), 1100–1112. <https://doi.org/10.1002/2015pa002844>
- Hermoso, M. (2016). Isotopic record of Pleistocene glacial/interglacial cycles in pelagic carbonates: Revisiting historical data from the Caribbean Sea. *Quaternary Science Reviews*, *137*, 69–78. <https://doi.org/10.1016/j.quascirev.2016.02.003>
- Hermoso, M., Candelier, Y., Browning, T. J., & Minoletti, F. (2015). Environmental control of the isotopic composition of subfossil coccolith calcite: Are laboratory culture data transferable to the natural environment? *GeoResJ*, *7*, 35–42. <https://doi.org/10.1016/j.grj.2015.05.002>
- Hermoso, M., Horner, T. J., Minoletti, F., & Rickaby, R. E. (2014). Constraints on the vital effect in coccolithophore and dinoflagellate calcite by oxygen isotopic modification of seawater. *Geochimica et Cosmochimica Acta*, *141*, 612–627. <https://doi.org/10.1016/j.gca.2014.05.002>
- Hermoso, M., McClelland, H.-L. O., Hirst, J. S., Minoletti, F., Bonifacie, M., & Rickaby, R. E. M. (2020). Toward the use of the coccolith vital effects in paleoceanography: A field investigation during the middle Miocene in the SW Pacific Ocean. *Deep Sea Research Part I: Oceanographic Research Papers*, *160*, 103262. <https://doi.org/10.1016/j.dsr.2020.103262>
- Hernández-Almeida, I., Ausin, B., Saavedra-Pellitero, M., Baumann, K.-H., & Stoll, H. M. (2019). Quantitative reconstruction of primary productivity in low latitudes during the last glacial maximum and the mid-to-late Holocene from a global *Florisphaera profunda* calibration dataset. *Quaternary Science Reviews*, *205*, 166–181. <https://doi.org/10.1016/j.quascirev.2018.12.016>
- Hernández-Almeida, I., Krumhardt, K., Zhang, H., & Stoll, H. (2020). Estimation of physiological factors controlling carbon isotope fractionation in coccolithophores in photic zone and core-top samples. *Geochemistry, Geophysics, Geosystems*, *21*, e2020GC009272.
- Holtz, L.-M., Wolf-Gladrow, D., & Thoms, S. (2017). Stable carbon isotope signals in particulate organic and inorganic carbon of coccolithophores—A numerical model study for *Emiliania huxleyi*. *Journal of Theoretical Biology*, *420*, 117–127. <https://doi.org/10.1016/j.jtbi.2017.01.030>
- Hopkinson, B. M., Dupont, C. L., Allen, A. E., & Morel, F. M. (2011). Efficiency of the CO<sub>2</sub>-concentrating mechanism of diatoms. *Proceedings of the National Academy of Sciences of the United States of America*, *108*(10), 3830–3837. <https://doi.org/10.1073/pnas.1018062108>
- Jansen, J. H. F., Kuijpers, A., & Troelstra, S. R. (1986). A mid-Brunhes climatic event: Long-term changes in global atmosphere and ocean circulation. *Science*, *232*, 619–622. <https://doi.org/10.1126/science.232.4750.619>
- Jasper, J. P., Hayes, J., Mix, A. C., & Prahl, F. G. (1994). Photosynthetic fractionation of <sup>13</sup>C and concentrations of dissolved CO<sub>2</sub> in the central equatorial Pacific during the last 255,000 years. *Paleoceanography*, *9*, 781–798. <https://doi.org/10.1029/94pa02116>
- Jin, X., Liu, C., Zhang, H., Zhou, C., Jiang, X., Wu, Z., & Xu, J. (2018). Evolutionary driven of *Gephyrocapsa* coccolith isotopic vital effects over the past 400 ka. *Earth and Planetary Science Letters*, *503*, 236–247. <https://doi.org/10.1016/j.epsl.2018.09.010>

- Key, R. M., Olsen, A., van Heuven, S., Lauvset, S. K., Velo, A., Lin, X., et al. (2015). *Global ocean data analysis project, version 2 (GLODAPv2), ORNL/CDIAC-162, ND-P093*, Carbon Dioxide Information Analysis Center, Oak Ridge National Laboratory, US Department of Energy.
- Kinkel, H., Baumann, K.-H., & Cepek, M. (2000). Coccolithophores in the equatorial Atlantic Ocean: Response to seasonal and Late Quaternary surface water variability. *Marine Micropaleontology*, 39, 87–112. [https://doi.org/10.1016/S0377-8398\(00\)00016-5](https://doi.org/10.1016/S0377-8398(00)00016-5)
- Köhler, P., Nehrbass-Ahles, C., Schmitt, J., Stocker, T. F., & Fischer, H. (2017). A 156 kyr smoothed history of the atmospheric greenhouse gases CO<sub>2</sub>, CH<sub>4</sub>, and N<sub>2</sub>O and their radiative forcing. *Earth System Science Data*, 9, 363–387. <https://doi.org/10.5194/essd-9-363-2017>
- Korte, L. F., Brummer, G. J. A., van der Does, M., Guerreiro, C. V., Mienis, F., Munday, C. I., et al. (2020). Multiple drivers of production and particle export in the western tropical North Atlantic. *Limnology & Oceanography*, 65(9). <https://doi.org/10.1002/lno.11442>
- Krumhardt, K. M., Lovenduski, N. S., Iglesias-Rodriguez, M. D., & Kleypas, J. A. (2017). Coccolithophore growth and calcification in a changing ocean. *Progress in Oceanography*, 159, 276–295. <https://doi.org/10.1016/j.pocean.2017.10.007>
- Lang, N., & Wolff, E. W. (2011). Interglacial and glacial variability from the last 800 ka in marine, ice and terrestrial archives. *Climate of the Past*, 7(2), 361–380. <https://doi.org/10.5194/cp-7-361-2011>
- Langer, G., Geisen, M., Baumann, K. H., Kläs, J., Riebesell, U., Thoms, S., & Young, J. R. (2006). Species-specific responses of calcifying algae to changing seawater carbonate chemistry. *Geochemistry, Geophysics, Geosystems*, 7, Q09006. <https://doi.org/10.1029/2005gc001227>
- Laws, E. A., Popp, B. N., Cassar, N., & Tanimoto, J. (2002). <sup>13</sup>C discrimination patterns in oceanic phytoplankton: Likely influence of CO<sub>2</sub> concentrating mechanisms, and implications for palaeoreconstructions. *Functional Plant Biology*, 29(3), 323–333. <https://doi.org/10.1071/pp01183>
- Leroy, L. (1939). Some small foraminifera, Ostracoda and otoliths from the Neogene of the Rokan-Tapanoeli area (central Sumatra). *Natuurkundig Tijdschrift voor Nederlandsch Indië*, 99(6).
- Lisiecki, L. E., & Stern, J. V. (2016). Regional and global benthic δ<sup>18</sup>O stacks for the last glacial cycle. *Paleoceanography*, 31, 1368–1394. <https://doi.org/10.1002/2016pa003002>
- Liu, C., Cheng, X., Zhu, Y., Tian, J., & Xia, P. (2002). Oxygen and carbon isotope records of calcareous nannofossils for the past 1 Ma in the southern South China Sea. *Chinese Science Bulletin*, 47, 798. <https://doi.org/10.1360/02tb9180>
- Locarnini, R., Mishonov, A., Antonov, J., Boyer, T., Garcia, H., Baranova, O., et al. (2013). World Ocean Atlas 2013. In S. A. Levitus (Ed.), & Mishonov Technical (Eds.), *Temperature* (Vol. 73, p. 40). NOAA Atlas NESDIS.
- Mann, K., & Lazier, J. (2006). *Vertical structure of the open ocean: Biology of the mixed layer: Dynamics of marine ecosystems*. Blackwell Publishing.
- McClelland, H., Bruggeman, J., Hermoso, M., & Rickaby, R. (2017). The origin of carbon isotope vital effects in coccolith calcite. *Nature Communications*, 8, 1–16. <https://doi.org/10.1038/ncomms14511>
- Mejia, L. M., Méndez-Vicente, A., Abrevaya, L., Lawrence, K. T., Ladlow, C., Bolton, C., et al. (2017). A diatom record of CO<sub>2</sub> decline since the late Miocene. *Earth and Planetary Science Letters*, 479, 18–33. <https://doi.org/10.1016/j.epsl.2017.08.034>
- Mejia, L. M., Ziveri, P., Cagnetti, M., Bolton, C., Zahn, R., Marino, G., et al. (2014). Effects of midlatitude westerlies on the paleoproductivity at the Agulhas Bank slope during the penultimate glacial cycle: Evidence from coccolith Sr/Ca ratios. *Paleoceanography*, 29, 697–714. <https://doi.org/10.1002/2013pa002589>
- Molino, B., & McIntyre, A. (1990). Precessional forcing of nutricline dynamics in the equatorial Atlantic. *Science*, 249, 766–769. <https://doi.org/10.1126/science.249.4970.766>
- Müller, P. J., Kirst, G., Ruhland, G., Von Storch, I., & Rosell-Melé, A. (1998). Calibration of the alkenone paleotemperature index U<sub>37K'</sub> based on core-tops from the eastern South Atlantic and the global ocean (60°N–60°S). *Geochimica et Cosmochimica Acta*, 62, 1757–1772. [https://doi.org/10.1016/S0016-7037\(98\)00097-0](https://doi.org/10.1016/S0016-7037(98)00097-0)
- O'Dea, S. A., Gibbs, S. J., Bown, P. R., Young, J. R., Poulton, A. J., Newsam, C., & Wilson, P. A. (2014). Coccolithophore calcification response to past ocean acidification and climate change. *Nature Communications*, 5, 1–7.
- Okada, H., & Honjo, S. (1973). The distribution of oceanic coccolithophorids in the Pacific. *Deep Sea Research and Oceanographic* (pp. 355–374). [https://doi.org/10.1016/0011-7471\(73\)90059-4](https://doi.org/10.1016/0011-7471(73)90059-4)
- Olsen, A., Key, R. M., van Heuven, S., Lauvset, S. K., Velo, A., Lin, X., et al. (2016). The Global Ocean Data Analysis Project version 2 (GLODAPv2)—An internally consistent data product for the world ocean. *Earth System Science Data*, 8(2), 297–323. <https://doi.org/10.5194/essd-8-297-2016>
- Orr, J., & Epitalon, J.-M. (2015). Improved routines to model the ocean carbonate system: Mocsy 2.0. (Vol. 8). *Geoscientific Model Development*. <https://doi.org/10.5194/gmd-8-485-2015>
- Pagani, M. (2014). 12.13 Biomarker-based inferences of past climate: The alkenone pCO<sub>2</sub> proxy. In H. D. Holland & K. K. Turekian (Eds.), *Treatise on geochemistry* (pp. 361–378). Elsevier. <https://doi.org/10.1016/B978-0-08-095975-7.01027-5>
- Pagani, M., Freeman, K. H., & Arthur, M. A. (1999). Late Miocene atmospheric CO<sub>2</sub> concentrations and the expansion of C<sub>4</sub> grasses. *Science*, 285, 876–879. <https://doi.org/10.1126/science.285.5429.876>
- Pagani, M., Huber, M., Liu, Z., Bohaty, S. M., Henderiks, J., Sijp, W., et al. (2011). The role of carbon dioxide during the onset of Antarctic glaciation. *Science*, 334, 1261–1264. <https://doi.org/10.1126/science.1203909>
- Perrin, L., Probert, I., Langer, G., & Aloisi, G. (2016). Growth of the coccolithophore *Emiliania huxleyi* in light- and nutrient-limited batch reactors: Relevance for the BIOSOPE deep ecological niche of coccolithophores. *Biogeosciences*, 13, 5983–6001. <https://doi.org/10.5194/bg-13-5983-2016>
- Peterson, R. G., & Stramma, L. (1991). Upper-level circulation in the South Atlantic Ocean. *Progress in Oceanography*, 26, 1–73. [https://doi.org/10.1016/0079-6611\(91\)90006-8](https://doi.org/10.1016/0079-6611(91)90006-8)
- Philander, S. (2001). *Atlantic Ocean equatorial currents*. Academic Press.
- Philander, S., & Pacanowski, R. (1986). A model of the seasonal cycle in the tropical Atlantic Ocean. *Journal of Geophysical Research: Oceans*, 91, 14192–14206. <https://doi.org/10.1029/jc091ic12p14192>
- Popp, B. N., Laws, E. A., Bidigare, R. R., Dore, J. E., Hanson, K. L., & Wakeham, S. G. (1998). Effect of phytoplankton cell geometry on carbon isotopic fractionation. *Geochimica et Cosmochimica Acta*, 62, 69–77. [https://doi.org/10.1016/S0016-7037\(97\)00333-5](https://doi.org/10.1016/S0016-7037(97)00333-5)
- Prahl, F. G., & Wakeham, S. G. (1987). Calibration of unsaturation patterns in long-chain ketone compositions for paleotemperature assessment. *Nature*, 330, 367–369. <https://doi.org/10.1038/330367a0>
- Prell, W., & Curry, W. (1981). Faunal and isotopic indices of monsoonal upwelling—Western Arabian Sea. *Oceanologica Acta*, 4, 91–98.
- Rae, J. W., Zhang, Y. G., Liu, X., Foster, G. L., Stoll, H. M., & Whiteford, R. D. (2021). Atmospheric CO<sub>2</sub> over the past 66 million years from marine archives. *Annual Review of Earth and Planetary Sciences*, 49. <https://doi.org/10.1146/annurev-earth-082420-063026>
- Rau, G. H., Riebesell, U., & Wolf-Gladrow, D. (1996). A model of photosynthetic <sup>13</sup>C fractionation by marine phytoplankton based on diffusive molecular CO<sub>2</sub> uptake. *Marine Ecology Progress Series*, 133, 275–285. <https://doi.org/10.3354/meps133275>

- Ravelo, A., & Fairbanks, R. (1992). Oxygen isotopic composition of multiple species of planktonic foraminifera: Recorders of the modern photic zone temperature gradient. *Paleoceanography*, 7, 815–831. <https://doi.org/10.1029/92pa02092>
- R Core Team. (2021). *R: A language and environment for statistical computing*. R Foundation for Statistical Computing. Retrieved from <http://www.R-project.org/>
- Rehfeld, K., Münch, T., Ho, S. L., & Laepple, T. (2018). Global patterns of declining temperature variability from the Last Glacial Maximum to the Holocene. *Nature*, 554, 356–359. <https://doi.org/10.1038/nature25454>
- Richardson, P., & Reverdin, G. (1987). Seasonal cycle of velocity in the Atlantic North Equatorial Countercurrent as measured by surface drifters, current meters, and ship drifts. *Journal of Geophysical Research*, 92, 3691–3708. <https://doi.org/10.1029/jc092ic04p03691>
- Rickaby, R. E., Henderiks, J., & Young, J. N. (2010). Perturbing phytoplankton: Response and isotopic fractionation with changing carbonate chemistry in two coccolithophore species. *Climate of the Past*, 6, 771–785. <https://doi.org/10.5194/cp-6-771-2010>
- Riegman, R., Stolte, W., Noordeoos, A. A. M., & Slezak, D. (2000). Nutrient uptake and alkaline phosphatase (ec 3:1:3:1) activity of *emiliana huxleyi* (PRYMNESIOPHYCEAE) during growth under n and p limitation in continuous cultures. *Journal of Phycology*, 36, 87–96. <https://doi.org/10.1046/j.1529-8817.2000.99023.x>
- Rigal-Hernández, A. S., Trull, T. W., Flores, J., Nodder, S. D., Eriksen, R., Davies, D. M., et al. (2020). Full annual monitoring of Subarctic *Emiliana huxleyi* populations reveals highly calcified morphotypes in high-CO<sub>2</sub> winter conditions. *Scientific Reports*, 10, 1–14. <https://doi.org/10.1038/s41598-020-59375-8>
- Romanek, C. S., Grossman, E. L., & Morse, J. W. (1992). Carbon isotopic fractionation in synthetic aragonite and calcite: Effects of temperature and precipitation rate. *Geochimica et Cosmochimica Acta*, 56, 419–430. [https://doi.org/10.1016/0016-7037\(92\)90142-6](https://doi.org/10.1016/0016-7037(92)90142-6)
- Schlitzer, R. (2008). *Ocean data view*.
- Seki, O., Foster, G. L., Schmidt, D. N., Mackensen, A., Kawamura, K., & Pancost, R. D. (2010). Alkenone and boron-based Pliocene pCO<sub>2</sub> records. *Earth and Planetary Science Letters*, 292, 201–211. <https://doi.org/10.1016/j.epsl.2010.01.037>
- Sett, S., Bach, L. T., Schulz, K. G., Koch-Klavnsen, S., Lebrato, M., & Riebesell, U. (2014). Temperature modulates coccolithophorid sensitivity of growth, photosynthesis and calcification to increasing seawater pCO<sub>2</sub>. *PLoS One*, 9, e88308. <https://doi.org/10.1371/journal.pone.0088308>
- Sosdian, S. M., Greenop, R., Hain, M., Foster, G. L., Pearson, P. N., & Lear, C. H. (2018). Constraining the evolution of Neogene ocean carbonate chemistry using the boron isotope pH proxy. *Earth and Planetary Science Letters*, 498, 362–376. <https://doi.org/10.1016/j.epsl.2018.06.017>
- Spero, H. J., Mielke, K. M., Kalve, E. M., Lea, D. W., & Pak, D. K. (2003). Multispecies approach to reconstructing eastern equatorial Pacific thermocline hydrography during the past 360 kyr. *Paleoceanography*, 18, 1022. <https://doi.org/10.1029/2002pa000814>
- Steph, S., Regenber, M., Tiedemann, R., Multiza, S., & Nürnberg, D. (2009). Stable isotopes of planktonic foraminifera from tropical Atlantic/Caribbean core-tops: Implications for reconstructing upper ocean stratification. *Marine Micropaleontology*, 71, 1–19. <https://doi.org/10.1016/j.marmicro.2008.12.004>
- Stoll, H. M., Guitian, J., Hernandez-Almeida, I., Mejia, L. M., Phelps, S., Polissar, P., et al. (2019). Upregulation of phytoplankton carbon concentrating mechanisms during low CO<sub>2</sub> glacial periods and implications for the phytoplankton pCO<sub>2</sub> proxy. *Quaternary Science Reviews*, 208, 1–20. <https://doi.org/10.1016/j.quascirev.2019.01.012>
- Stolz, K., & Baumann, K.-H. (2010). Changes in paleoceanography and paleoecology during Marine Isotope Stage (MIS) 5 in the eastern North Atlantic (ODP Site 980) deduced from calcareous nannoplankton observations. *Palaeogeography, Palaeoclimatology, Palaeoecology*, 292, 295–305. <https://doi.org/10.1016/j.palaeo.2010.04.002>
- Stramma, L., & Schott, F. (1999). The mean flow field of the tropical Atlantic Ocean. *Deep Sea Research Part II: Topical Studies in Oceanography*, 46, 279–303. [https://doi.org/10.1016/s0967-0645\(98\)00109-x](https://doi.org/10.1016/s0967-0645(98)00109-x)
- Takahashi, T., Sutherland, S. C., Wanninkhof, R., Sweeney, C., Feely, R. a., Chipman, D. W., et al. (2009). Climatological mean and decadal change in surface ocean pCO<sub>2</sub>, and net sea-air CO<sub>2</sub> flux over the global oceans. *Deep Sea Research Part II: Topical Studies in Oceanography*, 56(8–10), 554–577. <https://doi.org/10.1016/j.dsr2.2008.12.009>
- Tierney, J. E., & Tingley, M. P. (2018). BAYSPLINE: A new calibration for the alkenone paleothermometer. *Paleoceanography and Paleoclimatology*, 33, 281–301. <https://doi.org/10.1002/2017pa003201>
- Tremblin, M., Héros, M., & Minoletti, F. (2016). Equatorial heat accumulation as a long-term trigger of permanent Antarctic ice sheets during the Cenozoic. *Proceedings of the National Academy of Sciences of the United States of America*, 113, 11782–11787. <https://doi.org/10.1073/pnas.1608100113>
- Vink, A., Brune, A., Höll, C., Zonneveld, K. A., & Willems, H. (2002). On the response of calcareous dinoflagellates to oligotrophy and stratification of the upper water column in the equatorial Atlantic Ocean. *Palaeogeography, Palaeoclimatology, Palaeoecology*, 178, 53–66. [https://doi.org/10.1016/s0031-0182\(01\)00368-6](https://doi.org/10.1016/s0031-0182(01)00368-6)
- Volkman, J. K. (2000). Ecological and environmental factors affecting alkenone distributions in seawater and sediments. *Geochemistry, Geophysics, Geosystems*, 1(9), 1036. <https://doi.org/10.1029/2000gc000061>
- Waelbroeck, C., Kiefer, T., Dokken, T., Chen, M.-T., Spero, H., Jung, S., et al. (2014). Constraints on surface seawater oxygen isotope change between the Last Glacial Maximum and the Late Holocene. *Quaternary Science Reviews*, 105, 102–111. <https://doi.org/10.1016/j.quascirev.2014.09.020>
- Wilkens, R. H., Westerhold, T., Drury, A. J., Lyle, M., Gorgas, T., & Tian, J. (2017). Revisiting the Ceara Rise, equatorial Atlantic Ocean: Isotope stratigraphy of ODP Leg 154 from 0 to 5Ma. *Climate of the Past*, 13, 779–793. <https://doi.org/10.5194/cp-13-779-2017>
- Wilson, K. E., Maslin, M. A., & Burns, S. J. (2011). Evidence for a prolonged retroflexion of the North Brazil Current during glacial stages. *Palaeogeography, Palaeoclimatology, Palaeoecology*, 301, 86–96. <https://doi.org/10.1016/j.palaeo.2011.01.003>
- Yin, Q. Z., & Berger, A. (2012). Individual contribution of insolation and CO<sub>2</sub> to the interglacial climates of the past 800,000 years. *Climate Dynamics*, 38(3–4), 709–724. <https://doi.org/10.1007/s00382-011-1013-5>
- Young, J., Geisen, M., Cros, L., Kleijne, A., Sprengel, C., Probert, I., & Østergaard, J. (2003). A guide to extant coccolithophore taxonomy. *Journal of Nannoplankton Research, Special Issue*, 1, 1–132.
- Young, J. R., Thierstein, H. R., & Winter, A. (2000). Nannoplankton ecology and paleoecology. *Marine Micropaleontology*, 1(39), 7–9. [https://doi.org/10.1016/s0377-8398\(00\)00009-8](https://doi.org/10.1016/s0377-8398(00)00009-8)
- Zeebe, R. E. (1999). An explanation of the effect of seawater carbonate concentration on foraminiferal oxygen isotopes. *Geochimica et Cosmochimica Acta*, 63, 2001–2007. [https://doi.org/10.1016/s0016-7037\(99\)00091-5](https://doi.org/10.1016/s0016-7037(99)00091-5)
- Zhang, H., Stoll, H., Bolton, C., Jin, X., & Liu, C. (2018). A refinement of coccolith separation methods: Measuring the sinking characteristics of coccoliths. *Biogeosciences*, 15, 4759–4775. <https://doi.org/10.5194/bg-15-4759-2018>
- Zhang, Y. G., Henderiks, J., & Liu, X. (2020). Refining the alkenone-pCO<sub>2</sub> method II: Toward resolving the physiological parameter 'b'. *Geochimica et Cosmochimica Acta*, 281, 118–134. <https://doi.org/10.1016/j.gca.2020.05.002>



- Zhang, Y. G., Pagani, M., Liu, Z., Bohaty, S. M., & DeConto, R. (2013). A 40-million-year history of atmospheric CO<sub>2</sub>. *Philosophical Transactions of the Royal Society A: Mathematical, Physical & Engineering Sciences*, 371, 20130096. <https://doi.org/10.1098/rsta.2013.0096>
- Ziveri, P., Stoll, H., Probert, I., Klaas, C., Geisen, M., Ganssen, G., & Young, J. (2003). Stable isotope 'vital effects' in coccolith calcite. *Earth and Planetary Science Letters*, 210, 137–149. [https://doi.org/10.1016/s0012-821x\(03\)00101-8](https://doi.org/10.1016/s0012-821x(03)00101-8)
- Ziveri, P., Thoms, S., Probert, I., Geisen, M., & Langer, G. (2012). A universal carbonate ion effect on stable oxygen isotope ratios in unicellular planktonic calcifying organisms. *Biogeosciences*, 9, 1025–1032. <https://doi.org/10.5194/bg-9-1025-2012>

## References From the Supporting Information

- Bemis, B. E., Spero, H. J., Bijma, J., & Lea, D. W. (1998). Reevaluation of the oxygen isotopic composition of planktonic foraminifera: Experimental results and revised paleotemperature equations. *Paleoceanography*, 13, 150–160. <https://doi.org/10.1029/98pa00070>
- Boeckel, B., & Baumann, K.-H. (2004). Distribution of coccoliths in surface sediments of the south-eastern South Atlantic Ocean: Ecology, preservation and carbonate contribution. *Marine Micropaleontology*, 51, 301–320. <https://doi.org/10.1016/j.marmicro.2004.01.001>
- Bouvier-Soumagnac, Y., & Duplessy, J.-C. (1985). Carbon and oxygen isotopic composition of planktonic foraminifera from laboratory culture, plankton tows and Recent sediment; implications for the reconstruction of paleoclimatic conditions and of the global carbon cycle. *Journal of Foraminiferal Research*, 15, 302–320. <https://doi.org/10.2113/gsjfr.15.4.302>
- Buiteveld, H. (1995). A model for calculation of diffuse light attenuation (PAR) and Secchi depth. *Netherlands Journal of Aquatic Ecology*, 29(1), 55–65. <https://doi.org/10.1007/bf02061789>
- Dittert, N., Baumann, K.-H., Bickert, R., Henrich, R., Huber, R., Kinkel, H., & Meggers, H. (1999). Carbonate dissolution in the deep-sea: Methods, quantification and paleoceanographic application. In G. Fischer & G. Wefer (Eds.), *Use of proxies in paleoceanography: Examples from the South Atlantic* (pp. 255–284). Springer Verlag. [https://doi.org/10.1007/978-3-642-58646-0\\_10](https://doi.org/10.1007/978-3-642-58646-0_10)
- Fielding, S. R. (2013). *Emiliana huxleyi* specific growth rate dependence on temperature. *Limnology & Oceanography*, 58, 663–666. <https://doi.org/10.4319/lo.2013.58.2.0663>
- Flores, J.-A., Gersonde, R., Sierro, F., & Niebler, H.-S. (2000). Southern Ocean Pleistocene calcareous nannofossil events: Calibration with isotope and geomagnetic stratigraphies. *Marine Micropaleontology*, 40, 377–402. [https://doi.org/10.1016/s0377-8398\(00\)00047-5](https://doi.org/10.1016/s0377-8398(00)00047-5)
- Flores, J. A., & Marino, M. (2002). Pleistocene calcareous nannofossil stratigraphy for ODP Leg 177 (Atlantic sector of the Southern Ocean). *Marine Micropaleontology*, 45, 191–224. [https://doi.org/10.1016/s0377-8398\(02\)00030-0](https://doi.org/10.1016/s0377-8398(02)00030-0)
- Hermoso, M., Minoletti, F., Aloisi, G., Bonifacie, M., McClelland, H. L. O., Labourdette, N., et al. (2016). An explanation for the <sup>18</sup>O excess in Noelaerhabdaceae coccolith calcite. *Geochimica et Cosmochimica Acta*, 189, 132–142. <https://doi.org/10.1016/j.gca.2016.06.016>
- Hoefs, J., & Hoefs, J. (2009). *Stable isotope geochemistry*. Springer.
- Lin, J., Lee, Z., Ondrusek, M., & Du, K. (2016). Remote sensing of normalized diffuse attenuation coefficient of downwelling irradiance. *Journal of Geophysical Research: Oceans*, 121(9), 6717–6730. <https://doi.org/10.1002/2016jc011895>
- Murtugudde, R., Beauchamp, J., McClain, C. R., Lewis, M., & Busalacchi, A. J. (2002). Effects of penetrative radiation on the upper tropical ocean circulation. *Journal of Climate*, 15(5), 470–486. [https://doi.org/10.1175/1520-0442\(2002\)015<0470:eoprot>2.0.co;2](https://doi.org/10.1175/1520-0442(2002)015<0470:eoprot>2.0.co;2)
- Regenberg, M., Steph, S., Nürnberg, D., Tiedemann, R., & Garbe-Schönberg, D. (2009). Calibrating Mg/Ca ratios of multiple planktonic foraminiferal species with  $\delta^{18}\text{O}$ -calcification temperatures: Paleothermometry for the upper water column. *Earth and Planetary Science Letters*, 278(3–4), 324–336. <https://doi.org/10.1016/j.epsl.2008.12.019>



**Carbon isotopic fractionation of alkenones and *Gephyrocapsa* coccoliths over the Late Quaternary (Marine Isotope Stages 12 to 9) glacial-interglacial cycles at the western tropical Atlantic**

A. González-Lanchas<sup>1</sup>, I. Hernández-Alméida<sup>2</sup>, J.-A. Flores<sup>1</sup>, F.J. Sierro<sup>1</sup>, J. Guitian<sup>2</sup> and H. M. Stoll<sup>2</sup>

<sup>1</sup> Departamento de Geología, Universidad de Salamanca, Salamanca, Spain.

<sup>2</sup> Geological Institute, ETH Zürich, Zürich, Switzerland.

\*Corresponding author: Alba González-Lanchas (lanchas@usal.es)

## **Contents of this file**

Text S1 to S8  
Figures S1 to S7  
Tables S1 to S7

## **Introduction**

This supporting information files contains a detailed description of the procedures followed for estimating the  $p\text{CO}_2$  during the period of production of each sample, calculation of equilibrium calcification temperature relationships between the microplankton groups and species, the criteria for classification of the species contained in the *Gephyrocapsa* genus trough MIS 12 to MIS 9 and the analytical procedure for the parametrization of growth rates using micropaleontological proxies and temperature reconstructions. Results of the preservation of the coccolithophore assemblages in samples and the variation in the species composition of the *Gephyrocapsa* assemblage are also shown.

The complete results of the statistical multiple correlation analyses and visual correlation between coccolith carbon ( $\epsilon_{\text{coccolith}}$ ) and oxygen ( $\Delta\delta^{18}\text{O}_{\text{Gephyrocapsa-T. sacculifer}}$ ) vital effects with other parameters are presented in these files.

Data generated for this work is archived online at Mendeley as:

González-Lanchas, Alba; Stoll, Heather; Hernández-Alméida, Iván; Flores, José-Abel; Sierro, Francisco J.; Guitián, José (2020), “Carbon isotopic fractionation of alkenones and *Gephyrocapsa* coccoliths over the Late Quaternary (Marine Isotope Stages 12 to 9) glacial-interglacial cycles at the western tropical Atlantic”, Mendeley Data, (<https://data.mendeley.com/datasets/zhmwhjjs63>)

### **Text S1. $p\text{CO}_2$ Sample Assignment and $\text{CO}_2[\text{aq}]$ Estimation**

To derive the  $p\text{CO}_2$  values for each sample we used the equation obtained from the regression between the deep North Atlantic  $\delta^{18}\text{O}$  benthic stack LS16 (Lisiecki and Stern, 2016) and the  $p\text{CO}_2$  from the ice core compilation by Köhler et al. (2017) for the last 40 kyr:

$$p\text{CO}_2 = - 53.39 * \delta^{18}\text{O benthic Site 925} + 446.9$$

We obtained corresponding slope values in comparison with the equation from the regression between the spliced  $\delta^{18}\text{O}$  benthic at Site 925 (Wilkins et al., 2017) and  $p\text{CO}_2$  (Köhler et al., 2017) for the last 40 kyr.

We use the Henry's law formula for the estimation of  $\text{CO}_{2\text{aq}}$  after  $p\text{CO}_2$  sample assignment:

$$\text{CO}_{2\text{aq sample}} = K * p\text{CO}_{2\text{sample}}$$

$K$  is the  $\text{CO}_2$  solubility coefficient. A constant salinity value of 35 psu is used for calculation.

The  $p\text{CO}_2$ , SST, salinity and  $\text{CO}_{2\text{aq}}$  value for each sample is recorded in Table S1.

The same procedure for  $p\text{CO}_2$  sample assignment and  $\text{CO}_{2\text{aq}}$  estimation was applied for the samples in Zhang et al. (2013) corresponding to the Quaternary G/I period between 430 to 20 ka (MIS 12 to the Last Glacial Maximum; LGM). We selected the  $\delta^{18}\text{O}$  benthic at Site 925 (Wilkins et al., 2017), which most closely matched the upper and lower depth of each sampled interval for the  $\epsilon_p$  value reported in Zhang et al. (2013). The comparison of the slopes between  $\epsilon_p$  measured at Site 925 in our study and in Zhang et al. (2013) with  $\ln(\text{CO}_2[\text{aq}])$  calculated from the same protocol is presented in the Figure S3.

### **Text S2. Calculation of equilibrium calcification temperature relationships between *Gephyrocapsa* and the planktic foraminifera species**

For the calculation of the differences in equilibrium calcification temperatures between *Gephyrocapsa* and the planktic foraminifer species we use the culture equations

by Hermoso et al. (2016b) for *G. oceanica* and the equations for *G. ruber*, *T. sacculifer* and *N. dutertrei* summarized in Spero et al. (2003; Table S2).

To solve these calculations, a constant  $\delta^{18}\text{O}_{\text{sw}}$  is assumed; this relies in the small salinity-corrected gradient of 0.23 ‰ SMOW between 35 and 150 m depth obtained by applying the salinity -  $\delta^{18}\text{O}_{\text{sw}}$  equation for the tropical Atlantic by Regenberg et al. (2009) on the regional deep salinity gradient (36.25 – 35.75 psu annual salinity; WOA). We thus assume the constant  $\delta^{18}\text{O}_{\text{sw}}$  of 0.84 ‰ SMOW calculated for the Holocene (Waelbroeck et al., 2014) for our interglacial samples at MIS 11 and the MIS 10/MIS 9 transition. We further consider an offset of +1.25 ‰ SMOW for the glacial samples of MIS 12 and MIS 10 (Hoefs and Hoefs, 2009). These results are shown in Figure 2e.

We applied the same approach for the calculation of the paired differences in equilibrium calcification temperatures between the studied planktic foraminifer species *G. ruber*, *T. sacculifer* and *N. dutertrei* (Fig. S4).

### **Text S3. Species classification and structure of the *Gephyrocapsa* assemblage**

The taxonomy of *Gephyrocapsa*, which represents the major component of the assemblage, follows the criteria by Flores et al. (2000). The *Gephyrocapsa* specimens < 3  $\mu\text{m}$  with open central areas were grouped as small *Gephyrocapsa* (including *G. ericsonii* and *G. aperta*). Either smaller or larger than 3  $\mu\text{m}$  *Gephyrocapsa* specimens with closed central areas are grouped as *Gephyrocapsa caribbeanica* (small and medium *G. caribbeanica*). The medium *Gephyrocapsa* comprises all specimens > 3  $\mu\text{m}$  with open central area, mostly corresponding to the species *Gephyrocapsa oceanica*; very rarely specimens of *Gephyrocapsa muelleri* were present in samples and are included in this group.

The *Gephyrocapsa* assemblage is dominated by small *Gephyrocapsa* (open centrals) and medium *Gephyrocapsa*, respectively accounting 28 and 26 % in average of the total assemblage. Both alternate in the dominance within a very low range of variability (Fig. S5h). *G. caribbeanica* (small and medium) comprises 18 %, with modest relative increases in the interglacial samples (Fig. S5h). The number of *Gephyrocapsa* coccoliths per gram (N) of the different groups evidence together a decreasing trend across the interval. There is a final increase in values, which is particularly significant in *G. caribbeanica* (Fig. S5g).

### **Text S4. Preservation of coccoliths**

A dissolution estimation based on the preservation of different size species was generated by using the CEX dissolution index  $\text{CEX} = (\text{small } Gephyrocapsa) / (\text{small } Gephyrocapsa + \text{Calcidiscus leptoporus})$  by Boeckel and Baumann, (2004) following the ratio: based on the CEX index by Dittert et al. (1999). Higher values of CEX corresponds to lower dissolution levels, with a threshold of  $\text{CEX} = 0.63$  established to characterize a depositional environment below the calcite lysocline (Boeckel and Baumann, 2004).

According to visual criteria by Flores and Marino (2002), little or no evidence of dissolution and full preservation of the diagnostic characters of the specimens sets a "moderate" to "good" preservation. The constant high content of specimens more prone to dissolution, such as the small *Gephyrocapsa* individuals, together with high CEX well

above 0.63 prove a low dissolution effect on *Gephyrocapsa* coccoliths. This supports the concentration of *Gephyrocapsa* (N; coccoliths  $\text{g}^{-1}$ ) can be used to estimate primary productivity across the interval.

### **Text S5. Growth rate parametrization**

The growth rate parametrization method proposed by Krumhardt et al. (2017) is based on Sea Surface Temperature (SST) and nutrient limitation, as expressed in the formula:

$$\mu = \mu_{max} * \left( \frac{N}{N + K_M} \right)$$

A complete description of this model is available in the original publication (Krumhardt et al., 2017). Summarizing, this parametrization is based on the estimation of a maximum temperature dependent growth rate ( $\mu_{max}$ ) in relation with the concentration of a limiting nutrient (N), which corresponds to  $[\text{PO}_4^{3-}]$ , and  $\text{CO}_2$  concentrations.  $K_M$  is the half saturation constant for the nutrient  $[\text{PO}_4^{3-}]$  ( $K_M = 0.17\mu\text{M}$ ), and  $\mu_{max}$  corresponds to maximum growth rate at a given temperature according to the Fielding (2013) power function ( $0.1419 * T^{0.8151}$ ). The required temperature estimation is based on the  $U_{37}^{kl}$  SST record at Site 925.

### **Text S6. Calculation of Modern Photosynthetic Active Radiation (PAR)**

Calculation of light levels in depth was estimated using a model of penetration of photosynthetic active radiation (PAR) from surface to depth (Buiteveld, 1995; Murtugudde et al., 2002). Monthly climatology of PAR, and the diffuse attenuation coefficient for downwelling irradiance at 490 nm ( $K_d490$ ) were included in Equation 1 in Lin et al. (2016) to calculate PAR at each depth, extracted at the location from the MODIS Ocean products database (<http://oceancolor.gsfc.nasa.gov/cgi/l3>). Results are summarized in Table S7.

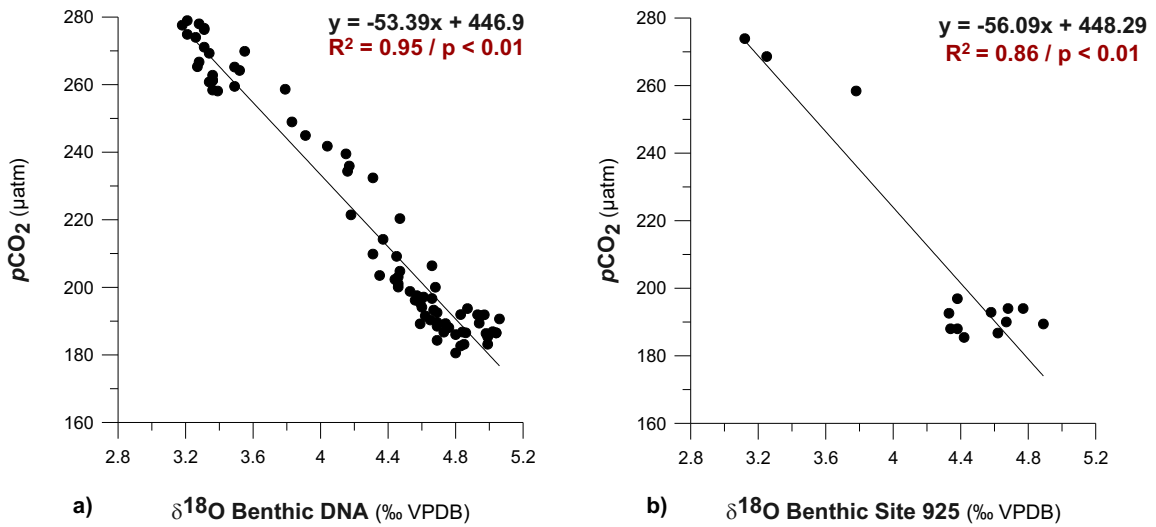


**Figure S1.** (a) Regression between the deep North Atlantic (DNA)  $\delta^{18}\text{O}$  benthic stack LS16 (Lisiecki and Stern, 2016) and  $p\text{CO}_2$  (Köhler et al., 2017) for the last 40 kyr; (b) Regression between the spliced  $\delta^{18}\text{O}$  benthic at Site 925 (Wilkins et al., 2017) and  $p\text{CO}_2$  (Köhler et al., 2017) for the last 40 kyr.

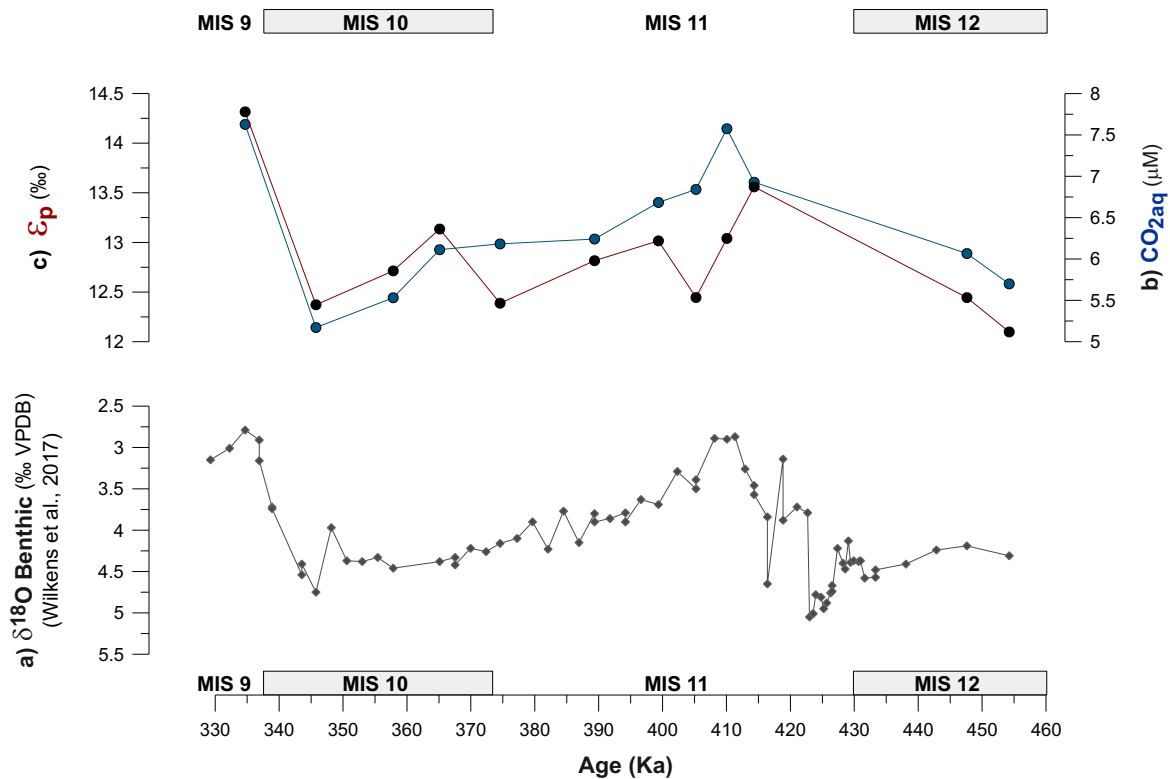


**Figure S2.** Time series of  $\epsilon_p$  record at Site 925 and the estimated  $\text{CO}_2[\text{aq}]$ . (a) spliced  $\delta^{18}\text{O}$  benthic profile at Site 925 (‰VPDB) by Wilkins et al. (2017); (b)  $\text{CO}_2[\text{aq}]$  estimated from

$p\text{CO}_2$  calculated from the regression between the deep North Atlantic (DNA)  $\delta^{18}\text{O}$  benthic stack LS16 (Lisiecki and Stern, 2016) and  $p\text{CO}_2$  (Köhler et al., 2017) for the last 40 kyr. **(c)**  $\epsilon_p$  measured at Site 925 (‰VPDB).

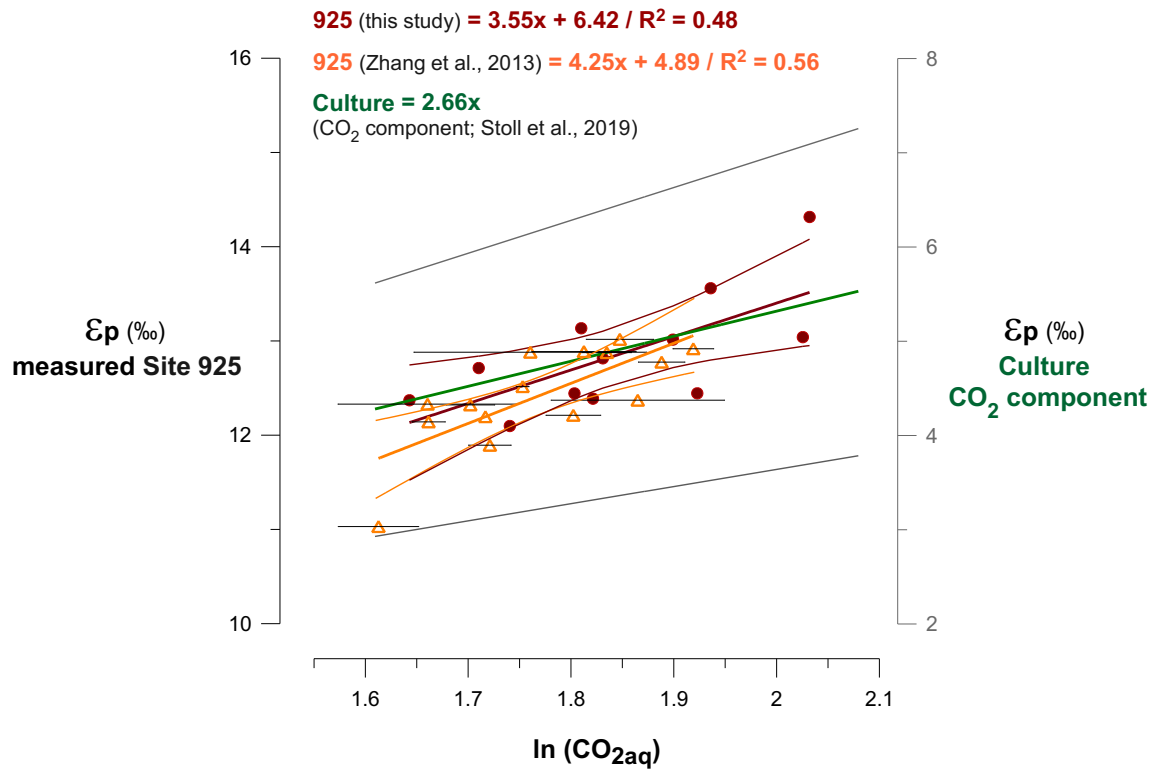


**Figure S3.** On the left y-axis: Regression of  $\epsilon_p$  measured at Site 925 and  $\ln(\text{CO}_{2\text{aq}})$  from the MIS 12 to 9 in this study, in red, and from the MIS 12 to the LGM from the data by Zhang et al. (2013) in orange. The horizontal bars on the series from Zhang et al. (2013) represent the range in the  $p\text{CO}_2$  using the nearest matching  $\delta^{18}\text{O}$  benthic at Site 925 by Wilkens et al. (2017) to apply the regression between the deep North Atlantic  $\delta^{18}\text{O}$  benthic



stack LS16 and the ice core  $p\text{CO}_2$ . The best fit (linear equation) and the 95% confidence intervals for the regression for both datasets, as in the Figure 7, is represented.

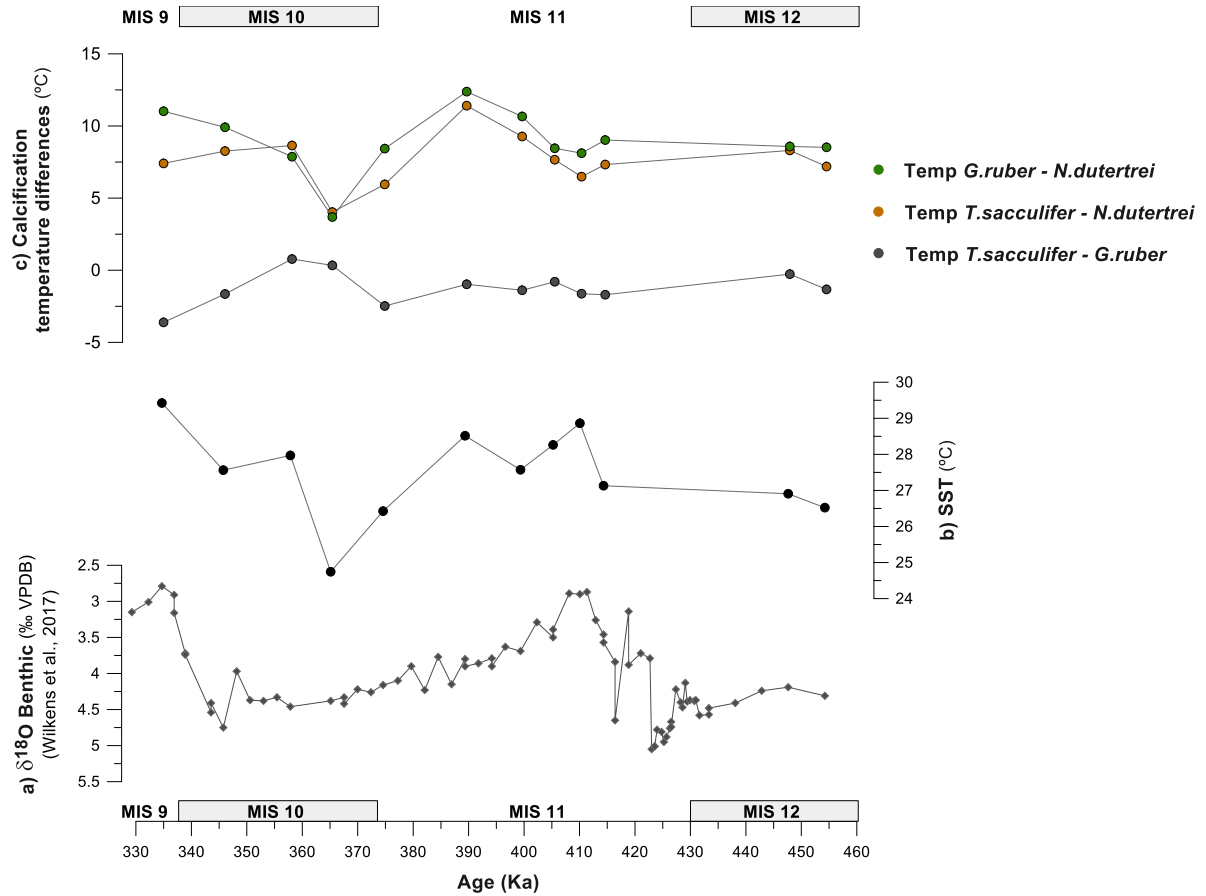


**Figure S4.** Difference in equilibrium calcification temperatures between the planktic foraminifera species. **(a)** spliced  $\delta^{18}\text{O}$  benthic profile at Site 925 ( $\text{‰ VPDB}$ ) by Wilkens et

al. (2017) **(b)**  $U_{37}^{k'}$  alkenone-derived SST ( $^{\circ}\text{C}$ ); **(c)** paired equilibrium calcification temperature relationships between the planktic foraminifera species ( $^{\circ}\text{C}$ ).

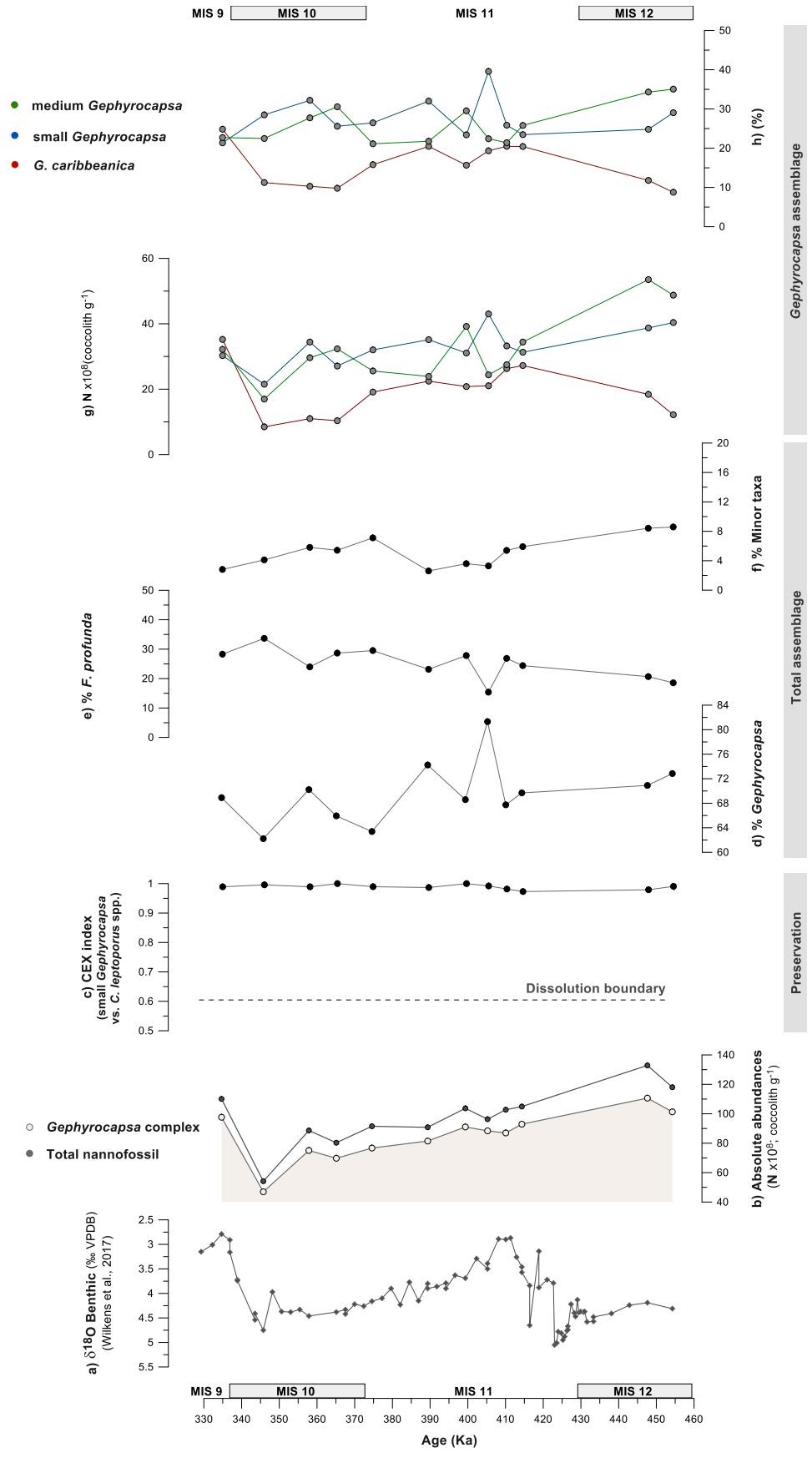


**Figure S5.** Composition and preservation state of the total coccolithophore assemblage and the species composing the *Gephyrocapsa* genus in the studied samples. **(a)** spliced  $\delta^{18}\text{O}$  benthic profile at Site 925 (‰ VPDB) by Wilkens et al. (2017); **(b)** Absolute abundances, N (coccolith  $\text{g}^{-1}$  sediment), of all the *Gephyrocapsa* specimens (colored section) and the total assemblage (black dots); **(c)** CEX index for the determination of the assemblage preservation. The dashed line corresponds to the dissolution boundary (0.63) established by Boeckel and Baumann (2004). Relative abundances (%) of **(d)** all the *Gephyrocapsa* specimens; **(e)** *F. profunda*; **(f)** other minor taxa present in the coccolithophore assemblage. **(g)** Absolute abundances, N (coccolith  $\text{g}^{-1}$  sediment), of each *Gephyrocapsa* species; **(h)** Relative abundances (%) of each *Gephyrocapsa* species.

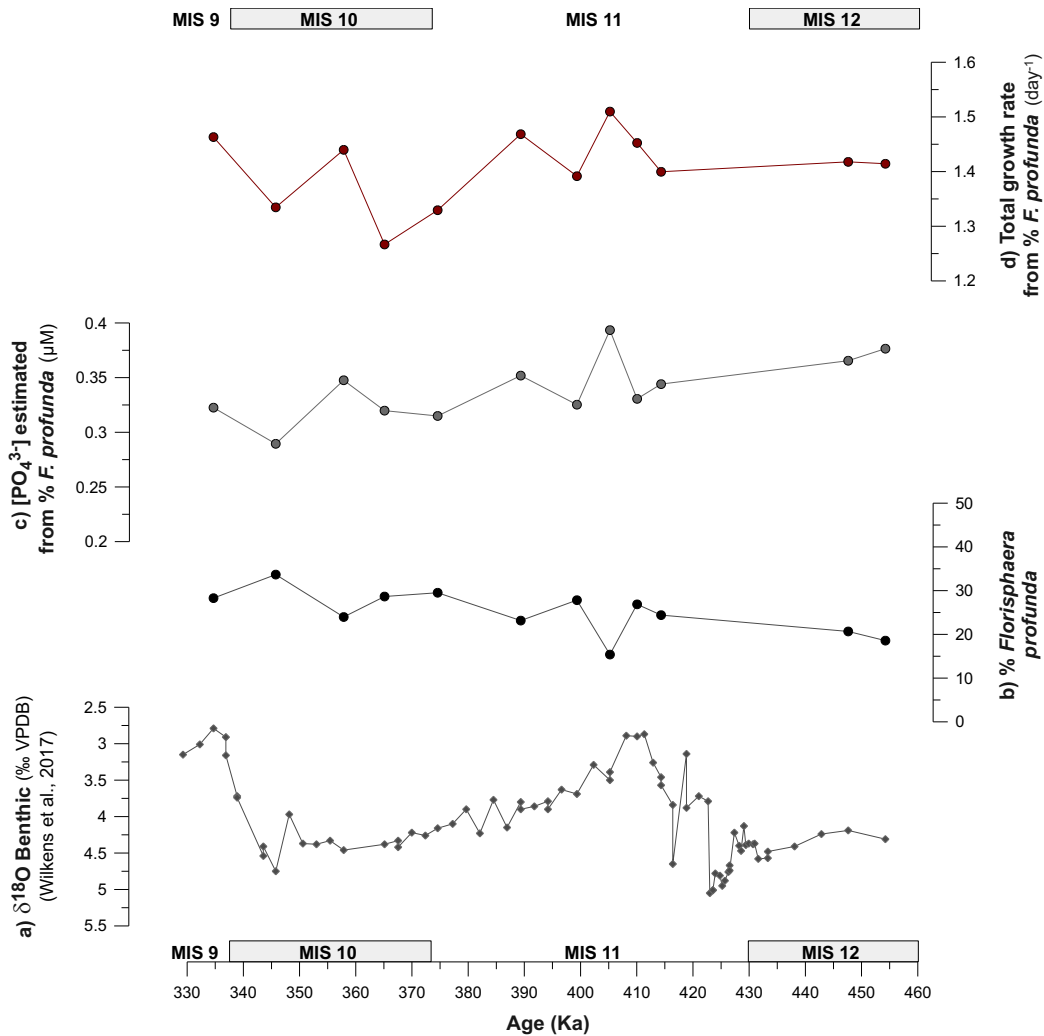


**Figure S6.** Absolute growth rate parametrization following Krumhardt et al. (2017) using **(a)** the % values of *F. profunda* converted into **(b)**  $[\text{PO}_4^{3-}]$  by the application of the

regression in Hernández-Alméida et al., (2020); **(c)** profile of the resulting total growth rate calculated in combination with  $U_{37}^{kl}$  alkenone-derived SST trough MIS 12 to 9 at Site 925.

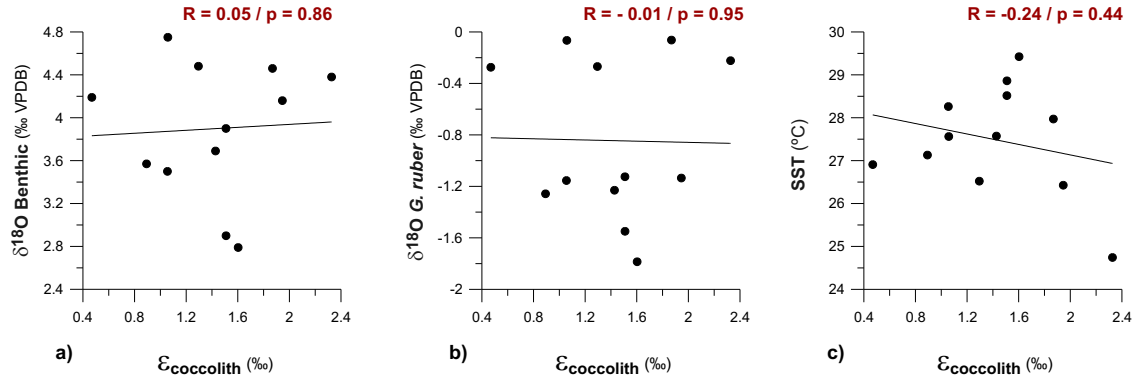


**Figure S7.** Correlation R between  $\epsilon_{\text{coccolith}}$  and the regional proxies at Site 925 of **(a)**  $\delta^{18}\text{O}$  benthic at Site 925 (‰ VPDB) by Wilkens et al. (2017); **(b)**  $\delta^{18}\text{O}$  *G. ruber* (‰ VPDB) and **(c)**  $U_{37}^{kl}$  alkenone-derived SST (°C) at Site 925.

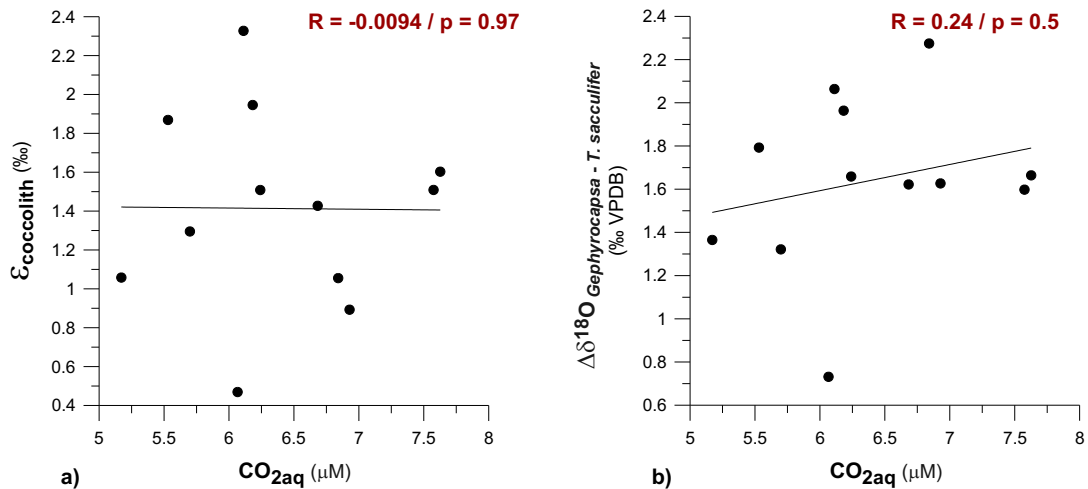


**Figure S8.** Correlation R between the carbon and oxygen vital effect profiles, respectively **(a)**  $\epsilon_{\text{coccolith}}$  and **(b)**  $\Delta\delta^{18}\text{O}_{\text{Gephyrocapsa-T. sacculifer}}$  with  $\text{CO}_2[\text{aq}]$ .

Age (ka)	$p\text{CO}_2$ ( $\mu\text{atm}$ )	$U_{37}^{k'}$	SST ( $^{\circ}\text{C}$ )	$K$	$\text{CO}_2[\text{aq}]$ ( $\mu\text{M}$ )
334.69	297.94	0.977	29.42	0.025597	7.63
345.77	193.30	0.934	27.56	0.026751	5.17
357.86	208.78	0.934	27.97	0.026490	5.53
365.13	213.05	0.870	24.74	0.028686	6.11
374.58	224.80	0.908	26.43	0.027502	6.18
389.35	238.68	0.950	28.52	0.026148	6.24
399.35	249.89	0.933	27.57	0.026744	6.68
405.23	260.04	0.954	28.26	0.026307	6.84
410.06	292.07	0.967	28.86	0.025936	7.58
414.33	256.30	0.931	27.13	0.027032	6.93
447.63	223.20	0.922	26.91	0.027179	6.07
454.24	207.71	0.917	26.52	0.027438	5.70

**Table S1.**  $p\text{CO}_2$  assigned to each sample.  $U_{37}^{k'}$  and  $U_{37}^{k'}$ -derived SST calibrated with BAYSPLINE. Solubility coefficient ( $K$ ) and the resulting  $\text{CO}_2[\text{aq}]$  estimated by the application of Henry's law.

Species	A	B	Reference
<i>G. oceanica</i>	22	-4.4	Hermoso et al. (2016)
<i>G. ruber</i>	14.9	-4.8	Bemis et al. (1998)
<i>T. sacculifer</i>	12	-5.67	Spero et al. (2003)
<i>N. dutertrei</i>	10.5	-6.58	Bouvier-Soumagnac and Duplessy (1985)

$$\text{Temperature equation (general): } T = A + B (\delta c - \delta w) \quad (1)$$

$$\text{Difference in equilibrium temperature: } T_i - T_{ii} = (A_i - A_{ii}) + B_i (\delta c_i) - B_{ii} (\delta c_{ii}) + \delta w (B_{ii} - B_i) \quad (2)$$

**Table S2.** Compilation of culture temperature equilibrium equations used for the calculation of the paired differences in equilibrium calcification temperatures. A and B are the coefficient values of each equation. Equation 1 is the general culture equations.  $\delta c$  is

the isotopical  $\delta^{18}\text{O}$  value of calcite measured in the specimens and  $\delta w$  the seawater  $\delta^{18}\text{O}$  value correspondent to depth habitat. Equation 2 is the constructed paired equation to solve the difference in equilibrium calcification temperatures between species i and species ii.

<b><math>N</math> <i>Gephyrocapsa</i> ~ % <i>F. profunda</i> + Mag. susceptibility; (n=12) <math>R^2 = 0.62</math></b>				
	Coefficients	p value	Lower CI	Upper CI
% <i>F. profunda</i>	1.44	0.06	-0.07	2.96
Mag. susceptibility	-1.26	0.09	-2.74	0.22

**Table S3.** Multiple regression of % *F. profunda* and magnetic susceptibility to explain the variability in the absolute concentration,  $N$ , of *Gephyrocapsa* coccolith.

<b>residual <math>\epsilon_p</math> ~ % <i>F. profunda</i> + C37/38.et; (n=12) <math>R^2 = 0.34</math></b>				
	Coefficients	p value	Lower CI	Upper CI
% <i>F. profunda</i>	0.03	0.27	-0.03	0.08
C37/38.et	-1.50	0.32	-4.75	1.75

**Table S4.** Multiple regression of % *F. profunda* and the alkenone C37/38.et ratio to explain the variability in the residual  $\epsilon_p$  (non- $\text{CO}_2$  variation in  $\epsilon_p$ ).

<b><math>\epsilon_{\text{coccolith}}</math> ~ C37/38.et + <i>Gephyrocapsa</i> coccolith mass; (n =12) <math>R^2 = 0.49</math></b>				
	Coefficients	p value	Lower CI	Upper CI
C37/38.et	-1.53	0.25	-4.33	1.28
<i>Gephyrocapsa</i> coccolith mass	0.54	0.04	0.04	1.04

**Table S5.** Multiple regression of the alkenone C37/38.et ratio and *Gephyrocapsa* coccolith mass to explain the variability in  $\epsilon_{\text{coccolith}}$ .

<b><math>\epsilon_{\text{coccolith}}</math> ~ C37/38.et + <i>Gephyrocapsa</i> coccolith mass + <math>\text{CO}_2[\text{aq}]</math>; (n=12) <math>R^2 = 0.59</math></b>				
	Coefficients	p value	Lower CI	Upper CI
C37/38.et	-1.33	0.29	-4.06	1.4
<i>Gephyrocapsa</i> coccolith mass	0.72	0.02	0.15	1.29
$\text{CO}_2[\text{aq}]$	0.25	0.19	-0.15	0.65

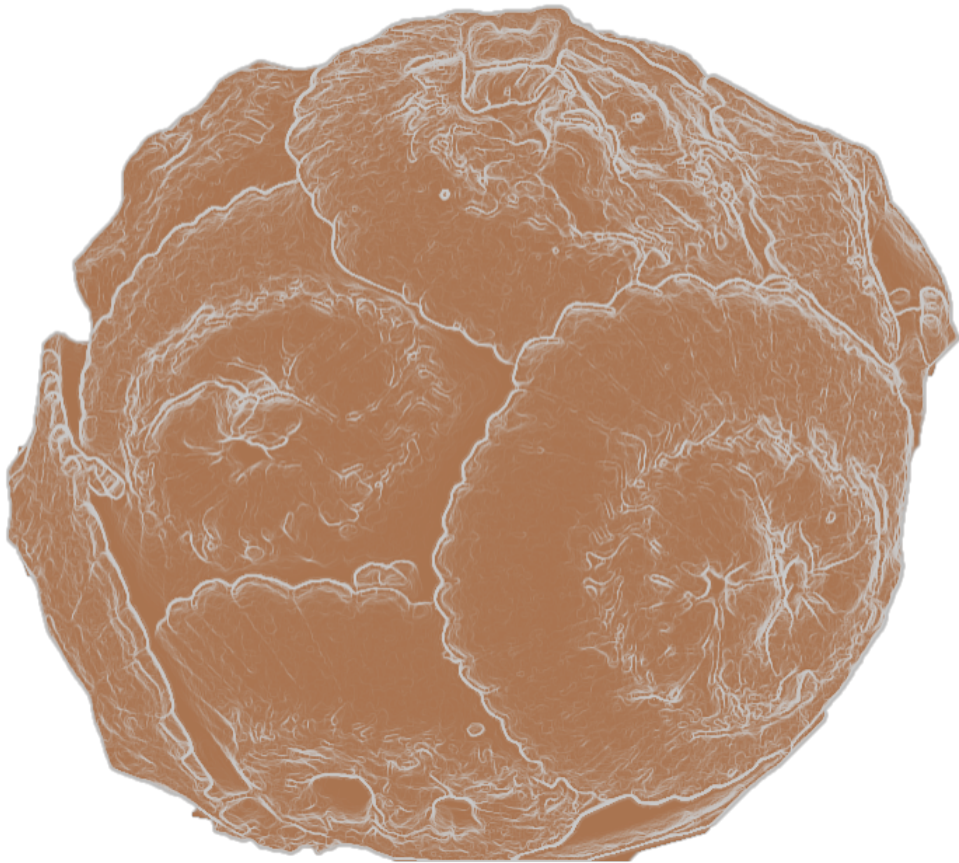
**Table S6.** Multiple regression of the alkenone C37/38.et, *Gephyrocapsa* coccolith mass and CO<sub>2</sub>[aq] values to explain the variability in  $\epsilon_{\text{coccolith}}$ .

Depth (m)	Jan.	Feb.	Mar.	Apr.	May.	Jun.	Jul.	Aug.	Sep.	Oct.	Nov.	Dec.	Average
50	114.65	100.36	124.99	108.02	111.39	112.36	86.50	101.69	114.03	126.46	129.66	130.62	<b>113.39</b>
60	87.17	73.61	93.16	78.60	83.18	83.57	60.11	71.66	81.81	93.12	97.80	101.93	<b>83.81</b>
70	66.28	53.99	69.43	57.19	62.12	62.16	41.77	50.50	58.70	68.58	73.76	79.54	<b>62.00</b>

**Table S7.** Monthly Photosynthetic Active Radiation (PAR) in  $\mu\text{E m}^{-2} \text{s}^{-1}$ , calculated at the different depths discussed in the text (section 6.2.3).







**Western Mediterranean deep-sea environmental conditions in response to surface organic productivity and regional circulation dynamics during the MIS 11**

(González-Lanchas et al.,)

Artículo en revisión en *Marine Geology*

## **CAPÍTULO 5. Artículo científico**

### **“Western Mediterranean deep-sea environmental conditions in response to surface organic productivity and regional circulation dynamics during the MIS 11”**

**Alba González-Lanchas**<sup>a</sup>, Javier Dorador<sup>b</sup>, Francisco J. Rodríguez-Tovar<sup>b</sup>, Francisco J. Sierro<sup>a</sup> y José-Abel Flores<sup>a</sup>

<sup>a</sup> Departamento de Geología, Universidad de Salamanca, 37008 Salamanca, España.

<sup>b</sup> Departamento de Estratigrafía y Paleontología, Universidad de Granada, 18002 Granada, España.

Artículo en revisión en *Marine Geology*

## Resumen

La fuerte conexión físico-biológica establecida en el sector occidental del Mar Mediterráneo, el Mar de Alborán, ha permitido considerar las reconstrucciones de productividad primaria en la región como una buena herramienta para la caracterización de su evolución paleoceanográfica, principalmente en lo referido a la intensidad de circulación Mediterránea en esta zona y en relación con la evolución climática en el Atlántico Norte a diferente escala de tiempo durante el pasado (Ausín et al., 2015; Bazzicalupo et al., 2018; Colmenero-Hidalgo et al., 2004). La precisión de la respuesta ecológica de los ambientes profundos de la cuenca Mediterránea occidental a los cambios en estas condiciones se plantea como una herramienta útil, en el sentido del análisis de las condiciones de transferencia entre superficie y ambiente profundo, y de la posible influencia de los procesos de ventilación del fondo, asociados a la circulación en la región, sobre los mismos (Pérez-Asensio et al., 2020). No obstante, esta cuestión ha sido escasamente abordada hasta la fecha

Las asociaciones macrobentónicas que se desarrollan en las profundidades oceánicas se encuentran influenciadas, principalmente, por los flujos de materia orgánica de procedencia superficial y por las condiciones de suministro de oxígeno disuelto hacia el fondo. El registro del hábitat de estos organismos durante el pasado se lleva a cabo a partir del análisis de sus trazas o pistas fósiles en el sedimento (Knaust y Bromley, 2012; Uchman y Wetzel, 2011). Aparte de afectar a las condiciones de supervivencia y adaptabilidad de determinados grupos macrobentónicos, ambos parámetros, aporte de nutrientes y condiciones de oxigenación, pueden registrarse también a modo de cambios de color en el sedimento, que evidencian un diferente grado de preservación de la materia orgánica en relación al balance entre disponibilidad y consumo (Dorador y Rodríguez-Tovar, 2016). En el Mar de Alborán, estas condiciones dependen, respectivamente, de la producción primaria asociada a los sistemas de surgencia (*upwelling*) que operan en la región (*Alboran Upwelling System*; González-Lanchas et al., 2020) y de las condiciones de intensidad circulación y renovación de las aguas profundas en este sector occidental de la cuenca Mediterránea. Este último parámetro se encuentra básicamente controlado por las tasas de formación de aguas profundas y también por las fuerzas de aspiración que

operan en el estrecho de Gibraltar (Rohling et al., 2015). De modo accesorio, los aportes terrestres y el aporte por vía lateral de partículas orgánicas pueden afectar al registro.

En este trabajo se lleva a cabo un análisis icnológico y de cambios de color en los sedimentos del testigo ODP *Site* 977, para el intervalo de tiempo correspondiente a la transición glacial/interglacial entre los estadios isotópicos marinos (MIS-*Marine Isotope Stage*) 12/11 o Terminación glacial V y el periodo interglacial MIS 11 completo, entre las edades de 430-374 mil años (ka), siguiendo el modelo de edad propuesto en González-Lanchas et al. (2020), que también se emplea para el cálculo de las tasas de sedimentación en este estudio. Este es un intervalo de tiempo que contiene cambios climáticos significativos afectando a las latitudes estudiadas (Oliveira et al., 2016) y de repercusión conocida en la dinámica paleoceanográfica superficial en la región de estudio (González-Lanchas et al., 2020; Marino et al., 2018). Para los análisis icnológicos y de cambios de color en el sedimento se emplearon técnicas de análisis de imagen, siguiendo la metodología respectivamente descrita en Dorador y Rodríguez-Tovar (2018) y Dorador y Rodríguez-Tovar (2014) sobre las imágenes de alta resolución disponibles en el repositorio virtual de IODP (<http://www-odp.tamu.edu>). La caracterización para el análisis se enfocó en la identificación del tipo y abundancia de la pista fósil indicativa de la presencia de determinadas especies y en la cuantificación del grado de bioturbación. La caracterización de color proviene del valor de color medio de píxel. Estos datos se integraron con el índice de productividad primaria, PPP, en González-Lanchas et al. (2020), durante el intervalo, y con otros marcadores procedentes del estudio de las asociaciones de cocolitóforos en el trabajo anterior, como las abundancias de nanofósiles retrabajados, potencialmente indicativos de procesos de circulación profunda en la región.

La relación existente entre el PPP y la disponibilidad de materia orgánica en el sustrato profundo, a partir del desarrollo y los cambios observados en la comunidad macrobentónica – representación de especies, abundancia y bioturbación – muestran una alta relación, donde modestos cambios en la tasa de sedimentación son responsables, exclusivamente, de una modulación de segundo orden.

Durante la Terminación V, las condiciones de alta productividad orgánica superficial por la activación completa del sistema del *Alboran Upwelling System* se transfirió al ambiente profundo, donde una baja renovación de las aguas profundas y la

consecuente reducción de la oxigenación beneficiarían la acumulación y preservación de la materia orgánica, resultando en la disminución de la actividad macrobentónica y la formación de una capa rica en materia orgánica (ORL – *Organic Rich Layer*). Durante la primera fase de intervalo de condiciones interglaciales plenas, MIS 11c, se identifica un ambiente macrobentónico oligotrófico, favorecido por una mejora de la oxigenación profunda y relacionado con las tasas de producción superficial moderadas. La producción orgánica superficial aumenta hacia la fase tardía del MIS 11c, incrementando la disponibilidad de materia orgánica en el ambiente profundo, lo que, junto con la reducción de la remoción de aguas profundas, habría favorecido la acumulación y preservación orgánica. Estas observaciones sugieren una influencia menor de la señal de oxigenación asociada a la intensidad de formación de aguas profundas en el ambiente macrobentónico en este intervalo y escala, lo que respalda la importancia del gradiente de densidad entre las masas de agua en el estrecho de Gibraltar y las fuerzas de aspiración de Bernoulli sobre la extracción y renovación de las aguas profundas en esta región (Rohling et al., 2015). Sin embargo, se necesitan más estudios para verificar esta observación, donde los enfoques que combinan marcadores superficiales y profundos, como el presentado, pueden servir como referencia.

En contraste, el ambiente profundo bien oxigenado y la diversidad de trazas fósiles y bioturbación durante los eventos de tipo *Heinrich*, Ht3 y Ht2, respaldan las determinaciones previas sobre el mantenimiento de la intensidad del *Alboran Upwelling System* y una probablemente intensa circulación del Mediterráneo occidental durante estos episodios que, en este caso, ejercería un impacto de primer orden sobre la oxigenación profunda y condiciones de hábitat macrobentónicas del Mar de Alborán.

## Referencias

- Ausín, B., Flores, J.-A., Sierro, F.-J., Bárcena, M.-A., Hernández-Almeida, I., Francés, G., Gutiérrez-Arnillas, E., Martrat, B., Grimalt, J.O., Cacho, I., 2015. Coccolithophore productivity and surface water dynamics in the Alboran Sea during the last 25 kyr. *Palaeogeography, Palaeoclimatology, Palaeoecology* 418, 126-140.
- Bazzicalupo, P., Maiorano, P., Girone, A., Marino, M., Combourieu-Nebout, N., Incarbona, A., 2018. High-frequency climate fluctuations over the last deglaciation in the Alboran Sea, Western Mediterranean: Evidence from

- calcareous plankton assemblages. *Palaeogeography, Palaeoclimatology, Palaeoecology* 506, 226-241.
- Colmenero-Hidalgo, E., Flores, J.-A., Sierro, F.J., Bárcena, M.A., Löwemark, L., Schönfeld, J., Grimalt, J.O., 2004. Ocean surface water response to short-term climate changes revealed by coccolithophores from the Gulf of Cadiz (NE Atlantic) and Alboran Sea (W Mediterranean). *Palaeogeography, Palaeoclimatology, Palaeoecology* 205, 317-336.
- Dorador, J., Rodríguez-Tovar, F.J., 2014. A novel application of digital image treatment by quantitative pixel analysis to trace fossil research in marine cores. *Palaios* 29, 533-538.
- Dorador, J., Rodríguez-Tovar, F.J., 2016. High resolution digital image treatment to color analysis on cores from IODP Expedition 339: Approaching lithologic features and bioturbational influence. *Marine Geology* 377, 127-135.
- Dorador, J., Rodríguez-Tovar, F.J., 2018. High-resolution image treatment in ichnological core analysis: initial steps, advances and prospects. *Earth-Science Reviews* 177, 226-237.
- González-Lanchas, A., Flores, J.-A., Sierro, F.J., Bárcena, M.Á., Rigual-Hernández, A.S., Oliveira, D., Azibeiro, L.A., Marino, M., Maiorano, P., Cortina, A., Cacho, I., Grimalt, J.O., 2020. A new perspective of the Alboran Upwelling System reconstruction during the Marine Isotope Stage 11: A high-resolution coccolithophore record. *Quaternary Science Reviews* 245, 106520.
- Knaust, D., Bromley, R. G. (Eds.). 2012. *Trace fossils as indicators of sedimentary environments*. Newnes.
- Marino, M., Girone, A., Maiorano, P., Di Renzo, R., Piscitelli, A., Flores, J.-A., 2018. Calcareous plankton and the mid-Brunhes climate variability in the Alboran Sea (ODP Site 977). *Palaeogeography, palaeoclimatology, palaeoecology* 508, 91-106.
- Oliveira, D., Desprat, S., Rodrigues, T., Naughton, F., Hodell, D., Trigo, R., Rufino, M., Lopes, C., Abrantes, F., Goni, M.F.S., 2016. The complexity of millennial-scale variability in southwestern Europe during MIS 11. *Quaternary Research* 86, 373-387.
- Pérez-Asensio, J.N., Frigola, J., Pena, L.D., Sierro, F.J., Reguera, M.I., Rodríguez-Tovar, F.J., Dorador, J., Asioli, A., Kuhlmann, J., Huhn, K., 2020. Changes in western Mediterranean thermohaline circulation in association with a deglacial Organic Rich Layer formation in the Alboran Sea. *Quaternary Science Reviews* 228, 106075.
- Rohling, E., Marino, G., Grant, K., 2015. Mediterranean climate and oceanography, and the periodic development of anoxic events (sapropels). *Earth-Science Reviews* 143, 62-97.
- Uchman, A., Wetzel, A., 2011. Deep-sea ichnology: the relationships between depositional environment and endobenthic organisms, *Developments in Sedimentology*. Elsevier, pp. 517-556.





**Western Mediterranean deep paleoenvironmental conditions in  
response to surface organic productivity and regional deep dynamics  
during MIS 11**

(González-Lanchas et al., *en revisión en Marine Geology*)

**Abstract**

Trace fossil assemblages is studied at Ocean Discovery Program Site 977 to characterize the response of the macrobenthic trace maker community to deep paleoenvironmental conditions during the Termination V (TV) and interglacial Marine Isotope Stage (MIS) 11 at the western Mediterranean Alboran Sea. An assemblage composed of *Chondrites*, *Planolites*, *Scolicia*, *Thalassinoides* and *Zoophycos* is identified, showing notable variations in ichnodiversity, abundance and bioturbation index that were analyzed in detail. The integration of ichnological information with sediment color and high-resolution coccolithophore records from Site 977 evidenced that variations in macrobenthic trace maker community are primarily controlled by oxygen availability, surface organic productivity patterns and deep transference. During TV, high surface organic productivity by intense *Alboran Upwelling System* enhanced the deep organic accumulation that, together with reduced deep-water removal, resulted in a decrease of bioturbation and the formation of an Organic Rich Layer. Moderate and stable surface production through MIS 11c reduced deep food availability, resulting in an oligotrophic and stable deep environment, reflected by relatively abundant trace fossils in lighter sediments. Intra-interglacial increase in surface organic production at ~ 405 ka is reflected as increased organic matter preservation. Minor impact of western Mediterranean circulation on deep water removal, but a plausible stronger control by Bernoulli aspiration intensities in the region, is, in overall, evidenced during these intervals. During the Heinrich-type (Ht) events 3 and 2, increased trace fossil diversity and well oxygenated environment is conducted by limited surface organic production, but rather evidence the effect of more intense western Mediterranean circulation on regional deep-water removal.

**Keywords:** Trace fossils, Primary Productivity, Deep oxygenation, Nannofossils, western Mediterranean, Marine Isotope Stage 11.

## 1. Introduction

Changes in deep water oxygen content and organic matter fluxes can lead important impacts on the deep-sea regional environments and macrobenthic trace maker communities (e.g., Wetzel, 1991; Rodríguez-Tovar et al., 2019). In the western Mediterranean – Alboran Sea region, these processes are mainly dependent on the balance between i) bottom-water ventilation, which supplies dissolved oxygen, ii) surface ocean productivity, controlling the organic matter fluxes that reach the seafloor and, complementary, iii) terrestrial input and eventual lateral advection of organic particles (see Pérez-Asensio et al., 2020 and references therein).

Bottom ventilation and deep-water removal in the Alboran Sea is controlled by two mechanisms. The first one is the deep-water injection, lifting the preexisting deep-water masses in the region; this mechanism entirely depends on the rates of Western Mediterranean Deep-Water (WMDW) formation at the Gulf of Lions. The second one, is the Bernoulli aspiration of water from below the sill depth (i.e., the depth of the Strait of Gibraltar), that depends on the velocity of the outflow and the density gradient existing below the sill depth. Both processes can act independently or in combination, indiscriminately (see Rohling et al., 2015 and references therein). Particularly, calculations accounting for Bernoulli aspiration, shows the capability of this mechanism itself to remove the deep waters from the entire western Mediterranean at the current outflow velocities, this is, solely controlled by the density gradient of water masses (Stommel et al., 1973; Rohling et al., 2015).

Surface phytoplankton primary productivity in the Alboran Sea is mainly controlled by the operation of the *Alboran Upwelling System* (see González-Lanchas et al., 2020). The regional changes in primary productivity evidenced a close relationship with North Atlantic climate evolution via atmospherical connection, from Holocene to older intervals during the Pleistocene (e.g. Ausín et al., 2015; Bazzicalupo et al., 2018, 2020; Colmenero-Hidalgo et al., 2004; Marino et al., 2018).

Accounting for this approach, paleoichnological analysis is revealed as a suitable tool in paleoenvironmental studies, including paleoceanography and paleoclimatology, providing useful information for the interpretation of parameters such as hydrodynamic energy, oxygenation, sedimentation rate or nutrient availability (Buatois and Mángano, 2011; Knaust and Bromley, 2012). Particularly, changes in ichnological features, such as

ichnodiversity, abundance of bioturbation, trace fossils size, or ichnofabrics, allow the interpretation of variations in paleoenvironmental conditions related to Pleistocene climates, at orbital to millennial scales (e.g., Heinrich Events), affecting macrobenthic tracemaker communities (Casanova-Arenillas et al., 2021; Goñi et al., 2019; Hodell et al., 2017; Rodríguez-Tovar et al., 2015a; Rodríguez-Tovar et al., 2019; Rodríguez-Tovar et al., 2015b; Rodríguez-Tovar et al., 2020b).

As case of study, the Marine Isotope Stage (MIS) 11 has traditionally been considered as a long-lasting (~30 kyr) and extremely warm interglacial on the recent Pleistocene history (e.g. Berger and Wefer, 2003; Hodell et al., 2000; PAGES, 2016; Raynaud et al., 2005; Yin and Berger, 2012), when the extreme collapse of high-latitude ice sheets conditioned an eustatic sea-level rise of about 20 m higher than today (Olson and Hearty, 2009; Raymo and Mitrovica, 2012; Reyes et al., 2014; Roberts et al., 2012). Against such stable interglacial conditions, mid-latitude climate-records has increasingly evidenced contrasting climate instabilities from ~ 406 ka on centennial (e.g. Koutsodendris et al., 2010; Prokopenko et al., 2010; Tye et al., 2016) to millennial timescales (Oliveira et al., 2016; Tzedakis et al., 2009). Suborbital-scale instabilities associated with the southward incursion of waters with an Arctic origin (Oppo et al., 1998) are comparatively well recorded towards the late MIS 11 (~ 395-374 kyr), as Heinrich-*type* (Ht) events at Iberian latitudes (de Abreu et al., 2005; Hodell et al., 2013; Martrat et al., 2007; Palumbo et al., 2013; Rodrigues et al., 2011; Stein et al., 2009; Voelker et al., 2010). In the Alboran Sea, such climate changes have been recognized from high-resolution coccolithophore records and suggested to impact the conditions of WMDW formation and western Mediterranean thermohaline circulation, responsible of differential stimulation of the *Alboran Upwelling System* and regional primary productivity (González-lanchas et al., 2020; Marino et al., 2018). Given this preamble and the intense dynamic behavior of the regional surface systems, and the overall high rates of regional primary production (Bárcena et al., 2004; Hernández-Almeida et al., 2011), it seems consistent to expect such a dynamical response recorded in deep-organic environments, a question that, however, has scarcely been addressed during the Holocene and Last Glacial Maximum (e.g., Pérez-Asensio et al., 2020), but absent for older intervals of the Pleistocene at this region.

The aim of this contribution is the use of ichnological features and sediment color as proxies to infer bottom conditions in the Alboran Sea environment during the TV and MIS 11. To solve the limitations that traditionally raised for the ichnological research of unconsolidated modern marine deposits, where the differences between biogenic structures and host sediment are weak ( Dorador et al., 2014a; Dorador and Rodríguez-Tovar, 2015) and in conjunction with software development, a high resolution image treatment improved visibility of ichnological features (Casanova-Arenillas et al., 2020; Dorador and Rodríguez-Tovar, 2018) and allowed detailed sediment color analysis (see methods). On this base, ichnological and sediment color information from modern cores have been frequently included in studies involving paleoenvironmental reconstructions, ocean-atmosphere dynamics and sedimentary basin analysis in the last years (e.g. Dorador and Rodríguez-Tovar, 2016; Evangelinos et al., 2020; Hodell et al., 2017; Miguez-Salas et al., 2019; Rodríguez-Tovar et al., 2015a; Rodríguez-Tovar et al., 2015b; Rodríguez-Tovar et al., 2020a; Rodríguez-Tovar and Dorador, 2014).

These data are integrated with production rates and surface environmental characterization by González-Lanchas et al. (2020), providing an opportunity to i) evaluate the transference of surface organic production to deep environment as organic matter fluxes and ii) discuss the influence of bottom ventilation and deep-water removal in the Alboran Sea during the studied interval. This novel multi-proxy approach improves the knowledge about important intra-basin processes and allows hypotheses about climate mechanisms affecting the Mediterranean scale and the evolution of its water exchange dynamics with the Atlantic in such a period of contrasted climate conditions.

## **2. Site ODP 977: the western Mediterranean sector**

The ODP Site 977 (36° 1.9' N; 1° 57.3' W) is located south of the Cabo de Gata, in the eastern sector of the Alboran Sea Basin (Fig. 1), at a water depth of 1984 meters.

The materials in this study are comprised between 67.49 to 58.64 corrected meters below sea floor (cmbsf). It corresponds to the cores 8H-5 to -1 and 7H-7 (and -CC) to -6 of the hole 977A and belongs to the lithological Unit I by Comas et al. (1996). As such, the studied sediments are predominantly composed of open marine-hemipelagic nannofossil and calcareous silty clay and clay facies; the background TOC and % CaCO<sub>3</sub> range respectively between 0.17 – 0.8 and 43.2 to 57.7 wt % (Comas et al., 1996).

The chronological determination of the material, the stage/substage identification and the sedimentation rate calculation is based on the age assignation proposed by González-Lanchas et al. (2020).

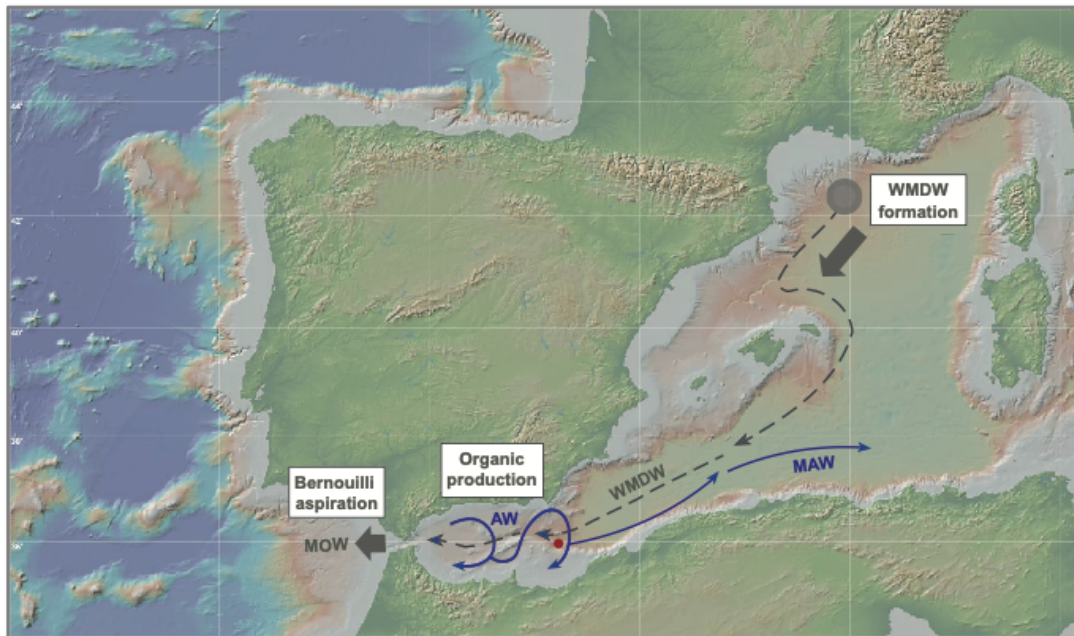


**Figure 1.** Location of the Site ODP 977 (red dot) and the main surface and deep currents (respectively, blue, and gray lines and arrows) at the region. Framed with a grid appear the three main mechanisms responsible for either the production of organic matter at the Alboran Sea (*Organic production*) and the oxygenation bottom waters (*Western Mediterranean Deep Water – WMDW – formation* and *Bernoulli aspiration* at the Strait of Gibraltar). AW: Atlantic Waters, MAW: Modified Atlantic Waters, MOW: Mediterranean Outflow Water. Map source <http://www.geomapapp.org/>.

In terms of water circulation dynamics, the Alboran Sea represents a transitional area between the semi-enclosed Mediterranean Sea and the adjacent Atlantic Ocean, connected by the narrow and shallow Strait of Gibraltar (Pistek et al., 1985). As such, the anti-estuarine Mediterranean circulation is intense in this region and characterized by the strong imprint of both the low saline Atlantic waters in surface (Atlantic Water, AW), and the deep outflow of the highly saline Mediterranean waters (Mediterranean Outflow Water, MOW) through the Strait of Gibraltar (Pistek et al., 1985).

The conditions for primary productivity in the region largely depend on the dynamics of the *Alboran Upwelling System*, a multi-cell upwelling system stimulated by the combined effects of i) westerly winds blowing over the southern Iberian coast (Fig.1)

and ii) the intensities of surface Atlantic waters entering the region in relation with the western Mediterranean circulation (Fig. 1; see González-Lanchas et al., 2020 for a complete description).

### **3. Methods**

#### **3.1. Ichnological analysis**

Ichnological research was supported by digital image analysis (Dorador et al., 2014 a,b; Dorador and Rodríguez-Tovar, 2014; Dorador and Rodríguez-Tovar, 2018; Rodríguez-Tovar and Dorador, 2015) applied to high-resolution images from the studied cores. The developed method facilitates ichnological analysis on modern cores, improving visualization of ichnological features. Digital image analysis enables the differentiation between trace fossils (i.e., bioturbational sedimentary structures with sharp outlines and a characteristic recurrent geometry) and biodeformational structures (i.e., with no distinct outlines and no recurrent geometry, determining a mottled background), ichnotaxonomy, relative abundance, cross-cutting relationships, and percentage of bioturbation. Ichnotaxonomic identification was approached to the ichnogenus level based on the recognition of ichnotaxobases in cores (Knaust, 2017).

#### **3.2. Sediment color analysis**

Color characterization was conducted on ODP 977 core digital images that are available in the OPD virtual repository <http://www-odp.tamu.edu>. The selected images were previously treated using Adobe Photoshop CC software to highlight color contrast following method described by Dorador et al. (2014a) based on image adjustments modification, but the same parameters values in all of them to avoid artefacts. Specifically, *levels* were adjusted to 30, 0.45 and 154; *brightness* and *contrast* was 0 and 74 respectively and finally, *vibrance* was slightly modified to +1 and *saturation* to -2. Then, color was characterized obtaining mean pixel values, using the 8-bits scale (i.e., 0-255), from 2.5 cm thick rectangular sections on the treated core images (Dorador and Rodríguez-Tovar, 2016), excluding the uppermost section to avoid errors associated to sediment core record. A more accurate characterization using thinner sections was discarded due to image resolution limitations.

### 3.3. Calcareous nannofossil-based proxies and sedimentation rates

Calcareous nannofossil analyses were performed on 181 sediment levels spaced 4 to 6 cm from the hole 977A.

For nannofossil-sample preparation, we followed the random settling technique by Flores and Sierro (1997), with which a homogeneous distribution of coccoliths in the samples is achieved from an initially controlled and regular sample amount. Coccolith identification and quantitative analysis were performed with the use of a double polarized-light Nikon Eclipse 80i petrographic microscope at 1000x magnification. Above the number of 400 coccoliths per sample were identified in a variable number of fields of view. A supplementary census count of 10 fields of view was performed to accurately determine the abundance of other taxa represented in samples with a proportion lower than 1 %. Identification of coccolithophore species were based in Young et al. (2003) and the guide of coccolithophore biodiversity and taxonomy Nannotax 3 ([ina.tmsoc.org/Nannotax3/index.html](http://ina.tmsoc.org/Nannotax3/index.html)). Nannofossil data are presented as N, the measure of nannofossil concentration per gram of sediment (nannofossil g<sup>-1</sup>), calculated following the procedure by Flores and Sierro, (1997). The Primary Productivity Proxy (PPP = N small *Gephyrocapsa* + *G. caribbeanica*) is considered an estimation of surface primary productivity used to trace the state of activation of the *Alboran Upwelling System* (see González-Lanchas et al., 2020 for a complete description). We consider the threshold of PPP under and over 20 x 10<sup>9</sup> nannofossil g<sup>-1</sup> to respectively identify the intervals with lower and higher surface primary production in the region related to the state of activation of the *Alboran Upwelling System*.

The specimens from older stratigraphic levels prior to the studied interval are termed “reworked nannofossil”. The presence of these specimens in the studied sediments is considered potentially indicative of depositional processes related to changes in the intensity of deep circulation in the western Mediterranean. These values were obtained in a separate counting in 10 fields of view and expressed as natural logarithm (Ln) of the N reworked (nannofossil g<sup>-1</sup>).

Sedimentation rates during the studied interval are derived from the adopted age model.

## 4. Results

### 4.1. Ichnological assemblage

Trace fossil assemblage through the studied interval mainly consists of *Chondrites*, *Planolites*, *Scolicia*, *Thalassinoides* and *Zoophycos* (Fig. 2), that can be assigned to the *Zoophycos* ichnofacies, typical of deep-sea environments, below storm-wave base in outer-shelf to slope deposits (Uchman and Wetzel, 2011). In this general context, significant variations in ichnodiversity, relative abundance and degree of bioturbation are observed:

The TV reveals a change in trace fossil assemblage and color, upward from cm 80 to cm 0 in core 8H-5. From cm 80 to around cm 35, frequent discrete traces of *Planolites* and *Thalassinoides* have been observed in light sediments. From that point to the top of the core, bioturbation degree and ichnodiversity show a decreasing trend. *Planolites* and *Thalassinoides* are absent and *Zoophycos* is registered as the dominant trace fossil. This is almost exclusive, except on top of the core where light filled *Thalassinoides* are observed. The presence of *Zoophycos* coincides with darker sediments (Fig. 2; Fig. 3c and f).

A significant change in the ichnological features is observed between TV and the beginning of the full interglacial MIS 11c, at cores 8H-4, 8H-3 and 8H-2 (Fig. 2), also revealed in the color analysis (Fig. 2; Fig. 3c and f). The lower part of MIS 11c, from cm 140 to around cm 90 in core 8H-4, is characterized by a totally bioturbated sediment, mainly consisting of *Scolicia*. After that, *Scolicia* disappears and a trace fossil assemblage with *Thalassinoides* and *Planolites* characterizes the rest of the full interglacial MIS 11c, from cm 90 in core 8H-4 to top of core 8H-2 (Fig. 2 and Fig. 3f).



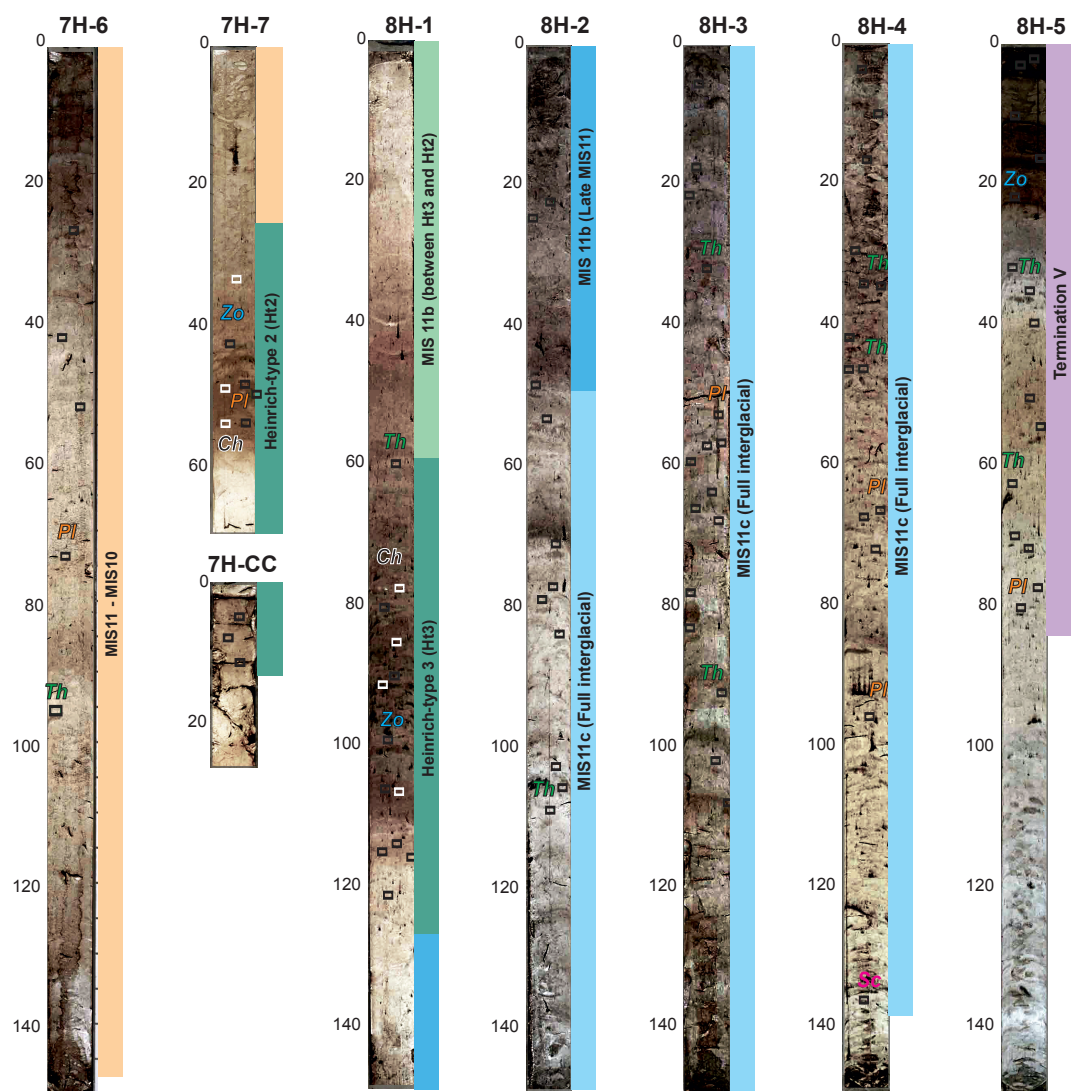


**Figure 2.** Schematic representation of the trace fossil assemblage identified in sediment cores 8H-5 to 7H-6 of Site ODP 977, corresponding to the time interval that includes Termination V and interglacial MIS 11. The limits between isotopic substages and the location of Heinrich type (Ht) events 3 and 2 were based on the  $\delta^{18}\text{O}$  *G. bulloides* and  $U^{k}_{37}$ -SST in González-Lanchas et al., (2020). Trace fossil assemblage *Scolicia* (*Sc*), *Planolites* (*Pl*), *Thalassinoides* (*Th*), *Zoophycos* (*Zo*) and *Chondrites* (*Ch*).

The late MIS 11 (MIS 11b) shows variations in ichnological features; the beginning of this part of the record, corresponding to cm 50 to 0 of the core 8H-2, shows the same previous pattern with the record of scarce *Thalassinoides* and *Planolites* in darker host sediments (i.e., similar to the full interglacial MIS11c). The rest of the late MIS 11 shows significant changes in the ichnological features and color record with a similar pattern in the two studied Heinrich types (Ht3 and Ht2; Fig. 2; Fig. 3c and f).

At the Ht3 and Ht2 the trace fossil assemblage is relatively abundant, mainly consisting of *Chondrites*, *Planolites*, *Thalassinoides* and *Zoophycos* (Fig. 2 and Fig. 3f). The interval between cm 130 to cm 30 of core 8H-1 in Ht3 can be correlated with the entire Ht2, at core 7H-CC and core 7H-7 (Fig. 2 and Fig. 3f). In general, a similar upward trend is observed in both Heinrich *types*: a lighter colored lower part, first scarcely bioturbated and then with the presence of *Planolites*, which upward shows a progressive increase in abundance of traces and ichnodiversity with *Chondrites*, *Thalassinoides* and *Zoophycos* associated to darker sediments.

At the MIS 11- MIS 10 transition, corresponding to the entire core 7H-6, it is observed a decrease in abundance and ichnodiversity respect to the previous Ht2, with scarce and disperse *Thalassinoides* and *Planolites*, showing similar pattern than that recorded at cm 50 to 0 in core 8H-2 at the late MIS 11 (Fig. 2 and Fig. 3f).

#### **4.1.1. Changes in sediment color**

Mean pixel color values characterization reveals significant sediment color changes through the studied intervals (Fig. 3c). From the bottom to the top, we can identify the following evolution. The first 40 cm show a medium color characterized by an average pixel value of 125, but it drastically decreases in the uppermost 20 cm of the 8H-5 core, associated to the last part of the TV (Fig. 3c), reaching 10 as the average value.

Then, an abrupt change to lighter sediments, 180 in average, is identified at the beginning of the full interglacial MIS 11c (Fig. 3c). From this point to 406 ka, approximately, the mean pixel value shows a gradual decreasing trend to darker sediments characterized by 70 as average value (Fig. 3c). This trend has some local and short intervals characterized by darker sediments, usually linked to a scarce presence of trace fossils. Finally, the last part of the full interglacial MIS 11c (i.e., approximately from 406 to 396 ka) is represented by light sediments with an average color value of 210 (Fig. 3c).

At MIS 11b, right after the full interglacial MIS 11c, a decreasing trend in color values is observed, reaching minimum values (40 as average) in the Heinrich *type* interval Ht3 (Fig. 3c). An increasing trend is observed until the end of the studied interval, interrupted by a decrease in the mean pixel color values during the Ht2, represented by an average mean pixel value of 60 (Fig. 3c).

## 4.2. Sedimentation rates

The sedimentation rate at Site 977 changed between 12 to 22 cm kyr<sup>-1</sup> during MIS 12/11 and MIS 11 (Fig. 3a).

The low sedimentation rates during the glacial period were followed by an average sedimentation rate of ~ 15 cm kyr<sup>-1</sup> between the onset of MIS 11 (~ 424 ka) until the end of the full interglacial MIS 11c (~ 387 ka). The sedimentation rate increased between 387 to 377 ka, in MIS 11b, and a final decrease towards an average of ~ 15 cm kyr<sup>-1</sup> is recorded at the end of the studied interval, towards the MIS 11/10 transition (Fig. 3a).

## 4.3. Changes in surface primary productivity and nannofossil-derived proxies

The average of the total N and PPP respectively range between 10 - 60 and 8 - 40 10<sup>9</sup> nannofossil g<sup>-1</sup> during the interval (Fig. 3b). Higher PPP, above 20 x 10<sup>9</sup> nannofossil g<sup>-1</sup>, is observed: i) between 428 and 423 ka at the TV; ii) from 406 to 392 ka, at the late phase of the period of full interglacial conditions, MIS 11c, and transition to the late stage of the MIS 11, MIS 11b, and iii) at two intervals with a large increase in the magnitude of the values between 389 to 386 ka and 383 to 376 ka of MIS 11b (Fig. 3b). Lower PPP, under the mentioned values, are observed: i) at the late phase of TV included in this record, until 428 ka; ii) continuously within the most part of the full interglacial MIS 11c, until 406 ka and iii) during the occurrence of Ht 3 and 2, respectively centered at ~ 390 and 383 ka (Fig. 3b).

The percentages of reworked values (expressed as natural logarithm, Ln, reworked), are comparatively higher in two intervals between: i) ~ 430 to 417 ka at the TV and the early MIS 11c, and ii) ~ 406 to 396 ka during the late phase of MIS 11c. Intermediate values with high variability are observed during the rest of the record (Fig. 3f).

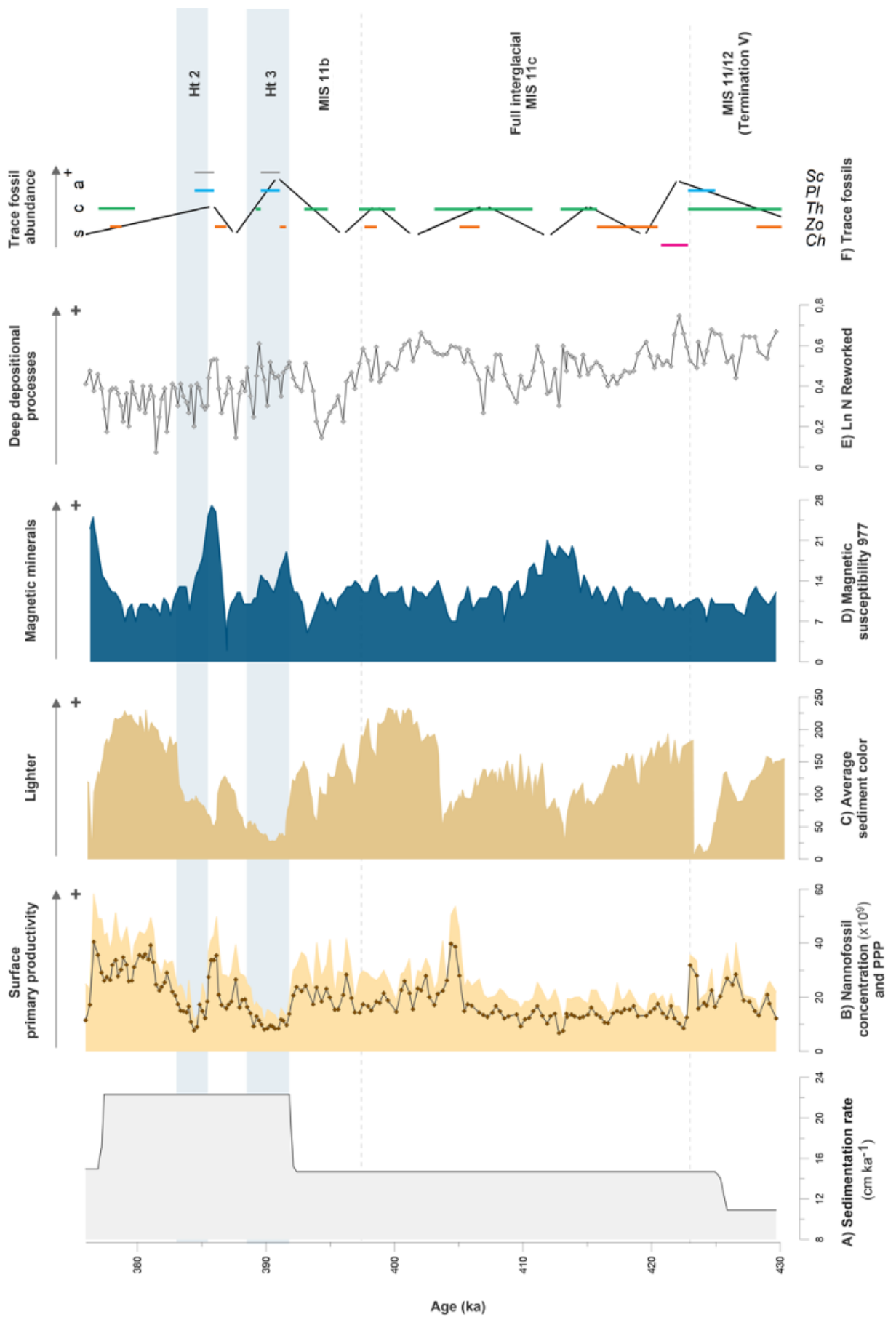


**Figure 3.** Integration of ichnological and sedimentological data with the calcareous nannofossil proxies and sedimentation rates during the studied interval. **A)** Sedimentation rate ( $\text{cm kyr}^{-1}$ ); **B)** Total amount of calcareous nannofossil in sediments (Total N) and Primary Productivity Proxy (PPP; nannofossil  $\text{g}^{-1} \times 10^9$ ); **C)** Sediment color profile (average pixel color); **D)** Magnetic susceptibility at Site 977 (Comas et al., 1996); **E)** Percentages of reworked nannofossil; **F)** Trace fossil assemblage; *Scolicia* (*Sc*), *Planolites* (*Pl*), *Thalassinoides* (*Th*), *Zoophycos* (*Zo*) and *Chondrites* (*Ch*). The abundance of the traces is summarized as *scarce* (s), *common* (c) and *abundant* (a) in the legend.

## 5. Discussion

In the following sections we discuss the relationship between conditions of surface organic production and deep oxygenation and live benthic environment, proposing a dynamic model integrating regional changes in deep water removal at the Alboran Sea and western Mediterranean circulation by climate forcing dynamics.

### 5.1. Termination V (TV)

The PPP evidences moderate values between 430 to 423 ka at the TV, with an increase centered at  $\sim 425$  ka. Sedimentation rates experiment, as well, an increase towards this interval that, however, does not follow the same pattern as the PPP. Thus, the increased N and PPP between 428 to 422 ka without a clear connection with the sedimentation rates are deduced to be the effect of an increase in surface primary production during the TV (Fig. 3a and b).

The replacement of frequent *Planolites* and *Thalassinoides* during late MIS 12 ( $\sim 429 - 425$  ka; Fig. 2 and 3f) by dominant *Zoophycos* near the onset of the full interglacial MIS 11c ( $\sim 423$  ka; Fig. 2 and 3f), a decrease in bioturbation abundance and ichnodiversity and a color shift from lighter to darker sediments indicate an abrupt change in bottom water properties at the end of TV (Fig. 3c and f). The enhanced surface production through this interval (Fig. 3b) seems to drove a progressive increase in the organic matter supply to the deep environment, triggering comparatively high food, which resulted in a eutrophic benthic habitat (Fig. 3f), as revealed by the presence of *Zoophycos* in dark color sediments (Rodríguez-Tovar et al., 2015b). *Zoophycos* is a deep tier structure produced by vermiform animals (Löwemark, 2015), whose presence in Quaternary materials has been related, in particular, to glacial periods of intensive seasonal productivity and high organic carbon fluxes at intermediate sedimentation rates from 5 to 20  $\text{cm ka}^{-1}$  (Dorador

et al., 2016; Dorador et al., 2019), and usually when bottom water ventilation is low (Rodríguez-Tovar et al., 2015b).

The increased total organic carbon to the values of 0.8 wt % at ~ 424.5 ka (Comas et al., 1996) together with the maxima reduction in average sediment color (Fig. 3c), suggest this must correspond to one of the levels of Organic Rich Layer formation at Site 977 (Murat, 1999). These are typically found during deglacial times in the Western Mediterranean (see Rogerson et al., 2008), occurring during the TV in this case. Organic Rich Layers can be formed by higher organic fluxes to the seafloor or by reduced rates of deep-water renewal. The correspondence of such type of organic depositions at Site 977 with periods of only moderate, to even minimum, insolation assessed early hypothesis about the important role of local intensifications in upwelling dynamics in strong connection with jet-like Atlantic inflow (von Grafenstein et al., 1999). An intensification of the *Alboran Upwelling System* between ~ 430 to 423 ka at TV (González-Lanchas et al., 2020), observed in the PPP increase (Fig. 3b), integrates those requirements. However, if organic carbon flux from the surface were the only cause of bottom reduction in oxygenation, an increase of higher magnitude in the carbon supply out of the mixed layer than that recorded in the PPP (Fig. 3b) would be required (see Bethoux and Gentili, 1999). In agreement with Rodríguez-Tovar et al. (2015a), lowered bottom water ventilation is required, as well, to produce an impoverished benthic environment comparable to that recorded during this interval (Fig. 2 and 3f). Thus, it seems plausible that a lower rate of deep-water renewal at the Western Mediterranean Deep Water in the Alboran Basin would be necessary as second mechanism involved to produce the reconstructed lower oxygenated bottom waters.

A lower renewal of bottom waters during TV is consistent with i) lowered rates of WMDW formation in the Gulf of Lions and/or ii) decreased aspiration at the Strait of Gibraltar (Rohling et al., 2015). An intensification of the *Alboran Upwelling System* between ~ 430 to 423 ka entails an enhanced western Mediterranean circulation during the TV by overall amelioration in WMDW formation after glacial stagnation (González-Lanchas et al., 2020). As such, we hypothesize about a reduction in the intensities of the Bernoulli aspiration at the Strait of Gibraltar during TV as plausible mechanism reducing the regional deep-water removal. This process, together with the enhanced local surface

production, seems to plausibly explain the recorded lowered deep oxygenation environment and ORL deposition (Fig. 2 and 3).

## 5.2. Full interglacial MIS 11c

The PPP profile is almost constant, with moderate values between 423 and 405 ka, from when a sudden increase is observed, leading to slightly higher values until 392 ka, after the end of the full interglacial MIS 11c, at MIS 11b (Fig. 3b). Intermediate sedimentation rates are constant for the complete interval, so the intra-interglacial N and PPP variability is interpreted as primarily modulated by an increase in surface primary production (Fig. 3a and b).

After the TV, surface primary production abruptly decreases at the onset of MIS 11c and increased bioturbation and abundant traces of *Scolicia* are observed in lighter sediments (Fig. 3b and f). These features represent an important shift in the deep environmental conditions, in which, aside the high amounts of benthic food availability, indicated by the presence of *Scolicia* (Kröncke, 2006; Wetzel, 2008), there is a substantial improvement in deep oxygenation conditions in comparison with the TV (Fig. 3f). Rapid burial of the organic matter reaching the bottom, triggered by the slightly increased sedimentation rates after TV (Fig. 3a), together with the reduced rate of surface organic production (Fig. 3b), avoided oxidation at the sea floor, resulting in wide availability into the substrate for *Scolicia* trace makers in a well oxygenated environment. These conditions in sediments are interpreted as the evidence of amelioration in deep oxygenation at western Mediterranean, assigned to an early increase/restoration in the intensity of the aspiration at the Strait of Gibraltar after the reduction in the intensity of the process during TV. Such increase in this mechanism could be responsible of abrupt re-depositional deep processes, as observed at this time though increased amount of reworked nanofossil in sediments (Fig. 3e).

*Scolicia* disappeared at ~ 419 ka, from where the dominance of *Thalassinoides* and *Planolites* in relatively light-colored sediments is observed as a constant feature, from ~ 416 ka during the rest of the full interglacial interval (Fig. 3c). This ichnological pattern indicates a change towards oligotrophic environment in comparison with the onset of MIS 11c, but still under relatively well oxygenated conditions. More specifically, the shallow tier habitat indicated by *Planolites* (see Keighley and Pickerill, 1995; Pemberton and

Frey, 1982; Rodríguez-Tovar and Uchman, 2004) and the shallow/middle tier *Thalassinoides* inhabiting soft cohesive sediments (see Ekdale, 1992; Ekdale et al., 1984; Fürsich, 1973; Rodríguez-Tovar and Uchman, 2004; Schlirf, 2000), restrict our reconstruction at the uppermost centimeters of the substrate.

In the absence of significant changes in sedimentation rate for the interval, such a limited diversity in the macrobenthic trace maker community seems to be consistent with the reduction of surface organic input by the reduced interglacial primary production up to 405 ka (Fig. 3b). Thus, the reconstructed relatively high oxygen content of bottom waters could be the result of the low deep oxygen consumption due to the weak surface supply of organic matter (Fig. 3b and c). Under relatively steady and oligotrophic deep environmental conditions as such, modest oscillations in surface organic productivity, as recorded up to 405 ka (Fig. 3b), could produce an amplified reduction in the bottom oxygen availability, explaining the recorded interruptions in bioturbation (Fig. 2 and 3f).

The intra interglacial increase in surface primary productivity, from 405 ka upward (Fig. 3b), had a strong impact on the deep environment, triggered by a progressive increase in the transference and accumulation of organic matter to the deep environment, as evidenced by the progression from lighter towards darker sediments toward this part of the record (Fig. 3c), together with a coupled decrease in magnetic susceptibility (Fig. 3d). Such intra interglacial change is considered to be representative of a change in the Iberian interglacial winter climates, from higher humidity to more arid conditions (Oliveira et al., 2016). In terms of western Mediterranean circulation, this shift has been proposed to exert the observed impact on surface organic production, from reduced to increased PPP triggered by an intensification in the *Alboran Upwelling System* at 405 ka (González-Lanchas et al., 2020). Such intra interglacial atmospherical control on coccolithophore communities and surface production is not an isolated fact, but also observed at the nearby Atlantic Site IODP U1385 (González-Lanchas et al., 2021a). The increased WMDW formation by higher wind winter stimulation at the Gulf of Lions at this time (González-Lanchas et al., 2020) does not seem, however, to have a clear imprint on deep oxygenation improvement. As such, we suggest that a coeval reduction in the Bernoulli aspiration, reducing deep water removal and favoring the organic accumulation and preservation, should occur associated to the interglacial progress. An imprint of this



mechanism reducing regional deep re-depositional processes can be supported by the reduction of reworked nannofossil (Fig. 3e) during this interval.

### **5.3. Heinrich-type (Ht) events 3 and 2**

The PPP is minimum during Ht3 (~ 391 ka) and Ht2 (~ 385 ka; Fig. 3b). The high sedimentation rates suggest that other non-biogenic materials could obscure the surface organic productivity signal, that could be slightly higher than reconstructed from the absolute N and PPP (Fig. 3a and b). This is well evidenced by the increased values of magnetic susceptibility at Ht3 and Ht2 (Fig. 3d).

Trace fossil assemblage during both episodes is relatively abundant and mainly characterized by a similar pattern: lighter colored sediments scarcely bioturbated are registered at the lower part of the sequences (Fig. 3f). Then, the presence of *Planolites* gives rise to a progressive upward increase in the abundance of traces and ichnodiversity, with *Zoophycos*, *Chondrites* and *Thalassinoides* associated to darker sediments towards the central part of Ht3 and Ht2 (Fig. 3f). The main difference between both records is the interval of scarce bioturbation identified in the uppermost part of Ht3 without correspondence in Ht2 (Fig. 2 and 3f).

Ichnological records at different latitudes in the Atlantic revealed the occurrence of two-phase conditions during Heinrich stadial of the last glacial cycle ( Baas et al., 1997; Baas et al., 1998; Rodríguez-Tovar et al., 2019), characterized, in overall, by: i) an early phase of important bottom-water stagnation and highly dysoxic conditions related to Atlantic Meridional Overturning Circulation (AMOC) slowdown, and ii) deep oxygen amelioration and re-established biodiversity in the trace maker community shortly after the deposition of the ice-rafted detritus (IRD) layer. As the Heinrich stadial, the occurrence of both Heinrich-type 3 and 2 during the late MIS 11 has been linked to AMOC disruptions from iceberg calving of British ice sheet origin (de Abreu et al., 2005; Rodrigues et al., 2011). Thus, a comparable deep dynamic during the occurrence of Ht is expected to occur in the Atlantic, and recently reinforced during Ht3 and Ht2 by the identification of an, as well comparable, surface hydrological structure of halocline formation and nutrient upward limitation at the Site U1385 (González-Lanchas et al., 2021a).

In the western Mediterranean, low primary productivity rates during Ht3 and Ht2 have been primarily related to the impact of the cold surface waters of subpolar origin entering the Strait of Gibraltar over the phytoplankton community at the Alboran Sea (González-Lanchas et al., 2020; Marino et al., 2018). Climatically, semi-arid conditions at the Mediterranean maintaining high rates of WMDW formation and intense *Alboran Upwelling System* have been proposed during the Ht3 and Ht2 (González-Lanchas et al., 2020). This idea agrees with the relatively light color of the sediments through these episodes at 977 (Fig. 3d) suggesting, indeed, that important changes in deep oxygen conditions did not play a determining role in the western Mediterranean during Ht events. Rather, a reduction in surface supply of organic matter (Fig. 3c) or the effect of the increased sedimentation rates and accumulation of detrital particles seems to be an important factor promoting a quick burial and the trace fossil scarcity recorded at the beginning of the sequences (Fig. 3f).

The progressive increase in organic matter supply to the deep environment through the upper part of each event Ht3 and Ht2 could be promoted by an improvement in surface conditions for organic production, potentially less cold-temperature limitation on coccolithophore proliferation (González-Lanchas et al., 2020; Marino et al., 2018) together with a well-oxygenated deep environment, favoring the increase in diversity and abundance of the trace fossil assemblage (Fig. 2 and Fig. 3f). The dilution effect caused by the increased accumulation of detrital minerals during both intervals (i.e., magnetic minerals recorded in the profile of magnetic susceptibility; Fig. 3d) could have obscured, in some extent, the surface productivity signal (Fig. 3c).

## 6. Conclusions

Our results evidence a preponderant connection of surface organic production rates with deep organic matter availability and macrobenthic conditions at the Alboran Sea, where the modest changes in sedimentation rate are, however, responsible of modulation of second order. During Termination V, the high surface organic productivity by intense *Alboran Upwelling System* were transferred to the deep environment, where reduced deep-water removal and oxygenation caused accumulation and preservation of organic matter, resulting in the decrease of macrobenthic activity and the formation of Organic Rich Layer. During the early full interglacial MIS 11c, improved deep oxygenation is

recorded, generating better conditions for macrobenthic tracemakers. This oligotrophic deep environment is the result of moderate and stable surface production and sedimentation rates. Intra-interglacial increase in surface production increased organic matter availability at deep environment, which, together with reduced deep-water removal favored the organic preservation. As common observation for these intervals, minor direct impact of the signal of WMDW formation at the Gulf of Lions on the regional benthic environment can be extracted from our results, suggesting its potential minor influence on the regional deep oxygenation at this time and scale. This observation supports the recent growing suggestions about the importance of the density gradient between water masses at the Strait of Gibraltar and the resulting intensities of the Bernoulli aspiration on deep water removal in this region. However, more studies are needed to verify this observation, where integrated surface to deep approaches, as conducted in this study, may serve as a reference. Well oxygenated deep environment and trace fossil diversity during Ht3 and Ht2 supports previous determinations about an intense *Alboran Upwelling System* together with intense western Mediterranean circulation during the occurrence of these extreme episodes.

## **Acknowledgments**

This study was supported by the predoctoral FPU contract FPU17/03349 awarded to A. González-Lanchas by the Spanish Ministry of Science, Innovation and Universities. The research by JD was funded through the Juan de la Cierva Program (IJC2019-038866-I) by the Spanish Ministry of Science and Innovation. Essential financial infrastructure was provided by the programs RTI2018-099489-B-100 of the Spanish Ministry of Science, Innovation and Universities granted to GGO (Grupo de Geociencias Oceánicas de la Universidad de Salamanca) and CGL2015-66835-P and PID2019-104625RB-100 of the Spanish Ministry of Science, Innovation and Universities and B-RNM-072-UGR18, P18-RT-4074 of the Andalusian Government granted to Ichnology and Palaeoenvironment RG (University of Granada).

## **Data statement**

Calcareous nannofossil data used in this study is stored in the public repository PANGAEA® as: González-Lanchas, Alba; Flores, José-Abel; Sierro, Francisco J.;

Bárcena, María Ángeles; Cortina, Aleix; Cacho, Isabel; Grimalt, Joan O (2020): Nannofossil, opal phytolith, stable isotopes and  $U^{k'}_{37}$  Sea Surface Temperature record from ODP Site 977 during the MIS 11. <https://doi.org/10.1594/PANGAEA.921235>. Regarding ichnological analysis, all data obtained during this study are summarized in the present article. Anyway, original images and datasets are available by request.

## References

- Ausín, B., Flores, J.-A., Sierro, F.-J., Bárcena, M.-A., Hernández-Almeida, I., Francés, G., Gutiérrez-Arnillas, E., Martrat, B., Grimalt, J.O., Cacho, I., 2015. Coccolithophore productivity and surface water dynamics in the Alboran Sea during the last 25 kyr. *Palaeogeography, Palaeoclimatology, Palaeoecology* 418, 126-140.
- Baas, J., Schönfeld, J., Zahn, R., 1998. Mid-depth oxygen drawdown during Heinrich events: evidence from benthic foraminiferal community structure, trace-fossil tiering, and benthic  $\delta^{13}C$  at the Portuguese Margin. *Marine Geology* 152, 25-55.
- Baas, J.H., Mienert, J., Abrantes, F., Prins, M.A., 1997. Late Quaternary sedimentation on the Portuguese continental margin: climate-related processes and products. *Palaeogeography, Palaeoclimatology, Palaeoecology* 130, 1-23.
- Bárcena, M. A., Flores, J. A., Sierro, F. J., Pérez-Folgado, M., Fabres, J., Calafat, A., Canals, M. 2004. Planktonic response to main oceanographic changes in the Alboran Sea (Western Mediterranean) as documented in sediment traps and surface sediments. *Marine Micropaleontology*, 53(3-4), 423-445.
- Bazzicalupo, P., Maiorano, P., Girone, A., Marino, M., Combourieu-Nebout, N., Incarbona, A., 2018. High-frequency climate fluctuations over the last deglaciation in the Alboran Sea, Western Mediterranean: Evidence from calcareous plankton assemblages. *Palaeogeography, Palaeoclimatology, Palaeoecology* 506, 226-241.
- Bazzicalupo, P., Maiorano, P., Girone, A., Marino, M., Combourieu-Nebout, N., Pelosi, N., Salgueiro, E., Incarbona, A., 2020. Holocene climate variability of the Western Mediterranean: Surface water dynamics inferred from calcareous plankton assemblages. *The Holocene*, 0959683619895580.
- Berger, W.H., Wefer, G., 2003. On the dynamics of the ice ages: Stage-11 paradox, mid-brunhes climate shift, and 100-ky cycle, *Geophysical Monograph Series*, pp. 41-59.
- Bethoux, J. P., Gentili, B. 1999. Functioning of the Mediterranean Sea: past and present changes related to freshwater input and climate changes. *Journal of Marine Systems*, 20(1-4), 33-47.
- Buatois, L.A., Mángano, M.G., 2011. *Ichnology: Organism-substrate interactions in space and time*. Cambridge University Press.

- Casanova-Arenillas, S., Rodríguez-Tovar, F.J., Martínez-Ruiz, F., 2020. Applied ichnology in sedimentary geology: Python scripts as a method to automatize ichnofabric analysis in marine core images. *Computers & Geosciences* 136, 104407.
- Casanova-Arenillas, S., Rodríguez-Tovar, F.J., Martínez-Ruiz, F., 2021. Ichnological analysis as a tool for assessing deep-sea circulation in the westernmost Mediterranean over the last Glacial Cycle. *Palaeogeography, Palaeoclimatology, Palaeoecology* 562, 110082.
- Colmenero-Hidalgo, E., Flores, J.-A., Sierro, F.J., Bárcena, M.A., Löwemark, L., Schönfeld, J., Grimalt, J.O., 2004. Ocean surface water response to short-term climate changes revealed by coccolithophores from the Gulf of Cadiz (NE Atlantic) and Alboran Sea (W Mediterranean). *Palaeogeography, Palaeoclimatology, Palaeoecology* 205, 317-336.
- Comas, M., Zahn, R., Klaus, A., 1996. Preliminary results of ODP Leg 161. *Proceeding Ocean Drilling Program, Preliminary Results* 161, 1-1679.
- de Abreu, L., Abrantes, F.F., Shackleton, N.J., Tzedakis, P.C., McManus, J.F., Oppo, D.W., Hall, M.A., 2005. Ocean climate variability in the eastern North Atlantic during interglacial marine isotope stage 11: A partial analogue to the Holocene? *Paleoceanography* 20, 1-15.
- Dorador, J., Rodríguez-Tovar, F.J., 2014. A novel application of digital image treatment by quantitative pixel analysis to trace fossil research in marine cores. *Palaios* 29, 533-538.
- Dorador, J., Rodríguez-Tovar, F.J., 2015. Application of digital image treatment to the characterization and differentiation of deep-sea ichnofacies. *Spanish Journal of Palaeontology* 30, 265-274.
- Dorador, J., Rodríguez-Tovar, F.J., 2016. High resolution digital image treatment to color analysis on cores from IODP Expedition 339: Approaching lithologic features and bioturbational influence. *Marine Geology* 377, 127-135.
- Dorador, J., Rodríguez-Tovar, F.J., 2018. High-resolution image treatment in ichnological core analysis: initial steps, advances and prospects. *Earth-Science Reviews* 177, 226-237.
- Dorador, J., Rodríguez-Tovar, F.J., Expedition, I., 2014a. Digital image treatment applied to ichnological analysis of marine core sediments. *Facies* 60, 39-44.
- Dorador, J., Rodríguez-Tovar, F.J., Expedition, I., 2014b. Quantitative estimation of bioturbation based on digital image analysis. *Marine Geology* 349, 55-60.
- Dorador, J., Rodríguez-Tovar, F.J., Mena, A., Francés, G., 2019. Lateral variability of ichnological content in muddy contourites: Weak bottom currents affecting organisms' behavior. *Scientific reports* 9, 1-7.
- Dorador, J., Wetzel, A., Rodríguez-Tovar, F.J., 2016. Zoophycos in deep-sea sediments indicates high and seasonal primary productivity: Ichnology as a proxy in palaeoceanography during glacial–interglacial variations. *Terra Nova* 28, 323-328.

- Ekdale, A., 1992. Muckraking and mudslinging: the joys of deposit-feeding. *Short courses in Paleontology* 5, 145-171.
- Ekdale, A.A., Bromley, R.G., Pemberton, S.G., 1984. Ichnology: the use of trace fossils in sedimentology and stratigraphy. *Society of Economic Paleontologists and Mineralogists*.
- Evangelinos, D., Escutia, C., Etourneau, J., Hoem, F., Bijl, P., Boterblom, W., van de Flierdt, T., Valero, L., Flores, J.-A., Rodriguez-Tovar, F.J., 2020. Late Oligocene-Miocene proto-Antarctic Circumpolar Current dynamics off the Wilkes Land margin, East Antarctica. *Global and Planetary Change* 191, 103221.
- Flores, J., Sierro, F., 1997. Revised technique for calculation of calcareous nannofossil accumulation rates. *Micropaleontology*, 321-324.
- Fürsich, F., 1973. A revision of the trace fossils Spongeliomorpha, Ophiomorpha and Thalassinoides. *Neues Jahrbuch für Geologie und Paläontologie, Monatshefte* 12, 719-735.
- González-Lanchas, A., Flores, J.-A., Sierro, F.J., Bárcena, M.Á., Rigual-Hernández, A.S., Oliveira, D., Azibeiro, L.A., Marino, M., Maiorano, P., Cortina, A., Cacho, I., Grimalt, J.O., 2020. A new perspective of the *Alboran Upwelling System* reconstruction during the Marine Isotope Stage 11: A high-resolution coccolithophore record. *Quaternary Science Reviews* 245, 106520.
- González-Lanchas, A., Flores, J.A., Sierro, F., Sánchez Goñi, M., Rodrigues, T., Ausin, B., Oliveira, D., Naughton, F., Marino, M., Maiorano, P., Balestra, B., 2021a. Control mechanisms of Primary Productivity revealed by calcareous nannoplankton from Marine Isotope Stages 12 to 9 at the Shackleton Site (IODP Site U1385). *Paleoceanography and Paleoclimatology*, e2021PA004246.
- Goñi, M.F.S., Ferretti, P., Polanco-Martínez, J.M., Rodrigues, T., Alonso-García, M., Rodríguez-Tovar, F.J., Dorador, J., Desprat, S., 2019. Pronounced northward shift of the westerlies during MIS 17 leading to the strong 100-kyr ice age cycles. *Earth and Planetary Science Letters* 511, 117-129.
- Hernández-Almeida, I., Bárcena, M. A., Flores, J. A., Sierro, F. J., Sanchez-Vidal, A., Calafat, A. 2011. Microplankton response to environmental conditions in the Alboran Sea (Western Mediterranean): One year sediment trap record. *Marine Micropaleontology*, 78(1-2), 14-24.
- Hodell, D., Crowhurst, S., Skinner, L., Tzedakis, P.C., Margari, V., Channell, J.E., Kamenov, G., Maclachlan, S., Rothwell, G., 2013. Response of Iberian Margin sediments to orbital and suborbital forcing over the past 420 ka. *Paleoceanography* 28, 185-199.
- Hodell, D.A., Charles, C.D., Ninnemann, U.S., 2000. Comparison of interglacial stages in the South Atlantic sector of the southern ocean for the past 450 kyr: implications for Marine Isotope Stage (MIS) 11. *Global and Planetary Change* 24, 7-26.
- Hodell, D.A., Nicholl, J.A., Bontognali, T.R., Danino, S., Dorador, J., Dowdeswell, J.A., Einsle, J., Kuhlmann, H., Martrat, B., Mleneck-Vautravers, M.J., 2017. Anatomy

- of Heinrich Layer 1 and its role in the last deglaciation. *Paleoceanography* 32, 284-303.
- Keighley, D.G., Pickerill, R.K., 1995. Commentary: the ichnotaxa *Palaeophycus* and *Planolites*: historical perspectives and recommendations.
- Knaust, D., 2017. Atlas of trace fossils in well core: *appearance, taxonomy and interpretation*. Springer.
- Knaust, D., Bromley, R.G., 2012. *Trace fossils as indicators of sedimentary environments*. Newnes.
- Koutsodendris, A., Müller, U.C., Pross, J., Brauer, A., Kotthoff, U., Lotter, A.F., 2010. Vegetation dynamics and climate variability during the Holsteinian interglacial based on a pollen record from Dethlingen (northern Germany). *Quaternary Science Reviews* 29, 3298-3307.
- Kröncke, I., 2006. Structure and function of macrofaunal communities influenced by hydrodynamically controlled food availability in the Wadden Sea, the open North Sea, and the deep-sea. A synopsis. *Senckenbergiana maritima* 36, 123-164.
- Löwemark, L., 2015. Testing ethological hypotheses of the trace fossil *Zoophycos* based on Quaternary material from the Greenland and Norwegian Seas. *Palaeogeography, Palaeoclimatology, Palaeoecology* 425, 1-13.
- Marino, M., Girone, A., Maiorano, P., Di Renzo, R., Piscitelli, A., Flores, J.-A., 2018. Calcareous plankton and the mid-Brunhes climate variability in the Alboran Sea (ODP Site 977). *Palaeogeography, palaeoclimatology, palaeoecology* 508, 91-106.
- Martrat, B., Grimalt, J.O., Shackleton, N.J., de Abreu, L., Hutterli, M.A., Stocker, T.F., 2007. Four Climate Cycles of Recurring Deep and Surface Water Destabilizations on the Iberian Margin. *Science* 317, 502-507.
- Miguez-Salas, O., Dorador, J., Rodríguez-Tovar, F.J., 2019. Introducing Fiji and ICY image processing techniques in ichnological research as a tool for sedimentary basin analysis. *Marine Geology* 413, 1-9.
- Murat, A., 1999. 41. Pliocene-Pleistocene occurrence of sapropels in the Western Mediterranean Sea and their relation to Eastern Mediterranean Sapropels, *Proceedings of the Ocean Drilling Program, Scientific Results*, pp. 519-527.
- Oliveira, D., Desprat, S., Rodrigues, T., Naughton, F., Hodell, D., Trigo, R., Rufino, M., Lopes, C., Abrantes, F., Goni, M.F.S., 2016. The complexity of millennial-scale variability in southwestern Europe during MIS 11. *Quaternary Research* 86, 373-387.
- Olson, S.L., Hearty, P.J., 2009. A sustained +21m sea-level highstand during MIS 11 (400ka): direct fossil and sedimentary evidence from Bermuda. *Quaternary Science Reviews* 28, 271-285.
- Oppo, D., McManus, J., Cullen, J., 1998. Abrupt climate events 500,000 to 340,000 years ago: Evidence from subpolar North Atlantic sediments. *Science* 279, 1335-1338.
- Past International Working Group of PAGES, 2016. Interglacials of the last 800,000 years. *Reviews of Geophysics* 54, 162-219.

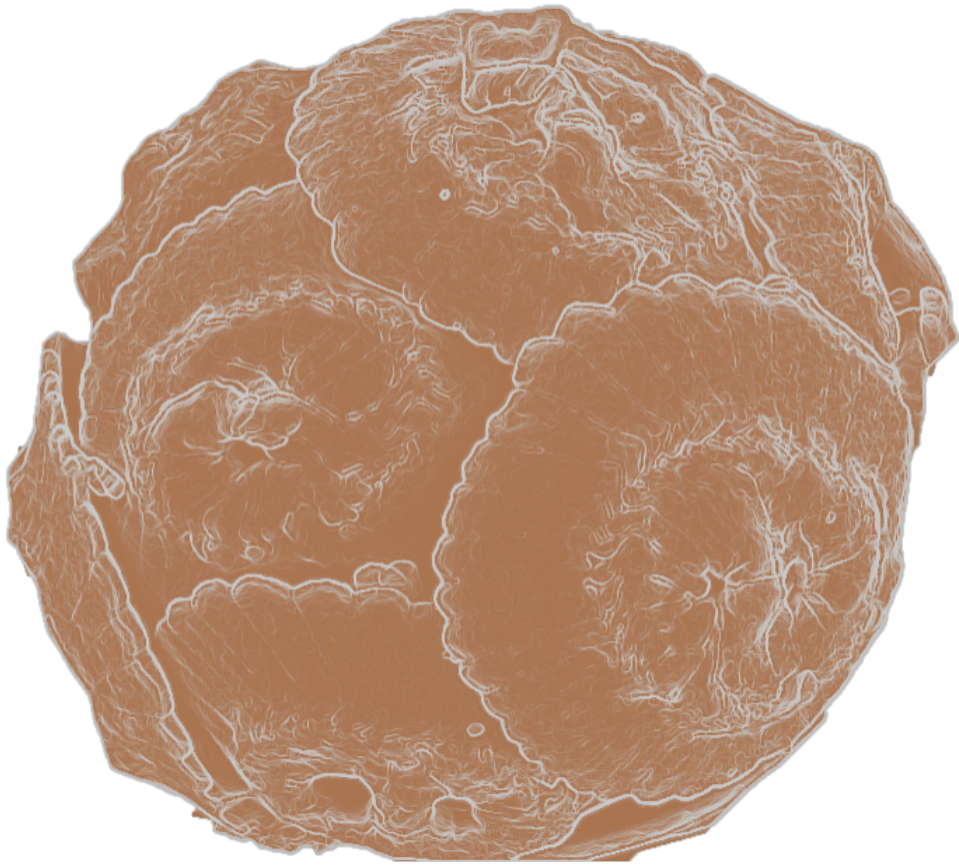
- Palumbo, E., Flores, J.A., Perugia, C., Emanuele, D., Petrillo, Z., Rodrigues, T., Voelker, A.H., Amore, F.O., 2013. Abrupt variability of the last 24 ka BP recorded by coccolithophore assemblages off the Iberian Margin (core MD03-2699). *Journal of Quaternary Science* 28, 320-328.
- Pemberton, S.G., Frey, R.W., 1982. Trace fossil nomenclature and the Planolites-Palaeophycus dilemma. *Journal of Paleontology*, 843-881.
- Pérez-Asensio, J.N., Frigola, J., Pena, L.D., Sierro, F.J., Reguera, M.I., Rodríguez-Tovar, F.J., Dorador, J., Asioli, A., Kuhlmann, J., Huhn, K., 2020. Changes in western Mediterranean thermohaline circulation in association with a deglacial Organic Rich Layer formation in the Alboran Sea. *Quaternary Science Reviews* 228, 106075.
- Pistek, P., De Strobel, F., Montanari, C., 1985. Deep-sea circulation in the Alboran Sea. *Journal of Geophysical Research: Oceans* 90, 4969-4976.
- Prokopenko, A., Bezrukova, E., Khursevich, G., Solotchina, E., Kuzmin, M., Tarasov, P., 2010. Climate in continental interior Asia during the longest interglacial of the past 500 000 years: the new MIS 11 records from Lake Baikal, SE Siberia. *Climate of the Past* 6, 31-48.
- Raymo, M.E., Mitrovica, J.X., 2012. Collapse of polar ice sheets during the stage 11 interglacial. *Nature* 483, 453.
- Raynaud, D., Barnola, J.-M., Souchez, R., Lorrain, R., Petit, J.-R., Duval, P., Lipenkov, V.Y., 2005. Palaeoclimatology: The record for marine isotopic stage 11. *Nature* 436, 39.
- Reyes, A.V., Carlson, A.E., Beard, B.L., Hatfield, R.G., Stoner, J.S., Winsor, K., Welke, B., Ullman, D.J., 2014. South Greenland ice-sheet collapse during marine isotope stage 11. *Nature* 510, 525.
- Roberts, D.L., Karkanas, P., Jacobs, Z., Mearns, C.W., Roberts, R.G., 2012. Melting ice sheets 400,000 yr ago raised sea level by 13 m: Past analogue for future trends. *Earth and Planetary Science Letters* 357, 226-237.
- Rodrigues, T., Voelker, A., Grimalt, J., Abrantes, F., Naughton, F., 2011. Iberian Margin sea surface temperature during MIS 15 to 9 (580–300 ka): Glacial suborbital variability versus interglacial stability. *Paleoceanography* 26.
- Rodríguez-Tovar, F., Miguez-Salas, O., Dorador, J., 2020a. Image processing techniques to improve characterization of composite ichnofabrics. *Ichnos* 27, 258-267.
- Rodríguez-Tovar, F.J., Dorador, J., 2014. Ichnological analysis of Pleistocene sediments from the IODP Site U1385 “Shackleton Site” on the Iberian margin: approaching paleoenvironmental conditions. *Palaeogeography, Palaeoclimatology, Palaeoecology* 409, 24-32.
- Rodríguez-Tovar, F.J., Dorador, J., 2015. Ichnofabric characterization in cores: a method of digital image treatment. *Annales Societatis Geologorum Poloniae*, pp. 465--471.
- Rodríguez-Tovar, F.J., Dorador, J., Grunert, P., Hodell, D., 2015a. Deep-sea trace fossil and benthic foraminiferal assemblages across glacial Terminations 1, 2 and 4 at



- the “Shackleton Site”(IODP Expedition 339, Site U1385). *Global and Planetary Change* 133, 359-370.
- Rodríguez-Tovar, F.J., Dorador, J., Hodell, D.A., 2019. Trace fossils evidence of a complex history of nutrient availability and oxygen conditions during Heinrich Event 1. *Global and Planetary Change* 174, 26-34.
- Rodríguez-Tovar, F.J., Dorador, J., Martin-Garcia, G.M., Sierro, F.J., Flores, J.A., Hodell, D.A., 2015b. Response of macrobenthic and foraminifer communities to changes in deep-sea environmental conditions from Marine Isotope Stage (MIS) 12 to 11 at the “Shackleton Site”. *Global and Planetary Change* 133, 176-187.
- Rodríguez-Tovar, F.J., Dorador, J., Mena, A., Francés, G., 2020b. Regional and global changes during Heinrich Event 1 affecting macrobenthic habitat: Ichnological evidence of sea-bottom conditions at the Galicia Interior Basin. *Global and Planetary Change* 192, 103227.
- Rodríguez-Tovar, F.J., Uchman, A., 2004. Trace fossils after the K–T boundary event from the Agost section, SE Spain. *Geological Magazine* 141, 429-440.
- Rohling, E. J., Marino, G., Grant, K. M. (2015). Mediterranean climate and oceanography, and the periodic development of anoxic events (sapropels). *Earth-Science Reviews*, 143, 62-97.
- Rogerson, M., Cacho, I., Jimenez-Espejo, F., Reguera, M., Sierro, F.J., Martinez-Ruiz, F., Frigola, J., Canals, M., 2008. A dynamic explanation for the origin of the western Mediterranean organic-rich layers. *Geochemistry, Geophysics, Geosystems* 9.
- Schlirf, M., 2000. Upper Jurassic trace fossils from the Boulonnais (northern France). *Geologica et Palaeontologica* 34, 145-213.
- Stein, R., Hefter, J., Grützner, J., Voelker, A., Naafs, B.D.A., 2009. Variability of surface water characteristics and Heinrich-like events in the Pleistocene midlatitude North Atlantic Ocean: Biomarker and XRD records from IODP Site U1313 (MIS 16–9). *Paleoceanography* 24.
- Stommel, H., Bryden, H., Mangelsdorf, P. (1973). Does some of the Mediterranean outflow come from great depth?. *Pure and Applied Geophysics*, 105(1), 879-889.
- Tye, G., Sherriff, J., Candy, I., Coxon, P., Palmer, A., McClymont, E., Schreve, D., 2016. The  $\delta^{18}\text{O}$  stratigraphy of the Hoxnian lacustrine sequence at Marks Tey, Essex, UK: implications for the climatic structure of MIS 11 in Britain. *Journal of Quaternary Science* 31, 75-92.
- Tzedakis, P., Pälike, H., Roucoux, K., De Abreu, L., 2009. Atmospheric methane, southern European vegetation and low-mid latitude links on orbital and millennial timescales. *Earth and Planetary Science Letters* 277, 307-317.
- Uchman, A., Wetzel, A., 2011. Deep-sea ichnology: the relationships between depositional environment and endobenthic organisms, *Developments in Sedimentology*. Elsevier, pp. 517-556.
- Voelker, A.H., Rodrigues, T., Billups, K., Oppo, D.W., McManus, J.F., Stein, R., Hefter, J., Grimalt, J.O., 2010. Variations in mid-latitude North Atlantic surface water

- properties during the mid-Brunhes (MIS 9–14) and their implications for the thermohaline circulation. *Climate of the Past*, 6, 531–552.
- von Grafenstein, R., Zahn, R., Tiedemann, R., Murat, A., 1999. Planktonic  $\delta^{18}\text{O}$  records at Sites 976 and 977, Alboran Sea: stratigraphy, forcing, and paleoceanographic implications. *Proceedings ODP, Scientific Results*, edited by: Zahn, R., Comas, MC, and Klaus, A., Ocean Drilling Program, College Station, TX, 469-479.
- Wetzel, A., 1991. Ecologic interpretation of deep-sea trace fossil communities. *Palaeogeography, palaeoclimatology, palaeoecology*, 85(1-2), 47-69.
- Wetzel, A., 2008. Recent bioturbation in the deep South China Sea: a uniformitarian ichnologic approach. *Palaios* 23, 601-615.
- Yin, Q.Z., Berger, A., 2012. Individual contribution of insolation and CO<sub>2</sub> to the interglacial climates of the past 800,000 years. *Climate Dynamics* 38, 709-724.
- Young, J.R., Bown, P.R. & Lees, J.A. (eds.) 2021. Nannotax3 website. International Nannoplankton Association. 1 Sep.2021. URL: <http://ina.tmsoc.org/Nannotax3>.
- Young, J. R., Geisen, M., Cros, L., Kleijne, A., Sprengel, C., Probert, I., & Østergaard, J., 2003. A guide to extant coccolithophore taxonomy. *Journal of Nannoplankton Research*, Special Issue, 1, 1-132.





**About the Mid-Brunhes interval and the role of the  
stumper coccolithophore *Gephyrocapsa* complex**

(González-Lanchas et al.,)

Artículo en preparación para *Nature Communications*

## **CAPÍTULO 6. Artículo científico**

### **“About the Mid-Brunhes interval and the role of the stumper coccolithophore *Gephyrocapsa* complex”**

**Alba González-Lanchas**<sup>a</sup>, Andrés S. Rigual-Hernández<sup>a</sup>, Francisco J. Sierro<sup>a</sup> Alonso-García<sup>a</sup> y José-Abel Flores<sup>a</sup>

<sup>a</sup> Departamento de Geología, Universidad de Salamanca, 37008 Salamanca, España

Artículo **en preparación** para ser enviado a *Nature Communications*

## Resumen

Las funciones vitales de fotosíntesis y calcificación en cocolitóforos intervienen, respectivamente, en las denominadas bombas de carbono orgánico e inorgánico, las cuales condicionan, por el mismo orden respectivo, bien la retirada una parte del CO<sub>2</sub> disuelto en la superficie del océano o la producción de una fuente de CO<sub>2</sub> a corto plazo (Rost y Riebesell, 2004; Rost et al., 2003). Así, la variación en la intensidad relativa de ambas funciones en el tiempo pudo modificar la capacidad de la superficie del océano para adquirir CO<sub>2</sub> y, con ello, el intercambio de CO<sub>2</sub> entre la superficie del océano y la atmósfera en el tiempo. El efecto final que ejerce el proceso de exportación del carbono orgánico e inorgánico producido por los cocolitóforos, mediante el hundimiento de los cocolitos hacia el fondo del océano hace, además, que el papel de este grupo de organismos influya a la tasa de acumulación de carbonatos y de carbono orgánico en el fondo de los océanos, ejerciendo, con ello, una función de amortiguación de la química oceánica y contribuyendo al almacenamiento de carbono en el reservorio oceánico (Archer y Maier-Reimer, 1994; Westbroek et al., 1993).

En este sentido, existen evidencias acerca del papel de los cocolitóforos pertenecientes a la familia de Noëlaerhabdaceae en el ciclo global del carbono, debido a la recurrencia de eventos de proliferación y aumento en la producción por parte de ciertas especies o morfotipos de esta familia a la escala de los ciclos de excentricidad orbital mínima de ~ 400 mil años (kyr) a lo largo del Pleistoceno. Si bien el registro de estos eventos es claro en los sedimentos de la franja ecuatorial, con aumento de la acumulación de carbonatos, reducción de la diversidad y predominio de especímenes de tamaño mediano de Noëlaerhabdaceae (Beaufort et al., 2020), la constatación de implicación global o cuasi global de este mecanismo no ha sido todavía puesta de manifiesto. Este aspecto es fundamental para explicar los procesos ambientales que mediaron entre el forzamiento orbital y la producción y adaptación de estos grupos, y a su vez un elemento que resultaría clave a la hora de desentrañar los procesos implicados en la regulación global del ciclo de carbono a esta escala orbital (De Vleeschouwer et al., 2020).

Uno de los principales ejemplos de estos episodios, es el que ocurrió durante el intervalo del Mid-Brunhes, entre los estadios isotópicos marinos (MIS-*Marine Isotope Stages*) 14 a 7 (~ 550 a 280 ka), dominado globalmente por el complejo *Gephyrocapsa* y

en particular por “*Gephyrocapsa caribbeanica*”, que eclosiona dentro de los límites de dicho intervalo (Flores et al., 2012).

En este estudio se presenta un análisis morfométrico detallado sobre los cocolitos de *Gephyrocapsa* durante este intervalo, con la aplicación de técnicas de análisis de imagen, que incluye la medida de talla y masa en testigos sedimentarios de diferentes localidades, que cubren un transecto latitudinal del Atlántico norte y Mediterráneo occidental: IODP Sites U1314, U1385, ODP Sites 977 y 925. Las medidas se realizaron, por separado, sobre los grupos de *Gephyrocapsa* pequeñas ( $<3 \mu\text{m}$ ; small *Gephyrocapsa*) y medianas ( $>3 \mu\text{m}$ ; medium *Gephyrocapsa*) y, siguiendo el procedimiento en Beaufort et al. (2020), se calcula el índice de divergencia morfológica (MDI-*Morphological Divergence Index*). Este parámetro y los resultados de este análisis muestran tendencias morfométricas (morfológicas, empleado indistintamente) homogéneas en todas las localidades estudiadas, donde el MDI reduce su valor y las tallas medias dominan en la parte central del intervalo. Siguiendo el razonamiento de Beaufort et al. (2020), este patrón de reducción del MDI se identifica con la eclosión de morfotipos adaptados al aprovechamiento rápido de condiciones proclives para el rápido crecimiento celular y producción. Estas evidencias se combinan con el análisis micropaleontológico de las asociaciones de *Gephyrocapsa* y con medidas biométricas del valor de ángulo del puente de la barra central en las *Gephyrocapsa* medianas, un elemento taxonómico característico de este grupo, considerado como índice de variabilidad taxonómica en este trabajo. Los resultados indican que, según las consideraciones taxonómicas tradicionales, la especie o morfotipo correspondiente a “*G. caribbeanica*” domina estos cambios. No obstante, una potencial inclusión de varios morfotipos dentro de este grupo no se descarta en este análisis y requiere, todavía, de una evaluación en profundidad de los datos disponibles.

A partir de los valores morfométricos anteriormente presentados, se lleva a cabo el cálculo de potenciales índices de calcificación, propuestos y empleados por otros autores previamente (Bolton et al., 2016; Jin et al., 2018 y autores referidos en estos trabajos). Estos parámetros son: el espesor normalizado (Size Normalized – SN – Thickness), el valor  $k$  y la estimación de la relación “PIC/POC”, cuyo cálculo se realiza siguiendo la determinación en los trabajos anteriormente referidos. La comparación de estos resultados para las diferentes latitudes y ambientes en este estudio, así como la valoración de su relación con un índice de disolución independiente, generado a partir de

la cuantificación de los fragmentos de foraminíferos planctónicos en el testigo IODP *Site* U1314 en este estudio, permite discutir su coherencia y discernir posibles sesgos o impactos regionales. Las tendencias del valor  $k$  y la estimación de PIC/POC son homogéneas y se consideran aplicables para la captura de los cambios en la calcificación de *Gephyrocapsa* en este estudio. Estos resultados confirman que, además de la respuesta de proliferación de este grupo durante el intervalo del Mid-Brunhes discutida por autores anteriores y la existencia de un patrón morfométrico, los coccolitóforos de este grupo también expresan una respuesta de incremento de la calcificación, potencialmente acoplada a la ciclicidad de  $\sim 400$  kyr, que domina estos cambios.

En esta propuesta, basándonos en la literatura existente, señalamos el efecto de la intensificación en la meteorización forzada por las condiciones de excentricidad mínima que acontecen durante el intervalo (Cheng et al., 2016), ya sea por un incremento neto del flujo o por la intensificación del proceso ante una mayor susceptibilidad del substrato a verse alterado (Caves et al., 2016). Este proceso incrementaría la alcalinidad neta del océano, un factor que se considera determinante en el impulso de la capacidad de calcificación de coccolitóforos en medios naturales, a esta escala (Bach et al., 2015), lo cual podría ser un factor potenciador de la respuesta de calcificación individual, a través de uno o más morfotipos de *Gephyrocapsa*. Independientemente o en conjunto con la respuesta de incremento en crecimiento y producción de este grupo ante condiciones ambientales favorables durante el intervalo, propuesta por autores previos (Flores et al., 2012; Rickaby et al., 2007), se sugiere la existencia de una respuesta de este grupo ante un cambio en la química del océano. Este aspecto podría explicar la entidad global o cuasi global de la respuesta observada en este estudio. Complementariamente, sugerimos que los cambios en la calcificación de los coccolitóforos y, en particular de Noëlaerhabdaceae, podrían ser explorados para su empleo como elementos de conexión de los procesos implicados en los cambios en la química del océano a la escala de  $\sim 400$  kyr.

## Referencias

- Archer, D., Maier-Reimer, E., 1994. Effect of deep-sea sedimentary calcite preservation on atmospheric CO<sub>2</sub> concentration. *Nature* 367, 260-263.
- Bach, L.T., Riebesell, U., Gutowska, M.A., Federwisch, L., Schulz, K.G., 2015. A unifying concept of coccolithophore sensitivity to changing carbonate chemistry embedded in an ecological framework. *Progress in Oceanography* 135, 125-138.



- Beaufort, L., L., Bolton, C., Sarr, A.-C., Suchéras-Marx, B., Rosenthal, Y., Donnadieu, Y., Barbarin, N., Bova, S., Cornuault, P., Gally, Y., Gray, E., Mazur, J.-C., Tetard, M., 2020. Cyclic evolution of phytoplankton forced by changes in tropical seasonality.
- Bolton, C.T., Hernández-Sánchez, M.T., Fuertes, M.-A., González-Lemos, S., Abrevaya, L., Mendez-Vicente, A., Flores, J.-A., Probert, I., Giosan, L., Johnson, J., 2016. Decrease in coccolithophore calcification and CO<sub>2</sub> since the middle Miocene. *Nature communications* 7, 1-13.
- Caves, J.K., Jost, A.B., Lau, K.V., Maher, K., 2016. Cenozoic carbon cycle imbalances and a variable weathering feedback. *Earth and Planetary Science Letters* 450, 152-163.
- Cheng, H., Edwards, R.L., Sinha, A., Spötl, C., Yi, L., Chen, S., Kelly, M., Kathayat, G., Wang, X., Li, X., 2016. The Asian monsoon over the past 640,000 years and ice age terminations. *Nature* 534, 640-646.
- De Vleeschouwer, D., Drury, A.J., Vahlenkamp, M., Rochholz, F., Liebrand, D., Pälike, H., 2020. High-latitude biomes and rock weathering mediate climate–carbon cycle feedbacks on eccentricity timescales. *Nature communications* 11, 1-10.
- Flores, J.A., Filippelli, G.M., Sierro, F.J., Latimer, J.C., 2012. The “White Ocean” hypothesis: a late Pleistocene Southern Ocean governed by coccolithophores and driven by phosphorus. *Frontiers in microbiology* 3, 233.
- Jin, X., Liu, C., Zhang, H., Zhou, C., Jiang, X., Wu, Z., Xu, J., 2018. Evolutionary driven of *Gephyrocapsa* coccolith isotopic vital effects over the past 400 ka. *Earth and Planetary Science Letters* 503, 236-247.
- Rickaby, R., Bard, E., Sonzogni, C., Rostek, F., Beaufort, L., Barker, S., Rees, G., Schrag, D., 2007. Coccolith chemistry reveals secular variations in the global ocean carbon cycle? *Earth and Planetary Science Letters* 253, 83-95.
- Rost, B., Riebesell, U., 2004. Coccolithophores and the biological pump: responses to environmental changes, *Coccolithophores*. Springer, pp. 99-125.
- Rost, B., Riebesell, U., Burkhardt, S., Sültemeyer, D., 2003. Carbon acquisition of bloom-forming marine phytoplankton. *Limnology and oceanography* 48, 55-67.
- Westbroek, P., Brown, C.W., van Bleijswijk, J., Brownlee, C., Brummer, G.J., Conte, M., Egge, J., Fernández, E., Jordan, R., Knappertsbusch, M., 1993. A model system approach to biological climate forcing. The example of *Emiliana huxleyi*. *Global and planetary change* 8, 27-46.



## About the Mid-Brunhes interval and the role of the stumper coccolithophore *Gephyrocapsa* complex

(González-Lanchas et al., en preparación para *Nature Communications*)

### Abstract

Noëlaerhabdaceae coccolithophores (the family of the modern *Emiliana huxleyi*) contributed to records of the global carbon cycle by increasing carbonate export and burial rates because of recurrent enhanced production at ~ 400 kyr cycles. Mid-sized morphotypes corresponding to “*G. caribbeanica*” lead these changes. If this variability also entailed a change in the degree of calcification is unknown, but plausible since regulation in the carbon cycle at this scale necessarily involve profound changes in the ocean carbonate chemistry. We propose that changes in the ocean carbonate chemistry trough ~ 400 kyr cycles can be captured using the changes in calcification as proxy. We analyzed the ~ 400 kyr low eccentricity cycle encompassing the Mid-Brunhes event from morphometric measurements (i.e., size and mass) in the *Gephyrocapsa* complex at a wide range of latitudinal environments across the Atlantic, providing a comprehensive record of coccolithophore calcification response. Calcification was enhanced during the period of domain of mid-sized *Gephyrocapsa*, where one or more morphotypes could lead this response. This feature is plausibly related to changes in seawater chemistry towards a more alkaline ocean trough weathering strengthening that, aside providing nutrients benefitting growth conditions, would have induced  $\text{HCO}_3^-$  increase of global or, at least, basin entity, sufficient to explain the homogeneous response of *Gephyrocapsa* calcification observed at all sites in this study.

## Introduction

Coccolithophores is a group of calcifying phytoplankton. They produce organic carbon via carbon fixation through photosynthesis and inorganic carbon, as calcium carbonated structures, named “coccoliths”, via intracellular biomineral precipitation through calcification (Rost et al., 2003). Both mechanisms take part in the so-called *organic* and *inorganic carbon pumps*, respectively. Each of these pumps have an opposite effect on each other: photosynthesis results in a net sink for dissolved CO<sub>2</sub> in the surface ocean (thereinafter referred as CO<sub>2</sub> [aq]), whereas coccolithophore calcification produces a short-term source of CO<sub>2</sub> within the sequence of chemical processes for calcium carbonate (CaCO<sub>3</sub>) formation (see Rost and Riebesell, 2004 for a review). The net relative intensity between the operation of these pumps can modulate the CO<sub>2</sub> exchange between the surface ocean and the atmosphere. Together with the ulterior coccolith sinking, such functions drive long-term carbonate export and accumulation (i.e., both inorganic and organic) processes in the deep ocean. Subsequently, the changes in coccolithophore photosynthesis and/or calcification could critically affect the sedimentary buffer capacity of ocean chemistry and the global carbon storage, ultimately, with large consequences for the global carbon cycle and climate feedbacks at geological time scales (Archer and Maier-Reimer, 1994; Broecker and Peng, 1987; Sigman and Boyle, 2000; Westbroek et al., 1993).

Coccolithophores belonging to the Noëlaerhabdaceae, one of the most successful and dominant coccolithophores families in fossil assemblages are thought to have played a major role in the control of the eccentricity forced ~ 400 kyr variability in the global carbon cycle due to the recurrence of events of enhanced proliferation and production of certain species and/or morphotypes (bloom episodes), as recently summarized during the Pleistocene by Beaufort et al. (2020). Several hypotheses trying to find an integrated explanation for the prolonged eccentricity-forced carbon cycle variability during the Pleistocene and older times during the Cenozoic includes, indeed, the enhanced ocean primary productivity and its impact over the net carbonate export and organic carbon burial (Hoogakker et al., 2006; Rickaby et al., 2007; Russon et al., 2010).

One of the best examples of these ~ 400 kyr Noëlaerhabdaceae bloom episodes is the one that occurred during the Mid-Brunhes (MB) interval, ranging between the Marine

Isotope Stages (MIS) 14 to 7 (~ 550 to 280 ka). The net pelagic CaCO<sub>3</sub> production was dominated by a group of species belonging to the genus *Gephyrocapsa*, in particular by “*Gephyrocapsa caribbeanica*”, that emerged and globally proliferated within the limits of this interval (Baumann and Freitag, 2004; Flores et al., 2012).

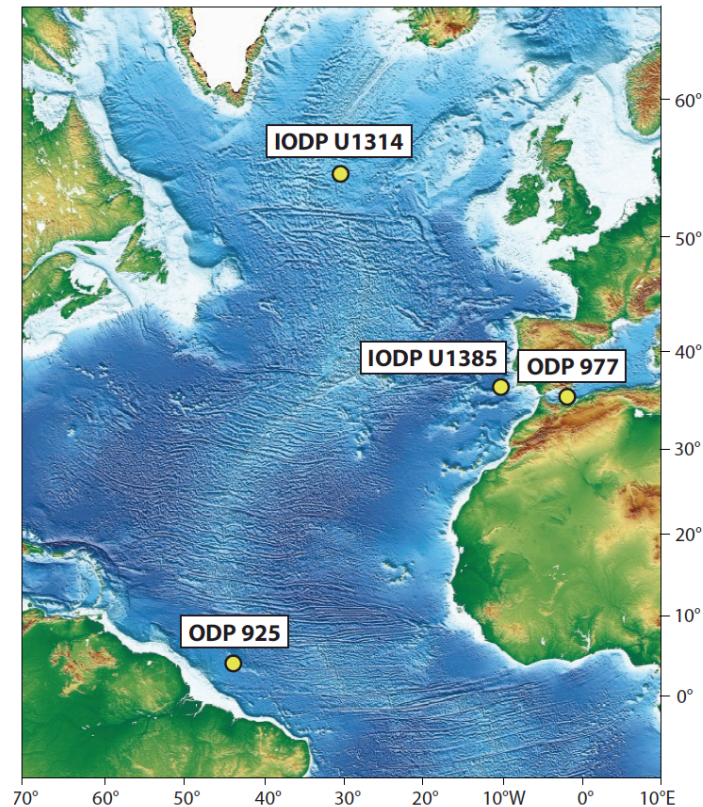


**Figure 1.** Map showing the location of the Sites in this study: IODP U1314, U1385, ODP 977 and 925. Map source: IODP ([www.iodp.org](http://www.iodp.org)). See details about locations, depths, and previous data of each of the materials used in this study in Material and Methods.

The Noëlaerhabdaceae bloom episodes during the ~ 400 kyr cycles, including that of the MB, are clearly preserved in the fossil record through increased carbonate accumulation, dominance of mid-sized specimens and reduced coccolith diversity in the pelagic sediments (Beaufort et al., 2020). However, there are still different perspectives to explain the environmental processes that mediated between orbital forcing over Noëlaerhabdaceae production and adaptation (Beaufort et al., 2020; Rickaby et al., 2007). There is debate on whether this event was of global or regional extent. This is a key aspect that could be critical in unraveling the overall combination of processes accounting for the global regulation of carbon cyclicity at this scale (De Vleeschouwer et al., 2020).

Findings during the last decade increasingly advocate the importance of eccentricity-forced weathering processes and monsoon evolution in the low latitudes, that should be integrated within the key processes controlling of such pattern (Ma et al., 2011; Ma et al., 2017; Tian et al., 2011; Wang et al., 2004).

One of the most robust evidence of the ~ 400 kyr global variability in the carbon cycle comes from the  $\delta^{13}\text{C}$  records from benthic foraminifera (Westerhold et al., 2020; Zachos et al., 2001). This proxy mirrors the isotopic composition of the dissolved inorganic carbon in deep ocean water masses,  $\delta^{13}\text{C}_{\text{DIC}}$ , that mainly changes by means of the interaction between the carbon reservoirs (i.e., ocean, atmosphere, and biosphere) and with the deep ocean (Zachos et al., 2001). Coccolithophore calcification in the natural environment is known to respond to the changes in seawater carbon chemistry as a first order driver (Bach et al., 2012;2013;2015). Thus, as eccentricity-forced rhythms in the carbon cycle entailed major changes in the seawater carbonate system, it seems plausible to expect that, at this scale, coccolithophores also express a calcification response. Surprisingly, analysis of the potential changes in coccolithophore calcification at the scale of the ~ 400 kyr, has not been addressed so far.

To shed light on this issue, we provide a detailed morphometrical analysis of *Gephyrocapsa* coccoliths in different locations covering a N-S latitudinal transect of the North Atlantic and the western Mediterranean Sea (IODP Sites U1385, U1314, ODP Sites 977 and 925; Fig. 1) with the use of image analysis techniques (C-calcita software; Fuertes et al., 2014) over the narrow *Gephyrocapsa* small (< 3  $\mu\text{m}$ ) and medium (>3  $\mu\text{m}$ ) size classes. From these values, we calculated coccolith Size Normalize (SN) Thickness,  $k$  value and the PIC/POC ratio (see Material and Methods), potential indicators of coccolithophore calcification (Bolton et al., 2016; Jin et al., 2018 and references therein). We discuss its coherence and present a comprehensive estimate of the changes in *Gephyrocapsa* coccolithophore calcification during the MB. Trends in values are homogeneous on a global scale and show that, in addition to the up-to-date well-known proliferation response of this group, coccolithophores individually express a response and regulation of calcification coupled to the path of the ~ 400 kyr global carbon cyclicity. Building up on the existing literature, we point to the effect of eccentricity-forced weathering, either by enhanced flow discharge or global intensification of the process (i.e., weatherability; Caves et al., 2016), conditioning a global net increase in ocean

alkalinity, as a determining factor on enhancing calcification response through one or more *Gephyrocapsa* morphotypes. In this way, we critically suggest that changes in coccolithophore calcification (i.e., Noëlaerhabdaceae family) can be used to identify seawater geochemical changes during the past and this to determine the type of processes involved in the climatical control of the carbon cycle at the orbital scale of ~ 400 kyr cycles.

## Results

### *Latitudinal homogeneity in the evolution of morphometric changes of the Gephyrocapsa complex*

Overall, the temporal variations of *Gephyrocapsa* coccolith size through the MB interval share high similarities between the different studied locations. When considering separately the two small and medium *Gephyrocapsa* fractions, the mean absolute size varied, respectively, between 2.3-2.7 and 3.2-4.7  $\mu\text{m}$  in all the sites (Fig. S1-S3). Coccolith mass is primarily controlled by changes in coccolith size through the interval and averages between 1.4-3 and 4-13 pg, for the small and medium *Gephyrocapsa* fractions, respectively (Fig. S4).

The significant correlation between size and mass changes (Fig. S4) agrees with early observations about the correspondence between size and mass changes (Young and Ziveri, 2000) and evidence that size changes in fossil coccoliths is the main determinant on changing mass values. Importantly, coccolith size and thickness are known to exhibit an allometric relationship, which implies that, in order to be able to compare the degree of calcification of coccoliths of different size on an equal footing coccolith thickness normalization is required (see Linge Johnsen et al., 2019).

The *Gephyrocapsa* complex display contraction in the divergence of the average size and mass values between the small and medium *Gephyrocapsa* populations throughout the MB, equally at all sites (Figs. S1-S3). This feature is summarized as reduction in the values of Morphological Divergence Index (MDI), calculated as in Beaufort et al. (2020; Fig. 2g). Such a feature is particularly well evidenced between MIS 13 to 11 and MIS 9 at all the studied sites (Fig. 2g and Figs. S1-S3). We agree with the previous author and consider the reductions in this index as indicative of a reduction in

the diversity in the Noëlaerhabdaceae coccolithophore population during blooming episodes: in this case, the MDI reduction reflect the domain of mid-sized morphotype or morphotypes, with an average coccolith size closer to  $\sim 3 \mu\text{m}$  (i.e., by a coeval increase/decrease in the average size values of small/medium *Gephyrocapsa* size classes) in all the studied sites (Fig. S1-S3). On the light of the correspondence of this pattern with the % “*G. caribbeanica*” (traditional identification, see Table S1) in the studied assemblages (Fig. 2f) and, according to previous authors, these morphological characteristics or size and mass reduction in the medium *Gephyrocapsa* population is identified with the domain of “*G. caribbeanica*” (Jin et al., 2018). However, we do not rule out that a variety of morphotypes can be included within this traditional grouping (Text S1).

Despite the coherence with the pattern for other low eccentricity-paced cycles in Beaufort et al. (2020), the coincidence, as well, of this coccolith morphometrical pattern with the timing of the Mid Brunhes Dissolution Interval (MBDI; Barker et al., 2006) could allow speculations about an impact of dissolution over morphometries (i.e., if this process could lead to a reduction in the average size of medium *Gephyrocapsa* size classes and a simultaneous increase in the average value of the small *Gephyrocapsa*, by, for example, preferential preservation of the larger and heavier morphotypes within this complex). However, two further observations clarify that calcite dissolution on coccoliths might have played a negligible role: i) the absence of clear correspondence between *Gephyrocapsa* MDI and the dissolution profile from % foraminiferal fragments for Site U1314 (Fig. 2e and g) and ii) the already pointed correspondence between the morphometrical trends and MDI values at the different studied sites (Fig. 2g and S1-S3), which are located at significantly different regional depths, latitudes, and environments (Fig. 1; Material and Methods).



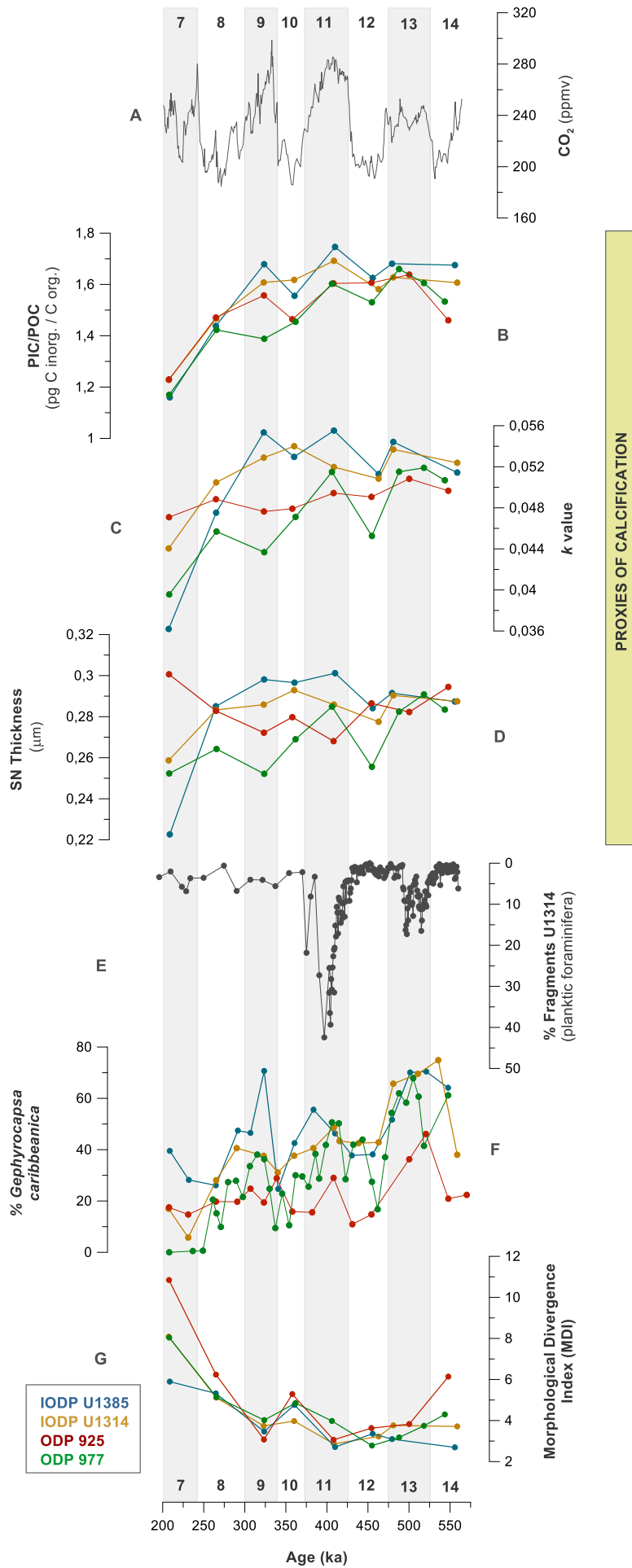


**Figure 2.** Relationship between **(a)**  $p\text{CO}_2$  changes during the Mid-Brunhes interval (Bereiter et al., 2015), the potential proxies for calcification: **(b)** SN Thickness, **(c)**  $k$  value and **(d)** PIC/POC; a dissolution estimate by **(e)** the percentages of fragments of planktic foraminifer in samples from Site IODP U1314, **(f)** percentage of “*Gephyrocapsa caribbeanica*” in samples and **(g)** the Morphological Divergence Index (MDI) for *Gephyrocapsa* in this study. The procedures for the calculation of indexes and values are found in the section Material and Methods.

### ***Enhanced calcification of the Gephyrocapsa complex***

The trends of the three potential proxies of calcification, the SN Thickness,  $k$  value and PIC/POC, are highly similar between them at all sites (Fig. 2b-d) and for both medium and small *Gephyrocapsa* size classes (Fig. S5), suggesting a common trend in the changes in cell size normalized calcite content implicit to these values (Bolton et al., 2016; Jin et al., 2018). Overall, the results evidence higher values during the MIS 13 to 9 interval and a pronounced decreasing trend through the MIS 7 (Fig. 2b-d).

Nonetheless, some slightly higher differences in the SN Thickness can be recognized between sites (Fig. 2d): conspicuous is the lower variability in the SN Thickness at Site 925 compared to that observed in other locations, a fact that suggests that the coccoliths dwelling at this low latitude system could have experienced some degree of extra dissolution. In fact, the western tropical Atlantic location is more prone to be affected by dissolution on depths above the lysocline, as a result of the changeable influence of Antarctic Bottom Water versus North Atlantic Deep Water during the Pleistocene (Pfuhl and Shackleton, 2004). In contrast, the  $k$  value and PIC/POC ratio display less variability between sites (i.e., highly similar range of values; Fig. 3) and correlation between locations (Table S1), a fact that suggest that these parameters are better suited for the reconstruction of coccolith calcification estimates from coccolith morphometries and lead us to its use for the following discussion (Fig. 3).

The coupling between maximum values in the pelagic carbonate concentration of sedimentary tracers (see Material and Methods for a detailed explanation) and the high concentrations of *Gephyrocapsa* coccolith at the different sites during the MB (Fig. 3) underscores the prevailing view that enhanced *Gephyrocapsa* production during this interval played a key role in the enhanced global carbonate burial (Barker et al., 2006; Flores et al., 2012; Rickaby et al., 2007; Wang et al., 2003). Notably, our results present new insights that evidence that, aside this increased carbonate production during the MB

due to the increased pelagic production by *Gephyrocapsa* (i.e., higher number of produced coccolith), there is an increase in the degree of individual coccolithophore calcification in *Gephyrocapsa* (i.e.,  $k$  values and PIC/POC). This feature has never been described and quantified before for the MB period, nor during the ~ 400 kyr Noëlaerhabdaceae blooming episodes of diversity contraction during the Pleistocene (Beaufort et al., 2020).

## Discussion

Recent findings by Beaufort et al. (2020) outlined that MDI reductions are due to be the result of environmental selective changes in Noëlaerhabdaceae morphotype dominance, occurring at low-latitudinal locations. The MDI for *Gephyrocapsa* in our study (Fig. 2g) shows good correlation with those observations in all the sites, strongly suggesting that this evolutive and/or adaptative change was not only constrained to the low latitudes during the MB. Our results evidence that, if the cyclicity observed in the MDI is exclusively a growth and production response that determines the proliferation of one or more mid-sized morphotypes, the triggering stimulus must have a global (or quasi-global) extent, or, at least, involve processes occurring at latitudes outside the tropical band. This observation is in agreement with previous research that pointed that global environmental controls were responsible for the amplification of the duration of the growth season during eccentricity minima (Rickaby et al., 2007), or an increase in the phosphorous delivery into the ocean (Flores et al., 2012). Both or any of these processes would result in an optimization of the growth conditions for *Gephyrocapsa*, thereby leading to a proliferation of certain morphotypes (i.e., “*G. caribbeanica*”) within the *Gephyrocapsa* complex. Our results are also in agreement with the recent approach by Zhang et al. (2021), who proposed the interplay of silica leakage at high latitudes together with the power of low-latitude monsoon strengthening to explain the conditions during this blooming event.

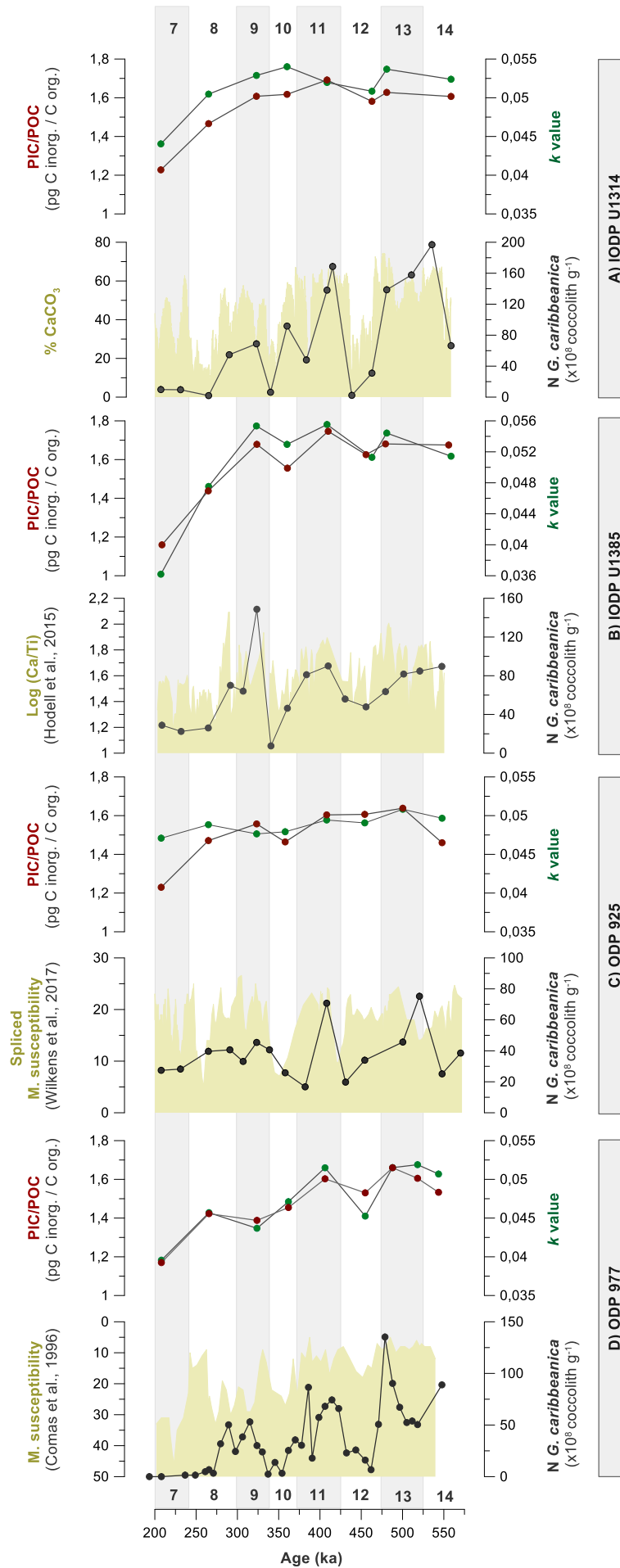


**Figure 3.** Connection between the calcification proxies:  $k$  values and PIC/POC, the absolute concentration of individuals belonging to “*G. caribbeanica*” (N values, as coccoliths  $g^{-1}$ ; see **Material and Methods**) and the estimation of pelagic carbonate concentration in sediments between MIS 14 to 7 from different sedimentological proxies (see Material and Methods) at the four Sites: **(a)** IODP U1314, **(b)** U1385, **(c)** ODP 925 and **(d)** 977.

Notably, coccolith size changes in calcifying nanoplankton is known to reflect a proportional change in cellular dimensions (Henderiks and Pagani, 2007). Smaller cells increase the relationship between surface area to volume, increasing Rubisco specificity (Tortell, 2000) and the power of intracellular carbon concentration mechanisms (Giordano et al., 2005), ultimately optimizing the photosynthesis capacity. At a macroevolutionary timescale, coccolithophore cell reduction has been observed coupled to long-term  $pCO_2$  decreases, as for example, from the Neogene into the Quaternary (i.e., Bolton et al., 2016; Suchéras-Marx and Henderiks, 2014). We propose that our results represent, in some extent, such a feature in size reduction, towards the domain of mid-sized individuals, at the short-term scale of  $\sim 400$  kyr (Fig. 2g). Assuming a similar physiological response of the coccolithophore populations during the MB than that observed in the above-mentioned studies, the change in coccolith and, consequently, cellular size, could most likely reflect an improvement in the capacity for the use of resources by the mid-sized “*G. caribbeanica*” morphotype or morphotypes. However, the  $pCO_2$  pattern at this scale does not seem to be a limiting resource for cell size change (Fig. 2a; Bereiter et al., 2015). Rather, following an inverse direction to postulates, the interglacial increases in  $pCO_2$  during MIS 13, 11 and 9, yielding  $\sim 240$ -280 ppmv, seems to accompany short-term reductions in the MDI during MIS 11 and 9 (Fig. 2g). This is: the short-term  $pCO_2$  increases, or, plausibility, the coupled interglacial increased surface temperatures could even favor the proliferation of “*G. caribbeanica*” individuals (Fig. S6).

A critical observation in this study is the coupling between the dominance of the mid-sized *Gephyrocapsa* and an increase in coccolith calcification (Fig. 3b-d). The homogeneous response in the wide range of environmental settings encompassed in this study (Fig. 2 and 3), implies that the underlying mechanism stimulating the development of the *Gephyrocapsa* complex must be a global phenomenon. Interestingly, the increase in coccolith thickness during the MB interval challenges the notion that a decrease in

coccolith size (i.e., in the case of the medium *Gephyrocapsa*) is coupled with a reduction of the degree of calcification (Suchéras-Marx and Henderiks, 2014).

Currently, it is unclear which environmental factors are responsible for the changes in cell-calcification coccolithophore in natural environments (see McClelland et al., 2016; Raven and Crawford, 2012). Among the most likely candidates are changes in seawater carbonate chemistry, as the changes in the amount of CO<sub>2</sub> [aq] and other carbonated species, together with changes in pH and total alkalinity have been shown to have an important role in coccolithophore calcification (Bach et al., 2015; Müller et al., 2021; Müller et al., 2015). There is consensus in that bicarbonate ion (HCO<sub>3</sub><sup>-</sup>) is the primary inorganic carbon source for calcification, implying that calcification rates increase with increasing aqueous HCO<sub>3</sub><sup>-</sup> transferred to the coccolithophore intracellular DIC carbon pool (i.e., the intracellular reservoir and source for calcification). The importance of the changes in HCO<sub>3</sub><sup>-</sup> over calcification at geological scale has also been suggested in the study by Bolton et al. (2016), who showed a clear decoupling between the *p*CO<sub>2</sub> and calcification relationships throughout the Pleistocene. But this has been never tested from natural fossil records before, neither at the scale of the ~ 400 kyr cyclical changes.

Several independent sedimentary and geochemical lines of evidence point to the operation of weathering feedbacks following carbon cycle perturbations in Earth history. In particular, the MB is known to be preceded by notable changes in the marine carbon reservoir, when massive fluvial discharges were coincident with the beginning of MIS 13 (i.e., Wang et al., 2003). Novel analysis estimating the tetrafluoromethane content in air bubbles trapped in ice cores supports the notion of intensified silicate weathering through the interval during the strong interglacial MIS 11 (Schmitt et al., 2013). Moreover, marine proxies also suggest a weathering intensification during the Quaternary due to either a greater reactivity of the exposed substrate (see Caves et al., 2016 and references therein) or increased “weatherability” (i.e., Penman et al., 2020; Rugenstein et al., 2019). Surface ocean enrichment in silicic acid (H<sub>4</sub>SiO<sub>4</sub>) through weathering entails HCO<sub>3</sub><sup>-</sup> and cation enrichment, in the form of Ca<sup>2+</sup>, Mg<sup>2+</sup>, Na<sup>+</sup> and K<sup>+</sup> (Meybeck, 1987). In other words, enhanced weathering results in an increase in seawater alkalinity, carbonate ion concentration ([CO<sub>3</sub><sup>2-</sup>]) and carbonate saturation state ( $\Omega$ ), thereby promoting CaCO<sub>3</sub> precipitation by marine calcifiers and subsequent preservation and burial in the sea floor

(Zeebe and Wolf-Gladrow, 2001). The physiological conceptualization by Bach et al. (2015) for coccolithophore calcification integrates these geochemical relationships from culture on a geological timescale, where both the  $\text{CaCO}_3$  sediment dissolution and the terrestrial weathering outstands as potential inputs of alkalinity to the ocean (i.e., increasing  $\text{HCO}_3^-$  and reducing  $\text{H}^+$ ) benefiting coccolithophore calcification at the scale in our study.

The latest contribution on the origin of the *Gephyrocapsa* bloom during the MB by Zhang et al. (2021), proposed the involvement of low-latitude monsoon enhancement from the minimum to maximum eccentricity cycle, between 400 to 200 ka (Cheng et al., 2016), stimulating nutrient supply through enhanced weathering and fluvial discharge. Our results agree with the latter studies and indicate that *Gephyrocapsa* blooming morphotype or morphotypes (included in the classical definition of “*G. caribbeanica*”) could be the result of an increase in seawater alkalinity entailed to these processes. This is: instead of a unique growth and productivity response outlined by previous authors (Barker et al., 2006; Flores et al., 2012; Rickaby et al., 2007; Zhang et al., 2021), we suggest a response to overall geochemical change, in which the homogeneity of the response in the different environments studied is more easily explained.

A rise in sea surface temperatures could also be invoked as an additional factor that would have accelerated the calcification metabolism in *Gephyrocapsa* (i.e., Sett et al., 2014). This idea agrees with the relationship between the relative contribution of “*G. caribbeanica*” and the high-resolution SST profiles at the mid latitude location of both the Mediterranean and Atlantic Iberian margins in González-Lanchas et al. (2020) and González-Lanchas et al. (2021a) (Fig S6).

Overall, our results offer the definitive perspective that calcification response in Noëlaerhabdaceae interacts as independent element to cell dimension and morphometrical coccolith size changes, potentially reflecting changes seawater carbonated chemical conditions, as well as constituting a key element involved in its modulation at the scale of ~ 400 kyr cycles. From the perspective acquired in this study, calcification reconstruction is a successful route to explore the seawater geochemical changes coupled to environmental drivers during the past and must be critically tested in older cycles modulated by low eccentricity through the Cenozoic, as a potential track of

the type of processes and that operated and sustained the carbon cycle oscillation under contrasted climatical background conditions.

## Main references

- Archer, D., Maier-Reimer, E., 1994. Effect of deep-sea sedimentary calcite preservation on atmospheric CO<sub>2</sub> concentration. *Nature* 367, 260-263.
- Bach, L.T., Bauke, C., Meier, K., Riebesell, U., Schulz, K.G., 2012. Influence of changing carbonate chemistry on morphology and weight of coccoliths formed by *Emiliana huxleyi*. *Biogeosciences* (BG) 9, 3449-3463.
- Bach, L.T., Mackinder, L.C., Schulz, K.G., Wheeler, G., Schroeder, D.C., Brownlee, C., Riebesell, U., 2013. Dissecting the impact of CO<sub>2</sub> and pH on the mechanisms of photosynthesis and calcification in the coccolithophore *Emiliana huxleyi*. *New Phytologist* 199, 121-134.
- Bach, L.T., Riebesell, U., Gutowska, M.A., Federwisch, L., Schulz, K.G., 2015. A unifying concept of coccolithophore sensitivity to changing carbonate chemistry embedded in an ecological framework. *Progress in Oceanography* 135, 125-138.
- Barker, S., Archer, D., Booth, L., Elderfield, H., Henderiks, J., Rickaby, R.E., 2006. Globally increased pelagic carbonate production during the Mid-Brunhes dissolution interval and the CO<sub>2</sub> paradox of MIS 11. *Quaternary Science Reviews* 25, 3278-3293.
- Baumann, K.-H., Freitag, T., 2004. Pleistocene fluctuations in the northern Benguela Current system as revealed by coccolith assemblages. *Marine Micropaleontology* 52, 195-215.
- Beaufort, L., L., Bolton, C., Sarr, A.-C., Suchéras-Marx, B., Rosenthal, Y., Donnadieu, Y., Barbarin, N., Bova, S., Cornuault, P., Gally, Y., Gray, E., Mazur, J.-C., Tetard, M., 2020. Cyclic evolution of phytoplankton forced by changes in tropical seasonality.
- Bereiter, B., Eggleston, S., Schmitt, J., Nehrbass-Ahles, C., Stocker, T.F., Fischer, H., Kipfstuhl, S., Chappellaz, J., 2015. Revision of the EPICA Dome C CO<sub>2</sub> record from 800 to 600 kyr before present. *Geophysical Research Letters* 42, 542-549.
- Bolton, C.T., Hernández-Sánchez, M.T., Fuertes, M.-A., González-Lemos, S., Abrevaya, L., Mendez-Vicente, A., Flores, J.-A., Probert, I., Giosan, L., Johnson, J., 2016. Decrease in coccolithophore calcification and CO<sub>2</sub> since the middle Miocene. *Nature communications* 7, 1-13.
- Bolton, C.T., Stoll, H.M., 2013. Late Miocene threshold response of marine algae to carbon dioxide limitation. *Nature* 500, 558-562.
- Broecker, W.S., Peng, T.H., 1987. The role of CaCO<sub>3</sub> compensation in the glacial to interglacial atmospheric CO<sub>2</sub> change. *Global Biogeochemical Cycles* 1, 15-29.



- Caves, J.K., Jost, A.B., Lau, K.V., Maher, K., 2016. Cenozoic carbon cycle imbalances and a variable weathering feedback. *Earth and Planetary Science Letters* 450, 152-163.
- Cheng, H., Edwards, R.L., Sinha, A., Spötl, C., Yi, L., Chen, S., Kelly, M., Kathayat, G., Wang, X., Li, X., 2016. The Asian monsoon over the past 640,000 years and ice age terminations. *nature* 534, 640-646.
- De Vleeschouwer, D., Drury, A.J., Vahlenkamp, M., Rochholz, F., Liebrand, D., Pälike, H., 2020. High-latitude biomes and rock weathering mediate climate–carbon cycle feedbacks on eccentricity timescales. *Nature communications* 11, 1-10.
- Flores, J.A., Filippelli, G.M., Sierro, F.J., Latimer, J.C., 2012. The “White Ocean” hypothesis: a late Pleistocene Southern Ocean governed by coccolithophores and driven by phosphorus. *Frontiers in microbiology* 3, 233.
- Fuertes, M.-Á., Flores, J.-A., Sierro, F.J., 2014. The use of circularly polarized light for biometry, identification and estimation of mass of coccoliths. *Marine Micropaleontology* 113, 44-55.
- Giordano, M., Beardall, J., Raven, J.A., 2005. CO<sub>2</sub> concentrating mechanisms in algae: mechanisms, environmental modulation, and evolution. *Annu. Rev. Plant Biol.* 56, 99-131.
- González-Lanchas, A., Flores, J.-A., Sierro, F.J., Bárcena, M.Á., Rigual-Hernández, A.S., Oliveira, D., Azibeiro, L.A., Marino, M., Maiorano, P., Cortina, A., Cacho, I., Grimalt, J.O., 2020. A new perspective of the Alboran Upwelling System reconstruction during the Marine Isotope Stage 11: A high-resolution coccolithophore record. *Quaternary Science Reviews* 245, 106520.
- González-Lanchas, A., Flores, J.A., Sierro, F., Sánchez Goñi, M., Rodrigues, T., Ausin, B., Oliveira, D., Naughton, F., Marino, M., Maiorano, P., Balestra, B., 2021. Control mechanisms of Primary Productivity revealed by calcareous nannoplankton from Marine Isotope Stages 12 to 9 at the Shackleton Site (IODP Site U1385). *Paleoceanography and Paleoclimatology*, e2021PA004246.
- Henderiks, J., Pagani, M., 2007. Refining ancient carbon dioxide estimates: Significance of coccolithophore cell size for alkenone-based *p*CO<sub>2</sub> records. *Paleoceanography* 22.
- Hoogakker, B., Rohling, E., Palmer, M., Tyrrell, T., Rothwell, R., 2006. Underlying causes for long-term global ocean  $\delta^{13}\text{C}$  fluctuations over the last 1.20 Myr. *Earth and Planetary Science Letters* 248, 15-29.
- Jin, X., Liu, C., Zhang, H., Zhou, C., Jiang, X., Wu, Z., Xu, J., 2018. Evolutionary driven of *Gephyrocapsa* coccolith isotopic vital effects over the past 400 ka. *Earth and Planetary Science Letters* 503, 236-247.
- Linge Johnsen, S.A., Bollmann, J., Gebuehr, C., Herrle, J.O., 2019. Relationship between coccolith length and thickness in the coccolithophore species *Emiliania huxleyi* and *Gephyrocapsa oceanica*. *PloS one* 14, e0220725.

- Ma, W., Tian, J., Li, Q., Wang, P., 2011. Simulation of long eccentricity (400-kyr) cycle in ocean carbon reservoir during Miocene Climate Optimum: Weathering and nutrient response to orbital change. *Geophysical Research Letters* 38.
- Ma, W., Wang, P., Tian, J., 2017. Modeling 400–500-kyr Pleistocene carbon isotope cyclicity through variations in the dissolved organic carbon pool. *Global and Planetary Change* 152, 187-198.
- McClelland, H., Barbarin, N., Beaufort, L., Hermoso, M., Ferretti, P., Greaves, M., Rickaby, R., 2016. Calcification response of a key phytoplankton family to millennial-scale environmental change. *Scientific reports* 6, 1-11.
- Meybeck, M., 1987. Global chemical weathering of surficial rocks estimated from river dissolved loads. *American journal of science* 287, 401-428.
- Müller, M.N., Brandini, F.P., Trull, T.W., Hallegraeff, G.M., 2021. Coccolith volume of the Southern Ocean coccolithophore *Emiliana huxleyi* as a possible indicator for palaeo-cell volume. *Geobiology* 19, 63-74.
- Müller, M.N., Trull, T.W., Hallegraeff, G.M., 2015. Differing responses of three Southern Ocean *Emiliana huxleyi* ecotypes to changing seawater carbonate chemistry. *Marine Ecology Progress Series* 531, 81-90
- Penman, D.E., Rugenstein, J.K.C., Ibarra, D.E., Winnick, M.J., 2020. Silicate weathering as a feedback and forcing in Earth's climate and carbon cycle. *Earth-Science Reviews*, 103298.
- Pfuhl, H., Shackleton, N., 2004. Two proximal, high-resolution records of foraminiferal fragmentation and their implications for changes in dissolution. Deep Sea Research Part I: *Oceanographic Research Papers* 51, 809-832.
- Raven, J.A., Crawford, K., 2012. Environmental controls on coccolithophore calcification. *Marine Ecology Progress Series* 470, 137-166.
- Rickaby, R., Bard, E., Sonzogni, C., Rostek, F., Beaufort, L., Barker, S., Rees, G., Schrag, D., 2007. Coccolith chemistry reveals secular variations in the global ocean carbon cycle? *Earth and Planetary Science Letters* 253, 83-95.
- Rost, B., Riebesell, U., 2004. Coccolithophores and the biological pump: responses to environmental changes, *Coccolithophores*. Springer, pp. 99-125.
- Rost, B., Riebesell, U., Burkhardt, S., Sültemeyer, D., 2003. Carbon acquisition of bloom-forming marine phytoplankton. *Limnology and oceanography* 48, 55-67.
- Rugenstein, J.K.C., Ibarra, D.E., von Blanckenburg, F., 2019. Neogene cooling driven by land surface reactivity rather than increased weathering fluxes. *Nature* 571, 99-102.
- Russon, T., Paillard, D., Elliot, M., 2010. Potential origins of 400–500 kyr periodicities in the ocean carbon cycle: A box model approach. *Global Biogeochemical Cycles* 24.
- Schmitt, J., Seth, B., Köhler, P., Willenbring, J., Fischer, H., 2013. Atmospheric CF4 trapped in polar ice—A new proxy for granite weathering. Goldschmidt Conference, Florence, Italy, 25 August 2013 - 30 August 2013.

- Sett, S., Bach, L.T., Schulz, K.G., Koch-Klavsen, S., Lebrato, M., Riebesell, U., 2014. Temperature modulates coccolithophorid sensitivity of growth, photosynthesis and calcification to increasing seawater  $p\text{CO}_2$ . *PloS one* 9, e88308.
- Sigman, D.M., Boyle, E.A., 2000. Glacial/interglacial variations in atmospheric carbon dioxide. *Nature* 407, 859-869.
- Suchéras-Marx, B., Henderiks, J., 2014. Downsizing the pelagic carbonate factory: Impacts of calcareous nannoplankton evolution on carbonate burial over the past 17 million years. *Global and Planetary Change* 123, 97-109.
- Tian, J., Xie, X., Ma, W., Jin, H., Wang, P., 2011. X-ray fluorescence core scanning records of chemical weathering and monsoon evolution over the past 5 Myr in the southern South China Sea. *Paleoceanography* 26.
- Tortell, P.D., 2000. Evolutionary and ecological perspectives on carbon acquisition in phytoplankton. *Limnology and Oceanography* 45, 744-750.
- Wang, P., Tian, J., Cheng, X., Liu, C., Xu, J., 2003. Carbon reservoir changes preceded major ice-sheet expansion at the mid-Brunhes event. *Geology* 31, 239-242.
- Wang, P., Tian, J., Cheng, X., Liu, C., Xu, J., 2004. Major Pleistocene stages in a carbon perspective: The South China Sea record and its global comparison. *Paleoceanography* 19.
- Westbroek, P., Brown, C.W., van Bleijswijk, J., Brownlee, C., Brummer, G.J., Conte, M., Egge, J., Fernández, E., Jordan, R., Knappertsbusch, M., 1993. A model system approach to biological climate forcing. The example of *Emiliana huxleyi*. *Global and planetary change* 8, 27-46.
- Westerhold, T., Marwan, N., Drury, A.J., Liebrand, D., Agnini, C., Anagnostou, E., Barnett, J.S., Bohaty, S.M., De Vleeschouwer, D., Florindo, F., 2020. An astronomically dated record of Earth's climate and its predictability over the last 66 million years. *Science* 369, 1383-1387.
- Young, J.R., Ziveri, P., 2000. Calculation of coccolith volume and its use in calibration of carbonate flux estimates. *Deep sea research Part II: Topical studies in oceanography* 47, 1679-1700.
- Zachos, J., Pagani, M., Sloan, L., Thomas, E., Billups, K., 2001. Trends, rhythms, and aberrations in global climate 65 Ma to present. *Science* 292, 686-693.
- Zeebe, R.E., Wolf-Gladrow, D., 2001. *CO<sub>2</sub> in seawater: equilibrium, kinetics, isotopes*. Gulf Professional Publishing.
- Zhang, H., Liu, C., Hernández-Almeida, I., Mejia, L.M., Stoll, H., 2021. High and low latitude controls on Mid-Brunhes coccolithophore bloom and its implications on ocean carbon cycle.

## Materials and methods

### *Sites and sampling*

The studied materials were collected from four Sites of different latitudes, covering northern subpolar, mid latitude and equatorial/tropical water masses in the North Atlantic: IODP Site U1314 in the southern *Gardar Drift* (56°21.8' N, 27°53.3' W; water depth 2.820 m), Site U1385 in the southwestern Iberian Margin (37°34.285' N, 10°7.562' W; water depth 2.578 m), ODP Site 925 in the western tropical Atlantic *Ceara Rise* (4°12.2' N, 43°29.3' W; water depth 3.040 m) and the Mediterranean Sea: ODP Site 977 in the Alboran Sea (36° 1.9' N, 1° 57.3' W; water depth 1.984 m; Fig. 1). The age models for Sites U1385, 925 and 977 are based on the isotope stratigraphy in comparison with the LR04 (Hodell et al., 2015; Wilkens et al., 2017) and, for Site U1314, by correlation of the color reflectance with the  $\delta^{18}\text{O}$ -dated nearby Site 983 (Gruetzner and Higgins, 2010).

A set of 8 samples corresponding to each isotopic stage from MIS 14 to MIS 7 were selected for image analysis and individual morphometric measurements of *Gephyrocapsa* coccoliths, whereas a higher resolution of 16 samples were considered for micropaleontological analysis of coccolithophore assemblages. Only in the case of Site 977 a higher number, of 37 samples were considered for micropaleontological analysis.

### *Micropaleontological analysis*

Samples for analysis of coccolithophore (coccolith) assemblage were prepared following the quantitative settling technique that produces an homogeneous distribution of coccoliths, by Flores and Sierro (1997), and studied with the use of a Nikon eclipse 80i petrographic microscope with 1000x magnification. A minimum of 400 coccoliths were counted for each sample in a variable number of fields of views. Initial taxonomic criteria for *Gephyrocapsa* species identification are summarized in Table S1.

Coccolith counts are presented as percentages (%) and absolute values (N; coccolith  $\text{g}^{-1}$  sediment) calculated following equation by Flores and Sierro (1997).

### *Morphometric measurements of *Gephyrocapsa* coccoliths*

Microscope slides were used for image analysis. Between 50 and 60 random fields of view per sample were imaged with the use of a Nikon DS-Fi1 8-bit colour digital camera installed on a Nikon eclipse LV100 POL microscope equipped with circular polarization. A detailed description of the circular polarization microscope set-up applied in this study can be found in Fuertes et al. (2014).

The birefringence-based method to provide coccolith size and mass measurements bases on the establishment of a direct relationship between the thickness of a calcite particle and the color generated under polarized light (Fuertes et al., 2014). For calibration consistency, microscopical light conditions and camera settings kept constant and calibration images of the same calcite particle were taken at every session: in this study, a *Rhabdosphaera* nannolith was used (Fuertes et al., 2014).

Images were processed with the use of C-Calcita software by Fuertes et al. (2014). Automatic selection of individual particles between 2 and 6  $\mu\text{m}$  were isolated with this software in between 50 and 60 random fields of view ensuring the obtention of a minimum of 100 *Gephyrocapsa* coccoliths belonging to each of the size ranges under and over 3  $\mu\text{m}$  (respectively termed small and medium *Gephyrocapsa*). Coccolith images were selected from the output files after visual evaluation. Birefringence limitations allows the applicability of the method only to coccoliths thinner than 1.5  $\mu\text{m}$  (Bolton et al., 2016); this does not interfere with our procedure because the thickness of *Gephyrocapsa* coccoliths is below this threshold. Coccolith length, width, area, and volume were automatically obtained with C- calcita (Fuertes et al., 2014)

### ***Calculations for coccolithophore calcification estimation***

Recent contributions (Linge Johnsen et al., 2019 and references therein) showed the existence of an allometric relationship between the changes in coccolith thickness and its length and mass, confirming that a size correction is always required to properly determine a calcification estimate from coccolith morphometrical data (Bolton et al., 2016; McClelland et al., 2016). Such a critical issue is overcome here by the corrections applied for the calculation of SN Thickness,  $k$  value and PIC/POC, following the procedures proposed by Bolton et al. (2016) and Jin et al. (2018), that summarize previous references included in these works. However, these parameters are not unequivocally exempt from being affected by post nucleation external effects, such as

dissolution. As such, the potential effect of preservation/dissolution over these measurements and calculations, and the adequacy of these proxies to be considered as indicators of cellular calcification are required to be discussed.

The thickness a coccolith is calculated as the relationship between the volume of a coccolith and its area:

$$\text{Coccolith Thickness (CT)} = \text{coccolith volume} / \text{coccolith area} \quad (2)$$

For the calculation of the coccolith area, the major and minor axes (Ma and ma, respectively) were integrated in the generic formula for ellipse area, that is considered the as the most representative geometry of Noëlaerhabdaceae (i.e., Bolton et al. (2016):

$$\text{Coccolith Area} = \pi * (\text{Ma} / 2) * (\text{ma} / 2) \quad (3)$$

To evaluate changes in coccolith thickness within the *Gephyrocapsa* complex in our samples, we normalized the thickness values as in Bolton et al., (2016) by applying the following the Size Normalized (SN) Thickness protocol by O’Dea et al. (2014):

$$\text{SN Thickness} = [(\text{ML} - \text{CL}) * \text{S}] + \text{CT} \quad (4)$$

Where: ML = mean coccolith length; CL = length of each individual coccolith in sample; S = slope of the regression between coccolith length and coccolith thickness for all coccoliths in sample; CT = original thickness of each individual coccolith in sample.

One of the most widely used and accurate approaches to estimate the coccolith volume of a given coccolithophore species is through the application of the following formula:

$$\text{Volume} = k l^3 \quad (5)$$

where volume is the volume of the coccolith, “l” is coccolith length and *k* is the shape factor. This parameter is specific for each coccolithophore species and represents the fraction of the volume of a cube defined by the surface length of a coccolith (see Young and Ziveri, 2000 for more details). This dimensionless number entails not only a change in the shape, but also a change in the degree of structural calcification, as recently discussed by Bolton et al. (2016) and Jin et al. (2018). Following these studies, we back-calculated the *k* values from the available coccolith mass and length values in this study using the formula by Young and Ziveri (2000):

$$k \text{ value} = \text{mass} / [2.7 * \text{length}^3] \quad (6)$$

where 2.7 is the density of calcite (pg/μm<sup>3</sup>). The coccolith length corresponds to Ma in this study.

The inorganic/organic carbon (PIC/POC) is the direct ratio of integrated rates of calcification to photosynthesis (Rost and Riebesell, 2004). For the calculation of this parameter, from the morphometrical parameters of length and thickness, we followed the approach in Jin et al., (2018) which is based in the application of the dimensional and volumetrical relationships in Aloisi (2015) and McClelland et al. (2016).

### ***Estimation of dissolution***

A foraminiferal test fragmentation index was produced at IODP Site U1314 (Fig. 2e), considered as an evidence of carbonate dissolution above the lysocline (Dittert and Henrich, 2000; Peterson and Prell, 1985; Thunell, 1976).

Counts of planktic foraminifera and fragments were performed in the 65–150  $\mu\text{m}$  fraction after cleaning with deionized water and dry-sieved through, respectively 63 and 150  $\mu\text{m}$  mesh.

### ***Considerations for the indicators of pelagic carbonate concentration***

Different type of data is considered indicative of the concentration of pelagic carbonate concentration in the sediments from the studied sites.

Only for Site U1314, the direct %  $\text{CaCO}_3$  values were available at resolution enough (Gruetzner and Higgins, 2010). At the Site U1385, the Log Ti/Ca is considered, where increase values are indicative of increased carbonated production and/or reduced terrigenous supply (Hodell et al., 2015). Magnetic susceptibilities are known to be the result of the standard ratio between detrital magnetic to non magnetic minerals. At the Site 925, this profile traces the influence of Amazon plumes dispersed in surface towards *Ceara Rise*, the location of the Site (e.g., Francois and Bacon, 1991), a fact observed by previous authors to result in stimulated biogenic blooming production at the location of the Site (e.g., González-Lanchas et al., 2021; Guerreiro et al., 2017; Korte et al., 2020). Thus, increased magnetic susceptibilities in the spliced profile at Site 925 by Wilkens et al. (2017) are interpreted as representative of increased pelagic carbonate accumulation in sediments. At Site 977, the balance between magnetic to non magnetic minerals is more likely controlled by deep processes of terrigenous transport, exerting dilution on the amount of pelagic carbonate; thus, increased magnetic susceptibilities at this location

(Comas et al., 1996) are simply representative of increased terrigenous accumulation and/or reduced biogenic carbonated production.

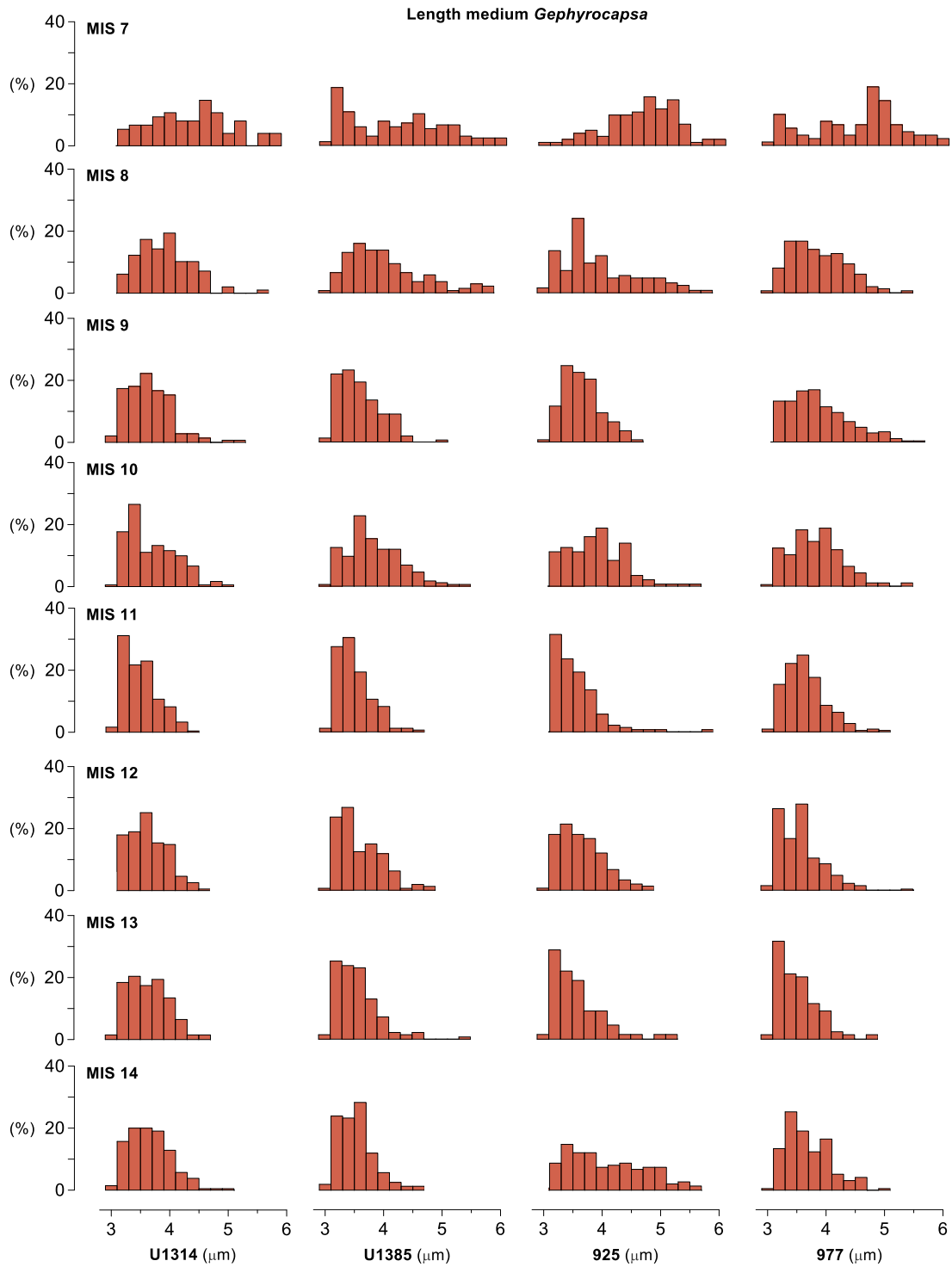
## Methods References

- Aloisi, G., 2015. Covariation of metabolic rates and cell size in coccolithophores. *Biogeosciences* 12, 4665-4692.
- Bolton, C.T., Hernández-Sánchez, M.T., Fuertes, M.-A., González-Lemos, S., Abrevaya, L., Mendez-Vicente, A., Flores, J.-A., Probert, I., Giosan, L., Johnson, J., 2016. Decrease in coccolithophore calcification and CO<sub>2</sub> since the middle Miocene. *Nature communications* 7, 1-13.
- Comas, M., Zahn, R., Klaus, A., 1996. Preliminary results of ODP Leg 161. *Proceeding Ocean Drilling Program, Preliminary Results* 161, 1-1679.
- Dittert, N., Henrich, R., 2000. Carbonate dissolution in the South Atlantic Ocean: evidence from ultrastructure breakdown in *Globigerina bulloides*. *Deep Sea Research Part I: Oceanographic Research Papers* 47, 603-620.
- Flores, J., Sierro, F., 1997. Revised technique for calculation of calcareous nannofossil accumulation rates. *Micropaleontology*, 321-324.
- Francois, R., Bacon, M.P., 1991. Variations in terrigenous input into the deep equatorial Atlantic during the past 24,000 years. *Science* 251, 1473-1476.
- Fuertes, M.-Á., Flores, J.-A., Sierro, F.J., 2014. The use of circularly polarized light for biometry, identification and estimation of mass of coccoliths. *Marine Micropaleontology* 113, 44-55.
- González-Lanchas, A., Hernández-Alméida, I., Flores, J.A., Sierro, F., Guitian, J., Stoll, H., 2021b. Carbon Isotopic Fractionation of Alkenones and Gephyrocapsa Coccoliths Over the Late Quaternary (Marine Isotope Stages 12–9) Glacial-Interglacial Cycles at the Western Tropical Atlantic. *Paleoceanography and Paleoclimatology* 36, e2020PA004175.
- Gruetzner, J., Higgins, S., 2010. Threshold behavior of millennial scale variability in deep water hydrography inferred from a 1.1 Ma long record of sediment provenance at the southern Gardar Drift. *Paleoceanography* 25.
- Guerreiro, C.V., Baumann, K.-H., Brummer, G.-J.A., Fischer, G., Korte, L.F., Merkel, U., Sá, C., De Stigter, H., Stuut, J.-B.W., 2017. Coccolithophore fluxes in the open tropical North Atlantic: influence of thermocline depth, Amazon water, and Saharan dust. *Biogeosciences* 14, 4577-4599.
- Hodell, D., Lourens, L., Crowhurst, S., Konijnendijk, T., Tjallingii, R., Jiménez-Espejo, F., Skinner, L., Tzedakis, P., Members, T.S.S.P., Abrantes, F., 2015. A reference time scale for Site U1385 (Shackleton Site) on the SW Iberian Margin. *Global and Planetary Change* 133, 49-64.
- Jin, X., Liu, C., Zhang, H., Zhou, C., Jiang, X., Wu, Z., Xu, J., 2018. Evolutionary driven of Gephyrocapsa coccolith isotopic vital effects over the past 400 ka. *Earth and Planetary Science Letters* 503, 236-247.

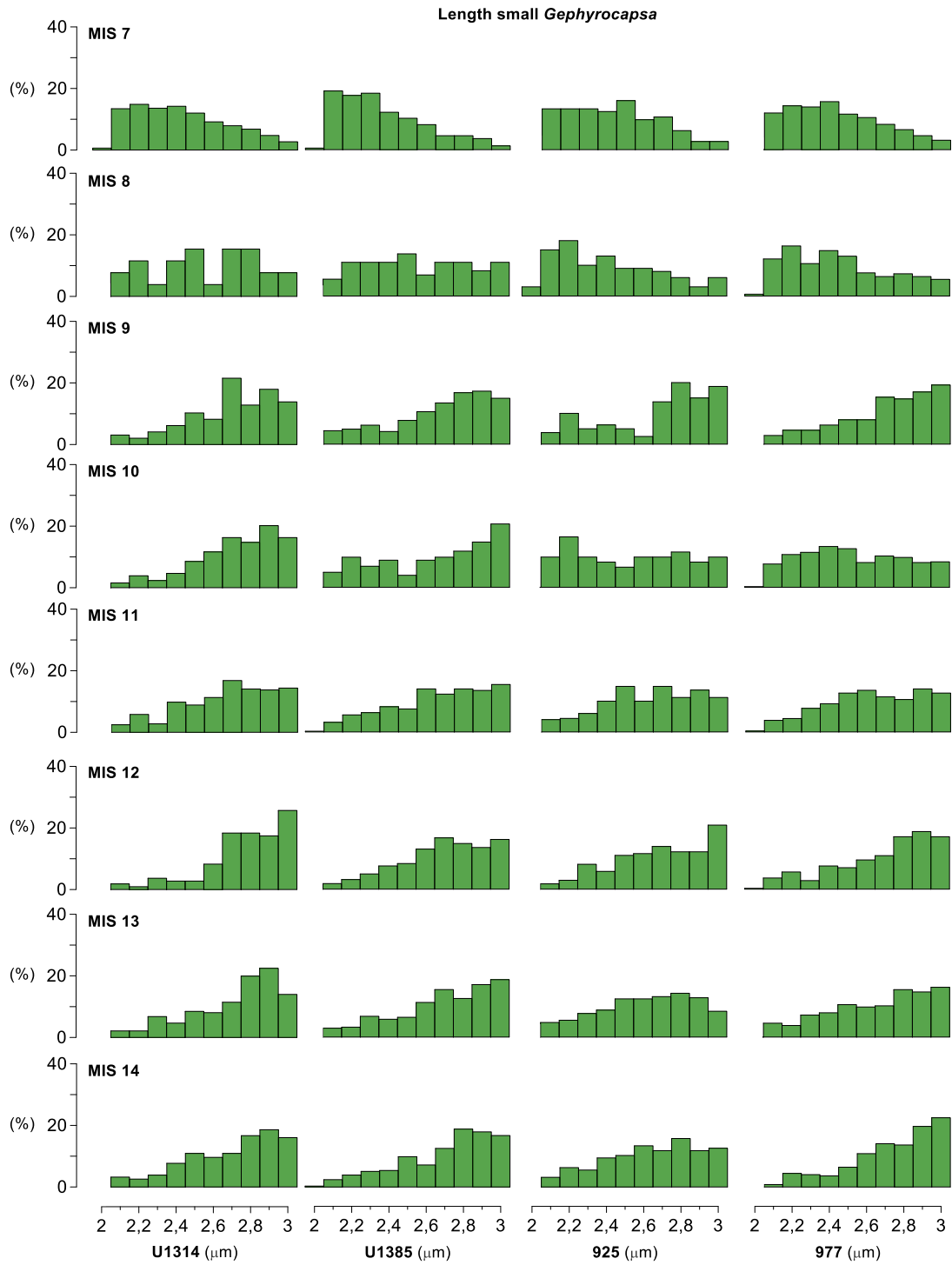


- Korte, L.F., Brummer, G.J.A., van der Does, M., Guerreiro, C.V., Mienis, F., Munday, C.I., Ponsoni, L., Schouten, S., Stuut, J.B.W., 2020. Multiple drivers of production and particle export in the western tropical North Atlantic. *Limnology and Oceanography* 65 (9).
- Linge Johnsen, S.A., Bollmann, J., Gebuehr, C., Herrle, J.O., 2019. Relationship between coccolith length and thickness in the coccolithophore species *Emiliana huxleyi* and *Gephyrocapsa oceanica*. *PloS one* 14, e0220725.
- McClelland, H., Barbarin, N., Beaufort, L., Hermoso, M., Ferretti, P., Greaves, M., Rickaby, R., 2016. Calcification response of a key phytoplankton family to millennial-scale environmental change. *Scientific reports* 6, 1-11.
- O’Dea, S.A., Gibbs, S.J., Bown, P.R., Young, J.R., Poulton, A.J., Newsam, C., Wilson, P.A., 2014. Coccolithophore calcification response to past ocean acidification and climate change. *Nature communications* 5, 1-7.
- Peterson, L., Prell, W., 1985. Carbonate dissolution in recent sediments of the eastern equatorial Indian Ocean: preservation patterns and carbonate loss above the lysocline. *Marine Geology* 64, 259-290.
- Rigual-Hernández, A.S., Trull, T.W., Flores, J.A., Nodder, S.D., Eriksen, R., Davies, D.M., Hallegraeff, G.M., Sierro, F.J., Patil, S.M., Cortina, A., Ballegeer, A.M., Northcote, L.C., Abrantes, F., Rufino, M.M., 2020. Full annual monitoring of Subantarctic *Emiliana huxleyi* populations reveals highly calcified morphotypes in high-CO<sub>2</sub> winter conditions. *Scientific Reports* 10.
- Rost, B., Riebesell, U., 2004. Coccolithophores and the biological pump: responses to environmental changes, *Coccolithophores*. Springer, pp. 99-125.
- Thunell, R.C., 1976. Optimum indices of calcium carbonate dissolution, in deep-sea sediments. *Geology* 4, 525-528.
- Wilkens, R.H., Westerhold, T., Drury, A.J., Lyle, M., Gorgas, T., Tian, J., 2017. Revisiting the Ceara Rise, equatorial Atlantic Ocean: isotope stratigraphy of ODP Leg 154 from 0 to 5Ma. *Climate of the Past* 13, 779-793.
- Young, J.R., Ziveri, P., 2000. Calculation of coccolith volume and its use in calibration of carbonate flux estimates. *Deep sea research Part II: Topical studies in oceanography* 47, 1679-1700.

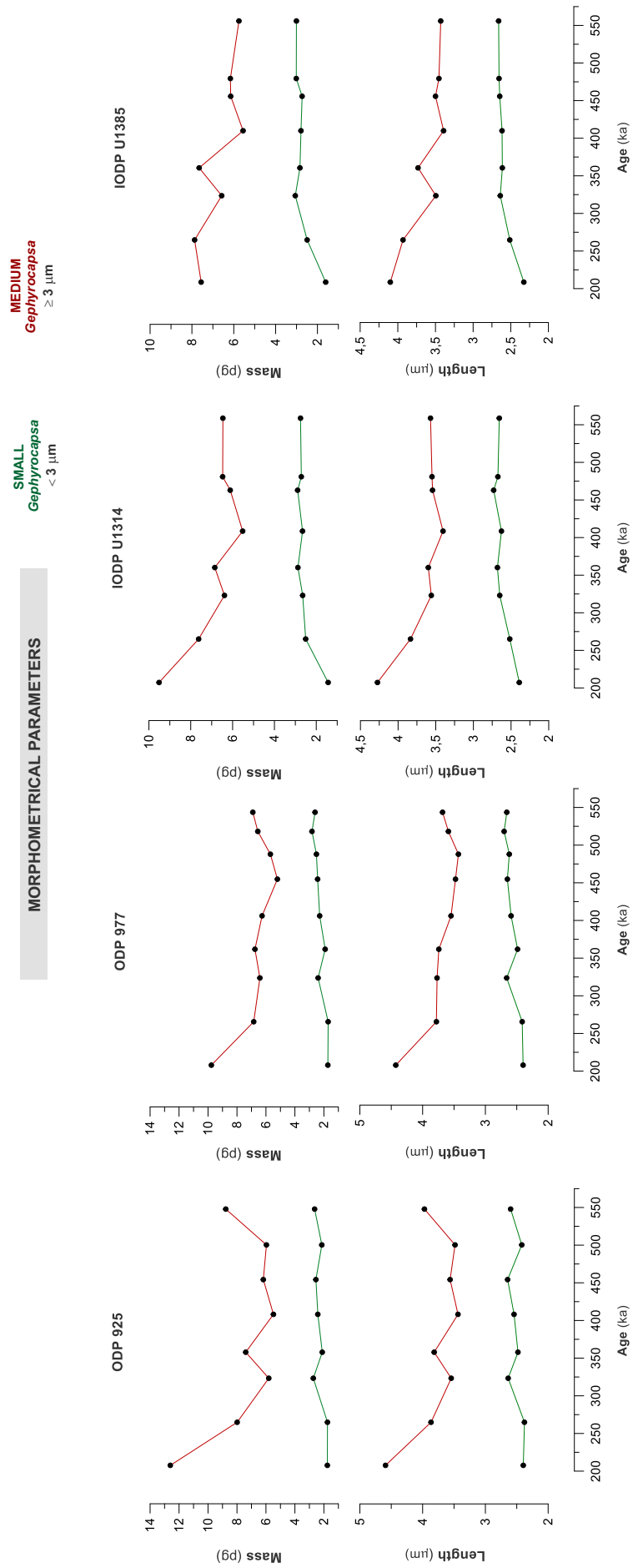
**Supplementary Information** for the article “*About the Mid-Brunhes interval and the role of the stumper coccolithophore Gephyrocapsa complex*” by Alba González-Lanchas et al.



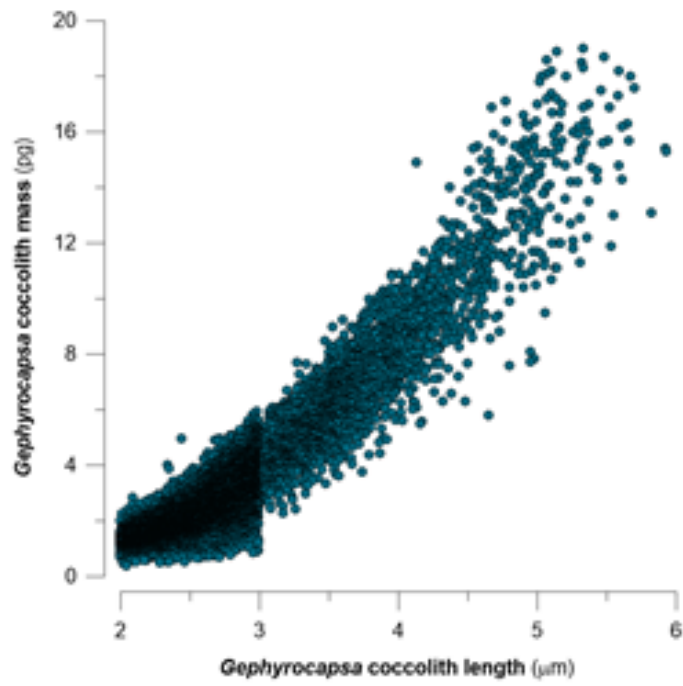
**Supplementary Figure 1 (Figure S1).** Histograms of frequency of the levels of variability in the values of length (coccolith size) in medium *Gephyrocapsa* coccoliths at the different locations over the MIS 14 to 7 interval.



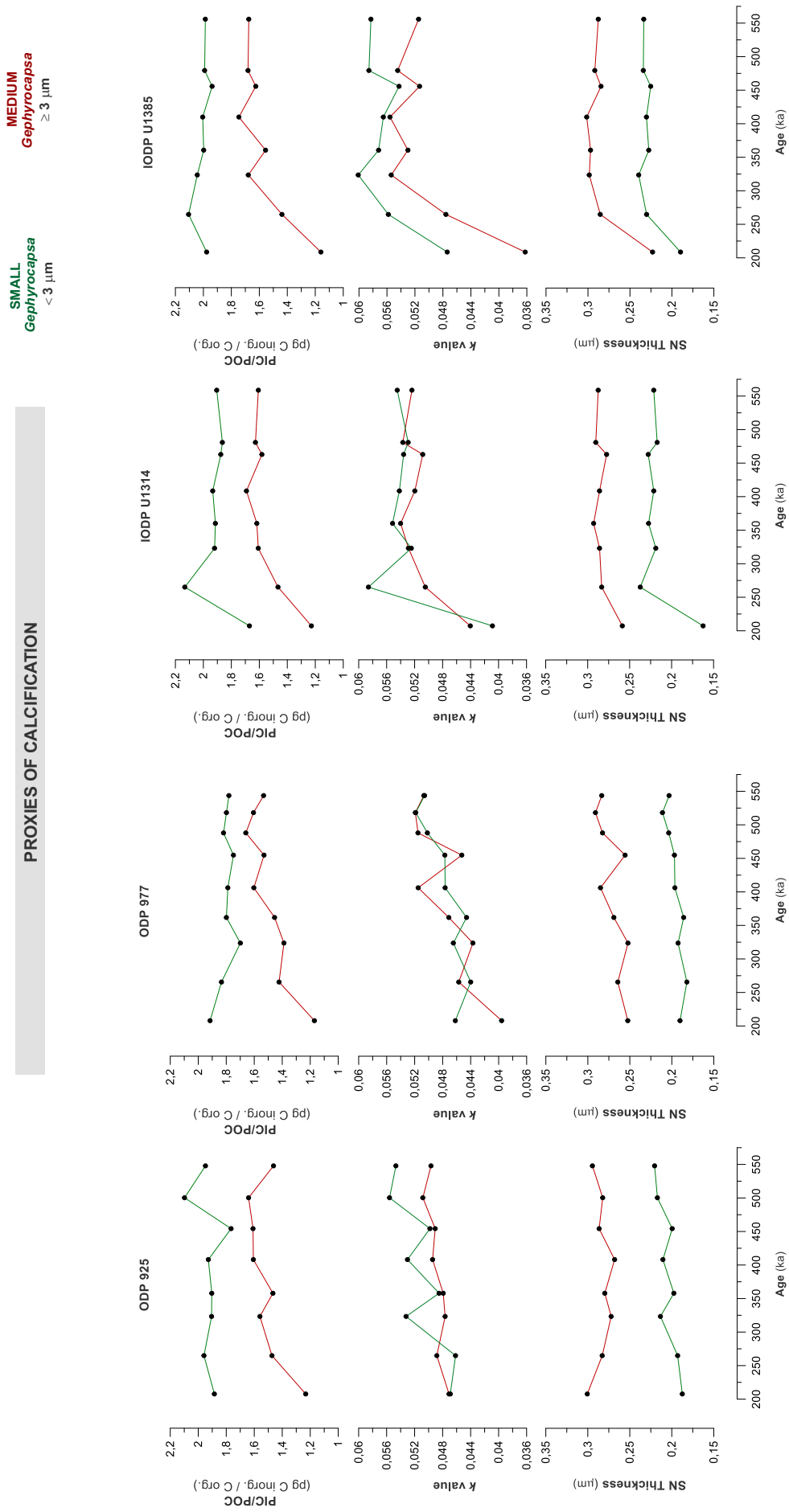
**Supplementary Figure 2 (Figure S2).** Histograms of frequency of the levels of variability in the values of length (coccolith size) in small *Gephyrocapsa* coccoliths at the different locations over the MIS 14 to 7 interval.



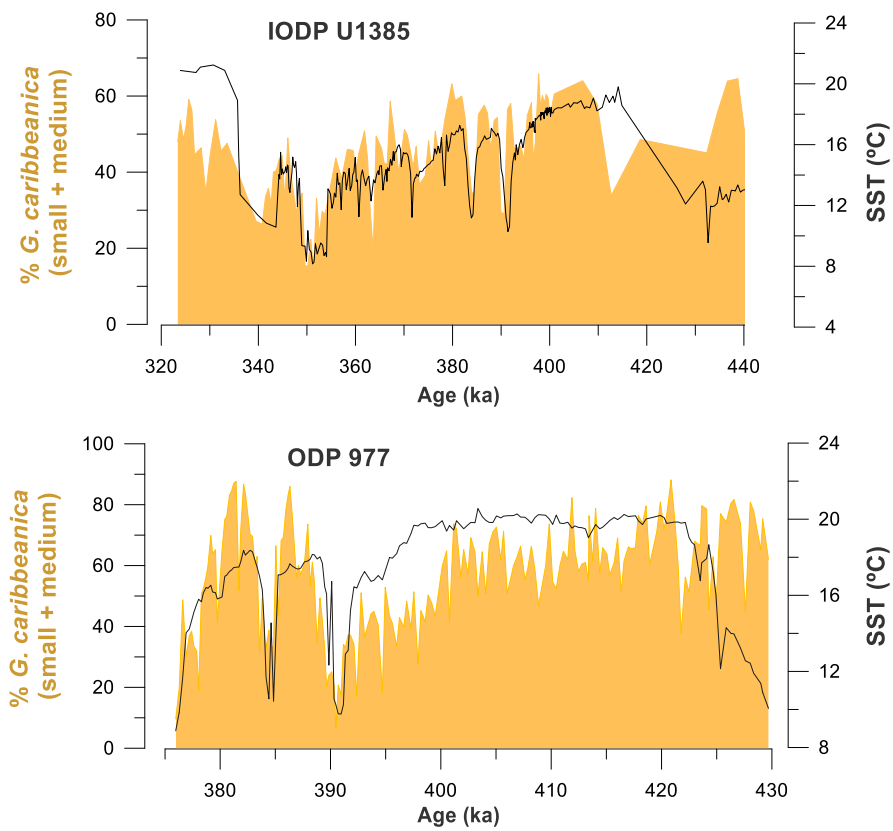
**Supplementary Figure 3 (Figure S3).** Time series plots of the evolution of the average values of coccolith length and mass in small (green) and medium (red) *Gephyrocapsa* at the different locations over the MIS 14 to 7 interval. The axes have been adjusted to yield the range that together includes both size classes.



**Supplementary Figure 4 (Figure S4).** Correlation between coccolith size and mass for each of the small and medium *Gephyrocapsa* classes measured in this study.

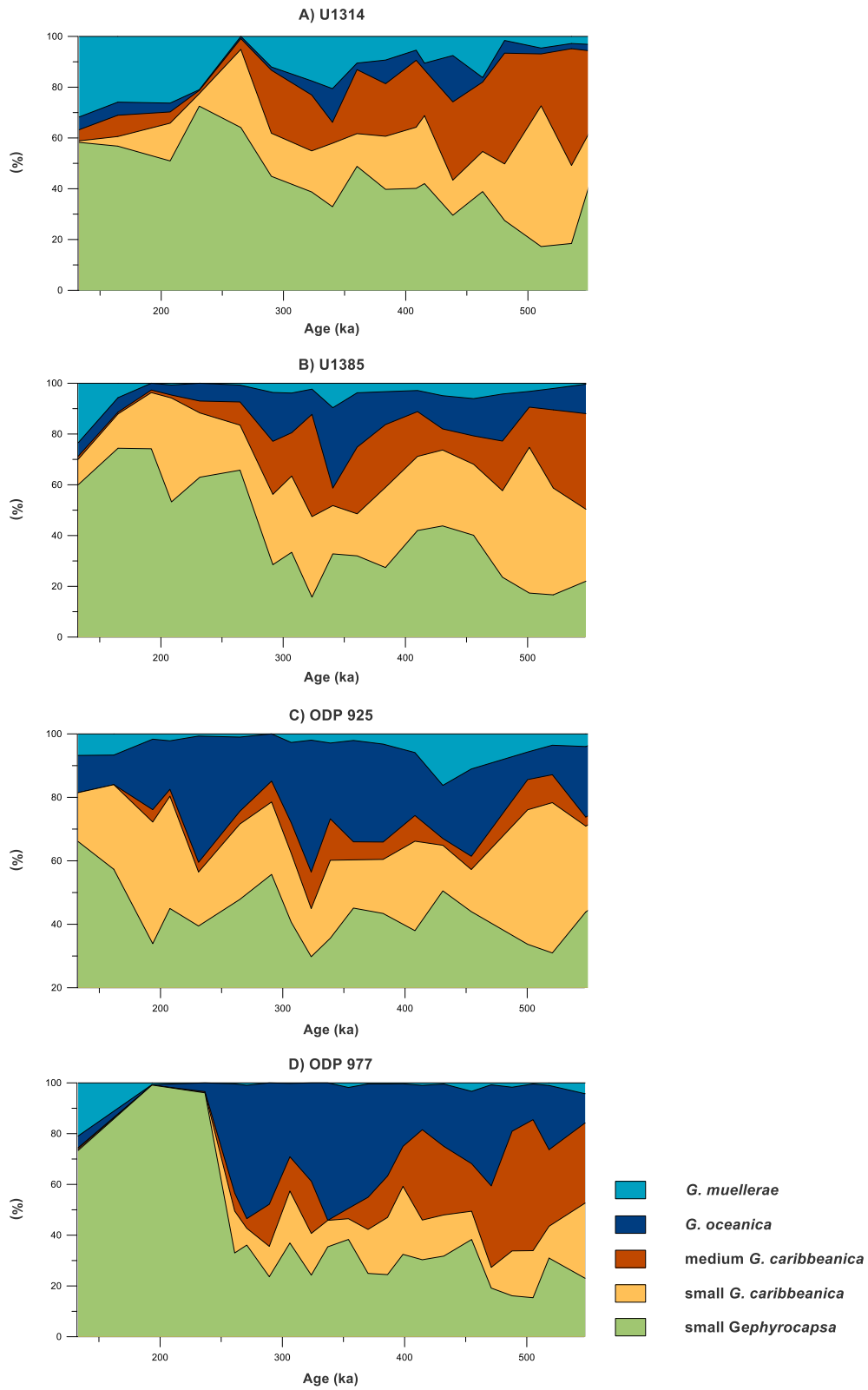


**Supplementary Figure 5 (Figure S5).** Time series plots of the evolution of the average values of Size Normalized (SN) Thickness,  $k$  value and the PIC/POC value in small (green) and medium (red) *Gephyrocapsa* at the different locations over the MIS 14 to 7 interval. The axes have been adjusted to yield the range that together includes both size classes.

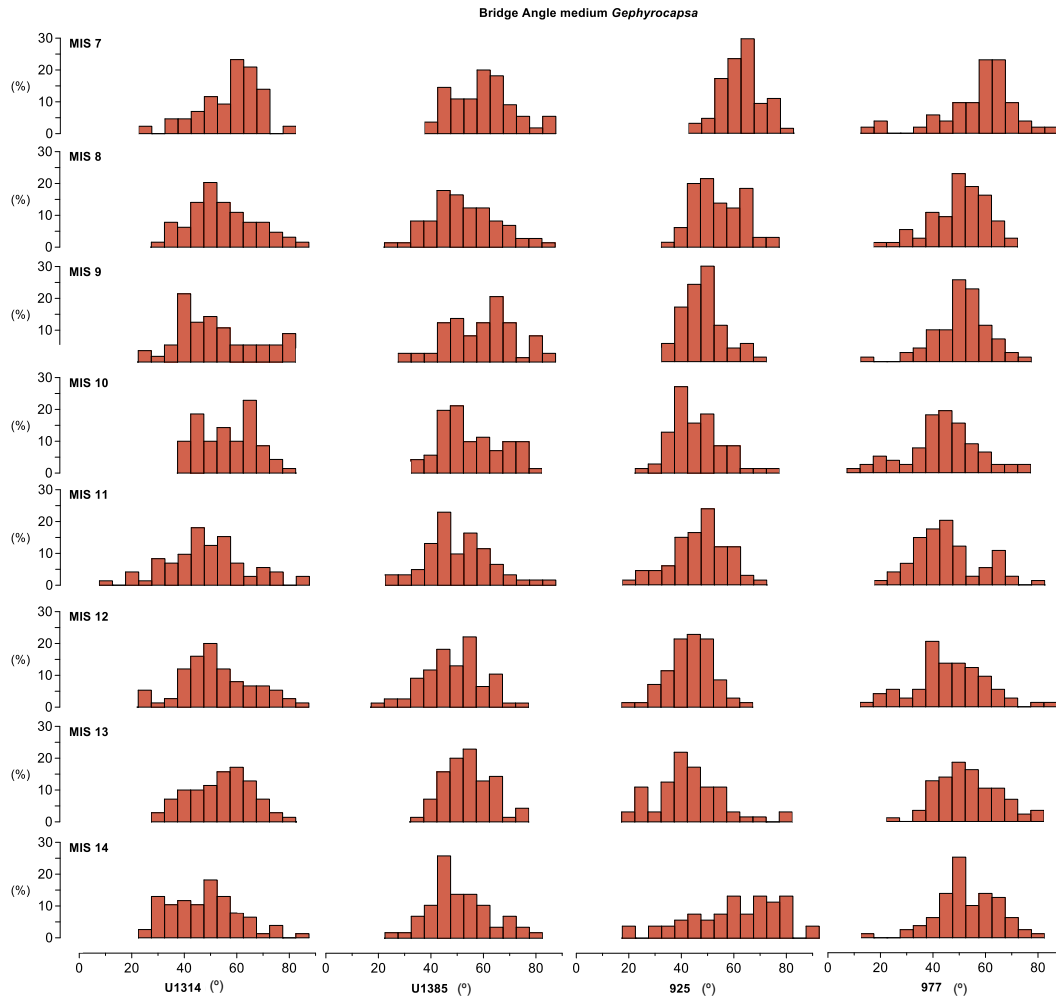


**Supplementary Figure 6 (Figure S6).** Visual correlation between high resolution % “*G. caribbeanica*” profiles and SST values at the Iberian Margin Sites ODP 977 (González-Lanchas et al., 2020) and IODP U1385 (González-Lanchas et al., 2021).





**Supplementary Figure 7 (Figure S7).** Percentage distribution of *Gephyrocapsa* species or groups in the studied sites.



**Supplementary Figure 8 (Figure S8).** Frequency histogram of the levels of variability in the values of bridge angle (inclination of the central bar respect to the major axis) in medium *Gephyrocapsa* coccoliths at the different locations over the MIS 14 to 7 interval.

### **Supplementary Text1 (Text S1). Bridge angle measurements in medium *Gephyrocapsa***

The bridge angle was manually measured and numerically computerized with the use of the software NIS-elements Advanced Research in a variable number between 50 to 70 of the randomly selected medium *Gephyrocapsa* coccoliths ( $>3 \mu\text{m}$ ) from each sample in the studied sites. The main results of this analysis are represented in the supplementary Figure S8.

Since the different *Gephyrocapsa* species are characterized by specific ranges of bridge angle inclination (Table S1), this parameter can be used as an independent indicator of species variety. Following the traditional taxonomical considerations (Table S1), a bridge angles ranging between  $40\text{-}50^\circ$  suggest that a shift towards an almost monomorphotypic assemblage of *Gephyrocapsa* led the coccolith size reduction observed during the MIS 13-11 intervals (Figure S8). The reduction in the bridge inclination is particularly visible in Sites 925 and 977, where its natural population is biogeographically more distant to the presence of *G. muelleriae*-type morphotypes of lower bridge angle (González-Lanchas et al., 2020; Kinkel et al., 2000), in comparison with the mid and high latitude Atlantic Sites U1385 y U1314 (González-Lanchas et al., 2021). The reduced variety towards the middle part of the Mid Brunhes in all sites confirm the domain of a unique morphotype driving the morphometrical coccolith size reduction. Under the classical perspective, that considers "*G. caribbeanica*" to all those individuals with an inclination of the central bridge around  $45^\circ$  (Table S1), this would be the group that led the size and mass reduction and the overall increase in calcification during the interval. The connection of calcification reconstruction profiles with the % "*G. caribbeanica*" also supports this preliminar idea (Fig. 3).

This study	small <i>Gephyrocapsa</i>	<i>G. muellerae</i> / <i>muellerae</i>	“ <i>G.</i> <i>caribbeanica</i> ”	<i>G. oceanica</i>
Maximum length	< 3 µm	> 3 µm	> 3 µm	> 3 µm
Bridge angle	-	< 25°/ < 40°	30-65° / closed central area	> 40°
Previous authors				
(Thierstein et al., 1977)	-	<i>G. caribbeanica</i>		
(Bréhéret and JG, 1978)	<i>G. ericsonii</i> / <i>G.</i> <i>aperta</i>	<i>G. muellerae</i>	<i>G. caribbeanica</i>	<i>G. oceanica</i>
(Samtleben, 1980)	<i>Gephyrocapsa</i> spp. (several)	<i>G. muellerae</i>	<i>G. caribbeanica</i>	<i>G. oceanica</i>
(Matsuoka and Okada, 1989)	<i>Gephyrocapsa</i> sp. D (small)	<i>Gephyrocapsa</i> sp. D	<i>Gephyrocapsa</i> sp. D (small)	<i>Gephyrocapsa</i> sp. D (large)
(Raffi et al., 1993)	small <i>Gephyrocapsa</i>	small <i>Gephyrocapsa</i>	small <i>Gephyrocapsa</i>	medium <i>Gephyrocapsa</i>
(Jordan et al., 1996)	<i>G. aperta</i> / <i>G.</i> <i>ericsonii</i>	<i>G. muellerae</i>	-	<i>G. oceanica</i>
(Bollmann, 1997)	<i>G. minute</i>	<i>G. cold</i>	<i>G. oligotrophic</i> / <i>G. transitional</i>	<i>G. large</i> / <i>G.</i> <i>equatorial</i>
(Flores et al., 2000)	small <i>Gephyrocapsa</i>	<i>G. muellerae</i>	<i>G. caribbeanica</i>	<i>G. oceanica</i>

**Supplementary Table 1 (Table S1)** Taxonomic criteria for *Gephyrocapsa* species identification based in previous authors detailed.

a)

<b>SN Thickness</b>	U1314	U1385	925	977
U1314	1			
U1385	<b>0.93</b>	1		
925	<b>-0.63</b>	<b>-0.79</b>	1	
977	<b>0.58</b>	<b>0.45</b>	<b>-0.13</b>	1

b)

<b>k value</b>	U1314	U1385	925	977
U1314	1			
U1385	<b>0.94</b>	1		
925	<b>0.53</b>	<b>0.53</b>	1	
977	<b>0.71</b>	<b>0.70</b>	<b>0.86</b>	1

c)

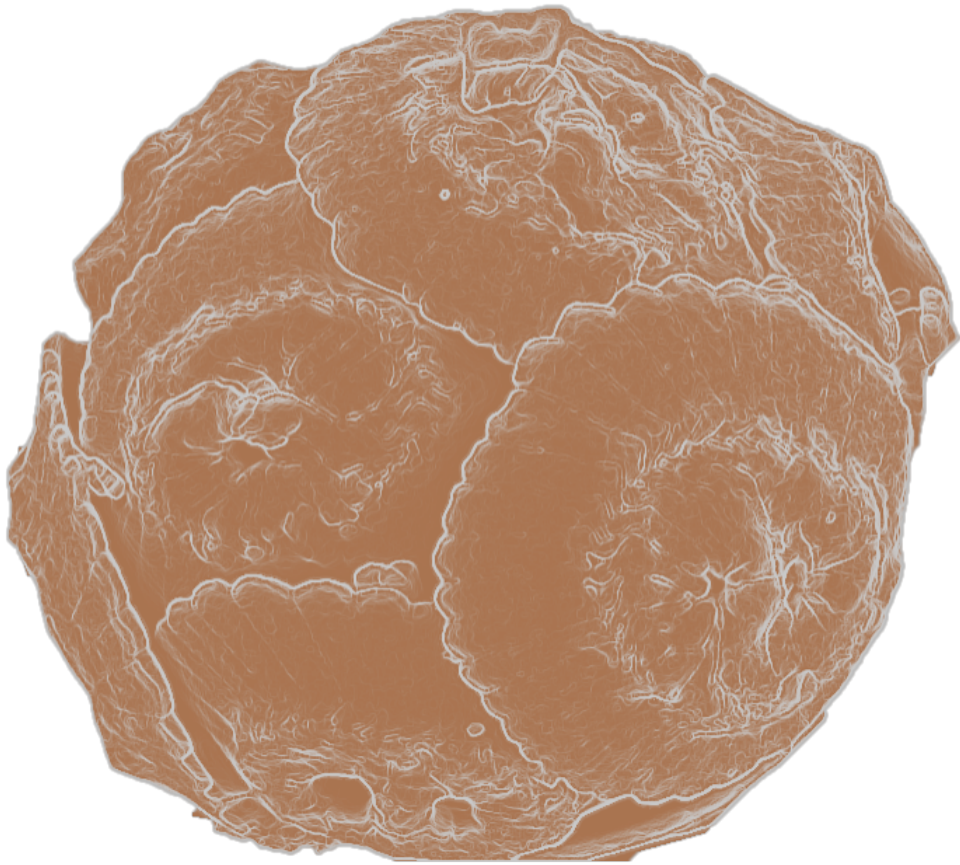
<b>PIC/POC</b>	U1314	U1385	925	977
U1314	1			
U1385	<b>0.97</b>	1		
925	<b>0.87</b>	<b>0.89</b>	1	
977	<b>0.85</b>	<b>0.87</b>	<b>0.82</b>	1

**Supplementary Table 2 (Tables S2a, S2b and S2c).** Matrix of correlation coefficients (R) for the three proxies of calcification, calculated for medium *Gephyrocapsa*, between the different sites: **a)** SN Thickness (SN Th), **b)** *k* value and **c)** PIC/POC.

## Supplementary References

- Bollmann, J., 1997. Morphology and biogeography of Gephyrocapsa coccoliths in Holocene sediments. *Marine Micropaleontology* 29, 319-350.
- Bréhéret, J., JG, B., 1978. Formes nouvelles quaternaires et actuelles de la famille des Gephyrocapsaceae (Coccolithophorides).
- Flores, J.-A., Gersonde, R., Sierro, F., Niebler, H.-S., 2000. Southern Ocean Pleistocene calcareous nannofossil events: calibration with isotope and geomagnetic stratigraphies. *Marine Micropaleontology* 40, 377-402.
- González-Lanchas, A., Flores, J.-A., Sierro, F.J., Bárcena, M.Á., Rigual-Hernández, A.S., Oliveira, D., Azibeiro, L.A., Marino, M., Maiorano, P., Cortina, A., Cacho, I., Grimalt, J.O., 2020. A new perspective of the Alboran Upwelling System reconstruction during the Marine Isotope Stage 11: A high-resolution coccolithophore record. *Quaternary Science Reviews* 245, 106520.
- González-Lanchas, A., Flores, J.A., Sierro, F., Sánchez Goñi, M., Rodrigues, T., Ausin, B., Oliveira, D., Naughton, F., Marino, M., Maiorano, P., Balestra, B., 2021. Control mechanisms of Primary Productivity revealed by calcareous nanoplankton from Marine Isotope Stages 12 to 9 at the Shackleton Site (IODP Site U1385). *Paleoceanography and Paleoclimatology*, e2021PA004246.
- Jordan, R., Zhao, M., Eglinton, G., Weaver, P., 1996. Coccolith and alkenone stratigraphy and palaeoceanography at an upwelling site off NW Africa (ODP 658C) during the last 130,000 years, *Microfossils and oceanic environments*. UWP, Aberystwyth, pp. 111-130.
- Kinkel, H., Baumann, K.-H., Cepek, M., 2000. Coccolithophores in the equatorial Atlantic Ocean: response to seasonal and Late Quaternary surface water variability. *Marine Micropaleontology* 39, 87-112.
- Matsuoka, H., Okada, H., 1989. Quantitative analysis of Quaternary nanoplankton in the subtropical northwestern Pacific Ocean. *Marine Micropaleontology* 14, 97-118.
- Raffi, I., Backman, J., Rio, D., Shackleton, N.J., 1993. Plio-Pleistocene Nannofossil Biostratigraphy and Calibration to Oxygen Isotope Stratigraphies from Deep Sea Drilling Project Site 607 and Ocean Drilling Program Site 677. *Paleoceanography* 8, 387-408.
- Samtleben, C., 1980. Die Evolution der Coccolithophoriden-Gattung Gephyrocapsa nach Befunden im Atlantik. *Paläontologische Zeitschrift* 54, 91-127.
- Thierstein, H., Geitzenauer, K., Molino, B., Shackleton, N., 1977. Global synchronicity of late Quaternary coccolith datum levels Validation by oxygen isotopes. *Geology* 5, 400-404.





## **Conclusiones**



## CAPÍTULO 7. Conclusiones

En este trabajo se han abordado distintos casos de estudio relacionados con la evolución de las condiciones paleoceanográficas y paleoclimáticas en el Atlántico Norte y el sector occidental del Mediterráneo durante el intervalo del Mid-Brunhes y la evolución del papel del complejo *Gephyrocapsa*. Más específicamente, los temas abordados en los artículos que constituyen esta tesis doctoral se agrupan en los tres bloques de reconstrucción paleoceanográfica de alta resolución en el margen ibérico, a partir de la señal del complejo *Gephyrocapsa* (Capítulos 2, 3 y 5), evaluación de la sensibilidad del fraccionamiento isotópico del carbono orgánico ( $\epsilon_p$ ) al CO<sub>2</sub> y de los efectos vitales de *Gephyrocapsa* en el sector Oeste del Atlántico tropical (Capítulo 4) y la caracterización morfométrica y de los cambios en la calcificación del complejo *Gephyrocapsa* a lo largo del transecto en el que se integran todos los testigos analizados en esta tesis doctoral, en el Atlántico Norte y el sector occidental del mar Mediterráneo (Capítulo 6).

Los cinco capítulos referidos con anterioridad contienen, además del desarrollo completo de las investigaciones individuales, la descripción extendida y con alto grado de detalle de las conclusiones independientemente establecidas, particularmente referidas a los objetivos y el planteamiento seguido en cada artículo. De este modo, a continuación, lejos de presentar de nuevo la totalidad de las conclusiones de los diferentes artículos en capítulos anteriores, lo que se presenta es una síntesis general en la que se extraen aquellas conclusiones principales, de carácter más general y de mayor relevancia acerca de la evolución del intervalo del Mid-Brunhes y del complejo *Gephyrocapsa*. No obstante, y para mayor claridad, se ha mantenido la agrupación de los tres bloques anteriormente mencionados, dentro de cada cual las conclusiones aparecen numeradas.

### **Reconstrucción paleoceanográfica de alta resolución en el margen ibérico a partir de la señal del complejo *Gephyrocapsa***

1. Las variaciones en el proxy de productividad primaria (PPP – *Primary Productivity Proxy*), construido a partir de los valores absolutos y/o de flujos de acumulación de los individuos del complejo *Gephyrocapsa* pertenecientes a los grupos de small *Gephyrocapsa* y “*G. caribbeanica*”, posibilitan la reconstrucción de la productividad primaria en los márgenes ibéricos Mediterráneo (Mar de Alborán - ODP Site 977) y

portugués (sector sur - IODP U1385), provocados por las variaciones en el estado de activación e intensidad de los sistemas de surgencia o *upwelling*.

2. La estimulación atmosférica es el principal control sobre los registros de PPP durante el periodo interglacial pleno del estadio isotópico marino (MIS) 11, en el que dos fases de productividad moderada y estimulada indican el efecto de la intensificación intra-interglacial de la célula atmosférica de Azores y, potencialmente, de los gradientes de presiones en el Atlántico Norte para la edad de  $\sim 406$  ka en ambas regiones. Este patrón se identifica como comparable a la operación de las dos fases del modo de la oscilación moderna del Atlántico Norte (NAO) durante el MIS 11, con una primera fase de preferencia de la fase negativa (-) y una segunda de preferencia de la fase positiva (+). Además del importante control de este mecanismo de entidad Atlántica ejerció sobre los diferentes sistemas de productividad en el Atlántico Norte y la región Mediterránea, esto sugiere la posible extensión de este mecanismo climático moderno durante fases interglaciales del Pleistoceno hasta el MIS 11.
3. A pesar de la existencia de unas condiciones atmosféricas y de circulación, en el caso del margen Mediterráneo, proclives a la estimulación de los sistemas de *upwelling*, la prevalencia del control atmosférico sobre los sistemas de productividad cesa durante los episodios de enfriamiento abrupto de tipo *Heinrich* (Ht). En el margen Mediterráneo, la limitación térmica asociada a las condiciones frías extremas durante estos eventos explicaría la mayor dificultad para la proliferación de las especies de cocolitóforos incluidas en el PPP. Estos anteriormente mencionados, y/o la formación de una haloclina regional en el margen portugués explica, por su parte, la reducción en la estimulación de los sistemas de *upwelling* alimentando al sector sur del margen ibérico portugués.
4. En el testigo ODP 977, la señal de PPP y los patrones de circulación asociados durante el MIS 11 muestra correspondencia con las condiciones de acumulación y preservación de materia orgánica en el sedimento durante el MIS 11.

**Evaluación de la sensibilidad del fraccionamiento isotópico del carbono orgánico ( $\epsilon_p$ ) al CO<sub>2</sub> y de los efectos vitales de *Gephyrocapsa* en el sector Oeste del Atlántico tropical**

1. El modelo clásico de adquisición pasiva de CO<sub>2</sub> es incapaz de explicar las relaciones de sensibilidad entre el CO<sub>2</sub> y el resto de los parámetros, directamente medidos o estimados, involucrados en el fraccionamiento isotópico del carbono durante la fotosíntesis ( $\epsilon_p$ ) en el intervalo comprendido entre los estadios isotópicos marinos (MIS) 12 y 9 sector Oeste del Atlántico Tropical.
2. Los cocolitóforos pertenecientes al complejo *Gephyrocapsa* muestran, sin embargo, una sensibilidad fotosintética a los cambios en las concentraciones de CO<sub>2</sub>, en esta región e intervalo, cercana al 50 %, una respuesta que es comparable a la recientemente observada en cultivos. Esta semejanza que permite la aplicación del modelo estadístico de variable múltiple disponible, basado en las relaciones empíricas en cultivos anteriormente referidas, para evaluar la influencia sobre  $\epsilon_p$  del resto de parámetros ambientales y/o fisiológicos, diferentes a CO<sub>2</sub>, y la capacidad de los indicadores micropaleontológicos y geoquímicos disponibles en este estudio para capturar estos cambios.
3. Los porcentajes de *Florisphaera profunda* y la ratio entre la concentración de los compuestos orgánicos C37/38, et tienen capacidad para explicar una parte del 50% de la variabilidad restante atribuida, potencialmente, los cambios en la disponibilidad de luz y en las tasas de crecimiento de los cocolitóforos analizados en esta región. Se observa que, por su parte, los cambios en las tallas celulares no tienen una repercusión importante sobre dicha variabilidad durante este intervalo y en esta región, donde, además, se demuestra, su incapacidad para producir valores de tasas de crecimiento aceptables mediante la aplicación de modelos de regresión recientemente propuestos.
4. Se demuestra la mayor robustez de las relaciones entre los parámetros obtenidas y presentadas en este estudio y en cultivos, para proporcionar estimaciones de  $p\text{CO}_2$  a partir de  $\epsilon_p$  durante el Neógeno, en comparación con aquellas obtenidas mediante la aplicación del modelo clásico para la reconstrucción de  $p\text{CO}_2$ .
5. Los modelos existentes, para oxígeno y carbono, hasta la fecha, son incapaces de explicar los efectos vitales en cocolitos de *Gephyrocapsa* observados en este estudio. No obstante, se constata la existencia de una correlación entre los efectos vitales de oxígeno y carbono durante el intervalo, lo que indicaría que las futuras propuestas de modelos para explicar los efectos vitales de, al menos, el género *Gephyrocapsa*,

deberían entrañar la existencia de un control conjunto sobre ambos sistemas de fraccionamiento de oxígeno y carbono.

### **Caracterización morfométrica y de los cambios en la calcificación del complejo *Gephyrocapsa* en el Atlántico Norte y el sector occidental del mar Mediterráneo**

1. El complejo *Gephyrocapsa* evidencia una evolución morfométrica similar en distintos puntos de diferente latitud y condiciones ambientales del Atlántico Norte y del Mediterráneo occidental durante el intervalo del Mid-Brunhes, comprendido entre el MIS 14 y 7, homogénea y coincidente para los puntos de diferente latitud y condiciones ambientales del Atlántico norte y del Mediterráneo oeste. Esta evolución morfométrica es indicativa de la eclosión del morfotipo de talla media predominante, que se identifica con el concepto clásico de “*G. caribbeanica*”.
2. La aplicación de relaciones dimensionales y volumétricas para la obtención de índices de calcificación a partir de parámetros morfométricos se establece como un buen procedimiento para la estimación de los cambios en la calcificación y respalda las evidencias previas acerca de la existencia de una relación alométrica entre la talla y el grosor de cocolitos.
3. Simultáneamente a los cambios morfométricos, el complejo de *Gephyrocapsa* expresa un incremento en la calcificación a lo largo del intervalo del Mid-Brunhes. El incremento en la calcificación del complejo *Gephyrocapsa* o la eclosión de morfotipos altamente calcificados podría ser la respuesta a un incremento en la alcalinidad global del océano.
4. Las ideas previas al respecto de una eclosión de la familia de Noëlaerhabdaceae estrictamente estimulada por la existencia de condiciones de producción y crecimiento más beneficiosas deben reconsiderar la inclusión de la perspectiva de la respuesta a cambios en la química oceánica. De este modo, la reconstrucción de los cambios en la calcificación de este grupo podría servir para analizar los cambios en la química oceánica a escala orbital.

## Conclusions

This PhD thesis integrates different studies related to the paleoceanographic and paleoclimatic evolution of the North Atlantic and the western Mediterranean, and the role of the *Gephyrocapsa* complex during the Mid-Brunhes interval. More specifically, different topics are addressed, which were grouped into the three blocks consisting of: high-resolution paleoceanographic reconstruction at the Iberian Margins based on micropaleontological analysis (Chapters 2, 3 and 5), evaluation of the sensitivity of carbon isotopic fractionation during photosynthesis ( $\epsilon_p$ ) to CO<sub>2</sub> and the *Gephyrocapsa* coccolith vital effects at the western tropical Atlantic (Chapter 4) and the characterization of changes in morphometry and calcification of the *Gephyrocapsa* complex along the North to South transect through different regions in the North Atlantic and the western Mediterranean Sea (Chapter 6). The five chapters above referred, independently contain the extended and highly detailed discussions in relation to each of the investigations. As it follows, we here present a general synthesis of the main and more general conclusions about the evolution of the Mid-Brunhes interval and the *Gephyrocapsa* complex. The grouping of the three blocks is maintained for better clarity. The conclusions are numbered within each of the blocks:

### **High-resolution paleoceanographic reconstruction at the Iberian Margin with the use of the *Gephyrocapsa* complex**

1. Variations in the primary productivity proxy (PPP), estimated from the values of absolute concentration and nannofossil accumulation rates of the small *Gephyrocapsa* and “*G. caribbeanica*” groups allow the reconstruction of primary productivity at the Mediterranean (Alboran Sea - ODP Site 977) and Atlantic (southern sector of the Portuguese coast – IODP Site U1385) Iberian margins, caused by the variations in the intensity of the regional upwelling systems.
2. Atmospheric stimulation is the main control over the PPP records. The identification of two-phase scenarios of moderate and increased productivity during the full interglacial marine isotopic stage (MIS) 11 is indicative of the intra-interglacial strengthening of the Azores atmospheric high-pressure cell (AH) at the age of ~ 406 ka in both regions. Such a pattern could indicate an intensification in the North to

South atmospheric pressure gradients in the North Atlantic and the operation of a North Atlantic Oscillation (NAO) - *like* mode during the MIS 11, shifting from the prevalence of the negative (-) mode during the early interglacial to the prevalence of the positive (+) towards the late full interglacial MIS 11.

3. The prevalence of an atmospheric control over regional productivity systems through upwelling in both regions is hampered during the occurrence of episodes of abrupt cooling and meltwater arrival towards Iberian latitudes, as during the Heinrich-*type* events (Ht). Thermal limitation by extreme surface cooling is invoked to explain the reduced proliferation of coccolithophores species included in the PPP at the Mediterranean; this and/or the formation of a regional halocline at the southern Portuguese Iberian coast is suggested to impede the complete development of the coastal upwelling systems.
4. The primary productivity record from PPP reconstruction at ODP Site 977 and circulation patterns during the MIS 11, show good correspondence to explain the conditions of accumulation and preservation of organic matter in the sediment during this interval.

**Evaluation of the photosynthetic sensitivity of *Gephyrocapsa* to CO<sub>2</sub>, from the values of carbon isotopic fractionation during photosynthesis ( $\epsilon_p$ ), and the *Gephyrocapsa* coccolith vital effects at the western tropical Atlantic**

1. The classical model of carbon isotopic fractionation during photosynthesis ( $\epsilon_p$ ), that considered a purely passive CO<sub>2</sub> acquisition, is unable to explain the sensitivity to CO<sub>2</sub> and the rest of non-CO<sub>2</sub> parameters, directly measured or estimated, in the western tropical Atlantic between MIS 12 and 9.
2. The photosynthetic sensitivity to CO<sub>2</sub> in this region, from the  $\epsilon_p$  values measured in *Gephyrocapsa*-produced alkenones, is close to 50%. The observed sensitivity and response are comparable to that recently observed in cultures. This similarity allows the application of the statistical multiple regression model, constructed from these empirical relationships, to evaluate the influence of the non-CO<sub>2</sub> parameters, (environmental and/or physiological) on  $\epsilon_p$  at this location and to evaluate the suitability of micropaleontological and geochemical indicators to capture such changes at this location.

3. The percentages of *Florisphaera profunda* and the ratio between the C37/38. et alkenones are able to explain part of the 50% remaining variability, attributed to changes in light availability and growth rates. On the other hand, *Gephyrocapsa* cell size changes are not shown to have impact over the non-CO<sub>2</sub> variability in this study, neither to provide acceptable estimates of growth rate.
4. The relationships in this study and cultures are proposed to provide better  $p\text{CO}_2$  estimates from  $\epsilon_p$  during Neogene, in comparison to those previously obtained by applying the classical diffusive model of passive CO<sub>2</sub> acquisition.
5. Existing models, for oxygen and carbon coccolith vital effects are unable to explain the results obtained from *Gephyrocapsa* coccolith analysis in this study. However, oxygen and carbon vital effects are correlated trough time, a fact that could indicate that future model proposals at least, for the *Gephyrocapsa* vital effects, should imply a coupled control over both oxygen and carbon systems.

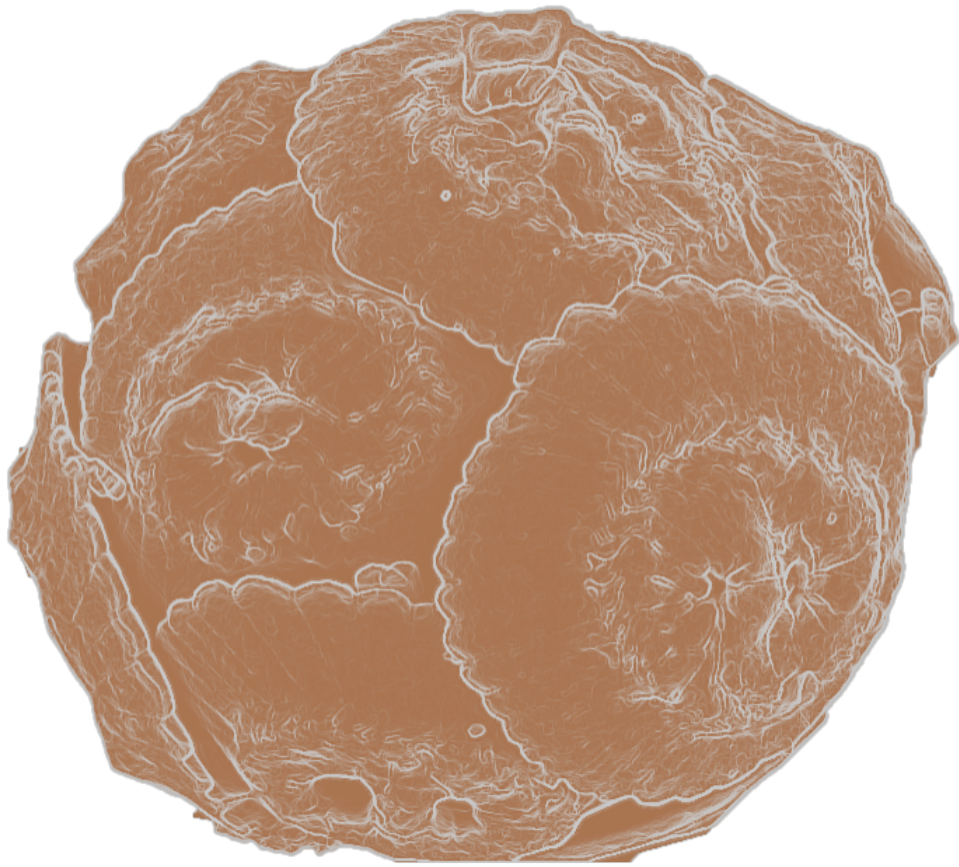
**Characterization of the changes in morphometry and calcification of the *Gephyrocapsa* complex along the North Atlantic and the western Mediterranean Sea**

1. The *Gephyrocapsa* complex shows a common morphometric evolution in different latitude and environments of the North Atlantic and the western Mediterranean during the Mid-Brunhes interval, between MIS 14 and 7. This morphometric evolution indicates the domain of mid-sized specimens, preliminarily identified with the classic definition of the domain of “*G. caribbeanica*”.
2. The application of calculations based in dimensional and volumetric relationships obtained from morphometrical measurements serves to capture the changes in coccolithophore calcification and supports previous evidence about the existence of an allometric relationship between coccolith size and thickness.
3. The *Gephyrocapsa* complex show an increase in calcification during the Mid-Brunhes interval. Such a pattern is suggested to be a response to global increase in seawater ocean alkalinity through the investigated period.
4. Previous ideas about the blooming response of Noëlaerhabdaceae under favorable growing and production conditions should consider the perspective of a response to changes in ocean chemistry. Thus, the reconstruction of the changes in

coccolithophore calcification during the past could serve to analyze the changes in ocean carbon chemistry at orbital scale.







**Anexos**

# ANEXOS

## Anexo I. Sistemática de los taxones estudiados

División HAPTOPHYTA Hibberd, 1972

Clase PRYMNESIOPHYCEAE Hibberd, 1976

Orden COCCOLITHALES Schwarz, 1932

**Familia CALCIDISCACEAE** Young y Bown, 1997

Género *Calcidiscus* Kamptner, 1950

Especie *Calcidiscus leptoporus* (Murray y Blackman 1898) Loeblich y Tappan, 1978

\*(*Calcidiscus leptoporus* subespecies)

*C. leptoporus* subsp. *leptoporus* (Murray y Blackman 1898) Loeblich y Tappan, 1978

*C. leptoporus* subsp. *small sensu* Young et al., 2003

*C. leptoporus* subsp. *quadriperforatus* (Kamptner 1937) Geisen et al., 2002

Género *Oolitothus* Cohen y Reinhardt, 1968

Especie *Oolitothus fragilis* Lohmann, 1912

Género *Umblicosphaera* Lohmann, 1902

Especie *Umblicosphaera foliosa* (Kamptner 1963) Geisen en Sáez et al., 2003

Especie *Umblicosphaera sibogae* (Weber-van Bosse) Gaarder, 1970

**Familia COCCOLITHACEAE** Poche, 1913 emend. Young y Bown, 1997

Género *Coccolithus* Schwarz, 1894

Especie *Coccolithus pelagicus* (Wallich 1877) Schiller, 1930

\*(*Coccolithus pelagicus* subespecies)

*C. pelagicus* subsp. *pelagicus* (Wallich 1877) Schiller, 1930

*C. pelagicus* subsp. *braarudii* (Gaarder 1962) Geisen et al., 2002

*C. pelagicus* subsp. *azorinus* Parente y Cachão en Parente et al., 2004

Orden ISOCHRYSIDIALES Pascher, 1910

**Familia NOËLAERHABDACEAE** Jerovic, 1970 emend. Young y Bown, 1997

Género *Gephyrocapsa* Kamptner, 1943

Especie *Gephyrocapsa caribbeanica* Bourdreaux y Hay, en Hay et al., 1967

Especie *Gephyrocapsa muelleriae* Bréhéret, 1978

Especie *Gephyrocapsa margerelli* Bréhéret, 1978

Especie *Gephyrocapsa oceánica* Kamptner, 1943

\*(small *Gephyrocapsa*)

Especie *Gephyrocapsa aperta* Kamptner, 1943

Especie *Gephyrocapsa ericsonii* McIntyre y Bé 1967

Especie *Gephyrocapsa ornata* Heimdal, 1973

Orden SYRACOSPHAERALES Hay, 1977 emend. Young et al. 2003

**Familia SYRACOSPHAERACEAE** Lohmann, 1902

Género *Syracosphaera* Lohmann, 1902

Especie *Syracosphaera pulchra* Lohmann, 1902

**Familia CALCIOSOLENIACEAE** Kamptner, 1927

Género *Calciosolenia* Gran, 1912

Especie *Calciosolenia brasiliensis* (Lohmann, 1919) Young en Young et al., 2003

Especie *Calciosolenia murrayi* Gran, 1912

**Familia RHABDOSPHAERACEAE** Haeckel, 1894

Género *Rhabdosphaera* Haeckel, 1894

Especie *Rhabdosphaera clavigera* Murray y Blackman, 1898

Orden ZYGODISCALES Young y Bown, 1997

**Familia HELICOSPHAERACEAE** Black, 1971

Género *Helicosphaera* Kamptner, 1954

Especie *Helicosphaera carteri* (Wallich, 1877) Kamptner, 1954

Especie *Helicosphaera inversa* (Gartner, 1977 ex. Gartner, 1980) Theodoridis, 1984

**Familia PONTOSPHAERACEAE** Lemmermann, 1908

Género *Pontosphaera* Lohmann, 1902

Especie *Pontosphaera multipora* (Kamptner, 1948) Roth, 1970

Especie *Pontosphaera discopora* Schiller, 1925

Grupo de nanolitos e *incertae sedis*

**Familia UMBELLOSPHAERACEAE** Young y Kleije, en Young et al., 2003

Género *Umbellosphaera* Paasche in Markali y Paasche, 1955

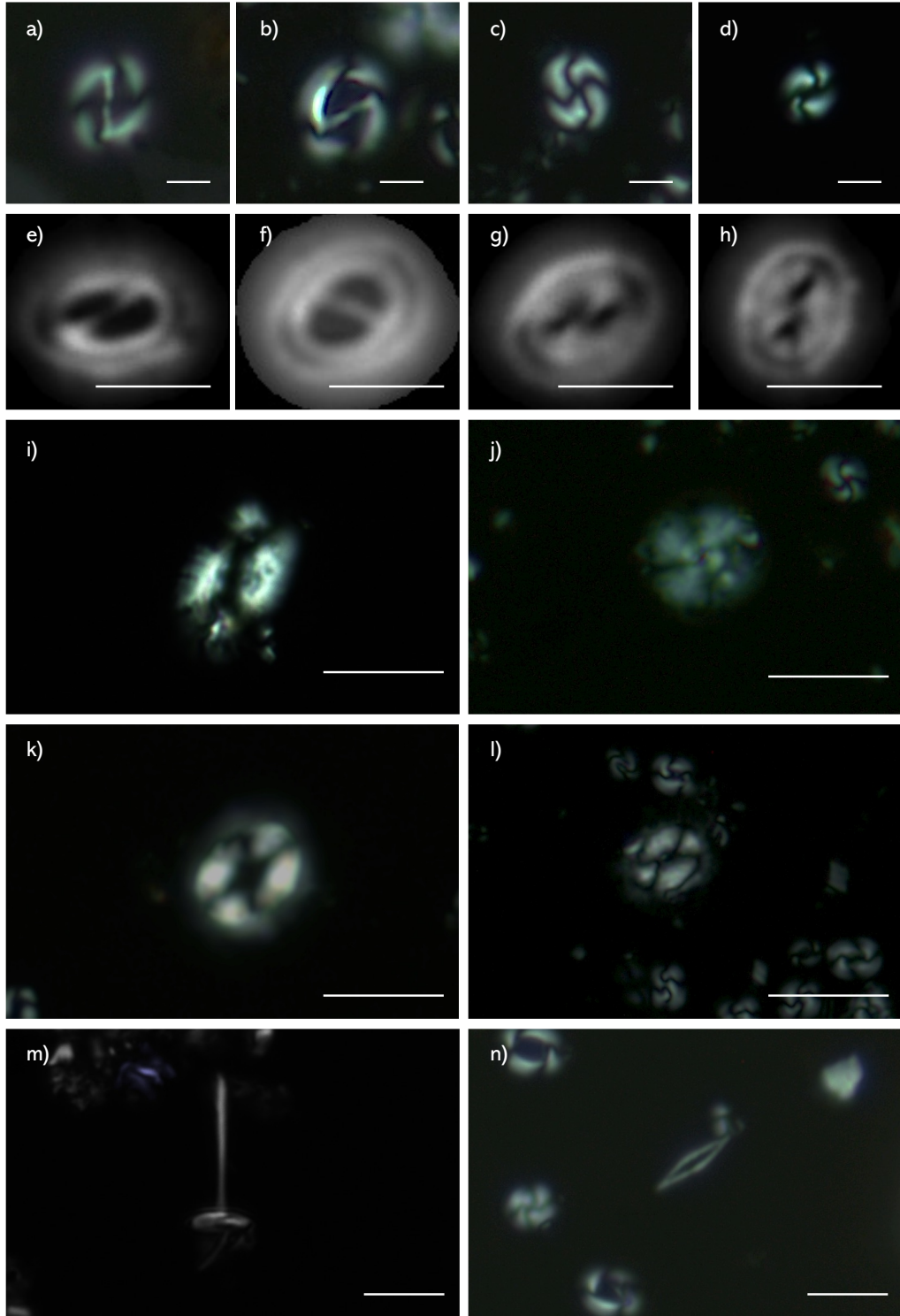
Especie *Umbellosphaera irregularis* Paasche in Markali y Paasche, 1955

Especie *Umbellosphaera tenuis* (Kamptner 1937) Paasche en Markali y Paasche,  
1955

Género *Florisphaera* Okada y Honjo, 1973

Especie *Florisphaera profunda* Okada y Honjo, 1973

## Anexo II. Lámina fotográfica



Las fotografías **a)** – **d)** corresponden a las principales especies pertenecientes al género *Gephyrocapsa* (complejo *Gephyrocapsa*) y fueron tomadas con técnicas de microscopía de óptica y polarización cruzada: **a)** *Gephyrocapsa muelleriae-margerelii*; **b)** *Gephyrocapsa oceánica*; **c)** y **d)** *Gephyrocapsa caribbeanica* (variedad mediana y pequeña). La escala representada para las imágenes **a)** – **d)** corresponde al tamaño de 2  $\mu\text{m}$ .

Las fotografías **e)** – **h)** corresponden a las principales especies de *Gephyrocapsa* y fueron tomadas con técnicas de microscopía óptica y polarización circular: **e)** *G. muelleriae-margerelii*; **f)** *G. oceanica*; **g)** y **h)** *G. caribbeanica*. La escala representada para las imágenes **e)** – **h)** corresponde al tamaño de 2  $\mu\text{m}$ .

Las fotografías **i)** – **n)** corresponden a algunas especies, de aparición minoritaria, presentes en los sedimentos estudiados y fueron tomadas con técnicas de microscopía óptica y polarización cruzada: **i)** *Helicosphaera carteri*; **j)** *Calcidiscus leptoporus*; **k)** *Coccolithus pelagicus* subsp. (subespecie) *braarudii*. El elemento característico de esta subespecie es su tamaño del eje mayor  $\geq 10 \mu\text{m}$ ; **l)** *Coccolithus pelagicus* subsp. (subespecie) *pelagicus*. El elemento característico de esta subespecie es su tamaño del eje mayor  $< 10 \mu\text{m}$ . La escala representada en ambas fotos corresponde a  $< 10 \mu\text{m}$ . **m)** *Rhabdosphaera clavigera* y **n)** *Calciosolenia brasiliensis*. La escala representada para las imágenes **m)** y **n)** corresponde al tamaño de 6  $\mu\text{m}$ .



## **Anexo III. Publicación adicional**

**“Middle Eocene calcareous nannofossils in the Jaca transect (South-central Pyrenees Eocene Basin, Aragón River valley, Huesca)”**

**Alba González-Lanchas**<sup>a,\*</sup>, Eduard Remacha<sup>b</sup>, Oriol Oms<sup>b</sup>, Francisco J. Sierro<sup>a</sup> y José-Abel Flores<sup>a</sup>

<sup>a</sup> Departamento de Geología, Universidad de Salamanca, 37008 Salamanca, España

<sup>b</sup> Departament de Geologia, Universitat Autònoma de Barcelona, 08193 Bellaterra, Barcelona, España

Artículo **publicado** en *Spanish Journal of Palaeontology*

DOI: [10.7203/sjp.34.2.16096](https://doi.org/10.7203/sjp.34.2.16096)



## Resumen

En este trabajo se analiza el contenido de nanoplancton calcáreo presente los sistemas turbidíticos del Grupo Hecho superior, de edad Eoceno medio, ubicado en la Cuenca de Jaca, perteneciente a la Cuenca Surpirenaica Central (España). La secuencia estudiada compone una sucesión sintética completa de 2.500 metros, que contiene sistemas con diferente origen genético y, particularmente, abarca desde la base de los sistemas de tipo turbidítico de la secuencia hasta los niveles de inestabilidades de Gracionepel, localizados dentro de las margas de talud de Larrés.

A partir del contenido en nanoplancton, se obtiene una caracterización bioestratigráfica detallada para la secuencia. La información bioestratigráfica en esta contribución, aporta datos cronostratigráficos de capital importancia para la mejora del marco previo existente de correlación temporal y espacial entre los diferentes sistemas de depósito, genéticamente asociados, a escala general de la Cuenca de Jaca y de la Cuenca Surpirenaica (Remacha y Fernández, 2003).

La asociación de nanofósiles calcáreos identificada se encuentra ampliamente dominada por las especies *Coccolithus pelagicus* (Wallich, 1877) Schiller, 1930 y *C. formosus* (Kamptner, 1962) Wise, 1973, así como por diferentes especies pertenecientes al género de *Reticulofenestra* Hay et al., 1966 y acompañados de contenido ocasional de varias especies del género *Sphenolithus* Deflandre en Grassé, 1952 y *Chiasmolithus* Hay et al., 1966.

Los resultados de este análisis bioestratigráfico permiten caracterizar los principales biohorizontes del Eoceno medio acorde los estándares bioestratigráficos globales (Agnini et al., 2014).

El depósito de la sucesión tuvo lugar durante las biozonas CNE11-CNE15 (Okada y Buckry, 1980) o NP15-NP16 (Martini, 1971), con una representación estratigráfica que abarca un rango temporal de ~ 3.45 Myr, comprendido entre los 43.96 y 40.51 Ma (Luteciense/Bartoniense). Como resultado significativo de este estudio, se precisa el inicio del Grupo Hecho superior, entre la megaturbidita de Roncal-Fiscal (MT-5) y las facies de inestabilidades de Gracionepel, en la parte terminal de la zona NP15 y se extiende dentro de la NP16.

El modelo de edad que se propone en esta contribución completa el existente para la Cuenca de Jaca y aporta nuevos datos críticos para el avance hacia una correlación más precisa entre eventos estratigráficos de otras secciones regionales. Esto facilita la comprensión de la evolución lateral y temporal de los sistemas estudiados, así como la mejora del marco paleogeográfico general de la Cuenca Surpirenaica Central.

## Referencias

- Agnini, C., Fornaciari, E., Raffi, I., Catanzariti, R., Pälike, H., Backman, J., Rio, D., 2014. Biozonation and biochronology of Paleogene calcareous nannofossils from low and middle latitudes. *Newsletters on stratigraphy* 47, 131-181.
- Deflandre, G., Grassé, P., 1952. Classe des Coccolithophoridés (Coccolithophoridae Lohmann, 1902). *Traite de Zoologie*. Masson, Paris, 439-470.
- Hay, W.W., Mohler, H., Wade, M.E., 1966. Calcareous nannofossils from Nal'chik (northwest Caucasus). *Eclogae Geologicae Helvetiae* 59, 379-399.
- Kamptner, E., 1962. Coccolithineen-Skelettreste aus Tiefseeablagerungen des Pazifischen Ozeans Eine nannopaläontologische Untersuchung. *Annalen des Naturhistorischen Museums in Wien*, 139-206.
- Martini, E. 1971. *Standard Tertiary and Quaternary calcareous nannoplankton zonation*. In: *Proceedings 2nd International Conference Planktonic Microfossils Roma* (ed. Farinacci, A.). Tecnoscienza, Rome 2, 739–785.
- Okada, H., Bukry, D. 1980. Supplementary modification and introduction of code numbers to the low-latitude coccolith biostratigraphic zonation (Bukry, 1973; 1975). *Marine Micropaleontology*, 5, 321-325.
- Remacha, E., Fernández, L. P. 2003. High-resolution correlation patterns in the turbidite systems of the Hecho Group (South-Central Pyrenees, Spain). *Marine and Petroleum Geology*, 20, 711-726.
- Schiller, J., 1930. Coccolithineae. Kryptogamen-Flora von Deutschland, Österreich und der Schweiz. 10. Akademische Verlagsgesellschaft, Leipzig.
- Wallich, G.C., 1877. XXXIV.—Observations on the Cocosphere. *Journal of Natural History* 19, 342-350.

Wise, S.W. 1973. Calcareous nannofossils from cores recovered during Leg 18, Deep Sea Drilling Project: biostratigraphy and observations on diagenesis. *Initial Report, Deep Sea Drilling Project* , 18, 569-615.





## Middle Eocene calcareous nannofossils in the Jaca transect (South-central Pyrenees Eocene Basin, Aragón river valley, Huesca)

Alba GONZÁLEZ-LANCHAS<sup>1\*</sup>, Eduard REMACHA<sup>2</sup>, Oriol OMS<sup>2</sup>, Francisco J. SIERRO<sup>1</sup>  
& José-Abel FLORES<sup>1</sup>

<sup>1</sup> Departamento de Geología, Facultad de Ciencias. Universidad de Salamanca, 37008 Salamanca, Spain; lanchas@usal.es, sierro@usal.es, flores@usal.es.

<sup>2</sup> Departament de Geologia, Universitat Autònoma de Barcelona, 08193 Bellaterra (Barcelona), Spain; eduard.remacha@uab.cat, joseporiol.oms@uab.cat.

\*Corresponding author

González-Lanchas, A., Remacha, E., Oms, O., Sierro, F.J. & Flores, J.A. 2019. Middle Eocene calcareous nannofossils in the Jaca transect (South-central Pyrenees Eocene Basin, Aragón river valley, Huesca). [Nanofósiles calcáreos del Eoceno medio en el transecto de Jaca (Cuenca eocena Surpirenaica Central, Valle del Río Aragón, Huesca)]. *Spanish Journal of Palaeontology*, 34 (2), 229-240.

Manuscript received 20 December 2017

<https://doi.org/10.7203/sjp.34.2.16096>

Manuscript accepted 10 June 2019

© Sociedad Española de Paleontología ISSN 2255-0550

### ABSTRACT

The calcareous nanoplankton is studied from the base of the turbidite systems of the Upper Hecho Group (Jaca Basin, middle Eocene of the South-central Pyrenean Basin) up to the Gracionepel instabilities, within the Larrés slope Marls. This new chronostratigraphic contribution is of crucial importance for the improvement of the detailed temporal and spatial correlation framework of the genetically related depositional systems at basin scale.

The calcareous nanofossil assemblage is largely dominated by *Coccolithus pelagicus* (Wallich, 1877) Schiller, 1930, *C. formosus* (Kamptner, 1963) Wise, 1973 as well as different species of *Reticulofenestra* Hay *et al.*, 1966, accompanied by occasional specimens of several species of *Sphenolithus* Deflandre in Grassé, 1952 and *Chiasmolithus* Hay *et al.*, 1966. The results obtained, based on the detailed biostratigraphic study of a composite succession 2,500 m thick, allow us to characterize the main biohorizons of the middle Eocene on the basis of global biostratigraphic standards. The studied succession was deposited during the CNE11-CNE15 or NP15-

### RESUMEN

Se estudia el contenido de nanoplancton calcáreo desde la base de los sistemas turbidíticos del Grupo Hecho superior (Cuenca de Jaca, Eoceno medio de la Cuenca Surpirenaica Central) hasta las inestabilidades de Gracionepel, dentro de las margas de talud de Larrés. Esta información cronostratigráfica es de capital importancia para mejorar el marco de correlación temporal y espacial detallado de los sistemas de depósito genéticamente asociados a escala de la cuenca.

La asociación de nanofósiles calcáreos identificada se encuentra ampliamente dominada por *Coccolithus pelagicus* (Wallich, 1877) Schiller, 1930, *C. formosus* (Kamptner, 1963) Wise, 1973 así como diferentes especies de *Reticulofenestra* Hay *et al.*, 1966, acompañados de especímenes ocasionales de varias especies de *Sphenolithus* Deflandre en Grassé, 1952 y *Chiasmolithus* Hay *et al.*, 1966. Los resultados obtenidos, basados en el estudio bioestratigráfico detallado de una sucesión sintética de 2.500 m, permiten caracterizar los principales biohorizontes del Eoceno medio acorde a los estándares bioestratigráficos globales. El depósito de la

NP16 biozones, within a time span of ~3.45 Myr, between 43.96 and 40.51 Ma (Lutetian/Bartonian). This age range is compatible with the existing scheme for the South-central Pyrenean Basin.

The Upper Hecho Group, between the Roncal-Fiscal megaturbidite (MT-5) and the instability facies of Gracionepel, starts in the uppermost part of Zone NP15 continues into Zone NP16.

The proposed biozonation provides new data for a correlation between stratigraphic events of other regional sections and facilitates the understanding of the lateral and temporal evolution of the studied systems, as well as the improvement of the general palaeogeographic framework of the basin.

**Keywords:** Calcareous nannofossils, middle Eocene, biostratigraphy, Jaca transect, Pyrenees (Spain).

sucesión tuvo lugar durante las biozonas CNE11-CNE15 o NP15-NP16, con una representación estratigráfica que abarca un rango temporal de ~3,45 Myr comprendido entre los 43,96 y 40,51 Ma (Luteciense/Bartoniense). Este modelo de edad completa el existente para la Cuenca Surpirenaica Central.

La propuesta de biozonación proporciona nuevos datos para una correlación más precisa entre eventos estratigráficos de otras secciones regionales, y facilita la comprensión de la evolución lateral y temporal de los sistemas estudiados, así como la mejora del marco paleogeográfico general de la cuenca.

El Grupo Hecho superior, entre la megaturbidita de Roncal-Fiscal (MT-5) y las facies de inestabilidades de Gracionepel, se inicia en la parte terminal de la zona NP15 y se extiende dentro de la NP16.

**Palabras clave:** Nanofósiles calcáreos, Eoceno medio, bioestratigrafía, transecto de Jaca, Pirineos (España).

## 1. INTRODUCTION

The Hecho Group (defined by Mutti *et al.*, 1972) is a worldwide reference model for deep-marine clastic sedimentation. Biostratigraphically, our research places the Upper Hecho Group in the depositional systems of the Jaca Basin, outcropping along the Aragón river valley (Fig. 1). The studied transect (Fig. 2) is characterised by the replacement up-section of basin floor turbidites by the slope-fan system of the lower Larrés Marls. In the study area, the lack of accurate age dating hampers the correlation of stratigraphic units between the proximal Aínsa and the Jaca Basin systems, as physical correlation is interrupted by erosion in the hinge zone of the Boltaña anticline and internal splitting by the Oturia thrust.

The available chronological data from the Hecho Group is rather limited, restricted to only a few general publications. The upper part of the group has been biostratigraphically studied in the Roncal Valley and partially located as late Lutetian (NP15 zone) by Labaume *et al.* (1985). Canudo & Molina (1988) locate the Upper Hecho Group and the younger deltaic succession of the eastern Jaca Basin to between late Lutetian and early Priabonian, i.e. from P.12 to the lower P.16 zones. Oms *et al.* (2003) carried-out a palaeomagnetic study in the Upper Hecho Group with samples obtained along the Aragón river valley. As a result, the Upper Hecho Group turbidite systems in the Aragón valley were deposited during the time span ranging from the upper C20r to the mid C18r (middle Lutetian to early Bartonian times; Fig. 2).

Previous regional correlations in the Jaca Basin (Labaume *et al.*, 1985; Remacha & Fernández, 2003) are challenged by Oms *et al.* (2003) and also by magnetostratigraphic and calcareous nannofossil studies

from the Aínsa Basin by Mochales *et al.* (2012) and Scotchman *et al.* (2015), respectively. Our study provides new data with the aim of resolving the controversial dating of the Jaca Basin and clarifying the general chronostratigraphic framework at basin scale.

## 2. GEOLOGICAL SETTING AND STRATIGRAPHY

The outcrop belt of the Paleogene Jaca Basin (South-central Pyrenees foreland basin system), forms an ESE-WNW elongated asymmetrical syncline developed west of the Boltaña anticline (Fig. 1). Its thicker northern limb consists of forward breaking thrust systems involving cover rocks (Mesozoic to upper Eocene), overlying a basement-involved duplex mostly comprising Paleozoic rocks (Cámara & Klimowith, 1985; Labaume *et al.*, 1985, 2016; Teixell, 1990, 1996; Cámara & Flinch, 2017) (Fig. 1). In the cover systems and overlying lower Eocene carbonates, the Hecho Group turbidites form a thick deep-marine clastic succession reaching up to 4,500 m in thickness. On the southern, passive margin of the basin, this group wedges-out by lateral onlap and horizontal facies change into the Burgui Marls Formation (Cámara & Klimowith, 1985). These marls are also the distal equivalents of the shallow-marine carbonates of the Boltaña and Guara formations (Soler-Sampere & Puigdefàbregas, 1970; Puigdefàbregas, 1975). To the east of the Boltaña anticline, the depositinally equivalent systems of the Jaca Basin are found in the Aínsa Basin. This last basin contains most of the architectural elements such as submarine canyons, turbidite channels and slope-fan systems. The general

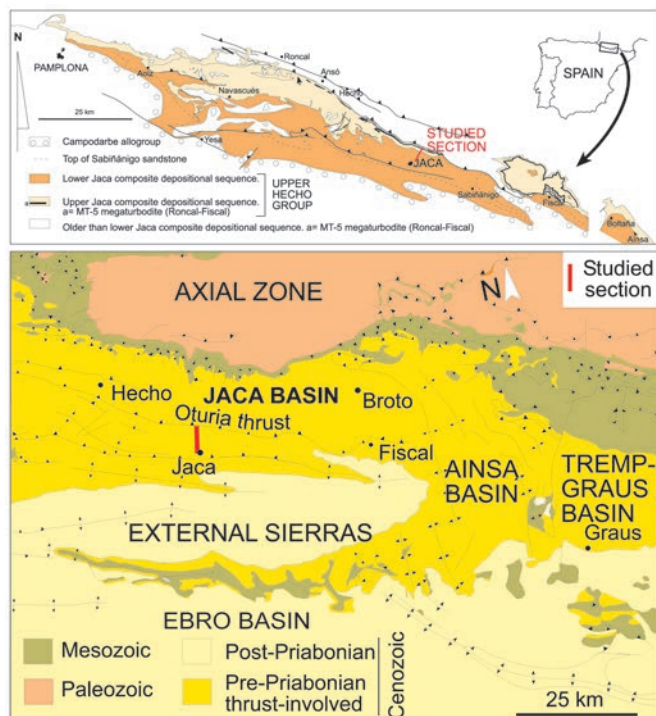


**Figure 1.** Geological setting of the studied section. Top: location on a sketch map of the Upper Hecho Group. Bottom: location in the central part of the South-central Pyrenees.

E-W-continuum of turbidite elements in the Jaca Basin comprises channel-lobe transition, sheet-like lobes and finally basin plain. Exceptions to the general distribution of architectural elements within the Hecho Group have been found in the uppermost part of the section in the Jaca Basin (Remacha *et al.*, 1987, 1995; Remacha & Picart, 1991), culminating in the northly-derived Rapitán turbidite system, the last turbidite system in the basin.

The studied section is ca. 2,500 m thick and is located north of Jaca, along the Aragón river valley. It is summarised in graphic form in Figure 2, together with the associated bio- and chronostratigraphic framework. The following section is a simplified review of the key depositional elements comprising the study transect.

At the base of the section and the starting point of the lower Jaca turbidite system (abbreviated hereinafter as LJSt), the Roncal-Fiscal megaturbidite (Mt-5) is found, bounded to the north by the Oturia thrust. The top of the section is marked by the Gracionepel instabilities (Gracionepel facies of Puigdefàbregas, 1975), within the Larrés Marls. These marls are interpreted as a slope fan, developing above the Rapitán turbidite channel of the upper Jaca turbidite system (abbreviated hereinafter as UJSt), and are genetically related to the Sabiñanigo Sandstone delta complex sealing the Eocene deep-marine clastic sediments in the South-central Pyrenees.

The basal ca. 1,100 m of the composite section (LJSt, see Fig. 2) contains the unit formerly known as the Banastón turbidites, represented in the Aragón valley by sheet-like lobe elements (Remacha & Fernández, 2003; Remacha *et al.*, 2005). LJSt contains three megaturbidites: Mt-5 (Roncal Fiscal), Mt-6 and Mt-7. In the Aragón section, the LJSt is sharply overlain by thick-bedded and very sand-rich facies forming the Torrijos Bridge lobes, comprising channel-lobe transition elements overlain by the Mt-8 megaturbidite.

The stratigraphic succession subsequently comprises a ca. 70 m thin-bedded package containing several distinctive, medium-scale cross-bedded sandstone beds. The following 50 m occurs in restricted outcrops, which are also thin-bedded with local sheet-like sandy intervals. The ensuing Charlé lobes are ca. 60 m thick and locally derived from the north. These lobes are relatively thick-bedded, sand-rich and sheet-like. The Charlé lobes are themselves overlain by 300 m of muddier, sheet-like lobes characterised by fewer thick beds and a net-to-gross of around 50%. The top of this unit is defined by a remarkable submarine erosional feature linked to the development of the Rapitán channel (Remacha *et al.*, 1987, 1995), the last turbidite system of the Hecho Group. In the studied section, the channel fill contains minor, thick-bedded, lenticular channel sand bodies separated by muddy debrites.

The upper part of the Rapitán channel evolves upward to the thin-bedded, lower Larrés Marls, which have a thickness of ca. 200 m. The latter are capped by the instabilities with abundant dolomite concretions of the Gracionepel facies, forming the slope and base-of-slope environments of the lower Sabiñanigo deltas (Remacha & Picart, 1991)

The Hecho Group has been placed within a framework of tectonosedimentary units (TSUs) by Remacha & Fernández (2003). These units are considered as second-order basinal divisions, each containing a number of third-order composite depositional sequences. Within the second-order framework, the upper Hecho Group comprises TSU-4 and TSU-5 (Remacha *et al.*, 1987; Remacha & Picart, 1991; Remacha & Fernández, 2003). The turbidites of TSU-4 and TSU-5 belong, respectively, to LJSt and UJSt.

A distinctive feature of the Upper Hecho Group in the Jaca Basin is the occurrence of the four, previously described, thick carbonate megaturbidites (Fig. 2). These megaturbidites, with a significant lateral extension, may be regarded as extremely useful time-line marker-beds. They provide first-order physical correlation and segregation of strictly time-equivalent stratal packages extending for significant distances within the Upper Hecho Group of the Jaca Basin (Labaume *et al.*, 1985; Remacha & Fernández, 2003; Remacha *et al.*, 2005).

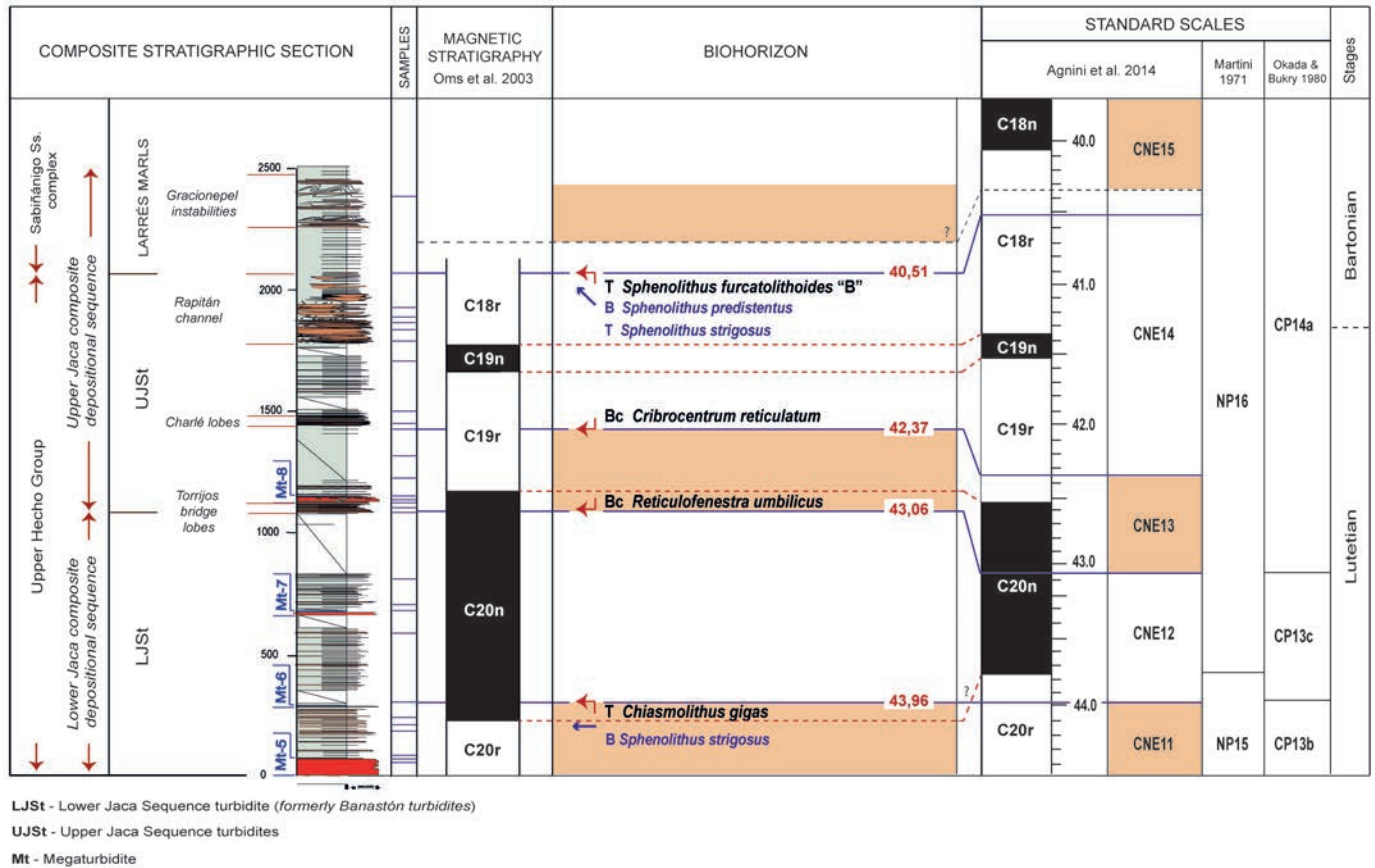


**Figure 2.** Integrated magneto-biostratigraphic data from the Aragón valley section. Lithostratigraphic section to the left contains: LJSt = Lower Jaca Sequence Turbidites (formerly Banastón turbidites); UJSt = Upper Jaca Sequence Turbidites; Mt = Megaturbidites. Calcareous nannofossil sampling levels and magnetostratigraphic record by Oms *et al.* (2003). Center: biostratigraphic results, with red arrows indicating significant bioevents (Agnini *et al.*, 2014) and blue arrows indicating other biomarkers (Perch-Nielsen, 1985; Bown & Dunkey Jones, 2006; Martini, 1971; Okada & Bukry, 1980). Right: Standard biozonation and magnetostratigraphic assignment for middle Eocene according to Agnini *et al.* (2014). Correspondence with standard scales of Martini (1971) and Okada & Bukry (1980). Eocene stages.

### 3. METHODS

A total of 29 samples were prepared following the Flores & Sierro (1997) settling technique, allowing for the generation of homogeneous and comparable data. For observation, a *Nikon eclipse 80i* polarized microscope was used at 1,000x magnification. The abundance of calcareous nannofossils was analyzed by systematic counting of the total content of non-reworked nannofossils in a pre-established area of 50 fields per sample (equivalent to 1 mm<sup>2</sup>). The quantitative pattern of selected biomarker taxa is expressed in percentages calculated in relation to the total number of nannofossils in each sample (Fig. 3).

Calcareous nannofossils were identified using the taxonomic concepts of Perch-Nielsen (1985), Bown (1998), Young *et al.* (1997, 2003, 2017). A total of 74 different species have been identified (Appendixes I and II).

### 4. CALCAREOUS NANNOFOSSIL ASSEMBLAGE

The calcareous nannofossil content in the studied samples is generally rich, although we have observed variations in nannofossil concentrations between sedimentary units. Despite this, a high diversity of species is constant throughout the Jaca section.

The preservation of coccoliths was good to moderate, with occasional low dissolution and partial breaking of large specimens, such as *Discoaster* Tan, 1927 and *Reticulofenestra* spp. For *Chiasmolithus* spp. only complete specimens with the central cross were identified.

The assemblages are dominated by *Reticulofenestra* spp., *Dictyococcites* Black, 1967, *Cribrocentrum reticulatum* (Perch-Nielsen, 1985), *Coccolithus pelagicus*, and *Coccolithus formosus*. For *Reticulofenestra umbilicus* (Levin, 1965) Martini & Ritzkowski, 1968 we have only considered specimens larger than 14 μm (Backman, 1986;



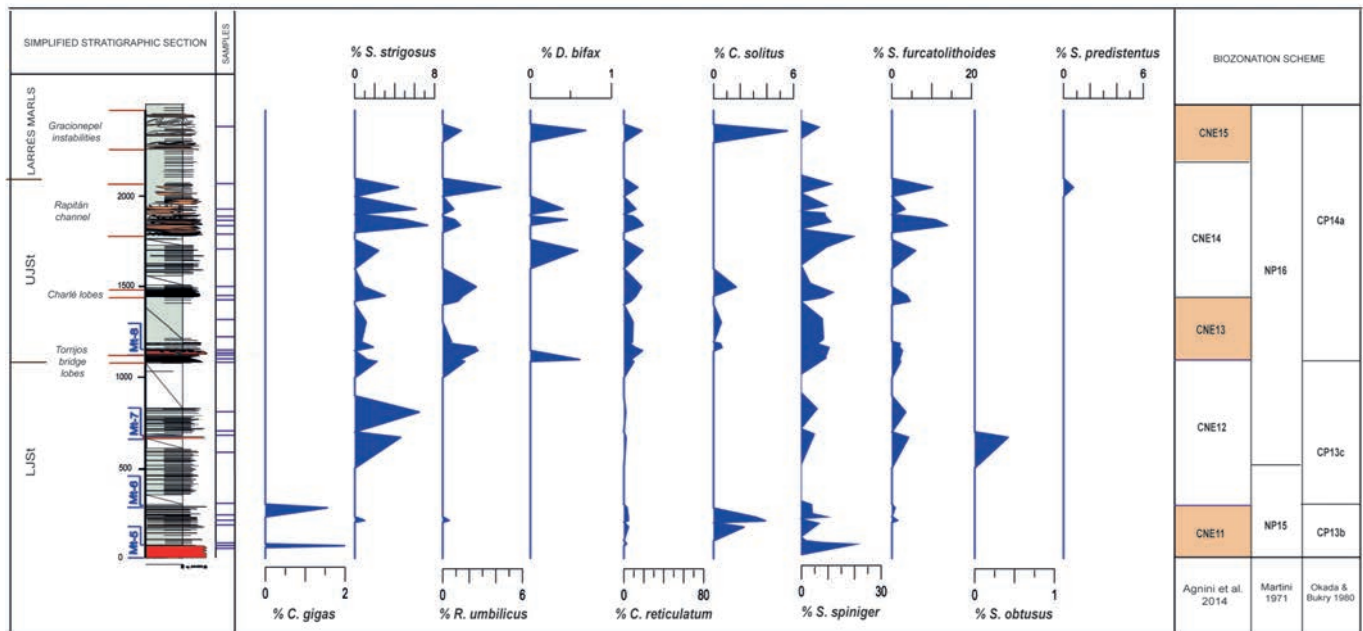


**Figure 3.** Percentage of abundance of biostratigraphically significant calcareous nannofossils and its position in relation to the simplified composite stratigraphic section (see more details in Fig. 2).

Backman & Hermelin, 1986; Wei & Wise, 1989; Fornaciari *et al.*, 2010; Norris *et al.*, 2014).

*Sphenolithus moriformis* (Brönnimann & Stradner, 1960) Bramlette & Wilcoxon, 1967, *Sphenolithus spiniger* Bukry, 1971, *Sphenolithus furcatolithoides* Locker, 1967, *Sphenolithus strigosus* Bown & Dunkley Jones, 2006, and *Sphenolithus predistentus* Bramlette & Wilcoxon, 1967 are also abundant. *Pemma* Klumpp, 1953, *Zygrhablithus bijugatus* (Deflandre in Deflandre and Fert, 1954) Deflandre, 1959, *Blackites* Hay & Towe, 1962, and *Lanternithus* Stradner, 1962 have a significant level of abundance. *Discoaster* spp. and *Chiasmolithus* spp., *Helicosphaera* Kamptner, 1954 and *Pontosphaera* Lohmann, 1902 are occasionally recorded. Cretaceous reworked nannofossils are consistently present but in low abundance.

Appendixes I and II show a summary of the identified calcareous nannofossil taxa.

## 5. BIOSTRATIGRAPHY

For this study we used the calcareous nannofossil biozonation and calibrated bioevents of Agnini *et al.* (2014), following the nomenclature of B (Base), Bc (Base common), T (Top) and Tc (Top common) for the lowest occurrence, first common record, last occurrence and highest common record in the studied section, respectively.

Some bioevents of the standard zonation of Martini (1971) and Okada & Bukry (1980) have also been identified. In addition, a few additional biomarkers

described by Perch-Nielsen (1985), Bown & Dunkley Jones (2006), and Fornaciari *et al.* (2010) have been identified, supporting the correlation between the standard schemes.

Table 1 is a summary of the identified chronographically calibrated events.

## 6. RESULTS AND DISCUSSION

Our results from the Upper Hecho Group, in the Aragón river valley are derived from the same section and outcrops studied for magnetostratigraphic purposes by Oms *et al.* (2003); i.e., in the succession formed by LJSSt, containing Mt-5, Mt-6 and Mt-7 megaturbidites, overlain by UJSt (between the Torrijos Bridge lobes to the top of the Rapitán channel system). Therefore, the magnetostratigraphic units, defined by Oms *et al.* (2003) in the Aragón valley, can be combined with the calcareous nannoplankton zones proposed here.

The presence of *Sphenolithus cuniculus* Bown, 2005 together with *Chiasmolithus gigas* (Bramlette & Sullivan, 1961) Radomski, 1968, from the lowest part of LJSSt, permits identification of zone CNE11 (*Sphenolithus cuniculus*/*Chiasmolithus gigas* Concurrent Range Zone), included in the Lutetian. Agnini *et al.* (2014) dated the Bc of *S. cuniculus* at 44.64 Ma. Consequently, the age of the materials studied here is younger (Fig. 2).

Zone CNE11 corresponds to the upper part of zone NP15 (Martini, 1971) and to upper part of Subzone CP13b (Okada & Bukry, 1980), also identified in the Jaca section

**Table 1.** List of calcareous nannofossil events: height (m), event, species, age (Ma) and magnetic chron. B = base; Bc = base common; T = Top; Tc = Top common. Additional information (reference work and time scale reference) is also provided.

High (m)	Event	Species	Ref.	Age (Ma)	Chron
2050	<b>B</b>	<i>Sphenolithus predistentus</i>	Bown & Dunkley Jones (2006)		
2050	<b>B</b>	<i>Sphenolithus furcatolithoides</i> (B)	Agnini <i>et al.</i> (2014)	40.51	C18r
2050	<b>T</b>	<i>Sphenolithus strigosus</i>	Bown & Dunkley Jones (2006)		
1450	<b>Bc</b>	<i>Criboecentrum reticulatum</i>	Agnini <i>et al.</i> (2014)	42.37	C19r
1090	<b>Bc</b>	<i>Reticulofenestra umbilicus</i>	Agnini <i>et al.</i> (2014)	43.06	C20n
280	<b>T</b>	<i>Chiasmolithus gigas</i>	Agnini <i>et al.</i> (2014)	43.96	C20r
210	<b>B</b>	<i>Sphenolithus strigosus</i>	Bown & Dunkley Jones (2006)		

based on the presence of *Blackites gladius* (Locker, 1967) Varol 1989, *Blackites inversus* (Bukry & Bramlette, 1969) Bown & Newsam, 2017, *Lanternithus arcanus* Bown, 2005, *Sphenolithus spiniger*, *Sphenolithus furcatolithoides*, and *Nannotetrina* Achuthan & Stradner, 1969 (Fig. 2).

The T of *C. gigas* marks the base of zone CNE12 (*Nannotetrina* spp. PRZ), dated at 43.96 Ma in chron C20r (Agnini *et al.*, 2014). This biohorizon is identified above the Mt-6 of the LJSt (Fig. 2).

The T of *B. gladius* marks the zone NP15-NP16 boundary (Martini, 1971), traditionally considered as correlative with the T of *C. gigas* (Okada & Bukry, 1980; Perch-Nielsen, 1985; Martini & Müller, 1986). In the Jaca section, *B. gladius* is still observed, although very scarce, within the LJSt unit, up to Mt-6 (CNE12). We cannot discard the possibility of some reworking or a certain degree of diachronism for this event, located by some authors within zone NP16 (Wei & Wise, 1989; Berggren & Aubry, 1984) and also at zone NP17 (Berggren & Aubry, 1984). Despite ambiguity surrounding the establishment of the zone NP15-NP16 boundary, we have elected here to follow the correlation of Agnini *et al.* (2014), which would place it within zone CNE12.

A high abundance of *S. strigosus* has also been observed within zone CNE12 in the Jaca section (Fig. 3). The B of this species is placed within zone NP16 (Bown & Dunkley Jones, 2006), supporting the correspondence of zones CNE12 and NP16 in this part of the section, above Mt-6 (Fig. 2). The observation of a few specimens in zone CNE11, corresponding to zone NP15 (Lutetian), is also described by Lupi & Wise (2006) and Fioroni *et al.* (2015).

The Bc of *R. umbilicus* ( $\geq 14 \mu\text{m}$ ) marks the base of zone CNE13 (*Reticulofenestra umbilicus* Base Zone) dated at 43.06 Ma in chron C20n (Agnini *et al.*, 2014). This biohorizon was identified in the Torrijos Bridge lobes, beneath Mt-8 of the lower UJSt unit (Fig. 2).

On the basis of the bioevents T of *C. gigas* and Bc of *R. umbilicus*, the LJSt unit should be chronostratigraphically defined as ranging from C20r to C20n (Fig. 2), which is in agreement with the proposal of Oms *et al.* (2003). In detail, the C20r-C20n polarity reversal, in this paper, is defined at stratigraphic levels below our placement of the T of *C. gigas* (Fig. 2). We should accordingly consider a possible diachronism associated with this event. In addition, we cannot discard reworking. Although the number of samples analysed for magnetostratigraphy, across this interval were indeed interpreted as a polarity reversal, a significant scattering of the declination and inclination values was also observed, so that, some slight modification of the exact position of the reversal event cannot be completely ruled out. A high-resolution revision is required here of both biostratigraphy and magnetostratigraphy in order to calibrate age assignments.

The Bc of *C. reticulatum* is used to define the base of zone CNE14 (*C. reticulatum* BZ) included in the Lutetian and dated at 42.37 Ma in chron C19r (Agnini *et al.*, 2014). This event was identified at the Charlé lobes stratigraphic level of UJSt (Fig. 2). Agnini *et al.* (2014) documented, nonetheless, a sporadic occurrence in zone CNE13. In the LJSt unit, specimens of *C. reticulatum* (with unclear central net) were sporadically observed.

The boundary between zones CNE14-CNE15 (*D. bisectus*-*S. obtusus* CRZ) is defined by the B of *Dictyococcites bisectus* (Hay *et al.*, 1966) Bukry & Percival, 1971 in the Bartonian and dated at 40.34 Ma in chron C18r (Agnini *et al.*, 2014). The scarce record of these specimens precludes a precise placement of the event, which, however, is identified within the LJSt unit. Other authors have considered this event as diachronic (Mita, 2001; Larrasoana *et al.*, 2008).

The T of *S. furcatolithoides* morphotype B (Agnini *et al.*, 2014) is constrained to the upper part of zone CNE14,

included in the Bartonian and dated at 40.51 Ma in chron C18r (Agnini *et al.*, 2014). This biohorizon was identified in the Rapitan channel system, in the upper part of UJSt unit (Fig. 2).

The UJSt unit is bounded by the Bc of *R. umbilicus* and the T of *S. furcatolithoides* (B) corresponding respectively to C20n and C18r (Fig. 2). This identification in the Jaca section is consistent with chron assignments by Oms *et al.* (2003), who defines the same polarity pattern for this part of the section. The intermediate location of C19r, according to Oms *et al.* (2003), is here also supported by the identification of Bc of *C. reticulatum* (Fig. 2).

The B of *S. predistentus* (Perch-Nielsen, 1985; Fornaciari *et al.*, 2010; Toffanin *et al.*, 2013) has been correlated by Agnini *et al.* (2014) with the lower part of zone CNE15, in the Bartonian. In the Jaca section, the T of *S. furcatolithoides* morphotype B was observed at the same stratigraphic level (Fig. 2). We used these two events to approximate the location of the CNE14-CNE15 boundary in the Rapitan channel system (Fig. 2).

The T of *C. solitus* has a range, which extends throughout the middle part of zone CNE15 (Agnini *et al.*, 2014), at the bottom of zone NP17 (Martini, 1971) and CP14b (Okada & Bukry, 1980). A scarce record of these specimens has been observed until the Gracionepel instabilities, in agreement with the base of zone CNE15 in the Bartonian (Fig. 2).

The B of *Sphenolithus obtusus* Bukry, 1971 and the Tc of *S. spiniger* (Fornaciari *et al.*, 2010) are correlated with the upper part of zone CNE15 (Agnini *et al.*, 2014). The abundance of *S. spiniger*, up to the top of the section is far from the prominent decrease described in Fornaciari *et al.* (2010) before the Tc (Fig. 3). The B of *S. obtusus* was dated at 39.64 Ma in chron C18n.2n (Fornaciari *et al.*, 2010). The absence of this taxon in the samples permits us to interpret this section as older than this date, in agreement with Oms *et al.* (2003) (Fig. 2).

The biostratigraphic results presented here validate the magnetostratigraphic data and correlation by Oms *et al.* (2003), reinforcing the methods of this paper in the sense that it is a rare example of magnetostratigraphic techniques applied to expanded deep-marine clastic systems.

The general correlation between sedimentary units of the Aínsa and Jaca Basins should be reconsidered, comparing our results with the proposal of Mochales *et al.* (2012) and Scotchman *et al.* (2015). First, the timing of the LJSt would correspond with the Guaso turbidite systems of the Aínsa Basin. Second, the overlying lowermost part of the UJSt would be the time equivalent of the Sobrarbe delta. Finally, the last turbidite system of the Hecho Group (Rapitán channel, established in the Jaca Basin) would be the deep-marine time equivalent of the continental sediments of the lower Escanilla formation in the Aínsa Basin. Although additional work is required, the above correlation should be taken as a guideline for any revised

palaeogeographic reconstruction involving the Aínsa and Jaca Basins.

## 7. CONCLUSIONS

Four age-calibrated calcareous nannofossil bioevents have been identified in the Jaca transect, establishing a biostratigraphic framework for the sedimentary units of the Upper Hecho Group and Larrés Marls. These results reinforce the magnetostratigraphic scheme and correlation established by Oms *et al.* (2003).

Sedimentation took place during the middle Eocene, including part of Lutetian and Bartonian stages, during biozones CNE11-CNE15 or NP15-NP16, covering a time-interval of at least ~3.45 Myr between 43.96 Ma (T of *C. gigas*) and 40.51 Ma (T of *S. furcatolithoides* morphotype B).

The correlation between the Aínsa and Jaca Basins should be revisited when integrating data by Mochales *et al.* (2012) and Scotchman *et al.* (2015). As an outline framework, the Upper Hecho Group, in the Jaca Basin, should correlate with the time span between the Guaso turbidite systems and the lower part of the already continental Escanilla Formation, with a slight overlap of the lower UJSt with the Sobrarbe Delta Formation.

## ACKNOWLEDGEMENTS

This work has been supported by the SEPAI-2016-07311 grant of the research aid program for young researchers awarded by the Spanish Society of Palaeontology (SEP) to Alba González-Lanchas for the development of the project “*Nanoplancton calcáreo del Eoceno medio y superior en el transecto de Jaca (Cuenca Eocena Surpirenaica Central)*” and by the program PGC2018-101575-B-I00 Spanish Ministry of Science, Innovation and Universities. Earlier version of this work benefitted from revision and comments by two anonymous reviewers and those of Dra. Adele Garzarella. We are indebted to Dr. Neil McDougall for the English revision of the text.

## REFERENCES

- Achuthan, M.V. & Stradner, H. 1969. Calcareous nannoplankton from the Wemmelian stratotype. In: *Proceedings of the First International Conference on Planktonic Microfossils* (eds. Brönnimann, P. & Renz, H.H.). 1 Brill, Leiden, Geneva, 1-13.

- Agnini, C., Fornaciari, E., Raffi, I., Catanzariti, R., Pälke, H., Backman, J. & Rio, D. 2014. Biozonation and biochronology of Paleogene calcareous nannofossils from low and middle latitudes. *Newsletters on Stratigraphy*, 47, 131-181; doi: 10.1127/0078-0421/2014/0042.
- Backman, J. 1986. Late Paleocene to middle Eocene calcareous nannofossil biochronology from the Shatsky Rise, Walvis Ridge and Italy. *Palaeogeography, Palaeoclimatology, Palaeoecology*, 57, 43-59; doi: 10.1016/0031-0182(86)90005-2.
- Backman, J. & Hermelin, J.O.R. 1986. Morphometry of the Eocene nannofossil *Reticulofenestra umbilicus* lineage and its biochronological consequences. *Palaeogeography, Palaeoclimatology, Palaeoecology*, 57, 103-116; doi: 10.1016/0031-0182(86)90009-X.
- Berggren, W.A. & Aubry, M.P. 1984. Rb-Sr glauconite isochron of the Eocene Castle Hayne Limestone, North Carolina: Further discussion. *Geological Society of America Bulletin*, 95, 364-370; doi: 10.1130/00167606(1984)95<364:RGIOTE>2.0.CO;2.
- Bown, P. 1998. *Calcareous Nannofossil Biostratigraphy*. Chapman and Hall, Kluwer Academic, London. 315 pp.
- Bown, P.R. 2005. Paleogene calcareous nannofossils from the Kilwa and Lindi areas of coastal Tanzania (Tanzania Drilling Project Sites 1 to 10, 2003-4). *Journal of Nannoplankton Research*, 27, 21-95.
- Bown, P.R. & Dunkley Jones, T. 2006. New Paleogene calcareous nannofossil taxa from coastal Tanzania: Tanzania Drilling Project Sites 11 to 14. *Journal of Nannoplankton Research*, 28, 17-34.
- Bown, P.R. & Dunkley Jones, T. 2012. Calcareous nannofossils from the Paleogene equatorial Pacific (IODP Expedition 320 Sites U1331-1334). *Journal of Nannoplankton Research*, 32, 3-51.
- Bown, P.R. & Newsam, C. 2017. Calcareous nannofossils from the Eocene North Atlantic Ocean (IODP Expedition 342 Sites U1403-1411). *Journal of Nannoplankton Research*, 37, 25-60.
- Black, M. 1967. New names for some coccolith taxa. *Geological Society of London*, 1640, 139-145.
- Bramlette, M.N. & Sullivan, F.R. 1961. Coccolithophorids and related nannoplankton of the Early Tertiary in California. *Micropaleontology*, 7, 129-188.
- Bramlette, M.N. & Wilcoxon, J.A. 1967. Middle Tertiary calcareous nannoplankton of the Cípero section, Trinidad, W.I. *Tulane Studies in Geology and Paleontology*, 5, 93-131.
- Brönnimann, P. & Stradner, H. 1960. Die Foraminiferen- und Dicoasteridenzonen von Kuba und ihre interkontinentale korrelation. *Erdoel-Z.*, 76, 364-9.
- Bukry, D. 1971. Cenozoic calcareous nannofossils from the Pacific Ocean. *San Diego Society of Natural History Transactions*, 16, 303-327.
- Bukry, D. & Bramlette, M.N. 1969. Some new and stratigraphically useful calcareous nannofossils of the Cenozoic. *Tulane Studies in Geology*, 7, 131-142.
- Bukry, D. & Percival, S.F., Jr. 1971. New Tertiary calcareous nannofossils. *Tulane Studies in Geology and Paleontology*, 8, 123-146.
- Cámara, P. & Flinch, J.F. 2017. The Southern Pyrenees: A salt-based fold-and-thrust belt. In: *Permo-Triassic Salt Provinces of Europe, North Africa and the Atlantic Margins* (eds. Soto, J.I., Flinch, J. & Tari, G.). Elsevier, pp. 395-415.
- Cámara, P. & Klimowitz, J. 1985. Interpretación geodinámica de la vertiente centro-occidental surpirenaica (Cuencas de Jaca-Tremp). *Estudios geológicos*, 41, 391-404.
- Canudo, J.I., & Molina, E. 1988. Biocronología con foraminíferos planctónicos de la secuencia deposicional de Jaca (Pirineo aragonés): Eoceno medio y superior. *Congreso Geológico de España, Comunicaciones*, 1, 273-276.
- Deflandre, G. 1952. Classe des Coccolithophoridés (Coccolithophoridae Lohmann, 1902). In: *Traité de Zoologie. Anatomie, Systématique, Biologie v. 1, part 1, Phylogénie. Protozoaires: généralités* (ed. Grasse, P.P.). Flagellés. Masson, Paris; 439-470.
- Deflandre, G. 1959. Sur les nannofossiles calcaires et leur systématique. *Revue de Micropaleontologie*, 2, 127-152.
- Deflandre, G. & Fert, C. 1954. Observations sur les coccolithophoridés actuels et fossiles en microscopie ordinaire et électronique. *Annales de Paléontologie*, 40, 115-176.
- Fioroni, C., Villa, G., Persico, D. & Jovane, L. 2015. Middle Eocene-Lower Oligocene calcareous nannofossil biostratigraphy and paleoceanographic implications from Site 711 (equatorial Indian Ocean). *Marine Micropaleontology*, 118, 50-62; doi: 10.1016/j.marmicro.2015.06.001.
- Flores, J.A. & Sierra, F.J. 1997. Revised technique for calculation of calcareous nannofossil accumulation rates. *Micropaleontology*, 43, 321-324.
- Fornaciari, E., Agnini, C., Catanzariti, R., Rio, D., Bolla, E.M. & Valvasoni, E. 2010. Mid-latitude calcareous nannofossil biostratigraphy and biochronology across the middle to late Eocene transition. *Stratigraphy*, 7, 229.
- Hay, W.W. 1977. Calcareous nannofossils. In: *Oceanic Micropaleontology* (ed. Ramsay, A.T. S.). Academic Press, London 1055-1200.
- Hay, W.W. & Towe, K.M. 1962. Electron microscope examination of some coccoliths from Donzacq (France). *Eclogae Geologicae Helveticae*, 55, 497-517.
- Hay, W.W., Mohler, H.P. & Wade, M.E. 1966. Calcareous nannofossils from Nal'chik (northwest Caucasus). *Eclogae Geologicae Helveticae*, 59, 379-399.
- Jerkovic, L. 1970. *Noëlaerhabdus* nov. gen. type d'une nouvelle famille de Coccolithophoridés fossiles: Noëlaerhabdaceae du Miocène supérieur de Yougoslavie. *Comptes Rendus Hebdomadaires des Séances de l'Académie des Sciences. Paris. Série D - Sciences Naturelles*, 270, 468-470.
- Kamptner, E. 1954. Untersuchungen über den Feinbau der Coccolithen. *Archiv für Protistenkunde*, 100, 1-90.
- Kamptner, E. 1963. Coccolithineen-Skelettreste aus Tiefseeablagerungen des Pazifischen Ozeans. *Ann. Naturh. Mus. Wien*, 66, 139-204.
- Klumpp, B. 1953. Beitrag zur Kenntnis der Mikrofossilien des Mittleren und Oberen Eozän. *Palaeontographica A*, 103, 377-406.

- Labaume, P., Meresse, F., Jolivet, M., Teixell, A. & Lahfid, A. 2016. Tectonothermal history of an exhumed thrust-sheet-top basin: An example from the south Pyrenean thrust belt. *Tectonics*, 35, 1280-1313; doi: 10.1016/j.crte.2015.10.010.
- Labaume, P., Séguret, M. & Seyve, C. 1985. Evolution of a turbiditic foreland basin and analogy with an accretionary prism: Example of the Eocene south-Pyrenean basin. *Tectonics*, 4, 661-685; doi: 10.1029/TC004i007p00661.
- Larrasoaña, J.C., Gonzalvo, C., Molina, E., Monechi, S., Ortiz, S., Tori, F. & Tosquella, J. 2008. Integrated magnetobiochronology of the Early/Middle Eocene transition at Agost (Spain): implications for defining the Ypresian/Lutetian boundary stratotype. *Lethaia*, 41, 395-415; doi: 10.1111/j.1502-3931.2008.00096.x.
- Levin, H.L. 1965. Coccolithophoridae and related microfossils from the Yazoo Formation (Eocene) of Mississippi. *Journal of Paleontology*, 39, 265-272.
- Locker, S. 1967. Neue Coccolithophoriden (Flagellata) aus dem Alttertiär Norddeutschlands. *Geologie, Berlin*, 16, 361-364.
- Locker, S. 1968. Biostratigraphie des Alttertiärs von Norddeutschland mit Coccolithophoriden. *Monatsberichte der Deutschen Akademie der Wissenschaften zu Berlin*, 10, 220-229.
- Lohmann, H. 1902. Die Coccolithophoridae, eine Monographie der Coccolithen bildenden Flagellaten, zugleich ein Beitrag zur Kenntnis des Mittelmeerauftriebs. *Archiv für Protistenkunde*, 1, 89-165.
- Lupi, C. & Wise, S.W., Jr. 2006. Calcareous nannofossil biostratigraphic framework for middle Eocene sediments from ODP Hole 1260A, Demerara Rise. *Revue de Micropaléontologie*, 49, 245-253; doi: 10.1016/j.revmic.2006.10.001.
- Martini, E. 1971. Standard Tertiary and Quaternary calcareous nannoplankton zonation. In: *Proceedings 2nd International Conference Planktonic Microfossils Roma* (ed. Farinacci, A.). Tecnoscienza, Rome 2, 739-785.
- Martini, E. & Müller, C. 1986. Current Tertiary and Quaternary calcareous nannoplankton stratigraphy and correlations. *Newsletters on Stratigraphy*, 16, 99-112.
- Martini, E. & Ritzkowski, S. 1968. Was ist das ‚Unter-Oligozän‘? Eine analyse der Beyrich'schen und v Koenen'schen Fassung der Stufe mit Hilfe des fossilen Nannoplanktons. *Nachr Akad Wiss Göttingen; II Mathematisch-Physikalische Klasse*, 13, 231-250.
- Mita, I. 2001. Data report: Early to late Eocene calcareous nannofossil assemblages of Sites 1051 and 1052, Blake Nose, northwestern Atlantic Ocean. *Proceedings of the Ocean Drilling Program, Scientific Results B*, 171, 1-28.
- Mochales, T., Barnolas, A., Pueyo, E.L., Serra-Kiel, J., Casas, A.M., Samsó, J.M., Ramajo, J. & Sanjuán, J. 2012. Chronostratigraphy of the Boltaña anticline and the Ainsa Basin (Southern Pyrenees). *Geological Society of America Bulletin*, 124, 1229-1250; doi:10.1130/B30418.1.
- Mutti, E., Luterbacher, H.P., Ferrer, J. & Rosell, J. 1972. Schema stratigrafico e lineamenti di facies del Paleogene marino della zona centrale sudpirenaica tra Tremp (Catalogna) e Pamplona (Navarra). *Memoria della Società Geologica de Italia*, 11, 391-416.
- Norris, R.D., Wilson, P.A., Blum, P. & the Expedition 342 Scientists. 2014. *Proceedings IODP, 342*. College Station, TX (Integrated Ocean Drilling Program); doi: 10.2204/iodp.proc.342.2014.
- Oms, O., Dinarès-Turell, J. & Remacha, E. 2003. Magnetic stratigraphy from deep clastic turbidites: an example from the Eocene Hecho group (southern Pyrenees). *Studia Geophysica et Geodaetica*, 47, 275-288; doi: 10.1023/A:1023719607521.
- Okada, H. & Bukry, D. 1980. Supplementary modification and introduction of code numbers to the low-latitude coccolith biostratigraphic zonation (Bukry, 1973; 1975). *Marine Micropaleontology*, 5, 321-325; doi: 10.1016/0377-8398(80)90016-X.
- Pascher, A. 1910. Chrysomonaden aus dem Hirschberger Grossteiche. *Monographien und Abhandlungen zur Internationalen Revue der gesamten Hydrobiologie und Hydrographie*, 1, 66.
- Perch-Nielsen, K. 1971. Elektronenmikroskopische untersuchungen an Coccolithen und verwandten Formen aus dem Eozan von Danemark. *Biologiske Skrifter. Kongelige Danske Videnskabernes Selskab*, 18, 1-76.
- Perch-Nielsen, K. 1985. Mesozoic calcareous nannofossils. In: *Plankton Stratigraphy* (eds. Bolli, H.M., Saunders, J.B. & Perch-Nielsen, K.). Cambridge University Press, Cambridge, 329-426.
- Poche, F. 1913. Das System der Protozoa. *Archiv für Protistenkunde*, 30, 125-321.
- Puigdefàbregas, C. 1975. La sedimentación molásica en la Cuenca de Jaca. *Monografías del Instituto de Estudios Pirenaicos, Jaca (Spain)*. 104, 187 p.
- Radomski, A. 1968. Calcareous nannoplankton zones in the Paleogene of the Western Polish Carpathian. *Annales de la Société Géologique de Pologne*, 38, 544-605.
- Remacha, E. & Fernández, L. P. 2003. High-resolution correlation patterns in the turbidite systems of the Hecho Group (South-Central Pyrenees, Spain). *Marine and Petroleum Geology*, 20, 711-726; doi: 10.1016/j.marpetgeo.2003.09.003.
- Remacha, E. & Picart, J. 1991. El complejo turbidítico de Jaca y el delta de la arenisca de Sabiñánigo. *Excursion Guide Book, 8. 1er. Congreso del Grupo Español del Terciario*. Vic Universitat de Barcelona.
- Remacha, E., Arbués, P. & Carreras, M. 1987. Precisiones sobre los límites de la secuencia deposicional de Jaca. Evolución de las facies desde la base de la secuencia hasta el techo de la arenisca de Sabiñánigo. *Boletín Geológico y Minero de España*, 98, 40-48.
- Remacha, E., Fernández, L.P. & Maestro, E. 2005. The transition between sheet-like lobe and basin-plain turbidites in the Hecho Basin (South-Central Pyrenees, Spain). *Journal of Sedimentary Research*, 75, 798-819; doi: 10.2110/jsr.2005.064.
- Remacha, E., Oms, O. & Coello, J. 1995. The Rapitán turbidite channel and its related eastern levee-overbank deposits, Eocene Hecho group, south-central Pyrenees, Spain. In: *Atlas of Deep Water Environments* (eds, Pickering, K.T., Hiscott, R.N., Kenyon, N.H., Ricci

- Lucchi, F. & Smith, R.D.A.). Springer Netherlands, 145-149. doi: 10.1007/978-94-011-1234-5\_22.
- Schiller, J. 1930. *Coccolithineae. Rabenhorst's Kryptogamen-Flora. Kryptogamen-Flora von Deutschland, Osterreich und der Schweiz*. Leipzig: Akademische Verlagsgesellschaft MBH.
- Schwartz, E.H.L. 1894. Coccoliths. *Annals and Magazine of Natural History*, Jun-14, 341-346.
- Scotchman, J.I., Bown, P., Pickering, K.T., BouDagher-Fadel, M., Bayliss, N.J. & Robinson, S.A. 2015. A new age model for the middle Eocene deep-marine Ainsa Basin, Spanish Pyrenees. *Earth-Science Reviews*, 144, 10–22; doi: 10.1016/j.earscirev.2014.11.006.
- Soler-Sampere, M. & Puigdefàbregas, C. 1970. Líneas generales de la geología del Alto Aragón Occidental. *Pirineos*, 95, 5-19.
- Stradner, H. 1962. Über neue und wenig bekannte Nannofossilien aus Kreide und Alttertiär. *Sonderabdruck aus den Verhandlungen der Geologischen Bundesanstalt*, 2, 363-377.
- Tan, S.H. 1927. Discoasteridae incertae sedis. *Proceedings of the Koninklijke Nederlandse Akademie van Wetenschappen, Sect Sci*, 30, 411-419.
- Teixell, A. 1990. Alpine thrusts at the western termination of the Pyrenean Axial Zone. *Bulletin de la Société Géologique de France*, 6, 241-249.
- Teixell, A. 1996. The Ansó transect of the southern Pyrenees: basement and cover thrust geometries. *Journal of the Geological Society*, 153, 301-310; doi: 10.1144/gsjgs.153.2.0301.
- Toffanin, F., Agnini, C., Rio, D., Acton, G., & Westerhold, T. 2013. Middle Eocene to early Oligocene calcareous nannofossil biostratigraphy at IODP Site U1333 (equatorial Pacific). *Micropaleontology*, 59, 69-82.
- Varol, O. 1989. Eocene calcareous nannofossils from Sile (northwest Turkey). *Revista Española de Micropaleontología*, 21, 273-320.
- Wallich, G.C. 1877. XXXIV - Observations on the Coccosphere. *Journal of Natural History*, 19, 342-350.
- Wei, W. & Wise, S.W. 1989. Paleogene calcareous nannofossil magnetobiochronology: results from South Atlantic DSDP Site 516. *Marine Micropaleontology*, 14, 119-152; doi: 0.1016/0377-8398(89)90034-0.
- Wise, S.W. 1973. Calcareous nannofossils from cores recovered during Leg 18, Deep Sea Drilling Project: biostratigraphy and observations on diagenesis. *Initial Report, Deep Sea Drilling Project*, 18, 569-615.
- Young, J.R. & Bown, P.R. 1997. Higher classification of calcareous nannofossils. *Journal of Nannoplankton Research*, 19, 15-20.
- Young, J.R., Bergen, J.A., Bown, P.R., Burnett, J.A., Fiorentino, A., Jordan, R.W., Kleijne, A., Niel, B.E., Van Romein, A.J.T. & Von Salis, K. 1997. Guidelines for coccolith and calcareous nannofossil terminology. *Palaeontology*, 40, 875–912.
- Young, J.R., Bown, P.R. & Lees, J.A. (eds.) 2017. Nannotax3 website. International Nannoplankton Association. 21 Nov. 2017. URL: <http://ina.tmsoc.org/Nannotax3>.
- Young, J.R., Geisen, M., Cros, L., Kleijne, A., Sprengel, C., Probert, I. & Østergaard, J. 2003. A guide to extant coccolithophore taxonomy. *Journal of Nannoplankton Research*, 1, 1-125.

## APPENDIX I: CALCAREOUS NANNOFOSSIL SYSTEMATICS

### Calcareous nannofossil biomarker genus and species

Order ISOCHRYSIDALES Pascher, 1910.

Family **Noelaerhabdaceae** Jerkovic, 1970 emend. Young & Bown, 1997.

Genus *Reticulofenestra* Hay, Mohler & Wade, 1966.

*Reticulofenestra umbilicus* (Levin, 1965) Martini & Ritzkowski, 1968.

(Fig. 4d)

Genus *Cribocentrum* Perch-Nielsen, 1971

*Cribocentrum reticulatum* (Perch-Nielsen, 1985)

(Fig. 4e)

Genus *Dictyococcites* (Hay, Mohler & Wade, 1966) Bukry & Percival, 1971.

*Dictyococcites bisectus* (Hay, Mohler & Wade, 1966) Bukry & Percival, 1971.

Order COCCOLITHALES Schwarz, 1932.

Family **Coccolithaceae** Poche, 1913 emend. Young & Bown, 1997.

Genus *Coccolithus* Schwarz, 1894

*Coccolithus gigas* (Bramlette & Sullivan, 1961) Radomski, 1968.

(Fig. 4a)

Genus *Chiasmolithus* Hay *et al.*, 1966.

*Chiasmolithus solitus* (Bramlette & Sullivan, 1961) Locker, 1968.

(Fig. 4f)

Order DISCOASTERALES Hay, 1977

Family **Sphenolithaceae** Deflandre, 1952

Genus *Sphenolithus* Deflandre in Grassé, 1952

*Sphenolithus furcatolithoides* Group sensu Bown & Dunkley Jones, 2012

*Sphenolithus furcatolithoides* Locker, 1967; morphotype "B" Perch-Nielsen, 1985

(Figs 4i, 4j)

*Sphenolithus strigosus* Bown & Dunkley Jones, 2006

(Figs 4b, 4c)

*Sphenolithus radians* Group sensu Bown & Dunkley Jones, 2012

*Sphenolithus spiniger* Bukry, 1971

(Figs 4g, 4h)

*Sphenolithus predistentus* Group sensu Bown & Dunkley Jones, 2012

*Sphenolithus predistentus* Bramlette & Wilcoxon, 1967

(Figs 4k, 4l)

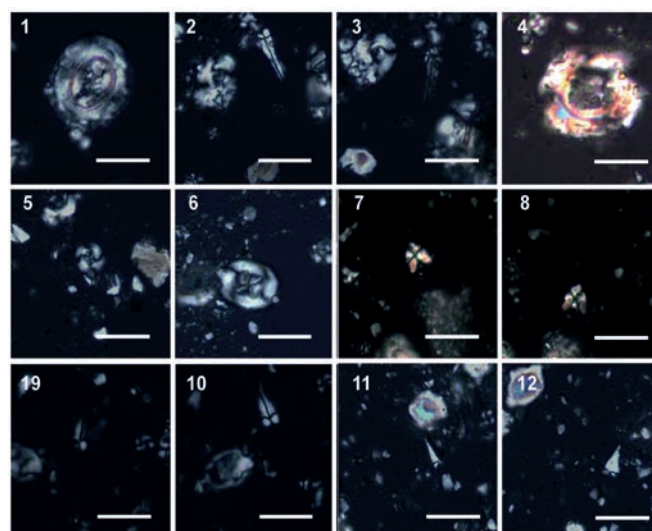


**Figure 4.** Microphotographs of Eocene calcareous nannofossil index species from the Jaca section. **a)** *Chiasmolithus gigas* (sample 6). **b)** *Sphenolithus strigosus* 0° (sample 7). **c)** *Sphenolithus strigosus* 45° (sample 11). **d)** *Reticulofenestra umbilicus* >10 μm (sample 20). **e)** *Cribocentrum reticulatum* (sample 22). **f)** *Chiasmolithus solitus* (sample 6). **g)** *Sphenolithus spiniger* 0° (sample 2). **h)** *Sphenolithus spiniger* 45° (sample 2). **i)** *Sphenolithus furcatolithoides* "B" 20° (sample 23). **j)** *Sphenolithus furcatolithoides* "B" 0° (sample 23). **k)** *Sphenolithus predistentus* 0° (sample 28). **l)** *Sphenolithus predistentus* 45° (sample 28). Scale bars 10 μm.

## APPENDIX II. OTHER TAXA CITED IN TEXT

- Blackites* Hay & Towe, 1962  
*Blackites gladius* (Locker, 1967) Varol, 1989  
*Blackites inversus* (Bukry & Bramlette, 1969) Bown & Newsam, 2017  
*Coccolithus* Schwartz, 1894  
*Coccolithus pelagicus* (Wallich 1877) Schiller, 1930  
*Coccolithus formosus* (Kamptner, 1963) Wise, 1973  
*Dictyococcites* Black, 1967  
*Dictyococcites bisectus* (Hay *et al.*, 1966) Bukry & Percival, 1971  
*Dictyococcites scrippsae* Bukry & Percival, 1971.
- Discoaster* Tan, 1927  
*Helicosphaera* Kamptner, 1954  
*Lanternithus* Stradner, 1962  
*Lanternithus arcanus* Bown, 2005  
*Lanternithus inversus* Bown, 2005  
*Nannotetrina* Achuthan & Stradner, 1969  
*Pemma* Klumpp, 1953  
*Pontosphaera* Lohmann, 1902  
*Sphenolithus* Deflandre in Grassé, 1952  
*Sphenolithus cuniculus* Bown, 2005  
*Sphenolithus moriformis* (Brönnimann & Stradner, 1960) Bramlette & Wilcoxon, 1967  
*Zygrhablithus* Deflandre, 1959  
*Zygrhablithus bijugatus* (Deflandre in Deflandre & Fert, 1954) Deflandre, 1959







## Anexo IV. Publicación adicional

### “Limited variability in the phytoplankton *Emiliana huxleyi* since the pre-industrial era in the Subantarctic Southern Ocean”

Andrés S. Rigual-Hernández <sup>a,\*</sup>, José Manuel Sánchez-Santos <sup>b</sup>, Ruth Eriksen <sup>c,d</sup>, Andrew D. Moy <sup>e,f</sup>, Francisco J. Sierro <sup>a</sup>, José-Abel Flores <sup>a</sup>, Fátima Abrantes <sup>g,h</sup>, Helen Bostook <sup>i</sup>, Scott D. Nodder <sup>j</sup>, **Alba González-Lanchas** <sup>a</sup> y Thomas William Trull <sup>c,d,e</sup>

<sup>a</sup> Departamento de Geología, Universidad de Salamanca, 37008 Salamanca, España

<sup>b</sup> Departamento de Estadística, Universidad de Salamanca, 37008 Salamanca, España

<sup>c</sup> CSIRO Oceans and Atmosphere, Hobart, Tasmania 7001, Australia

<sup>d</sup> Institute for Marine and Antarctic Studies, University of Tasmania, Private Bag 129, Hobart, Tasmania 7001, Australia

<sup>e</sup> Antarctic Climate and Ecosystems Cooperative Research Centre and Australian Antarctic Program Partnership, University of Tasmania, Hobart, Tasmania 7001, Australia

<sup>f</sup> Australian Antarctic Division, Channel Highway, Kingston, Tasmania 7050, Australia

<sup>g</sup> Portuguese Institute for Sea and Atmosphere (Takahashi et al.), Divisão de Geologia Marinha (DivGM), Rua Alferedo Magalhães Ramalho 6, Lisboa, Portugal

<sup>h</sup> CCMAR, Centro de Ciências do Mar, Universidade do Algarve, Campus de Gambelas, 8005-139 Faro, Portugal

<sup>i</sup> School of Earth and Environmental Sciences, University of Queensland, Brisbane, Queensland 4072, Australia

<sup>j</sup> National Institute of Water and Atmospheric Research, Wellington 6021, New Zealand

Artículo **publicado** en *Anthropocene*

DOI: [10.1016/j.ancene.2020.100254](https://doi.org/10.1016/j.ancene.2020.100254)

## Resumen

Los estudios climáticos actuales indican que el calentamiento experimentado por el Océano Austral avanza a un ritmo más rápido que el promedio del océano global (Shadwick et al., 2015). Además, debido a sus bajas temperaturas y alcalinidad moderada, esta región es particularmente vulnerable a acidificación del océano (Cao y Caldeira, 2008; Doney et al., 2009).

Los cocolitóforos son el grupo de fitoplancton calcificador más abundante y productivo, y un componente importante de los ecosistemas del Océano Austral (Tyrrell y Young, 2009).

Las observaciones y experimentos llevados a cabo en laboratorios, se centran en el estudio de la especie de cocolitóforos moderna más abundante, *Emiliana huxleyi*. Los resultados de estos análisis sugieren que esta especie altamente susceptible a las variaciones en la química del carbonato del agua del océano, lo cual implica un impacto en el ciclo del carbono (Langer et al., 2009; Westbroek et al., 1993). No obstante, hoy día, si existe una modificación ambiental durante la era industrial de origen antropogénico, y esta misma se encuentra ejerciendo un efecto determinado sobre las poblaciones de cocolitóforos del océano Austral, es un hecho todavía incierto.

En este estudio se analiza la composición de la asociación de cocolitóforos y los parámetros morfométricos de los cocolitos pertenecientes a la especie *E. huxleyi* en muestras tomadas de sedimentos de edad Holoceno procedentes del Sur de Tasmania. Los resultados del análisis sugieren que la disolución ejerció un efecto sobre la talla y la masa de los cocolitos existentes en el sedimento, reduciendo sus valores. No obstante, el valor de espesor de los cocolitos evidencia un desacoplamiento en la evolución de las tendencias de sus valores; es decir, estos valores no se encuentran afectados por la disolución. Este es un elemento determinante que posibilitó la comparación directa entre muestras con diferentes grados de preservación.

El patrón de distribución latitudinal del espesor de los cocolitos medidos refleja, además, el patrón latitudinal de los gradientes ambientales en la capa superficial, donde destaca la relación entre la distribución geográfica (horizontal) de los diferentes morfotipos de *E. huxleyi* sobre el control de la morfometría.

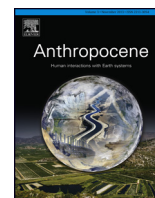
La comparación de estos datos procedentes del análisis de los cocolitos de *E. huxleyi* en los sedimentos, anteriormente detallados, con los de los registros anuales de acumulación de este grupo, procedentes de trampas de sedimentos localizadas en la zona subantártica, evidenció que los cocolitos modernos de *E. huxleyi* son menos robustos que durante la era preindustrial con una variabilidad del 2%. Esta variación relativamente ligera en el espesor del cocolito, contrasta marcadamente con trabajos anteriores en esta zona, que documentaron una pronunciado reducción en la calcificación de foraminíferos, un grupo para el que se registra una dramática disminución del peso de sus caparazones de entre el 30 y 35% y que se vincula, de igual modo, al efecto de la acidificación del océano (Moy et al., 2009).

Los resultados de este estudio subrayan, por lo tanto y de forma crítica, la existencia de una sensibilidad variable de los diferentes grupos de plancton calcificador marino al cambio ambiental en curso.

## Referencias

- Cao, L., Caldeira, K., 2008. Atmospheric CO<sub>2</sub> stabilization and ocean acidification. *Geophysical Research Letters* 35.
- Doney, S.C., Fabry, V.J., Feely, R.A., Kleypas, J.A., 2009. Ocean acidification: the other CO<sub>2</sub> problem. *Annual review of marine science* 1, 169-192.
- Langer, G., Nehrke, G., Probert, I., Ly, J., Ziveri, P., 2009. Strain-specific responses of *Emiliana huxleyi* to changing seawater carbonate chemistry. *Biogeosciences* 6, 2637-2646.
- Moy, A.D., Howard, W.R., Bray, S.G., Trull, T.W., 2009. Reduced calcification in modern Southern Ocean planktonic foraminifera. *Nature geoscience* 2, 276-280.
- Shadwick, E., Trull, T., Tilbrook, B., Sutton, A., Schulz, E., Sabine, C., 2015. Seasonality of biological and physical controls on surface ocean CO<sub>2</sub> from hourly observations at the Southern Ocean Time Series site south of Australia. *Global Biogeochemical Cycles* 29, 223-238.

- Takahashi, T., Sutherland, S.C., Wanninkhof, R., Sweeney, C., Feely, R.A., Chipman, D.W., Hales, B., Friederich, G., Chavez, F., Sabine, C., 2009. Climatological mean and decadal change in surface ocean  $p\text{CO}_2$ , and net sea–air  $\text{CO}_2$  flux over the global oceans. *Deep Sea Research Part II: Topical Studies in Oceanography* 56, 554-577.
- Tyrrell, T., Young, J., 2009. *Coccolithophores*.
- Westbroek, P., Brown, C.W., van Bleijswijk, J., Brownlee, C., Brummer, G.J., Conte, M., Egge, J., Fernández, E., Jordan, R., Knappertsbusch, M., 1993. A model system approach to biological climate forcing. The example of *Emiliana huxleyi*. *Global and planetary change* 8, 27-46.



## Limited variability in the phytoplankton *Emiliana huxleyi* since the pre-industrial era in the Subantarctic Southern Ocean

A.S. Rigual-Hernández<sup>a,\*</sup>, J.M. Sánchez-Santos<sup>b</sup>, R. Eriksen<sup>c,d</sup>, A.D. Moy<sup>e,f</sup>, F.J. Sierro<sup>a</sup>, J.A. Flores<sup>a</sup>, F. Abrantes<sup>g,h</sup>, H. Bostock<sup>i</sup>, S.D. Nodder<sup>j</sup>, A. González-Lanchas<sup>a</sup>, T.W. Trull<sup>c,d,e</sup>

<sup>a</sup>Área de Paleontología, Departamento de Geología, Universidad de Salamanca, 37008 Salamanca, Spain

<sup>b</sup>Departamento de Estadística, Universidad de Salamanca, 37008 Salamanca, Spain

<sup>c</sup>CSIRO Oceans and Atmosphere, Hobart, Tasmania 7001, Australia

<sup>d</sup>Institute for Marine and Antarctic Studies, University of Tasmania, Private Bag 129, Hobart, Tasmania 7001, Australia

<sup>e</sup>Antarctic Climate and Ecosystems Cooperative Research Centre and Australian Antarctic Program Partnership, University of Tasmania, Hobart, Tasmania 7001, Australia

<sup>f</sup>Australian Antarctic Division, Channel Highway, Kingston, Tasmania 7050, Australia

<sup>g</sup>Portuguese Institute for Sea and Atmosphere (IPMA), Divisão de Geologia Marinha (DivGM), Rua Alferedo Magalhães Ramalho 6, Lisboa, Portugal

<sup>h</sup>CCMAR, Centro de Ciências do Mar, Universidade do Algarve, Campus de Gambelas, 8005-139 Faro, Portugal

<sup>i</sup>School of Earth and Environmental Sciences, University of Queensland, Brisbane, Queensland 4072, Australia

<sup>j</sup>National Institute of Water and Atmospheric Research, Wellington 6021, New Zealand

### ARTICLE INFO

#### Article history:

Received 22 May 2020

Received in revised form 20 July 2020

Accepted 21 July 2020

Available online 24 July 2020

#### Keywords:

CO<sub>2</sub> emissions  
ocean acidification  
environmental change  
Southern Ocean  
coccolithophores  
*Emiliana huxleyi*

### ABSTRACT

The Southern Ocean is warming faster than the average global ocean and is particularly vulnerable to ocean acidification due to its low temperatures and moderate alkalinity. Coccolithophores are the most productive calcifying phytoplankton and an important component of Southern Ocean ecosystems. Laboratory observations on the most abundant coccolithophore, *Emiliana huxleyi*, suggest that this species is susceptible to variations in seawater carbonate chemistry, with consequent impacts in the carbon cycle. Whether anthropogenic environmental change during the industrial era has modified coccolithophore populations in the Southern Ocean, however, remains uncertain. This study analysed the coccolithophore assemblage composition and morphometric parameters of *E. huxleyi* coccoliths of a suite of Holocene-aged sediment samples from south of Tasmania. The analysis suggests that dissolution diminished the mass and length of *E. huxleyi* coccoliths in the sediments, but the thickness of the coccoliths was decoupled from dissolution allowing direct comparison of samples with different degree of preservation. The latitudinal distribution pattern of coccolith thickness mirrors the latitudinal environmental gradient in the surface layer, highlighting the importance of the geographic distribution of *E. huxleyi* morphotypes on the control of coccolith morphometrics. Additionally, comparison of the *E. huxleyi* coccolith assemblages in the sediments with those of annual subantarctic sediment trap records found that modern *E. huxleyi* coccoliths are ~2% thinner than those from the pre-industrial era. The subtle variation in coccolith thickness contrasts sharply with earlier work that documented a pronounced reduction in shell calcification and consequent shell-weight decrease of ~30–35% on the planktonic foraminifera *Globigerina bulloides* induced by ocean acidification. Results of this study underscore the varying sensitivity of different marine calcifying plankton groups to ongoing environmental change.

© 2020 The Authors. Published by Elsevier Ltd. This is an open access article under the CC BY-NC-ND license (<http://creativecommons.org/licenses/by-nc-nd/4.0/>).

## 1. Introduction

*Emiliana huxleyi* (Lohmann) Hay and Mohler is the most abundant and ubiquitous calcareous phytoplankton species and the only coccolithophore that regularly forms blooms in a wide range of environments, from polar to tropical systems and from

neritic to oceanic waters (Brown and Yoder, 1994; Tyrrell and Young, 2009). These blooms annually cover an areal extent of approximately  $1.0 \times 10^6$  km<sup>2</sup> equivalent to 0.28% of the global ocean (Brown and Yoder, 1994) and reach cell concentrations up to 10<sup>8</sup> cell per litre (Berge, 1962), thereby playing an important role in the marine carbon cycle (Westbroek et al., 1989). The underlying reason for the ecological success of *E. huxleyi* is due to its extensive genomic variability and consequent physiological adaptation repertoires (Read et al., 2013). Indeed, the high intraspecific

\* Corresponding author.

genetic divergence strongly suggests that *E. huxleyi* most likely represents a species complex, i.e. clades that are well separated according to most species definitions but are not always morphologically distinguishable (Read et al., 2013).

Carbon dioxide (CO<sub>2</sub>) emissions from anthropogenic sources have been altering the physical and chemical properties of the oceans beyond their natural state since the onset of the industrial era (Pachauri et al., 2014). In addition to increased warming, shallowing of mixed layers and changes in nutrient supply, enhanced oceanic uptake of anthropogenic CO<sub>2</sub> is lowering surface water pH and carbonate ion concentration, a process known as ocean acidification (Caldeira and Wickett, 2003). Ocean-carbon cycle models project that polar and subpolar ecosystems will be the first regions to become undersaturated with respect to calcium carbonate minerals in the coming decades (Orr et al., 2005; Feely et al., 2009). In particular, the mild alkalinity and low temperatures of the surface waters of the Southern Ocean, makes this region particularly vulnerable to ocean acidification (Cao and Caldeira, 2008; Fabry et al., 2009a; Shadwick et al., 2015).

Increased seawater acidification in laboratory experiments often results in reduced calcification rates in many calcified marine organisms, including planktonic foraminifera (Bijma et al., 2002), pteropods (Bednaršek et al., 2014; Manno et al., 2017), cold-water corals (Fabry et al., 2009b) and coccolithophorids (Meyer and Riebesell, 2015). Seawater carbonate chemistry manipulation experiments with *E. huxleyi* strains have come to different conclusions, with some studies pointing to enhanced calcification rates and net primary production at elevated partial pressure of CO<sub>2</sub> (pCO<sub>2</sub>) (e.g. Iglesias-Rodríguez et al., 2008), while others reported opposing effects (Riebesell et al., 2000). Reconciliation of these apparently conflicting findings is likely the result of the differing sensitivity to ocean acidification of the *E. huxleyi* strains employed in each study (Langer et al., 2009), including the possibility of contrasting positive responses to increased CO<sub>2</sub> availability versus negative responses to acidification (Bach et al., 2015). This notion is supported by Müller et al. (2015), who observed differing responses of three selected *E. huxleyi* strains isolated from the Southern Ocean to changing seawater carbonate chemistry. While laboratory experiments provide invaluable information of the physiological response of *E. huxleyi*, they also pose important limitations. The short duration of most laboratory manipulations preclude evolutionary adaptation to changing conditions (Langer et al., 2006; Schlüter et al., 2014), while the use of single isolated *E. huxleyi* strains eliminates the possibility of dominance shifts in the assemblage. These limitations introduce important uncertainties when extrapolating laboratory results to the natural field environment. It is, therefore, critical to perform field experiments (e.g. Triantaphyllou et al., 2018) to confirm or disprove the laboratory observations.

Comparison of sediment trap records with microplankton assemblages preserved in sea-floor sediments provides a valuable approach to assess the impact of climate change on plankton communities since the pre-industrial era (e.g. Jonkers et al., 2019). Moored time-series sediment traps are a reliable tool to reconstruct the seasonal cycles of specific plankton groups, including coccolithophores (e.g. Broerse et al., 2000b; Ziveri et al., 2000; Triantaphyllou et al., 2010, among others). Importantly, sediment trap records provide a resource to integrate annual coccolith fluxes and can be used to eliminate the effects of seasonality, therefore providing an important advantage versus plankton tows. These characteristics make annual sediment trap records a robust proxy for determining the state of modern coccolithophore communities. Similarly, coccolith assemblages from the uppermost layers of the sea-floor sediments represents an integrated assemblage of the past hundreds to thousands of years and therefore provides a baseline of the natural state of coccolithophore communities

before substantial human influences on the global environment. Together, the comparison of annual coccolith flux records with the assemblages preserved in the surface sediments provide a powerful means to assess changes in coccolithophore communities in response to ongoing environmental change.

The present study was partly prompted by earlier results from a field experiment comparing the weight of the planktonic foraminifera species *Globigerina bulloides* collected by sediment traps with those from the Holocene-aged sediments in the Australian sector of the Subantarctic Zone (Moy et al., 2009). Results from the latter study showed that modern *G. bulloides* populations are about 30–35% lighter than those in the Holocene sediments suggesting that ocean acidification could have caused a thinning of their shells. Following this approach, here we compare the annual coccolith assemblages of the key-stone species *E. huxleyi* collected by sediment traps deployed in the subantarctic surface waters south of Tasmania from an earlier study (Rigual-Hernández et al., 2020a) with a suite of Holocene-aged sediments samples retrieved in the same region. We characterized the coccolithophore assemblages in the sediment samples and determined the mass, length, and degree of calcification of *E. huxleyi* coccoliths, in order to answer the following research questions: (1) How do the seafloor sediments south of Tasmania preserve the record of the coccolith assemblages living during the pre-industrial era?; (2) Which and how natural and/or anthropogenic alterations to the marine environment, if any, have induced a change in the subantarctic *E. huxleyi* populations since the pre-industrial Holocene?; (3) How do any observed changes differ from those previously documented in planktonic foraminifera, the other major pelagic calcifiers in the Southern Ocean?

### 1.1. Oceanographic setting

The physical and chemical characteristics of the surface waters south of Tasmania exhibit pronounced latitudinal changes that occur as a series of steps or oceanographic fronts from north to south (Fig. 1). The Subtropical Front is characterized by a pronounced sea surface temperature gradient of approximately 4 °C that occurs in less than 0.5° of latitude (Rintoul et al., 1997) and represents the boundary between the subtropical gyres to the north and the Subantarctic Zone waters to the south. The Subantarctic Zone displays surface water pCO<sub>2</sub> well below atmospheric equilibrium, therefore acting as a large net sink for atmospheric CO<sub>2</sub> (~1 Gt C yr<sup>-1</sup>; Metzl et al., 1999; Lenton et al., 2013).

North of the Subtropical Front, the Zeehan current (an extension of the Leeuwin current) flows down the Tasmanian west coast (Ridgway, 2007). Along the east coast of Tasmania, an extension of the East Australian Current flows southward. Most of the East Australian Current extension that reaches south of Tasmania, is directed northwest as part of the Flinders Current, while the remaining flows poleward forming eddies (van Sebille et al., 2012; Pardo et al., 2019). South of the Subtropical Front, the general circulation is governed by the Antarctic Circumpolar Current that flows eastward connecting each of the major ocean basins (Rintoul et al., 2001). As a result of the different properties of the surface waters, the Subtropical and Subantarctic Zones exhibit different phytoplankton compositions (Odate and Fukuchi, 1995; Kopczynska et al., 2001; Eriksen et al., 2018).

The solubility of calcium carbonate minerals increases at lower seawater temperature and higher pressures, and thus their solubility increases with depth in the water column. Calcium carbonate preservation is largely controlled by changes in the carbonate ion concentration ([CO<sub>3</sub><sup>2-</sup>]) throughout the water column. The lysocline or saturation horizon is defined as the



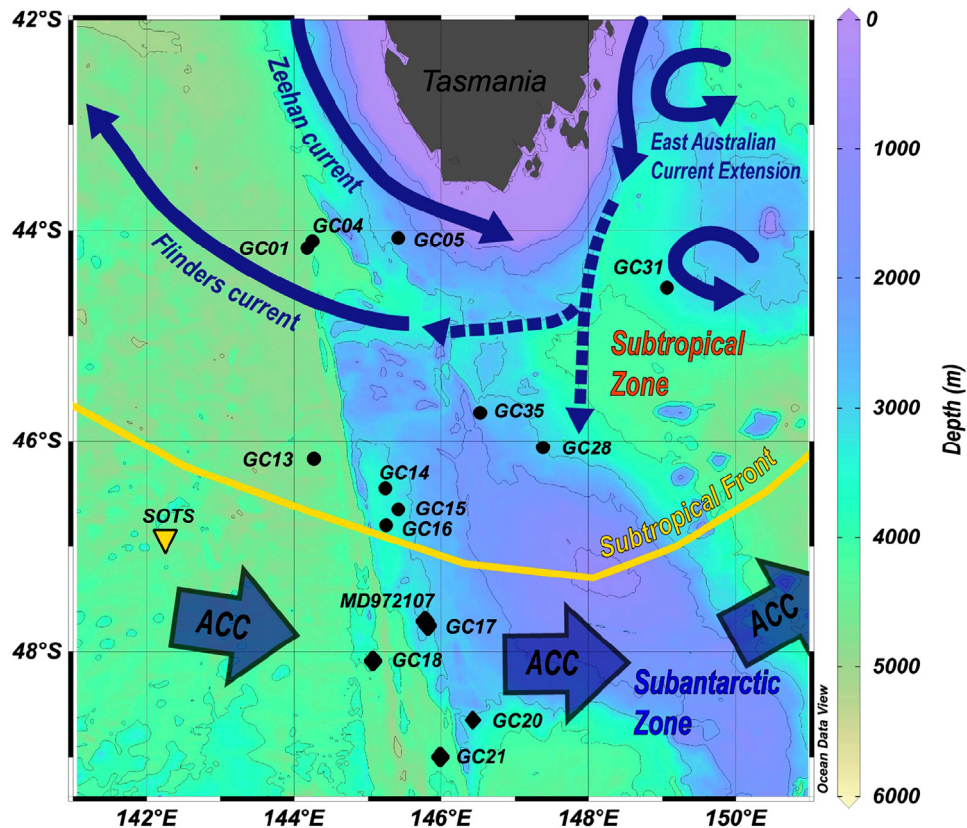


**Fig. 1.** Bathymetric map showing the location of Southern Ocean Time Series (SOTS) observatory sediment traps (yellow triangle) and Holocene core-top samples in the Subtropical Zone (black circles) and Subantarctic Zone (black diamonds) used in this study. Abbreviation: ACC – Antarctic Circumpolar Current. Oceanic fronts after Orsi et al. (1995). Ocean Data View software (Schlitzer, 2018) was used to generate this figure. Bathymetric data from General Bathymetric Chart of the Oceans (2020) (doi:10.5285/a29c5465-b138-234d-e053-6c86abc040b9).

depth in the water column where undersaturation ( $\Omega = 1$ ) with respect to a given  $\text{CaCO}_3$  phase (aragonite or calcite) occurs, therefore resulting in a pronounced increase in the rate of  $\text{CaCO}_3$  dissolution of that phase. In the subantarctic waters south of Tasmania, the calcite saturation horizon occurs at  $\sim 3400$  m (Moy et al., 2009; Bostock et al., 2011).

## 1.2. Distribution of *Emiliania huxleyi* morphotypes in the Southern Ocean

Based on the dimensions and fine structure of its coccoliths, *E. huxleyi* can be divided into different morphotypes. However, their precise delimitation can be difficult in some cases due to their overlapping features and size ranges (Young et al., 2003; Cook et al., 2011; Hagino et al., 2011). In the Southern Ocean, *E. huxleyi* largely dominates coccolithophore populations, displaying maximum abundances in the Subantarctic Zone and a general decline in its numbers moving poleward (Findlay and Giraudeau, 2000; Saavedra-Pellitero et al., 2014; Patil et al., 2017; Rigual Hernández et al., 2018). *E. huxleyi* populations in the waters south of Tasmania are primarily composed of three morphotypes: A overcalcified (A o/c), A and B/C (Cubillos et al., 2007; Cook et al., 2011; Cook et al., 2013), each of which is characterized by distinct coccolith structure and mass, photosynthetic pigment composition and differing responses to seawater carbonate chemistry variations (Cook et al., 2011; Cook et al., 2013; Krueger-Hadfield et al., 2014; Müller et al., 2015). These three morphotypes display important differences in their latitudinal distribution in the Australian sector of the Southern Ocean (Cubillos et al., 2007). The heavily-calcified type A o/c dominates *E. huxleyi* populations north of  $48^\circ\text{S}$  (i.e.

approximately the position of the Subantarctic Front), while the typical morphotype A extends roughly from the Subtropical Front to the Polar Front ( $\sim$ from  $44$  to  $55^\circ\text{S}$ ). Morphotype B/C displays the most southward distribution dominating from  $48$  to  $65^\circ\text{S}$  and becoming the only morphotype found in Antarctic Zone waters (Cubillos et al., 2007; Rigual Hernández et al., 2018). The light and delicate type B/C coccoliths are produced by the *E. huxleyi* var. *aurorae* ecotype, a Southern Ocean specialist with physiological adaptations that enable growth at cold temperatures ( $\sim 4^\circ\text{C}$ ) and low-light conditions (Cook et al., 2011).

## 2. Material and methods

### 2.1. The SOTS observatory

The Southern Ocean Time Series (SOTS) observatory is located at  $46^\circ 56' \text{S}$  and  $142^\circ 15' \text{E}$  (Fig. 1) and can be considered representative of a large swath of the Indian and Pacific sectors of the Subantarctic Zone ( $\sim 90$  to  $140^\circ\text{E}$ ; Trull et al., 2010). The SOTS facility consists of a set of three moorings platforms dedicated to measuring a range of physical, chemical, and biological processes, and the collection of ocean particles (Trull et al., 2010; Eriksen et al., 2018).

Rigual-Hernández et al. (2020a) analysed the seasonal variability of *E. huxleyi* coccolith assemblages collected by three vertically-moored sediment traps deployed from November 2009 to November 2010, to determine the seasonal variations of coccolith size and mass. Here, we take advantage of this study to obtain an approximation of the modern coccolithophore assemblages dwelling in the Subantarctic Zone. The potential source area (also

termed “statistical funnel”; Siegel et al., 1990; Siegel and Deuser, 1997) for the particles intercepted by a given sediment trap increases with depth. Therefore, to obtain the most robust representative of the modern conditions of Subantarctic Zone the three vertically-moored sediment trap records are represented as one composite sample (see section 2.6).

## 2.2. Holocene sediment samples

The sediment samples were retrieved from sediments underlying the subtropical and subantarctic waters south of Tasmania during the Australian Geological Survey Organisation Cruise 147 and IMAGES III cruise (Fig. 1 and Table 1). Most of the samples were collected from the South Tasman Rise, a large submarine plateau (approximately 500 km long) lying at depths ranging from 1000 to 4000 m. The majority of the samples were collected from locations above the top of the calcite saturation horizon and consequently expected to have good coccolith preservation. Based on the dated cores, sedimentation rates through the Holocene in the study area were low, with values ranging between 2–5 cm ky<sup>-1</sup>. The dated sediment samples suggest that the surface layer range between 3 to 7 kyrs BP (AMS <sup>14</sup>C dates for GC04 at a depth of 5–8 cm is 3160 yr BP, GC14 at 5–7 cm is 7373 yr BP (Connell and Sikes, 1997) and GC17 at 0–2 cm is 4440 yr BP (Moy et al., 2009)) therefore containing coccolithophore assemblages sedimented during the pre-industrial Holocene era.

## 2.3. Sample processing for calcareous nannoplankton analysis

Samples for calcareous nannoplankton analysis were prepared following a method adapted from Flores and Sierro (1997). Approximately 50 mg of dry sediment were suspended in a solution of sodium carbonate and sodium hydrogen carbonate (pH 8) with ammonia (2%). The samples were subject to gentle mechanical disaggregation on a rotating carousel for 24 hours (Stoll and Ziveri, 2002). Between 0.2 and 2 ml of sample were extracted with a micropipette and dropped onto a petri dish filled with buffered water and with a cover slip in its bottom. After settling 12 hours, the excess of water was removed using filter-paper strips. Then the cover slip was left to dry and mounted on a glass slide with Canada balsam. Coccoliths were identified to species level using a Nikon Eclipse 80i polarised light microscope at 1000x magnification. A minimum of 300 coccoliths were identified to the lowest taxonomic level possible. Only in GC18 sample, that contained extremely low coccolith abundance this target was not met, with only 45 coccoliths identified. Then, coccolith relative and absolute abundances were estimated.

A Carl Zeiss EVO HD25 Scanning Electron Microscope (SEM) was used to identify and classify about 100 *E. huxleyi* coccoliths per sample into morphotypes. Round glass cover slips were prepared following Flores and Sierro (1997), mounted on aluminium stubs and coated with gold. *E. huxleyi* morphotypes were identified following the same criteria as Rigual-Hernández et al. (2020a) which in turn is based on Young et al. (2003) and Hagino et al. (2005) with slight modifications adapted for Southern Ocean populations. Coccolithophore assemblage composition of most of the sediment samples analysed here had been previously characterized by Findlay and Giraudeau (2002). However, in order to be consistent and make the results comparable with the sediment trap results all the samples were recounted.

## 2.4. The *Calcidiscus leptoporus* – *Emiliana huxleyi* Dissolution Index (CEX)

Modern coccolith sinking assemblages in the subantarctic waters south of Tasmania are dominated by *E. huxleyi* (> 80% of the annual sinking assemblage) followed by *Calcidiscus leptoporus* (~10%) (Rigual-Hernández et al., 2020b). Although the coccoliths of these two species are placoliths, i.e. they are composed of a proximal and distal shield connected by a central column, they represent the two ends of the coccolith dissolution spectrum. While *E. huxleyi* produces fragile coccoliths with delicate T-shaped elements that make them particularly vulnerable to dissolution, and *C. leptoporus* producing heavily calcified shields highly resistant to dissolution. Since *E. huxleyi* and *C. leptoporus* have relatively similar ecological affinities, changes in this ratio could be potentially used as indicator of the intensity of dissolution in the sediments (e.g. Dittert et al., 1999; Boeckel and Baumann, 2004). If it is assumed that the proportion of these two species has remained similar through the Holocene until present, the *C. leptoporus* – *E. huxleyi* Dissolution Index (CEX) (Dittert et al., 1999) could be used to assess dissolution in the sediments. Previously, a ratio of 0.6 has been proposed as the critical boundary below which substantial carbonate dissolution occurs (Dittert et al., 1999; Boeckel and Baumann, 2004). The CEX index is calculated as follows:

$$CEX = \%E. huxleyi / (\%E. huxleyi + \%C. leptoporus)$$

## 2.5. Coccolith mass and size measurements

A minimum of 100 *Emiliana huxleyi* coccoliths were analysed in all samples with exception of GC16 and GC18 where 90 and 65 coccoliths were measured, respectively. A total of 1128 fields of view (FOV) were photographed using a Nikon Eclipse LV100 POL

**Table 1**

Summary of zonal system, latitude, longitude and water column depth of the sediment samples. STZ – Subtropical Zone, SAZ – Subantarctic Zone.

Core ID	Zonal system	Longitude (°E)	Latitude (°S)	Water column depth (m)
GC01	STZ	144.18	44.17	4262
GC04	STZ	144.25	44.10	2980
GC05	STZ	145.42	44.07	2334
GC13	STZ	144.27	46.17	4452
GC14	STZ	145.24	46.45	3360
GC15	STZ	145.42	46.65	3260
GC16	STZ	145.25	46.80	3523
GC17	SAZ	145.82	47.75	3001
GC18	SAZ	145.07	48.09	4368
GC20	SAZ	146.43	48.65	3300
GC21	SAZ	145.99	49.00	4132
GC28	STZ	147.38	46.06	3065
GC31	STZ	149.06	44.55	3402
GC35	STZ	146.53	45.73	2720
MD972107	SAZ	145.78	47.71	2950

microscope equipped with circular polarisation and a Nikon DS-Fi1 8-bit colour digital camera. C-Calcita software (Fuertes et al., 2014) extracted images of all particles between 1 and 8  $\mu\text{m}$  from each FOV photograph. Then, the output files of single *E. huxleyi* coccoliths were visually selected. *E. huxleyi* coccoliths were differentiated from *Gephyrocapsa* species – the other members of Noëlaerhabdaceae family present in the Subantarctic Zone with relatively similar coccolith dimensions – on the basis of the presence or absence of a conjunct bridge. Even when this bridge is missing, *Gephyrocapsa* coccoliths often display two conspicuous highly calcified thickenings that correspond with the base of the bridge allowing identification of members of this genus. Coccolith mass and length measurements on the output images of *E. huxleyi* coccoliths were performed automatically by C-Calcita software. Further details of the calibration and image analysis protocol can be found in Rigual-Hernández et al. (2020a).

The proportions between different morphometric parameters of a coccolith of a given species typically vary with size (i.e. allometric growth; Young and Ziveri, 2000). In particular, coccolith thickness has been documented to increase in proportion to its size (O’Dea et al., 2014). Therefore, in order to compare coccolith thickness across datasets beyond this relationship we calculated the size-normalized coccolith thickness, hereinafter SN thickness after O’Dea et al. (2014) and Bolton et al. (2016) using the following formula:

$$\text{SN thickness} = \text{CT} + [(\text{ML} - \text{DSL}) \times \text{S}]$$

where the first term, CT, is the coccolith thickness of coccolith A in sample X and the correction for size is given by the second term, in which ML is the mean coccolith length of all the samples analysed together (i.e. sediment trap plus sediment samples), DSL (distal shield length) is the length of *E. huxleyi* coccolith A in sample X, and S is the slope of the regression line between coccolith length (x axis) and thickness (y axis) in sample X.

## 2.6. Statistical Analyses

As the variables coccolith mass, DSL and SN thickness have a weighted composition, the weighted Kolmogorov-Smirnov test (Monahan, 2011) was performed instead of the classical test (Darling, 1957) to assess the difference in *E. huxleyi* coccolith mass, DSL and SN thickness between modern (Sediment trap) and pre-industrial (Holocene sediments) datasets. Since the sediment traps were deployed in the Subantarctic Zone, we also performed a second comparison with Subantarctic Zone seabed samples only – i.e. excluding all the sediment samples retrieved from the Subtropical Zone. The Kolmogorov-Smirnov comparison consists of a two-sample distribution-free test designed to identify possible deviations from the initial hypothesis that the distributions of the two compared populations are identical. If the p value is small, i.e. 0.05 or less, it can be concluded that the distributions of the two populations compared are significantly different.

The modern subantarctic assemblage, termed “sediment trap composite sample” was derived by integrating the coccolith flux time series collected during a year (from August 2011 until July 2012) from three vertically moored sediment traps placed at 1000, 2000 and 3800 m at the SOTS site from a previous study (Rigual-Hernández et al., 2020a). Since the relative abundance of *E. huxleyi* morphotypes display substantial latitudinal variations across the subtropical and subantarctic waters south of Tasmania (Findlay and Giraudeau, 2000; Cubillos et al., 2007) and each of these morphotypes are characterized by coccoliths with different degree of calcification and size ranges, we ran two different comparisons between the “sediment trap composite sample” and sediments: one with the whole sediment sample dataset – hereinafter termed

“sea-bed sediment group” – dataset and one with the subantarctic sediment samples only, hereinafter termed “subantarctic sediment group”.

Additionally, the Pearson’s correlation (Pearson, 1907) used to assess the degree of association between *E. huxleyi* morphometric parameters, CEX, latitude and water column depth of the seafloor samples.

## 3. Results

### 3.1. Coccolith assemblage composition and CEX index

With the exception of GC13, GC14, GC16 and GC18, the calcareous nannofossil assemblages were largely dominated by *E. huxleyi* that accounted for between 60 and 84% of the assemblage, followed by *C. leptoporus* (1–23%) and *Gephyrocapsa* group (including *G. muelleriae*, *G. oceanica*, *Gephyrocapsa* spp. < 3  $\mu\text{m}$  and *Gephyrocapsa* spp. > 3  $\mu\text{m}$ ; 4–28%) (Supplementary Table 1). GC13, GC14, GC16 and GC18 are among the samples retrieved from deepest locations and exhibit more pronounced signs of dissolution. These samples were dominated or co-dominated by the heavily calcified *C. leptoporus* (7–42%) and *Coccolithus pelagicus* (8–42%).

CEX values in most sediment samples were above 0.6 (Dittert et al., 1999; see also section 2.6), suggesting that post-depositional dissolution processes had not altered the composition of the coccolith assemblages. Only in samples GC13, GC16 and GC18 CEX was equal or below the 0.6 threshold, indicating that carbonate dissolution could have compromised the imprint of some taxa. CEX exhibited a significant correlation with water column depth ( $r = -0.66$ ,  $p < 0.01$ ,  $n = 15$ ) (Fig. 2) highlighting the intimate relationship between depth and calcite dissolution (Milliman, 1975). Note that the slightly different r coefficients between CEX and depth shown in Figs. 2 and 5 are due to the different number of samples used in each correlation.

### 3.2. Morphotype composition of *E. huxleyi* assemblages

Overall, SEM analyses on the Holocene sediment samples revealed that most of the *E. huxleyi* coccoliths were affected by dissolution. The total or partial loss of their T-elements and central area elements (e.g. Fig. 3a) precluded the identification to morphotype level of about 85% (average value) of the *E. huxleyi* coccoliths found in the sediment samples (Fig. 4 and Supplementary Table 2). GC05 and GC04 exhibited the best preservation with 49 and 37 % of the *E. huxleyi* coccoliths identifiable to morphotype

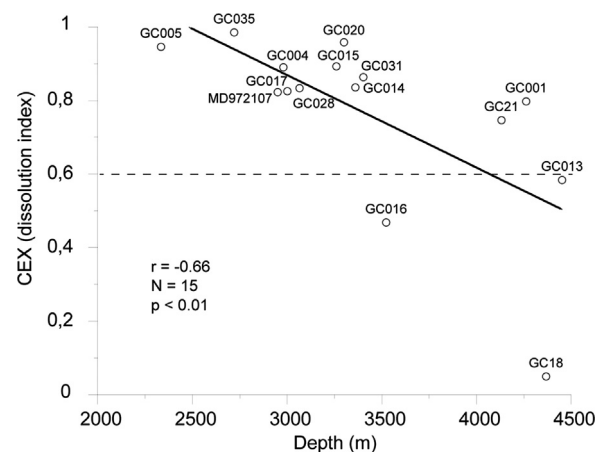
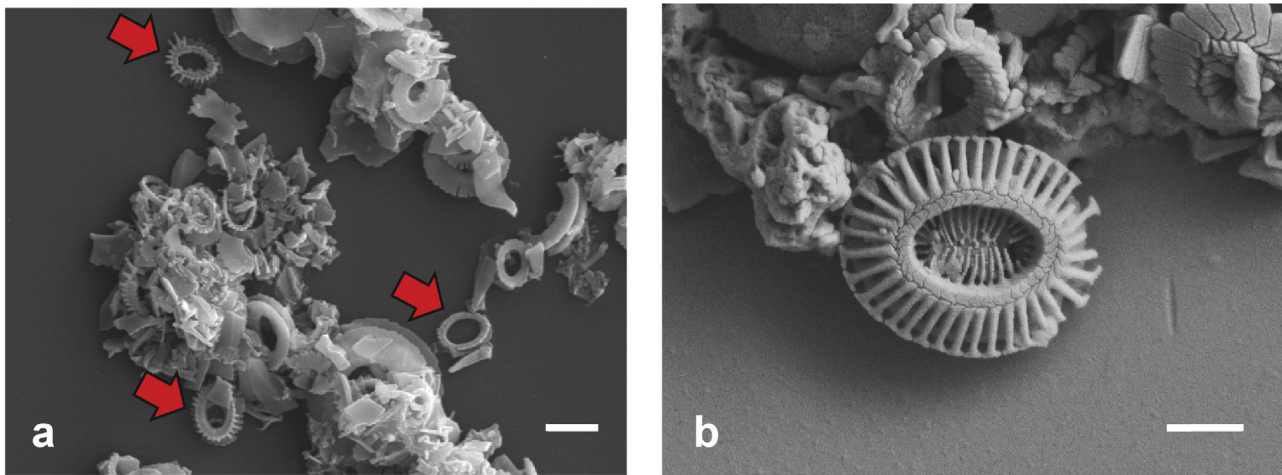
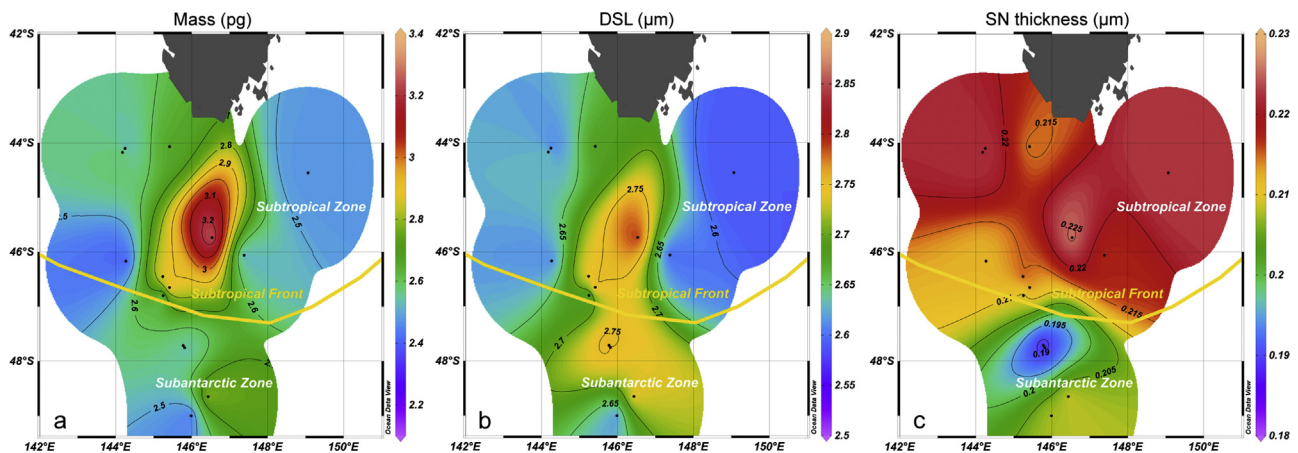


Fig. 2. Regression plot between the CEX index (*Calcidiscus leptoporus* – *Emiliania huxleyi* Dissolution Index) and water column depth of the sediment samples.



**Fig. 3.** Scanning Electron Microscope photographs showcasing the two ends of the preservation spectrum of *E. huxleyi* coccoliths in the sediments south of Tasmania: highly dissolved coccoliths (red arrows) (a) and well-preserved coccolith (type A) (b). Scale bars: a = 2  $\mu\text{m}$ ; b = 1  $\mu\text{m}$ .



**Fig. 4.** Relative abundance of *E. huxleyi* morphotype in (a) the Holocene sediments south of Tasmania in latitudinal order from north (left) to right (south) and (b) in the subantarctic SOTS sediment traps (composite sample grouping the three sediment traps). B/C and C morphotypes grouped together under B/C.

level. These two samples correspond to the northernmost locations of data set and displayed the highest concentrations of type A (29 and 22% for GC05 and GC04, respectively) and among the highest for type A o/c (13 and 15%) of the total coccoliths counted, in all samples (Fig. 4). In contrast the poorest preservation was observed in the subantarctic – and second deepest sample (depth 4368 m) – GC18, that was almost barren for *E. huxleyi* coccoliths. Very poor coccolith preservation was also documented in the samples located in GC13, GC14, GC15 and GC16 located in the western flank of the South Tasman Rise where > 98% of the *E. huxleyi* coccoliths were unidentifiable (Fig. 4). The poor preservation of the *E. huxleyi* coccoliths in the sediments contrasts with their good conservation in the SOTS sediment trap samples, where all coccoliths found in distal shield view were identifiable (Rigual-Hernández et al., 2020a).

### 3.3. Coccolith mass, length, and thickness distributions in the sediments south of Tasmania

A total of 1794 *E. huxleyi* coccoliths from the Holocene sediments south of Tasmania were visually identified and analysed for morphometric parameters. An average of 128 coccoliths per sample were analysed, ranging from 65 in sample GC20 to 189 in GC04. Average coccolith mass in the sediments is  $2.65 \pm 1.20$  pg

(average  $\pm$  standard deviation). Peak values are observed in the subtropical samples GC35 and GC15 ( $3.34 \pm 1.50$  and  $3.29 \pm 1.49$  pg) collected from the northern flank of the South Tasman Rise and minima in the nearby, but deeper (3523 m), GC16 site ( $2.16 \pm 1.23$  pg) depth) and in GC21 ( $2.35 \pm 0.95$  pg), located the southern flank of the South Tasman Rise. The spatial distribution of coccolith mass in the sediments south of Tasmania was similar to that of DSL (Fig. 6 a and b), exhibiting a strong and significant correlation between both parameters ( $r = 0.86$ ; Fig. 5). Unlike coccolith mass and DSL, SN thickness exhibits a clear latitudinal gradient with maximum values observed in the subtropical samples GC31, GC01 and GC35 and minima in the subantarctic samples GC17 and MD972107 (Fig. 6c). SN thickness was not correlated with either coccolith mass or DSL ( $r = 0.36$  and  $-0.13$ , respectively), but was significantly negatively correlated with latitude ( $^{\circ}\text{S}$ ) ( $r = -0.61$ ; Fig. 5).

### 3.4. Coccolith morphometrics: sediment trap versus Holocene sediment *E. huxleyi* assemblages

Annual flux-weighted coccolith mass, DSL and SN coccolith thickness for the sediment trap composite sample are 2.76 pg, 2.82  $\mu\text{m}$  and 0.192  $\mu\text{m}$ , respectively. Comparison of the coccolith mass distributions between datasets initially suggests that modern

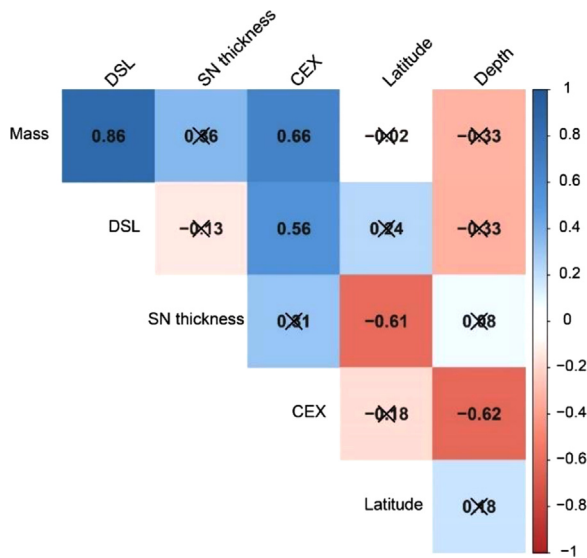


**Fig. 5.** Pearson correlation matrix for mean morphometric parameters of *E. huxleyi* coccoliths (mass, DSL and SN thickness), the dissolution index CEX, water column depth and latitude of the Holocene-aged sediment samples south of Tasmania. Non-significant correlations ( $p$  values  $> 0.05$ ) are crossed out.  $N = 14$  samples (no coccolith morphometric data for GC18).

*E. huxleyi* coccolith assemblages (i.e. those from the composite sediment trap sample) display a higher calcite content than their counterparts retrieved from the seafloor, both when all sediment samples are considered together, and when only subantarctic sediment samples are compared (Fig. 7a and b). For DSL distributions, the results of the Kolmogorov-Smirnov test yielded similar results to those for coccolith mass, with DSL of the sediment trap assemblages being greater than that of all the seafloor sediment samples (i.e. the sea-bed sediment group) and the subantarctic samples (Fig. 7c and d). Interestingly, the SN coccolith thickness comparison indicates that Holocene *E. huxleyi* populations were more calcified than modern ones (Fig. 7e). This statement holds true when we narrow the comparison to the subantarctic sediment group (Fig. 7f).

## 4. Discussion

### 4.1. Factors influencing the preservation and composition of coccolith sinking assemblages

The complex interaction of several physical, chemical and biological processes can alter the original coccolithophore assemblage since its initial production in the surface ocean until its eventual preservation in the sediments. Grazing by zooplankton is the first factor influencing the original coccolithophore assemblage produced in the surface layer and can have opposing effects on coccolith preservation. On the one hand, mechanical breakage of coccospheres and/or the effect of acidic food vacuoles (3–5 pH) of some zooplankton species may result in fragmentation of coccoliths and/or rapid calcite dissolution (e.g. Broerse et al., 2000a; Mayers et al., 2019). On the other hand, formation of faecal and algal aggregates can reduce the contact of the coccoliths with the environment and effectively increase their sinking rates, thereby facilitating their rapid transit through the water column and deposition on the seafloor (Ziveri et al., 2007). In the study area, Pearce et al. (2011) estimated that microzooplankton exerts a strong top-down control by removing about 80% of primary production during the austral summer, while Ebersbach et al. (2011) documented that the bulk of the particles sinking out of the mixed layer during summer occurs in the form of faecal aggregates. SEM observations indicate that the preservation of *E. huxleyi* coccoliths collected by the traps is excellent indicating that negligible dissolution occurs in the transit of the coccolithophores throughout the water column (Rigual-Hernández et al., 2020a). Taken together, all the above-mentioned studies suggest that grazing pressure in the subantarctic waters facilitates the rapid transit of coccoliths from the surface to the sea floor thereby optimizing their preservation. The good preservation of the coccoliths in the traps is consistent with Moy et al. (2009) who reported minimal dissolution of planktonic foraminifera *Globigerina bulloides* tests captured by sediment traps in the study region.

Once at the seabed, the accumulated coccoliths are exposed to several processes that can alter the preservation and composition of the original assemblage. Firstly, bioturbation can result in the mixing of sediment layers introducing a blurring effect on the information preserved in the sediment record (Boudreau, 1998). The AMS  $^{14}\text{C}$  dates (section 2.2) confirm that all the samples analysed here are Holocene (Connell and Sikes, 1997; Findlay and

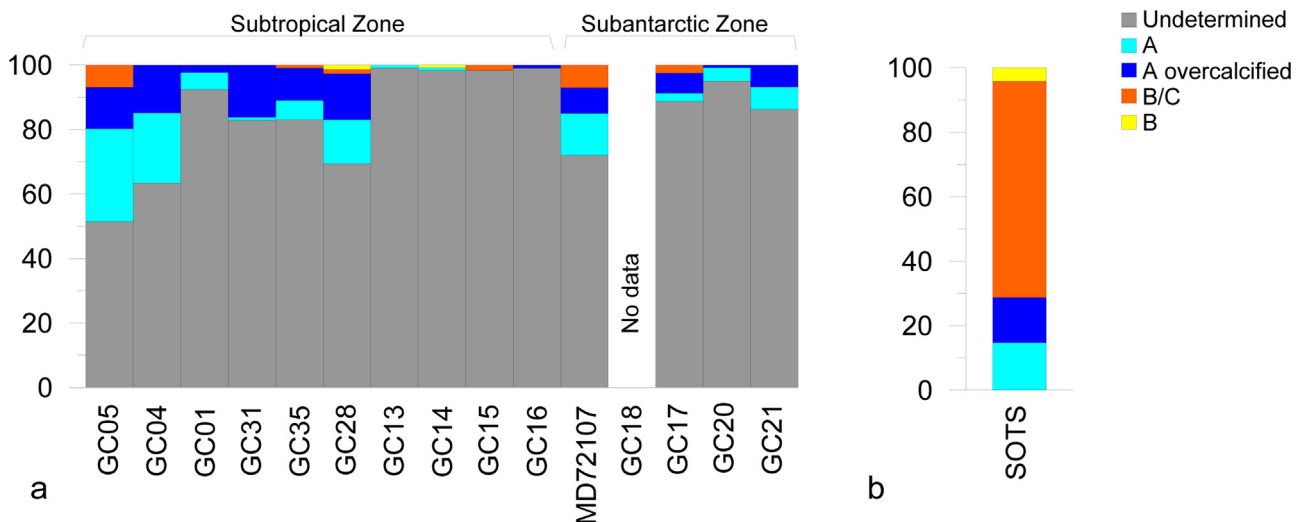


**Fig. 6.** Distribution of *E. huxleyi* coccolith mass (a), DSL (Distal Shield Length) (b) and SN thickness (c) in the seafloor Holocene sediments south of Tasmania. Black points identify location of sampling points. Ocean Data View software (Schlitzer, 2018) was used to generate this figure.

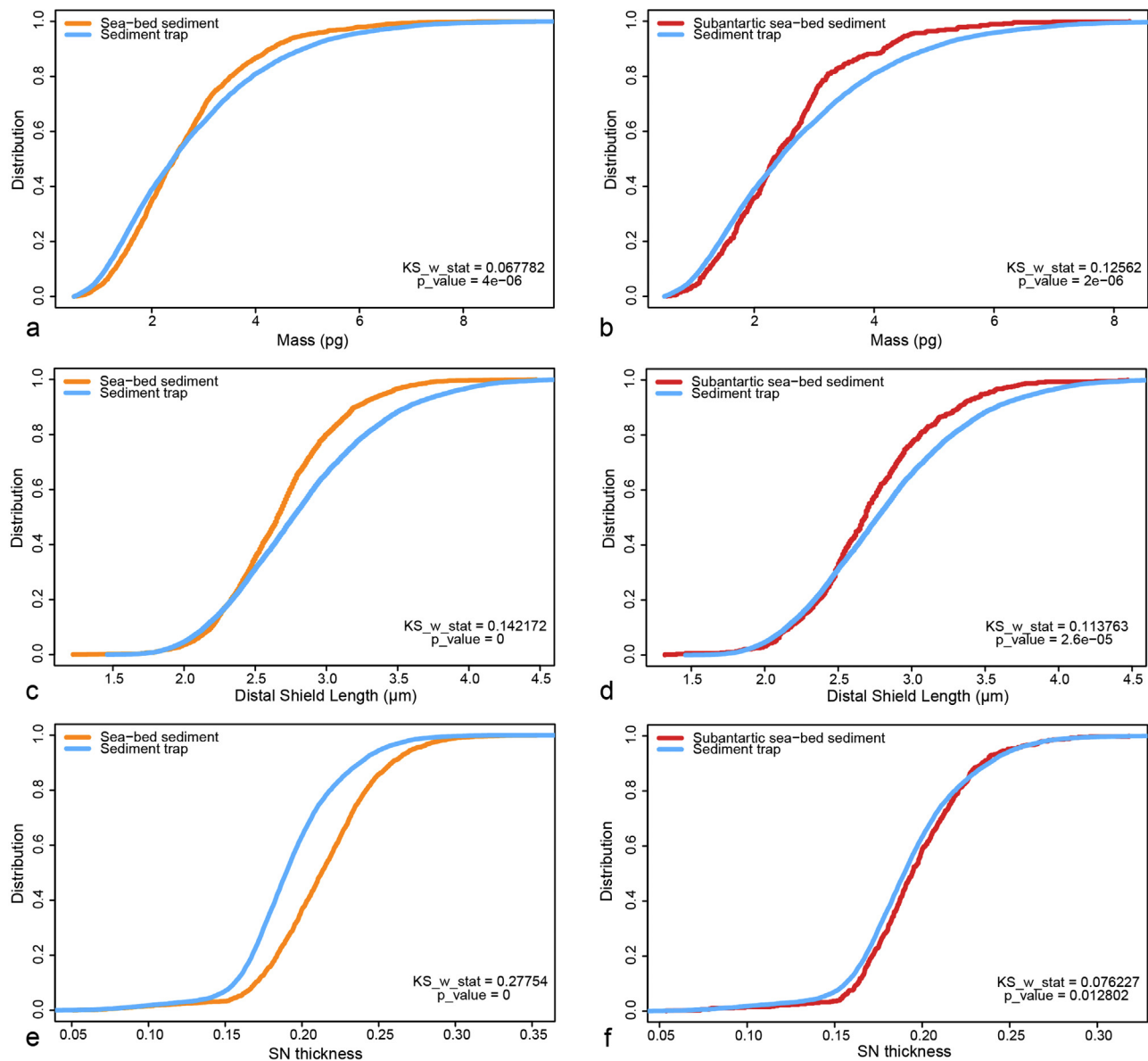


**Fig. 7.** Weighted Kolmogorov-Smirnov comparison of the distribution of *Emiliana huxleyi* coccolith mass, DSL and Size-Normalized (SN) coccolith thickness between: (i) sediment trap composite sample versus all sediment samples grouped together (a, c and e); (ii) and sediment trap composite sample versus subantarctic sediment samples grouped together (b, d and f).

Giraudeau, 2002; Moy et al., 2009). Secondly, carbonate dissolution is generally considered the most important factor altering the original coccolith assemblage. SEM observations indicate that most of the *E. huxleyi* coccoliths in all the sediment samples analysed have experienced a variable degree of dissolution and fragmentation of their elements and shields that precluded the identification to morphotype-level of a substantial number of coccoliths (Figs. 3 and 4). It is likely that supralysocline dissolution processes (Milliman et al. (1999) related to the guts and faeces of epipelagic grazers, and microbial oxidation of organic matter facilitated post depositional dissolution of the sea-floor samples.

#### 4.2. Biogeographical distribution patterns of *Emiliana huxleyi* coccoliths

The modern Subtropical and Subantarctic Zone waters host different proportions of *E. huxleyi* morphotypes, with type A and A o/c occurring more frequently in the Subtropical Zone, while the

subantarctic waters are dominated by morphotype B/C, endemic to the Southern Ocean (Cubillos et al., 2007). Notably, these morphotypes display important differences in their degree of calcification, with morphotype A and A o/c exhibiting substantially more calcified coccoliths than the weakly calcified type as reflected in their different coccolith shape factors ( $k_s = 0.04, 0.02$  and  $0.015$  for type A o/c, A and B/C, respectively; Young and Ziveri, 2000; Poulton et al., 2011). Therefore, we initially expected the *E. huxleyi* coccolith mass distributions in the sea floor to mirror the latitudinal gradient in the surface layer, displaying maximum coccolith mass in the northern stations and minima south of the Subtropical Front. The lack of a clear decreasing north-south gradient in both mass and length (Fig. 6a and b) is interpreted as resulting from substantial post depositional dissolution processes on the seafloor. This idea is supported by the significant correlations of coccolith mass and DSL with CEX (Fig. 5) suggesting that dissolution most likely altered these two parameters. In contrast, the SN thickness displays a clear latitudinal pattern

consistent with the distribution of morphotypes in the surface layer (Fig. 6) and is not correlated with the dissolution index CEX (Fig. 5). These observations suggest that the SN thickness is decoupled from coccolith preservation (O'Dea et al., 2014). Comparison of SN thickness distributions indicates that subtropical *E. huxleyi* coccoliths are 10% thicker than those preserved in the subantarctic sediments. We speculate that the variations in coccolith thickness along the latitudinal environmental gradient are intimately related to changes in the proportions of *E. huxleyi* morphotypes. Indeed, if we focus on the subtropical sample with the best preservation, i.e. sample GC05, the contribution of type A and type A o/c together accounts for ~40% of the assemblage (Fig. 4). And it is important to note that this value should be viewed as an underestimation because about half of the *E. huxleyi* coccoliths in sample GC05 were unidentifiable to morphotype level. Indeed, the contribution of type A and type A o/c together would increase up to 85% if the unidentified *E. huxleyi* coccoliths are not considered. Although the poor preservation of the *E. huxleyi* coccoliths in the subantarctic samples precludes estimation of morphotype proportions, previous research in the nearby New Zealand Subantarctic Zone indicates that type B/C is, by far the dominant morphotype in the surface sediments (Saavedra-Pellitero and Baumann, 2015). Taken together, all the above observations support the notion that changes in coccolith thickness along the north-to-south environmental gradient south of Tasmania are controlled by the morphotype composition of *E. huxleyi* populations.

#### 4.3. Comparison of modern and pre-industrial Holocene *Emiliania huxleyi* assemblages

Given the substantial variability in morphotype composition of *E. huxleyi* assemblages between the subtropical and subantarctic waters south of Tasmania (Findlay and Giraudeau, 2000; Cubillos et al., 2007; Rigual-Hernández et al., 2020a), we focus on the comparison of the SOTS sediment traps with the subantarctic sediment samples (Fig. 7b, d and f) to assess the changes of *E. huxleyi* populations in the subantarctic region since the pre-industrial era.

Since the coccolithophore populations captured by the SOTS sediment traps and those from the subantarctic Holocene-aged sediment samples display CEX values above 0.7, it can be inferred that a negligible to low number of *E. huxleyi* coccoliths had been completely removed from these samples. In other words, the results suggest that the bulk of *E. huxleyi* coccoliths that reached the seafloor in the Subantarctic Zone are still present in the sediments, thereby discarding the possibility that differential dissolution removed the most weakly calcified *E. huxleyi* coccoliths from the seafloor. However, this does not imply that *E. huxleyi* coccoliths were unaltered by dissolution. In fact, the SEM observations clearly indicate that most of the *E. huxleyi* coccoliths in the sediments experienced a variable degree of CaCO<sub>3</sub> loss that resulted in a reduction of both coccolith mass and DSL. In contrast, the results of this study (see section 4.2), along with previous research (O'Dea et al., 2014), indicate that SN thickness is unaffected by dissolution, this parameter can be used to compare to sediment trap and seafloor coccolith assemblages on an equal footing.

Comparison of the distributions of SN thickness indicates that modern *E. huxleyi* coccoliths are less calcified than Holocene ones from the subantarctic sediments (Fig. 7f). It is important to note that although this difference is significant (at p-value < 0.05), it is small with modern *E. huxleyi* coccoliths being 2% thinner than pre-industrial Holocene ones. Next, we examine the most probable environmental factors that could have driven this change between the Holocene and present.

Several lines of evidence strongly suggest that temperature is a critical factor controlling the biogeographical distribution of *E. huxleyi* morphotypes in the Southern Ocean (Cubillos et al., 2007; Charalampopoulou et al., 2016; Rigual Hernández et al., 2018; Saavedra-Pellitero et al., 2019). In particular, unpublished results from Hallegraef et al. (see Rigual-Hernández et al., 2020a for more information) have showed that Southern Ocean B/C strains are able to grow at 4, 10 and 17 °C, while types A and A o/c do not survive at 4 °C. Since the weakly calcified type B/C dominates the coccolithophore populations in the Subantarctic Zone, any substantial variation in water temperatures could potentially induce a change in the proportions of morphotypes, thereby driving a change in the average size and weight of the *E. huxleyi* populations (Bach et al., 2012). Sea surface temperature reconstructions based on alkenones of core GC17 (Fig. 1), indicate that surface temperatures in the Subantarctic Zone has decreased approximately 2.5 °C since the early Holocene (Sikes et al., 2009). Therefore, it is plausible that the warmer conditions during the early to mid Holocene (Sikes et al., 2009) favoured the development of *E. huxleyi* strains with affinity for higher SSTs, such as type A and A o/c (Cubillos et al., 2007; Cook et al., 2011), thereby explaining the thicker coccoliths recorded in the Holocene sediments. Moreover, seawater carbonate chemistry manipulation experiments with Southern Ocean *E. huxleyi* strains (corresponding to morphotypes B/C, A and A o/c) showed differing physiological responses to projected pCO<sub>2</sub> levels (Müller et al., 2015). In particular, type B/C was shown to be the most sensitive of the three morphotypes to high pCO<sub>2</sub>, almost ceasing calcification at pCO<sub>2</sub> levels above 1000 μatm. However, it is important to note that response of type B/C to increased pCO<sub>2</sub> was not linear, as it displayed an increase of up ~20% on its growth rates from pre-industrial pCO<sub>2</sub> concentrations (~250 μatm) to present industrial levels (~400 μatm) before reducing its growth rates at further higher pCO<sub>2</sub> concentrations. In turn, growth rates of type A strains remained constant between Holocene and industrial pCO<sub>2</sub> levels. Thus, it is possible that seawater carbonate chemistry changes in subantarctic waters induced by enhanced pCO<sub>2</sub> levels during the industrial era would have favoured the growth of B/C populations, thereby resulting in an overall ecologically-driven decrease in the calcification of subantarctic populations, as suggested by the results.

## 5. Conclusions

Comparison of the morphotype composition and morphometric parameters of *E. huxleyi* coccolith preserved in the Holocene-aged sediments south of Tasmania with assemblages from annual sediment-trap time series records permit answers to the research questions posed in this paper:

1- Results indicate that, whereas post depositional processes diminished the mass and distal shield length of *E. huxleyi* coccoliths preserved in the Holocene-aged sediments, the size normalized coccolith thickness is retained allowing comparison of modern and pre-industrial *E. huxleyi* assemblages using this variable.

2- Modern *E. huxleyi* populations in the Subantarctic Zone produce coccoliths about 2% thinner than those from the pre-industrial Holocene. This result suggests that ongoing anthropogenic-driven environmental change in the Subantarctic Zone has induced only minor changes in the composition or physiological response of *E. huxleyi* populations. The production of subtly thicker coccoliths during the pre-industrial Holocene attributable to the warmer conditions and/or lower pCO<sub>2</sub> levels could have possibly favoured the growth of *E. huxleyi* morphotypes other than the currently dominant, and weakly calcified, type B/C.

3- The limited variation in coccolith calcification of *E. huxleyi* since the pre-industrial era contrasts sharply with the 30–35% reduction in shell weight of the dominant class of calcifying zooplankton, foraminifera, as observed for the species *Globigerina bulloides* (Moy et al., 2009). Ocean acidification has been documented to have an overall negative effect on the calcification of both species (Meyer and Riebesell, 2015; Davis et al., 2017). However, the results of this study suggest that there are important differences in the sensitivity of both groups to the  $p\text{CO}_2$  increase since the onset of the industrial revolution (i.e. from  $\sim 250$  to  $\sim 400$   $\mu\text{atm}$ ) with *E. huxleyi* subantarctic strains being more resilient than *G. bulloides*.

Understanding the response of coccolithophores to environmental change is important to enable robust predictions of the impacts on higher trophic levels, and to carbon cycling on regional and global scales. While the results presented here indicate that critical ocean acidification thresholds for *E. huxleyi* calcification have not been reached, it is expected that they will be crossed in the coming decades (Müller et al., 2015). Moreover, recent research has provided evidence that less abundant but larger subantarctic coccolithophore species (such as *Calcidiscus leptoporus*) account for a greater fraction of  $\text{CaCO}_3$  export to the deep sea than *E. huxleyi* (Rigual-Hernández et al., 2020b). Therefore, it is of critical importance to maintain continuous sampling programs in key Southern Ocean locations and extend the monitoring to other ecologically important species to better evaluate the response of marine ecosystems to predicted environmental change.

#### Declaration of Competing Interest

The authors declare that they have no known competing financial interests or personal relationships that could have appeared to influence the work reported in this paper.

#### Acknowledgments

This project has received funding from the European Union's Horizon 2020 research and innovation programme under the Marie Skłodowska-Curie grant agreement number 748690 – SONAR-CO2 (ARH, JAF and FA). FA acknowledges FCT funding support through project UIDB/04326/2020. SN and HB were funded via the New Zealand Strategic Science Investment Fund to the 'Marine Geological Processes' programme in NIWA. The authors acknowledge the assistance of Vito Clericò and Enrique Diez (USAL-NANOLAB) in SEM analyses. Authors wish to thank José Ignacio Martín and Miguel Ángel Fuertes for their assistance in nannoplankton sample preparation and calibration of C-Calcita software, respectively. Authors would like to express our sincere thanks to two anonymous reviewers and editor Anne Chin for valuable comments that helped to improve the paper.

#### Appendix A. Supplementary data

Supplementary material related to this article can be found, in the online version, at doi:<https://doi.org/10.1016/j.ancene.2020.100254>.

#### References

- Bach, L.T., Bauke, C., Meier, K., Riebesell, U., Schulz, K.G., 2012. Influence of changing carbonate chemistry on morphology and weight of coccoliths formed by *Emiliania huxleyi*. *Biogeosciences* 9, 3449–3463.
- Bach, L.T., Riebesell, U., Gutowska, M.A., Federwisch, L., Schulz, K.G., 2015. A unifying concept of coccolithophore sensitivity to changing carbonate chemistry embedded in an ecological framework. *Progress in Oceanography* 135, 125–138.
- Bednaršek, N., Tarling, G.A., Bakker, D.C., Fielding, S., Feely, R.A., 2014. Dissolution dominating calcification process in polar pteropods close to the point of aragonite undersaturation. *PLoS one* 9, e109183.
- Berge, G., 1962. Discoloration of the sea due to *Coccolithus huxleyi* "bloom". *Sarsia* 6, 27–40.
- Bijma, J., Hönisch, B., Zeebe, R.E., 2002. Impact of the ocean carbonate chemistry on living foraminiferal shell weight: Comment on "Carbonate ion concentration in glacial-age deep waters of the Caribbean Sea" by W. S. Broecker and E. Clark. *Geochemistry, Geophysics, Geosystems* 3, 1–7.
- Boeckel, B., Baumann, K.-H., 2004. Distribution of coccoliths in surface sediments of the south-eastern South Atlantic Ocean: ecology, preservation and carbonate contribution. *Marine Micropaleontology* 51, 301–320.
- Bolton, C.T., Hernandez-Sanchez, M.T., Fuertes, M.-A., Gonzalez-Lemos, S., Abrevaya, L., Mendez-Vicente, A., Flores, J.-A., Probert, I., Giosan, L., Johnson, J., Stoll, H.M., 2016. Decrease in coccolithophore calcification and  $\text{CO}_2$  since the middle Miocene. *Nat Commun* 7.
- Bostock, H.C., Hayward, B.W., Neil, H.L., Currie, K.I., Dunbar, G.B., 2011. Deep-water carbonate concentrations in the southwest Pacific. *Deep Sea Research Part I: Oceanographic Research Papers* 58, 72–85.
- Boudreau, B.P., 1998. Mean mixed depth of sediments: The wherefore and the why. *Limnology and Oceanography* 43, 524–526.
- Broerse, A.T.C., Ziveri, P., Honjo, S., 2000a. Coccolithophore ( $-\text{CaCO}_3$ ) flux in the Sea of Okhotsk: seasonality, settling and alteration processes. *Marine Micropaleontology* 39, 179–200.
- Broerse, A.T.C., Ziveri, P., van Hinte, J.E., Honjo, S., 2000b. Coccolithophore export production, species composition, and coccolith- $\text{CaCO}_3$  fluxes in the NE Atlantic ( $34^\circ\text{N}21^\circ\text{W}$  and  $48^\circ\text{N}21^\circ\text{W}$ ). *Deep Sea Research Part II: Topical Studies in Oceanography* 47, 1877–1905.
- Brown, C.W., Yoder, J.A., 1994. Coccolithophorid blooms in the global ocean. *Journal of Geophysical Research: Oceans* 99, 7467–7482.
- Caldeira, K., Wickett, M.E., 2003. Oceanography: anthropogenic carbon and ocean pH. *Nature* 425, 365.
- Cao, L., Caldeira, K., 2008. Atmospheric  $\text{CO}_2$  stabilization and ocean acidification. *Geophysical Research Letters* 35 n/a-n/a.
- Charalampopoulou, A., Poulton, A.J., Bakker, D.C., Lucas, M.I., Stinchcombe, M. C., Tyrrell, T.J.B., 2016. Environmental drivers of coccolithophore abundance and calcification across Drake Passage (Southern Ocean), 13. , pp. 5917–5935.
- Connell, R.D., Sikes, E.L., 1997. Controls on Late Quaternary sedimentation of the South Tasman Rise. *Australian Journal of Earth Sciences* 44, 667–675.
- Cook, S.S., Jones, R.C., Vaillancourt, R.E., Hallegraeff, G.M., 2013. Genetic differentiation among Australian and Southern Ocean populations of the ubiquitous coccolithophore *Emiliania huxleyi* (Haptophyta). *Phycologia* 52, 368–374.
- Cook, S.S., Whittock, L., Wright, S.W., Hallegraeff, G.M., 2011. Photosynthetic pigment and genetic differences between two southern ocean morphotypes of *Emiliania huxleyi* (haptophyta). *Journal of phycology* 47, 615–626.
- Cubillos, J., Wright, S., Nash, G., De Salas, M., Griffiths, B., Tilbrook, B., Poisson, A., Hallegraeff, G., 2007. Calcification morphotypes of the coccolithophorid *Emiliania huxleyi* in the Southern Ocean: changes in 2001 to 2006 compared to historical data. *Marine Ecology Progress Series* 348, 47–54.
- Darling, D.A., 1957. The kolmogorov-smirnov, cramer-von mises tests. *The Annals of Mathematical Statistics* 28, 823–838.
- Davis, C.V., Rivest, E.B., Hill, T.M., Gaylord, B., Russell, A.D., Sanford, E., 2017. Ocean acidification compromises a planktic calcifier with implications for global carbon cycling. *Scientific Reports* 7, 2225.
- Dittert, N., Baumann, K.-H., Bickert, T., Henrich, R., Huber, R., Kinkel, H., Meggers, H., 1999. Carbonate dissolution in the deep-sea: methods, quantification and paleoceanographic application, Use of proxies in paleoceanography. Springer, pp. 255–284.
- Ebersbach, F., Trull, T.W., Davies, D.M., Bray, S.G., 2011. Controls on mesopelagic particle fluxes in the Sub-Antarctic and Polar Frontal Zones in the Southern Ocean south of Australia in summer—Perspectives from free-drifting sediment traps. *Deep Sea Research Part II: Topical Studies in Oceanography* 58, 2260–2276.
- Eriksen, R., Trull, T.W., Davies, D., Jansen, P., Davidson, A.T., Westwood, K., van den Enden, R., 2018. Seasonal succession of phytoplankton community structure from autonomous sampling at the Australian Southern Ocean Time Series (SOTS) observatory. *Marine Ecology Progress Series* 589, 13–31.
- Fabry, V.J., McClintock, J.B., Mathis, J.T., Grebmeier, J.M., 2009a. Ocean acidification at high latitudes: the bellwether. *Oceanography* 22, 160.
- Fabry, V.J., McClintock, J.B., Mathis, J.T., Grebmeier, J.M., 2009b. Ocean Acidification at High Latitudes: The Bellwether. *Oceanography* 22, 160–171.
- Feely, R.A., Doney, S.C., Cooley, S.R., 2009. Ocean Acidification Present Conditions and Future Changes in a High- $\text{CO}_2$  World. *Oceanography* 22, 36–47.
- Findlay, C.S., Giraudeau, J., 2000. Extant calcareous nannoplankton in the Australian Sector of the Southern Ocean (austral summers 1994 and 1995). *Marine Micropaleontology* 40, 417–439.
- Findlay, C.S., Giraudeau, J., 2002. Movement of oceanic fronts south of Australia during the last 10 ka: interpretation of calcareous nannoplankton in surface sediments from the Southern Ocean. *Marine Micropaleontology* 46, 431–444.
- Flores, J.A., Sierrro, F.J., 1997. A revised technique for the calculation of calcareous nannofossil accumulation rates. *Micropaleontology* 43, 321–324.
- Fuertes, M.-A., Flores, J.-A., Sierrro, F.J., 2014. The use of circularly polarized light for biometry, identification and estimation of mass of coccoliths. *Marine Micropaleontology* 113, 44–55.
- Hagino, K., Bendif, E.M., Young, J.R., Kogame, K., Probert, I., Takano, Y., Horiguchi, T., de Vargas, C., Okada, H., 2011. New evidence for morphological and genetic variation in the cosmopolitan coccolithophore *Emiliania huxleyi*



- (prymnesiophyceae) from the COX1b-ATP4 genes. *Journal of Phycology* 47, 1164–1176.
- Hagino, K., Okada, H., Matsuoka, H., 2005. Coccolithophore assemblages and morphotypes of *Emiliana huxleyi* in the boundary zone between the cold Oyashio and warm Kuroshio currents off the coast of Japan. *Marine Micropaleontology* 55, 19–47.
- Iglesias-Rodríguez, M.D., Halloran, P.R., Rickaby, R.E., Hall, I.R., Colmenero-Hidalgo, E., Gittins, J.R., Green, D.R., Tyrrell, T., Gibbs, S.J., von Dassow, P., 2008. Phytoplankton calcification in a high-CO<sub>2</sub> world. *Science* 320, 336–340.
- Jonkers, L., Hillebrand, H., Kucera, M., 2019. Global change drives modern plankton communities away from the pre-industrial state. *Nature* 570, 372–375.
- Kopczynska, E.E., Dehairs, F., Elskens, M., Wright, S., 2001. Phytoplankton and microzooplankton variability between the Subtropical and Polar Fronts south of Australia: Thriving under regenerative and new production in late summer. *Journal of Geophysical Research: Oceans* 106, 31597–31609.
- Krueger-Hadfield, S., Balestreri, C., Schroeder, J., Highfield, A., Helaouët, P., Allum, J., Moate, R., Lohbeck, K.T., Miller, P., Riebesell, U., 2014. Genotyping an *Emiliana huxleyi* (Prymnesiophyceae) bloom event in the North Sea reveals evidence of asexual reproduction. *Biogeosciences* 11, 5215–5234.
- Langer, G., Geisen, M., Baumann, K.-H., Kläs, J., Riebesell, U., Thoms, S., Young, J.R., 2006. Species-specific responses of calcifying algae to changing seawater carbonate chemistry. *Geochemistry, Geophysics, Geosystems* 7 n/a/n/a.
- Langer, G., Nehrke, G., Probert, I., Ly, J., Ziveri, P., 2009. Strain-specific responses of *Emiliana huxleyi* to changing seawater carbonate chemistry. *Biogeosciences* 6, 2637–2646.
- Lenton, A., Tilbrook, B., Law, R., Bakker, D.C., Doney, S.C., Gruber, N., Hoppema, M., Ishii, M., Lovenduski, N.S., Matear, R.J., 2013. Sea-air CO<sub>2</sub> fluxes in the Southern Ocean for the period 1990–2009. *Biogeosciences Discussions* 10, 285–333.
- Manno, C., Bednaršek, N., Tarling, G.A., Peck, V.L., Comeau, S., Adhikari, D., Bakker, D.C.E., Bauerfeind, E., Bergan, A.J., Berning, M.I., Buitenhuis, E., Burrige, A.K., Chierici, M., Flöter, S., Fransson, A., Gardner, J., Howes, E.L., Keul, N., Kimoto, K., Kohnert, P., Lawson, G.L., Lischka, S., Maas, A., Mekkes, L., Oakes, R.L., Pebody, C., Peijnenburg, K.T.C.A., Seifert, M., Skinner, J., Thibodeau, P.S., Wall-Palmer, D., Ziveri, P., 2017. Shelled pteropods in peril: Assessing vulnerability in a high CO<sub>2</sub> ocean. *Earth-Science Reviews* 169, 132–145.
- Mayers, K.M.J., Poulton, A.J., Daniels, C.J., Wells, S.R., Woodward, E.M.S., Tarran, G.A., Widdicombe, C.E., Mayor, D.J., Atkinson, A., Giering, S.L.C., 2019. Growth and mortality of coccolithophores during spring in a temperate Shelf Sea (Celtic Sea, April 2015). *Progress in Oceanography* 177, 101928.
- Metz, N., Tilbrook, B., Poisson, A., 1999. The annual fCO<sub>2</sub> cycle and the air–sea CO<sub>2</sub> flux in the sub-Antarctic Ocean. *Tellus B* 51, 849–861.
- Meyer, J., Riebesell, U., 2015. Reviews and Syntheses: Responses of coccolithophores to ocean acidification: a meta-analysis. *Biogeosciences (BG)* 12, 1671–1682.
- Milliman, J.D., 1975. Dissolution of aragonite, Mg-calcite, and calcite in the North Atlantic Ocean. *Geology* 3, 461–462.
- Milliman, J.D., Troy, P.J., Balch, W.M., Adams, A.K., Li, Y.H., Mackenzie, F.T., 1999. Biologically mediated dissolution of calcium carbonate above the chemical lysocline? *Deep Sea Research Part I: Oceanographic Research Papers* 46, 1653–1669.
- Monahan, J.F., 2011. Numerical methods of statistics. Cambridge University Press.
- Moy, A.D., Howard, W.R., Bray, S.G., Trull, T.W., 2009. Reduced calcification in modern Southern Ocean planktonic foraminifera. *Nature Geosci* 2, 276–280.
- Müller, M.N., Trull, T.W., Hallegraeff, G.M., 2015. Differing responses of three Southern Ocean *Emiliana huxleyi* ecotypes to changing seawater carbonate chemistry. *Marine Ecology Progress Series* 531, 81–90.
- O’Dea, S.A., Gibbs, S.J., Bown, P.R., Young, J.R., Poulton, A.J., Newsam, C., Wilson, P.A., 2014. Coccolithophore calcification response to past ocean acidification and climate change. *Nature Communications* 5, 5363.
- Odate, T., Fukuchi, M., 1995. Distribution and community structure of picophytoplankton in the Southern Ocean during the late austral summer of 1992. *Proc NIPR Symp Polar Biol* 86–100.
- Orr, J.C., Fabry, V.J., Aumont, O., Bopp, L., Doney, S.C., Feely, R.A., Gnanadesikan, A., Gruber, N., Ishida, A., Joos, F., 2005. Anthropogenic ocean acidification over the twenty-first century and its impact on calcifying organisms. *Nature* 437, 681–686.
- Orsi, A.H., Whitworth Iii, T., Nowlin Jr., W.D., 1995. On the meridional extent and fronts of the Antarctic Circumpolar Current. *Deep Sea Research Part I: Oceanographic Research Papers* 42, 641–673.
- Pachauri, R.K., Allen, M.R., Barros, V.R., Broome, J., Cramer, W., Christ, R., Church, J.A., Clarke, L., Dahe, Q., Dasgupta, P., 2014. Climate change 2014: synthesis report. Contribution of Working Groups I, II and III to the fifth assessment report of the Intergovernmental Panel on Climate Change. *Ippc*.
- Pardo, P., Tilbrook, B., van Ooijen, E., Passmore, A., Neill, C., Jansen, P., Sutton, A.J., Trull, T.W., 2019. Surface ocean carbon dioxide variability in South Pacific boundary currents and Subantarctic waters. *Scientific Reports* 9, 7592.
- Patil, S.M., Mohan, R., Shetye, S.S., Gazi, S., Baumann, K.-H., Jafar, S., 2017. Biogeographic distribution of extant Coccolithophores in the Indian sector of the Southern Ocean. *Marine Micropaleontology* 137, 16–30.
- Pearce, I., Davidson, A.T., Thomson, P.G., Wright, S., van den Enden, R., 2011. Marine microbial ecology in the sub-Antarctic Zone: Rates of bacterial and phytoplankton growth and grazing by heterotrophic protists. *Deep Sea Research Part II: Topical Studies in Oceanography* 58, 2248–2259.
- Pearson, K., 1907. On further methods of determining correlation. Dulau and Company.
- Poulton, A.J., Young, J.R., Bates, N.R., Balch, W.M., 2011. Biometry of detached *Emiliana huxleyi* coccoliths along the Patagonian Shelf. *Marine Ecology Progress Series* 443, 1–17.
- Read, B.A., Kegel, J., Klute, M.J., Kuo, A., Lefebvre, S.C., Maumus, F., Mayer, C., Miller, J., Monier, A., Salamov, A., Young, J., Aguilar, M., Claverie, J.-M., Frickenhaus, S., Gonzalez, K., Herman, E.K., Lin, Y.-C., Napier, J., Ogata, H., Sarno, A.F., Shmutz, J., Schroeder, D., de Vargas, C., Verret, F., von Dassow, P., Valentin, K., Van de Peer, Y., Wheeler, G., *Emiliana huxleyi* Annotation, C., Allen, A.E., Bidle, K., Borodovsky, M., Bowler, C., Brownlee, C., Mark Cock, J., Elias, M., Gladyshev, V.N., Groth, M., Guda, C., Hadaegh, A., Debora Iglesias-Rodríguez, M., Jenkins, J., Jones, B.M., Lawson, T., Leese, F., Lindquist, E., Lobanov, A., Lomsadze, A., Malik, S.-B., Marsh, M.E., Mackinder, L., Mock, T., Mueller-Roeber, B., Pagarete, A., Parker, M., Probert, I., Quesneville, H., Raines, C., Rensing, S.A., Riaño-Pachón, D.M., Richier, S., Rokitta, S., Shiraiwa, Y., Soanes, D.M., van der Giezen, M., Wahlund, T.M., Williams, B., Wilson, W., Wolfe, G., Wurch, L.L., Dacks, J.B., Delwiche, C.F., Dyhrman, S.T., Glöckner, G., John, U., Richards, T., Worden, A.Z., Zhang, X., Grigoriev, I.V., 2013. Pan genome of the phytoplankton *Emiliana huxleyi* underpins its global distribution. *Nature* 499, 209.
- Ridgway, K.R., 2007. Seasonal circulation around Tasmania: An interface between eastern and western boundary dynamics. *Journal of Geophysical Research: Oceans* 112.
- Riebesell, U., Zondervan, I., Rost, B., Tortell, P.D., Zeebe, R.E., Morel, F.M.M., 2000. Reduced calcification of marine plankton in response to increased atmospheric CO<sub>2</sub>. *Nature* 407, 364–367.
- Rigual-Hernández, A.S., Trull, T.W., Flores, J.A., Nodder, S.D., Eriksen, R., Davies, D.M., Hallegraeff, G.M., Sierro, F.J., Patil, S.M., Cortina, A., Ballegeer, A.M., Northcote, L. C., Abrantes, F., Rufino, M.M., 2020a. Full annual monitoring of Subantarctic *Emiliana huxleyi* populations reveals highly calcified morphotypes in high-CO<sub>2</sub> winter conditions. *Scientific Reports* 10, 2594.
- Rigual-Hernández, A.S., Trull, T.W., Nodder, S.D., Flores, J.A., Bostock, H., Abrantes, F., Eriksen, R.S., Sierro, F.J., Davies, D.M., Ballegeer, A.M., Fuertes, M.A., Northcote, L. C., 2020b. Coccolithophore biodiversity controls carbonate export in the Southern Ocean. *Biogeosciences* 17, 245–263.
- Rigual Hernández, A.S., Flores, J.A., Sierro, F.J., Fuertes, M.A., Cros, L., Trull, T.W., 2018. Coccolithophore populations and their contribution to carbonate export during an annual cycle in the Australian sector of the Antarctic zone. *Biogeosciences* 15, 1843–1862.
- Rintoul, S., Hughes, C., Olbers, D., 2001. The Antarctic circumpolar current system. In: Siedler, G., Church, J., Gould, J. (Eds.). *Ocean Circulation and Climate*. Academic Press, New York, pp. 271–302.
- Rintoul, S.R., Donguy, J.R., Roemmich, D.H., 1997. Seasonal evolution of upper ocean thermal structure between Tasmania and Antarctica. *Deep Sea Research Part I: Oceanographic Research Papers* 44, 1185–1202.
- Saavedra-Pellitero, M., Baumann, K.-H., 2015. Comparison of living and surface sediment coccolithophore assemblages in the Pacific sector of the Southern Ocean. *Micropaleontology* 61, 507–520.
- Saavedra-Pellitero, M., Baumann, K.-H., Flores, J.-A., Gersonde, R., 2014. Biogeographic distribution of living coccolithophores in the Pacific sector of the Southern Ocean. *Marine Micropaleontology* 109, 1–20.
- Saavedra-Pellitero, M., Baumann, K.H., Fuertes, M.A., Schulz, H., Marcon, Y., Vollmar, N.M., Flores, J.A., Lamy, F., 2019. Calcification and latitudinal distribution of extant coccolithophores across the Drake Passage during late austral summer 2016. *Biogeosciences* 16, 3679–3702.
- Schlitzer, R., 2018. Ocean Data View. .
- Schlüter, L., Lohbeck, K.T., Gutowska, M.A., Gröger, J.P., Riebesell, U., Reusch, T.B.H., 2014. Adaptation of a globally important coccolithophore to ocean warming and acidification. *Nature Climate Change* 4, 1024–1030.
- Shadwick, E.H., Tilbrook, B., Cassar, N., Trull, T.W., Rintoul, S.R., 2015. Summertime physical and biological controls on O<sub>2</sub> and CO<sub>2</sub> in the Australian Sector of the Southern Ocean. *Journal of Marine Systems* 147, 21–28.
- Siegel, D.A., Deuser, W.G., 1997. Trajectories of sinking particles in the Sargasso Sea: modeling of statistical funnels above deep-ocean sediment traps. *Deep Sea Research Part I: Oceanographic Research Papers* 44, 1519–1541.
- Siegel, D.A., Granata, T.C., Michaels, A.F., Dickey, T.D., 1990. Mesoscale eddy diffusion, particle sinking, and the interpretation of sediment trap data. *Journal of Geophysical Research* 95, 5305–5311.
- Sikes, E., Howard, W., Samson, C., Mahan, T., Robertson, L., Volkman, J., 2009. Southern Ocean seasonal temperature and Subtropical Front movement on the South Tasman Rise in the late Quaternary. *Paleoceanography and Paleoclimatology* 24.
- Stoll, H.M., Ziveri, P., 2002. Separation of monospecific and restricted coccolith assemblages from sediments using differential settling velocity. *Marine Micropaleontology* 46, 209–221.
- Triantaphyllou, M., Dimiza, M., Krasakopoulou, E., Malinverno, E., Lianou, V., Souvermezoglou, E., 2010. Seasonal variation in *Emiliana huxleyi* coccolith morphology and calcification in the Aegean Sea (Eastern Mediterranean). *Geobios* 43, 99–110.
- Triantaphyllou, M.V., Baumann, K.-H., Karatsolis, B.-T., Dimiza, M.D., Psarra, S., Skampa, E., Patoucheas, P., Vollmar, N.M., Koukousioura, O., Katsigera, A., 2018. Coccolithophore community response along a natural CO<sub>2</sub> gradient off Methana (SW Saronikos Gulf, Greece, NE Mediterranean). *PLoS one* 13, e0200012.
- Trull, T.W., Schulz, E., Bray, S.G., Pender, L., McLaughlan, D., Tilbrook, B., Rosenberg, M., Lynch, T., 2010. The Australian Integrated Marine Observing System Southern Ocean Time Series facility. *OCEANS 2010 IEEE - Sydney*, pp. 1–7.

- Tyrrell, T., Young, J.R., 2009. Coccolithophores. In: Steele, J.H., Turekian, K.K., Thorpe, S.A. (Eds.), *Encyclopedia of Ocean Sciences*. Academic Press, San Diego, pp. 3568–3576.
- van Sebille, E., England, M.H., Zika, J.D., Sloyan, B.M., 2012. Tasman leakage in a fine-resolution ocean model. *Geophysical Research Letters* 39.
- Westbroek, P., Young, J.R., Linschooten, K., 1989. Coccolith Production (Biomineralization) in the Marine Alga *Emiliana huxleyi*. *The Journal of Protozoology* 36, 368–373.
- Young, J., Geisen, M., Cross, L., Kleijne, A., Sprengel, C., Probert, I., Østergaard, J., 2003. A guide to extant coccolithophore taxonomy. International Nannoplankton Association.
- Young, J.R., Ziveri, P., 2000. Calculation of coccolith volume and its use in calibration of carbonate flux estimates. *Deep Sea Research Part II: Topical Studies in Oceanography* 47, 1679–1700.
- Ziveri, P., de Bernardi, B., Baumann, K.-H., Stoll, H.M., Mortyn, P.G., 2007. Sinking of coccolith carbonate and potential contribution to organic carbon ballasting in the deep ocean. *Deep Sea Research Part II: Topical Studies in Oceanography* 54, 659–675.
- Ziveri, P., Rutten, A., de Lange, G.J., Thomson, J., Corselli, C., 2000. Present-day coccolith fluxes recorded in central eastern Mediterranean sediment traps and surface sediments. *Palaeogeography, Palaeoclimatology, Palaeoecology* 158, 175–195.



## Anexo V. Publicación adicional

### **“Preliminary results of R/V METEOR cruise M149: Shipboard and Post-Cruise Analysis, Recurrence of tsunamigenic hazards from *MeBo* drilling records and hazard mitigation using *MeBo* observatories: BIOESTRATIGRAPHY”**

Andre Hüpers <sup>a</sup>, Rouven Brune <sup>a</sup>, Vitor Hugo da Silva Magalhaes <sup>b</sup>, Timo Fleischmann <sup>a</sup>, Tim Freudenthal <sup>a</sup>, **Alba González-Lanchas** <sup>c</sup>, Philipp Haberkorn <sup>a</sup>, Lina Heine <sup>a</sup>, Christopher Klaembt <sup>a</sup>, Peter Mazerath <sup>a</sup>, Walter Menapace <sup>a</sup>, William Meservy <sup>d</sup>, Katharina Moreno <sup>a</sup>, Samuel Pereira <sup>a</sup>, Werner Schmidt <sup>a</sup>, Katja Stanislawski <sup>a</sup> y Martin Stelzner <sup>e</sup>.

<sup>a</sup>MARUM - Zentrum für Marine Umweltwissenschaften der Universität Bremen, Bremen (Germany)

<sup>b</sup>IPMA - Instituto Português do Mar e da Atmosfera, Lisboa (Portugal)

<sup>c</sup>Universidad de Salamanca, Salamanca (España)

<sup>d</sup>Instituto de Ciencias del Mar, Barcelona (España)

<sup>e</sup>Deutscher Wetterdienst, Geschäftsfeld Seeschifffahrt (Germany)

Memoria científica **publicada** en *Berichte-MARUM* (Zentrum für Marine Umweltwissenschaften, Fachbereich Geowissenschaften, Universität Bremen)

DOI: [10.26092/elib/100](https://doi.org/10.26092/elib/100)

## Resumen

El análisis bioestratigráfico llevado a cabo durante la campaña oceanográfica M149 se centró en el análisis de las asociaciones de fósiles calcáreos procedentes del nannoplancton (nanofósiles calcáreos) existentes en los sedimentos recuperados en la campaña para el control de la edad y de los procesos de mezcla de los sedimentos.

Su estudio se llevó a cabo mediante identificación microscópica sobre las muestras preparadas mediante la técnica de preparación de “frotis” sobre un portaobjetos de vidrio para microscopio, que supone la dispersión manual de una pequeña porción del sedimento y su sellado. La toma de muestras se realizó en la parte inferior de todos los testigos recuperados en la campaña y en algunas secciones de interés tras la descripción visual de los materiales.

La taxonomía general para la clasificación de los taxones de nanofósiles calcáreos analizados siguió principalmente los conceptos explicados en las obras de referencia para calcáreos (Burnett et al., 1998; Perch-Nielsen et al., 1985). Las calibraciones de los eventos del Mioceno al Cuaternario se derivan principalmente de (Raffi et al., 2006), mientras que para la biozonización de nanofósiles calcáreos y la calibración de eventos del Paleógeno se siguió el trabajo y propuesta de calibración de (Agnini et al., 2014), basado en datos de latitudes bajas y medias. Además, se emplean los esquemas zonales estándar de Martini (1971) y Okada y Buckry (1980). La bioestratigrafía del Cretácico superior se describe tomando como referencia la escala global superior de (Burnett et al., 1998) y las modificaciones posteriores de (Perch-Nielsen, 1983; Perch-Nielsen et al., 1985).

Para cada muestra se llevó a cabo una observación semicuantitativa. La asignación de los eventos de edad de los nanofósiles calcáreos se basan en la siguiente terminología: “FO” = primera aparición, “LO” = última presencia, “FcO” = primera aparición común, “LcO” = última presencia común, “FaO” = primera aparición en abundancia, “LaO” = última presencia en abundancia, “LrO” = última presencia regular, “T” = techo, parte superior, “B” = base, parte inferior.

Con la aplicación de la metodología previamente detallada se llevó a cabo en estudio de las muestras procedentes de los volcanes de lodo, la zona de lineamientos y los domos salinos, localizados en el Golfo de Cádiz, así como de la zona de fallas de

deslizamiento del mar de Alborán. Los diferentes apartados contenidos en esta memoria incluyen información y esquemas que ilustran visualmente los resultados preliminares básicos de estas investigaciones.

## Referencias

- Agnini, C., Fornaciari, E., Raffi, I., Catanzariti, R., Pälike, H., Backman, J., Rio, D., 2014. Biozonation and biochronology of Paleogene calcareous nannofossils from low and middle latitudes. *Newsletters on stratigraphy* 47, 131-181.
- Burnett, J., Gallagher, L., Hampton, M., Brown, P., 1998. *Calcareous nannofossil biostratigraphy*. British Micropaleontological society publications series. Editor: Paul R. Bown.
- Martini, E. 1971. Standard Tertiary and Quaternary calcareous nannoplankton zonation. In: Proceedings 2nd International Conference Planktonic Microfossils Roma (ed. Farinacci, A.). Tecnoscienza, Rome 2, 739–785.
- Okada, H., Bukry, D. 1980. Supplementary modification and introduction of code numbers to the low-latitude coccolith biostratigraphic zonation (Bukry, 1973; 1975). *Marine Micropaleontology*, 5, 321-325
- Perch-Nielsen, K., 1983. Recognition of Cretaceous stage boundaries by means of calcareous nannofossils, *Symposium on Cretaceous stage boundaries*, Copenhagen, pp. 152-156.
- Perch-Nielsen, K., Bolli, H., Saunders, J., 1985. Mesozoic calcareous nannofossils. *Plankton stratigraphy* 1, 329-426.
- Raffi, I., Backman, J., Fornaciari, E., Pälike, H., Rio, D., Lourens, L., Hilgen, F., 2006. A review of calcareous nannofossil astrobiochronology encompassing the past 25 million years. *Quaternary Science Reviews* 25, 3113-3137.

## **Preliminary Results of R/V METEOR Cruise M149: Shipboard and Post-Cruise Analysis**

*Recurrence of tsunamigenic hazards from MeBo drilling records and  
hazard mitigation using MeBo observatories*

**Chief Scientist: A. Hüpers**

24.07.2018 – 24.08.2018,  
Las Palmas (Canary Islands, Spain) – Cadiz (Spain)



A. Hüpers, R. Brune, V. Magalhaes, M. Freitas, T. Fleischmann, T. Freudenthal, A. Gonzales Lanchas, P. Haberkorn, L. Heine, C. Klaembt, P. Mazerath, W. Menapace, W. Meservy, K. Moreno, S. Pereira, J. N. Schmidt, K. Stanislawski, M. Stelzner

MARUM – Zentrum für Marine Umweltwissenschaften  
Universität Bremen

# **Berichte aus dem MARUM und dem Fachbereich Geowissenschaften der Universität Bremen**

published by

## **MARUM – Center for Marine Environmental Sciences**

Leobener Strasse, 28359 Bremen, Germany

[www.marum.de](http://www.marum.de)

and

## **Fachbereich Geowissenschaften der Universität Bremen**

Klagenfurter Strasse, 28359 Bremen, Germany

[www.geo.uni-bremen.de](http://www.geo.uni-bremen.de)

The "Berichte aus dem MARUM und dem Fachbereich Geowissenschaften der Universität Bremen" appear at irregular intervals and serve for the publication of cruise, project and technical reports arising from the scientific work by members of the publishing institutions.

### **Citation:**

Hüpers, A., Brune, R., Magalhaes, V., Freitas, M., Fleischmann, T., Freudenthal, T., Gonzales Lanchas, A., Haberkorn, P., Heine, L., Klaembt, C., Mazerath, P., Menapace, W., Meservy, W., Moreno, K., Pereira, S., Schmidt, J. N., Stanislawski, K., Stelzner, M.: Preliminary results of R/V METEOR cruise M149: Shipboard and Post-Cruise Analysis, Recurrence of tsunamigenic hazards from MeBo drilling records and hazard mitigation using MeBo observatories, Las Palmas (Canary Islands) – Cadiz (Spain), 24.07.2018 – 24.08.2018. Berichte, MARUM – Zentrum für Marine Umweltwissenschaften, Fachbereich Geowissenschaften, Universität Bremen, No. 324, 200 pages. Bremen, 2020. ISSN 2195-9633.

An electronic version of this report can be downloaded from:

<http://nbn-resolving.de/urn:nbn:de:gbv:46-MARUM9>

Please place requests for printed copies as well as editorial concerns with [reports@marum.de](mailto:reports@marum.de)





Fig. 2.1 Group photo of the science party.

## 2.2 Participating Institutions

MARUM	Zentrum für Marine Umweltwissenschaften der Universität Bremen (Germany)
U.Salamanca	Universidad de Salamanca (Spain)
DWD	Deutscher Wetterdienst, Geschäftsfeld Seeschifffahrt (Germany)
IPMA	Instituto Português do Mar e da Atmosfera (Portugal)
ICM	Instituto de Ciencias del Mar (Spain)

## 2.3 Crew

Name	Rank	Name	Rank
Detlef Korte	Master	Piotr Bußmann	Ship Mechanic
Heike Dugge	Chief officer	Alexander Durst	Ship Mechanic
Dirk Kahnke	1st Officer	Hans-Joachim Behlke	Ship Mechanic
Magnus Keller	2nd Officer	Hubert Hildebrandt	Ship Mechanic
Michael Hinz	Ship's doctor	Torsten Kruzona	Ship Mechanic
Peter Neumann	Chief Engineer	Merlin Till Pleuler	Ship Mechanic
Ralf Heitzer	2nd Engineer	Michael Zeigert	Ship Mechanic
Björn Brandt	2nd Engineer	Rainer Götze	Chief Cook
Rudolf Freitag	Electrician	Peter Wernitz	2nd Cook
Heinz Voigt-Wenzel	Chief Electronics Eng.	Jan Parlow	Chief Steward
Harry Scholz	Electronics Engineer	Petra Zimmermann	Steward
Bernhard Bagyura	System Manager	Monika Jürgens	Steward
Gerhard Lange	Fitter	Guomin Zhang	Laundryman
Lukas Eller	Motorman	Tom Ederleh	Apprentice
Jannik Hageleit	Motorman	Christoph Weber	Apprentice
Klaus Kudraß	Motorman	Alexander Wolf	Bosun

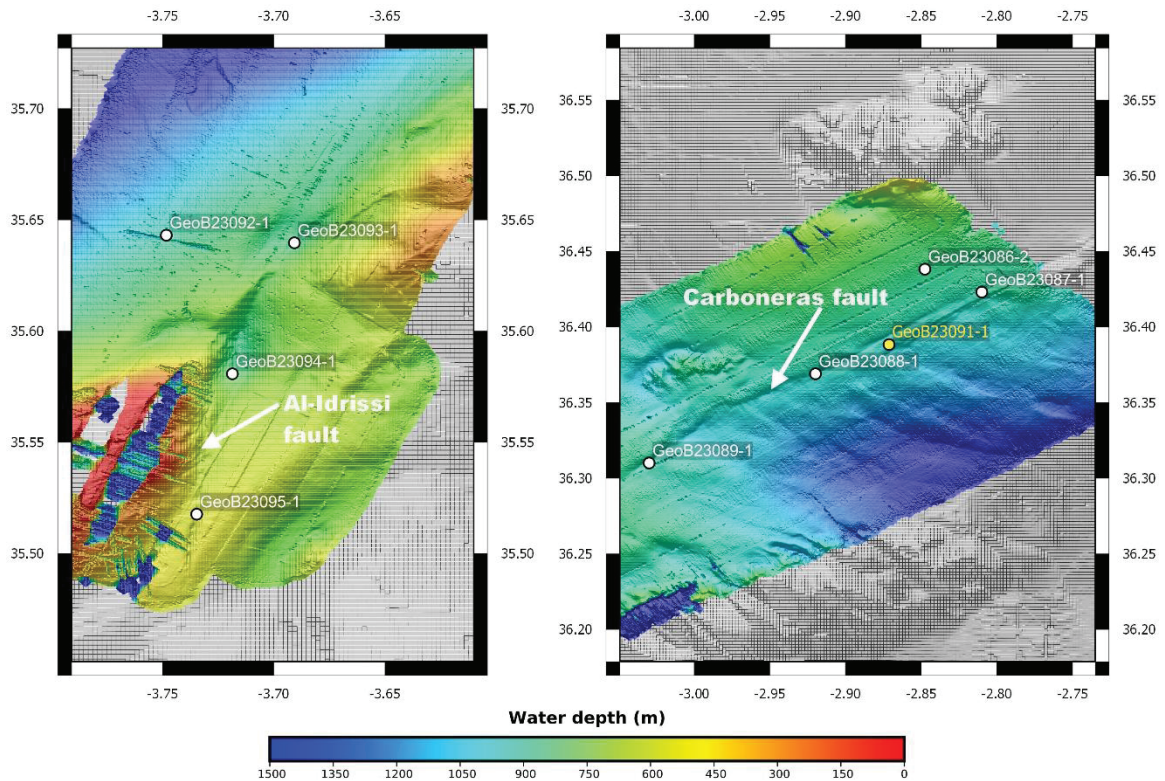


**Fig. 5.13** Bathymetric map showing the locations of gravity cores (white dots) and the MeBo core (yellow dot) in the Alboran Sea.

## 5.3 Biostratigraphy

(A. Gonzales Lanchas, P. Mazerath)

### 5.3.1 Methodology

Biostratigraphic analysis during cruise M149 focused on the calcareous nannoplankton fossils (calcareous nannofossils) assemblage in the recovered sediment. The nannofossils represent a powerful age control tool in ocean sedimentary sequences because of their small size, wide dispersion (since their first appearance in the Triassic) and full adaptation to different oceanic environments and photic zone water column depths. Micropaleontological samples for age control were obtained from the core catcher of every recovered core. Additional samples were selected during the core description to better characterize the lithologic variability of the sediment and to provide a more refined age determination. Those samples were also described regarding the percentage of the main components.

Nannofossils were studied for morphological species identification using an OLYMPUS transmitted-light microscope with a 1250 $\times$  magnification. For sample preparation, a small amount of sediment was placed on glass slide. Due to the small amount of sediment material required; the samples were taken from the archive half of the core. After adding a drop of distilled water, the samples were delicately spread on the slides with toothpicks. This was followed by a brief heating of the slides on a hotplate to dry the sediment. Then a drop of adhesive (Norland Optical Adhesive 61) was added to the cooled sediment sample which was covered with a MENZEL coverslip. For curing, the smear slides were placed under blacklight (UV) for  $\sim$  15 minutes.

For each sample a semiquantitative observation was made, in order to characterize the nannofossil assemblage. Calcareous nannofossil age events are assigned in core catcher samples and additional ones based on the following terminology: FO = first occurrence, LO = last occurrence, FcO = first common occurrence, LcO = last common occurrence, FaO = first abundant occurrence, LaO = last abundant occurrence, LrO = last regular occurrence, T = top, B = bottom, AB = acme bottom.

Several information sources are used for the classification of the calcareous nannofossil taxa. The general taxonomy mainly follows the concepts explained in the reference works for calcareous nannofossil biostratigraphy (Bown, 1998), Cenozoic calcareous nannofossils (Perch-Nielsen, 1985) and in the updated online dataset Nannotax (<http://ina.tmsoc.org/Nannotax3/index.php?dir=Coccolithophores>). The calibrations of the Miocene to Quaternary events are derived mainly from Raffi et al. (2006) and by correlation to the geomagnetic polarity timescale (GPTS) of Lourens et al. (2004a, b). Additionally, Martini (1971) and Okada and Bukry (1980) standard zonal schemes were adopted. For calcareous nannofossil biozonation and calibration of Paleogene events we followed Agnini et al. (2014), based on data acquired from key low- and middle-latitude deep-sea drilling sequences and marine onland sections of the Tethyan region (Agnini et al. 2014). Additionally, Martini (1971) and Okada and Bukry (1980) standard zonal schemes are adopted. Biostratigraphy of the Upper Cretaceous is described with reference to both the global Upper Cretaceous UC biozonation of Burnett (1998) and the older CC biozonation of Sissingh (1977), as modified by Perch-Nielsen (1979, 1983, 1985).

### **5.3.2 Gulf of Cadiz – Mud Volcanoes**

The analyses of the calcareous nannofossil assemblage in the recovered mud volcano sediments is based on the study of CC (core catcher) samples and additional samples from working half sections. Two well differentiated contexts, related to the content of calcareous nannofossils, have been observed in the samples that reflect the facies of the hemipelagic cover and the underlying mud breccia (Fig. 5.14).

For the hemipelagic cover the calcareous nannofossil content is always representative of an autochthonous nannoplankton assemblage, which is widely dominated by *Gephyrocapsa* spp. (small *Gephyrocapsa*, *G. caribbeanica*, *G. oceanica* and *G. muelleriae*), *Calcidiscus leptoporus* (subsp. *leptoporus*, *quadriperforatus* and small), *Coccolithus pelagicus* (subsp. *pelagicus*, *braarudi* and *azorinus*) *Umbilicosphaera* spp., *Syracosphaera* spp., *Rhabdosphaera clavigera*, *Florisphaera profunda*, *Helicospaera carteri*, *Helicospaera inversa* and *Calcisolenia brassilensis*. Due to the general absence of *Pseudoemiliana lacunosa*, a lower age limit of 0.47 Ma is established for the hemipelagic sediments based on the biohorizon top of that species. Presence of small placoliths of *Emiliana huxleyi* could not be specified on board due to technical limitations but, based on general shape of the *Gephyrocapsa* spp. assemblage (low relative *G. caribbeanica*), we assume the closeness or the later age of some of these sediments with respect to 0.29 Ma (biohorizon base of *E. huxleyi*). Only in few samples the clear presence of the large *Emiliana* morphotype (>4 µm) was detected, setting that sediments as younger than 0.29 Ma. In essence, the hemipelagic sediment cover represents a Quaternary age. Only in the cases in which lower intervals markers (lower Pleistocene - Pliocene) were identified a specific description has been made. Preservation of

calcareous nannofossils in the hemipelagic sediments is generally very good to excellent. Overgrowth and dissolution patterns are not observed in any case.

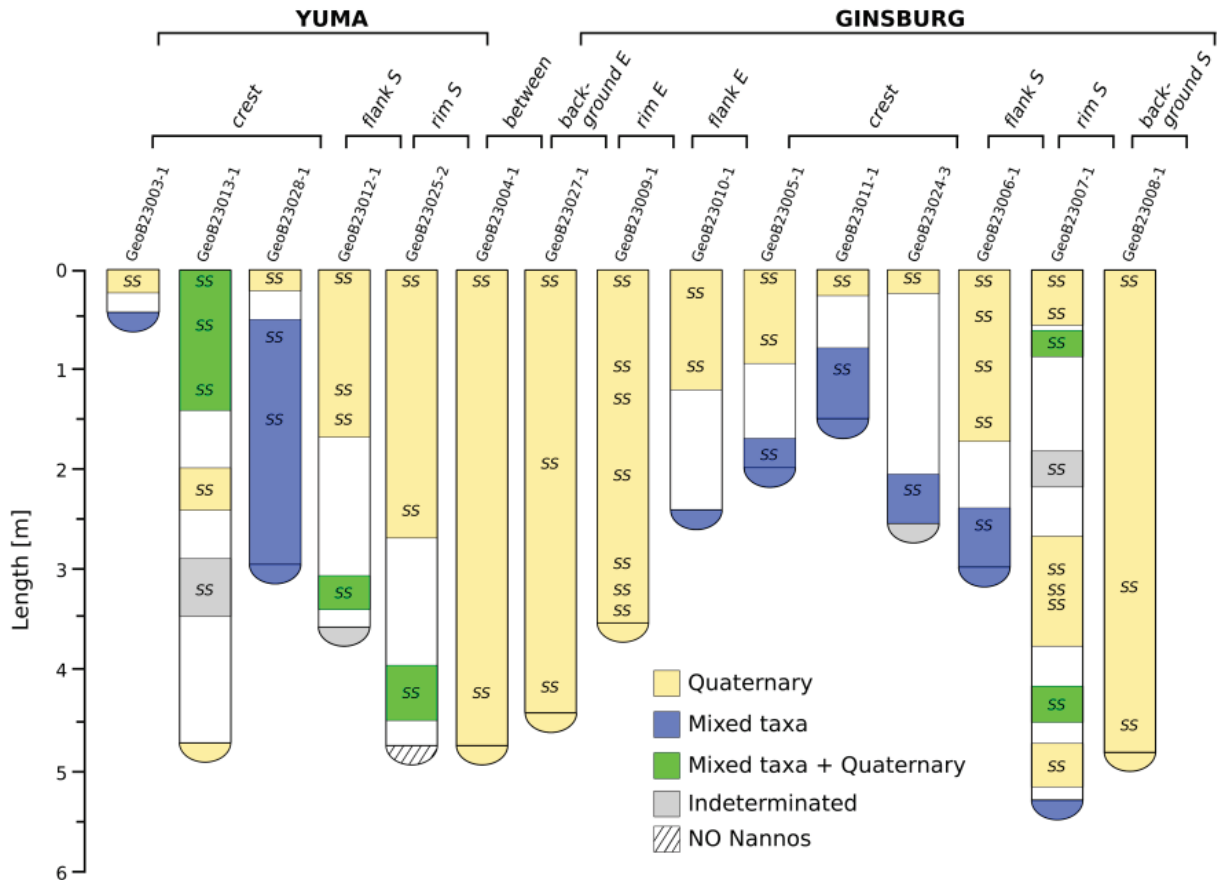


**Fig. 5.14** Summary of the biostratigraphic analyses showing the distribution of quaternary assemblages and mixing of specimens of different ages in mud breccias that constitute an unnatural species aggrupation non-representative of any nannoplankton specific age (=mixed taxa).

The calcareous nannofossil content in mud breccias is characterized by the mixing of specimens of different ages that constitute, in a similar proportion, an unnatural species aggrupation non-representative of any nannoplankton specific age assemblage. Because many species observed in the mud breccias are characterized by very broad age ranges / dispersion over time (i.e. *Reticulofenestra* spp., *Coccolithus* spp.), the observation focused on biomarkers with more narrow age dispersion, trying to delimit the main time interval or intervals of the materials. It is, therefore, a preliminary analysis lacking precise quantitative or semiquantitative character that could limit in-depth interpretations of these sediments. However, a mixture of taxa is observable, in which the Paleocene-Eocene and Middle Miocene biomarker content stands out. Some species with Oligocene and Pliocene-Pleistocene ranges are also present. Upper Cretaceous specimens also appear with a significantly higher proportion in certain cases. It is important to highlight the systematic observation of some nannofossils after Pleistocene age that are included in the mud volcano samples but always in a scattered proportion (e.g., *Gephyrocapsa* spp.). Only in those cases in which the Quaternary content is present in similar proportion to the old taxa, a mixing between both groups is referred to (Mixed taxa + Quaternary in Fig. 5.14). Preservation of nannofossils in mud breccia samples is moderate to poor. Evidence of regrowth, breakage

(especially significant in large species i.e. *Discoaster* spp.) and dissolution have been observed systematically in these specimens.

### 5.3.3 Gulf of Cadiz – Lineaments

Biostratigraphic analysis of sediments sampled along the lineaments and their branches focused on the small pull-apart basin structures – in particular the long MeBo cores (GeoB23069-1 along the Hermes fault (Fig. 5.09) and GeoB23073-1 along Lineament South (Fig. 5.11)). Calcareous nannofossil content in those cores is dominated, similar to the hemipelagic apron of the mud volcanoes, by *Gephyrocapsa* spp. (small *Gephyrocapsa*, *G. caribbeana*, *G. oceanica* and *G. muelleriae*), *Calcidiscus leptoporus* (subsp. *leptoporus*, *quadriperforatus* and small), *Coccolithus pelagicus* (subsp. *pelagicus*, *braarudi* and *azorinus*), *Umbilicosphaera* spp., *Syracosphaera* spp., *Rhabdosphaera clavigera*, *Florisphaera profunda*, *Helicosphaera carteri*, *Helicosphaera inversa* and *Calcisolenia brassilensis*. *Helicosphaera sellii*, *P. lacunosa* and *Reticulofenestra asanoi* are also present. Conservation of nannoplankton is high in almost all samples, showing a very good to excellent preservation state.

The calcareous nannofossils studied for MeBo core GeoB23069-1 (Hermes fault basin) is based on core catcher samples from core barrels GeoB23069-1\_19P to GeoB23069-1\_1P. The chronological framework for GeoB23069-1 is based on calcareous nannofossil events suggesting an age record until early to middle Pleistocene (Fig. 5.15). The identification of *Helicosphaera sellii* in the lowermost core catcher (CC), together with the absence of *Calcidiscus macintyreii*, limits the age of the lowermost sequence after 1.60 Ma, the biohorizon top of *Calcidiscus macintyreii*. Biohorizon top of *Helicosphaera sellii* (1.26 Ma) is placed in GeoB23069-1\_15P\_CC. Some specimens of *Reticulofenestra asanoi* are observed between GeoB23069-1\_12P\_CC and GeoB23069-1\_6P\_CC (Fig. 18). The age interval of 1.14 - 0.91 Ma for the range of occurrence of this species is assigned to GeoB23069-1\_10P\_CC - GeoB23069-1\_9P\_CC, where the morphotype larger than 6.5  $\mu\text{m}$  is observed in a high proportion in the assemblage (bloom). The stratigraphy of the last ~0.6 Ma is well-constrained up to the seafloor by the biohorizon base of the *Gephyrocapsa caribbeana* acme (0.60 Ma), located in GeoB23069-1\_10P\_CC. The interval of high relative abundance of this taxon relative to the other *Gephyrocapsa* species appears widely recorded in the sediment until the uppermost CC sample of the core, with a high content of *G. caribbeana* that dominates the complete assemblage in all samples. Biohorizon top of *P. lacunosa* (0.44 Ma; base Zone NN20) is well defined in sample GeoB23069-1\_3P\_CC (Fig. 5.15). Gravity core GeoB23066-1, which is also located in the Hermes fault basin (Fig. 5.9), shows an absence of *P. lacunosa*, placing the age of that sequence at least above 0.47 Ma (base Zone NN20). Gravity core GeoB23067-1 shows a calcareous nannoplankton assemblage corresponding to the same time interval. Despite that, some specimens of that taxon appear in a scattered occurrence together with other lower Pleistocene species up to the top of the sequence.

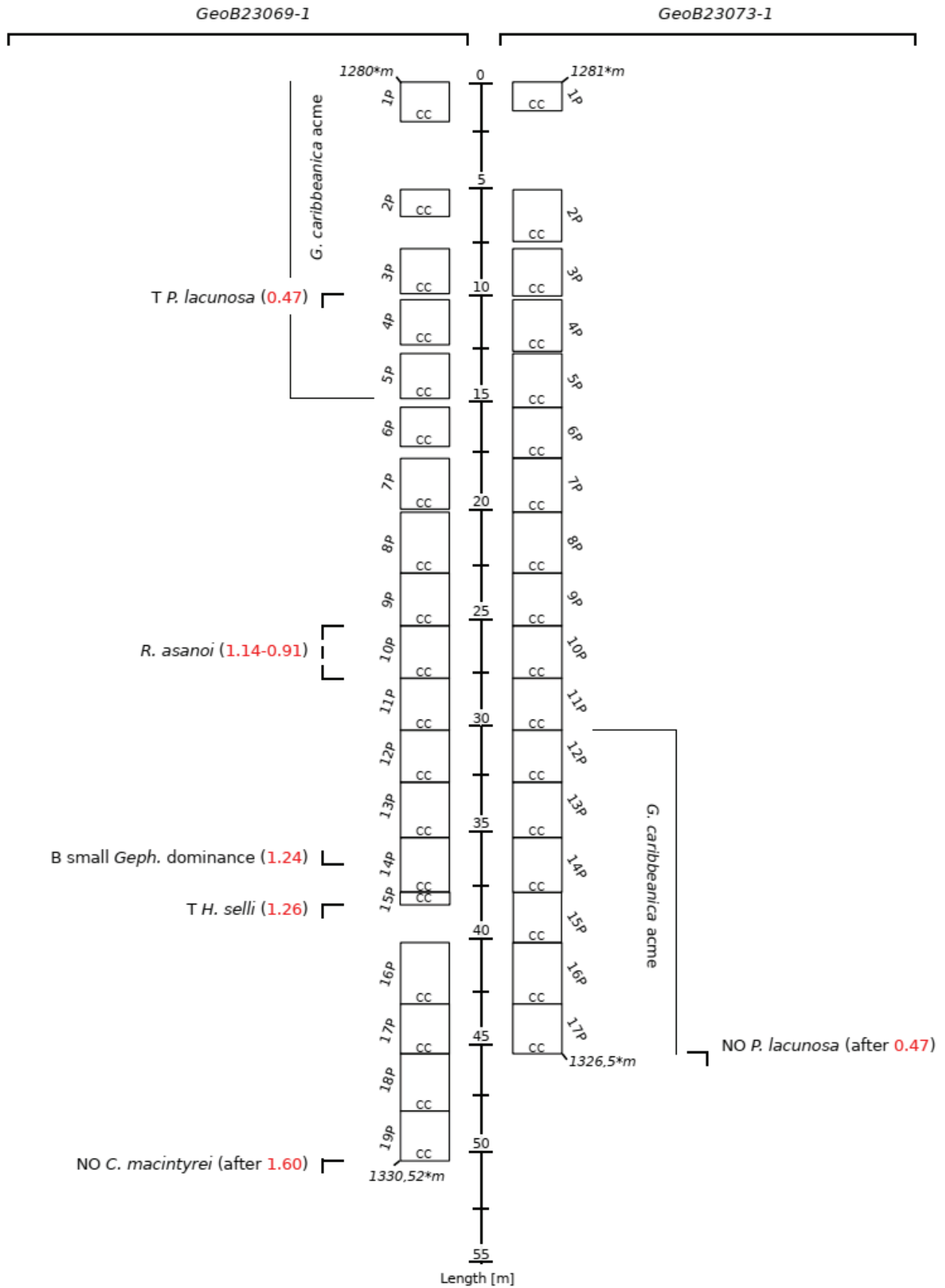


Fig. 5.15 Summary of the biostratigraphic analyses of calcareous nannofossils in core catcher samples from MeBo cores GeoB23069-1 (Hermes fault) and GeoB23073-1 (Lineament South). \* Water depth in (m).

The biostratigraphic record of MeBo core GeoB23073-1, located along the Lineament South, is based on the study of calcareous nannofossils in core catcher samples from core barrels GeoB23073-1\_17P to GeoB23069-1\_1P (Fig. 5.15). The chronological framework for GeoB23073-1 suggests a late Pleistocene (late Pleistocene/Holocene?) record. The interval between the lowermost GeoB23073-1\_17P\_CC and GeoB23073-1\_11P\_CC is characterized by the dominium of the assemblage by *Gephyrocapsa caribbeanica* (Fig. 5.15). The identification of the acme of this species, with no content of *P. lacunosa*, limits the age of the sequence to the last 0.47 Ma (biohorizon top of *P. lacunosa*). *E. huxleyi* was not clearly identified in the rest of the sequence. Calcareous nannofossil content in the gravity core GeoB23031-1, also located in the basin, registers to the late Pleistocene (late Pleistocene/Holocene?) with the absence of *P. lacunosa* in all samples. Some specimens of early to middle Pleistocene age (*C. macyntirei*, *H. selli* and *R. asanoi*) appear in a scattered occurrence up to the top of both sequences, with some samples in which the content of some older biomarkers is increased. Further gravity coring along Lineament South was conducted at stations GeoB23062-1, GeoB23063-1, GeoB23064-1 and GeoB23066-1 (Fig. 5.11). Similar to MeBo core GeoB23073-1, the nannofossil content in these cores is constrained to the last 0.47 Ma because the absence of *P. lacunosa*. A *G. caribbeanica* acme interval is also not identified in these samples. Instead the identification of scattered early to middle Pleistocene age biomarkers (*C. macyntirei*, *H. selli* and *R. asanoi*) is frequent in some samples. No *E. huxleyi* morphotypes have been clearly identified here.

#### **5.3.4 Gulf of Cadiz – Salt Domes**

Core catcher samples of gravity cores GeoB23078-3, GeoB23079-1 and GeoB23080-1 were studied to characterize the calcareous nannoplankton in the sediment covering the diapiric ridges and salt domes in the Seine abyssal plain (Fig. 5.12). The preservation of calcareous nannofossils in the investigated samples is very good to excellent showing a Quaternary age assemblage dominated by *Gephyrocapsa* spp. (small *Gephyrocapsa*, *G. oceanica* and *G. muellerae*), *Calcidiscus leptoporus* (subsp. *leptoporus*, *quadriperforatus* and small), *Coccolithus pelagicus* (subsp. *pelagicus*, *braarudi* and *azorinus*) and *Florisphaera profunda*. *Umbilicosphaera* spp., *Syracosphaera* spp., *Rhabdosphaera clavigera*, *Helicospaera carteri* are also present. Some specimens of large *Emiliana* are observed within the assemblage in GeoB23079-1\_CC and GeoB23080-1\_CC, allowing us to suggest an age after 0.29 Ma (biohorizon base *E. huxleyi*) for these sediments. This species was not clearly observed in GeoB23078-3\_CC. However, *P. lacunosa* is absent in all these samples, setting a lower age limit at 0.47 Ma (biohorizon top *P. lacunosa*).

#### **5.3.5 Alboran Sea – Strike-Slip Faults**

The preliminary study of the calcareous nannofossil content in cores recovered along the Carboneras and Al-Idrissi fault zones registers Quaternary age material. Calcareous nannofossils are abundant in these samples, with a very good to excellent preservation state. The assemblages are characteristically dominated by *Gephyrocapsa* spp. (small *Gephyrocapsa*, *G. oceanica* and *G. muellerae*), *Calcidiscus leptoporus* (subsp. *leptoporus*, *quadriperforatus* and small), *Coccolithus*

pelagicus (subsp. pelagicus, braarudi and azorinus) and Florisphaera profunda. Umbilicosphaera spp., Syracosphaera spp., Rhabdosphaera clavigera and Helicospaera carteri are also present as well as the large morphotype of E. huxleyi (>4 µm). The P. lacunosa biomarker is absent in all samples studied for this sector of Alboran Sea, limiting the age of the sediments to the last 0.47 Ma (biohorizon top of P. lacunosa). G. caribbeanica is also absent or appearing in rare morphotypes. The high abundance of large Emiliana is frequent through these samples (not in all), establishing a lower age limit of 0.29 (biohorizon base E. huxleyi) for these sediments (Fig.5.16).

The Carboneras fault sediments were biostratigraphically analyzed based on the study of calcareous nannofossils in core catcher samples from gravity cores GeoB23086-1, GeoB23087-1, GeoB23088-1 and GeoB23089-1 and from core catchers of MeBo core GeoB230691-1\_7P to GEOB 23069-1\_1P (Fig. 5.13). In cores GeoB23086-1 and GeoB23087-1 large Emiliana were identified as part of the calcareous nannoplakton assemblage, setting the lower age limit after 0.29 Ma (Fig.5.16). In GeoB23088-1\_CC and GeoB23089-1\_CC this precision could not be carried out because of an unclear observation of these species. In MeBo core GeoB23091-1 specimens of large Emiliana were only observed in the CC of the lowermost barrel (GeoB23091-1\_1P\_CC), setting for this core an age limit after 0.29 Ma (biohorizon base of E. huxleyi) (Fig.5.16).

Core catcher samples from the Al-Idrissi fault zone GeoB23092-1, GeoB23093-1, GeoB23094-1 and GeoB23095-1 were also studied for their calcareous nannofossil content (Fig. 5.13). P. lacunosa is absent in these samples, whereas large Emiliana species were identified in GeoB23092-1\_CC and GeoB23095-1\_CC. This sets the lower age limit to 0.29 Ma (biohorizon base of E. huxleyi) for these cores.

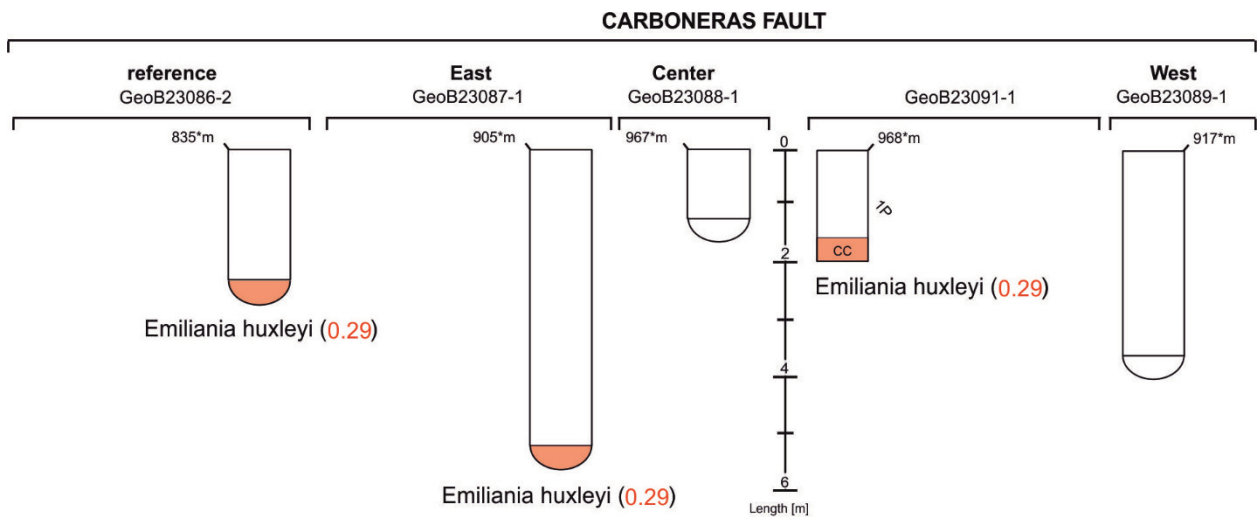


**Fig. 5.16** Summary of the biostratigraphic analyses of calcareous nannofossils in core catcher samples from cores sampled along the Carboneras fault. \*Water depth in (m).



